The hadronic properties of the photon in high-energy interactions*

T.H. Bauer ,† R. D. Spital,‡ and D. R. Yennie

Laboratory of Nuclear Studies, Cornell University, Ithaca, New York 14853

F. M. Pipkin

Department of Physics, Harvard University, Cambridge, Massachusetts 02138

High-energy photon interactions are discussed in terms of the hadronic structure of the photon, which is expressed by means of a formulation which is akin to, but somewhat more general than, vector-meson-dominance or specific generalized vector-dominance models. Experiments which demonstrate and yield information about this hadronic structure are discussed critically, and the resulting information is carefully evaluated. Special attention is paid to diffractive processes such as the photoproduction of vector mesons and to photon shadowing effects on nuclei. Relationships to other views of photon interactions, such as the parton model and the space-time description, are also discussed; these views are seen to complement the hadronic structure picture rather than to be in conflict. The general overview is that there is ample evidence which shows that the photon's hadronic structure plays a significant role in its interactions. What further work would most significantly enhance the understanding of the hadronic structure of the photon is also pointed out.

CONTENTS

*The preparation of this review was supported in part by the National Science Foundation (Cornell) and in part by the Energy Research and Development Administration (Harvard).

†Present address: Reactor Analysis and Safety Division, Argonne National Laboratory, Argonne, Il. 60439.

‡Present address: Pfizer Medical Systems, Columbia, Md. 21045.

I. INTRODUCTION

A. The internal structure of the photon

The concept of the photon originated in the first years of quantum mechanics, and the study of electromagnetic interactions with matter has played a prominent role throughout the history of quantum theory. At first, the photon was regarded as structureless, and the theory was very successful in predicting various spectral lines and their intensities and in understanding other processes such as the atomic photoeffect. As the scale of available energies increased, it was found that through an interaction with a Coulomb field the photons could materialize as pairs of electrons. Although not usually thought of in these terms, this phenomenon was the earliest manifestation of photon structure.

Pair production occurs because of the basic interactions

$$\gamma \rightleftarrows e^+ + e^-$$

required by relativistic quantum theory. These interactions are between "bare" states described by a "free Hamiltonian." Physical particle states, however, are eigenstates of the complete Hamiltonian. Therefore, a physical particle state contains not only the corresponding bare particle state, but also contributions from all bare states coupled to it by the interaction. We may think of the particles in these bare states as constituents of the physical particle.

Accordingly, with the above interaction, the physical photon has an electron-positron pair constituent. It is possible to think of pair production as arising through the scattering of this constituent by the Coulomb potential, permitting the pair to actually materialize, provided that the energy available is sufficiently high, i.e., $>2m_ec^2$. At low energies ($\ll 2m_ec^2$), the virtual e^+e^- pair does not manifest itself in a very pronounced way, although it does of course play an important role in refined quantum-electrodynamic effects. This illustrates the point that *at different energy scales, different aspects of the underlying dynamics become visible.*

When the first experiments on photoproduction of pions and electron scattering from nucleons were carried out,

the photon (real or virtual) was for purposes of hadronic interactions again regarded as structureless. (Of course, its structure due to electron pairs was taken into account through radiative corrections, which were in principle well understood.) That is, the photon was assumed to measure a charge density which is already present in hadrons or to induce a transition to an excited state (possibly involving particle production), with all the physical details being associated with the target, very much as in atomic physics.

Within the last fifteen years, there has been a growing awareness that this is too simple a view, and that in reality the photon has an internal structure which is very similar to that of hadrons, except that it occurs with a relative probability only of order $\alpha(\simeq 1/137)$. At lower energies, this hadronic structure of the photon is not apparent since the photon cannot materialize into these constituents by interacting with a target (in analogy with e^+e^- pair production, the energy available is far too low to excite this degree of freedom). However, as available photon energies have risen to the multi-GeV range, the similarities between photon interactions with hadrons and other hadron interactions have become increasingly apparent; an overview of these will be given in Sec. II.A. An elementary introduction to these ideas is provided in a *Scientific American* article by Murphy and Yount (1971). An intuitive discussion of the hadronic properties of the photon, based largely on the material in this review, was given by Yennie (1976) at the 1976 Cracow School of Theoretical Physics and also at the 1976 Latin American School of Physics in Caracas.

To avoid (or anticipate!) later confusion, it should be emphasized that there is no sharp distinction between effects due to the photon's internal structure, the target's internal structure, and the mutual properties of the interaction. To illustrate this point, we anticipate the fact that there is an interaction which permits a photon to transform to a vector meson (such as the ρ^0, ω, or ϕ)

$$\gamma \rightarrow V \tag{1.1}$$

and that this vector meson in turn couples to other hadrons. Such an interaction could affect the charge distribution seen in electron scattering experiments, as illustrated in Fig. 1(a). In this case, it has been usual to regard the modification due to (1.1) as being associated entirely with the target: V causes a change in the distribution of charge which is measured by the electron through a virtual photon. It is worth noting in this case that the photon is typically *highly* virtual (and spacelike: its energy $\ll$ its momentum). Another process is illustrated in Fig. 1(b). Here a real, high-energy photon transforms into a V before interacting with a target to produce a multiparticle final state. In this case it is more natural, as we shall argue in this paper, to regard the V as part of a "hadronic structure" of the photon since in particular the conversion to V often takes place well outside the normal structure of the target. We have described two extreme situations where the physical interpretation seems rather plausible, but there are also intermediate cases where the interaction and the structures must be considered as a unity. While it is strictly speaking meaningless to discuss the photon's structure in isolation from its subsequent interaction, we shall analyze the structure of a high-energy free photon in Sec. II.B, having in mind a target at rest with which it will ultimately interact.

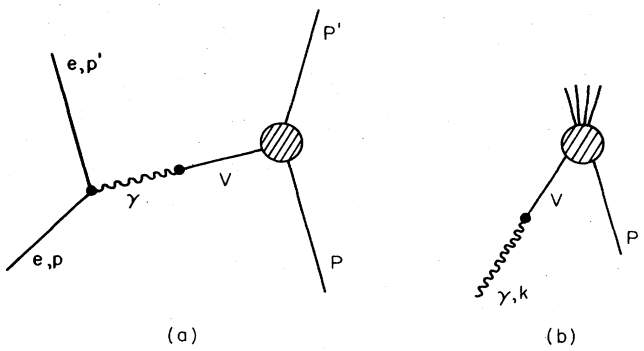

FIG. 1. Two situations where a photon interaction proceeds through an intermediate vector meson. (a) Elastic electron scattering with a virtual photon; here the vector meson is usually regarded as yielding a modification of the target charge distribution. (b) High-energy interaction of a real photon; the conversion takes place well outside the target and the vector meson is considered part of the photon's hadronic structure.

In a complete theory of high-energy electromagnetic interactions, the intuitive picture of how a collision takes place plays an interesting, but not a crucial, role. Lacking such a theory, the intuitive picture acquires a more important significance. It substitutes for a theory and aids us in developing models for interpreting and correlating experimental facts. One line of models [vector-meson-dominance or generalized(extended) vector-dominance] places the emphasis on the hadronic structure of the photon, while another (parton) concentrates on the structure of the target in an infinite momentum frame. The hadronic structure models are more natural and successful in describing the facts in one kinematic domain, and the parton models in another; they are not in conflict, but each seems "unnatural" when employed beyond its appropriate kinematic region (see Sec. II.D for further discussion).

The present paper is an assessment of the status of the hadronic structure picture. In spite of its length, we make no claim for a complete or balanced presentation. When originally conceived several years ago, the aim was to restrict the discussion to high-energy photon interactions with nuclei as a test of vector-meson dominance. Although the scope of the paper has been expanded, it is still largely oriented toward photon interactions with nuclei and emphasizes the role of lower-mass constituents of the photon (the ρ^0, ω, and ϕ). The various approaches to understanding the high-mass contributions are described in Secs. II.C, II.D, and VI.B as speculations. This is a reflection of our view that the role of these constituents, while undoubtedly important, is still only imperfectly understood. We were also not as successful as we would have liked in tying down the important numerical parameters of the model. Hopefully we have pinpointed the uncertainties of experiment and theory so that the next generation of work will produce more definitive conclusions. In the final chapter, we have tried to indicate areas where experiments could

add to our general understanding of the hadronic structure picture.

In the preparation of this article, we have benefitted from numerous review articles. Good sources of general information are the proceedings of recent lepton-photon conferences. Some conference summaries of particular relevance are as follows: 1971 Cornell conference (ed., Mistry, 1972); see papers by Wolf (1972), Gottfried (1972), K. Wilson (1972), and Kendall (1972). 1973 Bonn conference (eds., Rollnik and Pfeil, 1974); see papers by Strauch (1974), Gabathuler (1974), Moffeit (1974), and Preparata (1974). 1975 Stanford conference (ed., Kirk, 1975); see papers by Schwitters (1975), Gilman (1975), Silverman (1975), Mo (1975), Taylor (1975a), Llewellyn-Smith (1975), and Wolf (1975). 1977 Hamburg conference (ed. Gutbrod, 1977); see papers by Hand (1977), Marshall (1977), W. Y. Lee (1977), and Nachtman (1977). The 1970 Scottish Universities Summer School was devoted to electromagnetic interactions of hadrons (Cumming and Osborn, 1971); it has several articles related to this review (Leith, 1971; Gourdin, 1971; Harari, 1971; and Yennie, 1971). More recently, a collection of articles on the same subject has been edited by Donnachie and Shaw (1978a); we have had the benefit of some of these before publication (Donnachie and Shaw, 1978b; Grammer and Sullivan, 1978; and Leith, 1978). Feynman (1972) has prepared a book based on his lectures at Caltech. Some other reviews which we wish to cite are the following: Bauer (1972), Bjorken (1973), Gottfried (1970), Greco (1975), Harari (1967), Rosenfeld and Söding (1973), Sakurai (1968, 1969a,b, 1973, 1975), Schildknecht (1969, 1972, 1975), Schwitters (1977), Schwitters and Strauch (1976), Silverman (1969), Stodolsky (1970), Ting (1975), Weise (1974), Wolf (1971), Yan (1976), and Yennie (1977).

We tried to make the search of published literature complete to July 1, 1977. Some information which came to us since that date has been included where it seemed appropriate. We have, in general, not included material from the unpublished literature such as theses, laboratory reports, invited talks presented at meetings, etc., unless the information was unique or had special significance. We found it difficult to evaluate this material and were suspicious because it had not been published. Its limited accessibility also makes it of secondary value to the reader of this review. A glossary of notation is provided in Appendix E. Specialized material which may be skipped without breaking continuity is indicated by a mark (●) at the beginning of the paragraph.

B. Brief historical review

Our review of the development of ideas about the photon's hadronic structure will emphasize topics that are important for the remainder of the paper. It omits (without further apology) many interesting topics related to the development of vector-meson dominance. It also emphasizes the origin of concepts and early experiments rather than their subsequent refinements. These further developments are described in the detailed discussion of subsequent sections. We hope there are no serious distortions of the evolution of the subject.

The need for vector mesons was first indicated by some puzzles concerning the electromagnetic structure of nucleons. [However, Duerr (1956) and Teller (1956) had suggested earlier that vector mesons might play a role in nuclear forces.] A pre-vector-meson review of the situation was given by Yennie, Lévy, and Ravenhall (1957). Electron scattering experiments by Hofstadter *et al.* (McAllister and Hofstadter, 1956; Chambers and Hofstadter, 1956) had revealed that the proton had an extended charge distribution. Intuitively, this could be accounted for by a positive pion cloud in the proton. However, electron-neutron interactions (Hughes *et al.*, 1953; Melkonian *et al.*, 1956) as well as electron-deuteron scattering (McIntyre, 1956; McIntyre and Hofstadter, 1955) had revealed that the neutron had no appreciable charge structure, whereas charge symmetry had indicated it should have a negative pion cloud. A way out of this puzzle was suggested by Nambu (1957). He noted that if the electron and nucleon could exchange an isoscalar vector meson it would be possible to cancel the effect of the negative pion cloud in the neutron while enhancing the charge of the positive pion cloud in the proton. Another puzzle was noted by Drell (1958) in a careful review, presented at the 1958 CERN Conference, of the dispersion theory approach (Federbush *et al.*, 1958; Chew *et al.*, 1958) to the electromagnetic form factors. He pointed out the difficulty of simultaneously accounting for the magnitude and the radius of the isovector magnetic moment of the nucleon, which in the timelike region was thought to be dominated by intermediate pion pair states. After Drell's elaboration of the possibly important role of $\pi-\pi$ interactions in enhancing the low-mass region [which, incidentally, had also been suggested in an earlier, non-dispersion-theoretic paper by Holladay (1956)], Gell-Mann summarized the situation with the following comment:

"I understand from this talk that the theorists concerned with dispersion theory of G_2^v can get out of a very deep hole only if they suppose that the pion—pion system has a sort of resonance in the $I=1$, $J=1$ state, so that the form factor of the pion can correspond to a very spread-out pion. If so, it may be possible, using the observed magnetic moment and the observed structure of magnetic moment, to find very severe restrictions on what must be properties of this $I=1$, $J=1$ two-pion state, and one should formulate these, the energy and the lifetime of this state, and ask people to look for it in production experiments of two pions."

Subsequently, Frazer and Fulco (1959, 1960) found that they could explain the observed form factor in terms of a $\pi\pi$ resonance in the $I=1$, $J=1$ state with a total energy of roughly 550 MeV. A critical review of the studies of that era was provided by Drell and Zachariasen (1961).

During this same period, and moving further away from the picture of photons coupling with "loose" pions, Sakurai (1960) took advantage of a general gauge field theory (analogous to electromagnetic theory) proposed by Yang and Mills (1954) to develop a theory in which there was a whole family of vector mesons which were universally coupled to conserved isotopic spin, baryon, and hypercharge currents. Universality means that there is just one coupling constant for each type of vector me-

son; this is analogous to the universality of the electric charge. For example, the coupling of the $I=1$ vector mesons (ρ^+, ρ^0, and ρ^-) to both π mesons and to nucleons is given by the same constant (aside from isotopic spin factors). This coupling strength is defined at a certain value of the pion or nucleon isotopic spin form factor (namely at zero momentum transfer), and these form factors need not have the same momentum-transfer dependence. Sakurai's idea was extended by Gell-Mann (1962) to the higher symmetry scheme (eightfold way) although the additional strangeness-changing currents were not exactly conserved.

Gell-Mann and Zachariasen (1961) discussed the role of universality in the electromagnetic form factors. They argued that both the ρ^0 meson (for example) and the electromagnetic field ought to be coupled to the same unrenormalized isovector current. As a consequence, the matrix elements of the isovector part of the electromagnetic current should be proportional to the corresponding ρ^0 matrix elements. In the special case where the bare (unrenormalized) ρ^0 mass is infinite, their result reduces to an effective direct coupling of the photon to the ρ^0, and may be expressed

$$e\langle n|j_\mu^{em(I=1)}|m\rangle = \frac{e}{f_\rho}\,\frac{m_\rho^2}{Q^2+m_\rho^2}\,\langle n|J_\mu^{\rho 0}|m\rangle\ , \tag{1.2}$$

where $J_\mu^{\rho 0}$ is the source of the ρ^0. The direct $\gamma-\rho^0$ coupling is proportional to e/f_ρ, where f_ρ measures the coupling of the ρ^0 to its source. Q^2 is the negative mass-squared of the photon (see footnote 9). In the case of a particle form factor, (1.2) applies separately to the charge and magnetic moment form factors and is depicted graphically in Fig. 1(a). [Application of (1.2) including refinements such as the ρ^0's instability and the precise definition of f_ρ will be discussed in Sec. II.B.] In the same paper, they described how various meson decays could be related by assuming a basic $\pi\rho\omega$ coupling, together with direct couplings of the photon to the ρ or ω. The details of these relations were pursued in a subsequent paper by Gell-Mann, Sharp, and Wagner (1962); we shall not discuss this topic further in this review. This confluence of ideas marks the beginning of the vector-meson-dominance (VMD) model of electromagnetic interactions, a model which for simplicity and definiteness usually incorporates the *additional* assumption that vector-meson poles at $Q^2=-m_V^2$ dominate the Q^2 dependence of the particular matrix element under consideration.

Following up the suggestion that there might be a strong $\pi\pi$ attraction, several experiments were performed to determine the pion–pion scattering amplitude by studying the reaction

$$\pi+p\to N+\pi+\pi\ .$$

These first experiments were visualized through the Chew–Low extrapolation technique (1959), in which one scattered a real pion off a virtual pion in the nucleon. These experiments indicated a strong π-π resonance at a total energy of roughly 700 MeV. The first unambiguous evidence for this resonance was presented by Erwin, March, Walker, and West (1961). They analyzed bubble chamber data for the reactions

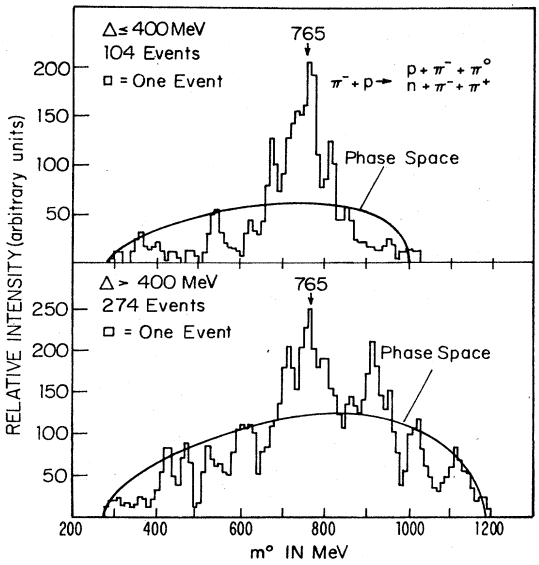

FIG. 2. The observed dipion mass spectrum of Erwin *et al.* (1961). Initial pion momentum ≈1.9 GeV (from Erwin *et al.*, 1961).

$$\pi^-+p\to\pi^-+\pi^0+p$$

$$\pi^-+p\to\pi^-+\pi^++n$$

by plotting the number of events versus the mass of the 2π system; see Fig. 2. This resonance was subsequently called the rho meson. It was found to have $m_\rho=760$, $\Gamma_\rho\simeq 150$ MeV, and the quantum numbers $I=1$, $J=1$.

A few months later Maglić, Alvarez, Rosenfeld, and Stevenson (1961) reported the discovery of the $I=0$ ω meson from an analysis of bubble chamber data for the reaction

$$p+\bar{p}\to 2\pi^++2\pi^-+\pi^0\ .$$

They plotted the number of events versus the invariant mass of the three-pion system (π^+,π^-,π^0), (π^+,π^+,π^-), (π^+,π^-,π^-) and found a strong enhancement in the π^+,π^-, π^0 channel at $m_\omega=787$ MeV with a width smaller than 30 MeV; see Fig. 3. This resonance was subsequently found to have the quantum numbers $J=1$, $I=0$.

During this same period McLeod, Richert, and Silverman (1961) used a photon beam at the Cornell 1.3 GeV synchrotron to look for a two-pion resonance. They found a strong enhancement in the cross section for a π-π mass of 720 MeV; see Fig. 4. This was the first evidence for the photoproduction of rho mesons.

A little later the second isoscalar vector meson predicted by Sakurai (1960) was discovered in a bubble chamber experiment at Brookhaven (Bertanza *et al.*, 1962) in the reaction

$$K^-+p\to\begin{cases}\Lambda^0+K^++K^-\\ \Lambda^0+K^0+\bar{K}^0\end{cases}\ .$$

The resonance, which is called the ϕ meson, occurred at $m_\phi=1020$ MeV with $\Gamma_\phi\leq 20$ MeV; Fig. 5 shows the observed mass spectrum. Its isotopic spin of zero is revealed by the presence of a K^+K^- mass peak in the reaction

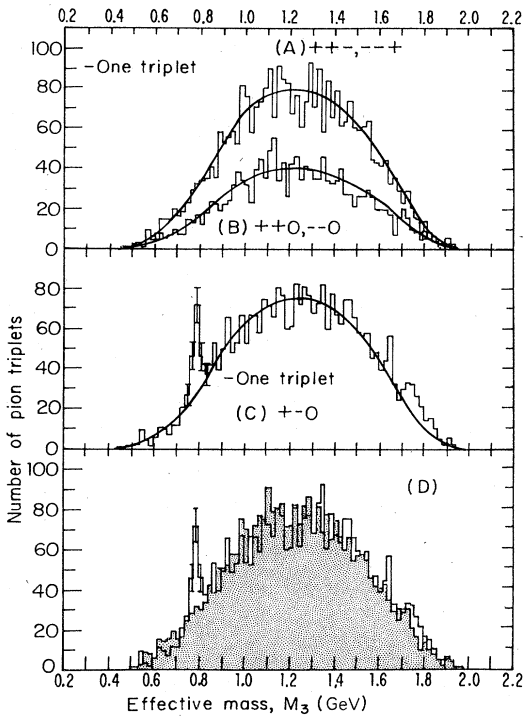

FIG. 3. The 3-pion mass spectrum in the reaction $p+\bar{p}\rightarrow 2\pi^+ +2\pi^- +\pi^0$ as observed by Maglić *et al.* (1961). Here (A), (B), and (C) show the data for pion triplets comprised of various charges. In (D) the combined data for charged triplets (A and B), shown shaded, is contrasted with the data for uncharged ($\pi^+\pi^-\pi^0$) triplets (C), heavy line (from Maglić *et al.*, 1961).

$$K^- + p \rightarrow \Sigma^0 + K^+ + K^-$$

but no similar K^-K^0 peak in

$$K^- + p \rightarrow \Sigma^+ + K^- + K^0 .$$

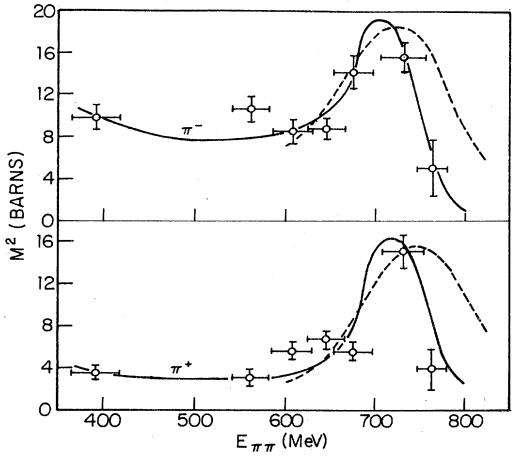

FIG. 4. The dipion mass spectrum observed by McLeod *et al.* (1961). The recoil proton and the indicated charged pion were detected in the final state. The energy of the π^+p and π^-p system was away from any resonance and held fixed while $E_{\pi^+\pi^-}$ was varied. Curves shown are theoretical models (from McLeod *et al.*, 1961).

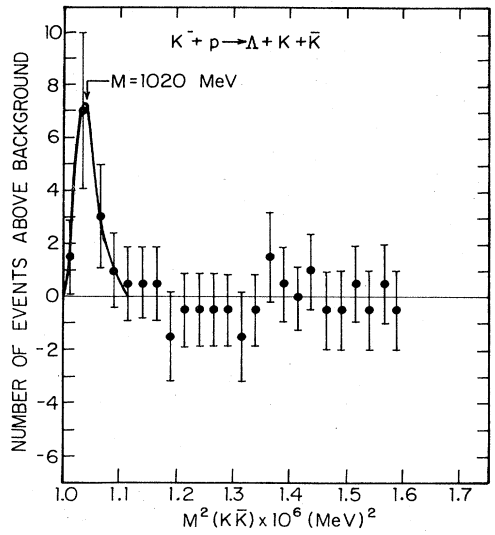

FIG. 5. The observed spectrum of $K\bar{K}$ pairs from the reaction $K^-p \rightarrow \Lambda K\bar{K}$ normalized to a phase space background (from Bertanza *et al.*, 1962).

The idea that *all* matrix elements of the isovector photon operator could be expressed in terms of those of the ρ^0-meson field operator was later called the "ρ-photon analogy" by Stodolsky (1964). This idea is equivalent to the *field-current identity* (FCI), which states that the isovector electromagnetic current is proportional to the ρ^0 field operator

$$j_\mu^{em(I=1)} = \frac{m_\rho^2}{f_\rho}\,\rho_\mu^0 . \tag{1.3}$$

This relationship was at first criticized by Feldman and Matthews (1963) on the basis of gauge invariance, but was subsequently justified by Kroll, Lee, and Zumino (1967), who gave it a Lagrangian field theory formulation. Joos (1967a) showed that (1.3) may be regarded as a suitable definition of the interpolating field of the ρ^0 meson. Clearly, the same idea may be extended to the isoscalar current so that

$$j_\mu^{em} = \frac{m_\rho^2}{f_\rho}\,\rho_\mu^0 + \frac{m_\omega^2}{f_\omega}\,\omega_\mu + \frac{m_\phi^2}{f_\phi}\,\phi_\mu . \tag{1.4}$$

There is no rigorous decomposition of $j_\mu^{em(I=0)}$ into interpolating fields for the ω and ϕ; it satisfies only the constraint that ω_μ not produce an on-mass-shell ϕ and vice versa. Nowadays we know that the electromagnetic current has substantial coupling to states other than the ρ^0, ω, and ϕ. Thus we must either extend the concept by including interpolating fields for higher-mass vector mesons or else use ρ_μ^0, ω_μ, ϕ_μ as interpolating fields for the whole hierarchy of states. Either alternative seems cumbersome, and the utility of the field-current identity is therefore diminished.

During these years there was a growing awareness that the ability of the photon to transform into vector mesons might play a broader role than in form factors and decay matrix elements. Such a virtual transition might also influence the description of high-energy photon reactions. An early version of these ideas is contained in

a paper by Berman and Drell (1964) in which they speculated on various models for photoproduction of vector mesons. One of these used an extension of the multiperipheral model of Amati, Fubini, and Stanghellini (1962). They concluded that these vector mesons could be produced by a diffractive mechanism and that the cross section would have approximately the same energy and momentum dependence as πp scattering. They used the universal coupling scheme to relate coupling constants, and their result may now be interpreted as equivalent to vector-meson dominance (VMD), albeit in a rather hidden form.

The first systematic study of rho-meson photoproduction was made at the Cambridge Electron Accelerator by the Cambridge bubble chamber group (Crouch *et al.*, 1964b) and by a Harvard counter group (Lanzerotti *et al.*, 1965), who showed that in hydrogen the cross section had a diffractive character. The cross section became energy independent above the resonance region, depended exponentially on momentum transfer, and was proportional to the πp scattering cross section. Measurements by the counter group of the production from complex nuclei (Lanzerotti *et al.*, 1965) showed that the cross section was coherent and increased more slowly than A^2. In fact, a whole series of early photoproduction measurements also indicated that in general photoproduction cross sections had a hadronic behavior and, to a good approximation, are given by multiplying the analogous pion cross sections by $\alpha/2\pi$ (Osborne, 1965).

Several influential papers on diffractive photoproduction of vector mesons appeared in 1966. Freund (1966) and Ross and Stodolsky (1966a) made the first application of VMD to these processes, assuming that the photoproduction amplitude was e/f_V (in our notation) times the elastic scattering amplitude of the vector meson, so that

$$\left(\frac{d\sigma}{dt}\right)_{\gamma p \to \rho^0 p} = \frac{e^2}{f_\rho^2}\left(\frac{d\sigma}{dt}\right)_{\rho^0 p \to \rho^0 p} . \tag{1.5}$$

Using SU(6), Freund suggested that the ρ^0 scattering amplitude should be about the same as that of the pion and made a remarkably good estimate of the forward production cross section ($\approx 100\,\mu b/\mathrm{GeV}^2$). He also used VMD to estimate the Compton scattering cross section. Ross and Stodolsky gave a more comprehensive discussion, containing most of our present ideas. They and Drell and Trefil (1966) pointed out the importance of experiments on nuclei to determine the two-body, total cross section (σ_ρ) of the unstable ρ^0. Their methods have stimulated other work on the determination of cross sections of unstable particles.

The first optical model analyses of the CEA counter experiments (Drell and Trefil, 1966) led to a preliminary (high) value of σ_ρ. Subsequently, a number of very substantial experiments were carried out to determine this and other important parameters of the reaction. These are discussed in Sec. III.C, and photoproduction from complex nuclei is reviewed in Sec. IV.C. One of Ross and Stodolsky's (1966 a, b) suggestions, the photoproduction of ω and ϕ with the aim to study their mixing, has never adequately been followed up.

By the time of the 1966 Berkeley conference on high-energy physics, the prominent features of ρ^0, ω, ϕ photoproduction had begun to emerge. In the talk by Jackson (1967), it was noted that ρ^0 photoproduction appeared to be diffractive with a decay angular distribution corresponding to s-channel helicity conservation, ω photoproduction could be accounted for as a combination of diffractive and one-pion exchange contributions, and ϕ photoproduction was much smaller than had been expected from SU(6). In the subsequent discussion, Joos pointed out that SU(6) together with smaller strange quark scattering cross sections [as suggested by Lipkin (1966)] could help explain this small cross section [see also Joos (1967b)]. In the following year, Harari (1967) wrote a critical review comparing various models of photoproduction of neutral vector mesons with the experimental facts.

At approximately the same time, Beder (1966) discussed how VMD and time-reversal invariance could be combined to relate photoproduction of π^+ (from the isovector part of the photon) to π^- production of ρ^0. The subject quickly developed into one of the most confusing in this general area of physics. Aside from a few general remarks we shall not attempt to review it here. The interested reader may find such a review and further references in the 1971 Erice lectures by Sakurai (1973). The essential difficulty is how to incorporate the supposed slow variation of the ρ^0 matrix element with mass (which varies from $Q^2 = 0$ to $-m_\rho^2$). The problem is that the real photons are necessarily transversely polarized, while ρ^0's are not; further, the separation of an amplitude into transverse and longitudinal parts is *not* a relativistically invariant concept (Fraas and Schildknecht, 1968; Białas and Zalewski, 1969). An amusing insight by an anonymous contemporary wit is shown in Fig. 6. Various authors have now been able to give a reasonably favorable interpretation of the VMD connec-

VECTOR DOMINANCE AND THE SPIN OF THE PHOTON

AABBCCDDEFG Collaboration

ABSTRACT

Vector Dominance[1] relates the two reactions

$\gamma + p \to \pi + N^*$ (1)

$\pi + N^* \to \pi_{tr} + p$. (2)

However, the Lorentz frame in which the transverse polarization of the Vector meson V is defined has not been uniquely specified. Various arguments have been proposed in favor of the helicity[2] frame, the conspiracy[3] frame, the Brickwall-Jackson[4] frame, The Breit-Wigner frame, the Dar-Weisskopf[1] frame and the Dontknowwho-Youguessim[5] frame.

This ambiguity has now been settled experimentally by direct measurements of the reactions (1) and (2), using Reggeized colliding beams. Although the experiment was performed in the Feynman gauge, the results are assumed to be gauge invariant and show that vector dominance is seriously violated in all frames unless the photon is assumed to have spin 3/2. Since it seems highly undesirable to discard the attractive vector dominance hypothesis,[6] we concludd that the photon has spin 3/2.

REFERENCESS AND FOOTNOTES

[1] Vector F. Weisskopf and Arnon Darminance, CERN report (unpublished)

[2] A.B. Helicity and F.C. Conspiracy, Phys. Rev. Letters 20, 37 (1968)

[3] F.C. Conspiracy and A. B. Helicity, Phys. Rev. Letters 20, 37 (1968)

[4] Also called the Stonewall Jackson frame.

[5] J.T. Dunnohue and J. HUguessin, Phys. Rev. Letters 20, 37 (1968)

[6] J.J. Sakurai, Any Paper

FIG. 6. A witty reaction to a simple theoretical picture overburdened with qualifications and subtle refinements.

tion between the two processes, including the extension to virtual (spacelike) photoproduction. A more dynamical analysis was carried out by Schmidt (1969) and Manweiler and Schmidt (1970, 1971) using the fixed-t dispersion relation formulation of photoproduction of pions. This incorporates variations in the mass which are not accounted for by the usual smoothness assumptions. In our opinion, the experiments show the presence of the VMD mechanism, but a good dynamical model is necessary in comparing experiment and theory. However, for fairly general reasons discussed in Secs. II.C and V.D, we believe some VMD violation is likely in these processes.

To sum up, this era was perhaps the high point of vector-meson dominance. It certainly seemed successful in explaining gross, overall features of photon interactions as well as diffractive production processes. Values of coupling constants as determined by quite different experiments seemed to be in approximate agreement [see, for example, Sakurai (1969)]. Moreover, as remarked by Stodolsky (1967), the total photon cross section could be estimated from forward vector-meson photoproduction using the relation

$$\sigma_\gamma^{(\mathrm{VMD})} = \sum_{V=\rho^0,\omega,\phi} \left(\frac{16\pi e^2}{f_V^2} \frac{d\sigma_{\gamma V}}{dt} \right)^{1/2} . \tag{1.6}$$

This estimate does yield a rough accounting for the observed total cross section. However, in trying to describe nondiffractive, very energy-dependent processes, VMD seemed a bit forced. A few reviews of the status of VMD at that time were given by Sakurai (1969a, 1969b, 1973), Gottfried (1972), Schildknecht (1972), and Leith (1971).

One idea which was emerging from the VMD picture was the possibility of photon shadowing in nuclei. Stodolsky (1967) pointed out that if a photon acts like a combination of ρ^0, ω, ϕ, the total photon cross section should be smaller than A times the single nucleon cross section [a similar argument had been given earlier by Bell (1964) for neutrino-nucleus cross sections]. Later authors (Brodsky and Pumplin, 1969; Gottfried and Yennie, 1969; Margolis and Tang, 1969; Nauenberg, 1969) showed that the effect should go away at lower (~ few GeV) energies.

It had always been felt that it was very difficult to measure the total photonucleon cross section. However, stimulated by the theoretical work on VMD and shadowing, groups at DESY (Meyer *et al.*, 1970; Heynen *et al.*, 1971), SLAC (Caldwell *et al.*, 1969, 1970, 1973), and Daresbury (Armstrong *et al.*, 1971, 1972; Brookes *et al.*, 1973) undertook systematic measurements of the total photon-nucleon cross section for H, D, and complex nuclei. These experiments all showed shadowing but not to the same degree or with the same A and energy dependence as predicted by VMD. These and subsequent experiments will be described in Sec. III.A and the analysis will be given in Sec. V.B. The model also predicts shadowing in individual channels such as photoproduction of pions or incoherent ρ^0 photoproduction (Gottfried and Yennie, 1969). Some such shadowing has been seen in experiments at SLAC (Boyarski *et al.*, 1969) and Cornell (McClellan *et al.*, 1969c; Meyer *et al.*, 1972). These experiments will be described in Sec. III.H and the analysis will be given in Sec. V.D. More recently, a DESY group has observed shadowing in Compton scattering from nuclei (see Sec. V.C). Shadowing experiments for virtual photons have been carried out at SLAC, Cornell, and Brookhaven. In all present cases the observed shadowing is small and comparison with theoretical expectations is inconclusive. The experiments are discussed in Sec. III.J and the theory in Sec. V.E.

The first gross breakdown of VMD came in the SLAC–MIT measurements (Bloom *et al.*, 1969; Breidenbach *et al.*, 1969) of inelastic electron scattering, a process which is thought to occur through interchange of a virtual photon. The SLAC group found that the inelastic electron scattering cross section was surprisingly large. The most striking feature of the data for highly virtual, highly energetic photons was "scaling"; that is, the functional form of the variation of cross sections with virtual photon mass and energy is predictable solely on the basis of dimensional analysis without reference to any other mass, cross section, etc. This scaling behavior had been earlier predicted on theoretical grounds by Bjorken (1969). Popularly, the measurements were understood by picturing the nucleon as made of pointlike objects called partons (Feynman, 1969). A quark was one possible candidate for a parton. More recent experiments (to be described in Sec. III.I) indicate slowly varying deviations from scaling at large Q^2 and ν.

Important support for the idea that the photon interacts (at least partially) through its hadronic structure was provided by a study of the space-time properties of high-energy photon interactions. Ioffe (1969) showed that the experimental data required a long longitudinal range, suggesting that the photon converts to hadrons before interacting with the nucleon. Pestieau, Roy, and Terazawa (1970) made a more quantitative analysis, and the role of the long range in diffractive interactions was further emphasized by suri and Yennie (1972). Thus over a wide kinematic range the principal qualitative feature of VMD, that of providing the photon with a hadronic structure, remains valid.

Early attempts to use VMD to explain inelastic electron scattering were not particularly successful; naive VMD predicted either too large a longitudinal cross section or too rapid a falloff with the mass of the virtual photon. At the same time, the colliding e^+e^- experiments (Sec. III.F) were revealing that the photon's hadronic structure is considerably richer than a simple superposition of ρ^0, ω, and ϕ. In fact, the probability for a photon to be in a higher-mass hadronic state is comparable to the probability for it to be in one of the low-lying vector-meson states. Most recently, the family of hadronic photon constituents has been enlarged by the discovery of the J/ψ (Aubert *et al.*, 1974; Augustin *et al.*, 1974a), indicating the presence of exciting new physics.

The first theoretical attempts to include the effects of additional photon constituents were made by Gribov (1969) and Brodsky and Pumplin (1969) in a generalization of VMD. Later, Fujikawa (1971), Sakurai and Schildknecht (1972), Brámon and Greco (1972), and Brámon, Etim, and Greco (1972) began detailed study of generalized vector-meson dominance, in which specific models of the higher-mass states are employed.

Around the same time, accurate data on the real photon total cross sections were becoming available and it was found that the VMD contribution (1.6) accounted for about 80% of the experimental value. The new states are easily adequate to supply the missing contribution. In fact, it is clear that the new states must interact with an appreciably *smaller* effective cross section than typical hadronic ones in order to account for real and virtual photon cross sections. These models, as well as other speculations about the role of higher-mass constituents, will be described in Sec. VI.B.

II. GENERAL FEATURES OF HADRONIC ELECTRODYNAMICS

The purpose of this section is to give the reader a bird's-eye view of the whole field. Later sections will provide detailed descriptions of the data and, in many cases, a closer examination of the theoretical arguments. It is suggested that the less dedicated reader may wish to read this section as a more or less self-contained "mini-paper," then glance at the figures and tables in Sections III, IV, and V, and return to a reading of Section VI for a summary and speculations.

A. Analogies between photon- and hadron-induced processes

High-energy hadron–hadron elastic scattering shows all the features that one would expect to flow from a strong interaction and the existence of a myriad of open channels: a total cross section that varies very slowly with energy; a forward amplitude that is dominantly imaginary; and virtually complete opacity at small impact parameters. Photon interactions, on the other hand, are very weak. There is no doubt that the low partial waves, corresponding to small impact parameters,

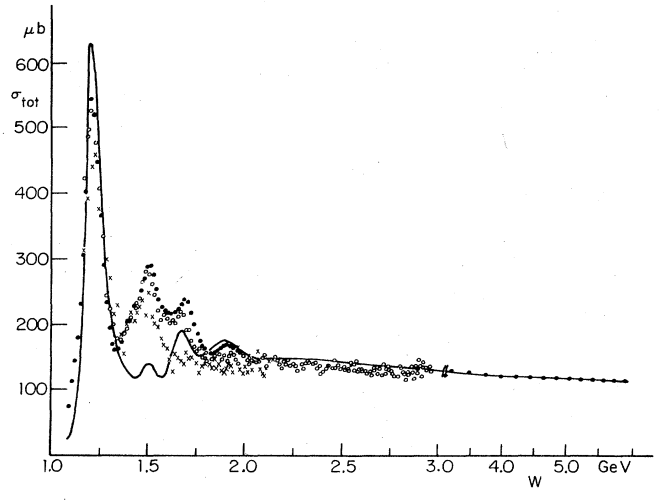

FIG. 7. A plot versus energy of the total hadronic cross section and the total photon cross section. The solid line is a plot of $(\sigma_{\pi^+p}+\sigma_{\pi^-p})/440$ using data taken from the compilation of Höhler and Jakob (1972). For the electromagnetic total cross sections see the compilation of Damashek and Gilman (1970) ($\sigma_{\gamma p}$:●) and Armstrong *et al.* (1972a, b) ($\sigma_{\gamma p}$:○; and $\sigma_{\gamma n}$:×). This figure was taken from Genz and Schmidt (1973).

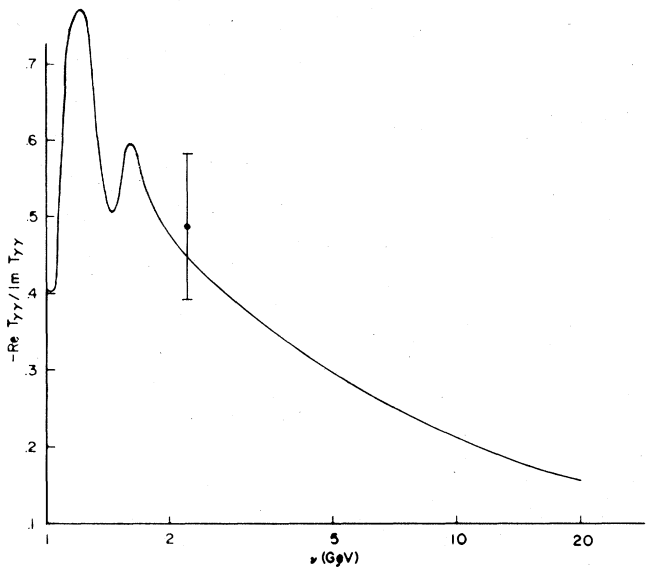

FIG. 8. A plot of $\mathrm{Re}T_{\gamma\gamma}/\mathrm{Im}T_{\gamma\gamma}$ for Compton scattering versus energy. The solid curve comes from the dispersion relation analysis of Damashek and Gilman (1970); the data point comes from the measurement of $\mathrm{Re}T_{\gamma\gamma}$ of Alvensleben *et al.* (1973), together with the optical-theorem value for $\mathrm{Im}T_{\gamma\gamma}$.

have only very small phase shifts, and that the total cross sections for photon-hadron collisions, $\sigma_{\gamma h}$, are nowhere near geometrical. At first sight one might therefore have expected photon-hadron scattering to bear no resemblance to that of hadrons by hadrons.

A host of experiments have shown that such expectations were quite wrong.[1] The most obvious similarity of photon and hadron interactions is the behavior of the total cross sections, which is illustrated in Fig. 7. Both show spectacular resonances at low energies, and above 3 GeV they level out and become structureless, apparently tending to a constant at high energies.[2] The limiting photon total cross sections on neutrons and protons are nearly the same, indicating that the photon interaction does not depend primarily on the charge of the target. The photon total cross sections are smaller than the hadronic ones by approximately the fine structure constant in order of magnitude. Except for its very small magnitude, the nucleon's Compton amplitude[3] $T_{\gamma\gamma}(s,t)$ is virtually indistinguishable from, say, the pion-nucleon amplitude (at least for $s \gg t$). For energies

[1] An excellent review of the evidence for the similarity of photon and hadron interactions is contained in the 1971 and 1973 Erice Lectures of Sakurai (1973, 1975). Yennie (1977) has also given a review at the 1972 Cargèse summer school, with emphasis on diffractive processes.

[2] Whenever we talk of "constant values" at large s, we do not mean to rule out the possible presence of terms rising logarithmically with s. A very recent experiment (Caldwell *et al.*, 1977) shows that photon cross sections develop this behavior which was previously well confirmed for hadronic reactions at CERN (Amaldi *et al.*, 1973; Amendolia *et al.*, 1973) and at FNAL (Carroll *et al.*, 1974).

[3] We denote the amplitude for the process $aN \to bN$ by T_{ab} throughout. N denotes that the target is a single nucleon. A detailed glossary of notation is contained in Appendix E.

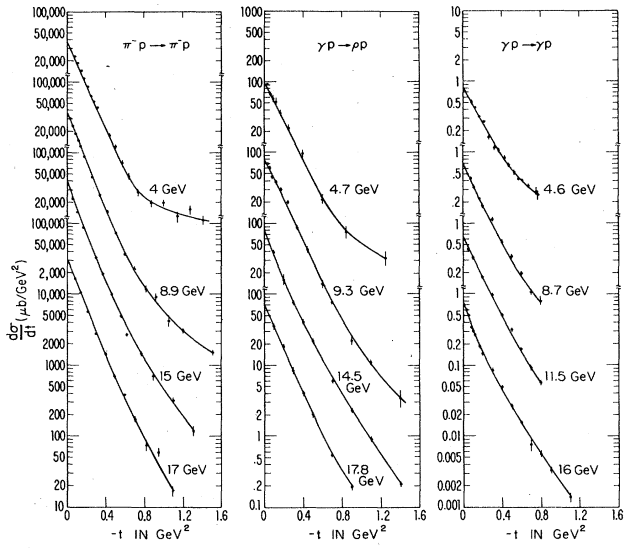

FIG. 9. Comparison of angular distributions: (a) Elastic π-N scattering; (b) Photoproduction of ρ^0 mesons; and (c) Compton scattering from protons. Here (a) is from the data of Foley *et al.* (1967) and (b) and (c) are adapted from the thesis of Kogan (1975).

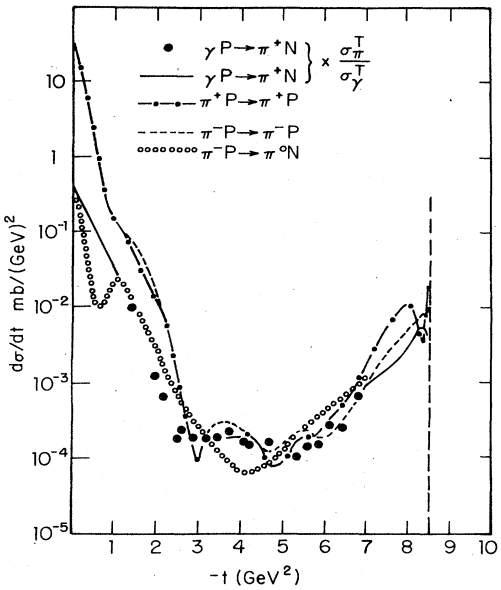

FIG. 10. Comparison of the 5 GeV data for the photoproduction reaction $\gamma p \to \pi^+ n$ with 5 GeV data for π^+ and π^- elastic scattering and $\pi^- p$ charge exchange. The figure was taken from R. L. Anderson *et al.* (1973b). The photoproduction data are from Boyarski *et al.* (1968) and R. L. Anderson *et al.* (1969, 1973b); the pion data are from Diddens (1972).

above the baryon resonances $T_{\gamma\gamma}$ has an angular falloff whose slope is similar to that of purely hadronic angular distributions; and the ratio $\mathrm{Re}T_{\gamma\gamma}(s,0)/\mathrm{Im}T_{\gamma\gamma}(s,0)$ shown in Fig. 8, as determined from the forward dispersion relation (Damashek and Gilman, 1970) and by direct measurement (Alvensleben *et al.*, 1973), is small and negative, as is the case for the πN and NN amplitudes. Typical angular dependences in elastic π scattering and in Compton scattering are compared in Fig. 9.

There is, of course, one important difference. Whereas the total elastic cross section in purely hadronic collisions is typically 15-20% of the total cross section, this cannot be the case for an electromagnetic process: $\sigma_{\gamma N}^{\mathrm{el}}$ is necessarily of order $\alpha\sigma_{\gamma N}$.[4] But this distinction between Compton amplitudes and purely hadronic amplitudes is "compensated" by diffractive photoproduction. Indeed the most striking feature of photoproduction is the copious production of neutral vector mesons V, most prominently the ρ^0. The amplitudes $T_{\gamma V}$ for V production[3] can be considered to be the photon analog of purely hadronic elastic amplitudes: they approach (nearly) s-independent[2] limits, and have the same typical falloff in t, as illustrated in Fig. 9. In the case of ρ^0 one has more detailed information: one knows that there is no helicity flip near $t=0$ (Ballam *et al.*, 1973), only a small difference between the production amplitude on neutrons and protons, and there are indications that $|\mathrm{Re}T_{\gamma\rho}| \ll \mathrm{Im}T_{\gamma\rho}$ (Alvensleben *et al.*, 1970d; Biggs *et al.*, 1971). Moreover, the portion of $\sigma_{\gamma N}$ attributable to V production is of the same magnitude as $\sigma_{\mathrm{el}}/\sigma_{\mathrm{tot}}$ in hadronic collisions.

Turning to finer details of high-energy cross sections, we note briefly two other similarities between photon and hadron interactions on nucleon targets. One is the general behavior of nondiffractive interactions leading to two-body final states. These can be described phenomenologically with Regge exchanges, and they are characterized by dips and peaks governed by common rules. An example is shown in Fig. 10. The other is inclusive cross sections which display sharply falling $p_\perp^2$ distributions and similar longitudinal momentum distribution properties, as illustrated in Fig. 11.[5] These

[4] $\sigma_{\gamma N}$ and $\sigma_{\gamma N}^{\mathrm{el}}$ refer, respectively, to the total cross section for a photon to interact with a nucleon and its elastic part (i.e., nucleon Compton scattering). A proton or neutron is distinguished by $N=p$ or n. Our interest in this paper lies in the purely hadronic interactions of the photon; but, of course, the electromagnetic process of electron pair production has a much higher cross section—the additional powers of α being overcome by the large scale which is set by the electron's Compton wavelength ($\lambda\!\!\!^{-}_e$). On the proton, the electromagnetic cross section is of order 100 times the hadronic cross section, while on nuclei the electromagnetic background grows worse with increasing Z because of coherence in the Coulomb field. This copious pair production presents difficult problems for the experimentalist who wishes to measure hadronic cross sections. It also presents an opportunity, as one can interfere electromagnetically produced pairs with those produced in strong interactions and thus determine phase relations (Alvensleben *et al.*, 1970c, d; Biggs *et al.*, 1970a, 1971; Alvensleben *et al.*, 1973). In studying Compton scattering directly, the dominant electromagnetic contribution is prominent only for near-forward scattering, and it may be avoided by studying events with momentum transfers $\gg\hbar/\lambda\!\!\!^{-}_e$.

[5] A crude attempt has been made by Yennie (1975) to analyze the forward π^- inclusive distribution in terms of the dipion constituent of the photon, with some qualitative success. The dipion constituent refers to the part of the physical photon which may be regarded as a $\pi^+\pi^-$ pair, as will be described in the following subsection. It includes the ρ^0, together with a nonresonant pion pair state.

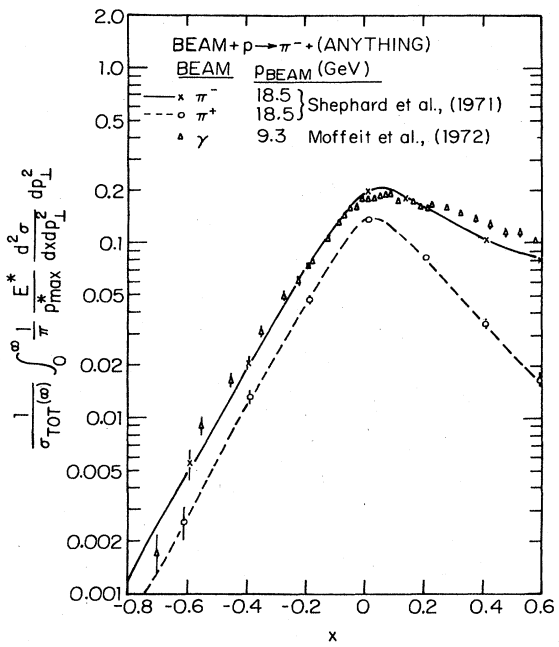

FIG. 11. A comparison between the invariant structure function found in photoproduction and that found in pion inclusive hadron reactions. Figure was taken from Moffeit *et al.* (1972). Curves are approximations to the hadron-induced data with representative data points shown.

relations become quantitative when the cross sections for particular photon and hadron processes are divided by the appropriate total cross sections. This shows that if one removes the small overall probability for photon interactions, there is a detailed correspondence. For a more complete account of these similarities, we refer the reader to the reviews by Sakurai (1973, 1975).

The final similarity between interactions of hadron and photon projectiles is absorption by nuclei, which is one main topic of this paper. Both hadron and photon interactions display shadowing, which is to say that the projectile's initial interaction is almost always with a nucleon on the incident side of the nucleus. The presence of photon shadowing is thus important in exploring our main supposition that photon interactions are due (in most cases) to the incident photon's being momentarily in an actual hadronic state. The general physical ideas of photon shadowing are discussed in Sec. II.E, experimental studies of photon shadowing are described in Secs. III.A, B, H, and J, and detailed analyses are made in Sec. V. Section VI includes some speculations as well as suggestions for photon (or virtual photon) experiments on nuclei which might shed further light on the hadronic properties of the photon.

B. The physical photon state and the notion of vector-meson dominance

As we have just seen, from a purely phenomenological viewpoint, photon interactions with hadrons bear many remarkable similarities to purely hadronic interactions. At a very crude level, this could be understood if the physical photon $|\gamma\rangle$ were a superposition of two types of states: a bare photon $|\gamma_B\rangle$, which at high energies accounts for a small, or perhaps negligible, portion of the interaction; and a small—of order $\sqrt{\alpha}$—hadronic component $\sqrt{\alpha}\,|h\rangle$ which undergoes conventional hadronic interactions. That is, we expect the important part of the physical photon state to be expressible as

$$|\gamma\rangle \cong \sqrt{Z_3}\,|\gamma_B\rangle + \sqrt{\alpha}\,|h\rangle\ , \tag{2.1}$$

where Z_3 is introduced to assure the proper normalization of $|\gamma\rangle$; all states in Eq. (2.1) have the same 3-momentum $\mathbf{k}$. Invariance considerations dictate that $|h\rangle$ should have the same symmetry quantum numbers as the photon, i.e., $J^{PC}=1^{--}$, $Q=B=S=0$. The copious photoproduction of the vector mesons ρ^0, ω, and ϕ suggests that they provide very important contributions to $|h\rangle$. The restrictive assertion that these three mesons are the sole hadronic constituents of the photon, and that the bare component $|\gamma_B\rangle$ cannot interact with hadrons, is the hypothesis of vector-meson dominance[6] (VMD) in its most naive and clear-cut form. The less restrictive assumption that all interactions result from $|h\rangle$, which has more constituents than ρ^0, ω, and ϕ, is referred to as generalized vector dominance (GVD).[6]

These ideas may be formulated more precisely by considering the structure of the state $|\gamma\rangle$ in conventional time-independent perturbation theory.[7] To lowest order in the electromagnetic interaction H' between photons and hadrons[8]

$$\sqrt{\alpha}\,|h\rangle = \mathbf{S}_n\ \frac{|n+\rangle\langle n+|H'|\gamma_B\rangle}{\nu - E_n}, \tag{2.2}$$

where $|n+\rangle$ is a completely interacting hadronic state (identified by particles emerging from the interaction region as time $\to +\infty$) and $|\gamma_B\rangle$ includes the exact hadronic vacuum, together with a bare photon of momentum $\mathbf{k}$. The energy of the photon is $\nu(\equiv|\mathbf{k}|$ for real photons and $(\mathbf{k}^2-Q^2)^{1/2}$ for virtual ones[9]), and the energy E_n is given by $(\mathfrak{M}^2+\mathbf{k}^2)^{1/2}$, where $\mathfrak{M}$ is the invariant mass of $|n+\rangle$. Here $\mathbf{S}_n$ stands for sums and integrals over all appropriate labels in n.

---

[6]Some references to VMD and GVD have been given in Sec. I and others will be given later in this section and in Secs. V.E and VI.B.

[7]The idea of using time-independent perturbation theory to discuss the photon's hadronic structure has been mentioned by several authors (Gottfried, 1972; Nieh, 1973). The most detailed discussion, which will be outlined here, was given by Yennie (1975).

[8]This interaction also produces a constituent with two bare photons plus hadrons, which we ignore since (except for Compton scattering) it does not contribute to hadronic interactions to lowest order in α. Interactions between photons and leptons are also ignored in the present discussion. However, when the generalization to virtual photons is made, $|\gamma\rangle$ originates from a deep-inelastic lepton scattering.

[9]It is not really correct to speak of virtual photon states since there are no such elements of the physical Hilbert space. However, it happens that the theoretical treatment of inelastic electron scattering is really an extension of the theory of real photon interactions in which an exchanged virtual photon has an off-mass-shell relation between its energy and momentum: $\nu^2-\mathbf{k}^2=k^2\equiv -Q^2$, where $Q^2>0$ for inelastic electron scattering. It is usual to characterize the "virtual photon" by its kinematic parameters ν and Q^2, together with its polarization.

As mentioned earlier, the invariance properties of H' assure that the states $|n+\rangle$ have the photon's symmetry quantum numbers. Possible examples of such states are $\pi^+\pi^-$, $\pi^+\pi^-\pi^0$, $K\bar{K}$, $N\bar{N}$, etc. Since the vector mesons ρ^0, ω, and ϕ are not stable under strong interactions, they actually do not appear as separate terms in the sum in (2.2). However, to the extent that they may be regarded as narrow resonances in the $\pi^+\pi^-$, $\pi^+\pi^-\pi^0$, and $K\bar{K}$ modes, respectively, their contributions may be separated off and replaced by equivalent elementary vector-meson states, which may then be regarded as interacting more or less like distinct physical particles (see below). We then recover the contributions expected from VMD or GVD.

At high energies, the expression (2.2) may be simplified and given a more familiar appearance.[10] This involves the following ingredients:

(1) The energy denominator of (2.2) may be approximated

$$\begin{aligned}\nu - E_n &= -\mathfrak{M}^2/2\nu \text{ (real photons, } \nu \gg \mathfrak{M}) \\ &= -(\mathfrak{M}^2+Q^2)/2\nu \text{ (virtual photons, } \nu \gg (\mathfrak{M}^2+Q^2)^{1/2}),\end{aligned} \tag{2.3}$$

(2) For fixed $\mathfrak{M}$, the center-of-mass motion may be explicitly separated out and (2.2) may be rewritten (Yennie, 1975)[11]

$$\sqrt{\alpha}\,|h_S\rangle = -(2\pi)^3 \int_{\mathfrak{M}_t^2}^{\infty} \frac{d\mathfrak{M}^2}{\mathfrak{M}^2+Q^2} \sum_{n_1} |\mathrm{k}, \mathfrak{M}, n_i\rangle \times \langle \mathrm{k}, \mathfrak{M}, n_i\,|\mathcal{H}'(0)|\,\gamma_B\rangle\,, \tag{2.4}$$

where the sum now extends over all internal quantum numbers holding k and $E_n = (\mathrm{k}^2+\mathfrak{M}^2)^{1/2}$ fixed, and $\mathcal{H}'$ is the interaction Hamiltonian density.[12] The label h_S means that (2.4) is valid only for the low-mass components of the photon.

(3) In a model in which the states $|n_i\rangle$ are transversely polarized vector mesons of definite mass, the matrix element of $\mathcal{H}'(0)$ is independent of k and the integral in Eq. (2.4) collapses to a discrete sum which is the usual VMD expansion for a photon state [the rhs of Eq. (2.6) below]. The Q^2 dependence is contained entirely in the denominator and is that of a vector-meson propagator. The vector-meson state has momentum k.

(4) More generally, the transverse matrix element of $\mathcal{H}'(0)$ is independent of k, and Eq. (2.4) is like a continuous superposition of vector-meson states, each of momentum k. Since the probability amplitude for these states depends on $\mathfrak{M}$, but not k, we say that the superposition is "frozen in."[13] For longitudinally polarized photons (possible only for $Q^2 \neq 0$), the matrix element of $\mathcal{H}'(0)$ does depend on k, but in a definite way. A slightly more detailed discussion is necessary [see Yennie (1975), Sec. IV], but one finds again that the longitudinal structure is frozen in.

(5) We note that the hadronic states occurring in (2.4) are precisely the ones seen in $e^+e^- \to$ hadrons and the probability per unit $\mathfrak{M}^2$, $P(\mathfrak{M}^2, Q^2)$, of their occurrence is given by the cross section of the latter reaction,[14] namely (for transverse photons)

$$\begin{aligned}P(\mathfrak{M}^2, Q^2) &= \frac{(2\pi)^6}{(\mathfrak{M}^2+Q^2)^2} \sum_{n_i} |\langle 0, \mathfrak{M}, n_i\,|\mathcal{H}'(0)|\,\gamma_B\rangle|^2, \\ &= \frac{\mathfrak{M}^4}{(\mathfrak{M}^2+Q^2)^2} \frac{\sigma_{\mathrm{tot}}(e^+e^- \to X(\mathfrak{M}))}{4\pi^2\alpha}\,.\end{aligned} \tag{2.5}$$

The e^+e^- annihilation experiments will be summarized in Sec. III.F. For masses $\lesssim$1 GeV, the resonances associated with the familiar vector mesons ρ^0, ω, and ϕ completely dominate the final states, confirming that they are the most important low-mass members of the photon's hadronic component. Additional very broad resonances have been observed (possibly excited states of these familiar vector mesons); and very recently some very narrow resonances and threshold behavior at high energies have been discovered (new particles and possibly new physics). At higher masses, most theoretical expectations had been that $P(\mathfrak{M}^2, 0)$ would decrease, probably as $1/\mathfrak{M}^2$ (see, for example, Bjorken, 1974). This behavior, known as "scaling," means the dependence of $\sigma_{\mathrm{tot}}(e^+e^- \to X(\mathfrak{M}))$ can be simply predicted from dimensional analysis, ignoring the importance of any mass except $\mathfrak{M}$, the center-of-mass energy. At the time of writing, the highest-energy data is suggestive of scaling behavior. In the next few years, the $\mathfrak{M}^2$ range will be extended by a large factor, and it will be seen whether this trend continues or new thresholds will appear. In any case, it is clear that higher masses give a large contribution to the photon's structure.

Let us consider the low-mass resonances in a little more detail. One might suspect that such states dominate Eq. (2.4) at low Q^2 because of the factor $1/(\mathfrak{M}^2+Q_2)$. As indicated previously, the hypothesis that such resonances do dominate (2.4) is called VMD. If a resonance

---

[10] It is often confusing to the newcomer to this type of discussion that our analysis of photon structure seems very dependent on the specific Lorentz frame. How can a high-energy photon have a structure that differs from a low-energy one? For a photon by itself there can be no difference, and the answer to our question must lie in the additional presence of an "observer" or target. It makes little sense to discuss the structure of the photon apart from its interaction with other objects, and without loss of generality the reader might envision each Lorentz frame as the rest frame of a hypothetical target. In the perturbation scheme we have employed, the photon structure seen by such a target *can* depend on energy (Lorentz frame) and is described by the analysis in the text.

[11] From now on, we write the expressions for virtual photons. The real photon results are obtained by setting $Q^2=0$ and dropping longitudinal photon terms.

[12] The transition from (2.2) to (2.4) uses the fact that the matrix element of H' is $(2\pi)^3$ times a momentum-conserving δ function times the corresponding matrix element of $\mathcal{H}'(0)$.

[13] The reader familiar with the parton model of deep-inelastic electron scattering will recognize that we have given an infinite momentum frame treatment of the photon, in which the internal state has become independent of the momentum of the photon. However, the particle labels in n_i are quite different from parton labels. These pictures are further compared and contrasted in Sec. II.D.

[14] This idea is stressed in the various papers on GVD: Gribov (1969); Brodsky and Pumplin (1969); Ritson (1971); Fujikawa (1971); Bjorken (1974); Sakurai and Schildknecht (1972); Bramon, Etim, and Greco (1972); Bramon and Greco (1972).

is very narrow, we may replace the $\mathfrak{M}^2$ in the denominator of (2.4) by its value at the position of the resonance and take it outside the integral. The remaining integral, including contributions from all decay channels (n_i), is then *defined* to be the appropriate vector-meson state. Thus we find

$$\sqrt{\alpha}\,|h_S\rangle_{\rm res} = \sum_V \frac{e}{\bar{f}_V}\,\frac{m_V^2}{m_V^2+Q^2}\,|V\rangle\ , \tag{2.6}$$

where $|V\rangle$ is an appropriately normalized state and the normalization constant is chosen *by convention* to be $e/\bar{f}_V$ for real photons.[15] When the ρ^0 resonance in the $\pi^+\pi^-$ channel is studied in detail (Yennie, 1975), it is found that $|\rho^0\rangle$ defined in this way corresponds to a spatially localized state. That is, it is very similar to any other physical particle.[16] It is expected that the other vector-meson states have the same property.

The VMD approximation (2.6) has great predictive power because it connects scattering amplitudes involving high-energy photons, $\gamma N \to X$, to analogous amplitudes involving vector mesons, $VN \to X$. We find, assuming the bare photon does not interact,

$$\langle X|S|\gamma N\rangle = \sum_V \frac{e}{\bar{f}_V}\,\frac{m_V^2}{Q^2+m_V^2}\langle X|S|VN\rangle\ , \tag{2.7}$$

where "S" is the S matrix operator of formal scattering theory. When restricted to the ρ^0 mode, Eq. (2.7) expresses the "ρ^0-photon" analogy alluded to in Sec. I. Equation (2.7) is a generalization of (1.3) and is illustrated by Fig. 1(b).

●[17]Our understanding of VMD may be enhanced by a slight detour into a version suggested by relativistic quantum field theory. In this context, photons and vector mesons are incorporated as elementary particles. Many pioneering papers in this field have employed this approach, so readers conversant with older literature might find this view more familiar. Whether or not this notion of "elementary particle" has any profound meaning, our point of view here will be to regard it as a useful formalism when only a few low-mass vector mesons are the photon's most important constituents.

●The basic idea is that a photon enters the world of hadrons through a direct coupling to the ρ^0, ω, and ϕ vector mesons, corresponding in lowest order in e to an interaction Lagrangian density $\mathfrak{L}_I(x)$[18] given by

$$\mathfrak{L}_I(x) = \sum_V \frac{e m_V^2}{f_V}\,V_\mu A^\mu\ , \tag{2.8}$$

where V_μ and A^μ are quantum field operators associated with the vector meson and photon. In Feynman diagram language this leads to a direct photon-vector-meson coupling of strength em_V^2/f_V.[18] By hypothesis, all photohadronic interactions involve the propagation of these vector mesons as intermediaries between the photon and the rest of the hadronic system.

●A basic constraint in all of this is that real ($Q^2=0$) photons couple to the conserved electromagnetic current with a universal strength "e." Sakurai (1960) proposed that these three vector mesons couple universally to the conserved hadronic currents: isospin, baryon number, and hypercharge. These universal coupling strengths must be such that the photon in the end properly couples to the electromagnetic current (a linear combination of these conserved hadronic currents). For example, in coupling a photon to charged pions we deal with an I-spin 1 system and need only consider the ρ^0 as an intermediary. Considering the direct γ-ρ^0 coupling and ρ^0 propagator $[\propto 1/(Q^2+m_\rho^2)]$ at $Q^2=0$ it is apparent (neglecting any $\rho-\pi^+\pi^-$ form factor and propagator effects) that the $\rho^0-\pi\pi$ coupling strength is simply f_ρ! A few paragraphs below, we shall see in discussing experimental determinations of f_V that this simple VMD picture of the charged-pion form factor is pretty well borne out.

●In any case this form of VMD [known commonly as the field-current identity (Gell-Mann and Zachariasen, 1961; Kroll, Lee, and Zumino, 1967) because the electromagnetic current is effectively identified with vector-meson fields] adds useful and more sophisticated predictive power to the present formulation of VMD, Eqs. (2.6) and (2.7). First of all, we easily recover (2.7) in the approximation of a "structureless" vector meson by incorporating a free particle vector-meson propagator $\propto 1/(Q^2+m_V^2)$ and neglecting any "off-the-mass-shell" (Q^2 differing from $-m_V^2$) modification of the vector-meson scattering amplitude. (With this set of approximations there is no distinction between $\bar{f}_V$ and f_V.[15]) How-

[15]Many different conventions for coupling constants are employed in the literature. Table I defines the ones used in the present paper. Because of the coupling of the vector mesons to their decay channels, the different conventions lead to quantitatively different values (at the 10%–15% level) of the coupling constants. These effects are discussed in Appendix C. Consistent use of any convention of course produces consistent results. (Note also that some authors use $e/2\gamma_V$ rather than $e/\bar{f}_V$.)

[16]This study also shows that replacing $\mathfrak{M}^2$ in the denominator of Eq. (2.4) by m_ρ^2 in the simplest model leads to a state vector $|\rho\rangle$ that cannot be normalized. If, instead, we retain the factor $\mathfrak{M}^2+Q^2$ in the denominator of (2.4), dividing by a factor $m_\rho^2+Q^2$ *outside* the integral and multiplying by the same factor inside the integral, we produce an equation similar in appearance to Eq. (2.6) but where the new state $|\text{"}\rho\text{"}\rangle$ can be normalized. However, $|\text{"}\rho\text{"}\rangle$ in this case depends on Q^2! Although this dependence on Q^2 is weak and to a first approximation can probably be ignored, the implication is that $|\text{"}\rho\text{"}\rangle$ does not represent a pure vector meson but rather a mixture of component states, i.e., a spatially localized vector meson plus a cloud of nonresonant $\pi^+\pi^-$ pairs. Yennie (1975) estimates that a contribution as large as 10% of the total probability may be associated with this nonresonant dipion state.

[17]This symbol (●) indicates a paragraph which may be skipped without breaking continuity in reading. It generally indicates somewhat more specialized material.

[18]The interaction (2.8) is not gauge invariant beyond lowest order, as was emphasized by Feldman and Matthews (1963). However, it is possible to replace (2.8) by a coupling of order e involving the field strengths associated with the photon and the V, together with a direct coupling of the photon to the current source of the V, which exactly produces the effect of (2.8) to lowest order and assures gauge invariance to all orders (Kroll, Lee, and Zumino, 1967). The f_V appearing here is different from $\bar{f}_V$ in Eq. (2.6). It corresponds to normalizing the vector-meson propagator at $Q^2=0$ rather than at $Q^2=-m_V^2$ —see Appendix C.

TABLE I. Definitions of different experimental coupling constants of vector mesons.

1. *From* $V \to e^+e^-$:

$$\frac{\bar{f}_V^2}{4\pi} = \frac{\alpha^3}{3}\frac{m_V}{\Gamma_{V\to e^+e^-}}$$

defines the coupling of the photon to the vector meson with the vector-meson propagator normalized at the resonance. A different normalization convention was adopted by Kroll, Lee, and Zumino (1967); in their convention, the vector-meson propagator is normalized at $k^2=0$, defining a coupling

$$\frac{f_V^2}{4\pi} = \frac{\bar{f}_V^2}{4\pi}\left(1-\frac{\bar{\Pi}_V(0)}{m_V^2}\right),$$

where $\bar{\Pi}_V$ is the vacuum polarization correction to the propagator [see Appendix C, Eqs. (C.1)–(C.11)]. Their coupling constant f_V appears as the natural choice in the field-current identity, Eq. (2.8).

2. *From diffractive photoproduction of* V:

$$\frac{\hat{f}_V^2}{4\pi} = \alpha\frac{|T_{VV}^2|}{|T_{\gamma V}|^2}.$$

This phenomenological coupling includes the effects of extrapolation in the external mass of the amplitudes.

3. *Strong interactions of the* V, *for example* ρ *decay*:

$$\frac{\bar{f}_{\rho\pi\pi}^2}{4\pi} = 12\frac{\Gamma_{\rho\to\pi\pi}}{m_\rho}\left(1-\frac{4m_\pi^2}{m_\rho^2}\right)^{-3/2}.$$

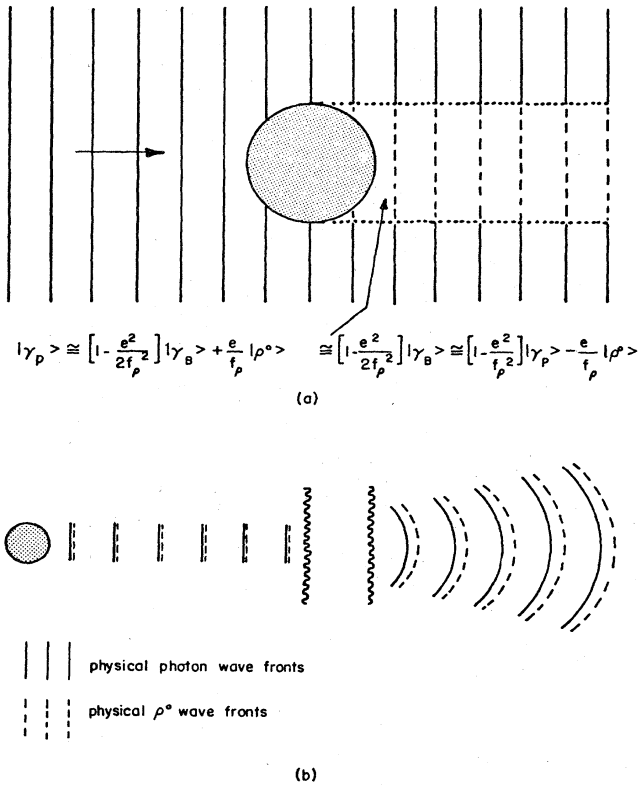

FIG. 12. Compton scattering and diffractive photoproduction of ρ^0 mesons in a simple model. (a) shows the situation in the vicinity of the target nucleon. The ρ^0 component of the physical photon is absorbed out, leaving a bare photon. The bare photon state may be reexpressed in terms of physical photon and physical ρ^0 states; the coefficient of the physical photon state is fixed by the condition that the state be correctly normalized to order e^2/f_ρ^2. Here (b) shows the modified portion of the wave reexpressed in terms of physical particles. Immediately behind the target nucleon, the two components are in phase and combine with the incident wave to reproduce a bare photon. Further along they become disentangled and represent real Compton scattering and ρ^0 production (from Yennie, 1975).

ever, by relaxing these last assumptions we can include in a single picture of photon structure all those additional hadronic states coupled by field theory to the vector mesons. A practical illustration of this appears a few paragraphs below.

Returning now to some general consequences of VMD, we note that the reactions $e^+e^- \to \pi^+\pi^-$, $\pi^-\pi^0\pi^+$, K^+K^-, and $K\bar{K}$ disclose the important parameters $\bar{f}_\rho$, $\bar{f}_\omega$, and $\bar{f}_\phi$, and also make possible internal tests of the theory. For example, by studying the "bump" in the $\pi^+\pi^-$ mode attributed to the ρ^0 (see Sec. III.F), we may readily see that its width is given by the $\rho-\pi^+\pi^-$ coupling strength ($\bar{f}_{\rho\pi\pi}$, see Table I; in VMD $\bar{f}_{\rho\pi\pi}=f_\rho=\bar{f}_\rho$ if finite width effects are ignored) and that its overall normalization is determined by the $\gamma-\rho^0$ coupling strength [$(e/\bar{f}_\rho)m_\rho^2$ in VMD]. The data seem to be quite consistent with this normalization/width relationship predicted by VMD (Benaksas *et al.*, 1972),[15] when account is taken of the finite width effects (Gounaris and Sakurai, 1968; Vaughn and Wali, 1968). Analyses for $\bar{f}_\omega$ and $\bar{f}_\phi$ in the other modes are similar but complicated somewhat by a variety of branching ratios (see Sec. III.F and Appendix C).

A process of great interest to us in this paper, which is very easy to analyze from the viewpoint of the photon's hadronic component, is the photoproduction of the vector mesons themselves. The target modifies the hadronic constituents (essentially by absorption at small impact parameters) so that behind the target the state corresponds to a slightly attenuated incident photon state plus physical hadrons. The mechanism is illustrated in Fig. 12(a) for the ρ^0 part of the photon. If we now make the further assumption that constituents are not mixed by the scattering, i.e., the "diagonal approximation," we can view ρ^0 production by an incident real photon as shown in Fig. 12(b). Under these circumstances, then, we clearly have the result

$$T_{\gamma V} = (e/\bar{f}_V)T_{VV} \tag{2.9}$$

for any vector meson V in the photon's hadronic component. Note that (2.9) depends only on the absence of bare photon contributions and the diagonal approximation; explicit VMD is not used in any way! In Table I we define a phenomenological photoproduction coupling by $\hat{f}_V$ in place of $\bar{f}_V$ in Eq. (2.9). The difference between these allows for off-diagonal VMD or non-VMD-type processes. Comparison of experimental values of $\bar{f}_V^2/4\pi$ and $\hat{f}_V^2/4\pi$ then provides a test of these hypotheses; such comparisons are made in Sec. IV.

While the diagonal approximation is often made as a simplifying assumption when VMD is applied, the two are really quite independent. There is nothing in VMD to prevent the scattering of V into V'; indeed, the neutron–proton difference in photoproduction is often attributed to ρ^0 scattering-into-ω contributions. More-

over, in the photoproduction of the isoscalar ϕ and ω mesons Eq. (2.9) might well be modified by an off-diagonal "mixing" term consistent with the VMD hypothesis. In the language of SU(3) both ω and ϕ mesons are mixtures of SU(3) singlet and octet states and in fact appear to be much closer to pure "quark" assignments, where the $\phi(\omega)$ consists of only strange (nonstrange) quarks; see Gourdin (1971). In any case one easily envisions a strong SU(3) violating coupling between ω and ϕ which in principle could lead to $\phi \rightleftarrows \omega$ transitions on nuclear targets. Ross and Stodolsky (1966b) were aware of this possibility and pointed out some of its implications in nuclear photoproduction of ϕ and ω. More recently Bauer and Yennie (1976), assuming diagonal scattering of strange (nonstrange) quarks and employing "exact" ϕ, ω quark content from experiment, have estimated that $\phi \rightleftarrows \omega$ transitions might reduce the rhs of Eq. (2.9) by 9% (6%) in the case of the $\phi(\omega)$.

● Concentrating specifically on ρ^0 photoproduction ($Q^2 = 0$), we mention that it is possible to apply VMD in the more sophisticated manner allowed by the field-current identity by taking into account the coupling of the photon (field-theoretically through the ρ^0) to $\pi^+\pi^-$ pairs. One can think of this as ρ^0 dominance, where the ρ^0 is itself structured by its coupling to pion pairs (Bauer, 1973) or, alternatively, as more of a "pion pair dominance," encompassing the ρ^0 as a prominent resonance (Yennie, 1975). These considerations lead to a modification of the mass spectrum of photoproduced $\pi^+\pi^-$ pairs from a Breit–Wigner shape to one which is skewed toward lower masses. Since a proper treatment of this line shape has been an irksome problem in the treatment of data, we shall give a brief discussion of the underlying physics here. (In Sec. IV.C the practical procedure for defining the ρ^0 cross section is given.) In addition to the amplitude for simple ρ^0 production, the interfering contribution from nonresonant pion pairs is rather important (Söding, 1966; Pumplin, 1970; Bauer, 1970, 1971). The model is similar to that described above leading to Eq. (2.9). Still within the confines of VMD several possibilities and results are illustrated in Fig. 13 (Yennie, 1975). The curve labeled R.S. [for the line shape predicted by Ross and Stodolsky (1966a)] corresponds to a model where the nonresonant pion pair state and the ρ^0 both interact with the same cross section; the result is a Breit–Wigner shape modified by a factor $(m_\rho^4/m_{\pi\pi}^4)$. The curve labeled D.S. [for the photoproduction model of Söding (1966), which incorporates the Drell amplitude (Drell, 1960)] assigns double strength to the nonresonant pion pair amplitude corresponding to the assumption that *each* pion has an interaction cross section comparable to that of the ρ^0. The preference of the data for this second model is then probably a rough indication of a physically real, nonresonant, two-pion component in the photon. Other approaches to the line shape problem have been given by Kramer and Uretsky (1969). Kramer and Quinn (1971), and Kramer (1972) using dispersion relations and by Satz and Schilling (1970), Dewey and Humpert (1971), and Uretsky (1973) in a dual model.

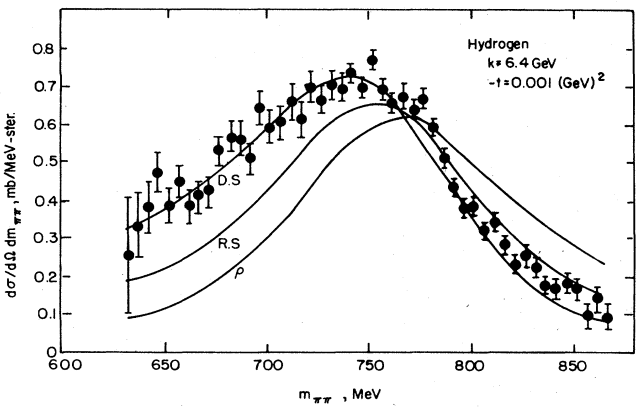

FIG. 13. The mass distribution of pion pairs in photoproduction from hydrogen. The curve labeled ρ^0 is the pure ρ^0 part of a best fit with an adjustable background (Spital and Yennie, 1974a). The curves labeled RS and DS refer to phenomenological models of Ross and Stodolsky (1966a) and Söding (1966). The data are from the DESY–MIT group (privately supplied by Professors U. Becker and S. Ting) (from Yennie, 1975).

Another very important process we shall consider in detail is the total photon-nucleon cross section. For $Q^2 = 0$ we can estimate the low-mass contributions rather simply. Returning to Fig. 12(a) and Eq. (2.6) we see that the photon state vector is modified in passing through the target, thus producing a contribution to Compton scattering. As mentioned earlier in the paper, we are favorably motivated by the fact that the energy and angular dependence, along with a predominantly imaginary phase of experimental Compton scattering, is similar to that of elastic vector-meson scattering. The VMD contribution to the Compton amplitude $T_{\gamma\gamma}$ is given in the diagonal approximation by

$$T_{\gamma\gamma}^{(\mathrm{VMD})} = \sum_V \frac{e^2}{f_V^2} T_{VV} \,. \tag{2.10}$$

The imaginary part of the VMD contribution to the forward Compton scattering amplitude yields (via the optical theorem) the VMD contribution to the total photon cross section $\sigma_{\gamma N}$, where

$$\sigma_{\gamma N}^{(\mathrm{VMD})} = \sum_V \frac{e^2}{f_V^2} \sigma_V \,. \tag{2.11}$$

[Actually, Eq. (1.6) is a better representation for $\sigma_{\gamma N}^{(\mathrm{VMD})}$ since it incorporates off-diagonal contributions.] At high energies we take from experiment[19] $(e^2/f_\rho^2)\sigma_\rho \approx 85$ μb, $(e^2/f_\omega^2)\sigma_\omega \approx 10$ μb, and $(e^2/f_\phi^2)\sigma_\phi \approx 7$ μb, which total up to $\approx$100 μb, in comparison to $\approx$120 μb, or a defect of order 20%. Finite width corrections (see Appendix C and Bauer and Yennie, 1976) can change these estimates slightly. Moreover $\phi \rightleftarrows \omega$ transitions (Ross and Stodolsky, 1966b) might easily reduce the total ϕ and ω content to about 12 μb (Bauer and Yennie, 1976). The role of VMD in the interaction of virtual photons with nucleon targets is discussed in Secs. C and D.

We have seen or mentioned that VMD is a quantitatively useful hypothesis in many contexts. On the other hand, it seems to break down as a complete description of processes whose cross sections decrease rapidly with en-

[19] A more complete discussion of these parameters is one of the objectives of this paper. For the moment, we indicate only very approximate estimates.

ergy, such as pseudoscalar meson photoproduction. In any case the contribution of such processes to the total cross section individually is relatively unimportant [as an example, $\sigma(\gamma p \to \pi^+ n) = 20/\nu^2$ μb, with ν between 1.8 and 16 GeV (Boyarski *et al.*, 1968)]. From a theoretical point of view, the space-time discussion of the next section suggests that such nondiffractive processes may be biased toward higher-mass photon components (or even direct photon interactions) involving delicate interference among many components. Our notion of absorption is more of a "bulk" effect; so it is not implausible that VMD should work best for diffractive amplitudes which correspond to the absorption mechanism we have described.

C. Space-time aspects of real and virtual photon interactions

Our discussion so far has been phrased in the language of stationary state perturbation theory. Our intuitive discussion of photon interactions assumed tacitly a *separability* of the problem into two stages: the internal structure of the photon is first worked out independently of the target, and then the various components are permitted to interact with the target. For this picture to be valid, the virtual hadrons must be present for a time sufficiently long so as to undergo collisions as if they were ordinary, "real" hadrons. They must be able to propagate like physical particles into the target as if they had become detached from the photon. They would then reflect their photonic origin only in their symmetry quantum numbers and the specifics of the superposition.[20]

In free space, the virtual hadrons never could become detached. The physical photon is always making transitions back and forth between a bare photon and hadronic states in such a way as to produce the steady state (2.1).[21] Such transitions are called vacuum polarization fluctuations, and we may regard interactions with the target as arising from the interception of a photon in its temporary hadronic state. For these interactions to satisfy the separability conditions it is necessary that the fluctuation lasts a typical time (called the formation time), which is relatively long compared to the interaction time with the target. The formation time may be estimated from a venerable uncertainty principle argument to be

$$t_f \sim \left| \frac{1}{\nu - E_n} \right| \sim \frac{2\nu}{Q^2 + \mathfrak{M}^2} \ . \tag{2.12}$$

For fixed Q^2 and $\mathfrak{M}^2$, this is directly proportional to the photon's energy. For example, the ρ^0 component inside a 10 GeV photon has a formation distance of order 7 F![22] That high-energy interactions can proceed over longitudinal dimensions that grow with energy was first realized by Gribov, Ioffe, and Pomeranchuk (1965). Application of this notion to inelastic electron scattering was initiated by Ioffe (1969), and its application to nuclear photoabsorption cross sections was initiated by Gribov (1969). Its importance for diffractive photon processes was stressed by Nieh (1970, 1973).

In the above example, the distance over which the photon can travel in its hadronic phase is much larger than the typical dimensions of hadrons. Since the interaction time is likely to be characterized by the nucleon radius, the separability condition should be well satisfied for contributions arising from the ρ^0 constituent. When the formation time becomes shorter (large $\mathfrak{M}^2$ and/or large Q^2), the hadron-mediated interactions may become practically indistinguishable from interactions due to the bare photon term.

Spital and Yennie (1976) have studied the separation of photon interactions into direct and hadron-mediated terms using time-dependent perturbation theory. They showed that the hadron-mediated term is a superposition over hadronic states of the amplitude for the photon to contain a hadron multiplied by the amplitude $\mathfrak{a}$ for that hadron to interact, which is just what one might expect from the preceding intuitive discussion. This result might seem to indicate that our comments about formation time are irrelevant, but this is not so. The amplitude $\mathfrak{a}$ is off the hadron's energy shell by the amount $|\nu - E_n| \approx (Q^2 + \mathfrak{M}^2)/2\nu = (t_f)^{-1}$. To the extent that $\mathfrak{a}$ is insensitive to this energy discrepancy, $\mathfrak{a}$ is the same as for a real incident particle and the separability condition is satisfied. We may regard the rate of change of $\mathfrak{a}$ with respect to $|\nu - E_n|$ as a measure of the interaction time. Whenever $\mathfrak{a}$ is slowly varying, the interaction time is small compared to the formation time, and hence the interaction does not sense the small discrepancy in frequency of the incoming hadron. When $\mathfrak{a}$ varies rapidly, the converse is true. Incidentally, if one expands $\mathfrak{a}$ in powers of $(\nu - E_n)$, the correction terms cancel the energy denominator in (2.2). Such corrections

[20] The specific details of the superposition could be quite important in determining the properties of various interactions. The superposition produces a localized state which interacts as a unit which may have very different properties from those suggested by the labels n_i occurring in (2.4). For example, in some circumstances it may be better to visualize this state as a quark pair rather than in terms of real physical particles.

[21] The superposition of bare photon and hadronic states that we called in Sec. II.B the "physical photon" is (to lowest order in e) an eigenstate of the full Hamiltonian. Apart from interactions with a target, no transitions occur among the various components. If, however, we *start* with a bare photon and allow it to evolve in time under the influence of the full Hamiltonian, time-dependent transitions do occur between the bare photon and the—as we now perceive it—developing hadronic structure. Regarding calculational techniques, e.g., a perturbation expansion, the two approaches differ only in being "steady state" or "time dependent." It is this latter view that we will emphasize in this section.

[22] We use the terms "formation distance" and "formation time" interchangeably since the hadronic component propagates essentially at the speed of light. The concept of formation time is discussed more fully in papers by Spital and Yennie (1976) and Yennie (1976). For narrow resonances, the hadronic component takes much longer to build up than t_f, but t_f is the more relevant time since it represents the coherence time for different contributions to act together constructively. If a broad mass distribution is important for a given process, the buildup time for the component could shorten and become comparable to the formation time. Then the concept of separability breaks down. An intuitive discussion of this point is contained in the lectures by Yennie (1976).

should then not be associated entirely with the photon's hadronic structure; rather they become inseparable from its direct interaction effects.

The remarkable property of a long formation distance must surely lead to observable consequences. In the following section we will describe the role that long-ranged interactions play in the scaling region. In Sec. II.E we shall describe how such effects should show up rather directly in photon reactions in nuclei. The remainder of this section will describe another compelling, if less intuitive, argument for evidence of long-range interactions.

The argument begins with the fact that the propagation of light through matter is completely determined by the commutation properties of the electromagnetic current density J_μ. This permits us to relate the imaginary part of the forward Compton scattering amplitude (or equivalently, through the optical theorem, the total photon-nucleon cross section) to the space-time behavior of the absorption and emission of photons. The derivation of this relationship is given in Appendix A. Here we shall describe briefly the arguments by which the long-range behavior is inferred from the data.

As explained in Appendix A, a phenomenological description of total photon-nucleon cross sections (nucleon spin averaged) requires knowledge of two independent structure functions $W_{1,2}(Q^2, k\cdot P)$, where k is the photon 4-momentum, $k \equiv (\nu, \mathbf{k})$. $Q^2 \equiv -k^2 = \mathbf{k}^2 - \nu^2$ is positive for inelastic electron or muon scattering and zero for real photons. In the laboratory frame we find $Q^2 \leq 2k\cdot P = 2M\nu$, where the equality holds for elastic lepton–nucleon scattering. Here P is the nucleon's 4-momentum ($\mathbf{P} \equiv 0$ in the lab) and M is its mass. Experimentally, the dimensionless quantities MW_1 and νW_2 are determined by "single-arm" inelastic electron or muon scattering, as described in Sec. III.I. They are also related to quantities called the transverse and longitudinal virtual photon total cross sections (σ_T and σ_L)[23] (Hand, 1963) by

$$MW_1 = \frac{2M\nu(1-x)}{8\pi^2\alpha}\,\sigma_T(Q^2,\nu)\,,$$

$$\nu W_2 = \frac{2Q^2(1-x)}{8\pi^2\alpha[1+(Q^2/\nu^2)]}\,[\sigma_T(Q^2,\nu)+\sigma_L(Q^2,\nu)]\,, \qquad (2.13)$$

[23]Aside from the limiting case $Q^2 = 0$, the quantities σ_T and σ_L do not have precisely the intuitive meaning of cross sections. The intuitive meaning derives from the probability of a particle in a beam to have a certain interaction; but there is, strictly speaking, no such thing as a beam of virtual particles. Aside from certain kinematical factors, the observed cross section corresponds to the imaginary part of the forward Compton scattering amplitude. For a real photon, this is proportional to $|\mathbf{k}|\,\sigma_{\rm tot}(\nu)$. In generalizing to virtual photons, Hand (1963) *chose* to replace $|\mathbf{k}|$ by the momentum of an equivalent real photon which would yield the same total center-of-mass energy as the virtual one, namely, $\nu - Q^2/2M$. This gives rise to the factor $(1-x)$ in Eq. (2.13), as compared to the result of replacing $|\mathbf{k}|$ by ν. Such differences in kinematical factors are of course entirely absorbed in the definition of σ_T and σ_L. It is only necessary that we adopt some convention and stick with it. Since the Hand convention is used fairly universally, we adopt it here. These remarks will be important later in deciding the appropriate way to implement VMD when $x \neq 0$.

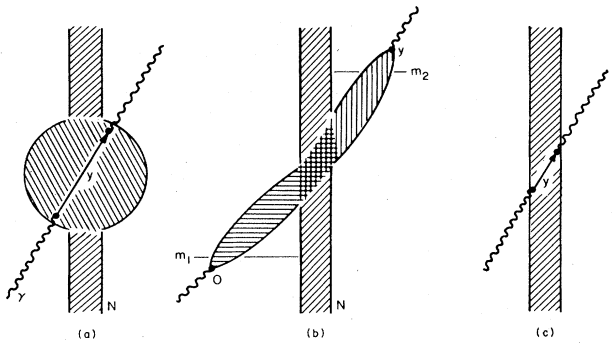

FIG. 14. The space-time dependence of forward Compton scattering. (a) The complete amplitude; y is the space-time separation between the annihilation of the incoming photon and creation of the outgoing photon. (b) The hadron-mediated contribution. (c) A short-range contribution.

where $x \equiv Q^2/2M\nu$ is the famous Bjorken scaling variable. The limiting behavior for small Q^2 is

$$\lim_{Q^2\to 0}\sigma_T(Q^2,\nu) = \sigma_{\gamma N}(\nu)\,,$$
$$\lim_{Q^2\to 0}\sigma_L(Q^2,\nu) = 0\,, \qquad (2.14)$$

where $\sigma_{\gamma N}(\nu)$ is the total real photon-nucleon cross section.

The result of the analysis given in Appendix A is that the forward Compton scattering amplitude may be expressed as a Fourier transform of a matrix element of the commutator of two current operators. Then, using various symmetry properties, it is possible to express W_1 and W_2 as space-time integrals. For example,

$$\nu W_2(k^2,\nu) = 2Q^2\nu M\int d^4y\,\sin(k\cdot y)\theta(y\cdot P)\theta(y^2)f_2(y^2, y\cdot P)\,. \qquad (2.15)$$

Here y is the 4-vector space-time separation between the points of absorption and reemission of the virtual photon and is illustrated in Fig. 14. $y\cdot P (= y_0 M$ in the laboratory frame) is called the "range." Note that y is *not* the difference between the coordinate of the photon's disappearance and the nucleon position. A critique of the idea of interaction range in the present context has been given by Miklavc and Woo (1973).

Simplest analyses of (2.15) assume $f_2(y^2, y\cdot P)$ to be regular and nonvanishing near the "light cone" ($y^2 = 0$). The singularity structure of the current commutator that leads to this behavior is "canonical." (If one evaluates the commutator with free field operators, the singularities obtained are called canonical.) These assumptions with $f_2(0, y\cdot P)$ a nontrivial function of $y\cdot P$ lead to Bjorken scaling (Bjorken, 1969). This means that as $Q^2, \nu \to \infty$ with $x = Q^2/2M\nu$ fixed, the structure functions MW_1 and νW_2 become functions $F_1(x)$ and $F_2(x)$ and do not depend on Q^2 and ν separately. The connection between canonical singularities and scaling has been shown by Brown (1969), Jackiw, van Royen, and West (1970), Brandt (1969, 1970), and Leutwyler and Stern (1970). Figure 15 illustrates that the data appear to have this behavior, at least over the SLAC kinematical range. At

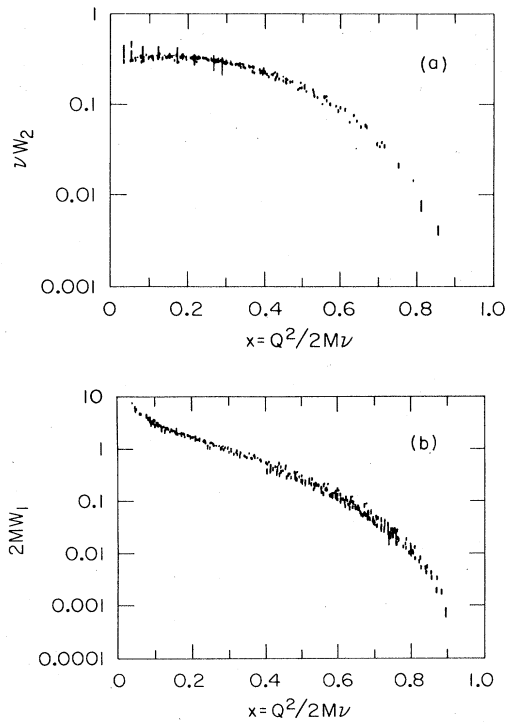

FIG. 15. Scaling of $2MW_1$ and νW_2 in deep-inelastic scattering (from Taylor, 1975). SLAC data with $Q^2 > 1$ GeV^2 and $W^2 (= M^2 + 2M\nu - Q^2) > 4$ GeV^2 are shown. Analysis was made assuming $R = \sigma_L/\sigma_T = 0$. Values of νW_2 are extracted from measurements where $\epsilon \geq 1/2$, those of $2MW_1$, where $\epsilon \leq 1/2$. The large vertical bars below $x = 0.3$ in the graph of νW_2 are from the muon experiment at Fermilab (Chang *et al.*, 1975).

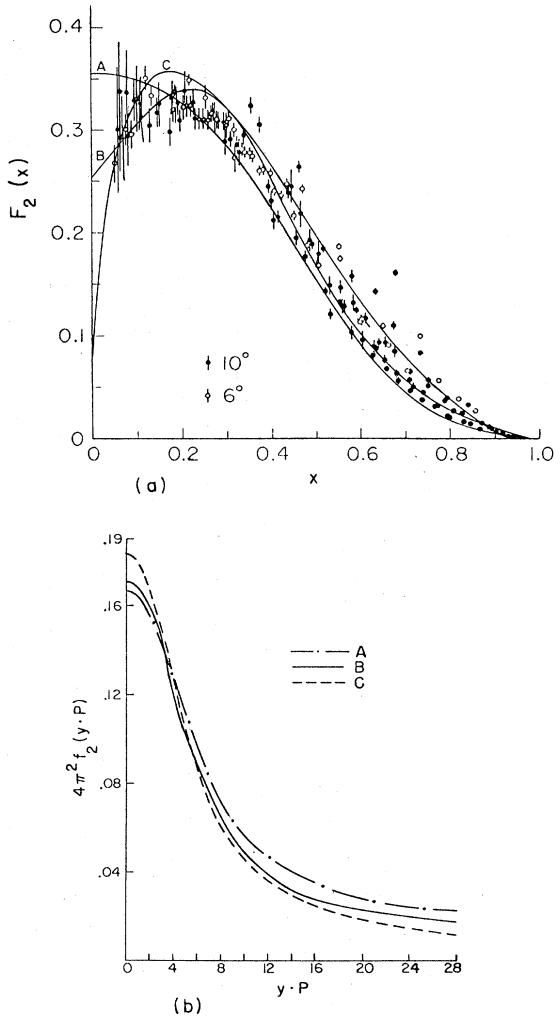

FIG. 16. The space-time analysis of Pestieau, Roy, and Terazawa (1970). (a) Three fits to the possible scaling limit of νW_2. (b) The dependence of the space-time function $f_2(0, y \cdot p)$ along the light cone for each of the three fits to the scaling limit.

higher energies, however, deviations from scaling appear—see Sec. III.I.[24]

●Other possibilities for the behavior of f_2 near the light cone have been studied. For example, anomalous dimensions [Wilson (1969); conference reviews were given by Wilson (1972) and Frishman (1972)] correspond to singularities with the behavior $(y^2)^\beta$ near the light cone. Most contemporary theoretical work suggests that light-cone singularities are *not* worse than canonical, i.e., they are either canonical, asymptotically free,[25] or have anomalous dimensions with $\beta > 0$.

We are particularly interested in the long-range (large $y \cdot P$) behavior of f_2 because of its possible connection with the hadronic structure of the photon. Ioffe (1969) first showed that the experimental data on inelastic electron scattering required a long range. Pestieau, Roy, and Terazawa (1970) then made a more quantitative analysis using a formula of Jackiw, van Royen, and West (1970) for inverting the scaling limit $F_2(x)$ of νW_2 to find $f_2(0, y \cdot P)$. Their results depend of course on the assumed form of F_2 since that quantity could only be guessed from finite energy data, and they are shown in Fig. 16. As was anticipated from Ioffe's work, the long-range behavior of f_2 turned out to be extremely sensitive to the small-x behavior of $F_2(x)$. If $\lim_{x \to 0} F_2(x) \neq 0$, the result is that $f_2 \propto y_0^{-1}$ for large y_0. Such a behavior is necessary to overcome the factor of Q^2 appearing explicitly in Eq. (2.15). For smaller y_0, the function changes behavior at $y_0 \sim R_p$ and remains finite as $y_0 \to 0$.

●The general idea of Ioffe's argument is as follows. Consider the sine function of Eq. (2.15) and rewrite $k_3 \approx \nu + Q^2/2\nu$ with $|\mathbf{k}| = k_3$. Then

$$k \cdot y \cong \nu(y_0 - y_3) - (Q^2/2\nu)\, y_3 . \tag{2.16}$$

For large ν, the rapid oscillations of the sine function force the major contribution to come from the vicinity

[24] Tests of scaling have been extended to very large values of Q^2 and ν using 56 and 150 GeV muons at Fermilab (Watanabe *et al.*, 1975; Chang *et al.*, 1975; H. L. Anderson *et al.*, 1976). Results show deviations from scaling as described in Sec. III.I, but it is remarkable that no large breakdown occurs.

[25] For present purposes, asymptotic freedom (Gross and Wilczek, 1973; Politzer, 1973) yields very small departures from scaling which vary only logarithmically with energy. See Sec. III.I for a comparison of theory and experiment.

of the light cone. If, in addition, f_2 were short ranged in $y\cdot P$ (hence in y_3), the result of the integration would depend on Q^2 only in the combination $Q^2/2\nu$. Ioffe showed that this is incompatible with certain features of the data and hence concluded that f_2 must be long ranged.

The study of the long-range behavior was elaborated further by suri and Yennie (1972). An outline of part of their treatment is given in Appendix A. They draw the following conclusions:

(1) If f_2 is short ranged, F_2 approaches 0 at least as fast as x^2 for small x. Experimental data plotted versus x are shown in Fig. 15. While the data suggest validity of scaling, F_2 appears more nearly to approach a constant for small x, and is certainly not proportional to x^2.

(2) If f_2 is short ranged, the real photon cross section should drop as $1/\nu^2$ for high energies. Contemporary data indicated that $\sigma_\gamma(\nu)$ approached a positive constant (~100 μb) as $\nu\to\infty$ (see Fig. 7); present data shows a logarithmic rise with ν.

(3) Since (1) and (2) appear to be in sharp disagreement with present data, long-range terms are necessary; and an asymptotic term like $h^{(1)}(y^2)/y_0$ (large y_0) will yield both a constant real cross section and an F_2 which is nonvanishing for small x:

$$f_2 \propto \frac{h(y^2)}{y_0} \to \sigma_\gamma \cong \text{const. and } \lim_{x\to 0} F_2(x) \neq 0 . \qquad (2.17)$$

●(4) Long-range terms with the structure $h^{(a)}(y^2)/y_0^a$ $(1<a<3)$ yield Regge-type energy behavior of the total cross section: $1/\nu^{a-1}$.

●(5) We mention for completeness that if one has a pure term $h^{(a)}(y^2)/y_0^a$ (i.e., if the asymptotic behavior is extended to $y_0=0$), the resulting contribution to νW_2 will be (for $\nu^2 \gg Q^2$)

$$\nu W_2^{(a)} = \frac{Q^2}{\nu^{a-1}} G^{(a)}(Q^2) , \qquad (2.18)$$

where for large $Q^2, G^a \to C(Q^2)^{a-2}$. With nonvanishing C, this gives a scaling contribution of the form $C' x^{a-1}$. Actually, there cannot be such pure terms since, aside from questions about whether such singularities are legitimate or not, they would violate the threshold condition that νW_2 should vanish for $x>1$.[26] Therefore the asymptotic behavior in y_0 is not continuable into small y_0. Somehow, the function is smoothed over, and the analysis of Pestieau, Roy, and Terazawa (1970) indicates that this smoothing takes place at around a proton radius.

To reinforce our conclusions that the long-range behavior expected from VMD or GVD is demanded by the data, let us look at the diffractive contributions in more detail. In the space-time analysis, these correspond to long-range terms as in Eq. (2.17). We would expect that if x is not too large, it should be possible to ignore the short-distance smoothing of f_2. The usual guess is that

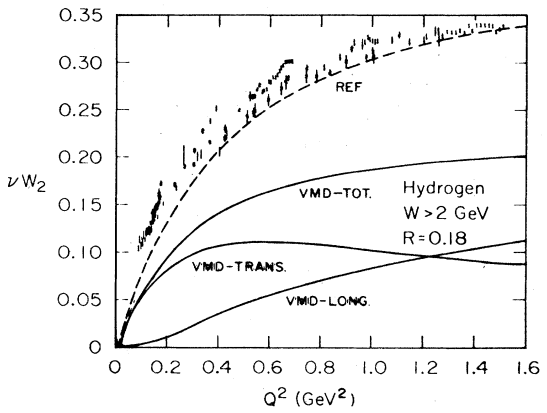

FIG. 17. νW_2 as a function of Q^2 in the small-x region. The data are for various values of x ranging from about 0.01 to about 0.15 (from Stein *et al.*, 1975). The VMD curves are based on Model I of Table XXXV, calculated for infinite energy ($x\to 0$), with only the ρ^0 assumed to give a longitudinal contribution specified by $\xi_\rho = 0.6$ in (2.20). The curve labeled "REF" is a reference curve to be used to compare data in different figures (Figs. 17 and 167). Its equation is $\nu W_2 = 0.89Q^2 \times (1+0.648Q^2)/(1+1.2Q^2)^2 \equiv A(Q^2)$. It has *no* physical significance. However, its slope at $Q^2=0$ has been adjusted to correspond to a real photon total cross section of 100 μb, which is close to the apparent asymptotic value; its asymptotic value for $Q^2 \to\infty$ is 0.40. It is probable that the experimental values of νW_2 in the region $0<Q^2<1$ GeV^2 will drop as ν increases, but no effort has been made to fit $A(Q^2)$ as the limiting curve.

$(R_p Q^2/2\nu) \ll 1$ where R_p is the radius of the proton (~$1/2m_\pi$). Thus we require $x \ll 2m_\pi/M = 0.3$. In practice, $x<0.1$ seems adequate and we expect the pure diffractive term to dominate and yield

$$\nu W_2^{(\text{diff})} = Q^2 G^{(1)}(Q^2) . \qquad (2.19)$$

A compilation of data plotted as a function of Q^2 from this region is shown in Fig. 17 and they seem to fall along a universal curve independent of ν as expected. Of course, other Regge contributions, as well as short-range smoothing, could be causing small systematic deviations from the ultimate curve (for $x\to 0$). The reader should note that Fig. 17 is not incompatible with scaling since it contains only small-Q^2 data.

Nondiffractive interactions display an intriguing difference. The rapid decrease of these cross sections with energy corresponds to a more rapid falloff of f_2 with y_0 than y_0^{-1} (suggesting short-range behavior—see suri and Yennie conclusions (2), (4), and (5) above). Thus the ability of long-range VMD to completely describe such processes is questionable. Intuitively, we might guess that interactions involving the changing of the internal quantum numbers of the target depend critically on the fine details of the overlap of the wave packets of the target and projectile. In order to have a significant probability of achieving the "right" overlap for a given nondiffractive process to occur, the photon may well have to disappear quite close to the important region of the target—hence the shorter range of such processes. (An indicator in pion photoproduction might be that the slope parameter B in $|T_{\gamma\pi}(t)|^2 \sim e^{Bt}$ is about 3 GeV^{-2}, in contrast to 6–8 GeV^{-2} in ρ^0 photoproduction—showing that

[26] Interestingly, the threshold behavior for $F_2(x)$ near $x=1$ also influences the behavior of $f_2(0,y_0)$ for large y_0. It requires an essential singularity in f_2 for (complex) $|y_0| \to\infty$. However, the limiting function is small and quite integrable for real y_0.

the effective interaction radius of π photoproduction is about a factor 2 smaller than in the ρ^0 case.)

Now we come full circle, and ask "What does VMD or GVD predict about the behavior of $\nu W_2^{(\mathrm{diff})}$?" Since there are many different versions of GVD, we shall restrict our discussion to VMD. There it is assumed that σ_T and σ_L are dominated by ρ^0, ω, and ϕ and

$$\sigma_T = \sum_V \frac{e^2}{f_V^2}\left(\frac{m_V^2}{m_V^2+Q^2}\right)^2 \sigma_V\,,$$
$$\sigma_L = \sum_V \frac{e^2}{f_V^2}\,\frac{\xi_V Q^2}{m_V^2}\left(\frac{m_V^2}{m_V^2+Q^2}\right)^2 \sigma_V\,, \tag{2.20}$$

where σ_V is the total cross section of the transversely polarized ($m=\pm 1$) vector particle. The factor ξ_V is introduced because the longitudinally polarized particle need not have the same total cross section (Sakurai, 1969c). The most important aspect of this assumption is that it yields a result of the form (2.20).[27] Although the form of the space-time behavior associated with vector mesons should be almost self evident from our discussion, it can be worked out explicitly. This has been done by Pestieau and Urias (1973) and by Spital and Yennie (1976). They find that f_2 is of the expected form $h(y^2)/y_0$ [Eq. (2.17)].

Historically, of course, deep-inelastic electron scattering was regarded as the first strong evidence against VMD. In first comparisons [in a conference report by Panofsky (1968)] using σ_T only, it was noted that the vector-meson contributions to νW_2 went to zero as $1/Q^2$ and therefore fell below the data. When σ_L was taken into account (with $\xi_\rho \approx 0.6$) (Sakurai, 1969c), it again appeared possible that VMD could account for the observations. However, this led to a large ratio $R(=\sigma_L/\sigma_T)$, which later was found to be in disagreement with experiment (Miller *et al.*, 1972). Thus the simplest version of VMD is inadequate to explain all the features of inelastic electron scattering.

If we do wish to "find VMD" in these data, we must first of all, in line with the above discussion, restrict ourselves to small x. Moreover, we should also restrict ourselves to small Q^2, which [see Eq. (2.15)] places greatest emphasis on the photon's low-mass components. Interestingly enough, if one looks at the small-x region of the present SLAC data (Friedman and Kendall, 1972; and Stein *et al.*, 1975), where machine energy limitations link small x with small Q^2, it appears that VMD contributions can account for a large fraction of the data (Yennie, 1975). This is shown in Fig. 17.[28]

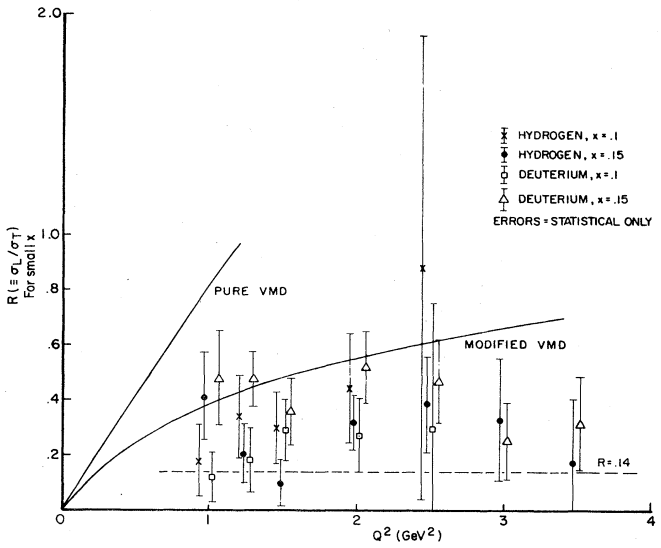

FIG. 18. Values of $R(=\sigma_L/\sigma_T)$ vs. Q^2 for various small values of x. The data are from Riordan *et al.* (1975). The curves are based on the same VMD model illustrated in Fig. 17. In both cases, the longitudinal part comes solely from the ρ^0. For the curve "Pure VMD," the transverse part arises from ρ^0, ω, and ϕ. For the curve "Modified VMD," the transverse part is given by the difference between $A(Q^2)$ (see caption of Fig. 17) and the longitudinal ρ^0 contribution to νW_2.

The ratio R also warrants more detailed study in the small-x region. Published SLAC data (Riordan *et al.*, 1974b, 1975) on R for $x \leq 0.15$ is shown in Fig. 18 plotted against Q^2. Naive VMD calculations predict that R monotonically increases with Q^2, a behavior tentatively suggested by the data for $1 \lesssim Q^2 \lesssim 2.5$ GeV^2 at which point R may be as large as 0.4–0.5 [published data for R at large x is typically of order 0.15; unpublished SLAC data reported by Hand (1977) in a conference summary talk yields $R \cong 0.35 \pm 0.16$]. In Fig. 18, the curve labeled "pure VMD" clearly disagrees with the data; but the one labeled "modified VMD," which incorporates a transverse non-VMD component, is of the right order of magnitude even though it overshoots the data at the large Q^2. Apart from this, the faint suggestion of the data that, around $Q^2 \approx 2-3$ GeV^2, R reaches a maximum is intriguing, and may indicate the Q^2 region where VMD breaks down as a viable qualitative description of the data. As more small-x data is obtained, hopefully over a wider range of ν and Q^2 (in attempting this at SLAC energies one rapidly encounters serious uncertainties in radiative corrections, as well as other systematic errors), it will

[27] In our opinion, it is actually the quantities $(1-x)\sigma_T$ and $(1-x)\sigma_L$ which should be approximated by the right-hand side of (2.20) in the small-x region. See Footnote 23 for a discussion of this additional factor. On the other hand, one might expect the VMD estimate to begin to break down when the formation time becomes comparable with the interaction time, which is perhaps of the order of the proton radius. The corrections would then be expected to be of relative order t_{int}/t_f or $R_p\,(Q^2+M^2)/2\nu \approx x[1+(\mathfrak{M}/Q^2)]$, which is a rather larger correction than the $1-x$ factor would give. The apparent absence of such a large dependence of the data on x in this region is perhaps an indication that the interaction time is much less than R_p.

[28] This figure differs from the original in several respects: Rather than the elaborate dipion calculation, a simple VMD result is shown here, using new parameters from Sec. IV. Also, the limiting curve for infinite energy is shown. The VMD results for finite energy (say 10 GeV) would be appreciably higher (perhaps 25%); but since there is some uncertainty about how to extend the nondiffractive terms to finite Q^2, we prefer to show only the limiting curve here.

be interesting to see whether or not these trends persist.

As we have seen, there is ample evidence that the small-x region of inelastic electron scattering is associated primarily with the hadronic structure of the photon. Within this framework (usually called GVD), we shall see that it is possible to fit the data in many ways, in all of which at small Q^2 the ρ^0, ω, and ϕ would make the dominant contributions. Unlike the original difficulty that VMD appeared to predict too low a cross section, the problem with GVD is how to suppress the effects of the very abundant higher-mass constituents that we have up to this point ignored. To see the problem most clearly, consider the total probability of the hadronic component (see Sec. II.B) using the data from e^+e^- interactions up to the currently available masses (up to around 5 GeV; see Sec. III.F). This turns out to be of order 1.3α, with the ρ^0 contributing 0.4α.[29] Unless the trend of these data changes drastically, the total hadronic component could be several times α. Clearly, it is not possible that this whole component be absorbed with a typical hadronic cross section of order 25 mb, which would lead to a total photon cross section of ~250 μb (to be compared with the experimental value of ~120 μb), as well as a large overestimate of νW_2. The cross sections of some of the higher-mass constituents must be considerably smaller.

At the present time, there is no generally accepted explanation for this apparently small interaction of the higher-mass components. Perhaps it indicates that the matter which is initially created in e^+e^- annihilation is not strongly interacting until some time has passed. That is, the higher-mass part of Eq. (2.2) represents a localized state which is completely unlike our usual picture of hadronic matter. Such a state may not have sufficient time to evolve and interact while passing through a nucleon. Various possibilities for the high-mass constituents are discussed in Sec. VI.B. In most of these the effective absorption cross section varies as $1/\mathfrak{M}^2$.

D. Scaling in high-energy photon interactions

Until this point, we have been emphasizing the role of the photon's hadronic structure in real and virtual photon interactions. Historically, when the first deep-inelastic electron scattering (DIES) results became known, it appeared that VMD was unable to account for the rather large observed cross sections and their slow decrease with Q^2. As a consequence, it has become more popular to discuss DIES in terms of parton models (Bjorken and Paschos, 1969; Feynman, 1969). The term "parton" conveys a mental image of a nucleon as made of internal constituents (partons) which are pointlike in their interaction with the electromagnetic field. In a simple way, these models were able to account for the observed scaling behavior of DIES. Most popularly, the partons are quarks and/or antiquarks (Kuti and Weisskopf, 1971). At the first level of understanding, the hadronic photon model and the parton model appear to be quite different, perhaps even incompatible. That they are in fact compatible and complementary to each other was pointed out by Nieh (1970). This section will first discuss the "naive" parton model, then describe how the hadronic photon can also account for scaling, and finally discuss how the two points of view may be reconciled. Grammer and Sullivan (1978) give a more complete and explicit discussion of this subject which is in general accord with the ideas presented here.

In the naive parton model, the most important property of the partons is their longitudinal momentum distribution in an infinite momentum frame. (If $\mathbf{p}$ is the proton's momentum with $|\mathbf{p}| \gg M$, $p_\parallel$ is the component of the parton's momentum parallel to $\mathbf{p}$.) When expressed as a fraction of the proton's total momentum ($\beta = p_\parallel/|\mathbf{p}|$), the distribution function $f(\beta)$ is assumed to be essentially independent of energy.[30] A crucial assumption is that for collisions involving extremely short times the parton behaves like an ordinary free particle. The limits Q^2, $\nu \to \infty$ are designed to make the scattering time sufficiently short, and the interaction is assumed to be the absorption of a highly virtual photon by a pointlike parton. As such a model contains no fundamental length—at large ν and Q^2 the parton's mass and transverse momentum is thought to be unimportant—it naturally leads to Bjorken scaling.[31] In detail, the kinematics of the free collision forces the virtual photon to pick out a parton whose $\beta = x \equiv Q^2/2M\nu$. Consequently, the scaling function $F_1(x)(F_2(x))$ is proportional to $f(x)(xf(x))$, apart from known factors depending on the spins of the partons (see, for example, Bjorken and Paschos, 1969; Kuti and Weisskopf, 1971). Experimental results on $R \equiv \sigma_L/\sigma_T$ (the most recent, Riordan *et al.*, 1974b, 1975) require the partons to have spin $\frac{1}{2}$ rather than 0.[32] A pedagogical discussion of the parton model has been given by West (1975); unfortunately, it is slightly marred by an error in the formal mathematical treatment of the bound state model. Kogut and Susskind (1973), Roy (1975), and Yan (1976) have given reviews of the status of the parton model.

An apparently opposite viewpoint is that scaling can be accounted for by hadron-mediated interactions [or generalized vector dominance (GVD)]. Many authors have followed this approach, with fairly specific assumptions

---

[29] We thank Mr. David Kaplan for evaluating this probability for us.

[30] Some field-theoretical models support this idea (see Drell, Levy, and Yan, 1969, 1970; Drell and Yan, 1971; note however that these models use a transverse momentum cutoff based on physical considerations outside a pure field theory approach), which is analogous to the "freezing in" of the photon's structure as described in Sec. II.B. However, it is not quite the same thing because the photon's structure was described in terms of physical hadrons, while the partons refer to some more primitive entities.

[31] Modified parton models predicting deviations from scaling behavior also exist. Examples are partons with form factors (Chanowitz and Drell, 1974) and partons within partons (Kogut and Susskind, 1974). Very recently, parton models have been improved to reflect features expected from quantum chromodynamics; for a review and references, see Nachtmann (1977).

[32] Because transverse momentum is assumed limited, the high-energy photon-parton collision is approximately one dimensional. The constraint of helicity conservation then makes it very difficult for longitudinal (transverse) photons to be absorbed by spin-$\frac{1}{2}$(0) partons (Callan and Gross, 1969).

about the vector states involved and how they interact. These approaches will be described in Sec. VI.B. Here we attempt a general, "all-encompassing" formulation and discussion.

Let us recall some of the main features of Secs. II.B and II.C. The amplitude for a mediating hadronic state to contribute to a definite final state was given by two factors:

(1) The amplitude for the vector state—which contains as factors the matrix element of $\mathcal{T}'(0)$ and the denominator $(Q^2+\mathfrak{M}^2)^{-1}$, and (2) the amplitude for the vector state to interact with the nucleon. The importance of the formation time ($t_f \sim 2\nu/(Q^2+\mathfrak{M}^2)$) relative to the collision time ($t_{\rm coll}$) was emphasized. Only if the ratio $t_f/t_{\rm coll}$ is large can we expect the vector state to interact more or less as an ordinary hadron. The fact that was emphasized at the end of Sec. II.C is that to account for the high-mass data on $e^+e^-\to$ hadrons, the factor (1) is surprisingly large, so that the factor (2) has to be strongly suppressed. This could happen either because the individual components have a cross section which decreases rapidly with increasing mass or because of destructive interference between components of different masses. Various speculations are described in Sec. VI.B.

A plausible representation for the hadron-mediated part of the cross section may now be written down. Taking into account the possible interference between different constituents of the photon, the transverse cross section (defined in Sec. II.C) takes the form (Spital and Yennie, 1976)[27]

$$(1-x)\sigma_T=\int\!\!\int_{\mathfrak{M}_{\rm th}^2}^{\infty}\frac{I_T(\mathfrak{M}_1^2,\mathfrak{M}_2^2,2\nu M,Q^2)}{(Q^2+\mathfrak{M}_1^2)(Q^2+\mathfrak{M}_2^2)}\,d\mathfrak{M}_1^2\,d\mathfrak{M}_2^2\,. \tag{2.21}$$

I_T incorporates the imaginary part of the amplitude for scattering of constituents of mass $\mathfrak{M}_1$ into those of mass $\mathfrak{M}_2$, as well as the matrix elements for the photon to convert into these constituents; the types of constituents occurring are summed over. The denominator factors come from the original energy denominator in (2.2).

●The fact that I_T should depend on $\mathfrak{M}_1^2$, $\mathfrak{M}_2^2$, and ν (i.e., the total energy) is obvious. However, its possible dependence on Q^2 is less direct. Mathematically it can come about because the momentum of the mediating hadrons (k) does not have the appropriate magnitude for hadrons of energy ν[namely $(\nu^2-\mathfrak{M}^2)^{1/2}$]. Or, in other words, the mediating hadrons are off the energy shell by $\sim(Q^2+\mathfrak{M}^2)/2\nu$. Rather than use these off-energy-shell variables directly, we have rearranged the arguments of I_T to include Q^2. Physically, this dependence describes the effects of the formation time relative to the collision time ($t_f/t_{\rm coll}$) and of the overall energy-momentum constraints, which require $Q^2<2M\nu$ for a real process. For small Q^2 ($\ll 2M\nu$), the integral emphasizes small $\mathfrak{M}^2$ and the formation times become large; in this limit, the dependence of I_T on Q^2 is expected to be unimportant. For higher Q^2, it is plausible that the reduction of the formation time causes I_T to decrease with increasing Q^2. Certainly near threshold (Q^2 close to $2M\nu$), I_T should vanish.

As an illustration of Eq. (2.21), diagonal VMD or GVD corresponds to[33]

$$I_T|_{\rm diag}=\sum_V\frac{e^2M_V^4}{f_V^2}\,\delta(\mathfrak{M}_1^2-\mathfrak{M}_V^2)\delta(\mathfrak{M}_2^2-\mathfrak{M}_V^2)\sigma_V(\nu)\,. \tag{2.22}$$

Off-diagonal VMD or GVD replaces this by a double sum, where $\sigma_{VV'}(\nu)$ denotes an off-diagonal scattering amplitude

$$I_T|_{\text{off-diag}}=\sum_{V,V'}\frac{e^2M_V^2M_{V'}^2}{f_Vf_{V'}}\,\delta(\mathfrak{M}_1^2-\mathfrak{M}_V^2)\delta(\mathfrak{M}_2^2-\mathfrak{M}_{V'}^2)\sigma_{VV'}(\nu)\,. \tag{2.23}$$

Specific models in GVD assume a definite spectrum of vector mesons extending to infinite masses. See Sec. VI.B.

It is evident that Eq. (2.21) has sufficient generality to account for any set of data without any direct photon terms. Thus it will be impossible to rule out hadron-mediated interactions as an explanation of the data.

What changes must be made to treat the longitudinal cross section σ_L? Gauge-invariance restrictions require the presence of a direct interaction term. However, this direct interaction term need be no larger than order Q^2/ν^2 compared to the hadron-mediated term (Yennie, 1975). Consequently, the assumption of GVD is still tenable, and the conclusion is that one obtains an expression similar to (2.21), but with an additional factor $Q^2/\mathfrak{M}_1\mathfrak{M}_2$:

$$(1-x)\sigma_L=Q^2\int\!\!\int_{\mathfrak{M}_t^2}^{\infty}\frac{I_L(\mathfrak{M}_1^2,\mathfrak{M}_2^2,2\nu M,Q^2)}{(Q^2+\mathfrak{M}_1^2)(Q^2+\mathfrak{M}_2^2)}\,\frac{d\mathfrak{M}_1^2}{\mathfrak{M}_1}\,\frac{d\mathfrak{M}_2^2}{\mathfrak{M}_2}\,. \tag{2.24}$$

What can we infer about I_T and I_L from experimental evidence, perhaps coupled with assumptions about canonical singularities? For small $Q^2(\lesssim 1.5\ \text{GeV}^2)$ and large $\nu(\gtrsim 5\ \text{GeV})$, we have seen that νW_2 is nearly a function of Q^2 alone[34] and that the low-mass VMD terms (ρ^0, ω, ϕ + nonresonant two pions) give a reasonable estimate of its order of magnitude. Accordingly, unless there are very significant interference terms involving the low-mass constituents, the contribution from the higher masses is small (~20% for $Q^2=0$ and somewhat larger for $Q^2\neq 0$). In this region, we expect the important arguments of $I_{T,L}$ to be $\mathfrak{M}_1^2,\mathfrak{M}_2^2$ (resonances, etc.) rather than Q^2; and in spite of the large probability associated with heavy masses, the integrals in (2.21) and (2.24) must cut off rather rapidly above the resonances.

However, if the factor I_T in (2.21) always cuts off the integral very strongly above the resonances, it is easy to see that the transverse contribution to νW_2 would at first rise as a function of Q^2, but would ultimately vanish as $1/Q^2$. This would lead to a vanishing transverse

[33]To agree with Eq. (2.20), a factor of $(1-x)$ would have to be placed on the left-hand side of that equation or on the right-hand side of (2.21).

[34]This experimental statement is based on the assumption that $\sigma_L/\sigma_T\cong 0.18$. Since this is not true in this region, the points in Fig. 17 may be modified slightly when the correct (and as yet not completely known) values of σ_L/σ_T are taken into account. It should be emphasized that the sensitivity to σ_L/σ_T is small since the experiment measures $(\sigma_T+\epsilon\sigma_L)$ with ϵ typically close to 1. Thus νW_2 is less uncertain than W_1.

contribution in the scaling region, in apparent disagreement with experiment. Moreover, we know the heavier masses are present. A strong cutoff is therefore unlikely; and it seems inevitable that the interaction mechanism for these higher masses must be rather different in character from that of the lower masses.

We shall now describe the general behavior of $I_{T,L}$ which leads to scaling. As usual, we assume in the absence of any fundamental length that when Q^2, $\mathfrak{M}_1^2$, $\mathfrak{M}_2^2$, and $2\nu M$ are sufficiently large, other masses in the problem become irrelevant. Then since I has dimensions $[M^{-2}]$, it should satisfy

$$I_T^{\text{asy}}(\lambda\mathfrak{M}_1^2, \lambda\mathfrak{M}_2^2, \lambda 2\nu M, \lambda Q^2) = \frac{1}{\lambda} I_T^{\text{asy}}(\mathfrak{M}_1^2, \mathfrak{M}_2^2, 2\nu M, Q^2) \tag{2.25}$$

where "asy" refers to the limiting behavior of the function when all arguments are large. On rescaling the mass integration $\mathfrak{M}_i^2 \to \xi_i^2 Q^2$ in (2.21), we find

$$(1-x)\sigma_T = \int\int_{\mathfrak{M}_t^2/Q^2}^{\infty} \frac{I_T(Q^2\xi_1^2, Q^2\xi_2^2, Q^2/x, Q^2)}{(\xi_1^2+1)(\xi_2^2+1)}\, d\xi_1^2 d\xi_2^2 .$$

Now we want to study this as Q^2 becomes very large, with x fixed. If I_T has no awkward behavior near the lower limit (resonances don't matter), we may use (2.25) with $\lambda = Q^2$. Then

$$(1-x)\sigma_T \to \frac{4\pi^2\alpha}{Q^2} F_T(x), \tag{2.26a}$$

where

$$4\pi^2\alpha F_T(x) \equiv \int\int_0^{\infty} \frac{I_T^{\text{asy}}(\xi_1^2, \xi_2^2, 1/x, 1)}{(\xi_1^2+1)(\xi_2^2+1)}\, d\xi_1^2 d\xi_2^2 . \tag{2.26b}$$

●A similar discussion for σ_L could run into trouble although the argument proceeds in the same formal way. The possible trouble is that the extra factor of $\xi_1\xi_2$ in the denominator could invalidate setting the lower limit equal to zero as $Q^2 \to \infty$. In particular, it is well known that the resonance contributions can lead to scaling of the longitudinal cross sections, and that a contribution from higher masses is not necessary to produce scaling.

We said earlier in this section that the parton and hadron-mediated views of photon interactions are *apparently* different. In fact, the intuitive pictures that these terms convey are quite different. Now we want to observe that these views are not necessarily in conflict (Nieh, 1970). By appropriate assumptions, either can account for scaling, and neither is "proved" if scaling is in fact confirmed. Either could be "improved" to account for any future breakdowns of scaling. Of course as a theoretical model becomes more specific and makes more detailed predictions, it is placed in greater jeopardy by experimental tests, and confirmations by experiment become more significant.

It is our feeling though that in the scaling region both of these pictures may be encompassing identical physics, but in two widely differing Lorentz frames (recall how dramatically the roles of electric and magnetic fields vary with the Lorentz frame classically): A proton infinite-momentum frame where the photon has too little energy to form any hadronic constituents during the time allotted for the scattering (Drell and Yan, 1971) would seem most appropriate to the parton model. On the other hand, as described in Sec. II.B, the hadronic structure model is most appropriate to the photon's infinite momentum or "lab" frame. For a true comparison we need a covariant picture that encompasses both limits. Such a covariant parton model was first described by Landshoff, Polkinghorne, and Short (1971) involving a fundamental-field-theoretic coupling between photons and pointlike partons and a phenomenological parton-nucleon interaction. The important contributions are illustrated in Fig. 19. It is simple enough to make assumptions that both follow experimental data and lead to scaling. For $Q^2, \nu \to \infty$, the picture is the naive parton model in the appropriate proton infinite-momentum frame, and the "aligned jet" hadronic structure model (described in Sec. VI.B) in the lab.

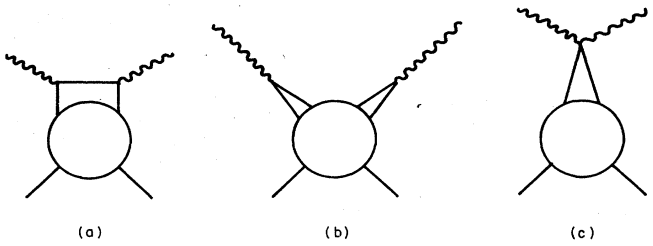

FIG. 19. Examples of graphs in the covariant parton model. (a) Believed to be the leading contribution as Q^2, $\nu \to \infty$. As seen in the infinite-momentum frame of the nucleon, this describes a photon interacting with a parton in the nucleon structure. In the lab frame, it could describe scattering where the photon is mediated by a parton pair. (b) A diagram that could include VMD contributions. (c) Sea-gull graphs which give a fixed-pole contribution.

A gauge-invariant extension of the covariant parton model for the complete Compton amplitude was given by Brodsky, Close, and Gunion (1972, 1973). These authors also show the equivalence between the covariant model and the infinite-momentum (time-ordered perturbation theory) calculations described above. It is clear that in all these calculations the extensive use of free particle dynamics in the parton model can only be valid within a typical hadronic relaxation time or hadronic confinement region in space. Jaffe (1972) has discussed the space-time properties of the parton model.

Apart from the question of Lorentz frame, the relative utility of the parton versus hadronic structure viewpoint may also be suggested by the region of "x" covered by the experiment. Since x is the fraction of the proton's momentum carried by the parton, it appears that the hadron-mediated view might be more useful in the small-x region ($\lesssim 0.15$, say) and certainly in the small-Q^2 region where the parton approach may be less sensible. Here, the large, nearly constant value of νW_2 (~ 0.35) is closely identified with hadron-mediated, diffractive behavior. As x increases, one sees a steady falling off of νW_2. As suggested previously, this could represent a weakening of the hadron-mediated cross section as the formation time is decreased and threshold effects become important. Thus the large area under the νW_2 curve *may not* be a reflection of pointlike charges in the nucleon (an idea popularized in the early days of

the parton model), but rather a reflection of the large diffractive contributions at small x. On the other hand, the parton view could be useful and correct for larger x. The experimental facts, together with the exercises we have just gone through, indicate that when the hadronic states have large masses and are far off the energy shell, the interactions are rather different from those of ordinary hadrons. Since, when $x \gtrsim 0.15$, the formation time is rather small, it becomes meaningless to think of the intermediate hadrons as really being present. Even in the lab frame, the photon therefore effectively interacts directly with the nucleon structure.

If we depart from predominantly diffractive interactions and deal with cross sections that fall rapidly with energy, the hadronic structure viewpoint may be less tractable, as the discussion of Sec. II.C points to these interactions as having a more short-range character. The analogous parton picture in the scaling limit may make more sense, as it involves only partons carrying a nonzero fraction of the proton's momentum ($x \neq 0$). Thus the study of νW_2(proton)-νW_2(neutron), in which diffractive contributions tend to cancel, will be of enhanced significance to the parton model.

● Further interesting theoretical contrast between the hadron-mediated approach and parton model calculations is the question of the existence of the "$J = 0$ fixed pole" in the Compton amplitude (Creutz, Drell, and Paschos, 1969; Damashek and Gilman, 1970). For the parton model, the fact that the two photons can interact at arbitrarily short distances with a charged parton leads immediately to a real contribution to the Compton amplitude that is, apart from normalization factors, independent of photon mass or energy. Such a term is "unhadronlike" and analogous to the Thomson limit in classical physics (see Brodsky, Close, and Gunion, 1972, 1973). [This is also a consequence of scaling, gauge invariance, and the existence of a dispersion relation for the Compton amplitude; see Cornwall, Corrigan, and Norton (1970, 1971).] On the other hand, this "local" two-photon contribution in the real Compton amplitude could strictly only arise in the hadron-mediated description from the infinite mass spectrum. Attempts to find such a term in experimental data using dispersion relations and a variety of hadronic models are still inconclusive— see Sec. III.B.

While we wish neither to indulge any naive model too seriously nor to comment on its ultimate veracity, the qualitative successes of the naive parton model nevertheless point out very dramatically a very important aspect of photohadronic interactions. This is that a photon is probably not a simple composite of hadrons in the sense that a hydrogen atom is a composite of an electron and proton or even the same sense as a hadron is alleged to be a composite of quarks. In these latter cases the hydrogen atom or hadron has a definite (unit) probability of being its appropriate constituents. In the case of the photon the total probability that it is made up of hadrons, $\int d\mathfrak{M}^2 P(\mathfrak{M}^2)$, in all likelihood diverges (Sec. II.B). This fact does not mean the hadronic picture or GVD is incorrect, only that the mix of constituents in any interaction will have to be carefully chosen. In contrast with the qualitative description in Sec. II.A, we will not always expect the photon's behavior to be analogous to that of a single or even a fixed superposition of hadrons. By emphasizing a "pointlike," noncomposite aspect of the photon, situations appropriate to the parton model tend then to highlight the breakdown of this, most naive, photon-hadron analogy.

E. Photon processes in nuclei

If the intuitive arguments about the long-range behavior of photon interactions are correct, how can this feature manifest itself experimentally? Clearly, if we deal with real photons incident on single nucleons, there is no direct experimental way of distinguishing long- from short-range effects. The data on energy dependence and deep-inelastic scattering, coupled with the theoretical assumption of canonical light-cone singularities, do of course imply this long-range behavior. However, the only intuitively clear way to demonstrate the long-range character of the interaction is to put obstacles in the way of the hadronic buildup and study how this alters the interaction. Very conveniently, nuclear matter supplies an appropriate density of nucleons for such a test. The idea is illustrated in Fig. 20, in which two mechanisms for interaction are contrasted. If the photon interacts only directly with each nucleon, the presence of the other nucleons should have no effect [Fig. 20(b)]. However, if the hadronic component is present over a long range,

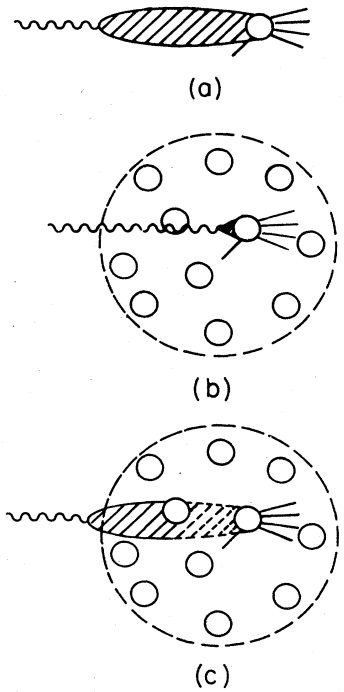

FIG. 20. Spatial visualization of photon interactions. (a) In interaction with a single nucleon the photon may convert to hadrons a long distance before reaching the nucleon. (b) The direct interaction of a photon with a nucleon in a nucleus. This would lead to no shadowing of photons. (c) With a long formation time, a photon cannot interact with a nucleon deep within the nucleus without initiating a reaction on another nucleon first. Thus the total cross section is reduced relative to that due to (b).

then interactions deep inside the nucleus will tend to be shadowed [Fig. 20(c)].

We would expect rather different experimental results in the two cases. If the interaction were primarily short ranged, then an incident photon would have an almost equal chance to interact with any nucleon—the conventionally calculated mean free path of a photon in nuclear matter is hundreds of fermis! In this case, the total cross section would be given by

$$\sigma(A)=A\sigma(1) \quad \text{(pure short range)}, \tag{2.27}$$

where $\sigma(1)$ is a suitably weighted average of total cross sections on neutrons and protons. On the other hand, if the interaction is primarily long ranged, the photon's initial interaction will be principally with the nucleons on the incoming side of the nucleus. Nucleons further along the photon trajectory may participate in secondary reactions which do not add to the total cross section. Stated in other language, the hadronic cloud of the photon is very quickly stripped off and the remaining bare photon is nearly incapable of interaction. Thus the photon penetrates nuclear matter quite freely, but its ability to initiate interactions is quickly shadowed. In consequence, we expect

$$\sigma(A)<A\sigma(1) \quad \text{(long range)}. \tag{2.28}$$

One often says that the absorption should be a surface effect and the total cross section should go as $A^{2/3}$. Of course, this power law is only meant to be suggestive as we are dealing with finite nuclei where the radius is not much greater than the mean free path and the surface thickness. This expectation for photon shadowing in the infinite energy limit was first pointed out by Stodolsky (1967) in the framework of vector-meson dominance (VMD). Subsequently, Gribov (1969) and Brodsky and Pumplin (1969) argued that it should be true more generally if interactions are mediated primarily by the hadronic constituents of the photon. More complete VMD analyses, taking into account the energy dependence of the formation time, were given by Brodsky and Pumplin (1969), Nauenberg (1969). Recent reviews of hadronic aspects of photon-nucleus interactions were given by Weise (1974) and Grammer and Sullivan (1978). At low energies the formation time will be short enough so that shadowing will be unimportant. This expectation is confirmed by specific model calculations which will be described later, in Sec. V.

In addition to the possibility of shadowing of the total photon cross section, there are other photon processes in nuclei which emphasize the hadronic structure of the photon. Examples are the diffractive photoproduction of states which are originally contained in the photon, and nondiffractive photoproduction of simple systems such as single pions. The idea of diffractive photoproduction was described in Sec. II.B and illustrated in Fig. 12. It is assumed that the only important constituent of the photon is a (nearly) stable ρ^0, which is completely absorbed in the target region leaving a "bare" photon. In this extreme example, it is this stripping away of the ρ^0 which renders the photon incapable of further interactions in the nucleus. When the state immediately behind the nucleon, or nucleus, is reconstituted in terms of a physical photon and physical ρ^0,[35] the distortion of the photon state from a plane wave leads to Compton scattering, and the presence of the real ρ^0 leads to diffractive photoproduction.

The great advantage of using nuclei for the photoproduction of ρ^0 was first appreciated by Ross and Stodolsky (1966a) and Drell and Trefil (1966). Those authors pointed out that, while it is impossible to construct a ρ^0 beam for conventional scattering experiments (a 10 GeV ρ^0 travels about 14F before decaying), a high-energy ρ^0 produced in the middle of a large nucleus has plenty of time to scatter or be absorbed on its way out; and through multiple scattering theory, study of the A dependence of nuclear photoproduction yields fundamental information, in particular the total ρ^0 cross section on a single nucleon. Incidentally, for this purpose it is not necessary that the production mechanism be diffractive; it need only be coherent (the nucleus remains in its ground state). In principle, this type of analysis could be applied to any type of coherent photoproduction, but the most comprehensive experiments and analysis have been carried out for ρ^0 production. The experiments will be described in Sec. III.C, and an analysis of the results will be presented in Sec. IV.C. Results for other vector-meson photoproduction will also be given in Secs. III.D, and III.E and analyzed in Sec. IV.D.

Nondiffractive, incoherent, photoproduction processes are harder to understand in terms of simple, VMD constituents—as discussed in Secs. II.B and C. In principle, each final channel may be sensitive to a different feature of the photon's hadronic structure. Each reaction may be regarded as a filter which "sees" some aspect of the structure. Experiments on nuclei may then be able to tell us whether the reaction selects a long-range or a short-range part of the photon's structure. This is in contrast to the VMD point of view which assumes that the components of importance are only the ρ^0, ω, and ϕ. We shall not attempt to review this complicated and controversial subject here,[36] but rather try to draw phenomenological conclusions from the experiments in Sec. V.

Before turning to a comparison of theory and experiment in the succeeding sections, we shall review very briefly the various assumptions underlying the theoretical analysis of high-energy processes in nuclei. The formalism itself is outlined in more detail in Appendix B. The basic approach to these processes was developed in a seminal paper by Glauber (1959), and such analyses are now a major industry.

The basic idea of the Glauber formalism is that the interaction of a high-energy particle with a nucleus can be built up from amplitudes on single nucleons. The incident projectile is assumed to interact with each nucleon in turn as it moves in a straight line (eikonal approximation) through the nucleus. The essential nuclear physics assumptions are:

(1) The nucleons do not move appreciably during collisions. This is certainly plausible, since, for a pro-

[35] A physical ρ^0 state takes the strong interaction into account exactly and also includes a bare photon component to order e.

[36] Recall the remarks of Sec. I.B.

jectile moving at the speed of light, the nuclear transit time is short compared to the evolution time scale of the nuclear wave function.

(2) Only the ground-state wave function is needed for the calculation. Although the nucleus is not restricted to remain in its ground state during the collision, the fact that the incident energy is large compared to the nuclear excitation energies enables one to use closure to sum over the intermediate excited states.

(3) The target nucleons do not overlap significantly so that the simultaneous collision of the projectile with two nucleons may be neglected. This assumption is hard to verify directly, but the theory's successes lend credence to it.

Less essential, but still necessary, assumptions involve the probability distribution of nucleons in the nucleus. The simplest such assumption is called the independent particle model (IPM) which neglects correlations between particles. The only improvement yet incorporated in the formalism is to include the effects of two-body correlations. These are as yet only imperfectly known, particularly in the nuclear surface; but fortunately for many purposes their effect is small.

The expressions calculated with the Glauber formalism depend on whether the process is coherent (nucleus remains in its ground state after the collision) or incoherent (state of nucleus changes). Ordinarily, experimental energy resolution is not sufficient to determine the nuclear final state. For coherent processes, this means that the data will have to be corrected for the additional events accepted ("incoherent background"). For incoherent processes one uses closure to evaluate the sum over nuclear final states.

Now let us try to visualize a high-energy process in a nucleus. The projectile, incident at some impact parameter **b**, hits the first nucleon. After the momentum and energy associated with the projectile have passed through the first target nucleon, we will find, in principle, a very complicated situation. One effect is that the initial channel will be partially depleted. This depletion (with a mean free path of 2 to 3F for incident hadrons) is responsible for both the total cross section for absorption of the projectile by the nucleus and elastic diffractive scattering. The probability removed from the incident channel reappears in various forms. Each time one of these new forms, or the remainder of the incident channel, strikes a new nucleon, it can be further transformed. Since different intermediate forms can interfere with each other at each state of development, this picture is too hopelessly general to be of any real practical interest. There is a natural tendency for high-energy physicists to contemplate this chaotic situation and conclude that no useful information can be drawn from experiments using nuclei. Experience has taught that this view is unduly pessimistic and that with reasonable further assumptions it is quite feasible to make many predictions which represent the actual physics. The more refined the prediction, however, the more likely that the complicated underlying nature of the process, along with unknown details of nuclear physics, will introduce significant uncertainties. In any given process, the various possible corrections should be estimated and the level of validity of the analysis evaluated.

For the types of reactions of interest to us, it is usual to assume that at most a few intermediate channels are of importance, and that these channels are simple in nature. In principle, for photon-initiated processes, one really needs to know how the entire hadronic superposition is modified as it passes through each nucleon. Gribov (1969) and Brodsky and Pumplin (1969) describe such an analysis for photon absorption in what would now be called a generalized vector-dominance treatment and, in line with our previous discussion, show that it leads to shadowing at high energies. The amount of shadowing obtained depends on the transition amplitudes from one hadronic component to another. This information is unavailable from simple two-body interactions, so for practical calculations it is necessary to make further assumptions or approximations.

For example, we might speculate that for diffractive interactions at high energies a hadronic system simply may not have time to make complicated internal transitions during its passage through the nucleus. (The time required for any internal transition is dilated by a factor proportional to the energy of the system.) Since the interaction is diffractive, i.e., no quantum numbers are exchanged with the nucleus, the net result may be that the projectile's internal "wave function" undergoes minimal changes inside the nucleus. If the incident particle is a hadron, we might think of the nucleus as providing a disturbance which results in particle production through projectile fragmentation.[37] If the incident particle is a photon, we might regard the nucleus as an analyzer of the photon's virtual hadronic component that channels the virtual constituents into various final states. The above picture may have to be drastically modified in the case of nondiffractive processes, which probably involve short-range photon interactions (see Secs. II.B and C).

Fortunately, we know that a large fraction of the real photon cross sections (~80%) can be attributed to its ρ^0, ω, and ϕ constituents—see estimates following Eq. (2.11). Thus the real photon cross section is dominated by rather well-known, low-mass constituents.[38] Most of our work will be concerned with the study of how these constituents participate in photon reactions in nuclei. In Sec. IV diffractive photoproduction on nuclei will be used to estimate the parameters associated with these chan-

---

[37] There is some experimental evidence for this point of view in the reaction $\pi A \to (n\pi)A$ (Bemporad *et al.*, 1971; Beusch, 1972). The absorption cross section for the final hadronic system in the nucleus is found to be much closer to σ_π than $n\sigma_\pi$, indicating that inside the nucleus the system is far from asymptotic and bears some resemblance to the projectile.

[38] It is interesting to speculate how well this picture holds up at *very* high energies (>100 GeV). As projectile energy increases it becomes kinematically possible to produce more and more states coherently from a nuclear target. Thus the Glauber picture could be complicated by the necessity of considering many more channels, and cross sections could be drastically altered from their values at lower energies (above and beyond small changes due to a nominal, slow variation of two-body cross sections with energy). In our view the resolution of this question must await future experiments.

nels. In Sec. V this information will be applied to other processes such as total absorption and incoherent particle production. Failure of this picture to predict the results of experiment, apart from problems with the optical models, will be taken as an indication of the presence of higher-mass constituents and/or short-range photon interactions. We refer to these loosely as "unshadowed contributions." The isolation and satisfactory treatment of these effects would require analyses of greatly increased complexity; such studies are still in their infancy—see Sec. VI.B.

III. EXPERIMENTAL RESULTS

In this chapter we review the major experimental work relating to the hadronic properties of the photon. In most cases, the phenomenological analyses and detailed theoretical implications of the data are discussed in other parts of the paper. In some cases material is included here for convenience and completeness even though it may not be essential to the remainder of the paper.

A. Total cross sections for real photons

As was emphasized in the previous chapter, measurements of the total hadronic photon cross sections on nucleons ($\sigma_{\gamma p}$ and $\sigma_{\gamma n}$) give one of the significant pieces of evidence for the hadronic structure of the photon. Aside from overall normalization (see Fig. 7), these cross sections are very similar to $\pi^+ p$ and $\pi^- p$ total cross sections, suggesting a similar underlying mechanism. The major part of the cross section can be attributed to the VMD mechanism (ρ^0, ω, ϕ contribution), but there is a need at the 15%–25% level for other contributions. A more subtle test of the hadronic structure picture, and the VMD model in particular, is provided by measurements of total photon-complex nuclei cross sections ($\sigma_{\gamma A}$), which are expected to show the effects of shadowing. In this section we shall first review the measurements for nucleons and then those for complex nuclei.

To measure total hadronic photoabsorption cross sections, it is necessary to determine the number of photons incident at a given energy and the fraction of these photons that interact hadronically in a target of known thickness and material. The fraction interacting can be determined either by observing the hadronic absorption and thus the absence of the photon or electromagnetic interaction products in the final state or by detecting the final-state hadrons. The successful counter experiments have used a combination of the two techniques to enhance the signal-to-noise ratio.

The measurement of the total cross section for photons is made difficult by the large cross sections for purely electromagnetic interactions such as electron–positron pair production. The ratio of the electromagnetic to hadronic interaction cross sections for the photon ranges from ~200 in hydrogen to ~2500 in lead. This large background makes it difficult to use the conventional attenuation method in which the total cross section is measured by observing the number of particles that disappear from the incident beam. It is necessary instead to use the observation of a produced hadron in coincidence with the disappearance of a photon from the beam. The successful experiments have combined the use of a tagged photon beam, a total absorption shower counter, and a geometrical method for separating hadronic and electromagnetic events.

To produce a tagged photon beam, one uses an incident monochromatic electron or positron beam in conjunction with a magnet and a set of scintillation counters. The apparatus determines the momentum of the electron or positron subsequent to its bremsstrahlung in a thin radiator, thereby giving electronically tagged photons of known energy. It is particularly important to have a clean incident beam with no halo and no low-energy contamination. It is also essential to use a thin radiator and to design the apparatus so as to minimize false tags due to trident production and multiple processes such as double bremsstrahlung in the photon radiator. A judicious arrangement of veto counters is generally used to reduce these backgrounds and to eliminate tagging signatures not accompanied by a photon.

The basis of the geometrical method is that the products of the pure electromagnetic interactions, such as pair production, are contained in an extremely small angular cone ($\theta \sim m_e/E$), while the products of hadronic interactions are more broadly distributed in angle. Thus by using hadronic counters with a hole in them one can eliminate most of the electromagnetic events. A total absorption shower counter is used to see if energy corresponding to that of the incident photon has disappeared from the beam. Since the shower detector has the same response to an electron–positron pair as the photon that produced the pair, it signals the hadronic disappearance of the photon. There is the additional advantage that for asymmetric electron-positron pair production in which one member of the pair is produced at a large angle and could be confused with a hadron, the forward member, which carries most of the energy, enters the shower counter.

Direct measurements of the total hadronic cross section $\sigma_{\gamma p}$ are now available from 0.275 GeV to 180 GeV and the cross section $\sigma_{\gamma d}$ from 0.275 GeV to 30 GeV. The data were obtained using a counter setup and a tagged photon beam [DESY-Hamburg (Meyer *et al.*, 1970); Santa Barbara–SLAC (Caldwell *et al.*, 1969, 1970, 1973; Hesse *et al.*, 1970); Glasgow-Sheffield–DNPL (Armstrong *et al.*, 1971; 1972a, b); Cornell (Michalowski *et al.*, 1977); Santa Barbara-Toronto-FNAL (Caldwell *et al.*, 1977)], an electron beam [Lebedev-Yerevan-Serpukhov (Belousov *et al.*, 1975)], bubble chamber experiments [Aachen–Berlin–Bonn–Hamburg–Heidelberg-Munchen Collaboration (ABBHHM) (Erbe *et al.*, 1968a, 1969)], and the combination of a bubble chamber and a monochromatic photon beam [SLAC–Berkeley (Ballam *et al.*, 1968); SLAC–Berkeley–Tufts (Ballam *et al.*, 1969a)]. The SLAC–MIT group (Bloom *et al.*, 1969b) has also determined the total cross section $\sigma_{\gamma p}$ by extrapolation to $Q^2 = 0$ of measurements of inelastic electron scattering; within the ±8% estimated systematic errors, the results are consistent with the direct measurements over the full range in which the data overlap, 0.265 GeV $< E_\gamma <$ 15 GeV. The total cross sections determined by the extrapolation to $Q^2 = 0$ of inelastic muon proton scattering data (Perl *et al.*, 1969) are also consistent with the re-

sults of the direct measurements. An extrapolation at very small Q^2 (<0.1 GeV^2) at 2 GeV has been carried out by Eickmeyer *et al.* (1976a) and gives agreement at the 10% level. In this review we shall concentrate on the more precise real photon counter experiments and merely cite the others as giving confirmation.

1. Description of experiments

Figure 21 shows a diagram of the apparatus used by the Santa Barbara–SLAC group (Caldwell *et al.*, 1973); Figure 22 shows a diagram of the apparatus used by the Glasgow–Sheffield–DNPL group (Armstrong *et al.*, 1972a, b); Figure 23 shows a diagram of the apparatus used by the DESY–Hamburg group (Meyer *et al.*, 1970). All three experiments used a tagged photon beam to count the number of photons within a fixed energy band, a carefully calibrated total absorption shower counter to determine whether or not the electromagnetic energy of the photon or its equivalent disappeared from the beam, and a hadron detector with a hole in it to suppress the detection of electromagnetic events. Two basic elements in the design of the experiments are the use of geometry to separate hadronic and electromagnetic processes and the fact that a shower counter has the same response to an electron-positron pair as to the photon that produced the pair. A judicious arrangement of veto counters is used to reject beam halo, low-energy beam contamination, and anomalous events (e.g., trident production) such as those produced by higher-order electromagnetic processes in the photon producing radiation. The basic signature of a hadronic event is a tagged photon, a small pulse in the downstream shower counter, and a detected hadron. It is crucial to have a good understanding of the tagging system and the total absorption shower counter.

For the Santa Barbara–SLAC group the tagged portion of the bremsstrahlung beam, which was produced by positrons of energy E_0, included four energy bins between $0.74E_0$ and $0.94E_0$. Wide-angle photons produced in the bremsstrahlung radiator were eliminated by the shower counter A0 located in front of the target. Those photons which did not interact in the target passed through central holes in the hadron detectors S2a and S2b and produced a large pulse in the total absorption counter S1. The major background, e^+e^- pair production, had the

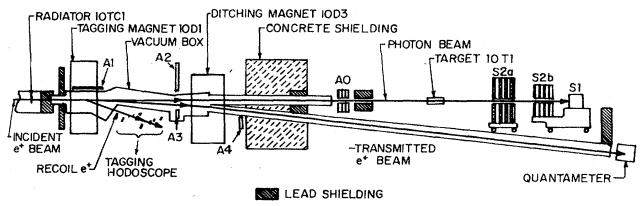

FIG. 21. Side view of the photon beam and experimental apparatus used by the Santa Barbara–SLAC group. Counters A1 through A4 are scintillation counters used to veto anomalous events; A0 is a shower counter used in anticoincidence to reject wide-angle bremsstrahlung events; S1 is the shower counter used to determine whether the equivalent gamma-ray energy is removed from the incident beam; S2a and S2b are the counters used to detect the produced hadrons (from Caldwell *et al.*, 1973).

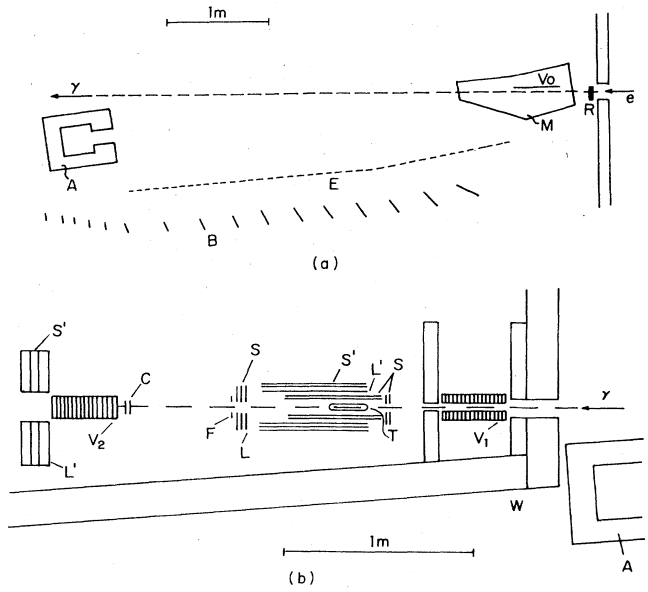

FIG. 22. Apparatus used by the Glasgow-Sheffield–DNPL group. (a) Illustration of tagging system. A weak electron beam strikes a radiator R. Tagging of γ rays is produced by the 64 electron counters E, associated in groups of four, with the backing counters B. (b) Schematic diagram of the detection system. The γ rays pass through the hole in the collimator veto counter V_1, to interact in the liquid-hydrogen cell T, 200-mm long and 44-mm in diameter. Hadronic events are detected in the surrounding box of paired scintillators S, and π^0 counters S′. L and L′ denote lead converters. Forward-going electromagnetic events are vetoed by the shower counter V_2, and electron counters C. A coincidence between a hadron counter and a tagging counter constitutes an event, and the channel number of the tagging counter is recorded on tape (from Armstrong *et al.*, 1972a).

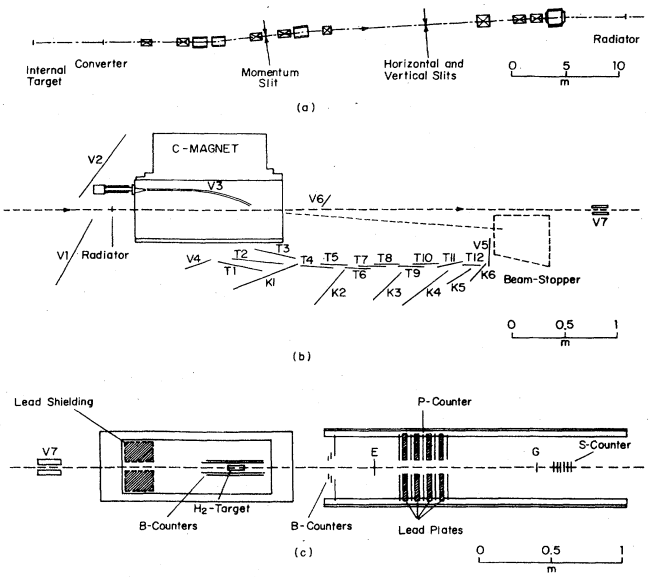

FIG. 23. Apparatus used by DESY–Hamburg group. (a) The beam transport system used to obtain the positron beam. (b) The tagging system (T1–T12, K1–K6) and the veto counters (V1–V7). (c) The target and detection system (from Meyer *et al.*, 1970).

same signature as a transmitted photon, since pairs had a sufficiently small angle to pass through the holes in S2a and S2b. Hadronic interactions were identified by a signal from one of the tagging channels in coincidence with a signal from the hadron detector S2, and no large coincidence pulse in S1. The S2 counters, each a four-layer sandwich of 2.5 cm lead followed by scintillator, were required to give either a four-pulse coincidence in S2a or S2b or a summed pulse height from the two counters equivalent to three minimum-ionizing particles passing through four scintillation planes, corresponding roughly to a 1 GeV electromagnetic shower. These criteria ensured a high efficiency for the detection of both charged and neutral pions, while greatly reducing the accidental coincidences caused by the background electromagnetic events. The positions of S2a and S2b were varied so as to study the electromagnetic contamination and the events missed due to wide-angle hadrons.

One of the chief difficulties faced by the Santa Barbara–SLAC group was due to the poor duty cycle of the Stanford Linear Accelerator. The electronic logic was arranged so that a tagged photon was specified by one and only one twofold coincidence in the accelerator gate and with no simultaneous signal from any of the anticounters A0 through A4. Circuits with different resolving time were used to monitor the major accidental rate—that between $T\overline{AS1}$ and S2. The accidental rate ranged from a few percent for hydrogen and deuterium targets to as high as 25% for a lead target.

The correction for geometric losses, because the solid angle subtended by S2 was less than 4π, was determined by a Monte Carlo calculation and found to be $\leq 2\%$ for the worst case. The correction due to the inefficiency in the S2 counters below 2 GeV varied from $(1.3 \pm 0.5\%)$ to $(0.5 \pm 0.5\%)$ in going from the lowest to the highest incident positron energies. The correction for contamination due to electron-positron pairs was in the worst case (Pb at 4 GeV) 10%. The total cross sections for the Santa Barbara–SLAC group cover the energy range from 3.7 to 18.3 GeV. They used essentially the same apparatus for the measurements on H, D, C, Cu, and Pb.

The Glasgow–Sheffield–DNPL group (Armstrong *et al.*, 1972a, b) used a tagging system (Brookes *et al.*, 1970) with much higher resolution so that they could make a detailed study of the total cross section in the resonance region. They used 64 tagging channels with a nominal non-overlapping width of ±12.5 MeV and an actual overlapping width of ±17.5 MeV. In addition to the analogs of the counters used by the Santa Barbara–SLAC group, they surrounded the target with a rectangular box of scintillation counters and with additional π^0 counters. They found these counters necessary for low-energy measurements. Auxiliary angular counters were used to estimate the small loss of hadronic events in the forward cone by extrapolating the observations to zero angle. The correction for losses in the forward direction ranged from 0 at the nominal 275 MeV point to +8% at the nominal 4.225 GeV point. The other corrections such as double bremsstrahlung losses and the corrections for randoms were much smaller and less than a few percent. The systematic error in the absolute cross sections for hydrogen and deuterium was estimated to be ±3%. The Glasgow–Sheffield–DNPL group used essentially the same apparatus for the measurements with deuterium and hydrogen targets. These data cover the range in photon energy from 0.265 GeV to 4.215 GeV.

A Sheffield–Glasgow–DNPL group (Brookes *et al.*, 1973) used a slightly different apparatus to measure the total hadronic photoabsorption cross sections for C, Al, Cu, Nb, Sn, Ta, and Pb over the energy range 1.7–4 GeV. The liquid hydrogen target used earlier was replaced by solid targets in the form of circular disks which were individually mounted on slides and moveable into and out of the photon beam by remote control. They used the space made available through removal of the liquid target and its refrigerator to improve the efficiency for detecting backward-going π^0's. The beam intensity was adjusted so that the random coincidence and veto rates were always kept at a level below 10% of the rate of real events. The data were corrected for hadronic events emitted in the forward cone of the vetoing shower counter (4% to 6%), double bremsstrahlung in the radiator (−2% to −4% for Pb), production of an x ray and an undetected electron followed by pair production with detection of the electron (−2% to −3%), pair production detected as hadronic events (for Pb ≃ 3%), and low-energy contamination in the beam (−2% to −3% for lead). The net overall mean systematic corrections ranged from 8% in C to −4% in Pb.

The experimental method employed by the DESY–Hamburg group (Meyer *et al.*, 1970) was very similar to that used by the Santa Barbara and Glasgow–Sheffield–DNPL groups. They used a tagged photon beam with 12 energy-defining counters each arranged to have $\frac{1}{3}$ overlap with both neighboring counters. The total energy range covered by the tagging counters was 2.0 GeV and the energy resolution, which was limited to ±50 MeV by the finite width of the counters, was independent of positron energy. Tagged photons were defined by a twofold coincidence between the smaller energy-defining counters and the corresponding back counters. The photon flux was measured by requiring a coincidence with a shower counter located at the end of the experiment. A number of veto counters V1 through V7 rejected background outside the beam (V1, V2), multiple processes in the radiator (V3–V6), and a halo of photons around the beam just in front of the target (V7). In addition to being vetoed in V7, the particles in the halo were stopped in a lead shield between V7 and the liquid target. The shield also prevented backward particles, from hadronic reactions in the target, from being vetoed by V7. Due to all these veto counters more than 95% of the tagged photon signals were accompanied by a high-energy photon.

A set of scintillation counters was used to detect charged particles from the target. Most hadronic reactions were seen by the A counters, which consisted of half cylinders surrounding the target. The B counters covered the forward angular range from 2° to 10° and were arranged as overlapping rings so as to give the angular distribution of the forward produced particles. A lead scintillator sandwich counter P identified electromagnetic particles. Counters G and E were used to monitor electron pairs from the target. To suppress purely electromagnetic reactions, the S counter, covering the small forward cone ($\simeq 1°$), was operated in anticoincidence with the hadronic counters A and B.

The accidental coincidences were measured in three different ways: (1) by recording delayed hadronic triggers, (2) by forming the hadronic trigger with three different resolving times of 22, 25, and 32 nsec, respectively, and (3) by recording the time overlap spectrum of the trigger pulse. The cross sections obtained by using each of the three methods were in good agreement with each other. An extrapolation procedure was used to correct for the forward hadronic events which were missed; the uncertainty in this procedure was estimated to be 2%. The correction due to double bremsstrahlung varied between 1.5 and 5.5% between 3 and 7 GeV with an estimated uncertainty of ±1%.

The DESY–Hamburg group (Heynen *et al.*, 1971) used essentially the same apparatus to measure the total cross sections for Be, C, Al, Ti, Cu, Ag, and Au at 5.4 GeV and to measure the energy dependence of $\sigma_{\gamma A}$ for Be, C, and Ti between 1.5 and 5.7 GeV. In addition to the corrections mentioned earlier, this experiment required a correction for the absorption of photons in front of and in the reaction target (~4%), and a correction for the finite veto efficiency of the shower counter S, which was given mainly by the conversion and detection probability for photons. This correction varied from 6% for Be to 25% for Au.

A Lebedev–Yerevan–Serpukhov group (Belousov *et al.*, 1975) used an electron beam produced from the 76 GeV Serpukhov proton accelerator to measure the total cross sections for hadronic photoabsorption by protons at energies from 12 to 38.8 GeV and by deuterons from 12 to 30 GeV. The apparatus, which is illustrated in Fig. 24, consisted of a 50 cm H_2 target which acted as the electron radiator and the photon absorber. The difference in the angular distributions of the electromagnetic and hadronic processes was used to separate the two processes. For energies above 10 GeV the secondary particles of the electromagnetic interactions remain essentially within the electron beam, while the hadrons are emitted at substantially greater angles.

The hadronic detectors each consisted of four scintillation counters with a circular aperture with a diameter of 10 cm. Between the counters were 3-cm thick lead plates with the same central opening. In addition there were two such plates in front of each detector. The large lead thickness was necessary to suppress the detection of low-energy electrons and photons emitted at large angles to the beam. The counters S_1 and S_2 were used to monitor the electron beam. A total absorption Cerenkov counter was used to measure the energy of the

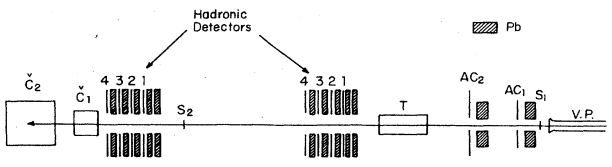

FIG. 24. Experimental arrangement used by Lebedev-Yerevan-Serpukhov group. S_1 and S_2, monitor counters; beam shapers consisting of collimators and guard counters AC_1 and AC_2; T target; hadron detectors consisting of counters 1–4; compound Cerenkov total-absorption spectrometer which includes counters $\check{C}_1$ and $\check{C}_2$ (from Belousov *et al.*, 1975).

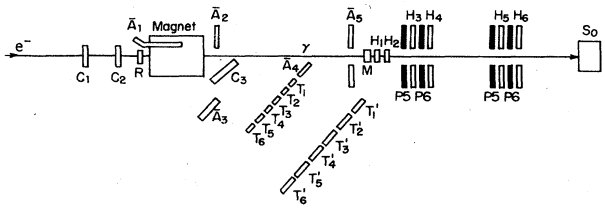

FIG. 25. Apparatus used by the Yerevan–Lebedev–IHEP group for their measurements of the total photoabsorption cross section for carbon (from Bayatyan *et al.*, 1975).

electrons which accompanied hadronic events and thus to determine the energy of the photon. The hadronic counters were empirically located in a position where their efficiency was 100%. The data were corrected for hadron electroproduction (6 to 16%), shape of the bremsstrahlung spectrum (0 to 8%), removal of photons through pair production (6.5%), counting losses due to analyzer dead time (<10%), other material in the beam, and in one case anomalous background contribution from electromagnetic processes.

A Lebedev–Yerevan–IHEP group (Bayatyan *et al.*, 1975) has used a more conventional tagged photon apparatus to measure the hadronic photoabsorption in carbon in the energy range 14–34 GeV. Figure 25 shows a diagram of their apparatus. A 40 GeV electron beam with momentum spread $\Delta p/p \simeq \pm 3\%$ was monitored by Counters C_1 and C_2 and struck a lead radiator of about 0.08 radiation lengths. The tagging hodoscope consisted of two arrays of counters coincident in pairs. Anticounters A_1-A_4 were used to prevent the spurious tags from low-energy positrons produced in the radiator. The coincidences between the tagging system and the shower counter S_0 gave the number of noninteracting photons.

The hadronic photoabsorption events were detected in the lead scintillator sandwich counters. A hadronic photoabsorption event was indicated by the coincidence of $(H_1H_2H_3H_4)$ or $(H_1H_2H_5H_6)$ with the tagged signal and no S_0 pulse. Photoabsorption events with only neutral hadrons were not detected with this setup. It is known that such events make up less than 2% of the total hadronic photoabsorption cross section at 2–4 GeV. The data were corrected for the absorption of the photon beam due to e^+e^- production, attenuation of the incident photon beam due to the inconsistency of its cross section with target area (5%), random coincidences (<1%), empty target (5 to 14%) multiple bremsstrahlung processes (10 to 15%), electromagnetic background (2%), geometric loss of ρ^0 events (0.5 to 1.5%), and hadron counter efficiency (8%).

A Cornell group (Michalowski *et al.*, 1977) has used a tagged photon beam in the energy range 1.0–10.5 GeV to measure the total hadronic cross section for hydrogen, deuterium, and complex nuclei. Incident electrons from the Cornell 12 GeV synchrotron struck a 0.002 radiation length thick tantalum target, and photons were tagged by deflecting the corresponding energy-degraded electrons in a magnet and detecting them with sixteen tagging scintillation counters. This system detected electrons in the energy band $1.08 \leq E_e \leq 4.40$ GeV.

Figure 26 shows a schematic view of the hadron detector and downstream veto counters used by the Cornell

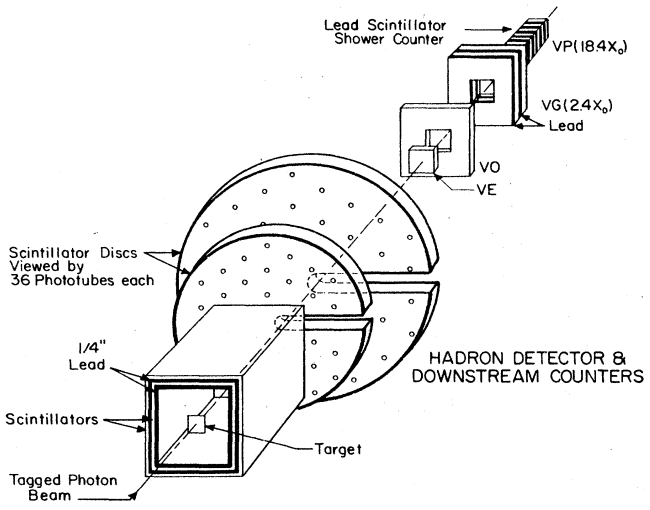

FIG. 26. Schematic view of the hadron detector and downstream veto counters used by the Cornell group. Angles less than 30 mrad were covered by an array of four counters directly in the beam, approximately 4m downstream of the target. These counters are VE, a thin scintillator ($0 < \theta < 12$ mrad), VO, a thin scintillator (12 mrad $< \theta <$ 30 mrad), VG, a scintillator with lead converter in front of it (12 mrad $< \theta <$ 30 mrad), and VP, an 18-radiation length counter ($0 < \theta < 12$ mrad) (from Michalowski *et al.*, 1977).

Group. The target was surrounded by scintillation counters and at large angles ($\gtrsim$ 350 mrad from the beam) particles were detected in scintillation counters forming a box around the target. At forward angles (30 mrad $< \theta <$ 450 mrad) the detector consisted of two large discs of scintillator each viewed by 36 phototubes. At all angles greater than 30 mrad the counters were preceded by two radiation lengths of lead to ensure good π^0 detection. Angles less than 30 mrad were covered by an array of four counters directly in the beam, approximately 4 m downstream of the target. There were in particular two thin scintillators (VE and V0), a scintillator preceded by a lead converter (VG), and an 18 radiation length shower counter.

The event trigger was a coincidence between a tagged photon and a "hadron" signaled by a count in the hadron counters surrounding the target. At all energies the trigger rate was dominated by electron–positron pairs where a low-energy electron or positron was scattered to an angle greater than 30 mrad. These were rejected by the pulses in VE and VP. For hydrogen the rejection of events with forward-going particles introduced a hadronic inefficiency of 8% at $E_\gamma = 10$ GeV and 2% at $E_\gamma = 2$ GeV. For high-Z elements occasionally both members of the electron pairs emerged at large angles and gave two "hadron" tracks with no counts in the downstream veto counters. Angular information from the two scintillator discs was used to reject all pairlike (observed multiplicity at one or two) events which were totally confined to a forward cone with angle chosen such that a Monte Carlo estimate of the residual e^+-e^- contamination was less than 2% of the observed hadronic cross section. This procedure has the disadvantage that it results in a significant inefficiency for detecting high-energy ρ^0 photoproduction and, since a large fraction of the rho cross section is coherent, could introduce an incorrect A dependence. Calculations using the published rho cross sections were used to determine this correction. The correction to the total cross section was as high as 12%; however, the correction to the shadowing factor was never more than 3%. For hydrogen the rho's were counted and the correction experimentally verified.

Data were obtained with 0.02 radiation length hydrogen and deuterium targets and with roughly 0.08 radiation length carbon, aluminum, copper, silver, gold, and uranium targets, at photon energies of 2.00, 3.27, 4.81, 6.21, 7.79, and 9.51 GeV, respectively. The worst case empty target rates were hydrogen (10%), carbon (2%), and gold (22%). The reported errors are statistical and do not include a further systematic uncertainty of 4%. As a check, the total electron–positron pair production cross section was extracted from the data. Over the range 1–10 GeV, and for all targets, the cross section agreed within 10% with the theoretical cross sections.

A Santa Barbara–Toronto–FNAL group (Caldwell *et al.*, 1978) has used a tagged photon beam at FNAL to measure the photon-proton total cross section from 30 to 180 GeV. Figure 27 shows a schematic drawing of the FNAL tagged photon beam. Protons struck a Be target and the neutral particles produced at 0° were separated by a sweeping magnet from charged particles. Photons from the primary neutral beam were converted to electrons and transported to the tagging system. Collimation in the beam transport system defined the energy to ±2.5% and reduced the pion contamination to typically 0.5%. The tagging system consisted of three magnets and a bank of hodoscopes and shower counters which measured the energy of electrons which radiated photons. Photons could be tagged in the energy range $0.45E_0 < E_\gamma < 0.93E_0$. The major sources of false tags were tridents and tridentlike events due to double conversion in the radiator. This source of false tags was largely eliminated by judiciously placed veto counters which detected the positrons. The veto counters, cuts, and requirements on signals in the tagging hodoscope kept the false tag rate below 0.05%.

Figure 28 shows a diagram of the hadron detector used by the Santa Barbara–Toronto–FNAL group. There were three hadron detectors which provided overlapping coverage in the forward center-of-mass hemisphere. Each of the hadron detectors had excellent efficiency for π^0, p, and $\pi^\pm$. Neutrons and K_L^0 were detected with an

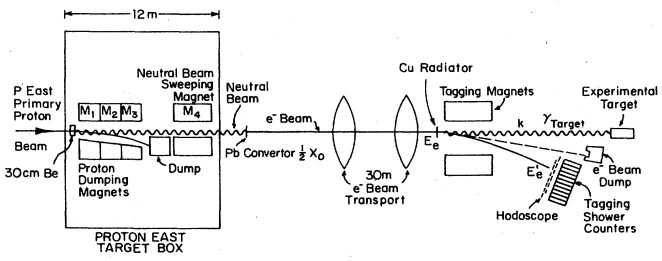

FIG. 27. Schematic diagram of the tagged photon beam used at the Fermi National Accelerator Laboratory by the Santa Barbara–Toronto–FNAL group (from Caldwell *et al.*, 1978).

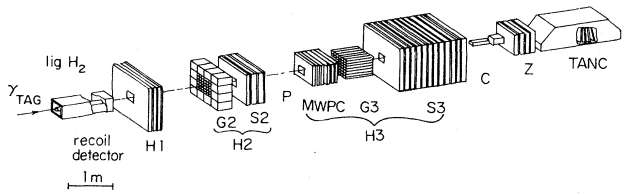

FIG. 28. A schematic diagram of the hadron detectors used by the Santa Barbara–Toronto–FNAL group at the Fermi National Accelerator Laboratory. H_1, 1.5 absorption length, 3-plane iron scintillator sandwich counter; H_2, 3 absorption length assembly consisting of 44 blocks of 30 cm Pb glass (G2) and a lead, scintillator, iron, scintillator, iron, scintillator sandwich counter (S2); H_3, 8 absorption length assembly consisting of a scintillation counter (P), a 6-plane multiwire proportional chamber (MWPC), a 7×7 lead-glass assembly (G3) with inner ring I, and 12 iron scintillator counter planes (S3); a 3.5 absorption length central hadron calorimeter (TANC) (from Caldwell *et al.*, 1978).

efficiency approaching 90% in the lead-steel scintillator S_2 and with nearly 100% efficiency in S_3. Most pairs were detected in the central counter, C, which covered ±3 mrad in the 90 GeV setting. Low-energy $e^{\pm}$ scattering outside of C and other rare electromagnetic channels were identified with the MWPC and G_3. The central hadrometer (Z + TANC) was used to spot events in which a γ (or $e^{\pm}$) interacted hadronically in C, as well as to detect hadrons which came through the central hole. The hadronic trigger consisted of a tag in coincidence with H_1 or H_2 or H_3 or $\bar{C}$. (I or P TANC). A simple calculation was used to subtract out double bremsstrahlung events.

Data were collected for electron beam energies of 40, 60, 90, 135, and 200 GeV with the detectors' positions approximately scaled for each energy. As a check on the double bremsstrahlung correction and other radiator-dependent effects, data were taken with several tagging radiator thicknesses. The systematic errors are estimated to be 0.8% with only half of the error applicable to effects that might vary with electron beam energy.

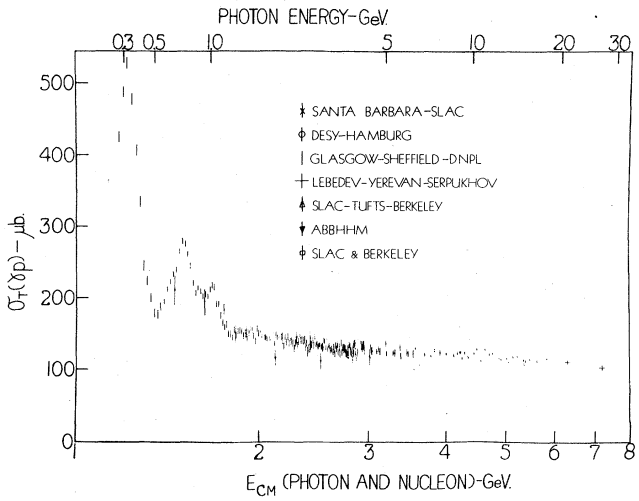

FIG. 29. A plot of the measured total photoabsorption cross section $\sigma_{\gamma p}$ versus energy for a hydrogen target. This figure was provided by G. N. Lewis (Glasgow).

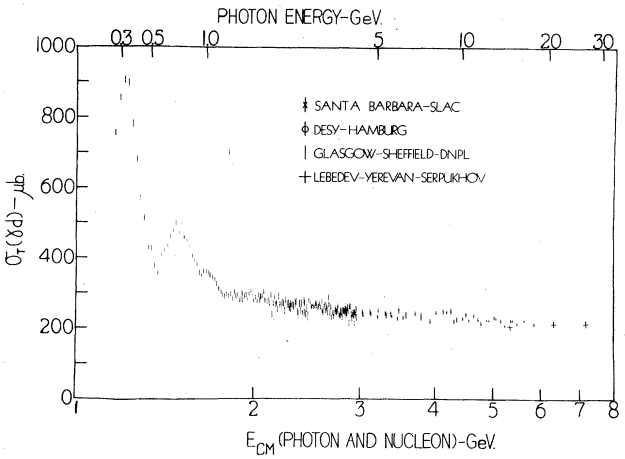

FIG. 30. A plot of the measured total photoabsorption cross section $\sigma_{\gamma d}$ versus energy for a deuterium target. This figure was provided by G. N. Lewis (Glasgow).

2. Results for $\sigma_{\gamma p}$ and $\sigma_{\gamma n}$

Figure 29 shows a plot of $\sigma_{\gamma p}$ versus energy of data for photon energies less than 30 GeV; Fig. 30 shows the corresponding plot for $\sigma_{\gamma d}$. These figures demonstrate the extent to which the data from the different groups agree. The agreement between the tagged photon counter experiments is quite satisfactory. The early measurements of the ABBHHM collaboration were made by summing the observed reactions, and one would expect them to be the least reliable.

Figure 31 shows the high-energy data from the Santa Barbara–Toronto–FNAL experiments. The cross section rises at high energy in the same manner as has been found for pion-proton total cross sections.

In order to extract the neutron cross sections from measurements with a deuterium target, it is necessary

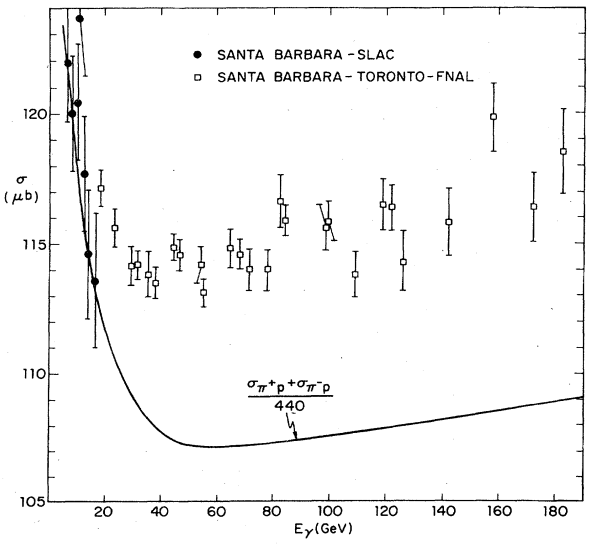

FIG. 31. Photon–proton total cross section as a function of energy determined by the Santa Barbara–Toronto–FNAL group in their FNAL experiment. The curve is a plot of $(\sigma_{\pi^+p}+\sigma_{\pi^-p})/440$, shown also in Fig. 7 (after Caldwell *et al.*, 1977).

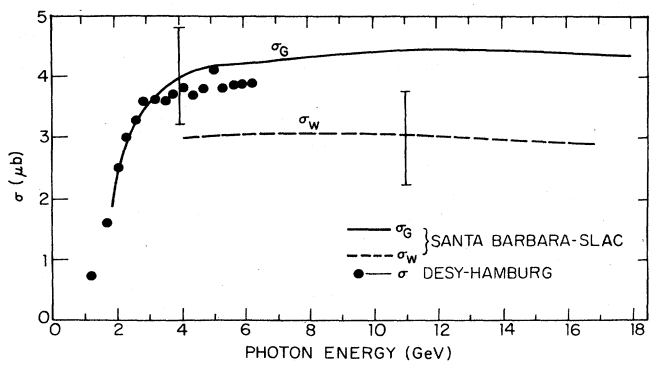

FIG. 32. The Glauber and West corrections for the deuteron used by the Santa Barbara–SLAC group. The dots show the calculation by the DESY–Hamburg group of the Glauber correction. Except where noted, we have corrected all deuteron data using these curves (from Caldwell *et al.*, 1973).

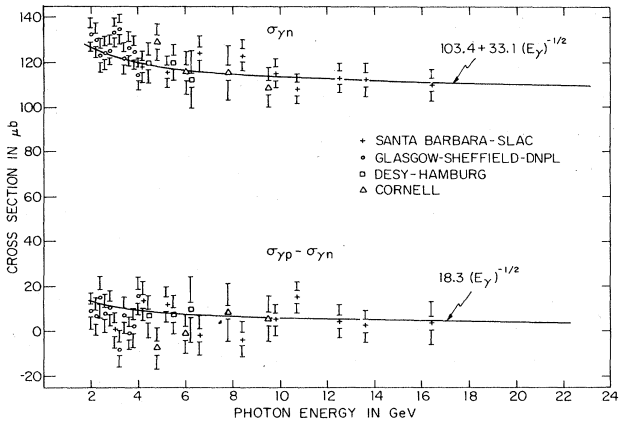

FIG. 33. A plot of $\sigma_{\gamma n}$, the total neutron cross section, versus energy, and of the proton-neutron difference. The inner error bars show an estimate of systematic uncertainties due to the deuteron corrections.

to apply certain theoretical corrections to the simple first approximation

$$\sigma_{\gamma d} \simeq \sigma_{\gamma p} + \sigma_{\gamma n} . \tag{3.1}$$

These corrections modify the value of $\sigma_{\gamma n}$ obtained from (3.1) by less than 10%; they are sufficiently uncertain, however, that they make it difficult to assess the error in the neutron-proton difference.

The first correction is the Glauber shadowing correction (Franco and Glauber, 1966). This correction is for the shadowing of one nucleon by the other. Since the phenomenon of shadowing for photons in nuclei is not well understood, this correction is somewhat uncertain. It is conventional to follow Brodsky and Pumplin (1969) and to assume that the shadowing is given by a calculation based on vector-meson dominance. Figure 32 shows the Glauber correction used by the Santa Barbara–SLAC group (Caldwell *et al.*, 1973) and the DESY–Hamburg group (Meyer *et al.*, 1970). This correction is small at low energy and then becomes a constant at high energy. A second correction is applied to account for "Fermi motion" in the deuteron (West, 1971)—see Appendix B.

The neutron cross section is then given by the equation

$$\sigma_{\gamma n} = \sigma_{\gamma d}/(1-\beta) - \sigma_{\gamma p} + \sigma_G , \tag{3.2}$$

where σ_G is the Glauber correction, and the $(1-\beta)^{-1}$ is the West correction for the Fermi motion of the nucleons. For the West correction, Dominguez, Gunion, and Suaya (1972) obtained $\beta = (1.3 \pm 0.3)\times 10^{-2}$. This agrees with the result of Atwood and West (1973) and the uncertainty covers the range of potentials from the Reid soft core to the Lomon–Feshbach potential. With the West correction defined as

$$\sigma_W = \sigma_{\gamma d}/(1-\beta) - \sigma_{\gamma d} \simeq \beta \sigma_{\gamma d} \tag{3.3}$$

the neutron cross section is given by

$$\sigma_{\gamma n} = \sigma_{\gamma d} - \sigma_{\gamma p} + \sigma_G + \sigma_W . \tag{3.4}$$

Frankfurt and Strikman (1976) argue that the West correction is incorrect and actually vanishes. In any case, there is sufficient uncertainty in the whole procedure that it is difficult to assess the real uncertainty in the neutron cross section and consequently in the neutron-proton difference. In this paper we have, unless stated otherwise, used the Glauber and West corrections shown in Fig. 32.

Figure 33 shows a plot of the neutron cross section versus energy calculated using (3.4), together with the proton-neutron difference. The inner error bars indicate the systematic uncertainty due to the deuteron corrections.

Figure 34 shows the details of the neutron cross section in the low-energy region determined by the measurements of the Glasgow–Sheffield–DNPL group (Armstrong *et al.*, 1972b).

●The similarity (see Fig. 7) in the shapes of the total hadronic photoabsorption cross sections and the total hadron-hadron cross sections suggests, in the region below 30 GeV before the cross section begins to rise with energy, a parametrization of the photon cross section as the sum of Regge-pole exchanges in the t channel. In the high-energy limit this corresponds to

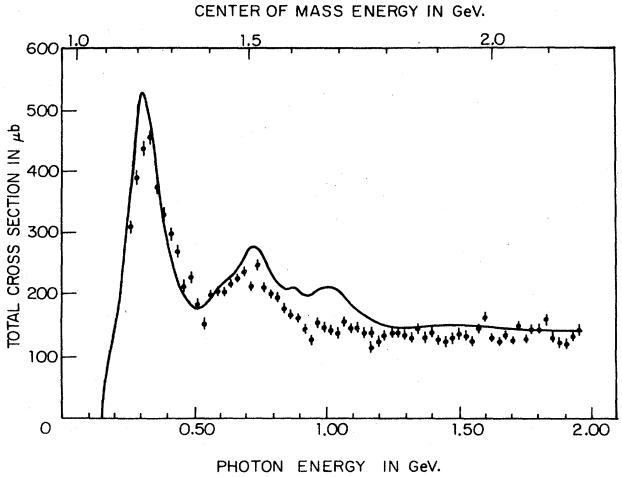

FIG. 34. A plot showing the detail of $\sigma_{\gamma n}$ in the low-energy resonance region (no West correction made in this plot). The solid line is the fit to $\sigma_{\gamma p}$ (from Armstrong *et al.*, 1972b).

$$\sigma_{\gamma p}(\nu) = \sum_i c_i \nu^{\alpha_i(0)-1}, \tag{3.5}$$

where the c_i are constants and the $\alpha_i(0)$ are the $t=0$ intercepts of the Regge trajectories, $\alpha_i(t)$, which are exchanged in the t channel. Such parametrizations give very good fits to the energy dependence of purely hadronic total cross sections (e.g., $\pi^{\pm}p$, $K^{\pm}p$, etc.). There it is found that the leading isospin 0 or 1 trajectories [those with $\alpha_i(0)>0$] are the Pomeron (corresponding to diffraction scattering and constant total cross section), which has $\alpha_p(0)=1$, and the P', A_2, ρ, and ω trajectories, all of which have $\alpha(0)\simeq 0.5$ as determined either from drawing the usual linear Regge trajectories (with slope $\simeq 1$ GeV^2) through the observed physical particle positions or from fits to the hadron-hadron total cross sections at high energies. For Compton scattering only t-channel trajectories with $C=+1$ contribute, so we can restrict our attention to only the P' and A_2 trajectories in addition to the Pomeron. We take $\alpha_p(0)=1$ and the effective intercept at $t=0$ of the P' and A_2 to be $\frac{1}{2}$. The total γP and γn cross sections may then be expressed in the form

$$\begin{aligned}\sigma_{\gamma p} &= c_p + (c_{p'} + c_{A_2})\nu^{-1/2} = a^p + b^p \nu^{-1/2} \\ \sigma_{\gamma n} &= c_p + (c_{p'} - c_{A_2})\nu^{-1/2} = a^n + b^n \nu^{-1/2}.\end{aligned} \tag{3.6}$$

In terms of the vector-meson-dominance model, A_2 exchange corresponds to diagrams in which the ρ^0 changes into an ω or ϕ or vice versa. Table II summarizes the Regge fits determined from the data from 4 to 18 GeV of the Santa Barbara–SLAC group (Caldwell *et al.*, 1973). Table III summarizes the Regge fits determined by the Russian group (Belousov *et al.*, 1975) using the data from 2 to 4.215 GeV of the Glasgow–Sheffield–DNPL group, the data from 2 to 6 GeV of the DESY–Hamburg group, the data from 4 to 18 GeV of the Santa Barbara–SLAC group, and the data from 12 to 30 GeV of the Lebedev–Yerevan–Serpukhov group. The data are consistent with a neutron–proton difference that goes to zero as the energy increases. The errors in the fits are statistical and only partially represent the real uncertainty. This is especially true for the neutron-proton difference. The data are not sufficiently precise to exclude expressions such as

$$\sigma_{\gamma p} = a + b\nu^{-1} \tag{3.7}$$

as suggested by suri and Yennie (1972), or

TABLE II. Regge fits using only the Santa Barbara–SLAC data to the form $\sigma = a + b\nu^{-1/2}$, where ν is the photon energy in GeV. Also given are the corresponding contributions for the Pomeron (c_p) and the energy-dependent isoscalar ($c_{p'}$) and isovector (c_{A_2}) contributions obtained from both the proton and neutron data (from Caldwell *et al.*, 1973).

$a^p = 98.7 \pm 3.6\mu$b	$\sigma_{\gamma p} = (98.7 + 65.0\nu^{-1/2})\mu$b
$b^p = 65.0 \pm 10.1\mu$b	
$a^n = 103.4 \pm 6.7\mu$b	$\sigma_{\gamma n} = (103.4 + 33.1\nu^{-1/2})\mu$b
$b^n = 33.1 \pm 19.4\mu$b	
$c_p = 101.9 \pm 2.9\mu$b	$\sigma_{\gamma p} - \sigma_{\gamma n} = (18.3 \pm 6.1)\nu^{-1/2}\mu$b
$c_{p'} = 50.9 \pm 8.5\mu$b	
$c_{A_2} = 9.1 \pm 3.0\mu$b	$c_{A_2}/c_{p'} = 0.18 \pm 0.06$

TABLE III. Regge fits to the neutron and proton photoabsorption cross section using all the available data from 2–38 GeV (from Belousov *et al.*, 1975).

Cross section	a (μb)	b (μb/GeV$^{-1/2}$)	χ^2	Number of points
$\sigma_{\gamma p}$	99.8 ± 1.6	57.0 ± 3.0	56	45
$\sigma_{\gamma n}$	98.5 ± 3.2	45.2 ± 6.3	38	41
$\sigma_{\gamma p} - \sigma_{\gamma n}$	•••	14.5 ± 1.9	50	41
$\sigma_{\gamma p} + \sigma_{\gamma n}$	198.2 ± 3.6	103.6 ± 7.1	29	41

$$\sigma_{\gamma p} = a + b\nu^{-1/2} + c\nu^{-3/2} \tag{3.8}$$

as suggested by Shibasaki *et al.*(1971).

3. Results for complex nuclei

Measurements on complex nuclei give direct evidence as to whether the hadronic structure of the photon gives rise to shadowing similar to that observed in hadronic reactions. The effect of shadowing is most easily seen for different nuclei in terms of the effective nucleon number, defined as

$$\frac{A_{\text{eff}}}{A} = \frac{\sigma_{\gamma A}}{Z\sigma_{\gamma p} + (A-Z)\sigma_{\gamma n}}. \tag{3.9a}$$

The Santa Barbara–SLAC group used this expression to report their measurements on C, Cu, and Pb targets. They first applied the West correction $1/(1-\beta)$ with $\beta = 0.013$ to $\sigma_{\gamma A}$ and assumed that the error was equal to the whole West correction. The West corrections for nuclei heavier than deuterium have been removed for the figures shown in this section. The Sheffield–Glasgow–DNPL group expressed their results for C, Al, Cu, Nb, Sn, Ta, and Pb in terms of (3.9a) but did not make the West correction. The DESY–Hamburg group expressed their results for Be, C, Al, Ti, Cu, Ag, and Au in terms of the expression

$$\frac{A_{\text{eff}}}{A} = \frac{\sigma_{\gamma A}}{A\bar{\sigma}_{\gamma N}}, \tag{3.9b}$$

where $\bar{\sigma}_{\gamma N}$ is the mean value for the cross sections on neutrons and protons. They did not make a West correction on $\sigma_{\gamma d}$. Since the difference induced by this procedure is less than the quoted systematic error, we have not corrected the DESY–Hamburg data to the form used by the other two groups. The Yerevan–Lebedev–IHEP group used Eq. (3.9a) to express their results for C; they did not make a West correction. The Cornell group expressed the shadowing in terms of the ratio

$$S = \frac{\sigma_{\gamma A}}{N\sigma_{\gamma d} - (N-Z)\sigma_{\gamma p}}, \tag{3.9c}$$

where $\sigma_{\gamma d}$ is their measured cross section for the deuteron, and no allowance has been made for the fact that the deuteron cross section is less than the sum of the neutron and proton cross section. We have used the Glauber and West corrections depicted in Fig. 32 to correct the Cornell data so that the shadowing is expressed with respect to the best estimates of the free neutron and proton cross sections. Figure 35 shows plots of A_{eff}/A as a function of photon energy for the measurements on

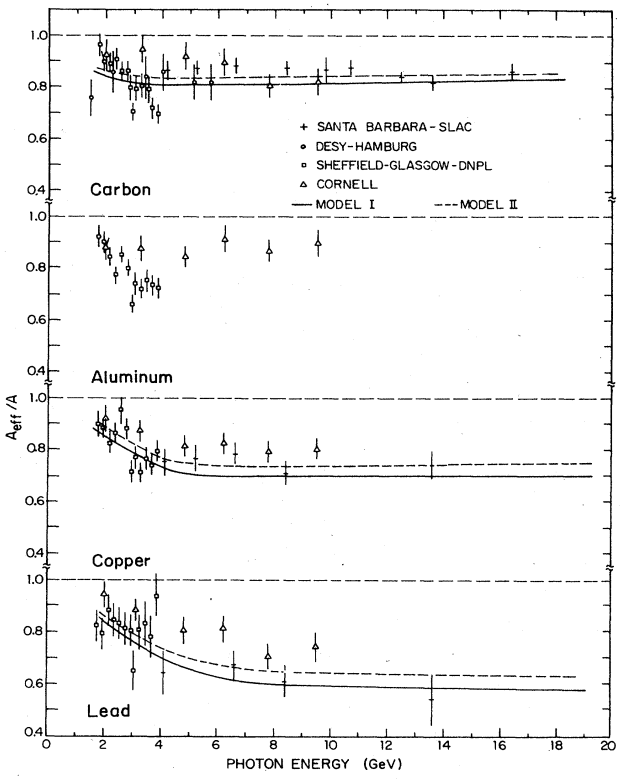

FIG. 35. A plot of A_{eff}/A for C, Al, Cu, and Pb from measurements by the DESY–Hamburg, Glasgow–Sheffield–DNPL, Santa Barbara–SLAC, and Cornell groups. The theoretical curves in Figs. 35–37 are described in Sec. V.B. They are repeated in Fig. 202, where they are compared with other models.

C, Cu, and Pb by the DESY–Hamburg (Heynen *et al.*, 1971), Sheffield–Glasgow–DNPL (Brookes *et al.*, 1973), Santa Barbara–SLAC (Caldwell *et al.*, 1973) and Cornell (Michalowski *et al.*, 1977) groups. Figure 36 shows a somewhat more extended plot for carbon which includes the data from the Yerevan–Lebedev–IHEP group (Bayatyan *et al.*, 1975). Figure 37 shows the energy dependence of A_{eff}/A for Be, C, and Ti observed by the DESY–Hamburg group. Figure 38 shows the shadowing observed for C, Al, Cu, Ag, Au, and U by the Cornell group. In these plots the errors bars include only the statistical errors and do not include the estimated systematic errors. With the exception of the Cornell experiment the systematic errors are estimated to be 3 to 5%

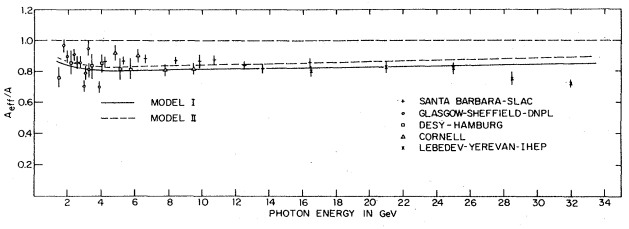

FIG. 36. A plot of A_{eff}/A for carbon for data from the DESY–Hamburg, Glasgow–Sheffield–DNPL, Santa Barbara–SLAC, Yerevan–Lebedev–IHEP, and Cornell groups.

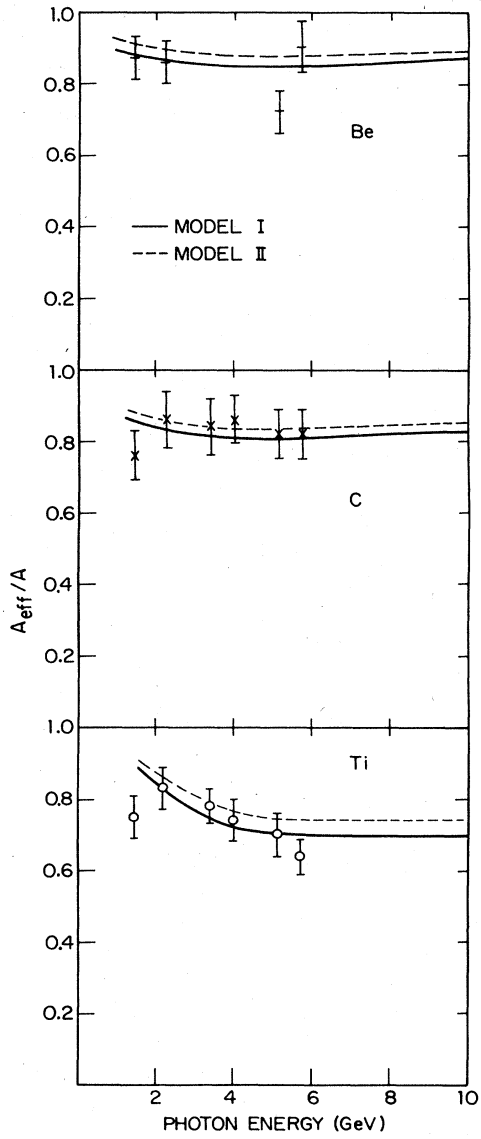

FIG. 37. The energy dependence of A_{eff}/A for Be, C, and Ti observed by the DESY–Hamburg group (from Meyer *et al.*, 1970).

for the low-Z nuclei and roughly 10 to 15% for the high-Z nuclei.

The Sheffield-Glasgow-DNPL data indicate a shadowing which turns on at a photon energy between 2 and 3 GeV. This observed energy dependence is greater for the light nuclei than for heavy nuclei. The DESY–Hamburg data give an A_{eff}/A which is less than 1 and thus suggestive of shadowing; they do not, however, show the energy dependence seen in the data of the Sheffield–Glasgow–DNPL group. The two experiments tend to agree at high energy and to disagree at low energy. The Santa Barbara–SLAC group finds an A_{eff}/A which is independent of energy and decreases significantly with A.

The Cornell data display a shadowing with a significant energy dependence for the heavy nuclei. The observed shadowing agrees roughly with that found by the Sheffield–Glasgow–DNPL and DESY–Hamburg groups but is

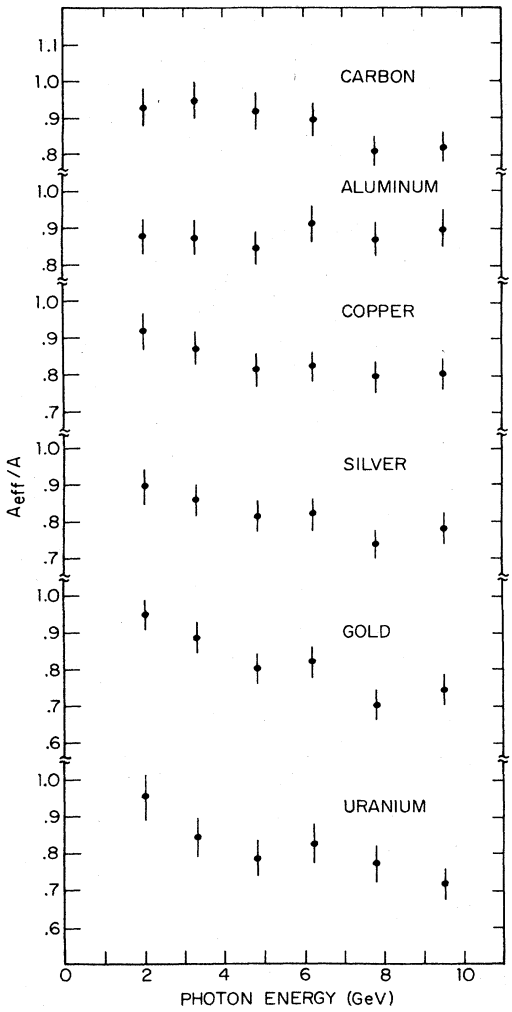

FIG. 38. The A_{eff}/A determined from the measurements of the Cornell group.

somewhat less for the heavy nuclei than that found by the Santa Barbara-SLAC group. Figure 39 shows the A dependence of A_{eff}/A determined by measurements of the Sheffield–Glasgow–DNPL group and the DESY-Hamburg group. These data indicate that there is a definite decrease in A_{eff}/A as the energy increases and that this decrease increases with A.

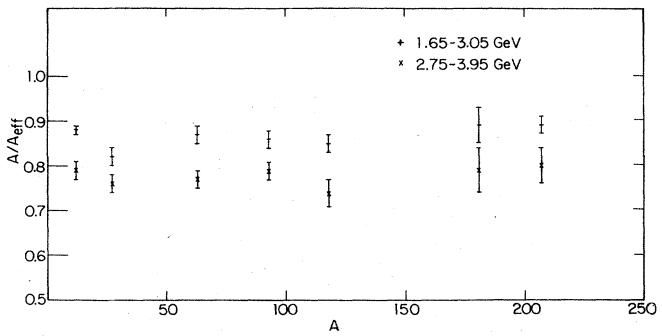

FIG. 39. The A dependence at various energies of A_{eff}/A determined from measurements of the Sheffield–Glasgow–DNPL and DESY–Hamburg groups.

In summary the data are consistent with the behavior expected for shadowing but display less shadowing than one would expect from the naive VMD models. The data are consistent with an increase of shadowing with energy which is slower for heavy nuclei than for light nuclei.

B. Compton scattering

The elastic scattering of photons from protons, which for historical reasons is called Compton scattering, is of fundamental importance. Below the threshold for meson production, Compton scattering is adequately described by a modification of the Klein–Nishina formula which takes into account the anomalous magnetic moment of the proton (Powell, 1949); above the threshold for meson production, the cross section increases with energy and depends upon the spin state of the proton. Early theoretical studies of Compton scattering were motivated by the desire to probe the mesonic structure of the nucleon (Sachs and Foldy, 1950; Capps and Holladay, 1955). Models were used to calculate the detailed scattering amplitude so that it could be compared with experiments. Somewhat later it was realized (Gell-Mann, Goldberger, and Thirring, 1954) that one could extend the analog of the Kramers–Kronig relations to field theory and use dispersion relations to relate Compton scattering to other photonuclear reactions. In particular, Compton scattering is related to the total hadronic photon cross section through the optical theorem and dispersion relations. It was subsequently proved under quite general assumptions (Low, 1954; Gell-Mann and Goldberger, 1954) that in the low-energy limit the Compton scattering amplitude contains the frequency-independent Thomson amplitude plus a term linear in the frequency which is determined by the static magnetic moment. Later, the vector-meson-dominance model kindled interest in the Compton scattering cross section at high energy. Compton scattering gives a direct test of VMD; if VMD is correct, Compton scattering should show the characteristic energy and momentum-transfer dependence found in hadron–hadron elastic scattering as well as a cross section which can be calculated from the cross sections for vector-meson photoproduction. Even if VMD fails as an adequate description, the more general "hadronic photon" picture described in Sec. II.B still predicts striking similarities to hadron-hadron elastic scattering. In this section we shall review the existing data on Compton scattering with particular emphasis on the region above the nucleon resonances.

1. Early measurements

The first measurements of nucleon Compton scattering were reported by Pugh *et al.* (1954). They employed a coincidence, anticoincidence telescope with lead converter to identify the gamma ray, followed by a large liquid scintillator to estimate the energy of the gamma ray. They used this setup to measure at 90° and 135° the absolute gamma-ray scattering cross section for Be, C, Al, Cu, Sn, Pb, and Bi in the energy range from 35 to 130 MeV. They found that for the elements heavier

than aluminum the agreement with Thomson scattering was adequate but for the lighter elements there was a clear disagreement corresponding to too large a backward scattering of high-energy photons.

The first measurements on hydrogen were reported by Oxley and Telegdi (1955). They used a converter telescope consisting of a 2.1 g/cm^2 carbon filter, an anticoincidence plastic scintillation counter, a 7.4 g/cm^2 lead converter, and a threefold telescope with 5.2 g/cm^2 of aluminum absorber interspersed to measure the scattering of 30 to 95 MeV photons by protons. They found that their measurements were adequately described by the Powell (1949) modification of the Klein–Nishina calculation. A somewhat more complete account of this effort was later reported by Oxley (1958).

Above the threshold for meson production, it is no longer possible to use a single counter to measure Compton scattering. The principal difficulty is the necessity of distinguishing the Compton scattered photons from the much larger number of photons coming from the decay of photoproduced π^0 mesons into two gamma rays. Since in a bremsstrahlung beam the energy of the incident photon is not defined, the measurement of the energy and angle of the recoil proton is not sufficient to distinguish between the two reactions. Two methods have been used to overcome this difficulty.

Figure 40 shows the apparatus used by an Illinois group (Bernardini *et al.*, 1960) for measurements in the range 100 MeV to 290 MeV. They detected in coincidence the scattered photon (with a lead-glass Cerenkov counter) and the proton (with a magnetic spectrometer). This enabled them to determine with precision the momentum of the recoil proton. Because for the same photon energy, Compton recoils carry greater energy than neutral pion recoils, the group could use the maximum photon energy to separate the two processes. Figure 41 shows a somewhat different setup that was used by a Cornell group (DeWire *et al.*, 1961) to measure the Compton cross section in the vicinity of 300 MeV. This group used a range telescope and made measurements at such angles that the recoil protons from Compton

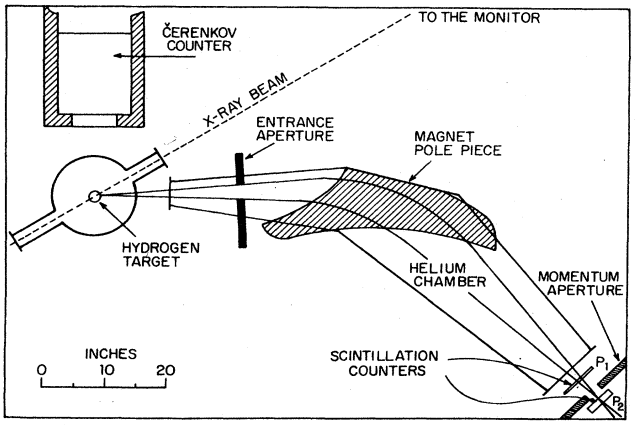

FIG. 40. A schematic drawing of the apparatus used by the Illinois group in their measurements of Compton scattering in the energy range from 100 MeV to 290 MeV (from Bernardini *et al.*, 1960).

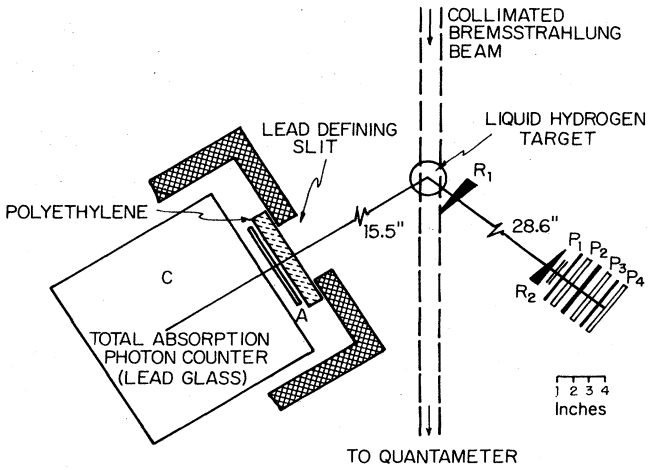

FIG. 41. A schematic diagram of the apparatus used by the Cornell group in their measurements of Compton scattering in the vicinity of 300 MeV (from DeWire *et al.*, 1961).

scattering were of longer range than from π^0 production with the available maximum photon energy. They also studied the angular correlation between the scattered photon and the recoil proton. For Compton scattering there is a unique correlation; for π^0 production the correlation is smeared out by the decay kinematics of the neutral pion.

With an increase in gamma-ray energy, it becomes more difficult to use the measured proton energy to separate Compton scattering from π^0 production, and it is necessary to make increased use of the angular correlation. Figure 42 shows the apparatus used by an

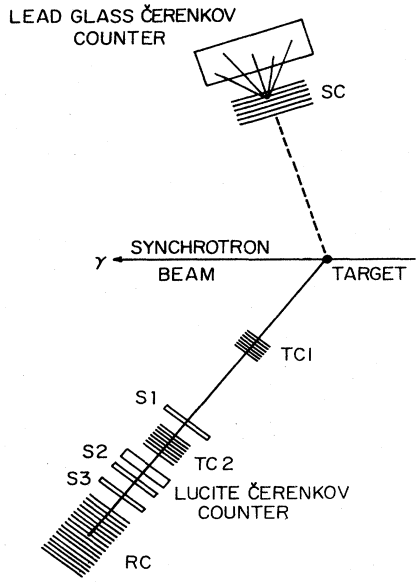

FIG. 42. Apparatus used by the MIT group in Compton scattering experiments carried out at Cornell. Spark chambers were used to determine the trajectories of the scattered gamma ray and the recoil proton; a lead-glass Cerenkov counter was used to determine the energy of the scattered photon; a range chamber was used to measure the energy of the recoil proton (from Stiening *et al.*, 1963).

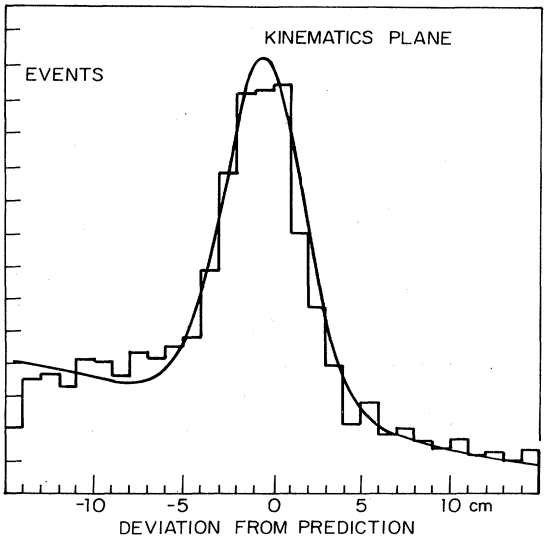

FIG. 43. Deviations of shower origins from the kinematically predicted direction in the reaction plane for an early experiment of the MIT group (from Stiening *et al.*, 1963).

MIT group (Stiening *et al.*, 1963) in pioneering experiments carried out at Cornell and at the Cambridge Electron Accelerator. They used spark chambers to determine the angles of the scattered gamma ray and the recoil proton. They also determined the energy of the proton with a range chamber and the energy of the gamma ray with a lead-glass Cerenkov counter. From the measured proton range and angle they computed the incident gamma-ray energy and the predicted angle of the scattered gamma ray on the assumption that it resulted from an elastic scattering event. Figure 43 shows a plot of the deviation of the observed direction from the predicted direction. There is a sharp peak at 0 deviation, representing elastic scattering, superimposed on a slowly varying background, due primarily to π^0 production. Rust *et al.* (1965) used a similar method at the Cornell 2 GeV synchrotron to measure proton Compton scattering from 450 to 1350 MeV near 90° in the center-of-mass system.

With two exceptions a combination of these techniques has been used in the reported measurements of Compton scattering. The disadvantage in using the recoil proton is that measurements cannot be made at very small momentum transfers.

2. Recent proton experiments

In this review our primary concern is measurements with E greater than 2 GeV. Measurements of the Compton cross section in this high-energy domain have been made at CEA–Cornell (2–4.5 GeV) (Deutsch *et al.*, 1973); at DESY (2–7 GeV) (Buschhorn *et al.*, 1970; 1971a,b), (5 and 6 GeV) (Criegee *et al.*, 1977); and at SLAC (5–17 GeV) (Anderson *et al.*, 1970a), (8 and 16 GeV) (Boyarski *et al.*, 1971). Table IV summarizes the reported measurements.

Figure 44 shows the apparatus used by one DESY group (Buschhorn *et al.*, 1970; 1971a). A 4×4 mm² collimated bremsstrahlung beam, typically 2×10^8 equivalent quanta/sec, traversed a 7-cm liquid hydrogen target and was monitored with a quantameter. The scattering angles θ_γ and ϕ_γ of the photon were measured by means of two crossed counter hodoscopes behind a 1-cm lead converter. Charged particles were either eliminated with a sweeping magnet or rejected by anticounters. A matrix of nine lead-glass shower counters provided a measurement of the photon energy. The recoil protons were detected with a wire spark chamber telescope. Five thin chambers served to measure the proton angles. They were followed by a system of three dE/dx counters of increasing thickness with which the energy of the recoil protons could be measured directly.

TABLE IV. A summary of the experiments which have reported measurements of Compton scattering from the proton.

Year	First author	Laboratory	Energy (GeV)
1954	Pugh	MIT	0.03–0.13
1955	Oxley	Univ. of Chicago	0.03–0.10
1957	Pugh	MIT	0.05–0.13
1958	Oxley	Univ. of Chicago	0.03–0.09
1959	Hyman	MIT	0.05–0.14
1960	G. Bernardini	Univ. of Illinois	0.13–0.29
1961	DeWire	Cornell	0.28–0.78
1962	Baranov	Lebedev	0.24–0.25
1963	Stiening	Cornell	0.54–0.84
1964	Nagoshima	INS–Tokyo	0.31–0.69
1965	Rust	Cornell	0.48–1.41
1966	Baranov	Lebedev	0.24–0.25
1967	Gray	Univ. of Illinois	0.19–0.34
1968	Barbiellini	Frascati	0.30–0.34
1969	Fujii	INS–Tokyo	0.70–0.80
1970a	R. L. Anderson	SLAC	5.50–17.00
1970	Buschhorn	DESY	5.00–7.00
1971	Boyarski	SLAC	8.00–16.00
1971a	Buschhorn	DESY	2.20–7.00
1971b	Buschhorn	DESY	3.20–3.70
1972	Barton	Daresbury	1.18–1.35
1972	Deutsch	CEA–Cornell	3.00–7.00
1972	Genzel	Bonn	0.24–0.43
1972	Kabe	INS–Tokyo	0.73–0.82
1973	Deutsch	CEA–Cornell	0.55–4.50
1974	Baranov	Lebedev	0.10
1975	Baranov	Lebedev	0.10
1977	Criegee	DESY	5.00–6.00

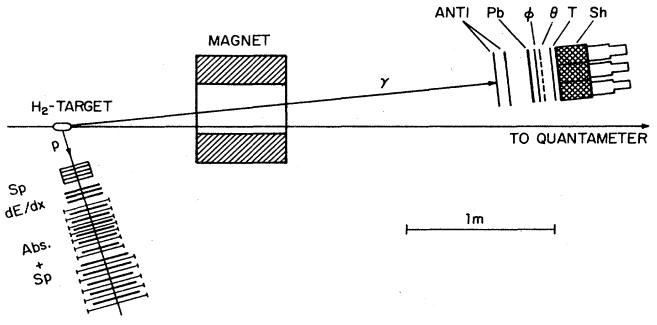

FIG. 44. Diagram of the apparatus used by the DESY group for Compton scattering measurements (from Buschhorn *et al.*, 1971a).

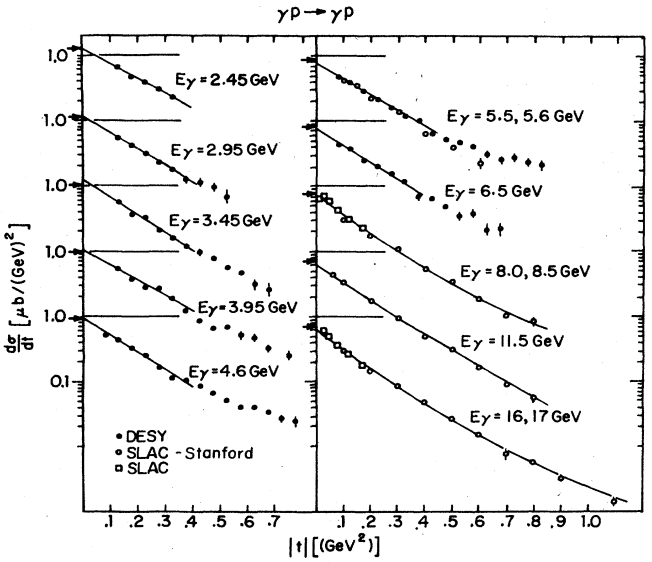

FIG. 45. A plot versus momentum transfer of the Compton scattering measurements reported by the DESY (Buschhorn *et al.*, 1970, 1971a), SLAC–Stanford (Anderson *et al.*, 1970a), and SLAC (Boyarski *et al.*, 1971) groups.

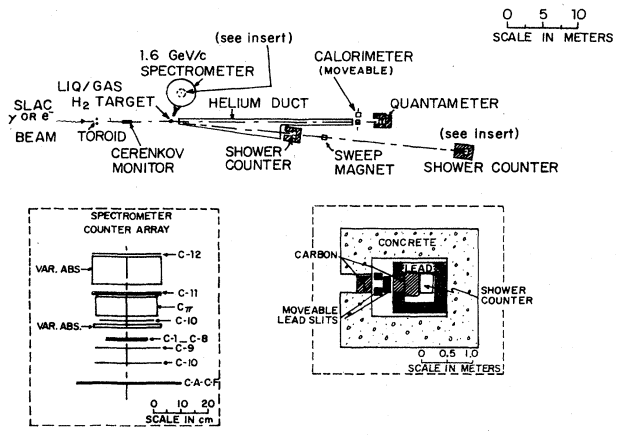

FIG. 46. Apparatus used by SLAC–Stanford group. The 1.6 GeV spectrometer is a 90° focusing spectrometer (from Anderson *et al.*, 1970a).

For protons with kinetic energy greater than 65 MeV the range was measured by a carbon plate wire chamber system. The results are plotted in Fig. 45. The plots include only the statistical errors. There is an estimated systematic error of ±7% which is due to the following contributions; background subtraction 3%; photon spectra 3%; target thickness 2%. For the energy range 3.7–4.2 GeV an additional systematic error of ±7% is due to the steep slope of the photon spectrum. The results of an exponential fit of the form $A\exp(Bt)$ for $0.06<t<0.4$ GeV^2 are given in Table V. All systematic errors except the normalization uncertainties (quantameter calibration and target thickness) have been taken into account in the fit.

The MIT group (Deutsch *et al.*, 1973) used a similar arrangement in their measurements of Compton scattering at the Wilson Synchrotron Laboratory and at the Cambridge Electron Accelerator. For one set of measurements they used a magnet rather than a range telescope to measure the momentum of the recoil protons. The result of the fits to their data are summarized in Table V. They estimated the normalization error of an individual run to be about ±7% with a common overall scale uncertainty of about ±10%.

Figure 46 shows the apparatus used by the SLAC–Stanford Group (R. L. Anderson *et al.*, 1970a). A coincidence experiment is made difficult by the poor duty cycle of the Stanford Linear Accelerator and thus special precautions were taken to shield the counters carefully. A lead-lucite shower counter 13 radiation lengths thick was used to detect the scattered gamma ray. The coun-

TABLE V. Results for $\gamma p\to\gamma p$. Fits to the data of the form $d\sigma/dt=A\exp(Bt)$ and $A\exp(Bt+Ct^2)$.

Experiment	E (GeV)	$-t$ range (GeV^2)	A (μb/GeV^2)	B (GeV^{-2})	C (GeV^{-4})
DESY (Buschhorn)	2.2–2.7	0.1 –0.4	1.26±0.13	5.2±0.5	◦◦◦
	2.7–3.2	0.1 –0.4	1.14±0.11	5.7±0.4	•••
	3.2–3.7	0.1 –0.4	1.24±0.11	6.2±0.4	•••
	3.7–4.2	0.1 –0.4	1.02±0.14	5.3±0.5	•••
	4.0–5.2	0.06 –0.4	0.92±0.09	6.0±0.4	◦◦◦
	5.0–6.2	0.06 –0.4	0.76±0.06	5.5±0.3	•••
	6.0–7.0	0.06 –0.4	0.76±0.07	5.9±0.4	•••
MIT	1.5–2.5	0.1 –0.25	1.25±0.13	5.3±0.5	◦••
	2.6–3.8	0.15 –0.4	0.99±0.10	5.0±0.3	•••
SLAC–Stanford	5.5	0.1 –0.6	0.88±0.15	6.9±1.3	1.3±1.9
	8.5	0.1 –0.8	0.6 ±0.1	6.2±0.8	0.7±0.9
	11.5	0.06 –0.8	0.63±0.06	6.5±0.6	0.8±0.7
	17	0.1 –1.1	0.55±0.05	6.6±0.4	1.1±0.4
SLAC	8.0	0.014 –0.17	0.82±0.04	7.7±0.5	•••
	16.0	0.014 –0.17	0.69±0.03	7.9±0.5	•••
Combination of SLAC–Stanford and SLAC	8.0	0.014 –0.8	0.79±0.03	7.6±0.4	2.3±0.5
	16.0	0.014 –1.1	0.64±0.02	7.3±0.3	1.7±0.3
DESY (Criegee)	5.0	0.002 –0.06	0.82±0.04	8.5±1.5	•••
	6.0	0.004 –0.08	0.79±0.04	8.6±1.2	•••

ter was placed inside a well shielded cave which could be moved remotely in angle and in height. The aperture of the counter was defined by remotely movable lead slits in front of the counter. The momentum and angle of the proton were measured by the SLAC 1.6 GeV spectrometer. The recoil proton and the incoming photon defined the plane of elastic scattering. Since the solid angle of the shower counter, which was matched to the spectrometer acceptance, was small compared with the 2γ π^0 decay cone, the π^0 contamination was strongly suppressed. The remaining π^0 contamination, including accidental counts, was measured directly by moving the shower counter out of the Compton plane. The main event selection was therefore made by the spectrometer, and the shower counter simply provided an additional kinematic constraint which was primarily geometrical and not strongly dependent on the energy resolution of the counter. The Compton data were corrected for counter efficiencies, loss from pair production of the scattered photon before the sweeping magnet, loss of incident photons before the secondary emission quantameter, and the change in the Δt acceptance of the spectrometer due to energy loss of the proton in the target. The total corrections were typically about 30% and were largely determined experimentally. The total uncertainty introduced by these corrections is estimated to be 20% of the correction.

Figure 45 shows a plot of the data versus momentum transfer. The data include all the errors except an overall normalization error of about 5%. Table V summarizes fits of the data to the form $A\exp(Bt+Ct^2)$.

Figure 47 shows the setup used by the SLAC group (Boyarski *et al.*, 1971). They did not observe the scattered proton; they used a pair spectrometer positioned 40 m from the 3.8 cm long hydrogen target to measure the angle and energy of the scattered photons. The pair spectrometer had a converter ($0.044X_0$ of copper, 10 cm wide × 13 cm high) in front of an 18D72 magnet with a 15 cm gap which was oriented to bend the pair-produced electrons and positrons in the vertical plane. Scintillation counters were used to determine the trajectories of the e^+ and e^-.

Two 14 radiation length lead-Lucite shower counters were used as part of the trigger. The bremsstrahlung beam was monitored by a secondary emission quantameter positioned 13 m behind the target and by a gas

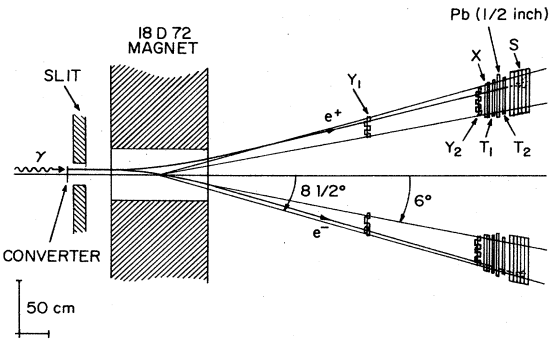

FIG. 47. A schematic diagram of the pair spectrometer used by the Stanford group. They observed only the scattered gamma ray (from Boyarski *et al.*, 1971).

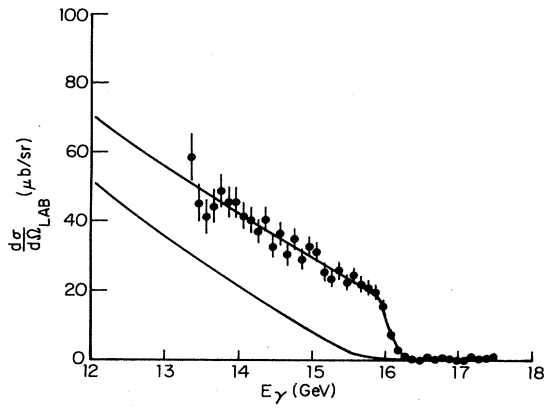

FIG. 48. A typical fit to the observed spectrum used by the SLAC group to measure the Compton cross section (from Boyarski *et al.*, 1971).

Cerenkov monitor and an ion chamber in front of the target. Data were taken at various angles from hydrogen and deuterium with the converter in and out. The cross section was then determined by fitting the observed spectrum with (a) a Compton step variable in height; (b) a fixed linear term beginning at the bremsstrahlung end-point energy computed from the processes $\gamma N\to\pi^0 N$, with $\pi^0\to\gamma\gamma$ and $\gamma N\to\eta N$ with $\eta\to\gamma\gamma$; (c) a fixed linear term starting at the final γ threshold for the process $\gamma N\to\omega N$ with $\omega\to\gamma\pi^0$; (d) a variable linear term starting at the final γ threshold for $\gamma N\to\pi^0\Delta(1230)$ with $\pi^0\to\gamma\gamma$; and (e) a variable flat background term describing chance triggers. The end-point energy was allowed to vary to account for any spectrometer energy miscalibration. These processes were folded with the bremsstrahlung spectrum, the e^+ and e^- straggling in the converter, and the spectrometer resolution. Figure 48 shows a typical spectrum together with the fitted Compton step. To account for the uncertainty in the fitting procedure a systematic error estimated at 3%(2%) for the 8(16) GeV fits has been added in quadrature to the statistical errors. An overall systematic error of ±3% common to all points has not been included. The results for a hydrogen target are plotted in Fig. 45. Fits to the form $A\exp(Bt)$ are tabulated in Table V; fits to the combined data of this experiment and those of Anderson *et al.* (1970a) to the form $A\exp(Bt+Ct^2)$ at 8.5 and 17 GeV are also summarized in Table V.

Figure 49 shows the setup used by a second DESY group (Criegee *et al.*, 1977a) to measure the Compton scattering from H_2 and D_2 at 5 and 6 GeV. They did not measure the energy or direction of the recoiling nucleon but detected only the scattered photon. The photon energy and angles were measured in a pair spectrometer consisting of a 4 mm thick Al converter, a bending magnet, and two telescopes equipped with seven spark chambers and one shower counter each. The energy resolution of the spectrometer was 1.3% (fwhm). The beam intensity and photon spectrum were continuously measured by a second pair spectrometer placed downstream in the main beam. The intensity was also monitored with a quantameter. The systematic error in the intensity measurement was ±1.2%. The contribution of

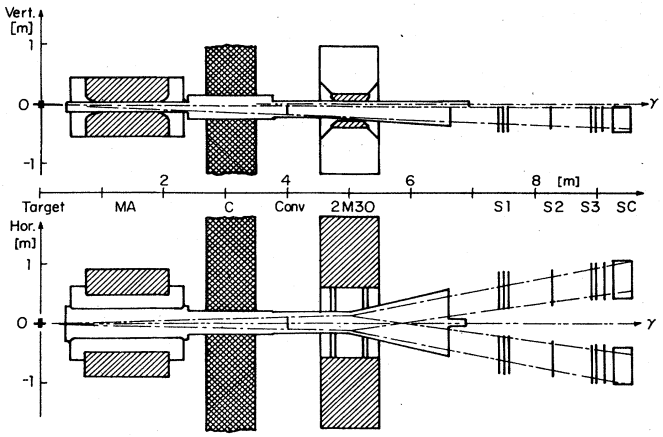

FIG. 49. A schematic diagram of the apparatus used by the DESY group for the measurement of Compton scattering from H, D, Be, C, Al, Ti, Cu, Ag, and Au (from Criegee *et al.*, 1977a).

inelastic hadronic reactions was separated through the different photon spectra they produce. The experiment concentrated on small momentum transfers ranging from -0.004 to -0.08 GeV^2 at 6 GeV, and from -0.002 to -0.06 GeV^2 at 5 GeV. The systematic error in the experiment resulted mainly from the uncertainty of the background (±1%), of the converter position (1.5%), and, in the case of the 6 GeV data, from the error in the telescope efficiencies (1.5%). By quadratic addition to the normalization error they obtained a total systematic error of 2.5% at 5 GeV and 3.6% at 6 GeV. Figure 50 shows a plot of the data for hydrogen and deuterium versus momentum transfer. The errors are statistical only and do not include the systematic error. Fits to the form $A\exp(Bt)$ are tabulated in Table V. For this experiment these fits include both statistical and systematic errors.

The plots in Fig. 45 and the fits tabulated in Table V show that the data from the five groups agree satisfactorily. They also show that the cross section displays the diffractive characteristics shown by hadron-hadron elastic scattering. That is, $d\sigma/dt$ is approximately constant with energy and has the characteristic exponential dependence on momentum transfer. For the wide-t region (e.g., $|t|<0.6$ GeV^2) the data definitely require a quadratic term in the exponential. For comparison, at 9 GeV the slope parameters for πp scattering for $|t|<1$ GeV^2 are $B=9.0\pm0.2$ GeV^2 and $C=2.5\pm0.3$ GeV^{-4}.

3. Deuteron experiments

Figure 51 shows the cross sections for hydrogen and deuterium obtained by the SLAC group (Boyarski *et al.*, 1971). For deuterium the data show a sharp forward peak due to coherent scattering together with an incoherent part that remains at larger t. With the neglect of spin effects and Fermi motion corrections, such as the West correction, the deuterium cross section is given by

$$(d\sigma/d\Omega)_d = 2|T_0|^2|1+F(4t)+2G(t)| + 2|T_1|^2|1-F(4t)| \tag{3.10}$$

(see Appendix B). Here T_0, T_1 are, respectively, the isoscalar and isovector t-channel exchange amplitudes of nucleons, $F(t)$ is the deuterium form factor, and $G(t)$ is the Glauber multiple scattering term. We have written

$$T_{n,p} = T_0 \mp T_1 . \tag{3.11}$$

The SLAC group used $F(t)=e^{14t}$ as determined from electron scattering (Rand *et al.*, 1967; Buchanan and Yearian, 1965) and $G(t)=0.069e^{-Bt/4}+0.07e^{-Bt/2}$ with

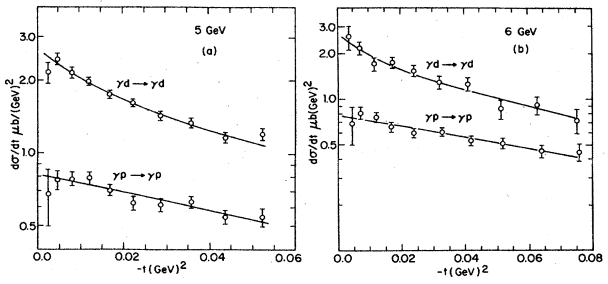

FIG. 50. A plot of the hydrogen and deuterium cross sections obtained by Criegee *et al.* (1977) at 5 and 6 GeV (from Criegee *et al.*, 1977a).

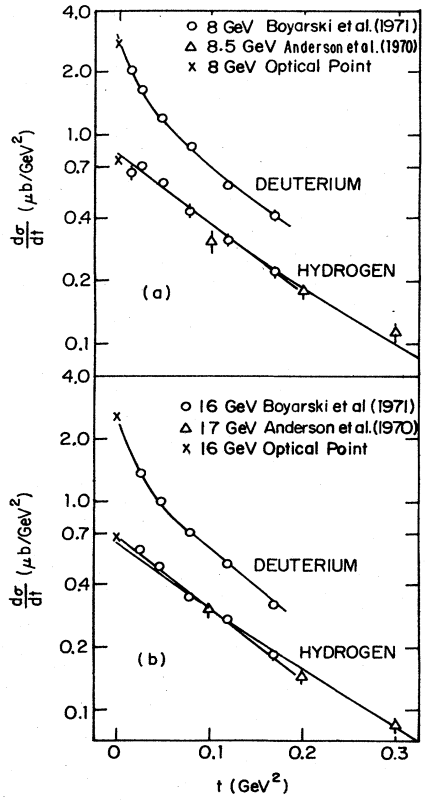

FIG. 51. A plot versus momentum transfer of the Compton cross section for hydrogen and deuterium obtained by the SLAC group (after Boyarski *et al.*, 1971).

TABLE VI. Tabulation of the determination of the isospin-0 and isospin-1 components by Criegee *et al.* from their data and from a reanalysis of the SLAC data of Boyarski *et al.* The * refers to the calculation with Hulthén wave function. The ** refers to an analysis of the data with the deuteron form factor and the Glauber correction obtained from a wave function following Reid (from Criegee *et al.*, 1977).

	$\frac{\lvert T_1\rvert^2}{\lvert T_0+T_1\rvert^2}$	$\frac{\mathrm{Re}(T_0T_1^*)}{\lvert T_0+T_1\rvert^2}$
Criegee *et al* (1977)		
5 GeV	0.13 ± 0.09	$0\ \pm0.03$
	$(0.08\pm0.10$	$0.02\ \pm0.03)$*
6 GeV	-0.12 ± 0.15	$0.10\ \pm0.04$
	$(-0.12\pm0.15$	$0.10\ \pm0.04)$*
Boyarski *et al.* (1971)		
8 and 16 GeV	0.03 ± 0.10	-0.043 ± 0.012
	$(0.02\pm0.12$	$0.02\ \pm0.02)$**
Criegee *et al.* together with Boyarski *et al.*	0.08 ± 0.05	$0.02\ \pm0.01$
Calculated using total cross section measurements of Meyer *et al.* (1970)	$\mathrm{Im}T_1/\mathrm{Im}T_0=0.042\pm0.008$	

$B=7.8$ GeV^2 as determined from a calculation by Ogren (1970).

The ratio of deuterium to hydrogen can be expressed by two unknown parameters; and from the combined 8 and 16 GeV data, fits to the D_2/H_2 ratios versus t give for these parameters

$$\mathrm{Re}(T_0^*T_1)/|T_0+T_1|^2=-0.049\pm0.012$$
$$|T_1|^2/|T_0+T_1|^2=0.03\pm0.10\,. \tag{3.12}$$

These parameters differ from those originally given by Boyarski *et al.* (1971) due to an error pointed out by G. Poelz (see the erratum to Boyarski *et al.*, 1971). On the assumption that T_0 and T_1 have the same t dependence, the negative real term implies that the differential neutron Compton cross section is larger than that for protons, unlike that seen in total cross sections. These results, together with the total γn and γp cross sections (Caldwell *et al.*, 1973), give for the isovector phase δ_1 and the isoscalar phase δ_0

$$\delta_1\simeq 0\,,$$
$$\delta_0\simeq \pi/2\,, \tag{3.12}$$

i.e., T_1 is almost pure real and T_0 is almost pure imaginary.

Criegee *et al.* (1977a) also used their deuterium and hydrogen data to determine the amplitudes for isospin 0 and isospin 1 exchange. They assumed that the deuterium cross section could be written in a form similar to Eq. (3.10). Table VI summarizes the two isospin ratios $|T_1|^2/|T_0+T_1|^2$ and $\mathrm{Re}|T_0^*T_1|/|T_0+T_1|^2$ obtained from fits to these data. This table includes only the statistical errors. Systematic uncertainties resulting mainly from the uncertainty in the background and in the precise converter position are about half of the statistical errors.

The isospin ratios depend sensitively on the assumed shape of $F(t)$ and $G(t)$. Criegee *et al.* used a deuteron wave function following Reid (1968) and calculated $G(t)$ in the ρ-dominance approximation. An analysis of these data starting from a Hulthen wave function yielded consistent but numerically different ratios. Criegee *et al.* also reanalyzed the data of Boyarski *et al.* using their Glauber correction. The results are given in Table VI.

All the ratios are compatible with a vanishing or at least small isospin-1 exchange contribution to the photon-nucleon interaction. They are also compatible with the measured ratio

$$\frac{\mathrm{Im}T_1}{\mathrm{Im}T_0}=\frac{\sigma_{\gamma p}-\sigma_{\gamma n}}{\sigma_{\gamma p}+\sigma_{\gamma n}}\,. \tag{3.14}$$

4. Shadowing in Compton scattering from nuclei

A DESY group (Criegee *et al.*, 1977b) used the pair spectrometer system described previously to measure Compton scattering from Be, C, Al, Ti, Cu, Ag, and Au targets at 3 and 5 GeV photon energies. The measurements covered the kinematic ranges $0.001\leq|t|\leq0.020$ (GeV)^2 and $0.002\leq|t|\leq0.060$ (GeV)^2 at 3 and 5 GeV, respectively. The method used to analyze the data was similar to that employed with the proton and the deuteron; a fit with an elastic plus an inelastic component was used to extract the elastic Compton scattering cross section. Figure 52 shows the observed t

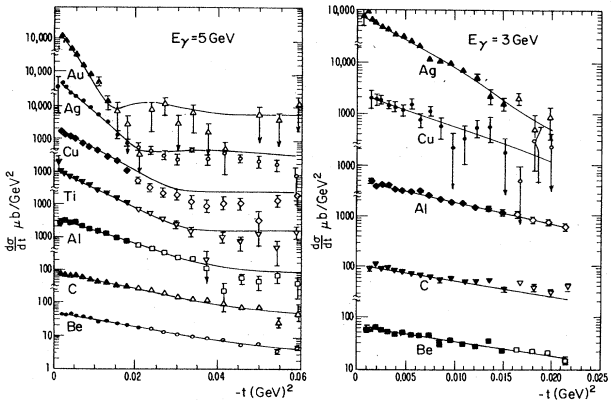

FIG. 52. The momentum transfer distribution for the scattering of 3 and 5 GeV photons from Be, C, Al, Ti, Cu, Ag, and Au nuclei (from Criegee *et al.*, 1977b).

dependence at 3 and 5 GeV; an optical-model calculation [including an incoherent component and with an overall scale factor and the nuclear radius (Wood–Saxon) as free parameters] was used to determine the forward differential cross section for elastic photon-nucleus scattering. The nuclear radii obtained with this procedure agreed satisfactorily with the tabulated values, thus demonstrating that high-energy photons give essentially the same nuclear sizes as high-energy electrons.

VMD optical-model calculations were used to compare the data with both measured single-nucleon cross sections and measured total cross sections via the optical theorem. The optical-model calculation is described in Sec. V.C. The shadowing effect can be expressed by the ratio R of the measured forward cross section to that expected for scattering on unshadowed nucleons through the expression

$$R \equiv \frac{d\sigma}{dt}(0)_A \Big/ \left[A^2 \frac{d\sigma}{dt}(0)_N\right]. \tag{3.15}$$

Owing to the difficulty in assessing the proton-neutron difference, choice of an "average" single-nucleon cross section is uncertain. Our choice is discussed in Sec. V.C and differs at the ~5 percent level with the choice of the group itself. Experimental results and optical-model calculations are shown in Fig. 53. Comparison of the data with corresponding total cross-section measurements and optical-model calculations of the ratio of real to imaginary part are displayed in Table XXXVI. The data show shadowing of a magnitude consistent with that seen in the total cross-section measurements.

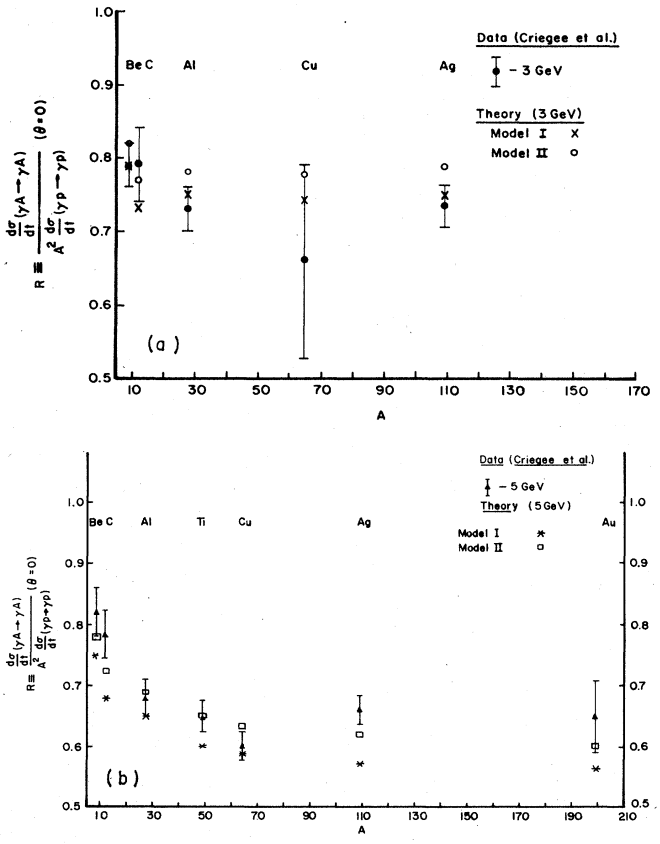

FIG. 53. Shadowing in Compton scattering represented by the ratio

$$R = d\sigma/dt\,(0)|_A / [A^2 d\sigma/dt\,(0)|_N]$$

(a) 3 GeV; (b) 5 GeV. Data are from Criegee *et al.* (1977b) and the models are described in Sec. V.C.

5. Polarization and spin effects

●A DESY group (Buschhorn *et al.*, 1971b) measured the elastic scattering of linearly polarized photons on protons for ν between 3.2 and 3.7 GeV and for four-momentum transfers ranging from −0.1 to −0.7 $(\text{GeV})^2$. The photon asymmetry is defined as

$$\Sigma = \frac{(d\sigma_\perp/dt - d\sigma_\parallel/dt)}{(d\sigma_\perp/dt + d\sigma_\parallel/dt)}, \tag{3.16}$$

where $d\sigma_\perp/dt$ and $d\sigma_\parallel/dt$ are the differential cross sections for photons with polarization vector perpendicular and parallel to the scattering plane. Figure 54 shows a plot of the observed asymmetry versus scattering angle. A linear fit gives

$$\Sigma(t) = -(0.08 \pm 0.18)|t|. \tag{3.17}$$

The predictions of three popular models are: 0^+ exchange and s-channel helicity conservation, $\Sigma = 0$; spin independence, $\Sigma = (1 - \cos^2\theta)/(1 + \cos^2\theta)$. For this experiment, spin independence corresponds to $\Sigma \cong 0.35|t|$. The s-channel helicity conservation or 0^+ exchange fit the data best, but the errors do now allow a definitive rejection of the other model. A similar result is obtained for ρ production (see Sec. III.C).

●There has been one measurement at the Cornell Wilson Synchrotron Laboratory by a MIT–Tufts Group of the polarization of the recoil protons (Deutsch *et al.*, 1972). For ν in the range 3–7 GeV and for t values from −0.2 to −0.54 $(\text{GeV})^2$, they obtained for the recoil proton an average polarization $P = 0.12 \pm 0.06$, where the error includes statistics only, with no evidence of any structure as a function of momentum transfer. In the DESY experiment (Buschhorn *et al.*, 1971b), which measured the photon asymmetry Σ, the recoil proton polarization was evaluated later and found to be $P = 0.01 \pm 0.18$. These

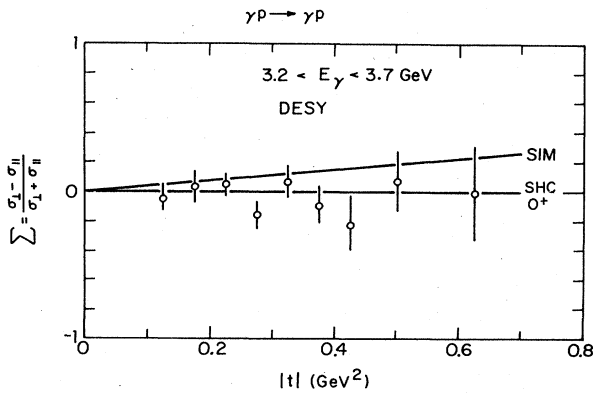

FIG. 54. A plot of the observed asymmetry versus momentum transfer for measurements with a polarized photon beam carried out by the DESY group (from Buschhorn *et al.*, 1971b).

results imply that the real part of the nucleon helicity flip amplitude is small relative to the diffractive part of the amplitude.

6. The real part of the Compton scattering amplitude

The forward Compton scattering amplitude is conventionally expressed in the laboratory frame in terms of the amplitudes $T_{\parallel}$ and $T_{\perp}$ through the equation (Damashek and Gilman, 1970)

$$T(\nu)=\chi_f^*[T_{\parallel}(\nu)\epsilon_2^*\cdot\epsilon_1+i\sigma\cdot(\epsilon_2^*\times\epsilon_1)T_{\perp}(\nu)]\chi_i\ . \tag{3.18}$$

Here χ_i and χ_f are the Pauli spinors characterizing the initial and final nucleons, and ϵ_1 and ϵ_2 are the polarization vectors of the incident and scattered photons, respectively. Since an average over nucleon spins leaves only $T_{\parallel}(\nu)$, $T_{\parallel}(\nu)$ is called the spin-averaged forward amplitude. The amplitudes $T_{\parallel}(\nu)$ and $T_{\perp}(\nu)$ are separable through experiments with polarized photons; $T_{\parallel}(\nu)$ corresponds to parallel, $T_{\perp}(\nu)$ to perpendicular linear polarization vectors of the initial and final photons, respectively. In terms of $T_{\parallel}$ and $T_{\perp}$, the two independent helicity amplitudes (photon and nucleon spins parallel, or antiparallel) for forward scattering are

$$T_{sp}(\nu)=T_{\parallel}(\nu)-T_{\perp}(\nu)\,, \tag{3.19a}$$

$$T_{sa}(\nu)=T_{\parallel}(\nu)+T_{\perp}(\nu)\,. \tag{3.19b}$$

Since the helicity amplitudes T_{sp} and T_{sa} are simply related by the optical theorem to the total hadronic photoabsorption cross section, we have

$$\mathrm{Im}T_{\parallel}(\nu)=\frac{\nu}{4\pi}\,\frac{\sigma_{sa}(\nu)+\sigma_{sp}(\nu)}{2}=\frac{\nu}{4\pi}\,\sigma_T(\nu)\,, \tag{3.20a}$$

where $\sigma_T(\nu)$ is the spin-averaged total cross section, and

$$\mathrm{Im}T_{\perp}(\nu)=\frac{\nu}{4\pi}\,\frac{\sigma_{sa}(\nu)-\sigma_{sp}(\nu)}{2}\ . \tag{3.20b}$$

For unpolarized targets and beams, the forward differential cross section is given by

$$\left(\frac{d\sigma}{d\Omega}\right)_{\theta=0^\circ}=|T(\nu)|^2=|T_{\parallel}(\nu)|^2+|T_{\perp}(\nu)|^2\,. \tag{3.21}$$

This yields

$$\left(\frac{d\sigma}{dt}\right)_{t=0}=\frac{\pi}{\nu^2}\,|T(\nu)|^2$$

$$=\frac{|\sigma_T(\nu)|^2}{16\pi}+\frac{\pi}{\nu^2}\,|\mathrm{Re}T_{\parallel}(\nu)|^2+\frac{\pi}{\nu^2}\,|T_{\perp}(\nu)|^2\,, \tag{3.22}$$

where t is the square of the four-momentum transfer. The real part of $T_{\parallel}(\nu)$ can be calculated from the imaginary part through the use of the dispersion relation

$$\mathrm{Re}T_{\parallel}(\nu)=-\frac{\alpha}{M}+\frac{\nu^2}{2\pi^2}\,P\int_{\nu_0}^{\infty}\frac{d\nu'\sigma_T(\nu)}{\nu'^2-\nu^2}\ . \tag{3.23}$$

Here M is the nucleon mass and ν_0 is the threshold for single-pion production. The constant, $-\alpha/M$, is the Thomson limit and it can be inferred from rather general theorems giving the behavior as $\nu\to 0$ (Low, 1954; Gell-Mann and Goldberger, 1954). Numerically $-\alpha/M=-3\,\mu$b-GeV.

●It has been suggested that the forward scattering amplitude $T_{\parallel}(\nu)$ might simulate an expression of an extended Regge-type, denoted by $T_{\parallel}^R(\nu)$, where

$$T_{\parallel}^R(\nu)=C-\sum_j\frac{c_j}{4\pi}\,\frac{1+e^{i\pi\alpha_j(0)}}{\sin\pi\alpha_j(0)}\,\nu^{\alpha_j(0)} \tag{3.24}$$

as $\nu\to\infty$. Attention is normally restricted to the Pomeron trajectory $\alpha_1(0)=1$ and the neighboring trajectory with $\alpha_2(0)=0.5$. Interest also centers on the possible existence of a real constant C which might be interpreted as a fixed pole. Regge theory leads to a sum rule

$$C=T_{\parallel}(0)-\frac{2}{\pi}\int_{\nu_0}^{N}\frac{d\nu'}{\nu'}\,\mathrm{Im}T_{\parallel}(\nu')+\frac{2}{\pi}\int_0^N\frac{d\nu'}{\nu'}\,\mathrm{Im}T_{\parallel}^R(\nu')\,, \tag{3.25}$$

where N is high enough that $\mathrm{Im}T_{\parallel}(\nu)=\mathrm{Im}T_{\parallel}^R(\nu)$ is valid for $\nu\geq N$. Explicitly Eq. (3.25) then gives

$$C=-3.0-\frac{1}{2\pi^2}\int_{\nu_0}^{N}\sigma_T(\nu')d\nu'+\frac{N}{2\pi^2}\left(c_1+\frac{2c_2}{N^{1/2}}\right)\,. \tag{3.26}$$

As discussed in Sec. II.D, it is of considerable interest whether or not C is zero.

●Several groups have used the dispersion relations (3.23) to calculate from the measured total cross section $\mathrm{Re}T_{\parallel}(\nu)$. The low-energy data (below ~2 GeV) are fit with a series of resonances of Breit–Wigner form plus a background term, and the high-energy data (above ~2 GeV) are parametrized with the Regge form

$$c_1+c_2\,\nu^{\alpha_2(0)-1}\,. \tag{3.27}$$

As was mentioned earlier the high-energy data are not sufficiently precise to allow a simultaneous fit to $\alpha_2(0)$. However, since any value of $\alpha_2(0)$ between 0.4 and 0.6 would seem reasonable, alternative fits have been performed for these two extremes. Calculations of the real part have been carried out by Dominguez *et al.* (1970), Damashek and Gilman (1970), the Glasgow-Sheffield–DNPL group (Armstrong *et al.*, 1972a), and the DESY group (Naroska, 1970). Each of these groups used a different source of data for the total cross section and hence different Regge parameters. Table VII summarizes parametrizations of the cross section and the resultant values of C for calculations by two of the groups. The data are consistent with there being a fixed pole C with a value in the neighborhood of the Thomson limit $-3\,\mu$b GeV.

Figure 55 gives a plot of the ratio of the real to imaginary part for proton Compton scattering as calculated by the Glasgow-Sheffield-DNPL group (Armstrong *et al.*, 1972a). It is essentially the same as that found by the other two groups.

The MIT–DESY group (Alvensleben *et al.*, 1973) has measured the real part of $T_{\parallel}$ through the interference between the Compton and Bethe–Heitler amplitudes by detecting the zero-degree electron pairs asymmetrically. Figure 56 shows a schematic drawing of the apparatus. Counter hodoscopes were used to determine the particle trajectories; Cerenkov and shower counters were used for particle identification. Figure 8 shows a comparison between the experimental result and the

TABLE VII. Regge parameters determined through use of the dispersion theory sum rule. A refers to the total cross-section measurements of Bloom *et al.* (1969), *B* to those of Caldwell *et al.* (1973), Meyer *et al.* (1971), and Ballam *et al.* (1968b, 1969a).

Calculator	Data set: Low energy	Data set: High energy	$\alpha(0)$	c_1 (μb)	c_2 (μb)	C (μb/GeV)
Damashek-Gilman	SLAC–Spec	*A*	0.6	100.5	68.1	−3.5
		B	0.6	93.5	61.7	−4.8
		A+*B*	0.6	89.9	72.9	−3.8
		A	0.5	107.5	64.0	−2.4
		B	0.5	99.2	59.6	−3.7
		A+*B*	0.5	96.6	70.2	−2.5
		A	0.4	112.2	62.5	−0.7
		B	0.4	102.9	59.9	−1.8
		A+*B*	0.4	101.2	70.1	−0.4
Glasgow-Sheffield-DNPL	Glasgow-Sheffield-DNPL	Glasgow Sheffield DNPL	0.6	80.7	80.0	−3.3
			0.5	91.0	71.4	−2.3
			0.4	97.9	66.2	−0.8

dispersion relation prediction. The agreement is satisfactory.

The results of these calculations can be used in conjunction with the measurements of the forward Compton cross section to set a limit on $T_\perp(\nu)$. Expressed in terms of the optical-theorem result

$$\left.\frac{d\sigma(\gamma p\to\gamma p)}{dt}\right|_{t=0}=\frac{\sigma_T^2}{16\pi}\left[1+\left(\frac{\mathrm{Re}T_\parallel(\nu)}{\mathrm{Im}T_\parallel(\nu)}\right)^2\right]+\frac{\pi}{\nu^2}|T_\perp(\nu)|^2 . \tag{3.28}$$

Figure 57 shows a comparison between the extrapolated forward Compton scattering differential cross sections and the first two terms of Eq. (3.28). The predicted cross section is about 10% higher than some of the more precise measurements. Whether this difference is due to systematic errors in the measurements, or to a failure of the straight line extrapolation at very small angles is unknown. The size of the difference certainly argues against a sizeable contribution due to the spin-dependent amplitude. We conclude from this comparison that

$$|T_\perp|^2<0.1|T_\parallel|^2 .$$

The Glasgow–Sheffield–DNPL (Armstrong *et al.*, 1972) group has used the data for a deuterium target as input to the dispersion relation to determine the real part of the spin-averaged forward scattering amplitude for the deuteron. Using a smooth fit over the resonance region and the high-energy fit

$$\sigma_{\gamma d}=(175+135\nu^{-1/2})\mu\mathrm{b}$$

they obtained the Argand diagram depicted in Fig. 58. They also found for the fixed-pole contribution $C=-1.7\mu$b GeV. This is close to that for the proton and suggests the neutron gives no contribution. Further analysis along these lines was carried out by Gunion and Suaya (1973).

●Dominguez, Gunion, and Suaya (1972) have independently extracted the neutron cross section $\sigma_{\gamma n}$ from the Glasgow-Sheffield–DNPL data for $\sigma_{\gamma d}$ and $\sigma_{\gamma p}$ and used this cross section to determine the fixed-pole contribution for the neutron. They obtained

$$C(\text{neutron})=0.0\pm1.5\ \mu\text{b-GeV} .$$

They also obtained values for the proton which were

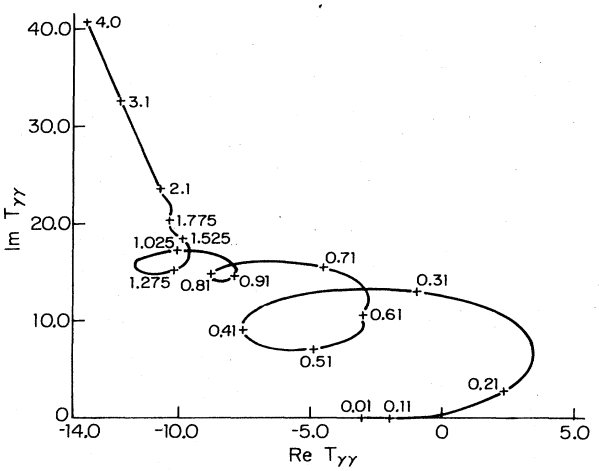

FIG. 55. Argand diagram for the forward scattering amplitude $T_\parallel(\nu)$ (in μb-GeV) for Compton scattering from the proton, plotted as ν goes from 0 to 4.0 GeV (from Armstrong *et al.*, 1972a).

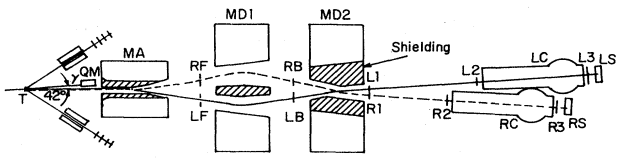

FIG. 56. Apparatus used by MIT–DESY group for the measurement of the real part of the spin-averaged forward amplitude for Compton scattering through the interference between the Compton and Bethe–Heitler amplitudes (from Alvensleben *et al.*, 1973).

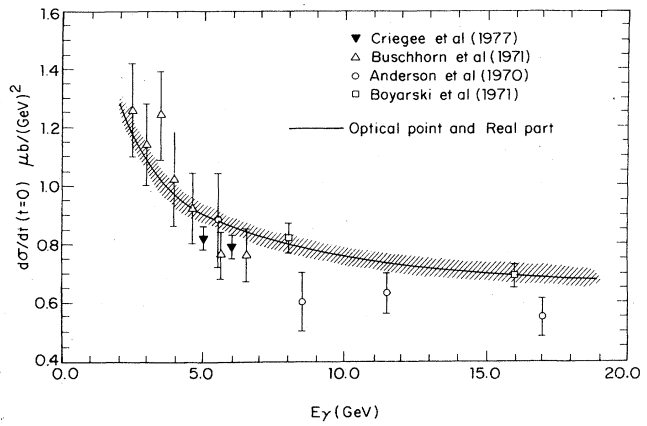

FIG. 57. A plot versus energy of the cross section for forward Compton scattering together with the optical-model dispersion theory predictions. The shaded area indicates the error of roughly 4% in $\sigma_{\gamma p}$.

consistent with the Thomson limit

$$C(\text{proton}) = -3.0 \pm 0.8\ \mu\text{b-GeV}\,.$$

We don't wish to leave the reader with the impression that there is overwhelming evidence in favor of the existence of a "fixed pole" in Compton scattering. The fine details of the hadronic model used are important to the computation. Analyses employing Regge exchanges more elaborate than simple poles (e.g., Tait and White, 1972; Moffat and Snell, 1972) point toward a much more ambiguous situation.

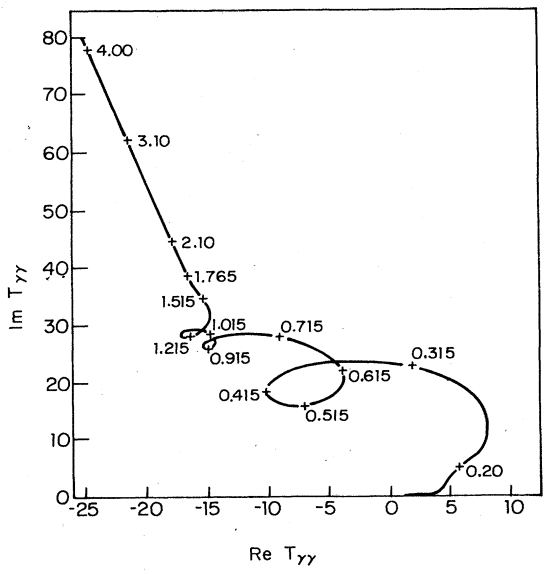

FIG. 58. Argand diagram showing the spin-averaged forward scattering amplitude $T_{\text{II}}^{0}(\nu)$ (in μb-GeV) for Compton scattering from the deuteron, plotted as ν goes from 0 to 4.0 GeV (from Armstrong *et al.*, 1972b).

C. Rho photoproduction

To a remarkable extent the rho meson dominates studies of high-energy photoproduction. Its production cross section is roughly one-sixth of the total hadronic photoproduction cross section; the rho is the dominant feature of the hadronic structure of the photon. In this section we shall review the present state of the knowledge of rho production.

The rho meson is an unstable particle whose mass and width are roughly 770 and 155 MeV, respectively. Its quantum numbers $I^G(J^P)C$ are $1^+(1^-)^-$ and its dominant decay mode is two charged pions. Once an axis of quantization has been chosen in the rho rest frame, the decay can be characterized by the orientation of the decay plane with respect to the plane of production and by the direction of the π^+ meson in the decay plane—see Fig. 211. The decay plane can be viewed as the plane of polarization of the rho meson. For production by polarized photons the angle between the polarization planes of the rho and photon can be directly related to the contributions in the production cross section from natural and unnatural parity exchanges in the t channel (Stichel, 1964; Stichel and Schulz, 1964; Schilling *et al.*, 1970). The decay distribution of the rho in the rho center-of-mass system gives a measure of the relative populations of the rho spin states with $m_z = \pm 1$ and $m_z = 0$. In Appendix D the relationships between the density matrix elements of the rho, the polarization of the photon, and the decay angular distribution are summarized. Here we wish to emphasize an important experimental result described near the end of this section; namely, if one chooses the z axis of the overall γp center-of-mass system to be opposite to the direction of the proton recoil (a choice known as the "helicity system"), the rho has the same polarization as the incident photon. This phenomenon is referred to as s-channel helicity conservation (Gilman *et al.*, 1970).

Four experimental methods have been used to study rho photoproduction—bubble chamber or streamer chamber experiments in which all three final-state particles are observed, counter-spectrometer experiments in which the two pions from the decay of the rho are observed, counter-spectrometer experiments in which only the recoil proton is observed, and counter-spectrometer experiments in which all three particles are observed over a limited solid angle.

1. Track chamber experiments

The feasibility of studying high-energy photoproduction in hydrogen by the track chamber technique was first demonstrated by Sellen *et al.* (1959; Chasan *et al.*, 1960) using a hydrogen-diffusion cloud chamber. In that work the authors studied photoproduction up to about 1 GeV and obtained first results on the production of the $\Delta(1236)$. Later, the production of the $\Delta(1236)$ and of the ρ^0 meson were studied in a heavy-liquid bubble chamber (Fretwell *et al.*, 1967). The first measurements with a hydrogen bubble chamber were carried out at the Cambridge Electron Accelerator by a Brown–CEA–Harvard–MIT–Padova group known as the Cambridge Bubble Chamber Group (Crouch *et al.*, 1964a, b).

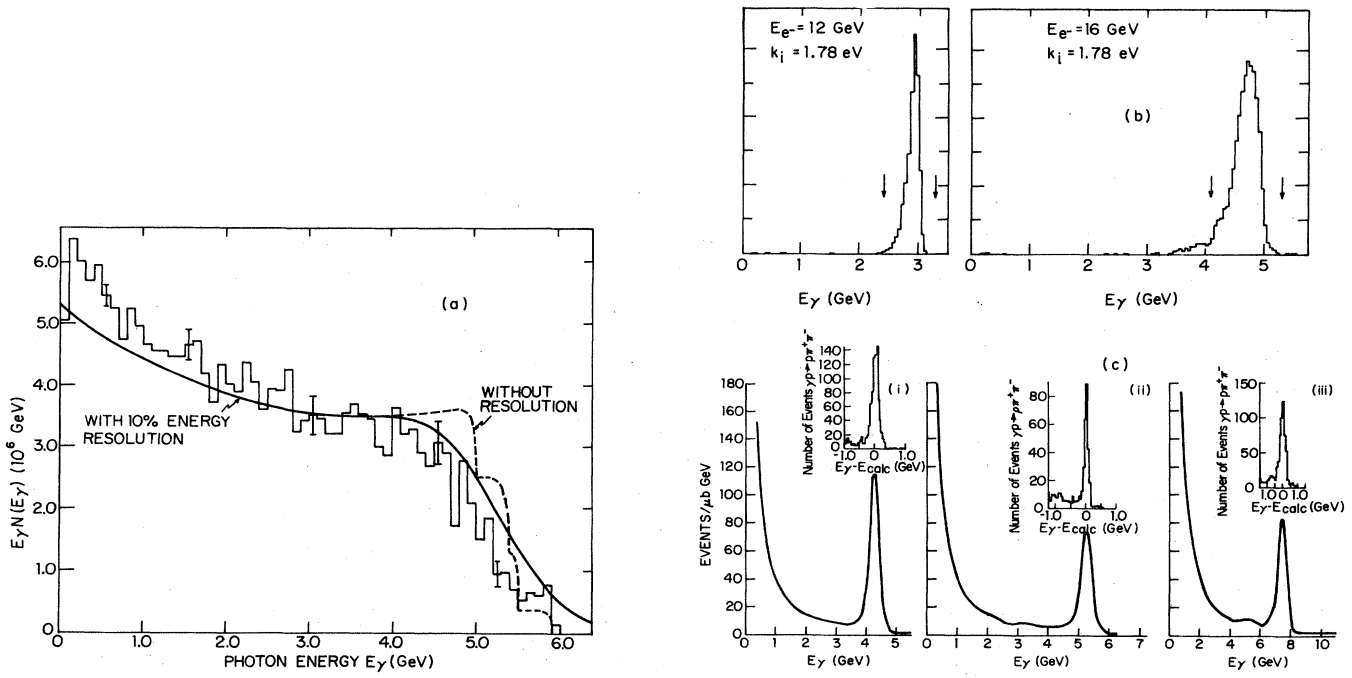

FIG. 59. (a) The photon-energy distribution obtained by the Cambridge bubble chamber group. The solid and dashed curves are sums of appropriately weighted bremsstrahlung distributions with and without a 10% energy resolution, respectively. This weighting is due to the fact that the experiment was not performed at a unique positron energy but rather at several positron energies. The theoretical curves are normalized to the energy above 0.1 GeV. Errors shown are statistical (from Crouch *et al.*, 1967b). (b) Unnormalized photon energy spectra for photons produced by backscattering of photons from a ruby laser (1.78eV) by electrons of 12 and 16 GeV. The arrows indicate the energy intervals used. The ordinate gives the number of photons (from Ballam *et al.*, 1972). (c) Spectra for photons produced by positron-electron annihilation. The incident direction of the positrons is monitored to ± 0.1 mrad by two positron beam indicators, while the outgoing photons are collimated into a beam at 7-11 mrad to the positron direction by two collimators, so that a vertical sheet of photons traverses the bubble chamber. The photon spectra in the bubble chamber were deduced from measurements of the reaction $\gamma p \to p\pi^+\pi^-$ and normalized to microbarn equivalents from e^+e^- pair production measurements. For (i) the positron energy was 8.5 GeV, the mean production angle 11.8 mrad; for (ii) $E_+ = 10$GeV, $\bar{\theta} = 9.4$ mrad; for (iii) $E_+ = 12$ GeV, $\bar{\theta} = 7.15$ mrad. The inserts show the distribution of energies E_γ found for 3-constraint fits about that calculated from the vertex position in the chamber (from Eisenberg *et al.*, 1972a).

Bubble Chamber experiments have been performed using a bremsstrahlung photon beam (Brall *et al.*, 1966; Crouch *et al.*, 1966; Erbe *et al.*, 1967, 1968; Hilpert *et al.*, 1970a, b; Schiffer *et al.*, 1972; Benz *et al.*, 1973, 1974), monochromatic beam produced by positron annihilation (Ballam *et al.*, 1968a, 1969; Eisenberg *et al.*, 1969, 1970, 1971, 1972) and monochromatic beam produced by the Compton scattering of a laser beam from a high-energy electron beam (Ballam *et al.*, 1970a, 1972, 1973; Bingham *et al.*, 1970; Alexander *et al.*, 1974, 1976; Eisenberg *et al.*, 1976; Gupta *et al.*, 1976; Bapu *et al.*, 1977). This latter technique gives not only monochromatic but linearly polarized photons. The incident photon beam is measured by using the number of e^+e^- pairs together with the known pair production cross section in hydrogen. The hydrogen pair production cross section is estimated to be accurate to 0.5% and has been verified to ±1%. The shape of the photon spectrum is usually determined from the energy spectrum of the e^+e^- pairs or from the $3C, p\pi^+\pi^-$ events. Figure 59 shows the three types of spectra that have been used.

Groups at SLAC (Davier *et al.*, 1968, 1969a, 1970; Park *et al.*, 1972; Liu *et al.*, 1972;) and DESY (Struczinski *et al.*, 1972, 1973, 1976) have used streamer chambers to study photoproduction. The SLAC group used the SLAC 2.2m streamer chamber and a 16 GeV bremsstrahlung beam to study photoproduction from hydrogen. The photon beam was monitored in a quantameter calibrated to a few tenths of 1% with electron and positron beams and the SLAC Faraday cup. The photon spectrum was checked by measuring the energies of pairs produced in the hydrogen gas target tube. The quantameter data, which were accurate to ±2.5%, were used in the final cross-section calculations. The scanning efficiency was (87 ± 3%), the measuring efficiency (88 ± 2%), the estimated systematic uncertainty in the absolute cross-section data ±8%.

The DESY streamer chamber group used an energy-tagged broadband photon beam together with a built-in liquid hydrogen target. They covered the laboratory energy range from 1.6 to 6.3 GeV, with the energy of the photons determined by the tagging system to ±1%. The photons passed through a liquid hydrogen target of 3.8 cm length and were counted in a totally absorbing shower counter. In determining the cross sections it was

necessary to make a large dead-time correction for the shower counter. Since the systematic uncertainties in determining the cross sections were of the order of 15% the group elected to normalize their data to the published total cross sections using the expression

$$\sigma_{\text{tot}} - \sigma_{1\text{ prong}} = \left(98.7 + \frac{64.9}{\sqrt{E_\gamma}} - \frac{80}{E_\gamma}\right)\ \mu\text{b}.$$

The chief disadvantage of the track chamber experiments is the small number of events and the consequent limited statistical precision. The chief advantages of the track chamber experiments are that the kinematic fit is overconstrained and one can observe the full angular distribution of the decay pions. The overconstraint allows one to eliminate unambiguously the inelastic events where the recoiling system is not a proton. The observation of the complete angular distribution of the decay pions eliminates the ambiguity due to the decay distribution and makes it possible to determine the decay matrix elements and to obtain information concerning the individual production helicity amplitudes.

For the study of ρ photoproduction the most serious correction to the track chamber experiments is for the loss of short proton tracks. This distorts the momentum-transfer spectrum at low $|t|$. Since the minimum momentum transfer decreases with energy, the inaccessible region increases with photon energy. The Weizmann–SLAC–Tel Aviv group (Eisenberg *et al.*, 1972a) reported in their study of photoproduction with positron annihilation radiation of 4.3, 5.25, and 7.5 GeV nominal energies that loss of short proton tracks was significant for $|t| < 0.06$ GeV^2. This effect was correlated with the number of pairs per frame but independent of track orientation. There was a ~13% loss for a photon energy >4 GeV. The ABBHHM group (Hilpert *et al.*, 1970b) studied this correction by measuring the spectrum of recoil protons in rho production from a deuterium target. Table VIII summarizes the corrections made in each of the major hydrogen bubble chamber experiments. The dominant error is generally due to the limited number of events. Figure 60 shows a plot of the total cross section for the channel $\gamma p \to p\pi^+\pi^-$ found by the track chamber and bubble chamber groups. The agreement between the measurements by the different groups is good.

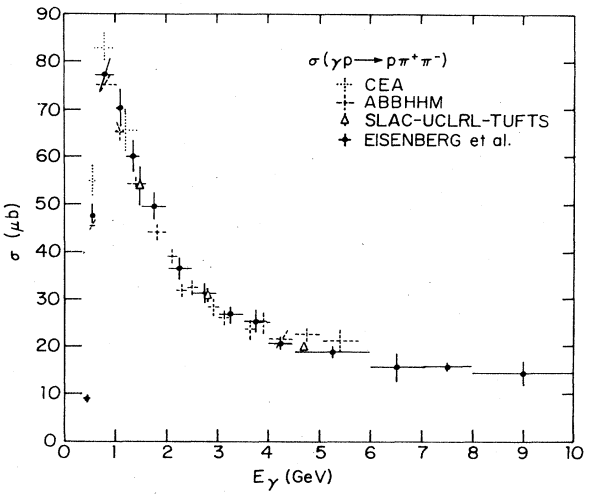

FIG. 60. Cross sections for the reaction $\gamma p \to p\pi^+\pi^-$ as a function of energy found in the several bubble chamber experiments (from Eisenberg *et al.*, 1972a).

2. Counter experiments

Figure 61 shows the counter-spectrometer system used by the Harvard group (Lanzerotti *et al.*, 1965; 1968) in their study of rho photoproduction at the Cambridge Electron Accelerator. The system consisted of two spectrometers, each of which used a half-quadrupole magnet and a number of scintillation counters to determine the momentum of the pions coming from the decay of the rho meson. Cerenkov counters and shower counters were used for particle identification. The two spectrometers were independently movable and the angular distribution of the rho decay could be observed by moving the spectrometers in the horizontal plane. Rho's produced at 0° and decaying at other than 90° in the rho center of mass could be observed by running the two spectrometers in an asymmetric configuration. A bremsstrahlung beam was used and a quantameter of the Wilson design was employed to determine the number of equivalent quanta. The chief disadvantages of this simple spectrometer system were its small solid angle and its inability to reject particles scattered from the magnets.

TABLE VIII. A summary of the exposures carried out with hydrogen-filled bubble chambers.

Group	Beam	Energy (GeV)	Type of chamber (cm)	Pictures	Systematic error	Small-t correction
CEA	Hardened	4.5	30	865 000	<5%	10% estimate
	Bremsstrahlung	6.0				lowest bin
ABBHHM	Hardened	5.45	85	1 700 000	<3%	No corrections made
	Bremsstrahlung	5.8				~15% for $E_\gamma > 2.5$ GeV
WST	Annihilation	4.3	100	300 000	<3%	Significant for
	Radiation	5.25		252 000		$\lvert t\rvert < 0.06$ GeV^2
		7.5		940 000		~13% for $E_\gamma > 4$ GeV
SBT	Laser-Compton	2.8	208	294 000	<3%	(-0.4 ± 0.4)% for $\lvert t\rvert \geq t_{\min}$
	(Polarized)	4.7		454 000		(3.4 ± 0.5)% for $\lvert t\rvert \geq t_{\min}$
		9.3		1 260 000		(7 ± 5)% for $0.02 < \lvert t\rvert \leq 0.05$

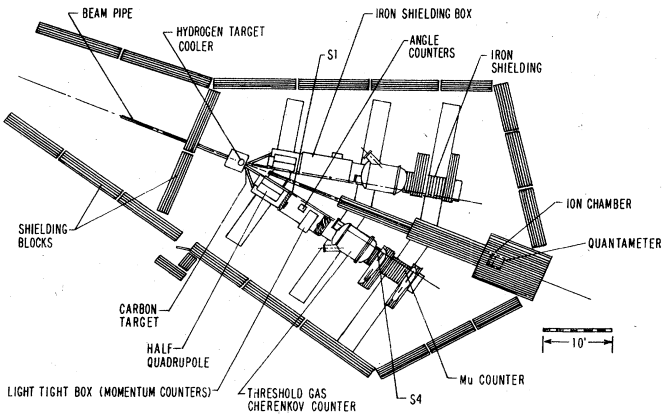

FIG. 61. The spectrometer system used by the Harvard group at the Cambridge Electron Accelerator in their study of rho photoproduction (from Lanzerotti *et al.*, 1968).

Figure 62 shows the system used at DESY by Blechschmidt *et al.* (1967) to study rho production from hydrogen, carbon, and aluminum. They used a tagged photon beam in conjunction with an optical spark chamber spectrometer equipped with a Cerenkov counter for particle identification. The principal disadvantages of this system were the limitation in rate due to the tagged beam and the necessity of scanning photographs of the optical spark chambers.

Figure 63 shows the spectrometer system used by the MIT–DESY group at DESY (Asbury *et al.*, 1967a; Alvensleben *et al.*, 1970b). This double-arm spectrometer was fixed in position and hodoscopes were used to determine the momentum and production angle of each of the pions. This information was then used to calculate the mass and production angle of the rho. The beam was monitored with a quantameter. This spectrometer has the virtues of large acceptance and good rejection of particles scattered from the magnets. The spectrometer recombines rays at constant $p_\pm\theta_\pm$ and therefore has a large acceptance and at the same time a good mass resolution. For a given spectrometer setting, the acceptance is $\Delta p/p \simeq 0.18$, $\Delta\theta/\theta \simeq \pm 0.14$, $\Delta m/m \simeq \pm 0.10$, and $\Delta\psi \simeq \pm 10$ mrad, where ψ is the projected vertical production angle. The hodoscopes defined an event to an accuracy of $\delta m = \pm 15$ MeV, $\delta p = \pm 150$ MeV, and $\delta t_\perp = \pm 0.001$ $(\text{GeV})^2$. The chief disadvantage of the setup was that only a limited range of production angles and a limited region of the rho-decay angular distribution could be seen. As a result, it was necessary to fold the t dependence and decay angular distribution into the acceptance.

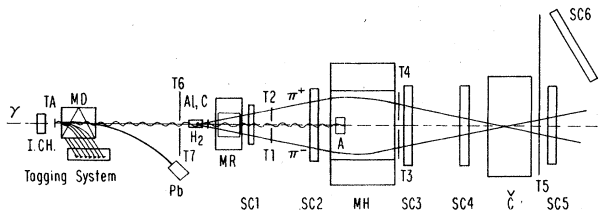

FIG. 62. Schematic diagram of the setup used by Blechschmidt *et al.* (1967) at DESY (from Blechschmidt *et al.*, 1967).

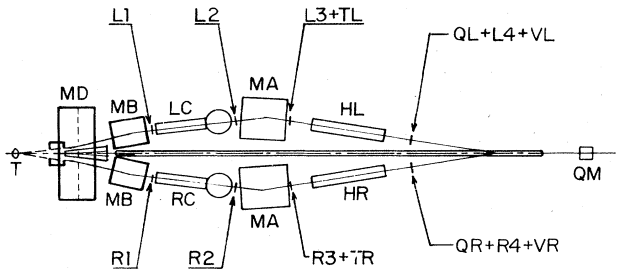

FIG. 63. Spectrometer system used by the MIT–DESY group at DESY (from Alvensleben *et al.*, 1970b).

It is estimated that the systematic uncertainty involved in using this apparatus is less than 5%.

Figure 64 shows the spectrometer used by the Daresbury group at DNPL (Biggs *et al.*, 1969). Each spectrometer consisted of two half-quadrupole magnets followed by a bending magnet. The optics were point-to-point focusing in the momentum (vertical) plane and parallel-to-point focusing in the θ (horizontal plane). The orthogonality of the momentum and angle planes enabled the production angles to be defined independently of momentum. For each spectrometer the important parameters were $\Delta\Omega = 0.67$ msr, $\Delta p/p = 0.14$, and $\Delta\theta = 19$ mrad. The mass resolution of the spectrometers was ±6 MeV; the total mass acceptance was of the order of 140 MeV. The two arms were independently adjustable in angle. The intensity of the photon beam was measured with a quantameter that had been calibrated in an electron beam against a Faraday cup. The total systematic uncertainty with this spectrometer system for measurements of hydrogen is estimated to be less than 3.5%.

Figure 65 shows a schematic plan view of the apparatus used by the Cornell group (McClellan *et al.*, 1969a, b, 1971b) at the Wilson Synchrotron Laboratory. The bremsstrahlung beam, which is monitored by a thin ion chamber upstream, passes through a 12 cm liquid hydrogen target and into a uranium beam stop. The π^+ and π^- from the decay of photoproduced ρ's pass through separate apertures in the pair spectrometer system. A six-fold coincidence in the scintillation counters triggers the optical spark chambers. The entire magnet sys-

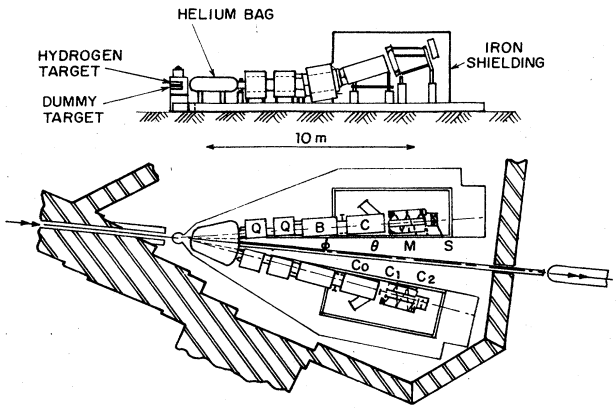

FIG. 64. Spectrometer system used by the Daresbury group at NINA (from Biggs *et al.*, 1969a).

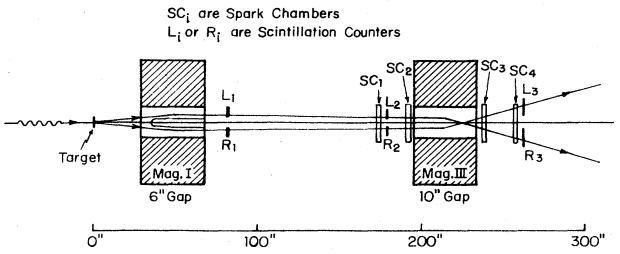

FIG. 65. Spectrometer system used by the Cornell group in their studies of rho photoproduction (from McClellan *et al.*, 1969).

tem is mounted on a platform which rotates vertically (to ~7°) about the target, thus varying the production angle. Typical acceptances (FWHM) are $\Delta m_{\pi\pi}/m_{\pi\pi} = \pm 4\%$ and $\Delta p_\rho/p_\rho = \pm 17\%$. The spark chambers were used for high-resolution analyses of the data taken on heavy nuclei, and served only for qualitative checks on the hydrogen-deuterium data. For the analysis of the data it was assumed that the ρ-decay angular distribution was given by $\sin^2\theta$, where θ is the center-of-mass polar angle relative to the ρ direction of flight. The overall systematic uncertainty in the hydrogen data was estimated to be ±7%.

In a subsequent experiment the Cornell group (Berger *et al.*, 1972) used a proton recoil hodoscope in coincidence with the pair spectrometer to eliminate the inelastic processes. The scintillation counter hodoscope, with an angular resolution of ±25 mrad, was placed below the hydrogen target, and the pair spectrometer was tilted vertically to vary the production angle from 0° to a maximum of 0.083 radians. Coplanarity of the recoil proton and vector meson was used as the criterion for two-body production.

Bulos *et al.* (1969) used at SLAC a wire chamber spectrometer based on a large-aperture magnet in conjunction with a monochromatic photon beam from positron annihilation to study rho production from hydrogen and complex nuclei. The data from this experiment has never been fully reported in the published literature.

Figure 66 shows a schematic diagram of the SLAC 1.6 GeV spectrometer used by the Ritson group at SLAC (Jones *et al.*, 1968; Anderson *et al.*, 1970b) to study vector-meson production through missing mass experiments in which the recoil particle was observed. It is a weak-focusing ($n = 0$), second-order-corrected, 90° vertical bend magnet with a radius of 254 cm. The spectrometer focused production angles and momenta onto a single focal plane. The resolution was ±0.08% in momentum and ±0.4 mrad in angle. For low $|t|$ values [$|t| < 0.4$ (GeV)^2] the protons were identified by range and pulse height using the first trigger counters. At higher $|t|$ values, a threshold Cerenkov counter was used to provide additional pion rejection. The primary beam monitor was a nonsaturating quantameter which had been calibrated against a Faraday cup. The net overall normalization uncertainty for cross sections determined using this apparatus is estimated to be (5 ± 1)%. The production of resonance particle X in the reaction $\gamma + p \rightarrow X + p$ corresponds to a step in the detected recoil proton yield measured as a function of angle for a fixed-photon end-point energy. This is evident from the equation

$$M_x^2 = 2k(p\cos\theta - T) - 2MT \qquad (3.29)$$

relating the missing mass and p, θ, M, and T which are, respectively, the momentum, angle, mass, and kinetic energy of the recoiling proton. Figure 67 shows measured proton yields for a peak bremsstrahlung energy of 11.5 GeV and for $t = -0.7$ (GeV)^2 and the breakdown of the yield into separate π^0, ρ^0, and ϕ peaks. This technique does not have sufficient resolution to separate out the ω, and other measurements must be relied on to make this correction.

Figure 68 shows the apparatus used by Gladding *et al.* (1973) to study vector-meson production from hydrogen at the Cambridge Electron Accelerator. They used a tagged photon beam and a recoil proton wire spark chamber spectrometer for primary identification. They also employed an array of large spark chambers downstream to observe some of the decay particles as an aid in separating the rho and omega.

A group from the California Institute of Technology (Barish *et al.*, 1973) used the SLAC 8 GeV spectrometer to study rho photoproduction from hydrogen by observing the recoil proton and using the missing mass to separate out the components due to π^0 and rho production. They used a bremsstrahlung beam and carried out measurements at photon energies of 6, 12, and 18 GeV for momentum transfers 0.5 to 3 GeV^2.

The chief disadvantage of the experiments in which one observes only the two pions is that one must make assumptions about the decay distribution in order to analyze the data. Those experiments which detect pion pairs

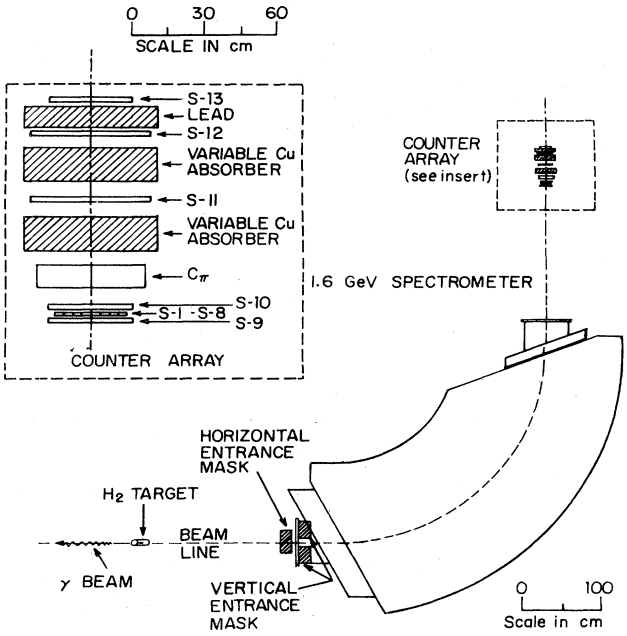

FIG. 66. Schematic diagram of the spectrometer system used by the Ritson group at SLAC to study vector-meson production through missing mass experiments in which the recoil particle was observed. The insert shows the detector system in more detail (from Anderson *et al.*, 1970b).

TABLE IX. Experiments on ρ^0 photoproduction, $\gamma p \to \rho^0 p$.

Experiment	Technique	Beam	Photon energy (GeV)	Particles detected	Number of rho events above 2 GeV	Remarks
CEA Collaboration	HBC	Bremsstrahlung	<6	p, π^+, π^-	500	
DESY (ABBHHM)	HBC	Bremsstrahlung	<6	p, π^+, π^-	2000	Final state $p\pi^+\pi^-$ is 3 (or 4) constrained; background from other reactions is negligible; no data below $\|t\| = 0.02$ GeV^2
SLAC–Weizmann–Tel Aviv	HBC	Quasi-monochromatic	2–8	p, π^+, π^-	3000	
SLAC–Berkeley Tufts	HBC	Laser beam, lin. pol. approx. monochromatic	2.8; 4.7 9.3	p, π^+, π^-	6000	
SLAC	Streamer-chamber	Bremsstrahlung	2–16	p, π^+, π^-	1700	
DESY (AHHM)	Streamer-chamber	Tagged γ beam	3–6	p, π^+, π^-	2000	
DESY (Blechschmidt *et al.*)	Spectrometer	Tagged γ beam	3–5	p, π^+, π^-	350	1 constraint, $\sin^2\theta$ assumed
Cornell	Spectrometer	Bremsstrahlung	4–8.5	$\pi^+\pi^-$	Many	Inelast. BG subtracted at 8.5 GeV 0 constraint, $\sin^2\theta$ assumed
DESY–MIT	Spectrometer	Bremsstrahlung	3–7	π^+, π^-	10^5	Inelast. BG not excluded
SLAC (Bulos *et al.*)	Spectrometer	Quasi-monochromatic	9		1400	1 Constraint
SLAC (Anderson *et al.*)	Spectrometer	Bremmsstrahlung	6–18	p	Many	1 Constraint, missing mass technique; resolution not good enough to separate ρ and ω production.
CEA (Gladding *et al.*)	Spectrometer	Tagged γ beam	3–4.7	p		ρ and ω separated
CEA (Lanzerotti *et al.*)	Spectrometer	Bremsstrahlung	2–6	$\pi^+\pi^-$	Many	0 Constraint $\sin^2\theta$ assumed
SLAC–ST (Davier *et al.*)	Spectrometer	Bremsstrahlung	16	$\pi^+\pi^-$	493	0 Constraint
CIT (Barish *et al.*)	Spectrometer	Bremsstrahlung	6,12,18	ρ	Many	1 Constraint, missing mass no ρ, ω separation

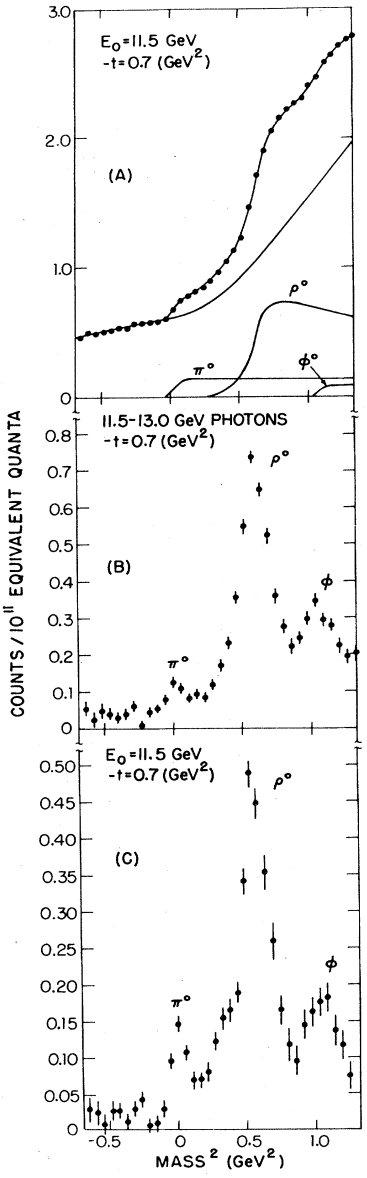

FIG. 67. (a) Measured proton yield for a peak bremsstrahlung energy of 11.5 GeV and for $t=-0.7$ GeV^2. The ordinate is the number of protons per hodoscope counter per 10^{11} E.Q. (equivalent quanta). The abscissa represents missing mass squared in GeV^2. The steps due to the onset of π^0, ρ^0, and ϕ production are clearly seen. The solid line through the data points represents a least squares fit to the data assuming π^0, ρ^0, and ϕ production in addition to the nonresonant background. The breakdown of the yield into separate contributions is also shown. (b) Subtracted proton yield curve in counts per hodoscope counter per 10^{11} E.Q. for photons between 13.0 and 11.5 GeV and for $t=-0.7$ GeV^2. This curve was obtained by subtracting the 11.5 GeV proton yield from the corresponding proton yield at 13 GeV end-point energy. The peaks due to π^0, ρ^0, and ϕ production are clearly seen. Because of multiple scattering of the recoil proton in traversing the target, the η is not clearly resolved from the ρ^0 peak. (c) Differential yield curve derived from integral curve in (a). Plotted is the difference, in counts per 10^{11} E.Q., between once-removed yield points versus missing mass squared. Note the subtracted yield curve in (b) (from Anderson *et al.*, 1970b).

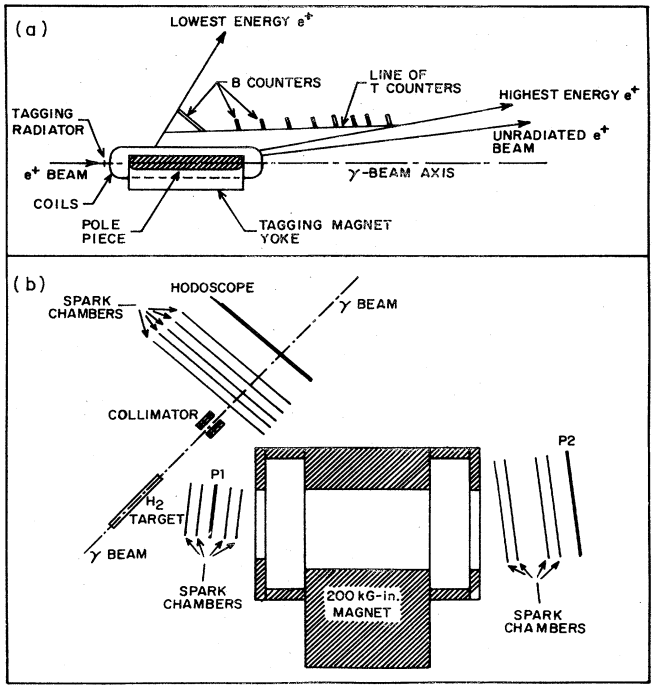

FIG. 68. Schematic diagram of the spectrometer used by Gladding *et al.* (1973) at the Cambridge Electron Accelerator. (a) Tagging system. (b) Spectrometer (from Gladding *et al.*, 1973).

near decay angles $\theta=\phi=90°$ actually measure

$$2(\rho^0_{11}+\rho^0_{1-1})(d\sigma/dt)\,.$$

[See "Angular Distribution of ρ^0 Decay" below (Sec. III.C.4.j).] Another difficulty is ruling out an inelastic component. The Cornell group (Berger *et al.*, 1972) has measured the inelastic contribution at 8.5 GeV in a separate experiment. They found for their running conditions that in the ρ mass region the contamination at small $|t|$ values is 5%-10% and increases to ~25% at $|t|=0.4$ GeV^2. The chief disadvantages of experiments in which only the recoil proton is observed are the uncertainties involved in unfolding the spectrum and the impossibility of measuring the angular distribution down to very small momentum transfer. Table IX summarizes all the reported experiments on rho photoproduction from hydrogen.

3. Treatment of the rho shape

A difficulty in the extraction of the rho cross section comes from the need to separate the observed mass spectrum into what is rho and what is background. Figure 69(a) shows a Dalitz plot for the reaction

$$\gamma p \to \pi^+ + \pi^- + p$$

for a photon energy of 9.3 GeV. These data were taken by the SLAC–Berkeley–Tufts group (Ballam *et al.*, 1973) using monochromatic photons produced by backscattering a laser beam by an electron beam. This plot shows a strong rho band and a relatively weak N^* band. It is clear that there is no problem due to the overlap of the bands since they are widely separated. Figure

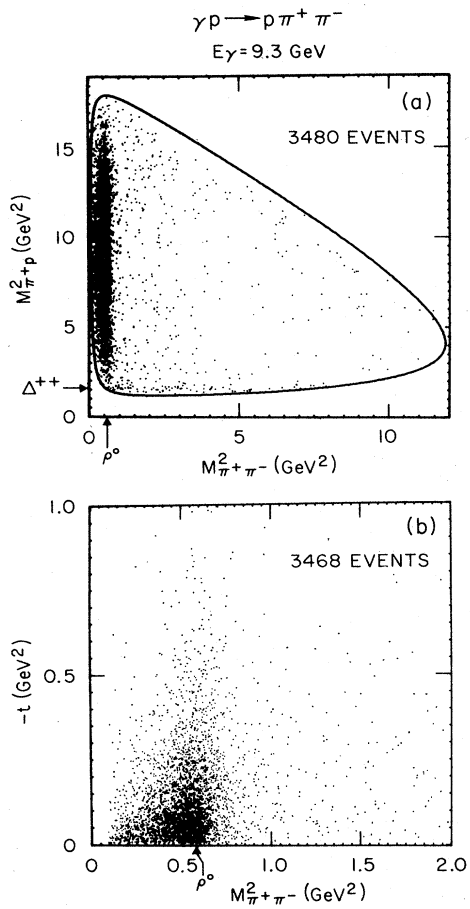

FIG. 69. Reaction $\gamma p \to p\pi^+\pi^-$ at 9.3 GeV. (a) Dalitz plot distribution for $|t| > 0.02$ GeV^2. (b) Chew–Low plot for $\pi^+\pi^-$ (from Ballam *et al.*, 1973).

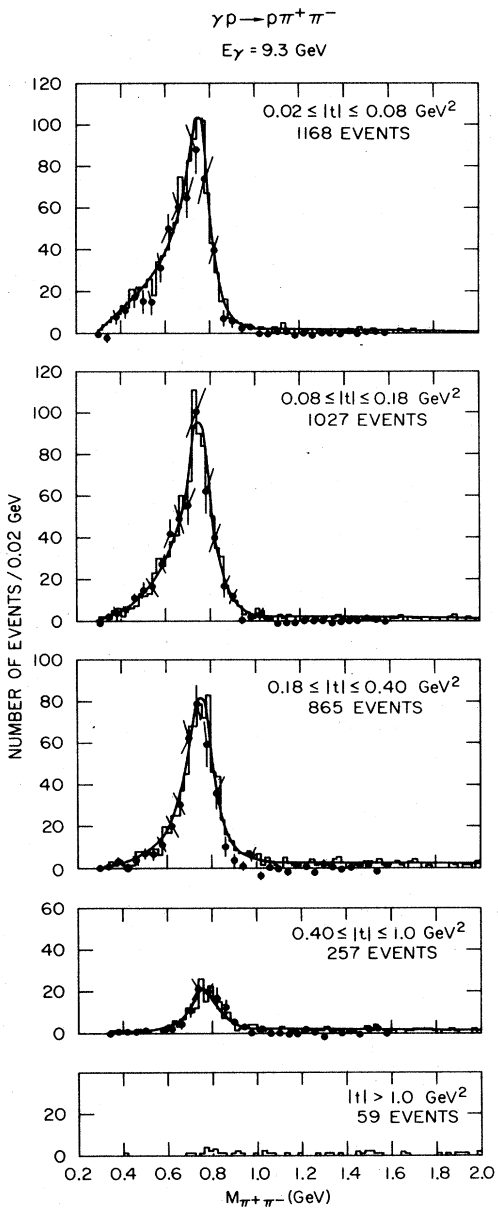

FIG. 70. Reaction $\gamma p \to p\pi^+\pi^-$ at 9.3 GeV. Distributions of the $\pi^+\pi^-$ mass for different t intervals. The helicity-conserving p-wave intensity, Π, is shown by the solid points. The curves give the result of a maximum-likelihood fit to the reaction using the Söding model (from Ballam *et al.*, 1973).

69(b) shows a Chew–Low plot for these same data. Figure 70 shows the projected mass plots for various ranges in momentum transfer. These plots show the major difficulties in the analysis of rho photoproduction. The mass peak is not symmetrical about the rho mass and the data cannot be represented as a simple Breit–Wigner plus a phase space background. In addition, there is a low-mass background which decreases as the momentum transfer increases.

The determination of the rho cross section from the mass spectrum has caused a lot of difficulty and produced a wide disparity in the reported cross sections. This problem is discussed at length in a recent paper by Spital and Yennie (1974a) and is reviewed in Sec. IV.C of this paper. It is generally believed that the background is chiefly due to a coherent "Drell mechanism" (Drell, 1960), as was first pointed out by Söding (1966). As argued by Bauer (1970, 1971) and Pumplin (1970), this background has the property of going to zero at the rho mass. Thus Spital and Yennie have suggested that the rho cross section be defined as

$$\frac{d\sigma}{dt} = \frac{1}{2}\pi\Gamma_\rho \left.\frac{d\sigma}{dt dm_{\pi\pi}}\right|_{m_{\pi\pi}=m_\rho}, \tag{3.30}$$

where m_ρ and Γ_ρ are taken from external sources such as colliding-beam measurements. The recommended procedure is to measure the whole spectrum, fit it appropriately, and use the fit to determine the cross section at the rho mass.

Two popular fitting functions to the entire spectrum are the p-wave Breit–Wigner with the Söding term added, and the p-wave Breit–Wigner with the Ross–Stodolsky modification which has the form

$$f_{BW}(m_\rho/m_{\pi\pi})^{n(t)}, \tag{3.31}$$

where the exponent $n(t)$ is variable. Fits of the first

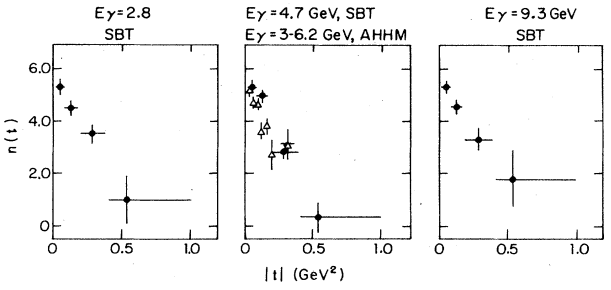

FIG. 71. Reaction $\gamma p \to p\rho^0$ at 2.8, 4.7, and 9.3 GeV. Fitted values for $n(t)$ using the parametrization $f_{BW}(m_\rho/m_{\pi^+\pi^-})^{n(t)}$ for the ρ^0 shape (from Wolf, 1972).

form are shown in Fig. 70. The fitted values of $n(t)$ to the same data using Eq. (3.31) are shown in Fig. 71. A similar behavior is observed at other energies.

There are several difficulties with the Spital–Yennie procedure. It does not prescribe a method for dealing with an incoherent background; it depends critically on values of m_ρ and Γ_ρ which are not well known; ρ-ω interference cannot be ignored; and it is sensitive to the absolute momentum calibration in the experiment. A further uncertainty at low t is given by the dependence of the minimum momentum transfer on the mass of the $\pi\pi$ system.

Various other definitions of the rho cross section are employed in the literature. Since it is not always feasible to convert these to the Spital–Yennie definition, we describe various other techniques which have been used; they have been used to obtain some of the results reported here.

(1) A "phenomenological Söding" ρ^0 cross section determined from the Spital–Yennie procedure [Eq. (3.30)] with $m_\rho = 770$ MeV and $\Gamma_\rho = 155$ MeV and using the fitting form (3.31). This agrees with the Spital–Yennie definition with a particular choice of the fitting function, and the results should be directly comparable to those derived from other fitting functions, e.g., using the Söding model.

(2) A so-called "Söding model" ρ^0 cross section derived from a fit of the Drell–Söding model to the data. This model includes helicity-conserving ρ production, two Drell diagrams, a rescattering term, and incoherently, Δ^{++} production and a phase space term. It is conventional (but not necessarily theoretically justified) to use the Ferrari–Selleri π-N form factors (Ferrari and Selleri, 1961) in conjunction with the Söding model. The fitting procedure removes the influence of the coherent background and gives a ρ^0 cross section which is proportional to the area of a ρ Breit–Wigner distribution integrated over the available phase space. This procedure is questionable because a formal integration over the Breit–Wigner form with the conventional mass-dependent p-wave width diverges. It would be better just to deal with the amplitude of the fitted curve, but in either case the cross section is still sensitive to the details of the Drell–Söding model.

(3) A "parametrization" ρ_0 cross section obtained by fitting the Dalitz plot to a matrix element consisting of phase space, Δ^{++}, and a ρ^0 whose shape is given by the form $f_{BW}(m_\rho/m_{\pi\pi})^{n(t)}$. Basically this procedure ignores the coherent background and yields a ρ^0 cross section through the assumption that all dipion pairs, other than those originating from Δ^{++} production and phase-space-like background, are from ρ^0 photoproduction.

(4) A model-independent cross section for p-wave $\pi\pi$ pairs called Π, which is determined from a moment analysis of the observed angular distribution for $\pi^+\pi^-$ pairs in the ρ^0 mass region.

Table X summarizes the fits of the form $(d\sigma/dt)|_{t=0} \times e^{Bt}$ made by the SLAC–Berkeley-Tufts (Ballam *et al.*, 1972; 1973) and Weizmann–SLAC–Tel Aviv (Eisenberg *et al.*, 1972) bubble chamber groups. The cross sections not only depend upon the method of analysis, but they vary significantly between the two groups. The discrepancies are disconcerting, and the differences in cross sections obtained by the two groups using the same method indicate that the quoted statistical errors do not adequately represent the real uncertainty in the determination of the cross sections.

Table XI summarizes the rho cross sections determined by the various groups, together with our best estimates of what the cross section would be using the Spital–Yennie procedure with $\Gamma_\rho = 155$ MeV, and in some cases correcting for the decay angular distribution using the density matrix elements measured in the bub-

TABLE X. Fits of the form $d\sigma/dt|_{t=0}e^{Bt}$ to the measurements of Ballam *et al.* (1972, 1973), Eisenberg *et al.* (1972a, 1972b) using different models to extract the rho cross section.

	$d\sigma/dt\|_{t=0}$ (μb GeV^{-2})			B (GeV^{-2})			
E_γ (GeV)	Söding	Param	Spital–Yennie	Söding	Param	Spital–Yennie	Group
2.0–2.5	143±14	138±20	215±24	5.4±0.5	5.9±0.7	6.7±0.9	Weizmann
2.5–3.0	170±17	179±27	219±30	6.4±0.6	7.7±0.9	7.5±1.1	
3.0–3.7	160±16	159±26	181±26	7.1±0.7	8.2±1.0	7.5±1.2	
3.7–4.7	100±10	130±13	125±12	6.5±0.5	7.5±0.6	6.8±0.7	
4.7–5.8	132±13	123±14	140±14	7.7±0.6	7.6±0.6	6.7±0.8	
6.8–8.2	102±10	104±11	107±12	7.1±0.6	7.5±0.6	7.0±0.8	
2.8	104±6	138±8	132±12	5.4±0.3	6.6±0.3	6.3±0.4	SBT
4.7	94±6	114±6	98±8	5.9±0.3	7.2±0.3	6.0±0.3	
9.3	86±5	95±4	79±4	6.5±0.2	7.3±0.2	6.3±0.3	

TABLE XI. Summary of determination of $\gamma p \to \rho^0 p$. The forward differential cross section $(d\sigma/dt)_{t=0}$ and the slope parameter B were determined from a fit of $d\sigma/dt$ to the form $(d\sigma/dt)_{t=0}e^{Bt}$. The total cross sections were determined in most cases by integration of the fitted curves.

Experiment	E_γ (GeV)	$-t$ Range (GeV^2)	Fit method	$(d\sigma/dt)_{t=0}$ (μb/GeV^2)	B (GeV^2)	$\sigma^T(\gamma\rho \to p\rho_0)$ (μb)
ABBHHM	2.5–3.5	0.05–0.5	$(M_\rho/M_{+-})^4$	147 ± 13	6.9 ± 0.4	21.3 ± 2.3
Erbe *et al.*	3.5–4.5			149 ± 19	8.1 ± 0.7	18.4 ± 2.8
(1968a)	4.5–5.8			130 ± 16	7.9 ± 0.7	16.5 ± 2.5
SLAC	2–4	$t_{\min} \to 0.5$	p-wave	178 ± 33	8.3 ± 1.0	19.2 ± 2.3
Davier *et al.*	4–8		Breit–Wigner	133 ± 34	8.9 ± 1.5	15.6 ± 1.7
(1970)	8–12			152 ± 65	11.1 ± 2.8	13.4 ± 3.6
SBT	2.8	0.02–0.4	$\Pi(t)$	144 ± 12	7.5 ± 0.6	19.2 ± 2.2
Ballam *et al.*			$(M_\rho/M_{+-})^{n(t)}$	138 ± 8	6.6 ± 0.3	20.9 ± 1.5
(1972)			Söding	104 ± 6	5.4 ± 0.3	19.3 ± 1.5
			Spital–Yennie	158 ± 13	6.3 ± 0.4	25.1 ± 2.6
	4.7	0.02–0.4	$\Pi(t)$	109 ± 8	7.6 ± 0.5	14.5 ± 1.4
			$(M_\rho/M_{+-})^{n(t)}$	114 ± 6	7.2 ± 0.3	15.8 ± 1.1
			Söding	94 ± 6	5.9 ± 0.3	15.9 ± 1.3
			Spital–Yennie	109 ± 8	6.0 ± 0.3	18.2 ± 1.6
Ballam *et al.*	9.3	0.02–0.4	$\Pi(t)$	84 ± 6	7.1 ± 0.4	11.8 ± 1.1
(1973)			$(M_\rho/M_{+-})^{n(t)}$	95 ± 4	7.3 ± 0.2	13.0 ± 0.7
			Söding	86 ± 5	6.5 ± 0.2	13.2 ± 0.9
			Spital–Yennie	94 ± 4	6.3 ±0.3	14.9 ± 1.0
Cornell[a]						
McClellan *et al.*	3.91	$t_{\min}$	Modified	211 ± 18		
(1971)	4.08		Spital–Yennie	188 ± 18		
	4.61		Corrected	175 ± 16		
	5.58	$t_{\min} - 0.23$	to $\Gamma = 155$ MeV	167 ± 8	8.50 ± 0.5	19.7 ± 1.5
	5.92			158 ± 11		
	6.53			136 ± 11		
	6.94			141 ± 13		
	7.40	$t_{\min} - 0.23$		135 ± 6	9.0 ± 0.6	15.0 ± 1.2
	8.24			134 ± 9		
Berger *et al.*						
(1972)	8.5	0.08–0.5		116 ± 7	6.9 ± 0.4	16.8 ± 1.1
DESY–MIT						
Alvensleben *et al.*						
(1969, 1970b)	3.0	$t_{\min}$	$(M_\rho/M_{+-})^4$	156.5 ± 11.5		
	3.6			132^{+22}_{-26}		
	4.2			127 ± 8		
	4.8			138 ± 5		
	5.4			125 ± 5		
	6.0			117 ± 3		
	6.4	$t_{\min}$	$(M_\rho/M_{+-})^4$	113 ± 5		
			Söding	119 ± 6		
	6.5	$t_{\min}$	$(M_\rho/M_{+-})^4$	117^{+4}_{-5}		
SWT						
Eisenberg *et al.*	2.0–2.5	0.06–0.4	$(M_\rho/M_{+-})^{n(t)}$	138 ± 20	5.9 ± 0.7	23.4 ± 4.4
(1972a)			Söding	143 ± 14	5.4 ± 0.5	26.5 ± 3.6
			Spital–Yennie	215 ± 24	6.7 ± 0.9	32.1 ± 5.6
	2.5–3.0		$(M_\rho/M_{+-})^{n(t)}$	179 ± 27	7.7 ± 0.9	23.3 ± 4.4
			Söding	170 ± 17	6.4 ± 0.6	26.6 ± 3.6
			Spital–Yennie	219 ± 30	7.5 ± 1.1	29.2 ± 5.9
	3.0–3.7		$(M_\rho/M_{+-})^{n(t)}$	159 ± 26	8.2 ± 1.0	19.4 ± 4.0
			Söding	160 ± 16	7.1 ± 0.7	22.5 ± 3.2
			Spital–Yennie	181 ± 26	7.5 ± 1.2	24.1 ± 5.2
	3.7–4.7		$(M_\rho/M_{+-})^{n(t)}$	130 ± 13	7.5 ± 0.6	17.3 ± 2.2
			Soding	100 ± 10	6.5 ± 0.5	24.6 ± 2.4
			Spital–Yennie	125 ± 12	6.8 ± 0.7	18.4 ± 2.6
	4.7–5.8		$(M_\rho/M_{+-})^{(t)}$	123 ± 14	7.6 ± 0.6	16.2 ± 2.2
			Söding	132 ± 13	7.7 ± 0.6	17.1 ± 2.2
			Spital–Yennie	140 ± 14	6.7 ± 0.8	20.9 ± 3.3
	5.8–8.2		$(M_\rho/M_{+-})^{n(t)}$	104 ± 11	7.5 ± 0.6	13.9 ± 1.8
			Söding	102 ± 10	7.1 ± 0.6	14.4 ± 1.9
			Spital–Yennie	107 ± 12	7.0 ± 0.8	15.3 ± 2.5

[a] In this experiment not the full ρ cross section, $d\sigma/dt$, but the quantity $2(\rho^0_{11} + \rho^0_{1-1})d\sigma/dt$ is measured (see text). The numbers given here for 5.58 and 7.40 GeV are the reported measurements and have not been corrected for the variation in density matrix elements; the cross section for 8.5 GeV has been corrected using the values of the density matrix elements determined by Ballam *et al.* (1973). $(2(\rho^0_{11} + \rho^0_{1-1}))$ was taken to be $(1 + 0.5t)$.

ble chamber experiments. It is our conviction that the Spital–Yennie procedure gives the most unambiguous measure of the rho, and when making comparisons between the different sets of data, we have used the cross section determined in this manner.

4. Experimental results

a. Hydrogen

Figures 72 shows differential cross sections at 4.7 GeV determined by the SLAC–Berkeley–Tufts (Ballam *et al.*, 1972) and ABBHHM (Erbe *et al.*, 1968) bubble chamber groups and the SLAC 1.6 GeV spectrometer group (Anderson *et al.*, 1970b). Figure 73 shows a comparison between data from the SLAC–Berkeley–Tufts group (Ballam *et al.*, 1973) and data from the Cornell (Berger *et al.*, 1972) and Ritson (Anderson *et al.*, 1970b) groups. The counter experiments give in the forward direction somewhat larger cross sections than are expected by simple extrapolation of the bubble chamber cross sections.

Figure 74 shows a plot of the forward cross section as a function of energy together with the cross section calculated using the quark model and $\hat{f}_\rho^2/4\pi = 2.18$. Part (a) shows data as listed in the publications by the various groups who have studied rho photoproduction. Part (b) shows the cross sections obtained from a reevaluation of the published data using the Spital–Yennie procedure with the assumption that $\Gamma_\rho = 155$ MeV. The data used for the quark model calculation are summarized in Table XII. The agreement of the data obtained by the

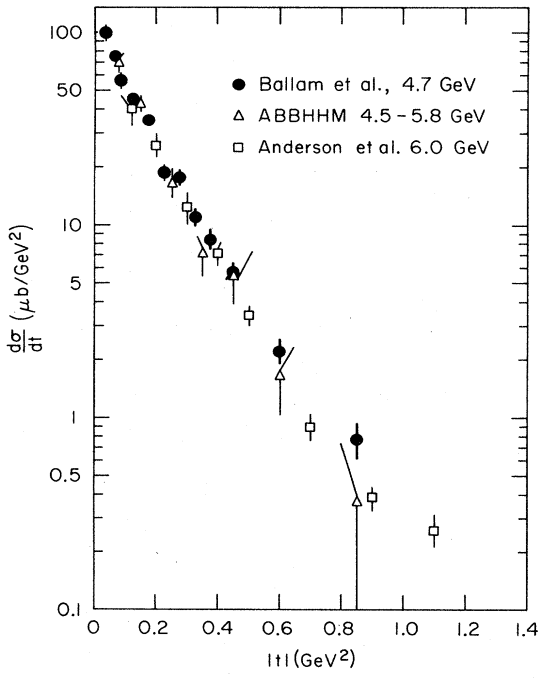

FIG. 72. The differential cross section for ρ^0 production: (●) at 4.7 GeV using the parametrization technique from Ballam *et al.* (1973); from the ABBHMM collaboration at 4.5–5.8 GeV (Erbe *et al.*, 1968a) (△); from Anderson *et al.* (1971) (□) at 6 GeV (figure from Ballam *et al.*, 1972).

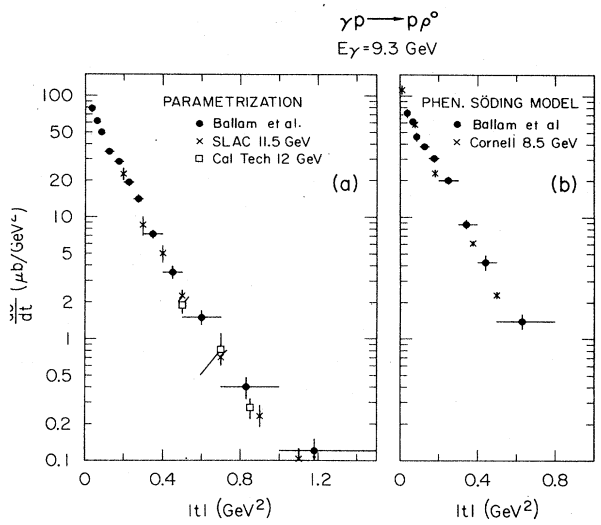

FIG. 73. Reaction $\gamma p \to p\rho^0$ at 9.3 GeV. Differential cross sections from (a) parametrization method and (b) phenomonological Söding model. The points labeled SLAC 4.5 GeV, Caltech 12 GeV, and Cornell 8.5 GeV are from Anderson *et al.* (1970), Barish *et al.* (1974), and Berger *et al.* (1972), respectively (figure from Ballam *et al.*, 1973).

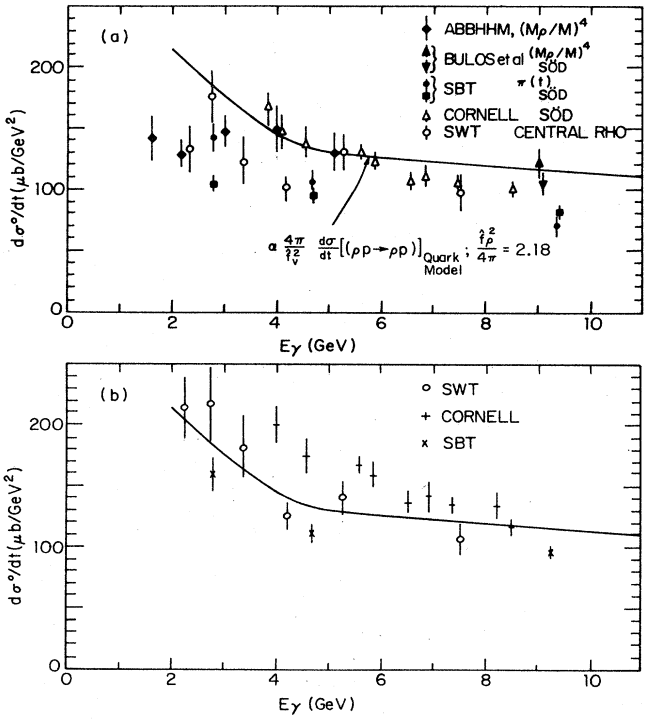

FIG. 74. The forward differential cross section for the reaction $\gamma p \to p\rho^0$. Part (a) shows the cross sections reported by the various groups using the several techniques that have been employed for determining the cross section. Part (b) shows the cross sections obtained when one uses the Spital–Yennie procedure with $\Gamma_\rho = 155$ MeV. The solid curve is, in both parts (a) and (b), the quark model-VMD prediction calculated using the measured pion-nucleon scattering cross sections with the assumption that $\hat{f}_\rho^2/4\pi = 2.18$. Part (a) follows a figure in Ballam *et al.*, 1973.

TABLE XII. A summary of the data used to calculate the ρ and ω photoproduction cross sections expected for the simple quark model plus vector-meson dominance. The cross sections are expressed in the form $A\exp(Bt+Ct^2)$, where t is in GeV^2. The strong interaction cross sections are in mb/GeV^2 and the photoproduction cross sections are in μb/GeV^2.

Reaction	Momentum (GeV)	Source of data	Real part	A	B	C
$\pi^+p\to\pi^+p$	3.0	Coffin *et al.* (1967)	−0.31	53.0	6.74	0.19
	4.0	Coffin *et al.* (1967)	−0.34	40.0	6.68	0.44
	8.5	Hartung *et al.* (1965)	−0.25	32.5	7.45	0.72
	16.7	Foley *et al.* (1963)	−0.18	31.5	8.73	2.55
$\pi^-p\to\pi^-p$	3.0	Coffin *et al.* (1967)	−0.16	53.0	7.80	1.04
	4.0	Coffin *et al.* (1967)	−0.16	46.1	7.95	1.28
	8.5	Hartung *et al.*	−0.12	38.1	8.54	1.84
	16.0	Foley *et al.* (1963)	−0.11	31.5	8.83	2.12
ρ^0p–ρ^0p	3.0			53.0	7.25	0.60
ωp–ωp	4.0			43.0	7.31	0.86
	8.5			35.5	7.99	1.28
	16.4			31.5	8.79	2.36
$\gamma p\to\rho^0p$	3.0	$\hat{f}_\rho^2/4\pi=2.18$		177.7	7.25	0.60
	4.0			144.0	7.31	0.86
	8.5			119.1	7.99	1.28
	16.4			105.6	8.79	2.36
$\gamma p\to\omega p$	3.0	$\hat{f}_\omega^2/4\pi=18.4$		20.7	7.25	0.60
	4.0			17.1	7.31	0.86
	8.5			14.2	7.99	1.28
	16.4			12.6	8.79	2.36

various groups is poor. The cross section determined by the Spital–Yennie procedure agrees satisfactorily with the quark–VMD model.

Figure 75 shows the total cross section obtained for ρ^0 photoproduction in the region below 12 GeV. Part (a) shows the data taken indiscriminately from the literature; part (b) shows only data obtained with the Spital–Yennie procedure with the assumption that $\Gamma_\rho=155$ MeV. The solid curve is the quark–VMD prediction with the assumption that $\hat{f}_\rho^2/4\pi=2.18$. The data obtained with the Spital–Yennie procedure are in quite good agreement with the quark–VMD prediction.

In an experiment carried out at FNAL with a 147 GeV muon beam incident on a 1.19 m liquid hydrogen target and a spectrometer based on the Chicago cyclotron magnet, Francis *et al.*, (1977) studied the muon production of rho mesons at high energy. With the assumption that $\sigma_\rho(Q^2)=\sigma_\rho(0)(1+Q^2/m_\rho^2)^{-2}$ they determined the photoproduction cross section by extrapolating measurements with $Q^2\leq 0.3$ (GeV)^2 to $Q^2=0$. Figure 76 shows a plot of their results, together with representative lower-energy data and vector-dominance-model predictions calculated using the pion-nucleon elastic cross sections (quark model) and the $\hat{f}_\rho^2/4\pi=2.18$.

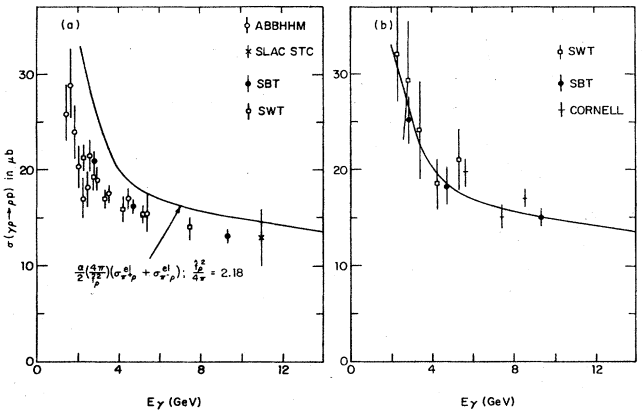

FIG. 75. The total cross section for the reaction $\gamma p\to p\rho^0$. Part (a) shows the cross section reported by the various groups using the several techniques that have been employed for determining the cross section. Part (b) shows cross sections obtained by using the Spital–Yennie procedure with $\Gamma_\rho=155$ MeV. The solid curve is the quark model–VMD prediction calculated using the measured pion-nucleon scattering cross section with the assumption that $\hat{f}_\rho^2/4\pi=2.18$. Part (a) follows a figure in Wolf, 1972.

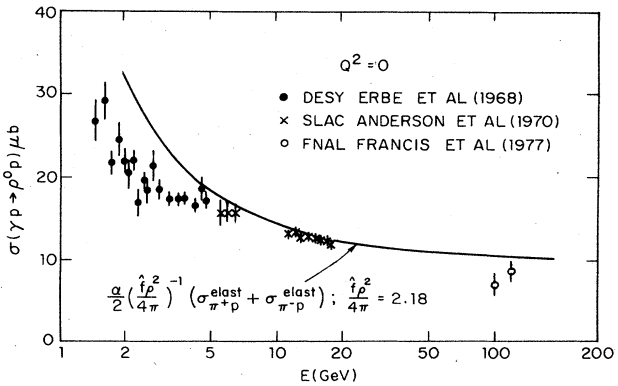

FIG. 76. A plot of the total rho photoproduction data obtained from extrapolation to $Q^2=0$ of ρ^0 muoproduction cross section obtained by Francis *et al.* (1977) together with representative lower-energy data and the quark model–VMD prediction. The predicted curve is an extension to high energy of the curve shown in Fig. 75.

b. Comparison of dσ/dt for hydrogen from different experiments

Given all these data the question arises what is the best value for the rho photoproduction cross section. There are clearly unresolved discrepancies in the measurements. The bubble chamber data become unreliable at low t; the counter data require at high t a correction due to the unmeasured density matrix elements. Part of this discrepancy can be removed by assuming the t dependence is not a simple exponential but is given by the more general expression

$$A\exp[Bt+Ct^2]. \tag{3.32}$$

The data from individual experiments are not sufficiently precise and do not extend over a sufficiently wide t range to obtain a meaningful fit with this generality. One suspects, however, that the cross section is very similar to that found in pion-nucleon scattering.

In order to display this relationship we have used the quark model–VMD expressions

$$\frac{d\sigma}{dt}(\gamma\rho^0\to\rho^0 p)=\alpha\left(\frac{4\pi}{\hat{f}_\rho^2}\right)\frac{d\sigma}{dt}(\rho^0 p\to\rho^0 p) \tag{3.33}$$

$$\frac{d\sigma}{dt}(\rho^0 p\to\rho^0 p)=\left[\frac{1}{2}\left(\frac{d\sigma}{dt}(\pi^+ p)\right)^{1/2}+\frac{1}{2}\left(\frac{d\sigma}{dt}(\pi^- p)\right)^{1/2}\right]^2 \tag{3.34}$$

together with a simple parametrization of the available pion–nucleon scattering data to obtain a reference cross section with respect to which the photoproduction data can be displayed. Table XII summarizes the data that were used for this calculation. For the pion data the optical point with the tabulated real part was added to the measured differential cross section and all the data

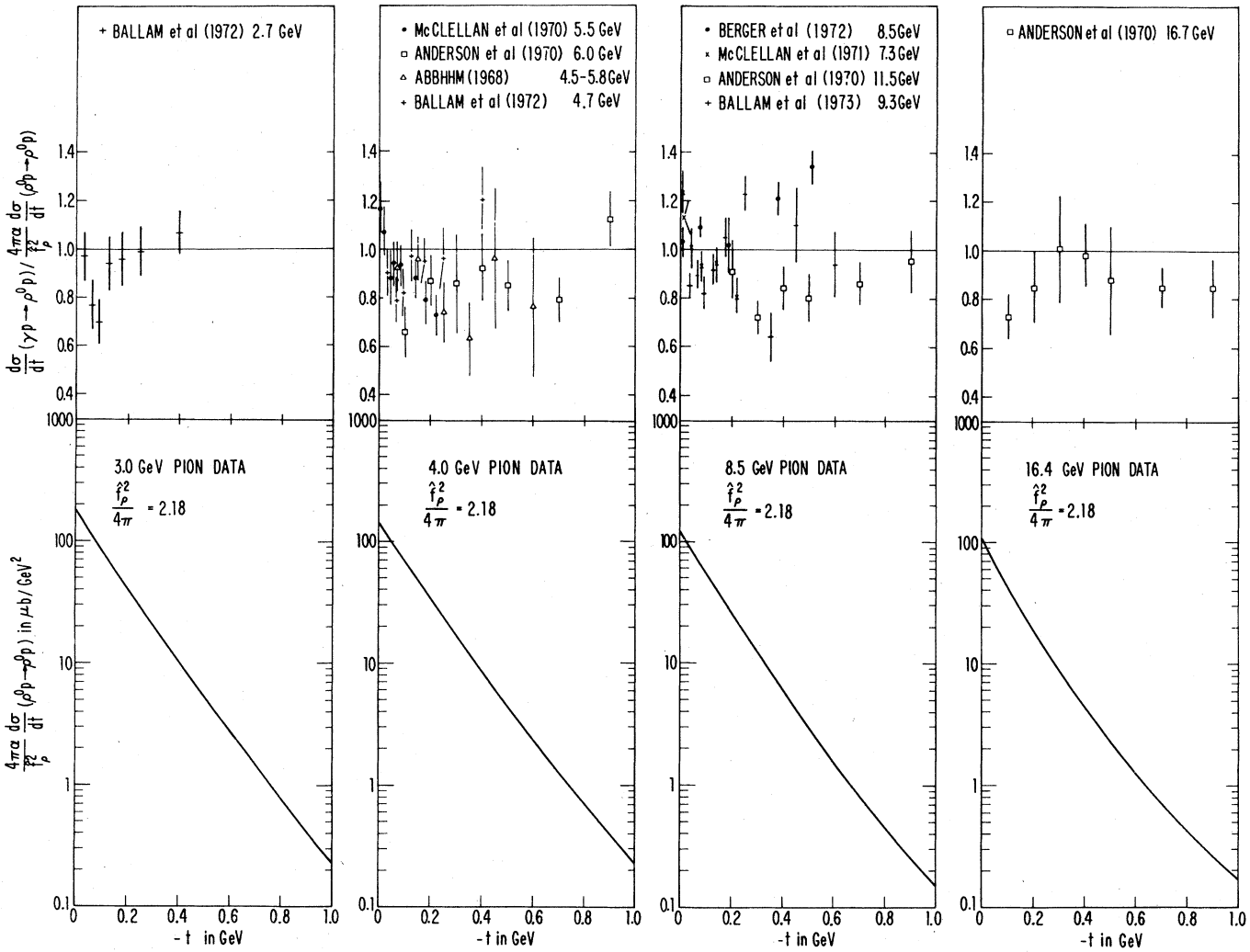

FIG. 77. A comparison of the experimental differential cross sections obtained by using, where possible, the Spital-Yennie procedure with Γ_ρ =55 MeV, with the quark model-VMD prediction based on the measured pion-nucleon cross section and assuming $\hat{f}_\rho^2/4\pi$=2.18. The data used as input to this calculation and the predicted cross sections are summarized in Table XII. The predicted energy dependence of the forward cross section (solid curve in Fig. 74) has been used to correct the measurements to the energy noted in the lower part of the figure.

in the restricted range $0.03\ (\mathrm{GeV})^2 < |t| < 0.8\ \mathrm{GeV}^2$ were fit to the expression given by Eq. (3.32). The real parts were taken from the analysis of Hendrick and Lautrup (1975). These fits were then used together with Eq. (3.34) to obtain the best expression of the form of Eq. (3.32) for the ρp differential cross section. This cross section was then used with Eq. (3.33) and with the assumption that $\hat{f}_\rho^2/4\pi = 2.18$ to calculate the ρ^0 photoproduction cross section.

Figure 77 shows the ratio of the measured cross sections obtained with the Spital–Yennie procedure with $\Gamma_\rho = 155$ MeV or from measurements with recoil protons to the quark model–VMD expressions. The calculated energy dependence of the forward cross section (solid line in Fig. 74) has been used to extrapolate the measurements to the closest of the energies at which the pion–nucleon data were used to determine the ρ^0-nucleon cross section. Figure 77 shows in a more immediately apparent manner the degree to which the cross sections determined by the different experiments agree and the extent to which they agree with the quark model–VMD prediction. At 2.7 GeV the measurements of Ballam *et al.* agree satisfactorily with the model. At 4 GeV, with the exception of the 5.5 GeV forward cross section reported by McClellan *et al.*, the data of the different groups agree satisfactorily with one another and with the VMD–quark model. At 8.4 GeV the agreement of the measurements of the different groups is satisfactory at low t, but not good at high t. The highness of the measurements by Berger *et al.* suggests that the correction made for the unmeasured density matrix elements was too large. At 16.7 GeV the data are somewhat low but not in serious disagreement with the quark model–VMD calculation. In general the data of the various groups agree with one another at the 15% level and with the quark model–VMD prediction. The quark–VMD model may in fact be a more accurate representation of the true cross section than the data.

c. Deuterium

Data on ρ^0 production from deuterons can be used to obtain information on the relative size of the isospin-0 and isospin-1 t-channel exchange contributions to the reaction $\gamma N \to \rho^0 N$. As described in Appendix B the differential cross section for production from deuterium, summed over all possible final states of the two-nucleon system, is given in the closure approximation by

$$d\sigma_d/d\Omega = 4\{|T_0|^2 \tfrac{1}{2}|1+F(4t)| + |T_1|^2 \tfrac{1}{2}|1-F(4t)| + |D(t)|^2 + |T_0|^2 G(t)\}. \quad (3.35)$$

Here $T_{0,1}$ is the amplitude for isospin-0, 1 exchange, $F(t)$ is the deuteron's elastic form factor, $D(t)$ is the single-scattering term arising from the spin-dependent portion of T, and $|T_0|^2\, G(t)$ is the Glauber correction. This form ignores the West correction. The predicted ratio of the deuterium-to-hydrogen cross section, assuming only isospin-0 exchange, is $R(t=0) = 3.75$. This estimate differs from that reported by McClellan *et al.* (1969b) due to use of a smaller value of σ_ρ (25 mb in place of 38 mb; see also McClellan *et al.*, 1971b). We estimate the theoretical uncertainty in R to be 0.05. The Cornell group (McClellan *et al.*, 1969b) found for the deuterium-to-hydrogen cross section at $t=0$ (averaged over energy), $R(t=0) = 3.26 \pm 0.10$. If the discrepancy between the experimental and theoretical values for R is attributed to the isospin dependence, then Eq. (3.35) gives

$$\mathrm{Re}\, T_0^* T_1 / |T_1 + T_0|^2 = 0.01 \pm 0.02 \quad (3.36)$$

from the incoherent part and then

$$\left|\frac{T_1}{T_1+T_0}\right|^2 = 0.11 \pm 0.06 \quad (3.37)$$

from the coherent part.

In a bubble chamber experiment, a Weizmann group (Eisenberg, 1974) measured the forward cross section for coherent photoproduction from deuterium by observing events in which there was a recoil deuteron. They then calculated from the ratio of this cross section to the proton cross section that

$$\frac{|T_1|^2}{|T_0|^2} = 0.06 \pm 0.16\,, \qquad \phi = 70^\circ \pm 30^\circ\,, \quad (3.38)$$

where ϕ is the phase angle between T_0 and T_1; this is consistent with the results obtained by the Cornell group.

In another bubble chamber experiment a DESY group (Hilpert *et al.*, 1970b) measured the $\gamma d \to \rho^0 d$ cross section over a t range $0.04 < |t| < 0.20\ \mathrm{GeV}^2$ for energies from 1.8 to 5.7 GeV. They then compared the measured cross sections for hydrogen and deuterium and obtained a value for $|T_1/T_0|^2$ consistent with that of the Cornell group. This group (Hilpert *et al.*, 1970b) also measured the cross section for the reaction $\gamma n \to \rho^- p$ and found, for energies above 3.5 GeV, $\sigma(\gamma n \to \rho^- p) = (1.0 \pm 0.4)\mu\mathrm{b}$. Then with the assumption that the ρ and A_2 exchange contribu-

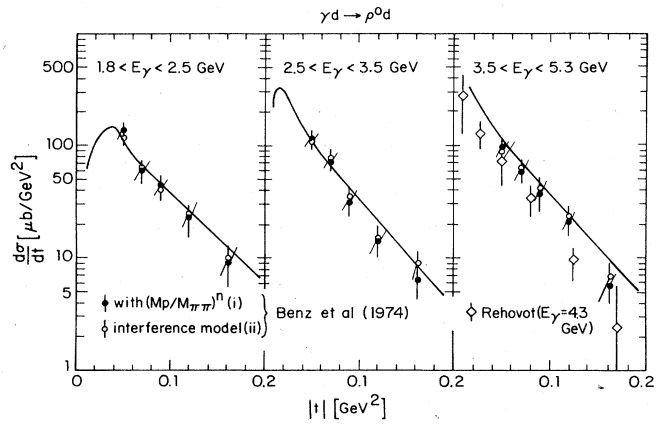

FIG. 78. Differential cross sections determined by Benz *et al.* (1974) for the reaction $\gamma d \to \rho^0 d$. The black dots and open circles refer to two different methods for determining the rho cross section. Also shown are the data of Eisenberg *et al.* (1972b). The curves are predictions from the reaction $\gamma p \to \rho^0 p$ assuming equal ρ^0 production amplitudes for neutrons and protons (from Benz *et al.*, 1974).

TABLE XIII. Results of fitting an exponential $A\exp(Bt)$ to the differential cross sections $d\sigma/dt|_{t=0}$ (corrected for finite-width effects) for coherent ρ^0 production $\gamma d \to \rho^0 d$, in the t range $0.04 < |t| < 0.20$ GeV^2. The models refer to different methods for fitting to the mass spectrum and determining the rho cross section (from Benz *et al.*, 1974).

E_γ (GeV)	1.8–2.5	2.5–3.5	3.5–5.3	1.8–5.3	Model
A (μb GeV^{-2})	467 ± 144	541 ± 148	335 ± 77	410 ± 67	$(M_\rho/M_{\pi\pi})^{n(t)}$ + phase space
B (GeV^{-2})	25.5 ± 3.9	29.5 ± 3.2	24.2 ± 2.5	25.5 ± 1.8	
A (μb GeV^{-2})	468 ± 108	470 ± 120	312 ± 75	383 ± 60	Diffractive amplitude + Drell
B (GeV^{-2})	23.8 ± 2.7	26.5 ± 3.1	22.6 ± 2.8	23.7 ± 1.8	one-pion exchange terms
A (μb GeV^{-2})	481 ± 111	501 ± 129	327 ± 83	402 ± 65	Alternate definition of resonant
B (GeV^{-2})	24.0 ± 2.7	26.9 ± 3.2	22.9 ± 2.9	24.0 ± 1.8	part of the amplitude

tions to ρ^- production do not tend to cancel, they estimated that

$$\frac{|T_1|^2}{|T_0|^2} < 0.05 . \tag{3.39}$$

Benz *et al.* (1974) studied the reaction $\gamma d \to \rho^0 d$ at DESY using the 85 cm deuterium bubble chamber and a 5.5 GeV bremsstrahlung beam. In their analysis they restricted themselves to three-prong events with a visible deuteron track. They found 1061 events in the momentum-transfer photon energy range $0.04 < |t| < 0.20$ (GeV)^2 and $0.9 < E_\gamma < 5.3$ GeV, respectively. Figure 78 shows the $d\sigma/dt$ obtained with the different fits to the mass distribution together with the data of Eisenberg *et al.* (1972b). The kinematic turnover at low $|t|$ arises from the fact that for fixed E_γ the kinematically possible maximum value of $M_{\pi^+\pi^-}$ depends on t, thus producing a variable cutoff in the mass distribution of a wide resonance like the rho. Correcting for this cutoff and fitting the data to the exponential form, $A\exp(Bt)$ yields the values of A and B summarized in Table XIII. With the assumption that $d\sigma/dt$ is exponential throughout and with the correction for the finite width effect, the average total cross section for the region $1.8 < E_\gamma < 5.3$ GeV is (13.2 ± 2) μb.

Benz *et al.* (1974) also used their deuterium data to study the reaction $\gamma n \to \rho^- p$. Figure 79 shows a plot of the total cross section as a function of energy; Fig. 80 shows the measured differential cross section for $1.2 < E_\gamma < 2.5$ GeV. The first point at $|t| = 0.084$ GeV^2 is corrected by + 20% for kinematic inaccessibilities due to the mass dependence of the minimum momentum transfer.

Benz *et al.* (1974) used their deuterium data to set a limit on the $I = 1$ amplitude for rho photoproduction. With the assumption that $\mathrm{Re}T_0/\mathrm{Im}T_0 = -0.20$ and using the data of Erbe *et al.* (1968) for $d\sigma/dt(\gamma p \to \rho^0 p)$ they found

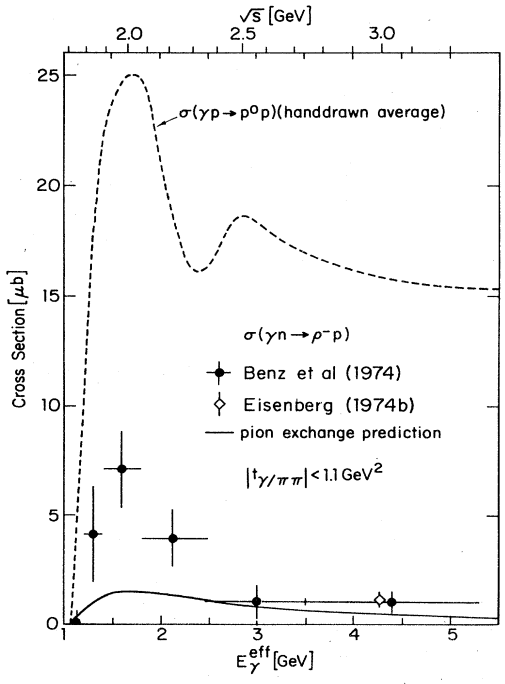

FIG. 79. Total cross section for the reaction $\gamma n \to \rho^- p$, with the restriction $|t| < 1.1$ GeV^2 as a function of E_γ^{eff}. The full curve shows the pion exchange prediction for $\gamma n \to \rho^- p$; the dashed curve shows the qualitative energy behavior of $\sigma(\gamma p \to \rho^0 p)$ (from Benz *et al.*, 1974).

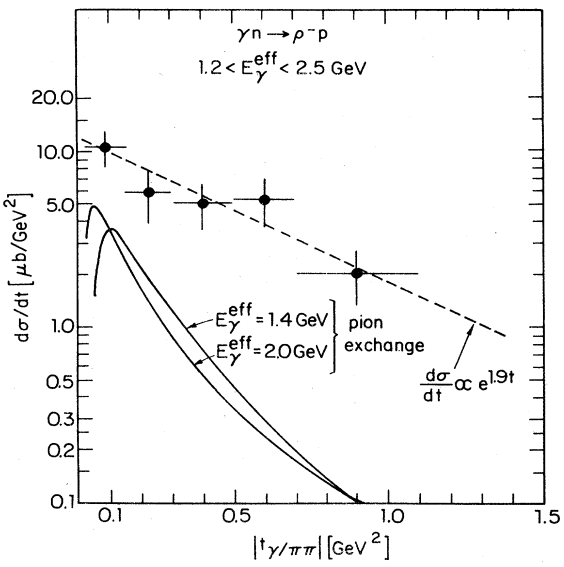

FIG. 80. Differential cross section for the reaction $\gamma n \to \rho^- p$ in the E_γ^{eff} interval $1.2 < E_\gamma^{\mathrm{eff}} < 2.5$ GeV. The full curves show the pion exchange prediction. The dashed line is an exponential with a slope of 1.9 GeV^{-2} (from Benz *et al.*, 1974).

that

$$R \equiv \frac{d\sigma/dt(\gamma d \to \rho^0 d)\text{cal}}{d\sigma/dt(\gamma d \to \rho^0 d)\text{meas}} = \frac{|T_0 + T_1|^2}{|T_0|^2}$$
$$= 1 + \frac{|T_1|}{|T_0|} 2\cos\Delta\Phi + \frac{|T_1|^2}{|T_0|^2} \quad (3.40)$$

was for the energy range 1.8 to 5.3 GeV consistent with unity to 10%. They then concluded that if $\Delta\Phi > 0$, $|T_1|/|T_0| < 0.3$ within one standard deviation for the energy range $1.8 < E_\gamma < 5.3$ GeV. With the assumption that ρ and A_2 exchange in ρ^- production do not effectively cancel they estimated from their ρ^- data for $E_\gamma > 3.5$ GeV

$$\frac{\sigma(\gamma p \to \rho^0 p)|_{I=1}}{\sigma(\gamma p \to \rho^0 p)_{\text{Total}}} \leq 0.05 . \quad (3.41)$$

In summary, all the measurements are in agreement with one another and indicate that the isospin-1 t-channel exchange contribution to ρ^0 photoproduction is small. The data are not sufficiently precise, however, to rule out an amplitude for isospin-1 exchange that is 25% of the isospin-0 exchange amplitude.

d. Complex nuclei

The first measurements of rho production from complex nuclei were carried out at the Cambridge Electron Accelerator by Lanzerotti *et al.* (1965, 1968) using the previously described spectrometer and a photon beam. They used data for H, C, Al, and Cu to demonstrate the diffractive, coherent nature of rho production and to show its simple relationship to pion-nucleon scattering. The realization by Drell and Trefil (1966) that such data could be used to determine the rho-nucleon total cross section stimulated a whole series of measurements. The early literature is somewhat confused by inadequately reported data and analyses, and we recommend Sec. IV.C as a guide.

In 1967 Asbury *et al.* (1967a) used their double-arm magnetic spectrometer system at DESY to measure rho production from Be, C, Al, Cu, Ag, and Pb for rho momenta of 2.8, 3.04, 3.5, and 4.5 GeV and peak incident bremsstrahlung energies 4.35 and 6.02 GeV. They used the model of Drell and Trefil (1966) to fit the A dependence with the nuclear radius parameter r_0 in the expression $R = r_0 A^{1/3}$ and the rho-nucleon total cross section as free parameters. With this relatively crude model, they obtained $r_0 = (1.29 \pm 0.04)F$ and $\sigma_\rho = (31.3 \pm 2.3)$ mb. They also demonstrated that the data showed the same energy dependence as the total $\pi^- p$ cross section.

The same year, Blechschmidt *et al.* (1967) reported measurements made at DESY of rho production from H, C, and Al at photon energies between 3.2 and 4.9 GeV. They used other data to determine the total ρ-nucleus cross sections and found an A dependence somewhere between opacity and transparency.

Asbury *et al.* (1968) subsequently used their apparatus to make more detailed measurements on C, Cu, and Pb nuclei. They showed that their data agreed with the diffraction production model and then used it to determine $\hat{f}_\rho^2/4\pi$ from the expression

$$\left.\frac{d\sigma(\gamma A \to \rho^0 A)}{dt}\right|_{t=0} = \frac{1}{4}\frac{k_\gamma}{p_\rho}\frac{\alpha}{\hat{f}_\rho{}^2}\sigma_T{}^2(\rho A \to \rho A) . \quad (3.42)$$

Using the optical-model analysis reported earlier, they found $\hat{f}_\rho{}^2/4\pi = 1.76 \pm 0.40$.

The next study of ρ^0 photoproduction from complex nuclei was reported by McClellan *et al.* (1969a). They used the Cornell 10 GeV synchrotron and the pair spectrometer system described earlier to measure rho production from C, Mg, Cu, Ag, Au, and Pb for a 6 GeV photon energy. McClellen *et al.* used these data together with their H and D data in conjunction with a generalization of the Drell–Trefil model to determine σ_ρ and $\hat{f}_\rho^2/4\pi$. They found for their best results $\sigma_{\rho N} = (38 \pm 3)$ mb, $\hat{f}_\rho^2/4\pi = 4.40 \pm 0.60$. These values disagreed with the results of Asbury *et al.* and with the results expected from simple theoretical models.

At roughly the same time Bulos *et al.* (1969) used at SLAC their wire chamber spectrometer system to study rho production from Be, C, Al, Cu, Ag, and Pb in the energy range from 5 to 16 GeV. From an optical-model analysis of the data they found $\sigma_\rho = 31 \pm 4$ mb and $f_\rho^2/4\pi = 4.82 \pm 0.04$. This value for $\hat{f}_\rho^2/4\pi$ seemed to support the analyses of McClellan *et al.*; the value of σ_ρ supported Asbury *et al.*

This disagreement provoked a great deal of controversy. It was pointed out by Swartz and Talman (1969) that all the analyses had neglected the real part of the rho-nucleon amplitude and were therefore suspect. The importance of the real part was noted also by Gottfried and Julius (1970).

Behrend *et al.* (1970a), at the 10 GeV Cornell synchrotron, then used a 9.15 GeV bremsstrahlung beam and a spectrometer system based on a large-aperture magnet with a magnetostrictive readout wire spark chamber array behind the magnet to measure rho production from Be, C, Al, Cu, Sn, W, and Pb targets. They used an optical-model analysis with the inclusion of a real part for the rho-nucleon scattering amplitude to determine from the 0° cross sections σ_ρ and $\hat{f}_\rho^2/4\pi$. They found $\sigma_\rho = (29.2 \pm 2.5)$ mb and $\hat{f}_\rho^2/4\pi = 2.48 \pm 0.48$. They attributed the difference between their results and the earlier measurements to the inclusion of a real part and a small hydrogen cross section.

Stimulated by the disagreement, effort was made at both DESY and Cornell to make more definitive measurements and to carry out a more definitive analysis. At DESY Alvensleben *et al.* (1970a, 1970b) used their magnetic spectrometer to measure rho photoproduction from Be, C, Al, Ti, Cu, Ag, Cd, In, Ta, W, Au, Pb, and U. The measurements covered 20 intervals in dipion mass from 400 to 1000 MeV, six intervals in momentum from 4.8 to 7.2 GeV, and 20 intervals in transverse momentum from $t_{\min}$ to -0.04 GeV^2. They also measured hydrogen (Alvensleben *et al.*, 1969) at forward production angles with incident photon energies between 2.6 and 6.8 GeV and in the dipion mass region from 500 to 1000 MeV. From an extensive optical-model analysis taking α_ρ, the ratio of the real to imaginary ρ^0-nucleon amplitude, equal to -0.2 they found

$$\sigma_\rho = (26.7 \pm 2.0) \text{ mb} \quad (3.43a)$$

$$d\sigma/dt\,|_{t=0} \text{ (extrapolated to } H) = (118 \pm 6)\mu\text{b/GeV}^2 \quad (3.43b)$$

$$\hat{f}_\rho^2/4\pi = 2.28 \pm 0.40 \quad (3.43c)$$

$$R=(1.12\pm0.02)A^{1/3}\ . \tag{3.43d}$$

At Cornell, McClellan *et al.* (1971b) extended their measurements and refined the analysis of their data. They used their spectrometer to take detailed mass spectra at $\langle E_\rho\rangle=4.4$ GeV for D, C, and Pb, at $\langle E_\rho\rangle=6.5$ GeV for C and Cu, and at $\langle E_\rho\rangle=8.8$ GeV for C, Cu, and Pb. They reported cross sections near the "peak" of the rho photoproduction for D, C, Mg, Ag, and Pb at 6.1, 6.5, 8.8 GeV, for Be and Au at 6.1 GeV, and for In at 8.8 GeV. For their optical-model analysis they used nuclear radii determined by nuclear or electron scattering experiments and took $\hat{f}_\rho^2/4\pi$ and σ_ρ as free parameters with the real part α_ρ as an adjustable parameter. For $\alpha_\rho=-0.24$ and the nuclear radii taken from electron scattering experiments they found

$$\sigma_\rho=(25.9\pm1.0)\text{ mb} \tag{3.44a}$$

$$d\sigma/dt\,|_{t=0}=(106\pm11)\mu\text{b/GeV}^2 \tag{3.44b}$$

$$\hat{f}_\rho^2/4\pi=2.52\pm0.08\ . \tag{3.44c}$$

The agreement with the results of Alvensleben *et al.* is satisfactory.

Coddington *et al.* (1975) used at Daresbury a tagged photon beam and an optical spark chamber system to study rho production from Be, C, Al, Cu, Ag, and Au in the 2.75 to 4.35 GeV energy range. There was no magnetic analysis of the hadrons, and three banks of heavy-plate optical spark chambers were used to separate electrons from hadrons. With this apparatus the low-mass background was much greater for the heavy nuclei than for the low-mass nuclei; this is the opposite situation of that found in the spectrometer experiments. They analyzed the data both in terms of the total cross section $\sigma(\gamma A\to\rho A)$ and in terms of the forward differential cross sections $(d\sigma/dt)_{\theta=0}(\gamma A\to\rho A)$. With the assumption that $\alpha_\rho=-0.2$ they found

$$\sigma_\rho=(22.5\pm2.7)\text{ mb} \tag{3.45a}$$

$$d\sigma/dt\,|_{\theta=0}(\gamma p\to\rho p)=(72.7\pm8)\mu\text{b/GeV}^2 \tag{3.45b}$$

$$\hat{f}_\rho^2/4\pi=2.60\pm0.48\ . \tag{3.45c}$$

These values for σ_ρ and $d\sigma/dt\,|(\gamma p\to\rho p)$ differ considerably from the other reported measurements. They can not be explained by the estimated systematic uncertainty of $\pm10\%$. This experiment is not as clean as the DESY and Cornell experiments and thus is suspect.

Section IV.C of this paper reports a reanalysis of the DESY and Cornell experiments which was carried out by Yennie and Spital. It is in substantial agreement with the latest DESY and Cornell analyses, and we shall use it to extract ρ^0 parameters for future reference.

There is a moral to this saga of rho photoproduction from complex nuclei. Much of the uncertainty and some of the duplication in measurement could have been eliminated if the early data and analyses had been more completely reported so that the discrepancies could have been localized. It was particularly puzzling why the two DESY–MIT experiments, which supposedly yielded the same cross sections gave compatible results for the ρ parameters with two quite different optical-model analyses. As the story unfolded, some people felt that the information presented was so sketchy that the results of the experiments were strongly prejudiced by existent theory.

e. ρ-ω interference

A feature which somewhat complicates the analysis of the rho photoproduction experiments is ρ-ω interference. The ω has a small amplitude to decay into $\pi^+\pi^-$ and the presence of this amplitude distorts the shape of the mass spectrum in the region of the rho. This effect can be taken into account by adding a term for the ω contribution to the pion-pair production amplitude, amounting to a replacement of the ρ propagator $(m^2-m_\rho^2+im_\rho\Gamma_\rho)^{-1}$ by

$$\frac{1}{m^2-m_\rho^2+im_\rho\Gamma_\rho}+\frac{\xi e^{i\alpha}}{m^2-m_\omega^2+im_\omega\Gamma_\omega}\ . \tag{3.46}$$

Four experimental groups have studied this phenomenon in photoproduction by carefully measuring the shape of the mass spectrum of the rho. Figure 81 shows the mass spectrum observed by the Daresbury group (Biggs *et al.*, 1970b) for ρ photoproduction from carbon. From a detailed analysis in which the rho shape was given by the Jackson form of the p-wave Breit–Wigner with the Ross–Stodolsky modification, they found

$$\xi=0.0097\pm0.008\ , \tag{3.47a}$$

$$\alpha=(104.0\pm5.1)^\circ\ , \tag{3.47b}$$

$$\Gamma_{\omega\to2\pi}=\left(0.091^{+0.031}_{-0.025}\right)\text{MeV} \tag{3.47c}$$

$$\Gamma(\omega\to2\pi)/\Gamma(\omega\to3\pi)=\left(0.80^{+0.28}_{-0.22}\right)\%\ . \tag{3.47d}$$

A Rochester-Cornell (Behrend *et al.*, 1971b) group used a spectrometer system consisting of a single bending magnet and a set of wire spark chambers with magnetostrictive readout to measure the interference between ρ^0 and ω in the 2π mode from carbon, aluminum,

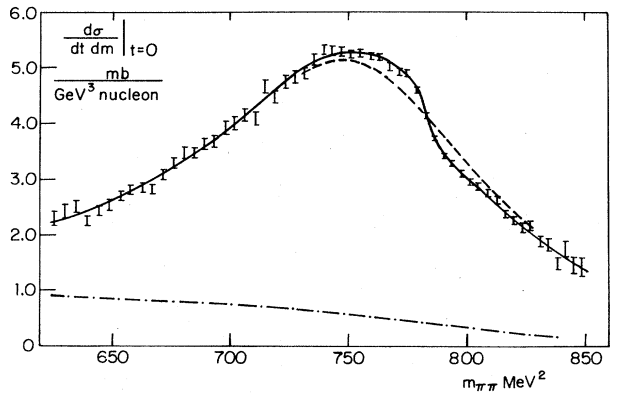

FIG. 81. Differential cross section $d\sigma/dtdm|_{t=0}$ for the reaction $\gamma C\to C\pi^+\pi^-$ in mb GeV^{-3} nucleon^{-1} as a function of invariant mass determined in measurements by Biggs *et al.* (1970b). The solid line is the best fit to the data using a model which incorporates $\rho\omega$ interference. The dashed line shows the same fit with $\xi=0$ (no ω contribution) and the chain line shows the incoherent background (from Biggs *et al.*, 1970b).

and lead. They concluded that there was no dependence on the target and

$$\xi \approx 0.013 \ , \tag{3.48a}$$

$$\Gamma(\omega \to 2\pi)/\Gamma(\omega \to 3\pi) = (2.8 \pm 0.6)\% \ , \tag{3.48b}$$

$$\alpha = (63 \pm 16)^\circ \ . \tag{3.48c}$$

The DESY–MIT (Alvensleben *et al.*, 1971a) group also used their spectrometer system to study the ρ-ω interference in dipion photoproduction in the energy range 5–7 GeV from hydrogen, carbon, and lead. Figure 13 shows their mass distribution for H at 6.4 GeV. They found

$$\xi = 0.0106 \pm 0.0012 \ , \tag{3.49a}$$

$$\Gamma(\omega \to 2\pi)/\Gamma(\omega \to 3\pi) = (1.36 \pm 0.33)\% \ , \tag{3.49b}$$

$$\alpha = (96 \pm 15)^\circ \ . \tag{3.49c}$$

In a low-statistics experiment carried out with a hydrogen bubble chamber, Moffeit *et al.* (1971) verified the ρ-ω mixing and obtained results that agreed with those of Biggs *et al.* for carbon. Considering the difficulty of the experiments, the agreement is surprisingly good.

f. Leptonic decay of the ρ^0

The initial suggestion that the ρ^0 meson dominates the pion form factor stimulated many experiments to measure the leptonic branching ratio $\Gamma(\rho \to l^+ l^-)/\Gamma(\rho \to all)$ in order to determine the γ-ρ coupling constant. Table XIV summarizes the reported measurements using hadron or photon beams; it does not include the colliding-beam measurements. The early experiments did not have sufficient resolution to study the ρ-ω interference and in the analysis it was usually necessary to make some assumption about the ω contribution.

g. Real part of production amplitude

A DESY–MIT (Alvensleben *et al.*, 1970d, 1971d) group measured the phase of the ρ photoproduction amplitude by observing the large-angle electron pairs from the reaction $\gamma + \mathrm{Be} \to \mathrm{Be} + e^+ + e^-$ in the e^+e^- invariant mass region $610 < M_{e^+e^-} < 850$ MeV/c^2. The measurement depends upon the interference between the real Bethe–Heitler amplitude and the Compton amplitude in which the ρ decays to an electron-positron pair. Since this interference vanishes in the symmetric case, one measures it by observing asymmetric electron–positron pairs. The DESY–MIT group found that the phase of the photoproduction amplitude of the ρ meson at 4.1–6.1 GeV deviated from pure imaginary by $(11.8 \pm 4.40)^\circ$. This corresponds to a ratio of the real to imaginary ρ-nucleon amplitude of $\alpha_\rho = -0.2 \pm 0.1$. A similar measurement using a carbon target with 4 GeV photons was carried out by the Daresbury group (Biggs *et al.*, 1971). They found $\alpha_\rho = -0.30 \pm 0.12$. These measurements are discussed further in Sec. IV.E.

h. ω-ρ relative phase

The Daresbury group (Biggs *et al.*, 1970a) also measured the electron-positron mass spectrum in the process $\gamma + \mathrm{C} \to e^+ + e^- + \mathrm{C}$ in the invariant mass region between 675 and 850 MeV/c^2 as a means of determining the relative phase of the ρ-ω photoproduction amplitudes. Figure 82 shows a plot of the observed spectrum. The mean photon energy was 4.2 GeV. From a detailed analysis they found

$$\hat{f}_\rho^2/4\pi = 2.00^{+0.48}_{-0.40} \tag{3.50a}$$

$$\hat{f}_\omega^2/4\pi = 14.0 \pm 4.8 \tag{3.50b}$$

$$\phi_{\omega\rho} = \left(100^{+38}_{-30}\right)^\circ \ . \tag{3.50c}$$

In a similar experiment carried out with a Be target at 5.1 GeV, the DESY–MIT group (Alvensleben *et al.*, 1970c, 1971c) obtained the spectrum shown in Fig. 83. From a detailed analysis they found

$$\phi_{\omega\rho} = (41 \pm 20)^\circ$$
$$\hat{f}_\omega^2/\hat{f}_\rho^2 = 9.4^{+2.6}_{-1.6} \ . \tag{3.51}$$

TABLE XIV. A summary of the measurements of the leptonic branching ratio for the ρ made using hadron or photon beams as a source of rho mesons.

Group	Experiment	$10^5 \times \frac{\Gamma(\rho \to l^+ l^-)}{\Gamma(\rho \to \mathrm{all})}$	Comments
Zdanis *et al.* (1965) (AGS)	$\pi^- + p \to e^+ + e^-$	5.0^{+6}_{-3}	Calculated ω correction
de Pagter *et al.* (1966) (CEA)	$\gamma + C \to \mu^+ + \mu^-$	$3.3^{+1.6}_{-0.7}$	Assumed ω negligible
Khachaturyon *et al.* (1967) (Dubna)	$\pi^- + p \to e^+ + e^-$	3.9 ± 1.2	Calculated ω correction
Hyams *et al.* (1967) (CERN)	$\pi^- + p \to \mu^+ + \mu^-$	$9.7^{+2.0}_{-2.3}$	ω excluded by mass selection
Wehmann *et al.* (1966, 1969) (AGS)	$\pi^- + (\mathrm{Fe\ or\ } C) \to \mu^+ + \mu^-$	5.6 ± 1.1	Calculated ω correction
Asbury *et al.* (1967b) (DESY)	$\gamma + C \to e^+ + e^-$	6.5 ± 1.4	Assumed ω negligible
Rothwell *et al.* (1969) (CEA)	$\gamma + C \to \mu^+ + \mu^-$	8.2 ± 1.6	Assumed ω negligible
Biggs *et al.* (1970) (DNPL)	$\gamma + C \to e^+ + e^-$	$4.9^{+1.2}_{-1.5}$	Good resolution ρ-ω separation

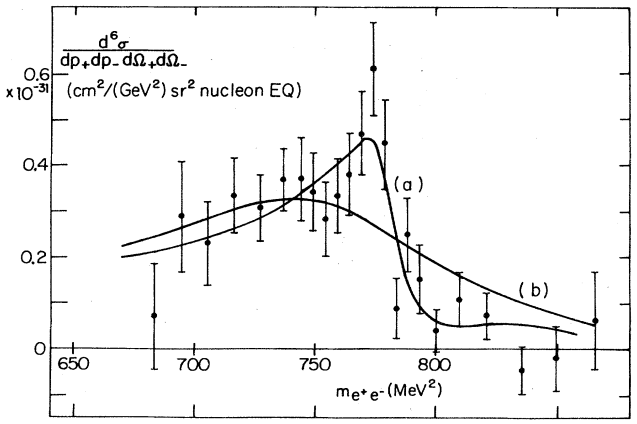

FIG. 82. Differential cross section for the reaction $\gamma C \rightarrow e^+e^-C$ determined in measurements by Biggs *et al.* (1970a). The curves shown in the figure are best fits to the data assuming (a) $\rho-\omega$ interference and (b) no ω contribution (from Biggs *et al.*, 1970a).

The reason for the discrepancy between the two measurements of $\phi_{\omega\rho}$ is unknown. The measurements are quite difficult and the final result depends on a relatively few critical points (see Sec. IV.E).

i. Independent determination of σ_ρ

The Ritson group at SLAC (Anderson *et al.*, 1971) used a measurement of the differential cross section for the reaction $\gamma + d \rightarrow \rho^0 + d$ in the high-momentum transfer region to determine the total ρ^0-nucleon cross section and the ρ^0-γ coupling constant. Figure 84 shows a plot of the measured cross section determined by measuring the yield of recoil deuterons as a function of missing mass. The change in slope around $t = -0.4$ GeV^2 is due to the onset of rescattering. This rescattering term, or Glauber correction, has a much weaker t dependence than ρ^0 production from a single bound nucleon. In rescattering, a large total momentum transfer may be shared between the two nucleons in such a way that the internal momentum transfer which must be made up by the deuteron

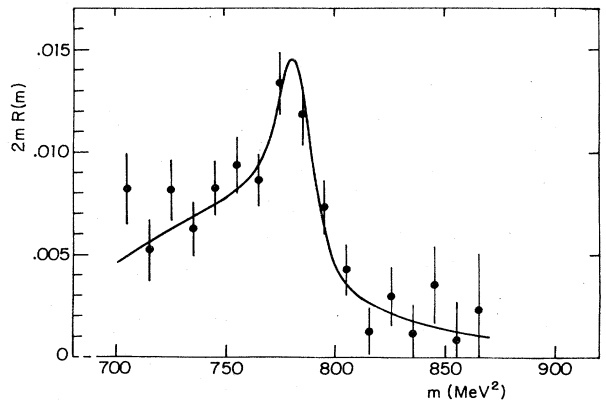

FIG. 83. The experimental mass spectrum for the reaction $\gamma \mathrm{Be} \rightarrow \mathrm{Be}\, e^+e^-$ determined from measurements by Alvensleben *et al.* (1970c). The curve is the best fit using a model which incorporates $\rho-\omega$ interference (from Alvensleben *et al.*, 1970c).

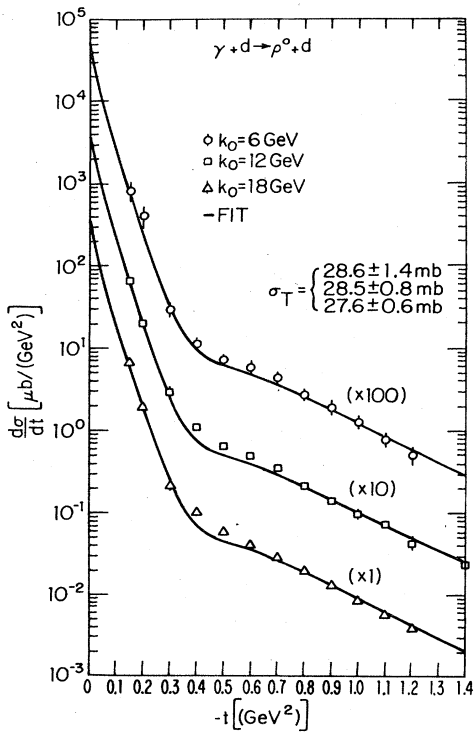

FIG. 84. Differential cross sections for the reaction $\gamma d \rightarrow \rho^0 d$ determined in measurements by Anderson *et al.* (1971). The solid lines are a fit using a double scattering model in which the ρ produced on one nucleon is scattered from the second nucleon (from Anderson *et al.*, 1971).

wave function is much smaller than if all momentum transfer were absorbed by one of the nucleons. Thus, if the deuteron is to hold together at increasingly large t, rescattering becomes the dominant mechanism. A ρ^0-nucleon scattering cross section may be extracted from such data. The results of Anderson *et al.* (1971) are summarized in Table XV. This measurement provides a satisfying confirmation of the VMD analysis of complex nuclei.

j. Angular distribution of ρ^0 decay

● The reader is referred to the formalism of Appendix D. In the rho rest frame the decay is characterized by θ and ϕ, the polar and azimuthal angles of the π^+ meson (Fig. 211). In this frame the rho has three polarization states and its production can be completely characterized by the spin-density matrix $\rho^\alpha_{i\,k}$ which may be obtained from experiment.

TABLE XV. A summary of the ρ coupling parameters and the total ρ-nucleon total cross section determined from the deuterium experiment of R. L. Anderson *et al.* (1971).

Energy (GeV)	$\hat{f}_\rho^2/4\pi$	σ_T (mb)
6	2.44±0.24	28.6±1.4
12	2.80±0.16	28.5±0.8
18	2.80±0.12	27.6±0.6

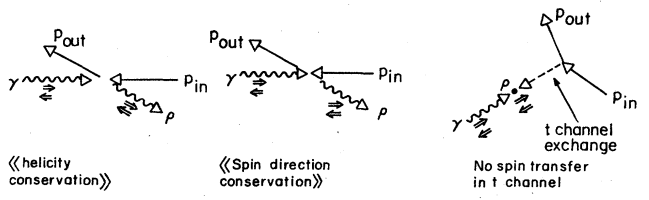

FIG. 85. A schematic diagram showing the preferred frames of reference for rho production depending on whether there is s-channel helicity conservation, conservation of spin direction, or no spin transfer in the t channel (from Rosenfeld and Söding, 1973).

● It is convenient to discuss the angular distribution of the ρ^0 decay in three reference systems which differ in the choice of the spin-quantization axis (z axis) of Fig. 211: the Gottfried–Jackson system, where the z axis is the direction of the incident photon in the ρ^0 rest system; the helicity system, where the z axis is opposite the direction of the recoil proton in the overall $\gamma\rho$ center-of-mass system; and the Adair system, where the z axis is along the direction of the incident photon in the overall γp center-of-mass system.

● Depending upon the production mechanism, the spin of the ρ^0 may be aligned along the z axis in one of these three systems (Gilman *et al.*, 1970). The system which gives the simplest description of the ρ^0 is then: (1) The Gottfried–Jackson system for t-channel helicity conservation; (2) the helicity system for s-channel helicity conservation (SCHC); (3) the Adair system for "spin independence" in the s-channel system. Figure 85 shows a schematic representation of these three coordinate systems.

● It has been shown that to leading order in energy, the overall production cross section (σ) may be split into noninterfering contributions σ^N and σ^U from natural- and unnatural-parity exchanges in the t channel by linear combinations of the density matrix parameters. The parity asymmetry is defined by

$$P_\sigma = \frac{\sigma^N - \sigma^U}{\sigma^N + \sigma^U} \quad . \tag{3.52a}$$

At high energies

$$P_\sigma = 2\rho^1_{1-1} - \rho^1_{00} \quad . \tag{3.52b}$$

(See Appendix D for definitions of the ρ^α_{ik}.) Since P_σ is invariant under rotations about the normal to the production plane, it is the same in the three coordinate systems defined earlier.

● In the counter experiments with polarized photons it is conventional to measure

$$\Sigma = \frac{\sigma_\parallel - \sigma_\perp}{\sigma_\parallel + \sigma_\perp} = \frac{\rho^1_{11} + \rho^1_{1-1}}{\rho^0_{11} + \rho^0_{1-1}} \quad , \tag{3.53}$$

where $\sigma_\parallel$ and $\sigma_\perp$ are cross sections for the pions from symmetric ρ decay to emerge in the plane of the photon polarization ($\Phi = \pi/2$) and perpendicular to it ($\Phi = 0$). When the helicity flip density matrix elements ρ^1_{00}, ρ^1_{11}, ρ^0_{00}, ρ^0_{1-1} are zero, Σ is equal to P_σ.

● If the ρ^0 production mechanism conserves s-channel helicity, i.e., if the ρ^0 is transverse and linearly polarized like the photon, then in the helicity system (D.1)

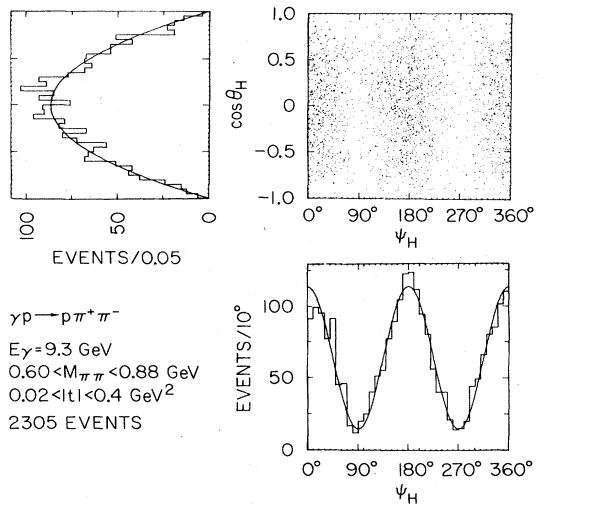

FIG. 86. Reaction $\gamma p \to p\rho^0$ at 9.3 GeV. Decay angular distribution of events in the ρ^0 region in the helicity system. The curves are calculated for an s-channel helicity-conserving $\gamma - \rho^0$ transition and incident photon polarization of 77% (from Ballam *et al.*, 1973).

implies

$$\rho^1_{1-1} = -\,\mathrm{Im}\rho^2_{1-1} = \frac{1}{2} \tag{3.54}$$

and all other ρ^α_{ik} in (D.1) are 0. In these circumstances ψ (see Fig. 211) is the azimuthal angle in the helicity system of the decay π^+ with respect to the ρ^0 polarization plane, and the decay angular distribution is proportional to $\sin^2\theta\cos^2\psi$ (D.4).

● Figure 86 shows the distribution of $\cos\theta$ vs ψ in the helicity system observed by the SLAC–Berkeley collaboration (Ballam *et al.*, 1973) at 9.3 GeV. The distribution, which is of the form $\sin^2\theta\cos^2\psi$, indicates zero helicity flip contributions and dominant natural spin-parity exchange. A more detailed study of the density matrix elements shows that in both the Gottfried–Jackson and Adair systems the helicity flip terms increase rapidly off the forward direction. This rules out dominance by an elementary 0^+ exchange and spin independence.

● Figure 87 shows the dipion spin-density matrix elements in the helicity system and the parity asymmetry as a function of t in the ρ^0 region. At small momentum transfers the helicity flip elements are zero, and s-channel helicity is conserved at the $\gamma\rho$ vertex. This indicates that in the center-of-mass system the rho behaves like a photon with its spin along the direction of flight. A more complete analysis shows that the amplitudes for helicity flip contribute less than 10% of the cross section for $|t| < 0.4$ GeV^2. Figure 88 (Chadwick *et al.*, 1973) shows a comparison between helicity flip elements for the ρ and those for pion-nucleon scattering. The similarity is striking.

● The data in Fig. 87 for the parity asymmetry show that rho production is completely dominated by natural-parity exchange, as one would expect for a diffraction mechanism. The fraction of unnatural-parity exchange

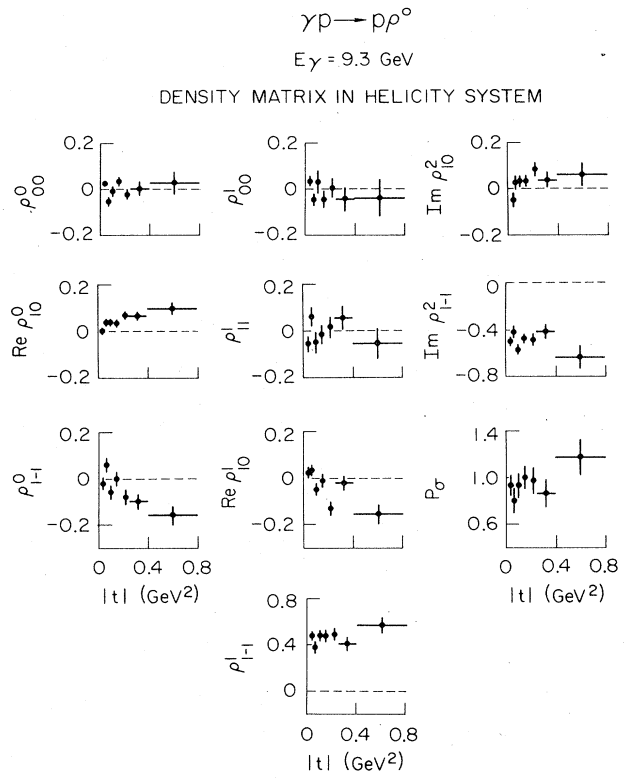

FIG. 87. Reaction $\gamma p \to p\pi^+\pi^-$ at 9.3 GeV. Dipion spin-density matrix elements in the helicity system and parity asymmetry as a function of t in the ρ^0 region (from Ballam *et al.*, 1973).

is consistent with the contribution expected from one-pion exchange.

● Counter experiments (Diambrini-Palazzi *et al.*, 1970; Criegee *et al.*, 1968, 1970) have also been carried out with linearly polarized photons to determine the asymmetry parameter Σ which measures the relative contributions from natural- and unnatural-parity exchange to the combination $(\rho^0_{11} + \rho^0_{1-1})$. Figure 89 shows the energy dependence of Σ for small momentum transfers.

● Measurements with deuterium targets (Eisenberg *et al.*, 1976) show a behavior for the density matrix elements for deuterium similar to that observed for hydrogen. The density matrix elements, in particular, reveal a helicity flip amplitude of the same sign and magnitude as for hydrogen. This, together with the absence of a large helicity flip amplitude in ω photoproduction, implies that the isospin of the helicity flip exchange amplitude is zero.

● With the assumptions that rho production is predominantly natural-parity exchange, that the helicity flip amplitudes are small, and that the nonflip amplitude is imaginary, Leith (1978) estimated the ratio of single and double helicity flip amplitudes to the dominant nonflip amplitude. He found that the single flip amplitude was ~10–15% in magnitude and of the same sign as the nonflip amplitude and that the double flip amplitude was roughly the same size but opposite in sign. Both helicity flip amplitudes are predominantly natural-parity exchange.

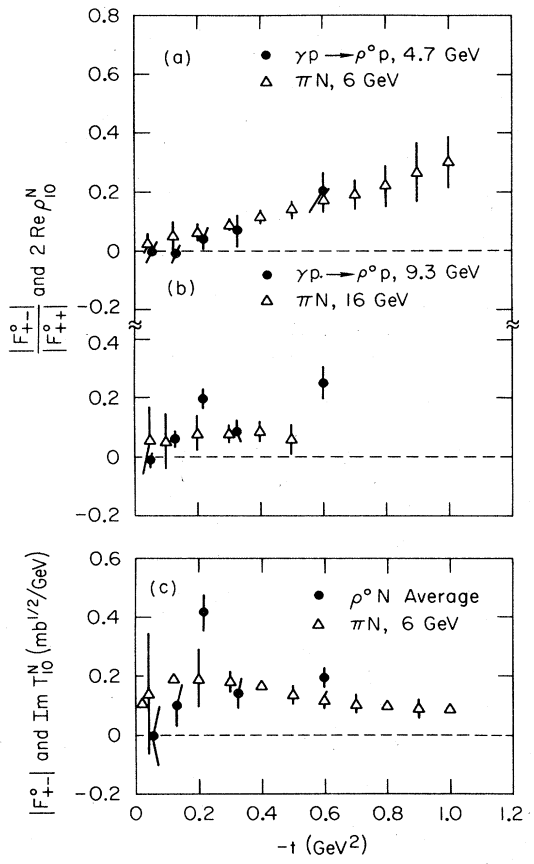

FIG. 88. (a), (b) $2\,\mathrm{Re}\rho^N_{10}$ for the reaction $\gamma p \to \rho^0 p$ and $|F^0_{+-}|/|F^0_{++}|$ for πN scattering. Open triangles are from de Lesquem *et al.* (1972) and Cozzika *et al.* (1972). (c) $|F^0_{+-}|$ for πN scattering at 6 GeV/c and average $\mathrm{Im}T^N_{10}$ for ρ^0 photoproduction at 4.7 and 9.3 GeV, normalized by the choice $\hat{f}^2_\rho/4\pi = 2.4$ (from Chadwick *et al.*, 1973).

● These general characteristics, together with the similarity to πN elastic scattering, indicate that small helicity flip is a common characteristic of diffraction processes.

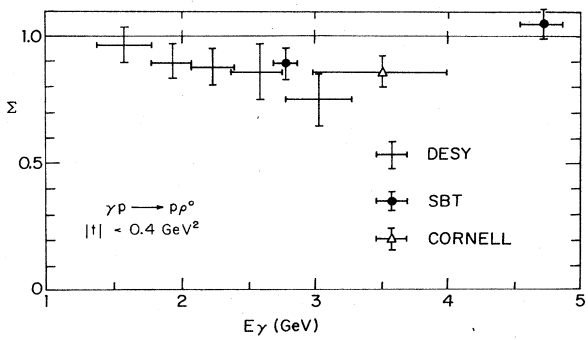

FIG. 89. The energy dependence for the polarization asymmetry Σ as determined in counter, bubble chamber, and streamer chamber experiments. Data are from DESY (Criegee *et al.*, 1970), SBT (Ballam *et al.*, 1970, 1972), and Cornell (Diambrini–Palazzi *et al.*, 1970) (figure after Wolf, 1972).

D. Omega photoproduction

The omega meson is an unstable particle with a mass of (782.7 ± 0.6) MeV and a width of (10.0 ± 0.4) MeV. Its quantum numbers $I^G(J^P)C$ are $0^-(1^-)^-$ and its dominant decay modes are $\pi^+\pi^-\pi^0((90.0\pm0.6)\%)$, $\pi^0\gamma((8.7\pm0.5)\%)$, and $\pi^+\pi^-((1.3\pm0.3)\%)$. Since the ω has a much larger width for the $\pi^0\gamma$ decay mode than the rho, one-pion exchange plays a larger role in ω photoproduction, and at low energies dominates the photoproduction cross section.

1. Production from hydrogen

Five experimental techniques have been used to study omega photoproduction—hydrogen bubble chamber experiments in which the $p\pi^+\pi^-$ are observed (Crouch *et al.*, 1966, 1967; Erbe *et al.*, 1968a, 1969; Ballam *et al.*, 1970, 1973; Eisenberg *et al.*, 1972a), deuterium bubble chamber experiments in which the $d\pi^+\pi^-$ are observed (Benz *et al.*, 1974; Eisenberg *et al.*, 1976; Alexander *et al.*, 1975), counter-spark chamber experiments in which the $\pi^+\pi^-\pi^0$ decay mode is observed (Behrend *et al.*, 1970, 1971a; Abramson *et al.*, 1976; Morris *et al.*, 1976), counter experiments in which the $\pi^0\gamma$ decay mode is observed (Braccini *et al.*, 1970), and counter experiments in which the recoil proton and some of the decay particles are observed (Gladding *et al.*, 1973).

The observation of the ω-decay angular distribution with a linearly polarized incident photon beam gives a particularly important piece of information, since it makes it possible to separate the portions of the cross section due to natural $[(-1)^J]$ and unnatural $[-(-1)^J]$ parity exchange in the t channel, and thus to separate the diffractive and one-pion exchange components of the cross section. The same formalism that was used to describe the ρ^0 angular distribution can be used to describe the ω (Schilling *et al.*, 1970). The reader may refer to the relevant discussion and definitions in Sec. III.C and Appendix D. The only distinction to be made here is that the matrix element which describes ω decay is proportional to $\hat{\epsilon}_\omega \cdot (\hat{k}_{\pi^+} \times \hat{k}_{\pi^-})$, whereas for the ρ^0 it is proportional to $\hat{\epsilon}_\rho \cdot \hat{k}_{\pi^+}$. Thus, for the ω, the direction normal to the decay plane $(\hat{k}_{\pi^+} \times \hat{k}_{\pi^-})$ plays the same role that the direction of $\hat{k}_{\pi^+}$ does for the ρ^0.

Early bubble chamber studies of ω photoproduction were carried out by the Cambridge bubble chamber group (Crouch *et al.*, 1966, 1967) and by the DESY bubble chamber group (Erbe *et al.*, 1968a, 1969). They showed that the total cross section for ω production decreases rapidly with energy, and can be viewed as due to diffractive production plus a large component due to one-pion exchange.

The most extensive bubble chamber data for production from hydrogen comes from the 2.8, 4.7, and 9.3 GeV runs by the SLAC–Berkeley group at SLAC (Ballam *et al.*, 1970, 1971, 1973) with the laser-produced polarized photon beam and the 208 cm bubble chamber. Since the presence of a neutral particle in the final state made it difficult to obtain a clean sample for the reaction

$$\gamma p \to p\omega, \quad \omega \to \pi^+\pi^-\pi^0,$$

it was necessary to investigate the bias coming from the event selection criteria. Corrections were made for ω events which (a) were excluded because they fit the three-constraint hypothesis $\gamma p \to p\pi^+\pi^-$; (b) had a reconstructed mass outside the ω region (0.67–0.90 GeV); (c) were lost because of short recoil protons; or (d) had a decay mode other than $\pi^+\pi^-\pi^0$. In addition, for the 2.8 and 4.7 GeV exposures, it was required that the calculated photon energy lie within a specified range. Without including (d), the combined correction factors were, respectively, 1.12, 1.22, and 1.29 at 2.8, 4.7, and 9.3 GeV. The correction factor for other decay modes was 1.11.

Figure 90 displays scatter plots for the reaction $\gamma p \to p\pi^+\pi^-\pi^0$ at 2.8, 4.7, and 9.3 GeV. There is a strong signal at the ω mass and no evidence for other resonant

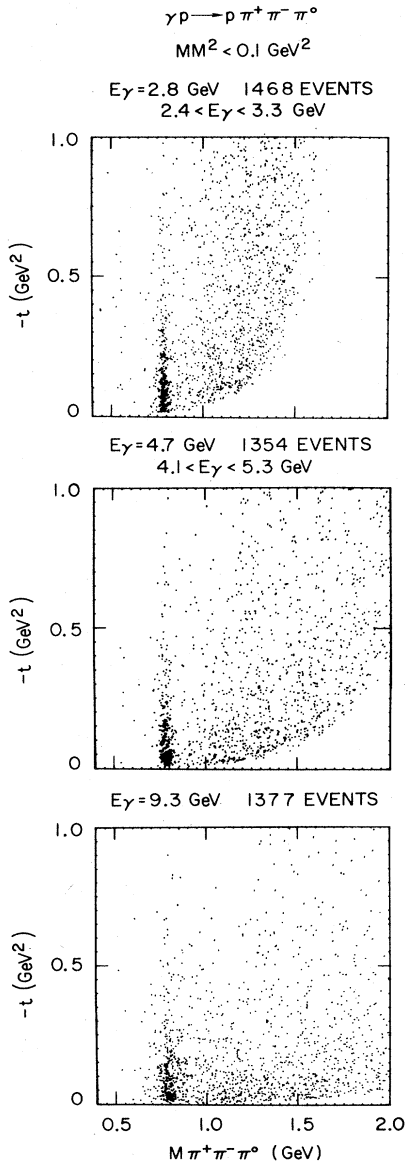

FIG. 90. Scatter plots of the $\pi^+\pi^-\pi^0$ mass versus momentum transfer t for the reaction $\gamma p \to p\pi^+\pi^-\pi^0$ at 2.8, 4.7, and 9.3 GeV (from Ballam *et al.*, 1973).

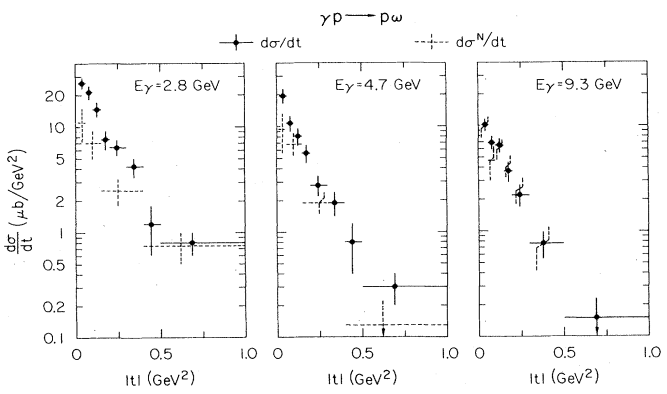

FIG. 91. Differential cross sections (•) and natural-parity exchange contributions to the differential cross section (---) for the reaction $\gamma p \to p\omega$ at 2.8, 4.7, and 9.3 GeV (from Ballam *et al.*, 1973).

states. Figure 91 shows the ω differential cross section $d\sigma/dt$; Fig. 92 shows the total cross section for ω production as determined by the SLAC-Berkeley experiment and the other bubble chamber experiments. The agreement between the different bubble chamber experiments is satisfactory.

Figure 93 shows the decay angular distributions in the helicity system and the parity asymmetry P_σ [Eq. (3.52)] for events in the ω mass region $0.74 \leq M_{\pi^+\pi^-\pi^0} \leq 0.84$ and in the momentum-transfer interval $0.02 < |t| < 0.3$ GeV^2. (We refer the reader to Fig. 211 for definitions of the various angles. Additional theoretical discussion can be found in Appendix D.) At the lower energies there is little structure in ψ, but at 9.3 GeV the characteristic $\cos^2\psi$ signal observed in rho production appears. The parity asymmetry is zero at 2.8 GeV and approaches 1 at 9.3 GeV.

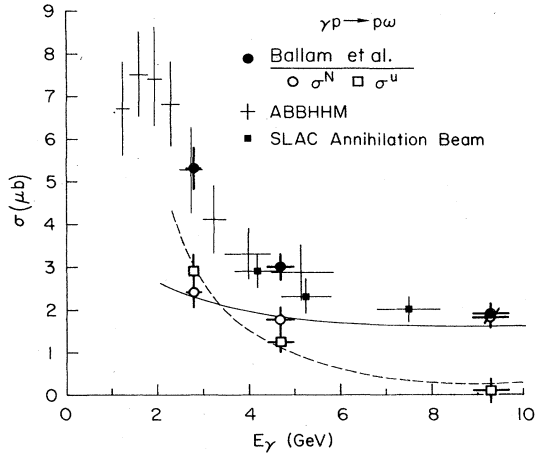

FIG. 92. Total cross sections for the reaction $\gamma p \to p\omega$ as a function of incident photon energy. The points labeled ABBHHM and SLAC Annihilation Beam are from Erbe *et al.* (1968a) and Eisenberg *et al.* (1972), respectively. Also shown are the contributions of natural- and unnatural-parity exchange in the t channel. The solid and dashed curves give the contributions of a diffractive process and OPE, respectively, as obtained from the fit described in the text (from Ballam *et al.*, 1973).

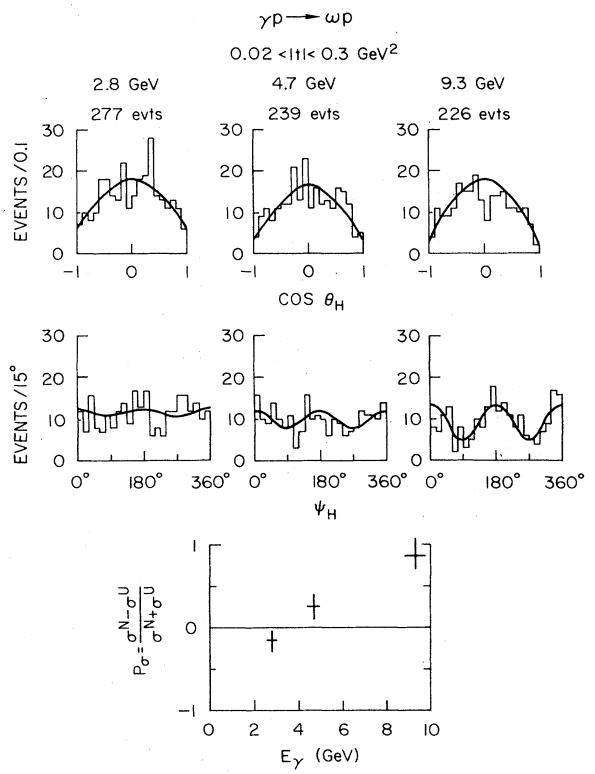

FIG. 93. Reaction $\gamma p \to p\omega$ at 2.8, 4.7, and 9.3 GeV. Decay angular distributions in the helicity system and parity asymmetry, P_σ, for events in the ω mass region $0.74 \leq M_{\pi^+\pi^-\pi^0} \leq 0.84$ MeV and in the momentum-transfer interval $0.02 < |t| < 0.3$ GeV^2. Curves are calculated from the fitted density matrix elements (from Ballam *et al.*, 1973).

Figures 91 and 92 also show the decomposition of the cross section into contributions arising from natural-(σ^N) and unnatural-(σ^U) parity exchanges in the t channel through the expression

$$\sigma^{N,U} = \frac{1}{2}(1 \pm P_\sigma)\sigma \ . \tag{3.55}$$

TABLE XVI. The reaction $\gamma p \to p\omega$ at 2.8, 4.7, and 9.3 GeV. Total cross sections and forward differential cross sections $d\sigma/dt|_{t=0}$ and slopes B from a fit of the form $d\sigma/dt = d\sigma/dt|_{t=0} e^{Bt}$ (from Ballam *et al.*, 1973).

	E_γ (GeV) 2.8	4.7	9.3
$\sigma(\mu b)$	5.3 ± 0.5	3.0 ± 0.3	1.9 ± 0.3
$\left.\frac{d\sigma}{dt}\right\|_{t=0}$ (μb/GeV^2)	33.2 ± 3.6 [a]	22.0 ± 3.2	13.7 ± 1.6 [a]
B (GeV^{-2})	6.8 ± 0.6 [a]	7.9 ± 0.9 [a]	7.5 ± 0.8 [a]
$\sigma^N(\mu b)$	2.4 ± 0.4	1.7 ± 0.3	1.8 ± 0.3
$\left.\frac{d\sigma^N}{dt}\right\|_{t=0}$ (μb/GeV^2)	14.5 ± 5.1 [b]	14.6 ± 4.8 [b]	11.4 ± 2.1 [b]
B^N (GeV^{-2})	7.3 ± 2.4 [b]	8.5 ± 2.4 [b]	6.6 ± 1.1 [b]
$\sigma^U(\mu b)$	2.9 ± 0.4	1.3 ± 0.3	0.1 ± 0.2

[a] Fit interval $0.02 \leq |t| \leq 0.5$ GeV^2.
[b] Fit interval $0.014 \leq |t| \leq 0.4$ GeV^2.

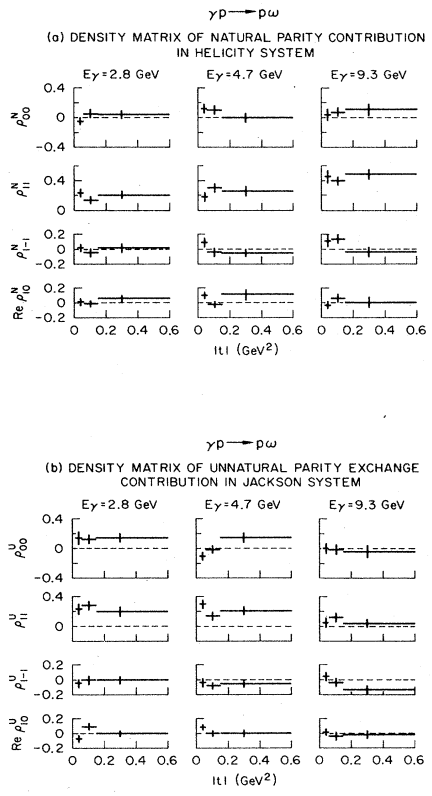

FIG. 94. Reaction $\gamma p \to p\omega$ at 2.8, 4.7, and 9.3 GeV. (a) Density matrix elements of the natural-parity exchange contribution in the helicity system. (b) Density matrix elements of the unnatural-parity exchange contribution in the Gottfried–Jackson system (from Ballam *et al.*, 1973).

Table XVI summarizes the fits of the differential cross sections to the form $d\sigma/dt = d\sigma/dt\,|_{t=0} e^{Bt}$. σ^U decreases rapidly with increasing energy; σ^N is approximately constant with energy.

Figure 94 shows separately the density matrix elements for the natural- and unnatural-parity exchange components. Since it is suspected that the unnatural component is due to one-pion exchange, this component of the density matrix elements has been expressed in the Gottfried–Jackson system. The natural spin-parity component has been expressed in the helicity system. These "systems" were discussed in Sec. III.C; see Gilman *et al.* (1970) for additional information. The natural spin-parity component is consistent with the behavior expected for an s-channel helicity-conserving γ-ω transition. It is also consistent with the same fraction of small helicity flip contributions that were observed for the ρ^0. The unnatural-parity exchange density matrix elements do not completely support t-channel helicity conservation ($\rho^U_{00} \ll \rho^U_{11}$), as would be expected from a naive one-pion exchange (OPE) model.

The SLAC–Berkeley group fit the data at all energies to a simple model in which ω photoproduction was described as a sum of diffractive and OPE components. Specifically they wrote

$$\frac{d\sigma}{dt} = \frac{d\sigma^N}{dt}\bigg|_{t=0} e^{B^N t} + W \frac{d\sigma^{\mathrm{OPE}}}{dt}(E_\gamma, t) \ . \tag{3.56}$$

(Wherever the superscript N appears in this section, it denotes natural spin-parity exchange.) Since the final states are orthogonal, there is no interference between the diffractive and one-pion exchange amplitudes. For the OPE calculation they used the formulation of Wolf (1969) (using Benecke-Dürr form factors) and the value of $\Gamma_{\omega\to\pi\gamma} = 0.90$ MeV for the radiative width. To allow for an energy dependence of $d\sigma^N/dt\,|_{t=0}$, they assumed

$$\frac{d\sigma^N}{dt}\bigg|_{t=0} = C\left(1 + \frac{D}{E_\gamma}\right) . \tag{3.57}$$

From a χ^2 fit to the differential cross sections and P_σ at the three energies in the interval $0.02 < |t| < 0.5$ GeV^2, they obtained

$$\begin{aligned} C &= (9.3 \pm 1.7)\ \mu\mathrm{b/GeV}^2 \ , \\ D &= (1.4 \pm 1.2)\ \mathrm{GeV} \ , \\ B^N &= (6.7 \pm 0.6)\ \mathrm{GeV}^{-2} \ , \\ W &= 0.97 \pm 0.09 \ . \end{aligned} \tag{3.58}$$

The resultant decomposition is shown in Fig. 92.

A Rochester group carried out two separate studies of ω photoproduction from hydrogen and deuterium at the Wilson Synchrotron Laboratory using a counter-spark chamber system. Figure 95 shows a diagram of the apparatus used in the initial experiment (Behrend *et al.*, 1971a). Omega mesons produced by a 9.1 GeV bremsstrahlung beam incident on a hydrogen target were detected through the $\pi^+\pi^-\pi^0$ decay mode. The charged pions from ω decay were momentum analyzed with a wire spark chamber system. The momentum and mass of the π^0 were determined by the measurement of the energy and opening angle of the γ rays. Since in the initial experiment the direction, but not the energy, of

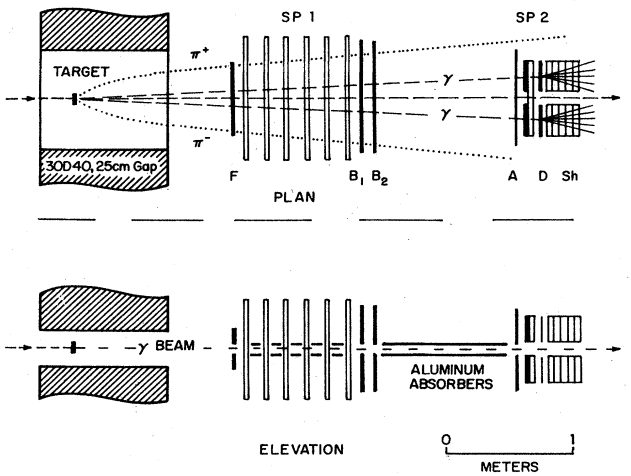

FIG. 95. Geometry of the apparatus used by the Rochester group (Behrend *et al.*, 1970) for detecting photoproduced ω mesons through their $\pi^+\pi^-\pi^0$ decay. SP1 is a wire spark chamber system used to determine the trajectories of the charged pions; SP2 is a strip spark chamber array used to measure the position of the gamma rays subsequent to the $1\frac{1}{2}$ radiation length lead converter. F_1, B_1, and B_2 are scintillation trigger counters; A is an anticounter. Sh is a segmented shower counter (from Behrend *et al.*, 1970b).

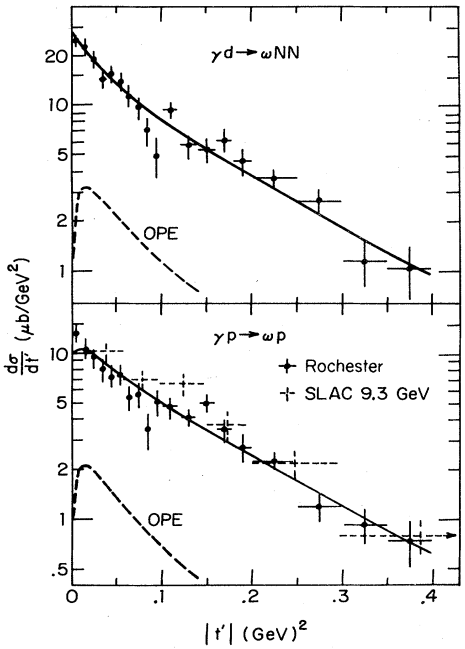

FIG. 96. Differential cross sections for $\gamma d \to \omega NN$ and $\gamma p \to \omega p$. Solid curves are fit to a diffractive component plus OPE. The dashed curves are the OPE contributions used in the fits. Data points labeled SLAC are from Ballam *et al.* (1973) and those labeled Rochester are from Abramson *et al.* (1976) (figure from Abramson *et al.*, 1976).

the primary photon beam was known, they could determine all the kinematical variables of the photoproduced ω but not the degree of excitation of the target. Thus they obtained cross sections summed over elastic ($\gamma N \to \omega N$) and inelastic ($\gamma N \to \omega N^*$) channels.

The Rochester group subsequently used a tagged photon beam with an improved version of their spectrometer to measure the cross sections from hydrogen and deuterium targets at a mean energy of 8.9 GeV (Abramson *et al.*, 1976). The tagged photon beam enabled them to determine the target excitation and to study separately the $\gamma N \to \omega N$ and $\gamma N \to \omega \Delta$ channels. Figure 96 shows the measured differential cross sections; also shown in this figure are the measurements of the SLAC–Berkeley bubble chamber group. In addition to the errors shown, there is an overall normalization uncertainty in each of the experiments. The Rochester group cited ±10% as the overall normalization uncertainty; the bubble chamber group did not give a figure for this uncertainty but increased their errors to take it into account. The two groups agree on the shape of the cross section but differ systematically by 22%. This difference in normalization may be compatible with the overall systematic uncertainties in the two experiments. A fit to the form $A_p \exp(B_p t') +$ one-pion exchange, where $t' \equiv t - t_{\min}$ is the square of the four-momentum transfer to the nucleon minus its value for forward production, gave

$$A_p = (8.8 \pm 0.7)\ \mu\text{b/GeV}^2\ , \qquad B_p\ (7.1 \pm 0.5)\text{GeV}^{-2}\ . \tag{3.59}$$

These values are compatible with those obtained by the SLAC–Berkeley bubble chamber group. The Rochester group also measured the density matrix elements for ω production from hydrogen. They found values in agreement with those of Ballam *et al.* and confirmed the deviation from SCHC at large momentum transfer.

TABLE XVII. A comparison between the measured natural spin-parity cross section for ω photoproduction and the cross section calculated from the quark-VMD model with the assumption that the $\hat{f}_\omega^2/4\pi$ has the colliding values of 18.4.

Source of data	Energy (GeV)	$\left.\frac{d\sigma}{dt}\right\|_{t=0}$ (μb/GeV^2)	B (GeV^{-2})
Ballam *et al.* (1973)	9.3	11.4 ± 2.1	6.6 ± 1.1
Abramson *et al.* (1976)	8.9	8.8 ± 0.7	7.1 ± 0.5
Quark-VMD model (see Table XII)	8.5	14.2	7.99

Gladding *et al.* (1973) used a tagged photon beam and the spectrometer system described earlier to study ω^0 production at the Cambridge Electron Accelerator in the energy range from 2.9 to 4.7 GeV. They observed the recoil proton and the direction of the decay pions. They used the decay pions to eliminate the rho channel and thus enhance the ω signal. They obtained differential cross sections which were roughly 40% lower than those obtained by Ballam *et al.* (1973). Gladding *et al.* did not quote an overall systematic error, but the statistical errors are large and it appears that their measurements and those of Ballam *et al.* are marginally compatible. Gladding *et al.* reported that for $3.7 < E_\gamma < 4.7$ GeV, the ratio of the differential cross sections for ω and ρ^0 production was consistent with a constant as a function of t. They interpreted this as an indication that the OPE contribution had already disappeared. In this they differed from Ballam *et al.* who concluded that the OPE component was roughly three-fourths of the diffractive component in this energy interval.

In summary, work by Abramson *et al.* and by Gladding *et al.* confirms certain aspects of the work of Ballam *et al.*, refutes none of it, but suggests that the absolute normalization is high. Table XVII gives a comparison between the measured spin-parity cross sections for hydrogen and the cross section calculated from the quark–VMD model summarized in Table XII.

2. Production from deuterium

It is particularly interesting to study ω production from deuterium. The observation of the coherent production from deuterium gives a direct measure of the isospin-zero part of the natural-parity exchange component. This cross section can then be combined with the natural-parity exchange component of the hydrogen cross section to determine the component of the cross section due to isospin-one exchange. The major natural-parity candidate for isospin-one exchange is the A_2 meson.

Figure 97 shows some natural-parity exchange diagrams for Compton scattering and ρ^0 and ω photoproduction in the spirit of the VMD model. Only the isospin-zero exchange diagrams contribute to coherent ρ^0 and ω photoproduction on the deuteron. VMD connects isospin

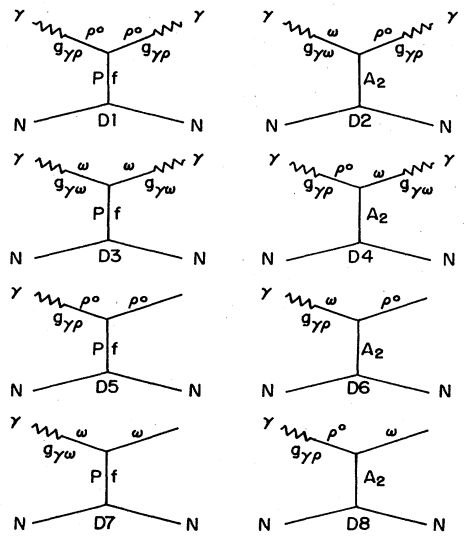

FIG. 97. Vector-meson-dominance diagrams for natural-parity exchange Compton scattering, ρ^0 photoproduction, and ω photoproduction (after Kogan, 1975).

exchange in forward ρ^0 and ω photoproduction with that in forward Compton scattering. The latter can be obtained via the optical theorem from the total γp and γd cross sections and their energy dependence. Regge fits to the total cross sections including P, f, and A_2 exchange have indicated the presence of a small isovector exchange amplitude. At $E = 4.3$ GeV,

$$\tau = \frac{\sigma_{\gamma p} - \sigma_{\gamma n}}{\sigma_{\gamma p} + \sigma_{\gamma n}} = \frac{\mathrm{Im}T_1(\gamma N \to \gamma N)}{\mathrm{Im}T_0(\gamma N \to \gamma N)} = (0.024 \text{ or } 0.035) \pm 0.011 \ , \tag{3.60}$$

where T_0 and T_1 are the isospin-0 and isospin-1 amplitudes, and where the two values in parentheses stem from two fits (Caldwell *et al.*, 1973; Dominguez *et al.*, 1972). *As discussed in Sec. III.A such estimates involving* $\sigma_{\gamma p} - \sigma_{\gamma n}$ *must be regarded with caution.* It was first pointed out by Harari (1970) that one might expect A_2 exchange to be more important in the natural-parity exchange component for ω photoproduction than for ρ^0 photoproduction. To a good approximation using the forward scattering amplitudes we obtain

$$\delta \equiv 2\,\frac{\mathrm{Re}[\,T_0^N(\gamma N \to \omega N) T_1^{N*}(\gamma N \to \omega N)]}{|\,T_0^N(\gamma N \to \omega N)\,|^2}$$

$$\text{“}\simeq\text{”}\ 2\,\frac{\mathrm{Im}T_1^N(\gamma N \to \omega N)}{\mathrm{Im}T_0^N(\gamma N \to \omega N)} \ , \tag{3.61a}$$

where the “$\simeq$” in Eq. (3.61a) is based on the assumption that $T_0^N(\gamma N \to \omega N)$ is nearly purely imaginary. Under these circumstances and assuming VMD applies to the amplitudes in Eq. (3.60),

$$\delta \simeq (\hat{f}_\omega^2/\hat{f}_\rho^2)\tau = 0.17 \pm 0.08 \ , \tag{3.61b}$$

where $\hat{f}_\omega^2/\hat{f}_\rho^2$ is taken equal to the colliding-beam value $\bar{f}_\omega^2/\bar{f}_\rho^2 = 7.14 \pm 1.0$. With a more complete analysis, the Rochester group (Abramson *et al.*, 1976) finds

$$\delta = 1.3(\hat{f}_\omega^2/\hat{f}_\rho^2)\tau \ , \tag{3.62}$$

where the factor 1.3 arises in part from the diagonal contribution of ω and ϕ to the Compton scattering diagrams, and in part from the nonzero real part of the isospin-zero amplitude. Non-VMD contributions to the amplitudes of Eq. (3.62) were not taken into account.

The Rochester group measured the cross section for the reaction

$$\gamma d \to \omega(d \text{ or } np)$$

and then used the expression

$$d\sigma/dt = 2\,|\,T_0^N\,|^2[\,1 + F(4t) - G_0(t)] + |\,T_1\,|^2[\,1 - \tfrac{1}{3}F(4t) - G_1(t)] \tag{3.63}$$

to analyze the data (see Appendix B). Here $|\,T_0^N\,|^2 = A_d \exp(B_d t)$ and $|\,T_1\,|^2$ are the spin-nonflip $I=0$ exchange and spin-flip $I=1$ exchange contributions for a single nucleon. The one-pion exchange calculation was used for $|\,T_1\,|^2$. The Glauber corrections G_0 and G_1 were taken to be 0.12. Figure 96 shows the data together with the fit. The fit gave

$$A_d = (7.4 \pm 0.5)\ \mu\text{b/GeV}^2 \ ,$$

$$B_d = (6.9 \pm 0.5)\text{GeV}^{-2} \ .$$

When comparing the forward cross section with the results of other groups, it should be remembered that there is an additional uncertainty in the overall normalization of $\pm 10\%$. The Rochester group also studied the density matrix elements and found less deviation from SCHC for deuterium than for hydrogen.

For the p-n cross-section difference for ω production, the Rochester group obtained $\delta = 0.20 \pm 0.12$. For the slope difference, $B_p - B_d$, they obtained (0.15 ± 0.74) GeV^{-2}, a result which is consistent either with zero or with that expected from A_2 exchange. If B_p and B_d are constrained to be equal, then the fitted cross sections change slightly, and the results yield $\delta = 0.18 \pm 0.09$. Both of these values of δ are compatible with the amount of A_2 exchange suggested by the $p-n$ total hadronic cross-section difference.

Four bubble chamber experiments have studied ω production from deuterium (Benz *et al.*, 1974; Eisenberg *et al.*, 1972, 1976; Alexander *et al.*, 1975). Benz *et al.* used the 85 cm bubble chamber at DESY to study ω photoproduction from a 5.5 GeV bremsstrahlung beam. Since $\gamma d \to \omega d$ was only a kinematic 0C fit reaction, they relied heavily on the narrowness of the mass distribution to separate this reaction from the background. Their data covered the kinematic range $1.4 < E_\gamma < 5.3$ GeV and $0.05 < |t| < 0.20$ GeV^2. For the total ω cross section in this region they found $(0.64 \pm 0.17)\mu$b. They then combined this value with the similarly measured total cross section for ρ^0 production $(4.6 \pm 0.4)\mu$b, to obtain

$$\frac{\hat{f}_\omega^2}{\hat{f}_\rho^2} \simeq \frac{\sigma(\gamma d \to \rho^0 d)}{\sigma(\gamma d \to \omega d)} = 7.2\ {}^{+2.7}_{-1.6} \ . \tag{3.64}$$

Equation (3.64) is based on the assumption of equal diffractive scattering amplitudes for ρ^0 and ω mesons.

A Weitzmann Institute group (Eisenberg *et al.*, 1976) reported γd measurements at 4.3 GeV using the SLAC laser-backscattered linearly polarized photon beam and the 208 cm deuterium-filled bubble chamber. Figure 98

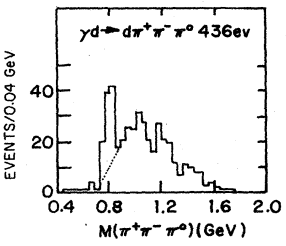

FIG. 98. $\pi^+\pi^-\pi^0$ mass distribution of 3-prong events in the reaction $\gamma d \to d\pi^+\pi^-\pi^0$. The dashed line represents the estimated background under the ω peak (from Eisenberg *et al.*, 1976).

shows the mass distribution of the $\pi^+\pi^-\pi^0$ combinations for $\gamma d \to d\pi^+\pi^-\pi^0$. A clear ω signal with a full width at half-maximum of 60 MeV is observed above a rising background. The background under the ω in each t bin was estimated on the Chew–Low plot, and the total background is plotted as dots in the figure.

The differential cross section for the coherent reaction $\gamma d \to d\omega$ in the range $0.02 < |t| < 0.20$ GeV^2 was obtained from the number of events in each t bin with $0.72 < M_{\pi^+\pi^-\pi^0} < 0.84$ GeV. This required the measurement of recoil deuteron tracks as short as 1.5 mm. After the background was subtracted, a correction was made for the loss of 3-prong events into the 2-prong sample. The correction ($< 10\%$) was estimated by imposing azimuthal symmetry of the outgoing deuteron track around the beam direction. An additional combined correction of 20% was introduced for ω events lost in the tails of the mass distribution, because of the missing mass cut and the incoming E_γ cut. The cross section was then corrected for the neutral ω-decay modes (10%). The systematic error was estimated as $\pm 20\%$ and has been added to all the total and forward cross sections.

Figure 99 shows the differential cross section. The integrated cross section is (1.2 ± 0.3) μb for $0.02 < |t| < 0.20$ GeV^2. For the interval $0.05 < |t| < 0.20$ GeV^2, the cross section for ω production is (0.61 ± 0.18) μb. This is consistent with the result (0.64 ± 0.17) μb obtained by Benz *et al.* (1974) for $1.4 < E_\gamma < 5.3$ GeV.

The coherent reaction $\gamma d \to d\omega$ was fit to the Glauber theory expression

$$\frac{d\sigma}{dt}(\gamma d \to d\omega) = 4\,|T_0^N|^2\,[F^2(t)e^{B_d t} - F(t)G_1 e^{3B_d t/4}] \,. \tag{3.65}$$

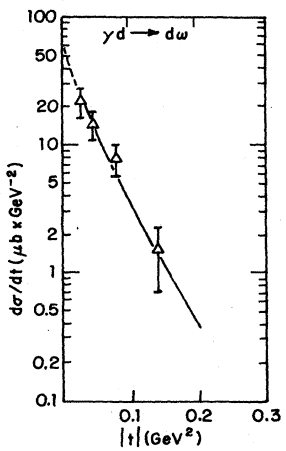

FIG. 99. $d\sigma/dt$ for the coherent reaction $\gamma d \to d\omega$. The curve gives the result of a least squares fit to (3.65) for $0.02 < |t| < 0.20$ GeV^2 (from Eisenberg *et al.*, 1976).

Here F is the form factor for the deuteron, and G_1 is the Glauber shadowing correction for $t = 0$. The ω slope parameter B_d was taken as 7.2 GeV^{-2}, the value found in similar measurements of ρ^0 production. The fitted curve is shown in Fig. 99. The derived forward cross section is

$$d\sigma/dt(\gamma d \to d\omega)\big|_{t=0} = (69 \pm 17)\ \mu\text{b/GeV}^2 \,. \tag{3.66a}$$

This gives

$$|T_0^N|^2\big|_{t=0} = (18.5 \pm 4.5)\ \mu\text{b/GeV}^2 \,. \tag{3.66b}$$

Because of the need to have $|t|$ large enough to observe recoil deuterons, the determination of the $t = 0$ cross sections required an extrapolation of roughly a factor of 3. The total resonance cross section for $|t| > t_{\min}$ was (1.8 ± 0.4) μb. This is close to the value (2.2 ± 1.2) μb obtained by this group (Eisenberg *et al.*, 1972b) in an earlier experiment using annihilation radiation.

Combining the above value of $|T_0|^2|_{t=0}$ with a reanalysis of the SLAC–Berkeley data at 4.7 GeV with an imposed slope of 7.2 GeV^{-2}, which yields

$$\frac{d\sigma^N}{dt}(\gamma p \to p\omega)\big|_{t=0} = |T_0^N + T_1^N|^2\big|_{t=0} = (12.6 \pm 2.4)\ \mu\text{b/GeV}^2 \,, \tag{3.67}$$

gives

$$\delta = -0.3 \pm 0.3 \,.$$

This is marginally consistent with the quoted predictions using the total γp and γn cross sections.

The coherent cross sections $\gamma d \to d\omega$ and $\gamma d \to d\rho^0$ can also be used to obtain the ratio $\hat{f}_\rho^2/\hat{f}_\omega^2$ (3.64). Eisenberg *et al.* (1976) found

$$\frac{d\sigma}{dt}(\gamma d \to d\rho^0)\big|_{t=0} = (466 \pm 27)\ \mu\text{b/GeV}^2 \,, \tag{3.68a}$$

where we have adjusted the cross section so that the width used is 155 MeV. Combining this value with (3.66a) yields

$$\frac{\hat{f}_\omega^2}{\hat{f}_\rho^2} \approx \frac{d\sigma/dt(\gamma d \to d\rho)}{d\sigma/dt(\gamma d \to d\omega)} = 6.7^{+2.1}_{-1.3} \,. \tag{3.68b}$$

It should be emphasized that the same slope was used to analyze both the ρ and ω data.

In an earlier experiment with the quasimonochromatic e^+ annihilation photon beam at 4.3 GeV, Eisenberg *et al.* (1972b) obtained

$$\frac{d\sigma}{dt}(\gamma d \to d\rho^0)\big|_{t=0} = (351 \pm 30)\ \mu\text{b/GeV}^2 \,, \tag{3.69a}$$

$$\frac{d\sigma}{dt}(\gamma d \to d\omega)\big|_{t=0} = (52 \pm 26)\ \mu\text{b/GeV}^2 \,, \tag{3.69b}$$

$$\frac{\hat{f}_\omega^2}{\hat{f}_\rho^2} = 6.8^{+6.7}_{-2.3} \,. \tag{3.69c}$$

A Tel Aviv group (Alexander *et al.*, 1975) studied ρ and ω photoproduction using the SLAC 208 cm bubble chamber exposed to a 7.5 GeV linearly polarized photon beam. From a fit of the data to the expression

$$d\sigma/dt = A_v(\exp(Bt))\,|F(t)|^2 \tag{3.70}$$

with the assumption that $B = 7.5$ GeV^2, they obtained

$$A_\rho = (300 \pm 11)\ \mu\text{b/GeV}^2\ , \tag{3.71a}$$

$$A_\omega = (42 \pm 9)\ \mu\text{b/GeV}^2\ . \tag{3.71b}$$

This measurement is discussed further in Sec. III.G. Figure 143 shows a plot of the observed differential cross section. This experiment gives for the ω

$$|T_0^N|^2|_{t=0} = (11.2 \pm 2.5)\ \mu\text{b/GeV}^2 \tag{3.72}$$

and for the ratio of the coupling constants

$$\frac{\hat{f}_\omega^2}{\hat{f}_\rho^2} = \frac{300 \pm 11}{42 \pm 9} = 7.1^{+2}_{-1.2}\ . \tag{3.73}$$

A Lancaster group (Morris *et al.*, 1976) used a tagged photon beam and an array of heavy-plate optical spark chambers to measure at the Daresbury synchrotron the cross section for ω photoproduction from deuterium at an average photon energy of 3.9 GeV. The reaction $\gamma d \to \pi^+\pi^-\pi^0 X$ was twice underdetermined since the recoil nucleons were not detected and the $\pi^\pm$ momenta were not measured. In addition, the gamma-ray energies from the decay of the π^0 were only crudely measured. An iterative procedure based heavily on a Monte Carlo calculation was used to analyze the data. The group found the cross section for the coherent process $\gamma d \to d\omega$ to be $(1.4 \pm 0.4)\mu$b, and that for the incoherent process $\gamma d \to np\omega$ to be $(3.3 \pm 0.7)\mu$b. Then they estimated the forward differential cross section for $\gamma d \to d\omega$ to be

$$\left.\frac{d\sigma}{dt}\right|_{t=0} = (54 \pm 20)\mu\text{b/GeV}^2\ . \tag{3.74a}$$

This gives, with the inclusion of the Glauber correction,

$$|T_0^N|^2|_{t=0} = (14.5 \pm 5.4)\mu\text{b/GeV}^2\ . \tag{3.74b}$$

Because of the lack of kinematic constraints and the poor resolution, this experiment should not be given great weight.

Combining the total cross section for coherent ω photoproduction from deuterium and the cross section for coherent ρ^0 photoproduction from deuterium ($9.9 \pm 1.2\ \mu$b) measured in another experiment (Hilpert *et al.*, 1970b), the Lancaster group obtained, using the approximation (3.64),

$$\frac{\hat{f}_\omega^2}{\hat{f}_\rho^2} \approx \frac{\sigma(\gamma d \to \rho^0 d)}{\sigma(\gamma d \to \omega d)} = 7.1^{+4.0}_{-2.1}\ . \tag{3.75}$$

The forward cross sections per nucleon for the four experiments just described are:

Rochester	8.9 GeV	$7.4 \pm 0.9\ \mu\text{b/GeV}^2$
Tel Aviv	7.5	11.2 ± 2.5
Weizmann	4.3	18.5 ± 4.5
Lancaster	3.9	14.5 ± 5.4

The claimed accuracy of the Rochester experiment is twice that of the bubble chamber experiments, and three times that of the Lancaster experiment. The only significant disagreement is between the Rochester and Weizmann results, which differ by 2.5 Weizmann standard deviations, and 12 Rochester standard deviations. That the experiments are not at the same energies is not expected to make much difference. Between 4.3 and 8.9 GeV, the ρ^0 production cross section falls by a factor of 1.25, the ω natural-parity exchange cross section on hydrogen by a factor of 1.15. The weighted mean of the four experiments is $(10.1 \pm 1.0)\ \mu\text{b/GeV}^2$ at a mean energy of 7.2 GeV. The SLAC $\gamma p \to \omega p$ natural-parity cross section at this energy is 11.0 $\mu\text{b/GeV}^2$, employing $\delta = +0.1$, with errors of ± 0.1 from the deuterium measurement, and ± 0.2 from the hydrogen measurement.

One can calculate values of δ from each of the individual deuterium measurements, using SLAC hydrogen bubble chamber results for the $\gamma p \to \omega p$ cross section where necessary

D_2	H_2	Energy	δ	"Theory"(3.60–3.64)
Rochester	Rochester	8.9	$+0.20 \pm 0.12$	$0.26 \pm .10$
Tel Aviv	SLAC	7.9	-0.01 ± 0.3	0.28
Weizmann	SLAC	4.3	-0.3 ± 0.3	0.38
Lancaster	SLAC	3.9	$-0.14^{+0.5}_{-0.3}$	0.39

As previously mentioned, the Rochester results are two standard deviations from zero and consistent with "theory." All other results are consistent with zero. The Tel Aviv and Lancaster results are sufficiently imprecise to be also consistent with "theory"; the Weizmann result disagrees with theory by 2-1/2 standard deviations. [Again, the reader is cautioned against assigning much significance to agreement with the "theory" column. See the remarks following Eq. (3.60)].

The following summarizes the deuterium work:

The high-statistics Rochester experiment is in conflict with the low-statistics Weizmann experiment; the Tel Aviv experiment favors the Rochester result, but not strongly. The Lancaster experiment is technically weak, and should be given low weight. The Rochester deuterium result was obtained simultaneously with a hydrogen result by the same experimental technique. The agreement (at the 20% level) between Rochester and SLAC $\gamma p \to \omega p$ results provides a check on the Rochester deuterium result. The Weizmann deuterium results

come from a difficult experiment, requiring measurement of very short recoil deuteron tracks. Further experiments are required to resolve the discrepancies.

3. Production from complex nuclei

Two groups have studied ω production from complex nuclei as a means for determining the ωN cross section and $\hat{f}_\omega^2/4\pi$. In an early experiment the Rochester group (Behrend *et al.*, 1970b) used the apparatus described previously in conjunction with a bremsstrahlung beam to measure the photoproduction of ω mesons from Be, C, Al, Cu, and Pb at a mean energy of 6.8 GeV. This experiment had good resolution in π^0 mass, ω mass, and t, but no ability to detect target excitation. The t distribution showed a forward peak characteristic of a coherent diffractive process and a considerable cross section at large t characteristic of an incoherent production mechanism. Figure 100 shows the t distributions observed for Cu and Be. The contribution of the inelastic and incoherent events was calculated using the expression

$$\left(\frac{d\sigma}{dt}\right)^{\mathrm{OPE}} = A_{\mathrm{eff}}\left[\left(\frac{d\sigma}{dt^*}\right)_{\omega\Delta} + G(t)\left(\frac{d\sigma}{dt}\right)_{\omega N}\right]. \tag{3.76}$$

Here A_{eff} is the effective number of nucleons contributing to incoherent photoproduction; its value was taken from large-angle ρ^0 photoproduction (McClellan *et al.*, 1969c) and π^+ photoproduction in complex nuclei (Boyarski *et al.*, 1969). $(d\sigma/dt^*)_{\omega\Delta}$ and $(d\sigma/dt)_{\omega N}$ are cross sections for the processes $\gamma N \to \omega\Delta$ (1236) and $\gamma N \to \omega N$ calculated by Wolf (1969) using an OPE model. The cross section for $\gamma N \to \omega\Delta$ was taken at a different value t^* to take into account that, in this experiment, the momentum transfer was reconstructed assuming elastic production. $G(t)$ is a correction factor calculated by von Bochmann, Margolis, and Tang (1969) to take into account the suppression of incoherent processes at small t because of nuclear correlations. The solid lines in Fig. 100 were obtained by fitting

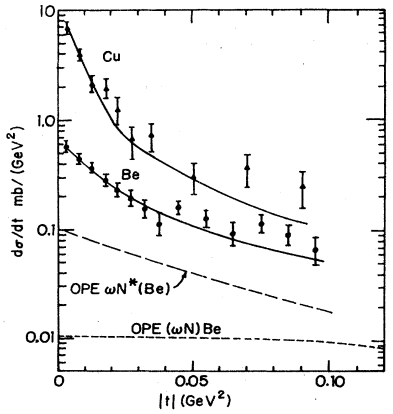

FIG. 100. Differential cross section for ω production in beryllium and copper. The two dashed lines give the contribution due to $\gamma\mathrm{Be} \to \omega N^*$ and $\gamma\mathrm{Be} \to \omega N$ as calculated using the OPE model. The solid lines are fits to the data using the method described in the text (from Behrend *et al.*, 1970b).

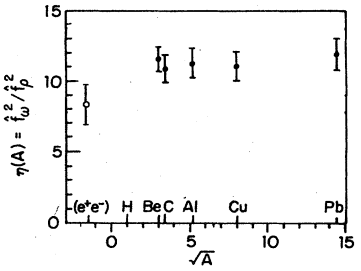

FIG. 101. The closed circles give the ratio $\eta(A) = (d\sigma/dt)_{\gamma A\to\rho A}/(d\sigma/dt)^{\mathrm{diff}}_{\gamma A\to\omega A}$ observed using the fit described in the text. The open circle gives $\bar{f}_\omega^2/\bar{f}_\rho^2$ as determined from colliding-beam experiments (after Behrend *et al.*, 1970b).

$$\left(\frac{d\sigma}{dt}\right)_{\omega A} = \left(\frac{d\sigma}{dt}\right)^{\mathrm{diff}}_{\omega A} + \left(\frac{d\sigma}{dt}\right)^{\mathrm{OPE}} \equiv \frac{1}{\eta(A)}\left(\frac{d\sigma}{dt}\right)_{\rho A} + \left(\frac{d\sigma}{dt}\right)^{\mathrm{OPE}} \tag{3.77}$$

to the data. Here $(d\sigma/dt)_{\rho A}$ is the measured photoproduction cross section for ρ^0 mesons on the same nucleus, and $\eta(A)$ is a fitting parameter which gives the ratio between diffractive ρ^0 and ω photoproduction cross sections. Fig. 101 shows the value of η as a function of A. With the assumption that the nuclear parameters are the same for both processes, this procedure gives an accurate determination of the ratio $\hat{f}_\omega^2/\hat{f}_\rho^2$. The ratio obtained is considerably higher than $\bar{f}_\omega^2/\bar{f}_\rho^2$ found in the colliding-beam experiments.

With the assumption that $\alpha_\omega = \alpha_\rho = -0.2$, the Rochester group obtained the following best fit values:

$$\sigma_\omega = (33.5 \pm 5.5)\,\mathrm{mb}\,, \tag{3.78a}$$

$$(d\sigma/dt)_{\omega N} = (11.4 \pm 1.9)\,\mu\mathrm{b/GeV}^2\,, \tag{3.78b}$$

$$\hat{f}_\omega^2/4\pi = 38.0 \pm 3.4\,. \tag{3.78c}$$

With the additional assumption that $\sigma_\omega = \sigma_\rho = (27 \pm 2)\,\mathrm{mb}$, they obtained

$$(d\sigma/dt)_{\omega N} = (9.6 \pm 1.2)\,\mu\mathrm{b/GeV}^2\,, \tag{3.79a}$$

$$\hat{f}_\omega^2/4\pi = 29.2 \pm 4.0\,. \tag{3.79b}$$

A Pisa–DESY group (Braccini *et al.*, 1970) used a somewhat different technique to study ω photoproduction from C, Al, Zn, Ag, Ta, and Pb at a mean photon energy of 5.7 GeV. These experimenters used a system of lead-glass counters to detect the $\pi^0\gamma$ decay mode of the photoproduced ω mesons. They did this by detecting the photon as well as one high-energy photon from the decay of the π^0. This system did not have sufficient angular resolution to measure the t dependence, and they had to rely on a Monte Carlo calculation to determine the diffractive component. Figure 102 shows the observed peaks.

This group used several models to subtract out the incoherent component. Figure 103 shows the t dependence predicted by the four models. The normalization of the incoherent cross section was determined by fitting the large-angle data of each angular distribution separately. After subtraction of the incoherent component according to the four models, an overall fit to the corresponding sets of coherent data was used to determine the unknown

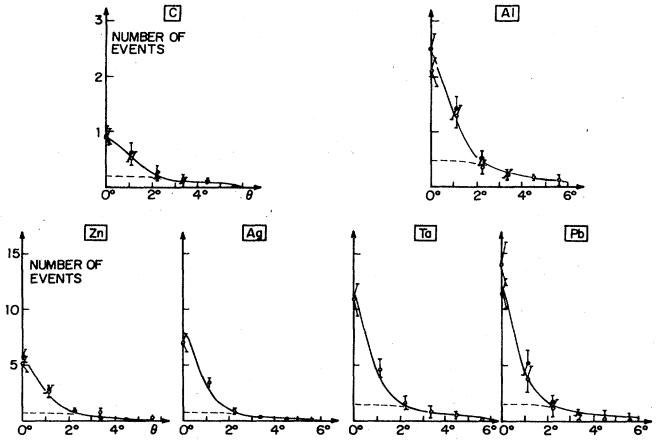

FIG. 102. ω yields in units of 10^{-35} (nucleons/cm^2)$^{-1}$ (eq. quant.)$^{-1}$ in the experiment of Braccini *et al.* (1970) as a function of angle. Full points and open points correspond to two different sets of measurements performed independently in order to check the reproducibility of the apparatus. The full lines are the best fit curves calculated according to model 4 which is illustrated in Fig. 103; the incoherent production at small angles is shown with dotted lines under the coherent peak (from Braccini *et al.*, 1970).

parameters $\hat{f}_\omega^2/4\pi$, σ_ω, and α_ω. For $\alpha_\omega=-0.3$, all the models gave values of σ_ω consistent with the total ρ^0-nucleon cross section. In particular, with model 4 and $\alpha_\omega=-0.3$,

$$\sigma_\omega=\left(27^{+6.0}_{-5.5}\right)\ \text{mb} \tag{3.80a}$$

$$\hat{f}_\omega^2/4\pi=22.0\pm5.4 \tag{3.80b}$$

$$\left.\frac{d\sigma}{dt}\right|_{\omega N}^{\text{diff}}=(13.5\pm3.3)\mu\text{b/GeV}^2\ . \tag{3.80c}$$

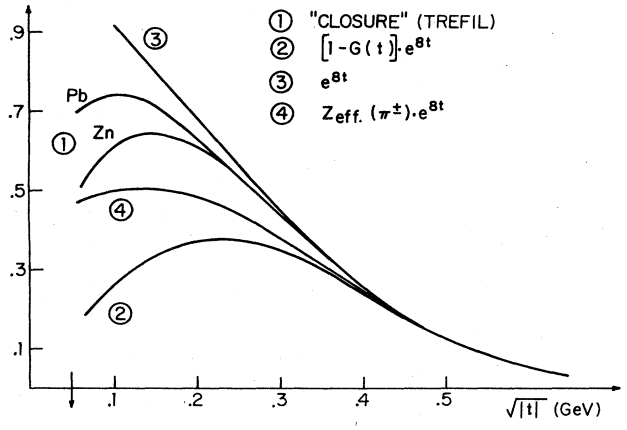

FIG. 103. Momentum-transfer dependence of the incoherent cross section, normalized at large t, according to the four different models used in the analysis of Braccini *et al.* (1970). Model 2 is the only one giving an A-dependent suppression factor. In this model the suppression factor is also slightly dependent on the energy. At large $|t|$ the incoherent cross sections follow the assumed common behavior e^{8t}. The arrow indicates the minimum of $\sqrt{|t|}$ in the experiment (from Braccini *et al.*, 1970).

These values differ somewhat from those quoted by Braccini *et al.* in that they include a more recent value for the $\omega\to\pi^0\gamma$ branching ratio and are corrected for $\rho^0\to\pi^0\gamma$ using $\Gamma(\rho\to\pi^0\gamma)=35\pm10$ keV. Whichever of the four models was used to evaluate the incoherent component, the fit to the large-angle points gave a hydrogen cross section $d\sigma/dt_{\gamma\omega}$ a factor of roughly 2 larger than the measured cross section for the reaction $\gamma p\to\omega p$. This suggests that other processes were contributing to the incoherent production. The results of this experiment are compatible with those of the Rochester experiment.

Since the Rochester value of $\hat{f}_\omega^2/4\pi$ was in considerable disagreement with the value then available from e^+e^- colliding-beam work, the experiments were subjected to considerable scrutiny. The following questions were raised concerning the two experiments on complex nuclei: (a) was inelastic production correctly subtracted, (b) was the assumption $\alpha_\omega\approx\alpha_\rho$ correct; (c) was it necessary to correct for A_2 exchange in nuclei having unequal numbers of neutrons and protons? This latter correction was not made initially. Item (a) is particularly important for the Bonn–Pisa experiment, because of its poor t resolution.

The Rochester group carried on further work to address these issues. By studying the A dependence of the ρ^0-ω phase difference in the 2π decay mode they determined that $\tan^{-1}\alpha_\omega-\tan^{-1}\alpha_\rho=-17^0\pm17^0$, consistent with the assumption questioned above in (b) (Behrend *et al.*, 1971c). They then restudied ω photoproduction from hydrogen, deuterium, beryllium, and copper, detecting $\omega\to\pi^+\pi^-\pi^0$, as in their 1970 experiments, but using a tagged photon beam (Abramson *et al.*, 1976). The group's $\gamma p\to\omega p$ and $\gamma d\to\omega NN$ results have already been discussed. The value of δ determined thereby was used to apply the small correction referred to in question (c) above. The reactions $\gamma p\to\omega\Delta(1236)$, $\gamma d\to\omega N\Delta(1236)$, $\gamma p\to\omega X$, and $\gamma d\to\omega NX$, $2.2\le m_X^2\le10.0$ GeV^2, were also studied. The cross sections measured for these reactions were used to obtain improved inelastic subtractions for the 1970 complex nuclei measurements, thus answering item (a). Corrections ranged from 3.5% to 10%. Finally, the new measurements for elastic ω photoproduction on Be and Cu, obtained with a tagged photon beam and therefore free of inelastic contamination, were compared with the corrected 1970 cross sections, and found to be in good agreement (10% lower,

TABLE XVIII. Summary of the deuterium data used to determine the ratio $\hat{f}_\omega^2/\hat{f}_\rho^2$ from measurements of the forward cross section.

Group	Energy	$\left.\frac{d\sigma}{dt}\right\|_{t=0}^{(\rho)}$	$\left.\frac{d\sigma}{dt}\right\|_{t=0}^{(\omega)}$	$\hat{f}_\omega^2/\hat{f}_\rho^2$
Abramson *et al.* (1976)	8.9	•••	28 ± 2	•••
Alexander *et al.* (1975)	7.5	300 ± 11	42 ± 9	$7.1^{+2.0}_{-1.2}$
Eisenberg *et al.* (1972b)	4.3	351 ± 30	52 ± 26	$6.8^{+6.7}_{-2.3}$
Eisenberg *et al.* (1976)	4.3	466 ± 27	69 ± 17	$6.7^{+2.1}_{-1.3}$
McClellan *et al.* (1971b)	4.08	447 ± 21	•••	•••
McClellan *et al.* (1971b)	4.61	432 ± 24	•••	•••
Unweighted Average		399 ± 65	47 ± 17	$8.4^{+9.7}_{-2.3}$

TABLE XIX. A summary of the $|T_0^N|^2$, $\sigma_{\omega N}$ and $\hat{f}_\omega^2/4\pi$ determined in the several ω photoproduction experiments. It has been assumed that $\hat{f}_\rho^2/4\pi = 2.18$.

Experiment	Energy	Target	Measured quantities	$\lvert T_0^N\rvert^2$ (μb/GeV^2)	$\sigma_{\omega N}$ (mb)	$\hat{f}_\omega^2/4\pi$	Assumptions	Comments
SLAC–Berkeley Ballam *et al.* (1973)	9.3	H	$\left.\frac{d\sigma}{dt}\right\|_\omega$	11.4 ± 2.1	···	25.3 ± 4.7	$\sigma_{\omega N} = 27$ mb $\alpha_\omega = -0.24$ $\left.\frac{d\sigma}{dt}\right\|_{t=0} = \lvert T_0^N\rvert^2$	No correction for A_2 exchange
Rochester Abramson *et al.* (1976)	8.3	D, Be, C, Al Cu, Pb	$\left.\frac{d\sigma}{dt}\right\|_{t=0}$	7.4 ± 0.5	25.4 ± 2.7	30.4 ± 4.8	$\alpha_{\omega N} = -0.24$	Corrected for A_2 exchange
Tel Aviv Alexander *et al.* (1975)	7.5	D	$\left.\frac{d\sigma}{dt}\right\|_\omega$	11.2 ± 2.5		25.7 ± 6.5	$\sigma_{\omega N} = 27$ $\alpha_\omega = -0.24$	
Tel Aviv Alexander *et al.* (1975)	7.5	D	$\left.\frac{d\sigma}{dt}\right\|_{\rho,\omega}$ $\left.\frac{d\sigma}{dt}\right\|_\rho \Big/ \left.\frac{d\sigma}{dt}\right\|_\omega = 7.1^{+2.0}_{-1.2}$	···	···	$15.5^{+7.0}_{-2.8}$	$\hat{f}_\omega^2/\hat{f}_\rho^2 = \left.\frac{d\sigma}{dt}\right\|_\rho \Big/ \left.\frac{d\sigma}{dt}\right\|_\omega$ $\hat{f}_\rho^2/4\pi = 2.18$	The rho cross section was anomalously low
Pisa–Bonn Braccini *et al.* (1970)	5.7	C, Al, Zn, Ta, Ag, Pb	Smeared cross section	13.5 ± 3.3	$27.0^{+6.0}_{-5.5}$	22.0 ± 5.4	$\alpha_{\omega N} = -0.3$	Poor t resolution and uncertainties in background correction
Weizmann Eisenberg *et al.* (1976)	4.3	D	$\left.\frac{d\sigma}{dt}\right\|_\omega$	18.5 ± 4.5	···	15.6 ± 3.8	$\sigma_{\omega N} = 27$ mb $\alpha_{\omega N} = -0.24$	
Weizmann Eisenberg *et al.* (1976)	4.3	D	$\left.\frac{d\sigma}{dt}\right\|_\rho$ $\left.\frac{d\sigma}{dt}\right\|_\rho \Big/ \left.\frac{d\sigma}{dt}\right\|_\omega = 6.7^{+2.1}_{-1.3}$	···	···	$14.6^{+4.9}_{-3.0}$	$\hat{f}_\omega^2/\hat{f}_\rho^2 = \left.\frac{d\sigma}{dt}\right\|_\rho \Big/ \left.\frac{d\sigma}{dt}\right\|_\omega$ $\hat{f}_\rho^2/4\pi = 2.18$	
Harvard–CEA Gladding *et al.* (1973)	4.2	H	$\left.\frac{d\sigma}{dt}\right\|_{\rho,\omega}$ $\left.\frac{d\sigma}{dt}\right\|_\rho \Big/ \left.\frac{d\sigma}{dt}\right\|_\omega = 7.7 \pm 0.12$			16.8 ± 2.8	$\hat{f}_\omega^2/\hat{f}_\rho^2 = \left.\frac{d\sigma}{dt}\right\|_\rho \Big/ \left.\frac{d\sigma}{dt}\right\|_\omega$ $\hat{f}_\rho^2/4\pi = 2.18$	No correction for OPE or A_2 exchange
ABHHM Benz *et al.* (1974)	1.3–5.3	D	$\sigma_{\rho,\omega}$ $\frac{\sigma(\rho)}{\sigma(\omega)} = 7.2^{+2.7}_{-1.6}$			$15.7^{+6.2}_{-3.7}$	$\hat{f}_\omega^2/\hat{f}_\rho^2 = \frac{\sigma(\gamma d \to \rho d)}{\sigma(\gamma d \to \omega d)}$ $\hat{f}_\rho^2/4\pi = 2.18$	
Lancaster Morris *et al.* (1976)	3.9	D	$\left.\frac{d\sigma}{dt}\right\|_{\rho,\omega}$	14.5 ± 5.4		15.3 ± 6.4	$\hat{f}_\omega^2/\hat{f}_\rho^2 = \frac{\sigma(\gamma d \to \rho d)}{\sigma(\gamma d \to \omega d)}$ $\hat{f}_\rho^2/4\pi = 2.18$	Poor-resolution experiment
Colliding beams						18.4 ± 1.8		

well within the statistical uncertainty of the measurements). The forward cross sections for Be, C, Al, Cu, and Pb, from the 1970 experiment (as corrected), and those for D, Be, and Cu from the 1976 experiment were subjected jointly to an optical-model analysis, under the assumption $\alpha_\omega = -0.24$. Results of the fit were $\sigma_\omega = (25.4 \pm 2.7)$ mb; $\hat{f}_\omega^2/4\pi = 30.4 \pm 4.8$. The statistical error on σ_ω is considerably reduced because of the extended range in A that results from the inclusion of deuterium data. The value of $\hat{f}_\omega^2/4\pi$ is little changed from the 1970 value.

The Bonn–Pisa experiment could be reanalyzed using the new data on ω inelastic photoproduction in the incoherent subtraction, and applying the small correction for δ. To our knowledge, this has not been done.

Summarizing the complex nuclei work, both experiments support $\sigma_\omega = \sigma_\rho$, the Rochester experiment to quite good accuracy. The 1976 Rochester experiment confirms their 1970 result, $\hat{f}_\omega^2/4\pi = 30.4$. The Bonn–Pisa experiment prefers a somewhat lower value, but (a) is not in serious disagreement (1.2 standard deviations), and (b) requires reanalysis to put the incoherent subtraction on firm ground.

It is instructive to consider together the data for coherent ρ^0 and ω photoproduction that can be used to determine $\hat{f}_\omega^2/\hat{f}_\rho^2$. These data are summarized in Table XVIII. The individual measurements for the ρ^0 and ω cross sections from deuterium are not in good agreement, and it appears rather meaningless to take a weighted average. The average value for $\hat{f}_\omega^2/\hat{f}_\rho^2$ in the table was obtained using the average cross sections.

Table XIX summarizes the cross sections and the values for $\hat{f}_\omega^2/4\pi$ and σ_ω determined by the various groups. The agreement between the various measurements is marginal and indicates that either some of the data are bad or there are systematic errors due to the mode of analysis.

Included in Table XIX are simultaneous measurements of ρ^0 and ω production from protons to obtain $\hat{f}_\omega^2/\hat{f}_\rho^2$ by Gladding *et al.* (1973). They found for $3.7 < E_\gamma < 4.7$ GeV

$$\frac{d\sigma/dt(\gamma p \to \rho p)}{d\sigma/dt(\gamma p \to \omega p)} = 7.7 \pm 1.2 \tag{3.81a}$$

and inferred using Eq. (3.64) a similar value for $\hat{f}_\omega^2/\hat{f}_\rho^2$. If it is assumed that the OPE contribution to the ω cross section is as found by Ballam *et al.* (40% at their energy), then

$$\hat{f}_\omega^2/\hat{f}_\rho^2 = 13.5 \pm 3.6 \ . \tag{3.81b}$$

Allowing for isospin exchange could boost their value as much as 50%. Because the value of δ at these low energies is so uncertain, and because of the large OPE cross section, which enlarges the error on the ratio, the results of Gladding *et al.* do not provide a useful result for $(\hat{f}_\omega/\hat{f}_\rho)^2$.

Figure 104 summarizes the measured values of $\hat{f}_\omega^2/\hat{f}_\rho^2$. The agreement between the various photoproduction experiments is good. They, however, give a value somewhat lower than that found in the colliding-beam experiments. The value obtained by the Rochester group is high and disagrees by two standard deviations with the colliding-beam value. The weight of the evidence supports the colliding-beam result.

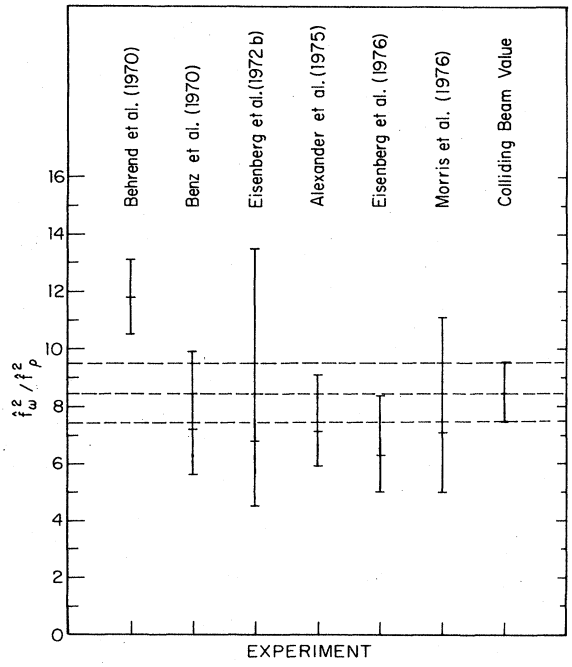

FIG. 104. A plot of $\hat{f}_\omega^2/\hat{f}_\rho^2$ versus E_γ for the various experiments.

The present data for ω photoproduction is quite unsatisfactory. There are several bubble chamber experiments but none with enough events to provide definitive results. There is only one high-statistics counter experiment. What is needed is another high-statistics track chamber or counter experiment with a sufficiently large number of events to provide a definitive arbitration between the presently available data.

It is our conclusion that the natural-parity exchange component of the omega photoproduction cross section is somewhat less than that given by the quark-VMD model and that otherwise the cross section has the expected character.

E. Phi photoproduction

The phi meson is an unstable particle with a mass of (1019.7 ± 0.3) MeV and a width of (4.1 ± 0.2) MeV. Its quantum numbers $I^G(J^P)C$ are $0^-(1^-)^-$ and its dominant decay modes are $K^+K^-((46.6 \pm 2.3)\%)$, $K_L K_S((35.0 \pm 2.0)\%)$, $\pi^+\pi^-\pi^0((16.4 \pm 1.5)\%)$, $\eta\gamma((2.0 \pm 0.4)\%)$, and $\pi^0\gamma((0.14 \pm 0.05)\%)$.

The ϕ meson is quite interesting from a number of standpoints. In addition to its being one of the three major vector mesons, it was pointed out on the basis of quite general arguments (Freund, 1967; Barger and Cline, 1970; Joos, 1967b; Kajantie and Trefil, 1967) that ϕp elastic scattering should proceed only through Pomeron exchange. This is a consequence of the most simple form of the quark model in which the ϕ is made up of only two strange quarks which are barred from resonant reactions with nonstrange hadrons. Thus, on the basis of diagonal VMD, one would expect ϕ photoproduction to be due dominantly to Pomeron exchange

and hence to provide an excellent source of information concerning the Pomeron (Leith, 1973; Moffeit, 1974; Dass and Fraas, 1975). There is, however, some evidence (such as $\phi \to \pi^+\pi^-\pi^0$) of a small admixture of non-strange quarks in the ϕ that could modify this simple view.

1. Production from hydrogen

Several experimental techniques have been used to study ϕ photoproduction: hydrogen bubble chamber experiments in which the K^+K^- pair is observed, counter experiments in which the K^+K^- pair is observed, counter experiments in which the recoil proton is observed, and counter experiments in which the K^+K^- pair and the recoil proton are observed. The first bubble chamber measurement was carried out at the Cambridge Electron Accelerator with a bremsstrahlung beam of 6 GeV by the Cambridge bubble chamber group (Crouch *et al.*, 1967). They obtained only a few events and were unable to study the details of the photoproduction reaction. Somewhat more extensive data were obtained at DESY by the ABBHHM collaboration using the DESY bubble chamber in conjunction with a 7.5 GeV bremsstrahlung beam (Erbe *et al.*, 1966, 1968a). The most extensive bubble chamber measurements were carried out at SLAC by the SLAC–Berkeley bubble chamber group (Ballam *et al.*, 1973).

Figure 105 shows a comparison between the data from the SLAC–Berkeley bubble chamber group (Ballam *et al.*, 1973), taken with a monochromatic photon beam, and the predictions of the s-channel helicity conservation model. The data are consistent with SCHC and pure natural-parity exchange. The bubble chamber data on the ϕ are not extensive, and additional experiments, in

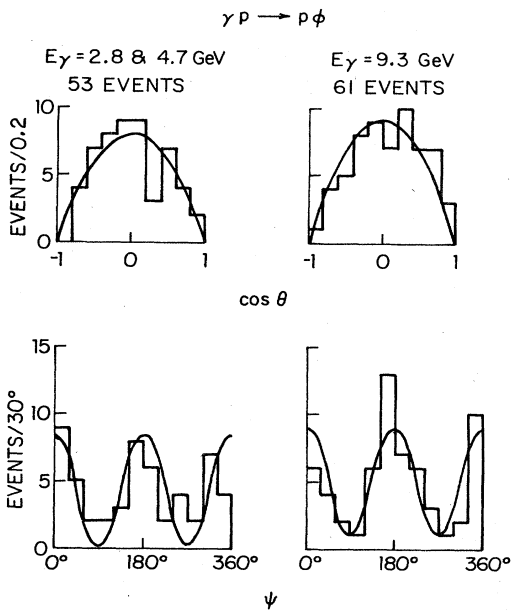

FIG. 105. A comparison between the decay angular distributions for ϕ photoproduction observed with a polarized photon beam and the predictions of the s-channel helicity conservation model with natural spin-parity exchange in the t channel (from Ballam *et al.*, 1973).

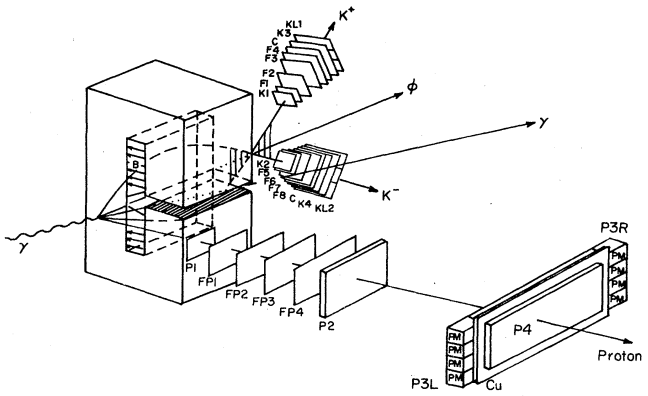

FIG. 106. Diagram of the apparatus used by the Bonn group to study ϕ photoproduction (from Besch *et al.*, 1974).

which the complete decay angular distribution is measured as a function of momentum transfer, are warranted. In particular, the SLAC–Berkeley bubble chamber experiments at 2.8, 4.7, and 9.3 GeV obtained only 114 events in the ϕ mass region.

Several counter groups have carried out measurements of ϕ photoproduction. The first counter experiment was carried out by a Cornell group using a pair spectrometer system at the 2 GeV electron synchrotron (Mostek *et al.*, 1968). Another Cornell group, working at the 10 GeV electron synchrotron, first used a pair spectrometer system (McClellan *et al.*, 1971a) and then supplemented the pair spectrometer system with a set of counters for observing the recoil proton in coincidence with the K^+K^- pair (Berger *et al.*, 1972). An MIT–DESY group used a pair spectrometer system to study ϕ production through observation of the K^+K^- decay mode (Alvensleben *et al.*, 1972). A SLAC–Wisconsin group carried out measurements in which they observed the recoil proton with a magnetic spectrometer and used a simple spectrometer system to observe the coincident K^+K^- pair (Halpern *et al.*, 1972). The group also made measurements in which they observed only the recoil proton (Jones *et al.*, 1968; Anderson *et al.*, 1973a). A Bonn group (Besch *et al.*, 1974) used a special spectrometer system to observe ϕ production by detection of the K^+K^- pair in coincidence with the recoil proton. Figure 106 shows a diagram of their apparatus. More recently a DESY–Karlsruhe group (Behrend *et al.*, 1975) used a pair spectrometer system in conjunction with a tagged photon beam to study ϕ photoproduction in the energy range $4.6 \leq E_\gamma \leq 6.7$ GeV. A Cerenkov counter was used to reject pions. Figure 107 shows a diagram of their apparatus. Table XX summarizes the reported measurements of ϕ photoproduction.

For the analysis of the counter experiments in which the two kaons are observed, it is necessary to assume a decay angular distribution for the ϕ. It is necessary to know that the decay distribution is the $\sin^2\theta$ characteristic of the SCHC model. Two of the counter groups (DESY–MIT and Bonn) presented evidence for the validity of this model for decay angles near 90° in the ϕ center-of-mass system. The later measurements by the Cornell group, in which they observed the two kaons and the recoil proton, showed that their earlier measure-

TABLE XX. A summary of the measurements of ϕ photoproduction from hydrogen.

Group	Accelerator	Energy (GeV)	Range in t (GeV^{-2})
Erbe *et al.* (1968a)	DESY	2.5–5.8	$0.02 < \|t\| < 1.6$
Anderson *et al.* (1970b)	SLAC	5.0–17.8	$0.12 < \|t\| < 1.4$
Alvensleben *et al.* (1972)	DESY	5.2	$t_{min} < \|t\| < 0.02$
Berger *et al.* (1972)	Cornell	8.5	$t_{min} < \|t\| < 0.5$
Ballam *et al.* (1973)	SLAC	2.8, 4.7, 9.3	$0.02 < \|t\| < 1.6$
Anderson *et al.* (1973)	SLAC	12	$0.2 < \|t\| < 1.0$
		6–19	$\|t\| = 0.6$
Besch *et al.* (1974)	Bonn	2.0	$0.23 < \|t\| < 0.73$
Behrend *et al.* (1975)	DESY	4.6–6.7	$t_{min} < \|t\| < 0.4$

ments, in which they observed only the two kaons, gave cross sections which were 12% to 20% too high. The discrepancy is presumably due to inelastic production.

Figures 108 and 109 show the momentum-transfer behavior of the cross section determined by the counter experiments at low and high momentum transfer, respectively. Figure 110 shows a comparison between the bubble chamber data and the counter data. The agreement between the counter data and the less precise bubble chamber data is satisfactory. Figure 111 shows on one plot all the data for ϕ photoproduction. Figures 108 through 111 indicate that the data lie on a universal curve, and that the parameter giving the exponential dependence on momentum transfer decreases with increasing $|t|$.

The data are striking in that they show little evidence for the shrinkage of the diffraction peak that one would expect from Pomeron exchange (see previous references). In order to make a more definitive test for shrinkage, the SLAC–Wisconsin group (Anderson *et al.*, 1973a) measured precisely the energy dependence of the cross section at $t = -0.6$ GeV^2 for $s = 5$ to $s = 36$ GeV^2. Figure 112 shows their result together with a lower energy point from measurements by the Bonn group (Besch *et al.*, 1974). There is clearly no evidence for shrinkage. Similar data for K^+p and pp scattering show strong shrinkage.

A fit of the form

$$\frac{d\sigma}{dt} = \left.\frac{d\sigma}{dt}\right|_{t=0} e^{Bt} \tag{3.82}$$

to the DESY–Karlsruhe data gives

$$B = (5.6 \pm 0.3)(\text{GeV})^{-2} \tag{3.83a}$$

$$\left.\frac{d\sigma}{dt}\right|_{t=0} = (2.49 \pm 0.15)\ \mu\text{b}/(\text{GeV})^2 \ . \tag{3.83b}$$

A similar fit to the Bonn data gives

$$d\sigma/dt = (1.47 \pm 0.22)\exp[(4.01 \pm 0.23)t] \ . \tag{3.84}$$

This fit is shown as a solid line in Fig. 108. Figure 113 shows the results for $\left.d\sigma/dt\right|_{t=0}$ and B determined by fitting the data for selected ($>1C$) experiments. The shaded area gives the slope of the theoretically extracted, "pure" Pomeron contribution in the reactions $\pi^\pm p \to \pi^\pm p, K^+p \to K^+p$, and $\gamma p \to \rho^0 p$ (Davier, 1972; Höhler and Jakob, 1974; Chadwick *et al.*, 1973; Lasinski *et al.*, 1972). Eisenberg (1974) has studied the question of the shrinkage of the forward $d\sigma/dt$ slope in ϕ photoproduction by using K^+p, K^-p, π^-p total cross sections and quark model relations. He concluded that existing data were not inconsistent with forward shrinkage, if $d\sigma/dt$ was expressed in the form $A\exp(Bt + Ct^2)$ in the $|t|$ range $0 \to 0.6$ GeV^2.

Kemp and Marshall (1975) have reexamined the energy and t dependence of ϕ photoproduction using all the available data. They found the fits

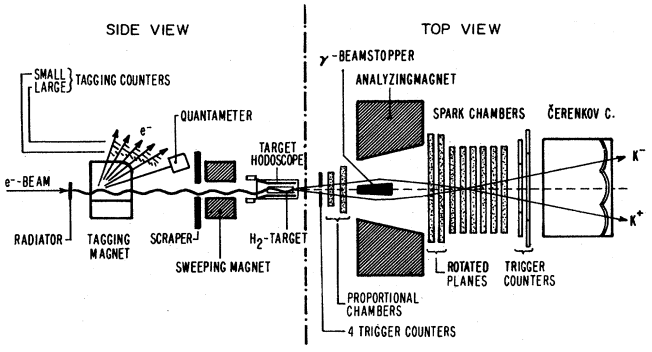

FIG. 107. Experimental setup used by DESY–Karlsruhe group to study ϕ photoproduction (from Behrend *et al.*, 1975).

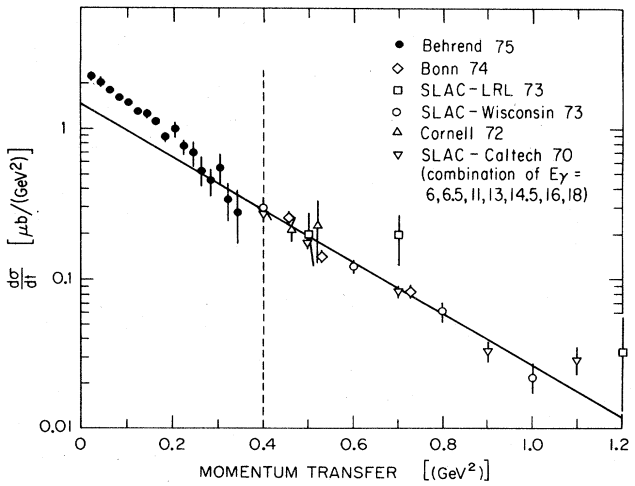

FIG. 108. A plot of $d\sigma/dt$ versus t determined in the reported ϕ photoproduction experiments (from Silverman, 1975).

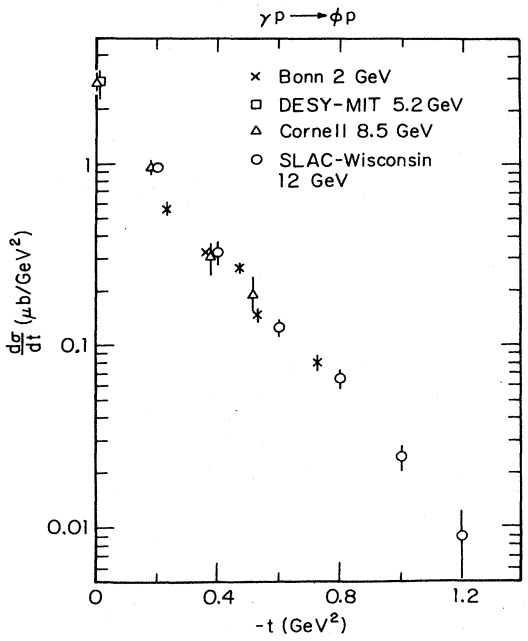

FIG. 109. A plot versus t of the ϕ photoproduction data obtained by the Bonn, DESY–MIT, Cornell, and SLAC–Wisconsin counter experiments (from Silverman, 1975).

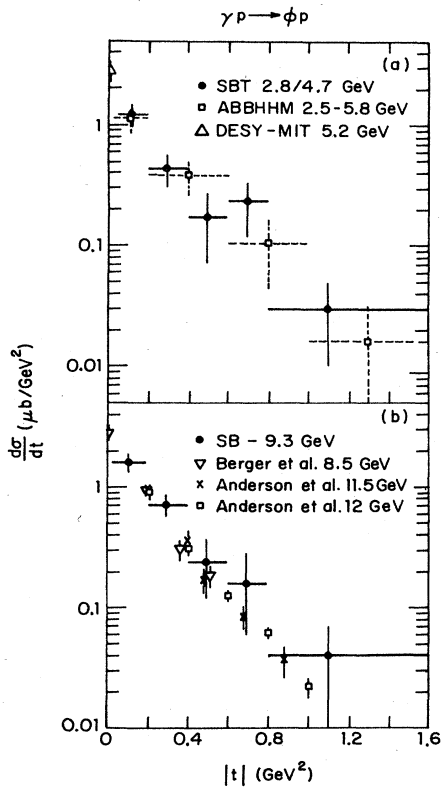

FIG. 110. A comparison of the ϕ photoproduction cross sections obtained by the counter and bubble chamber experiments (from Ballam *et al.*, 1973).

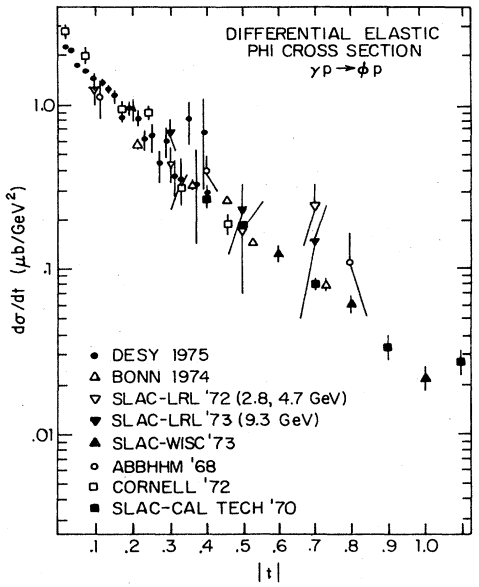

FIG. 111. A plot versus t of all the available data for ϕ photoproduction showing the striking energy-independent behavior of the cross section.

$$d\sigma/dt = (2.59 \pm 0.18)\exp[(5.9 \pm 0.3)t + (1.4 \pm 0.3)t^2] \tag{3.85a}$$

with $\chi^2/DF = 69/58$ (C.L. = 15.3%) and

$$d\sigma/dt = s^{2[\alpha(t)-1]}(1.34 \pm 0.10)\exp[(4.8 \pm 0.5)t + (1.7 \pm 0.5)t^2]. \tag{3.85b}$$

where

$$\alpha(t) = (1.14 \pm 0.05) + (0.27 \pm 0.08)t\ . \tag{3.85c}$$

with $\chi^2/DF = 54/56$(C.L. = 55.7%). Here $\alpha(t)$ may be regarded as an effective Pomeron trajectory. Thus this analysis slightly favors the possibility that the $t=0$ cross section rises with energy although, statistically, the case is not strong. In summary, the evidence appears to favor some shrinking of the forward diffraction peak.

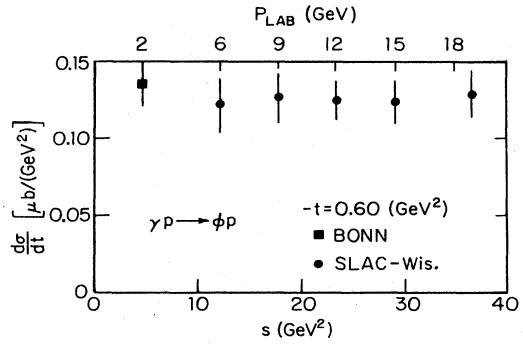

FIG. 112. A plot versus energy of the data obtained for ϕ photoproduction by the Bonn and SLAC–Wisconsin groups for $t=-0.60$ GeV^2 (from Anderson *et al.*, 1973a).

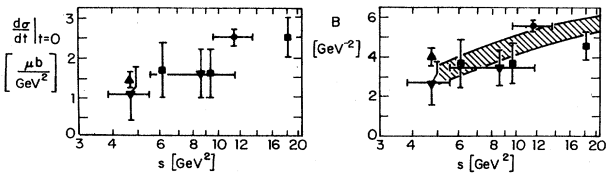

FIG. 113. Results for $d\sigma/dt|_{t=0}$ and B obtained from fitting all the data of the DESY–Karlsruhe group to the form $d\sigma/dt = d\sigma/dt|_{t=0}e^{Bt}$ together with corresponding results from other selected ($\geq 1C$) experiments. The symbols for the different experiments are: ■, Ballam *et al.*, 1973a; ▲, Besch *et al.*, 1974; ▼, Erbe *et al.*, 1968a. The shaded area represents the slope of the (model-dependent) Pomeron contributions in elastic meson-nucleon scattering (from Behrend *et al.*, 1975).

2. Asymmetry parameter

In an experiment in which they observed both the decay kaons and the recoil proton, the SLAC–Wisconsin group (Halpern *et al.*, 1972) measured the asymmetry parameter, $\Sigma(3.53)$, for production by polarized photons at 8.14 GeV, with $|t| = 0.2$ GeV^2, and found

$$\Sigma = 0.985 \pm 0.12 \tag{3.86}$$

in excellent agreement with the prediction of pure Pomeron exchange. This result discredited an earlier Cornell measurement (McClellan *et al.*, 1971c) in which a smaller asymmetry was observed. The Cornell experiment observed only the decay kaons and presumably the ϕ production was contaminated with inelastic events.

3. Production from deuterium

The Cornell group (McClellan *et al.*, 1971a) measured the ratio of the cross sections for production from deuterium and hydrogen and found, by extrapolating to $t = 0$, $R = 3.6 \pm 0.6$. The predicted ratio, assuming no isospin exchange (no proton-neutron difference) is $R(0) = 3.89$. The data are thus consistent with this assumption, lending some support to the hypothesis of pure Pomeron exchange.

4. Real part of production amplitude

The MIT–DESY group (Alvensleben *et al.*, 1971b) used their pair spectrometer system to measure for a carbon target the interference between the $\phi \to e^+e^-$ decay and the Bethe–Heitler production of electron-positron pairs. From these data they found for the ratio of the real to the imaginary part of the ϕ production amplitude, with $6 < E_\gamma < 7.4$ GeV,

$$\alpha_\phi = \frac{\mathrm{Re}T_\phi}{\mathrm{Im}T_\phi} = -0.48\,^{+0.33}_{-0.45} . \tag{3.87}$$

This ratio is quite large and suggests that ϕ production may not be due simply to Pomeron exchange, for which the amplitude is purely imaginary, or that there is a large Thomson-like amplitude (see Sec. IV.F). This is a difficult experiment and it should be repeated. We know of no theoretical prediction for α_ϕ.

5. Leptonic decay

The MIT-DESY group (Becker *et al.*, 1968 Alvensleben, *et al.*, 1971b) also measured the branching ratio for the decay of the ϕ into electron-positron pairs. In experiments with a carbon target, they found

$$\frac{\Gamma(\phi \to e^+e^-)}{\Gamma(\phi \to all)} = (2.8 \pm 0.4) \times 10^{-4} . \tag{3.88}$$

From this and $\Gamma_\phi = 4.0$ MeV, they calculated

$$\frac{\bar{f}_\phi^2}{4\pi} = 16.0 \pm 2.8 . \tag{3.89}$$

This is to be compared with the colliding-beam value $\bar{f}_\phi^2/4\pi = 13.2 \pm 0.6$.

6. Production from complex nuclei

A Cornell group (McClellan *et al.*, 1971a) measured ϕ photoproduction from a series of complex nuclei to determine σ_ϕ. The experimenters used a pair spectrometer system to measure the ϕ photoproduction from hydrogen, deuterium, carbon, magnesium, copper, silver, and lead targets. The system had a large aperture, and they used the optical model in conjunction with the assumption of a $\sin^2\theta$ angular distribution in the ϕ rest frame to analyze the data (see Appendix D, Fig. 211). They made no correction to the data for an inelastic contribution to the cross section, and placed an upper limit of 12% on the contamination of the forward hydrogen cross section by extrapolating to zero degrees measurements in which the recoil proton was also observed. Figure 114 shows a plot of the 0° cross section versus A. The group used optical-model calculations and various hypotheses concerning α_ϕ, σ_ϕ, and $\hat{f}_\phi^2/4\pi$ to fit the data. Table XXI summarizes their results. It is disturbing that $\hat{f}_\phi^2/4\pi$ comes out so much larger than the colliding-beam value $\hat{f}_\phi^2/4\pi = 13.2 \pm 0.6$ (Table XXVII).

The DESY–MIT group (Alvensleben *et al.*, 1972) made careful measurements of ϕ photoproduction from a hy-

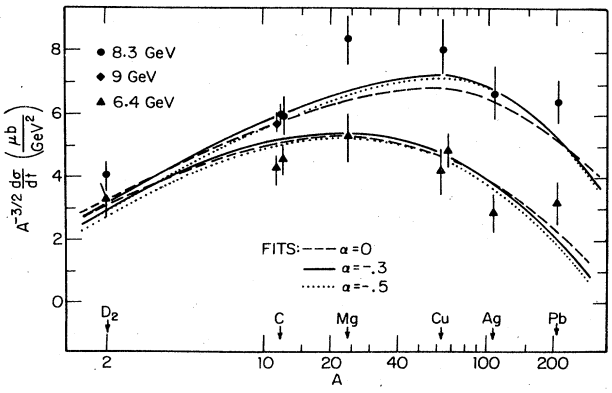

FIG. 114. A dependence of the 0° cross sections for the data of the Cornell group (McClellan *et al.*, 1971a). The curves are the results of simultaneous fits to the data at 6.4 GeV and the combined data at 8.3 and 9 GeV. The three indicated values of $\alpha_{\phi N}$ were used in the analysis (from McClellan *et al.*, 1971a).

TABLE XXI. Parameters from the A-dependence experiment of McClellan *et al.* (1971a). In the last four fits σ_ϕ is constrained to 12 mb, the quark-model value.

α_ϕ	σ_ϕ	$\hat{f}_\phi^2/4\pi$	Description
−0.5	9.2±2.8	17.2±8.4	All data
−0.3	12.1±3.0	23.6±9.6	All data
−0.0	17.6±4.3	42.8±16.4	All data
−0.25	12	22.0	8.3 GeV only
−0.35	12	25.2	6.4 GeV only
−0.12	12	21.2	D_2 excluded
−0.22	12	21.6	D_2 reduced by 10%

drogen target and used the expression

$$\frac{d\sigma}{dt} = \frac{\alpha}{16\pi}\left(\frac{\hat{f}_\phi^2}{4\pi}\right)^{-1}[1+(\alpha_\phi)^2](\sigma_\phi)^2 \tag{3.90}$$

to determine σ_ϕ through the use of their previously determined values of $\hat{f}_\phi^2/4\pi$ and α_ϕ. They found $\sigma_\phi = (9.8^{+2.9}_{-3.3})$mb. The DESY–Karlsruhe group (Behrend *et al.*, 1975) repeated this analysis using their data. If σ_ϕ is fixed at a quark-model value of (13.0±1.5)mb, then $\hat{f}_\phi^2/4\pi$ is found to be 25.6±6.4 (28.0±7.2) for $\alpha_\phi = 0(-0.3)$. Conversely, if $\hat{f}_\phi^2/4\pi$ is fixed at the storage ring value, $\hat{f}_\phi^2/4\pi = 13.2\pm0.6$, then σ_ϕ is found to be 10.2±0.6(9.7±0.6) for $\alpha_\phi = 0(-0.3)$.

A small amount of ω-ϕ mixing could have a considerable effect on the deviation of $\hat{f}_\phi^2/4\pi$ and σ_ϕ from the colliding-beam and quark-model values, and affect the value of σ_ϕ determined from the experiments on complex nuclei. This is discussed further in Sec. IV.

It is instructive to compare the observed ϕ cross section with that predicted by the quark-VMD model. We have used the expressions

$$\frac{d\sigma}{dt} = \alpha\left(\frac{4\pi}{\hat{f}_\phi^2}\right)\frac{d\sigma}{dt}(\phi p \to \phi p) \tag{3.91}$$

$$\frac{d\sigma}{dt}(\phi p) = \left[\left(\frac{d\sigma}{dt}(K^+p)\right)^{1/2} + \left(\frac{d\sigma}{dt}(K^-p)\right)^{1/2} - \left(\frac{d\sigma}{dt}(\pi^-p)\right)^{1/2}\right]^2 \tag{3.92}$$

to calculate from measurements of the kaon-proton and pion-proton cross sections the expected ϕ cross section. For this calculation $\hat{f}_\phi^2/4\pi$ was taken to be the earlier colliding-beam value 13.2. Table XXII summarizes the data used in these calculations and the results for the ϕ photoproduction cross section. In these calculations the measured total cross sections were used via the optical theorem to determine the cross section at 0°.

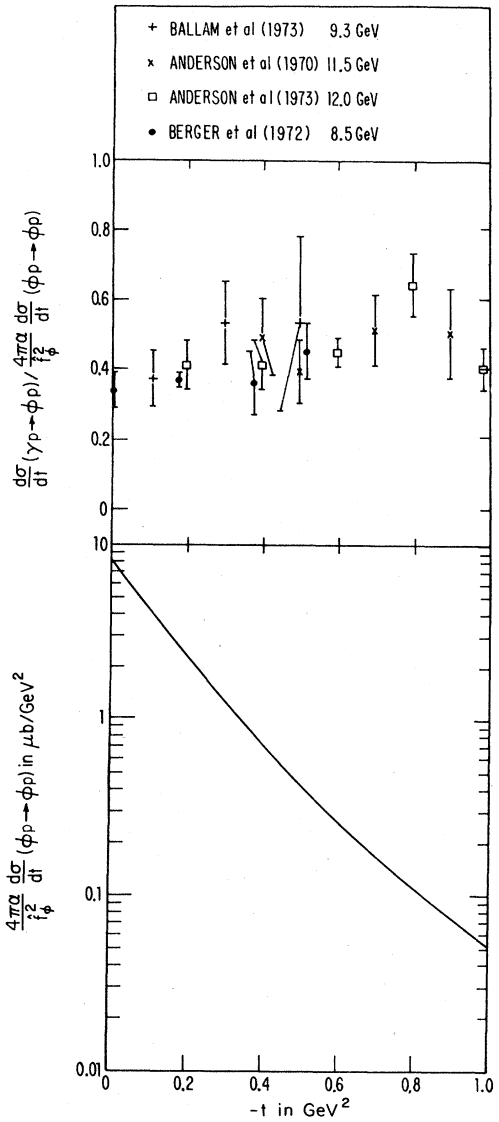

FIG. 115. A comparison between the phi reference cross section and representative portions of the available data. The data used are summarized in Table XXII.

Figure 115 shows a comparison between the measured ϕ cross sections and the quark–VMD model prediction.

TABLE XXII. A summary of the data used to calculate the ϕ photoproduction cross section expected for the simple quark model plus vector-meson dominance. The cross section has been expressed in the form $A\exp(Bt + Ct^2)$ where t is in the GeV^2, the strong interaction cross sections are in mb/GeV^2, and the photoproduction cross sections are in μb/GeV^2.

Reaction	Momentum GeV/c	Source of data		A	B	C
$\pi^-p \to \pi^-p$	8.5	Hartung *et al.* (1965)	−0.12	38.1	8.54	1.84
$K^+p \to K^+p$	9.8	Foley *et al.* (1963)[b]	−0.4	19.3	6.01	0.57
$K^-p \to K^-p$	9.0	Foley *et al.* (1963)[b]	+0.25	32.8	9.73	3.25
$\phi p \to \phi p$	9.1			14.9	6.72	1.66
$\gamma p \to \phi p$	9.1	$\hat{f}_\phi^2/4\pi = 13.2$		8.24	6.72	1.66

The model predicts the correct t dependence but is off by a factor of roughly 2 in the cross section. This discrepancy reveals a serious weakness in the understanding of ϕ photoproduction. Some possible contributing factors are: the ϕ scattering amplitude may be smaller than the quark model suggests; $\phi-\omega$ mixing may contribute destructively to ϕ photoproduction; and the VMD extrapolation from $k^2=m_\phi^2$ to $k^2=0$ may suppress the production amplitude relative to the scattering amplitude. None of these possibilities is very well understood at a quantitative level.

F. Electron-positron annihilation experiments

As described in Sec. II.B, e^+e^- annihilation experiments provide direct information about the hadronic states which contribute to the structure of the photon. Figure 116 shows some general diagrams for the production of hadrons through electron–positron collisions. The processes of interest to us are represented by Fig. 116(a) in which there is a single timelike virtual photon; according to Eq. (2.5), the resulting cross section provides a direct measure of the hadronic content of the photon. There is little or no evidence for the other types of processes illustrated in Fig. 116.

Since the intermediate state has only a virtual photon, the final hadronic state has $J=1$, $C=-1$, $P=-1$, $I=0$ or 1, and $S=0$. If it has only pions, its G parity is $(-1)^{I+1}$; i.e., the number of pions is odd for $I=0$ and even for $I=1$. Since the total angular momentum is 1, the angular dependence of any feature, such as the single-hadron distribution or jet axis distribution, is limited to the form

$$d\sigma/d\Omega=\sigma_T+\sigma_L+(\sigma_T-\sigma_L)(\cos^2\theta+P^2\sin^2\theta\cos2\phi)\ , \tag{3.93}$$

where $\sigma_T(\sigma_L)$ corresponds to a virtual photon polarized perpendicular (parallel) to the observed direction and P is the equal and opposite transverse polarization of the beams.

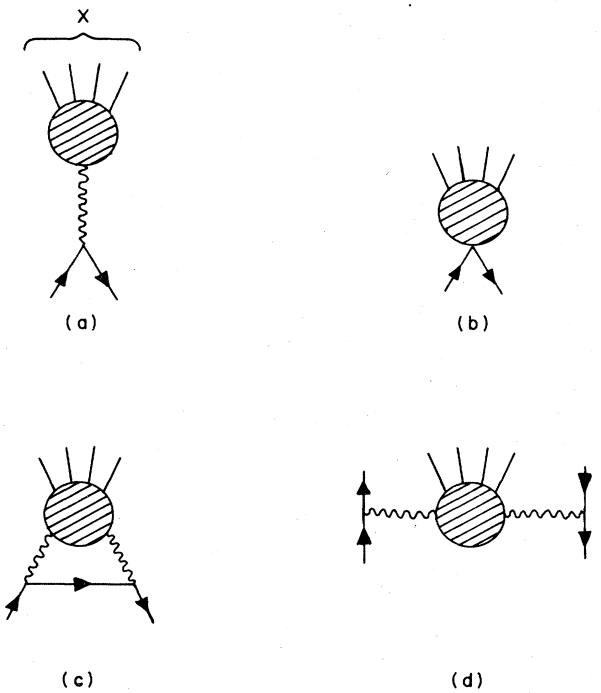

FIG. 116. Examples of hadron production in e^+e^- collisions. (a) Annihilation with a one-photon intermediate state. (b) A hypothetical direct coupling of e^+e^- to hadrons. (c) Annihilation with a two-photon intermediate state. (d) Photon-photon interaction, which should become relatively important at higher energies.

Some recent reviews of colliding-beam experiments have been given by Bernardini (1972), Silvestrini (1973), Strauch (1974), Richter (1974), Feldman and Perl (1975, 1977), Schwitters (1975, 1977), Feldman (1975), Bemporad (1975), Schwitters and Strauch (1976), and Wiik and Wolf (1977). For a summary of related theory, see Gilman (1975). Here we do not attempt to present a balanced view of this very active research area. Rather, we emphasize those topics which are of greatest interest to the remainder of the paper, particularly the determination of the parameters of the lower resonances.

1. Colliding-beam facilities

In order to obtain sufficient energy in the electron–positron center-of-mass system, it is necessary to use a colliding-beam system. The first colliding-beam facility which yielded interesting results was the e^-e^- storage rings which were originally proposed by O'Neill and were built at Stanford through a Princeton–Stanford collaboration (O'Neill, 1956; Barber *et al.*, 1959). This machine consisted of two separate intersecting rings and it was used to test quantum electrodynamics (Barber *et al.*, 1966). The development of electron–positron storage rings started in Europe in 1960 with the construction of the first ring, ADA, for electron and positron beams of 250 MeV each (Bernardini *et al.*, 1960, 1962). In 1964 Bernardini *et al.* reported the definite proof of electron–positron collisions in ADA through the detection of single bremsstrahlung of one beam on the other (Bernardini *et al.*, 1964). The first e^+e^- results of importance were obtained by the 2×700 MeV Novosibirsk storage ring, VEPP2, and the 2×550 MeV Orsay storage ring, ACO. The experiments performed with these rings included tests of quantum electrodynamics and investigations of the neutral vector mesons ρ^0,ω,ϕ and their link to the electromagnetic field. Subsequently the 2×1.5 GeV Frascati storage ring, ADONE, was completed (Amman *et al.*, 1969) and it was used to make new tests of quantum electrodynamics and to study the production of hadronic events of a nonresonant character in the total energy range from 1.4 to 2.4 GeV. It was found, in particular, that the production of multihadron events was surprisingly large. The conversion of the Cambridge Electron Accelerator (CEA) into a storage ring through the addition of a positron source and a bypass, made it possible to test quantum electrodynamics at higher energy and to study the total cross section for production of hadrons at center-of-mass energies of 4 and 5 GeV. These measurements showed that the ratio of the total hadronic cross section to the total μ-pair cross section was large and rising with energy. More recently new storage rings at SLAC and DESY have been

TABLE XXIII. Parameters of storage ring facilities.

Name	Location	Initial operation	Type	Status	Maximum total energy (GeV)	Nominal luminosity[a] ($cm^2\,sec^{-1}$)
ADA	Frascatti	1960	Single ring	Closed down	0.5	
ACO	Orsay	1966	Single ring	Closed down	1.1	10^{29}
ADONE	Frascatti	1970	Single ring	Operating	3.1	10^{30}
DCI	Orsay	1976	Two rings four beams	Operating	3.6	(10^{32})
CEA	Cambridge	1972	Synchrotron bypass	Closed down	5.0	3×10^{28}
VEPP-2	Novosibirsk	1966	Single ring	Closed down	1.3	3×10^{28}
VEPP-3	Novosibirsk	1973	Single ring	Testing	4.0	10^{32}
VEPP-4	Novosibirsk	1976	Single ring	Under construction	10–14	10^{32}
SPEAR 1	SLAC	1973	Single ring	Closed down	5.0	5×10^{30}
SPEAR 2	SLAC	1974	Single ring	Operating	9.0	10^{31}
DORIS	DESY	1974	Two rings	Operating	9.0	10^{31}
PETRA	DESY	1979	Single ring	Under construction	38.0	(10^{32})
PEP	SLAC	1980	Single ring	Under construction	38.0	(10^{32})
CESR	Cornell	1979	Single ring	Under construction	16.0	(10^{32})

[a] ( ) projected luminosities.

put into operation. They have made possible measurements up to a total center-of-mass energy of 7.8 GeV. These measurements have verified the large hadronic cross section and revealed a whole new family of resonances.

● When speaking of storage rings it is conventional to characterize them by their luminosity. The luminosity is defined as the number by which the cross section must be multiplied to obtain the event rate. Table XXIII summarizes characteristics of the e^+e^- colliding-beam machines which have either been used or are under construction.

2. Purely electromagnetic processes

● The study of electromagnetic processes is important for two reasons. On the one hand, quantum electrodynamics is the only field theory where cross sections can be calculated with arbitrarily good precision (due to the smallness of α). Thus accurate measurements provide a basic test of the assumptions of local quantum field theory. On the other hand, observation of these processes in kinematic regions where there is no question of the validity of the theory provides a means of determining the luminosity experimentally.

● All of the machines have been used to study the reactions

$$e^+ + e^- \to e^+ + e^- ,$$

$$e^+ + e^- \to \gamma + \gamma ,$$

$$e^+ + e^- \to \mu^+ + \mu^- ,$$

as a means of determining the validity of quantum electrodynamics at small distances (Alles-Borelli *et al.*, 1972; Borgia *et al.*, 1972; Balakin *et al.*, 1971b; M. Bernardini *et al.*, 1973c; Newman *et al.*, 1974; Beron *et al.*, 1974; Augustin *et al.*, 1975). The quantum-electrodynamic cross sections are based on the assumption that leptons are pointlike Dirac particles, that Maxwell's equations describe the photon, and that contributions from higher-order diagrams can be taken into account through radiative corrections. No deviations from QED have been reported in measurements up to a total center-of-mass energy of 7.4 GeV (Augustin *et al.*, 1975; O'Neill *et al.*, 1976). The assumption of a single form factor for spacelike and timelike photons gives cutoffs of $\Lambda_+ > 35$ GeV and $\Lambda_- > 47$ GeV, where the Λ's are defined through the form-factor parametrization

$$F_\pm(Q^2) = (1 \pm Q^2/\Lambda_\pm^2)^{-1} . \tag{3.94}$$

No physical significance is to be attributed to this form; it merely gives a convenient parametrization of a possible breakdown.

● For the reaction

$$e^+ + e^- \to \mu^+ + \mu^- ,$$

when it is assumed that the muons are spin-$\frac{1}{2}$ point Dirac particles, the differential cross section is

$$\frac{d\sigma_{\mu\mu}}{d\Omega} = \frac{\alpha^2\beta}{4s}\left[(1+\cos^2\theta) + (1-\beta^2)\sin^2\theta\right] , \tag{3.95}$$

where s is the square of the total center-of-mass energy, and $\beta = p_\mu/E_\mu$. A simple integration gives for the total cross section

$$\sigma_{\mu\mu} = \frac{2\pi\alpha^2}{3s}\beta(3-\beta^2) \tag{3.96}$$

which becomes, in the limit $\beta \to 1$,

$$\sigma_{\mu\mu} = \frac{4\pi\alpha^2}{3s} = \frac{21.71\,nb}{E^2} \tag{3.97}$$

where E is the single beam energy in GeV. In discussing hadronic final states, it is conventional to express the total hadronic cross section $e^+ + e^- \to$ hadrons in terms of $\sigma_{\mu\mu}$ through the expression

$$R_{e^+e^-}(s) = \frac{\sigma_{\rm had}(s)}{\sigma_{\mu\mu}(s)} . \tag{3.98}$$

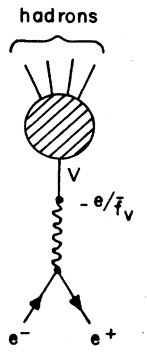

FIG. 117. Coupling of a virtual photon to hadrons through a vector meson which produces a resonance peak.

3. Resonance production formalism

In Sec. II.B, we saw how a collection of states in resonance could be combined to produce a photon constituent which should behave in many respects as a physical vector meson (see Footnote 16 for a caveat). Before discussing the data on resonance production, we shall summarize the formalism. Production of hadrons through an intermediate vector meson is illustrated in Fig. 117. Here it is assumed that the coupling of the photon to the resonance, $e/\bar{f}_V$, is independent of s (any deviation from constancy could be regarded as part of the nonresonant, but interfering, background contribution). If we also ignore modifications of the real part of the vector-meson propagator (see Appendix C for further discussion of this point), the part of the total hadronic cross section described by the resonance is

$$\sigma_{V,h}(s)=\frac{12\pi m_V^2\,\Gamma(V\to e^+e^-)\Gamma(V\to h)}{s[(s-m_V^2)^2+m_V^2\Gamma_V^2]}\ , \tag{3.99}$$

where m_V is the mass of the resonance, Γ_V is its total width, $\Gamma(V\to h)$ is its partial width for hadronic decay, and $\Gamma(V\to e^+e^-)$ is its partial width for the decay $V\to e^++e^-$.[39] [The distinction between Γ_V and $\Gamma(V\to h)$ is unimportant for the broader resonances, but it becomes important for the ψ and ψ' where $\Gamma(V\to e^+e^-)$ is an appreciable fraction of Γ_V.] The electron pair width is given by

$$\Gamma(V\to e^+e^-)=\frac{\alpha^2}{3}\left(\frac{\bar{f}_V^2}{4\pi}\right)^{-1}m_V\ . \tag{3.100}$$

The decay into a given channel f is given by

$$\sigma_{V,f}=\sigma_V\frac{\Gamma(V\to f)}{\Gamma_V}\ , \tag{3.101}$$

where $\Gamma(V\to f)$ is the partial width for that channel. The height of the resonance at the peak is

$$\sigma_{V,h}(m_V^2)=\frac{12\pi}{m_V^2}\frac{\Gamma(V\to e^+e^-)\Gamma(V\to h)}{\Gamma_V^2}\ . \tag{3.102}$$

A measure of the total strength of a resonance is its area. In the narrow width approximation [$\Gamma_V\ll m_V$, and $\Gamma(V\to h)$, Γ_V approximated by constants], this is

$$\int_{s_{\rm th}}^{\infty}\sigma_{V,h}(s)ds\approx 12\pi^2\frac{\Gamma(V\to e^+e^-)}{m_V}\frac{\Gamma(V\to h)}{\Gamma_V}\ . \tag{3.103}$$

Thus, if the branching ratio to hadrons is known, the area gives $\Gamma(V\to e^+e^-)$ and hence the coupling constant, $f_V^2/4\pi$. The narrow width form of Eq. (3.99) may be more familiar to some readers:

$$\sigma_{V,f}\cong\frac{3\pi}{m_V^2}\frac{\Gamma(V\to e^+e^-)\Gamma(V\to f)}{(\sqrt{s}-m_V)^2+\frac{1}{4}\Gamma_V^2}\ . \tag{3.104}$$

An important special case is the ρ^0 resonance which decays primarily into $\pi^+\pi^-$

$$e^++e^-\to\rho^0\to\pi^++\pi^-\ .$$

The overall reaction can always be expressed in terms of the electromagnetic form factor of the pion

$$\frac{d\sigma_{V,\pi^+\pi^-}}{d\Omega}=\frac{\alpha^2\beta^3\sin^2\theta\,|F_\pi(s)|^2}{8s}\ , \tag{3.105a}$$

$$\sigma_{V,\pi^+\pi^-}=\frac{\pi\alpha^2\beta^3|F_\pi(s)|^2}{3s}\ , \tag{3.105b}$$

where

$$\beta=p_\pi/E_\pi=\left(1-\frac{4m_\pi^2}{s}\right)^{1/2}\ . \tag{3.105c}$$

When the reaction proceeds through the ρ^0 resonance, which has a decay coupling constant $\bar{f}_{\rho\pi\pi}$ (measured at the ρ^0 mass), one finds (C.7)

$$m_\rho\Gamma_\rho(s)=\frac{1}{3}\frac{\bar{f}_{\rho\pi\pi}^2}{4\pi}\frac{p_\pi^3}{E_\pi}\ . \tag{3.106}$$

In the neighborhood of the resonance, the form factor becomes

$$F_\pi(s)=\frac{m_\rho^2(\bar{f}_{\rho\pi\pi}/\bar{f}_\rho)}{s-m_\rho^2+im_\rho\Gamma_\rho(s)}\ . \tag{3.107}$$

Using Eqs. (3.100), (3.106), and (3.107), it is easy to see that (3.105b) reduces to (3.99). As discussed in Appendix C, the factor $\bar{f}_{\rho\pi\pi}/\bar{f}_\rho=[1-\bar{\Pi}_\rho(0)/m_\rho^2]$ agrees with the results of Gounaris and Sakurai (1968) and Vaughn and Wali (1968). The various coupling constant conventions are defined in Table I.

The $\pi^+\pi^-$ channel is actually made more complicated by the interference of the ω resonance (which decays predominantly into $\pi^+\pi^-\pi^0$) with the ρ^0 contribution changing the pion form factors (3.107) to

$$F_\pi(s)=\frac{m_\rho^2(\bar{f}_{\rho\pi\pi}/\bar{f}_\rho)}{s-m_\rho^2+im_\rho\Gamma_\rho}+\xi e^{i\phi}\frac{m_\omega^2}{s-m_\omega^2+im_\omega\Gamma_\omega}\ , \tag{3.108a}$$

where

$$\xi=\frac{6[\Gamma(\omega\to\pi^+\pi^-)\Gamma(\omega\to e^+e^-)]^{1/2}}{\alpha m_\omega(\beta)^{3/2}}\ . \tag{3.108b}$$

The parameters to be determined by measurements of this channel are usually m_ρ, Γ_ρ, $\bar{f}_{\rho\pi\pi}/\bar{f}_\rho$, ξ, and ϕ; m_ω, Γ_ω, and $\Gamma(\omega\to e^+e^-)$ are taken as input.

4. The low-lying resonances: $\rho^0,\omega,\phi,\rho'(1250)$, and $\rho''(1600)$

At Orsay three sets of apparatus have been used to study the electron–positron annihilation into ρ^0, ω, and ϕ. The first apparatus consisted of a symmetrical arrangement of spark chambers and scintillation counters.

[39] Note that here s is synonymous with the $\mathfrak{M}^2$ of Sec. II.B.

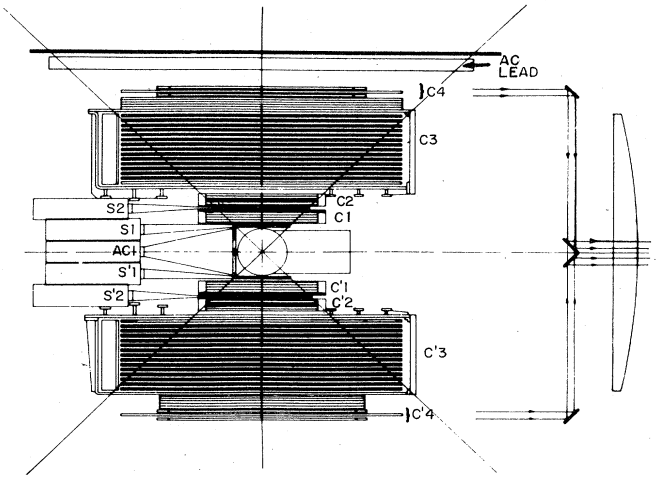

FIG. 118. Side view of the first Orsay detector: C_1C_1', thin-plate spark chambers; $C_2C_2'C_3C_3'C_4C_4'$, thick-plate spark chambers; $S_1S_2S_1'S_2'$, coincidence counters; ACI, machine background veto counter; and AC, cosmic ray background veto counters (from Augustin *et al.*, 1969a).

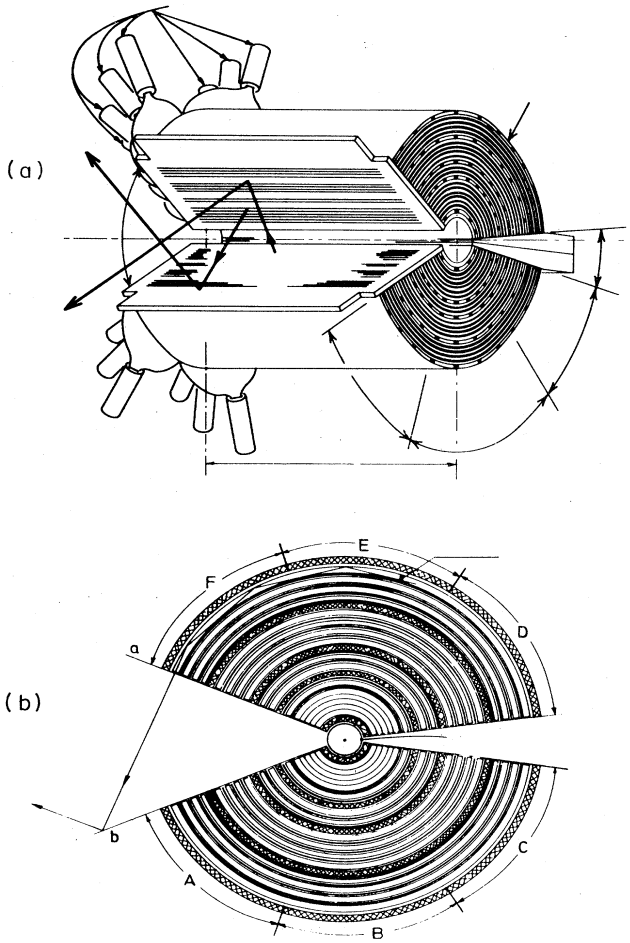

FIG. 119. Second Orsay detector. (a) General view. (b) Cross section (from Benaksas *et al.*, 1972a).

In each array a four-gap thin-plate chamber was used to determine particle trajectories. Two thick-plate chambers were used as shower and range chambers to identify electron and pion tracks. Veto chambers were used to reject cosmic rays. Figure 118 shows a side view of the apparatus.

The second apparatus used by the Orsay group was a cylindrical system with the beam along the cylindrical axis. Figure 119 shows a drawing of the apparatus. This setup includes 2×16 optical spark chambers and 2×15 sets of counters arranged in six sectors. The direction of the charged particles is measured in the five spark chambers. Electron and photon showers are observed in a sandwich of 11 lead sheets (0.5 radiation lengths each) interspaced between the last 11 spark chambers. Transverse and longitudinal views are photographed through an optical system by a single camera. Counters are used to veto cosmic rays. For the observation of the ϕ through the detection of the two kaons, the Orsay group used a special setup consisting of four double-gap spark chambers and four scintillation counters arranged so as to minimize the energy loss required for particle detection.

A group at Orsay has subsequently used the magnetic detector *DM*1 to study the reaction

$$e^+ + e^- \rightarrow \pi^+ + \pi^-$$

in the center-of-mass energy range from 480 to 1100 MeV. This detector has a $0.95T$ solenoidal field with four cylindrical proportional chambers with anode and

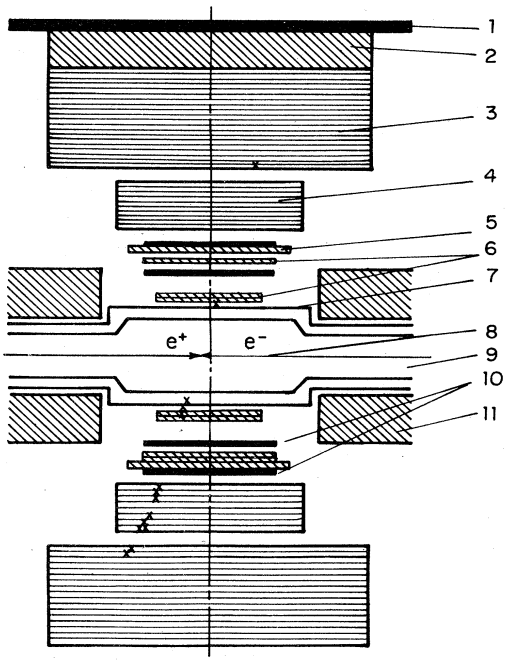

FIG. 120. Novosibirsk spark chamber system: 1, anticoincidence scintillation counter; 2, lead layer 20 cm thick; 3, range spark chamber; 4, shower spark chamber; 5, Duraluminum layer 24-mm thick; 6, thin-plate spark chambers; 7, window of outer vacuum chamber; 8, region of collision; 9, inner vacuum chamber; 10, scintillation counters; 11, storage ring magnet (from Auslander *et al.*, 1967).

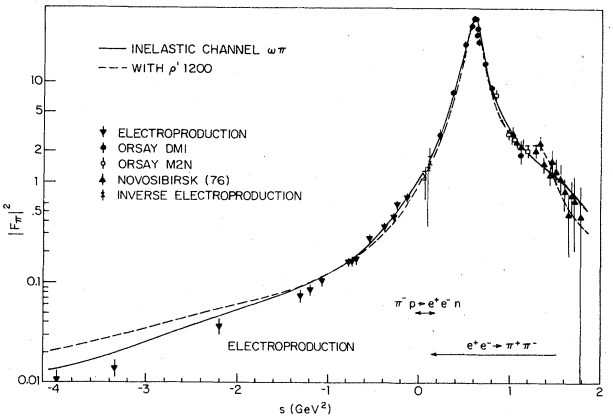

FIG. 121. A plot of the pion form factor versus energy as determined from colliding beams, inverse electroproduction, and electroproduction measurements. The solid curve is a fit assuming an inelastic $\omega\pi$ channel; the dashed curve is a fit assuming a contribution due to the $\rho'(1200)$ (from Quenzer *et al.*, 1977).

cathode readout used to track the particles. Those chambers are only $7\times10^{-4}\,X_0$ thick in the radial direction and are used in conjunction with a beam vacuum chamber consisting of a stainless steel foil 38μ thick. This system is described more completely in articles by Jeanjean *et al.* (1974) and Cordier *et al.* (1976).

The Novosibirsk group used a setup consisting of two identical parts with the layout shown in Fig. 120. The spark chambers next to the target were used to determine the particle direction and to locate the vertex. The particles were identified by observing their interaction in the shower and range chambers.

Measurements of the reaction

$$e^+ + e^- \to \pi^+ + \pi^-$$

have been carried out at Orsay (Augustin *et al.*, 1968, 1969a, b; Benaksas *et al.*, 1972a; Quenzer *et al.*, 1975; 1977), Novosibirsk (Auslander *et al.*, 1967, 1969; Balakin *et al.*, 1971a, 1972) and Frascati (Bernardini *et al.*,

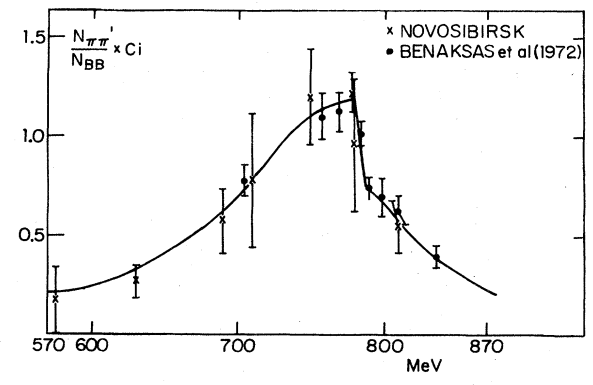

FIG. 122. A detailed plot of the $e^+e^-\to\pi^+\pi^-$ cross section in the region of the ρ^0 mass. The data are from Orsay III (Benaksas *et al.*, 1972a) and Novosibirsk (Auslander *et al.*, 1969). The asymmetry is due to rho-omega mixing. The solid curve is the fit number referred to in the text (from Benaksas *et al.*, 1972a).

TABLE XXIV. ρ^0 and ω parameters from two of the fits to the Orsay data.

	Fit 2	Fit 3
M_ρ(MeV)	775.4 ± 7.3	772.3 ± 5.9
Γ_ρ (MeV)	149.6 ± 23.2	135.8 ± 15.1
$\sigma(e^+e^-\to\rho)$ (μb)	1.00 ± 0.13	1.04 ± 0.12
$B(\rho\to e^+e^-)$ ($\times10^5$)	4.1 ± 0.5	4.2 ± 0.4
$\Gamma(\rho\to e^+e^-)$ (keV)	6.1 ± 0.7	5.8 ± 0.5
$(B(\omega\to\pi^+\pi^-))^{1/2}$	0.19 ± 0.05	0.17 ± 0.05
ϕ (degrees)	85.7 ± 15.3	88.3 ± 15.8
$f_\rho^2/4\pi$	2.26 ± 0.25	2.38 ± 0.18
$f_{\rho\pi\pi}/4\pi$	2.84 ± 0.50	2.60 ± 0.32

1973a, 1973b). The most detailed measurements in the vicinity of the rho meson come primarily from Orsay; the Novosibirsk measurements are less extensive; the Frascati measurements are limited to the region above 1.0 GeV center-of-mass energy. Figure 121 summarizes the total cross section for the $\pi^+\pi^-$ production expressed in terms of the pion form factor. The dominant feature is the large peak at the rho mass. Figure 122 shows the detail in the region around the rho mass. The peak is not symmetrical and gives evidence for rho-omega mixing.

The Orsay group carried out four experiments in which they studied the $\pi^+\pi^-$ production at the rho mass. The cross sections obtained differed substantially for unknown reasons. We shall report here details from the analysis of the last two experiments (Benaksas *et al.*, 1972a; Quenzer *et al.*, 1977). It is these data and the data from measurements by the Novosibirsk group (Auslander *et al.*, 1969) that are plotted in Fig. 122. Among other things, the Orsay group analyzed their data in terms of Eq. (3.105) and a form for F_π equivalent to Eq. (3.108).

Benaksas *et al.* (1972a) made three different fits to the data. The values for Γ_ω, m_ω, and $\Gamma(\omega\to e^+e^-)$ were taken from the experiment studying $e^+e^-\to\pi^+\pi^-\pi^0$.[40] The first fit used all the Orsay data from $2E = 705$ MeV to 990 MeV. The second fit eliminated the 990 MeV point on the assumption that it was influenced by the tail of a possible ρ' resonance and the opening of the $\omega\pi^0$ channel at 920 MeV. The third fit used both the Orsay data and the Novosibirsk data. The rho-omega parameters derived from fits two and three are summarized in Table XXIV. The solid curve in Fig. 122 is fit number two. The interference parameter from this experiment is approximately twice as large as from the DESY and Daresbury $\pi^+\pi^-$ photoproduction experiments (Sec. III.C, D). Since such a large difference is not expected on the basis of theoretical models (a smaller difference is plausible), Dr. G. Parrour has, at our request, redone the fits with the interference parameter fixed at the photoproduction value and m_ρ and Γ_ρ assigned different values compatible with photoproduction. These fits are summarized in Table XXV (the one shown excludes the 990 MeV data point). The results agree with ones obtained at Cornell

[40] "Old" values of $B(\omega\to e^+e^-) = (0.898\pm0.045)\times10^{-4}$ and $\Gamma_\omega = (9.2\pm1)$ MeV were actually used in this fit.

TABLE XXV. Determination of $\bar{f}_\rho^2/4\pi$ from $e^+e^- \to \pi^+\pi^-$, for various choices of m_ρ and Γ_ρ; also, the $\rho^0-\omega$ interference parameter is fixed at the photoproduction values ($\xi = 0.01$). The number of degrees of freedom is 8, so all fits are acceptable. Comparison of the last two columns gives an indication of the validity of the assumption of point couplings as discussed in Appendix C.

Γ_ρ	m_ρ	χ^2	$\frac{\bar{f}^2_{\rho\pi\pi}}{4\pi}$	$\frac{\bar{f}^2_\rho}{4\pi}$	$\frac{\bar{f}^2_{\rho\pi\pi}}{\bar{f}^2_\rho}$	$[1-\Pi_\rho(0)/m_\rho^2]^2$
135	767	3.53	2.61	2.21 ± 0.07	1.18 ± 0.04	1.18
145	774	3.99	2.77	2.20 ± 0.06	1.26 ± 0.04	1.19
155	776	5.14	2.95	2.12 ± 0.06	1.39 ± 0.04	1.20

by Mr. D. Kaplan using a less sophisticated radiative correction treatment.

Quenzer *et al.* (1977) found that the simple model in which only the ρ^0 and ω were present did not give an adequate fit to the Orsay I, Orsay II, and *DM*1 data over the range 480–1100 MeV. They then employed three different methods to obtain a satisfactory fit. The first method included the $\rho'(1200)$ as a second resonance, the second method assumed there was ρ, ρ' mixing, the third method used the formalism of Costa de Beauregard *et al.* (1977) to include the inelastic $\omega\pi$ channel. In each case they included the constraint $F_\pi(0) = 1$. As input to the fit they used the data from *DM*1, the high-energy ($\sqrt{s} > 0.95$ GeV) data of Orsay II, and the high-energy data ($\sqrt{s} > 0.95$ GeV) of Novosibirsk. Table XXVI summarizes the fit parameters; Figure 123 shows the fit in graphic form.

The Orsay group carried out two experiments (Augustin *et al.*, 1969c; Benaksas *et al.*, 1972b) in which they studied the reaction

$$e^+e^- \to \omega \to \pi^+\pi^-\pi^0 .$$

They used the large solid-angle detector which permitted the detection of both charged and neutral particles. Figure 124 shows the measured excitation curve. They used the equivalent of Eq. (3.99) to fit the data and thus determine Γ_ω and the cross section at $\sqrt{s} = m_\omega$. They obtained

$$\sigma(e^+e^- \to \omega \to 3\pi)\big|_{\sqrt{s}=m_\omega} = (1.80 \pm 0.20)\mu\text{b} . \tag{3.109a}$$
$$\Gamma_\omega = (9.1 \pm 0.8)\ \text{MeV} .$$

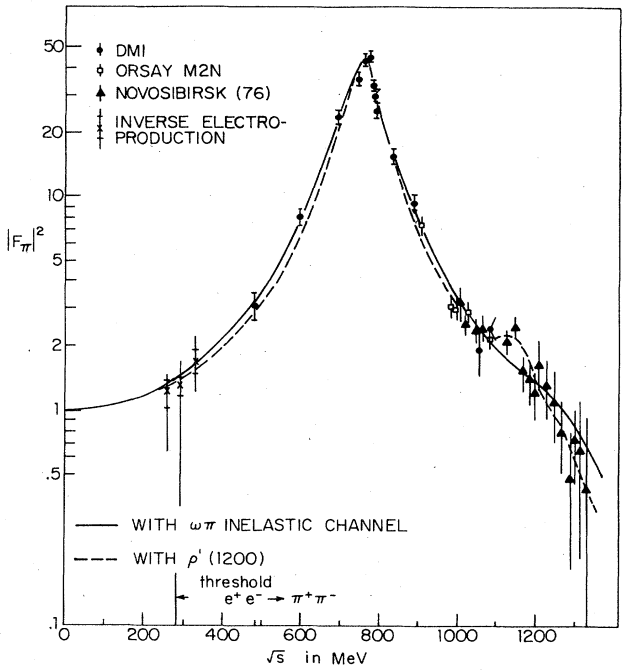

FIG. 123. The plot of the pion form factor obtained using the DMI data (Quenzer *et al.*, 1977), the high-mass data of Orsay III, and the high-mass data of Novosibirsk. The solid curve is the fit obtained assuming ρ, ω, and a contribution from an inelastic $\omega\pi$ channel; the dashed curve assumes ρ, ω, and $\rho'(1200)$ (from Quenzer *et al.*, 1977).

They then used Eq. (3.102) together with the known branching ratio

$$B(\omega \to \pi^+\pi^-\pi^0) = 0.895 \pm 0.045 \tag{3.109b}$$

to obtain

$$B(\omega \to e^+e^-) = (0.83 \pm 0.10) \times 10^{-4} , \tag{3.110a}$$
$$\Gamma(\omega \to e^+e^-) = (0.76 \pm 0.08)\ \text{keV} . \tag{3.110b}$$

Using Eq. (3.100) they obtained

$$\bar{f}_\omega^2/4\pi = 18.4 \pm 1.8 . \tag{3.111}$$

These results differed somewhat from earlier reported

TABLE XXVI. The ρ^0 and ω parameters determined by Quenzer *et al.* (1977) and Quenzer (1977) in their fit to the DM1 data, the high-energy data ($\sqrt{s} > 0.95$ GeV) of Orsay II, and and the high-energy data ($\sqrt{s} > 0.95$ GeV) of Novosibirsk. Case I refers to the situation in which the ρ' (1200) appears as a separate resonance; Case II refers to the situation in which there is $\rho'\rho$ mixing; inelastic $\omega\pi$ refers to the analysis using the formalism of Costo de Beauregard *et al* (1977).

Parameter	Inclusion of ρ' Case I	Case II	Inelastic $\omega\pi$
d	0.51 ± 0.023	0.31 ± 0.2	0.50 ± 0.02
m_ρ (MeV)	780.3 ± 3.5	780.3 ± 3.5	777.2 ± 3.7
Γ_ρ (MeV)	143.3 ± 4.2	143.3 ± 4.3	158.9 ± 4.7
$[B(\omega \to \pi^+\pi^-)]^{1/2}$	0.178 ± 0.39	0.178 ± 0.39	0.141 ± 0.033
$\phi_{\rho\omega}(^0)$	118.8 ± 12.4	101.8 ± 12.4	$102. \pm 14$
$\phi_{\rho\rho'}(^0)$	106 ± 10.8	95.8 ± 11.1	...
χ^2/dF	21.4/29	21.4/29	26.5/31

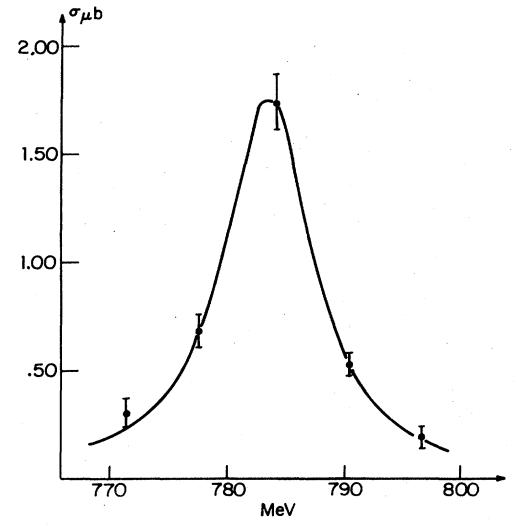

FIG. 124. Excitation curve for the reaction $e^+e^- \to \omega \to \pi^+\pi^-\pi^0$ (from Benaksas *et al.*, 1972b).

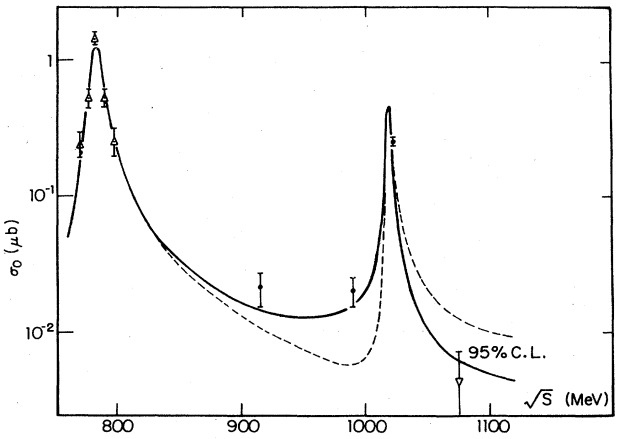

FIG. 125. $e^+e^- \to \pi^+\pi^-\pi^0$ data showing the interference between ω and ϕ intermediate states. The curves correspond to opposite relative signs for the two amplitudes: solid for the opposite sign for couplings $\omega \to 3\pi$ and $\phi \to 3\pi$, and dotted for the same sign (from Parrour *et al.*, 1976a).

measurements by the same group. The Orsay group recommends that one take the new results as correct.

In a later experiment the Orsay group (Parrour *et al.*, 1976a) studied $\pi^+\pi^-\pi^0$ production more carefully around the ϕ and in the region between the ω and ϕ resonances. In the same experiment they determined the position and width of the ϕ resonance from the $K_S^0K_L^0$ channel. They found that the magnitude and energy dependence of the experimental cross section (in the whole energy range 770 to 1076 MeV) was well described by an "interfering propagator" model given by Renard (1974). This is shown in Fig. 125. The interference effect clearly corresponds to an opposite sign between the $\omega \to 3\pi$ and $\phi \to 3\pi$ coupling constants.

Several studies of ϕ production have been made by the Orsay group (Augustin *et al.*, 1969d; Bizot *et al.*, 1970; Cosme *et al.*, 1974a, b; Parrour *et al.*, 1976a, b). In their first experiment, the Orsay experimenters used their first spark chamber setup to study the $K_S^0K_L^0$ and 3π decay modes. A form of Eq. (3.109) was used to extract values of $\Gamma(\phi \to \text{all})$, $\Gamma(\phi \to e^+e^-)$, $B(\phi \to K_S^0K_L^0)$, $B(\phi \to K^+K^-)$, and $B(\phi \to \pi^+\pi^-\pi^0)$. The results are summarized in Table XXVII as Orsay 1. In their second experiment, they used a specially constructed apparatus to study the K^+K^- decay mode. These results were then combined with those of the earlier experiment to obtain $\Gamma(\phi \to e^+e^-)$ and the other ϕ parameters (Orsay 2, Table XXVII). Using their large-angle cylindrical detector, the Orsay experimenters studied the $K_L^0K_S^0$ decay mode in detail. From these measurements they found

$$\Gamma_\phi = (3.81 \pm 0.37)\ \text{MeV}\,,$$
$$\sigma(e^+e^- \to K_L^0K_S^0)\big|_{\text{peak}} = (1.48 \pm 0.08 \pm 0.12)\ \mu\text{b}\,, \tag{3.112}$$

where the quoted errors in σ are, respectively, statistical and systematic. They also used the cylindrical detector to study the $\pi^+\pi^-\pi^0$ decay mode. The combination of these two cylindrical detector studies leads to the ϕ parameters listed in Table XXVII as Orsay 3. The group's recent work on the $\pi^+\pi^-\pi^0$ mode over a wide energy range (Parrour *et al.*, 1976a, b) plus new measurements of the $\eta\gamma$ and $\pi^0\gamma$ decay modes (Cosme *et al.*, 1976b) are given in Table XXVII as Orsay 4.

Also summarized in Table XXVII (as Novo 1) are the results of the Novosibirsk group (Balakin *et al.*, 1971a). The group used its apparatus described earlier to study simultaneously the three ϕ decay modes K^+K^-, $K_L^0K_S^0$, and $\pi^+\pi^-\pi^0$. Figure 126 shows the observed excitation

TABLE XXVII. Phi parameters from Orsay and Novosibirsk.

Data/Group	Orsay 1	Orsay 2	Novo 1	Orsay 3	Orsay 4
$B(\phi \to K^+K^-)$	0.486 ± 0.024	0.493 ± 0.044	0.540 ± 0.034	0.500 ± 0.053	···
$B(\phi \to K_S^0K_L^0)$	0.308 ± 0.016	0.301 ± 0.041	0.257 ± 0.030	0.322 ± 0.031	···
$B(\phi \to 3\pi)$	0.206 ± 0.040	0.206 ± 0.036	0.203 ± 0.042	0.150 ± 0.019	0.136 ± 0.007
$B(\phi \to \eta\gamma)$ $(\times 10^2)$	···	···	···	2.5 ± 0.7	1.5 ± 0.4
$B(\phi \to \pi^0\gamma)$ $(\times 10^3)$	···	···	···	···	1.4 ± 0.5
$B(\phi \to e^+e^-)$ $(\times 10^4)$	3.96 ± 0.62	3.45 ± 0.27	2.81 ± 0.25	3.3 ± 0.3	···
$\Gamma(\phi \to e^+e^-)$ (keV)	1.64 ± 0.26	1.41 ± 0.12	1.31 ± 0.12	1.27 ± 0.11	1.30 ± 0.06
Γ_ϕ (MeV)	4.2 ± 0.9	4.09 ± 0.29	4.67 ± 0.42	3.8 ± 0.4	4.2 ± 0.2
$f_\phi^2/4\pi$	11.0 ± 1.7	12.9 ± 1.1	13.8 ± 1.29	14.3 ± 1.2	13.2 ± 0.6
$\sigma_{\text{all}}(2E = M_\phi)$ (μb)	5.5 ± 1.0	4.89 ± 0.39	3.96 ± 0.35	4.7 ± 0.4	4.4 ± 0.44 [a]

[a] World averages.

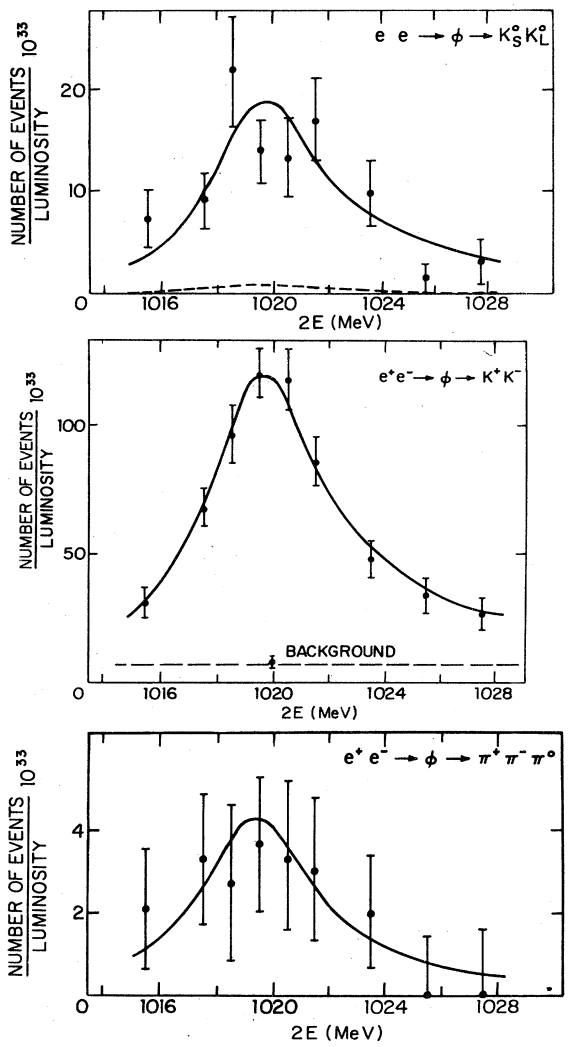

FIG. 126. Excitation curves for the ϕ resonance decaying into the indicated channels (from Balakin *et al.*, 1971a).

curves for the three decay modes. Figure 127 shows the excitation of the $K_L^0 K_S^0$ decay mode in a recent Novosibirsk experiment. The overall agreement among the various experiments contributing to Table XXVII is quite satisfactory.

The Frascati $\mu\pi$ group (Grilli *et al.*, 1973; Conversi *et al.*, 1974) has reported evidence for a higher-mass vector meson decaying into hadrons through observation of the reaction

$$e^+e^- \to \rho'' \to \pi^+\pi^-\pi^+\pi^- .$$

The group used a detector consisting of two identical counter-spark chamber telescopes located horizontally on opposite sides of one of the straight sections of ADONE. Figure 128 shows a plot of the observed cross section versus energy. If this "bump" is analyzed as a resonance, a Breit–Wigner fit gives $M_{\rho''} = (1550 \pm 60)$ MeV, $\Gamma_{\rho''} = (360 \pm 100)$ MeV, and $\sigma_{\text{peak}} = (17 \pm 5)$ nb. From an analysis of the data it was concluded that the ρ'' decayed through the channel

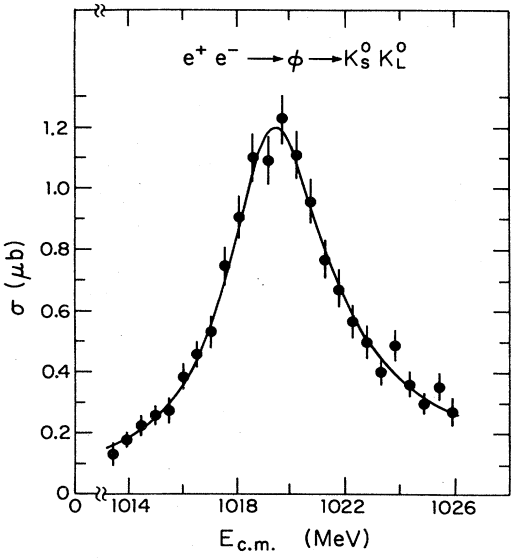

FIG. 127. Excitation curve for $e^+e^- \to \phi \to K_S^0 K_L^0$ (from Schwitters, 1975).

$$\rho''(1600) \to \rho^0(770) + \epsilon^0(800) .$$

With the assumptions that

$$\sigma(e^+e^- \to \rho^0\epsilon^0 \to \pi^+\pi^-\pi^0\pi^0) = 0.5\sigma(e^+e^- \to \rho^0\epsilon^0 \to \pi^+\pi^-\pi^+\pi^-)$$

and the $\rho'' \to \pi^+\pi^-$ mode is highly depressed, it was found that

$$\bar{f}^2_{\rho''}/4\pi = 17 \pm 5 . \qquad (3.113a)$$

With the assumption that the $\omega\pi^0$ system is produced at the same rate as the $\rho^0\epsilon^0$ system in the $\pi^+\pi^-\pi^0\pi^0$ state, it was found that

$$\bar{f}^2_{\rho''}/4\pi = 13 \pm 5 . \qquad (3.113b)$$

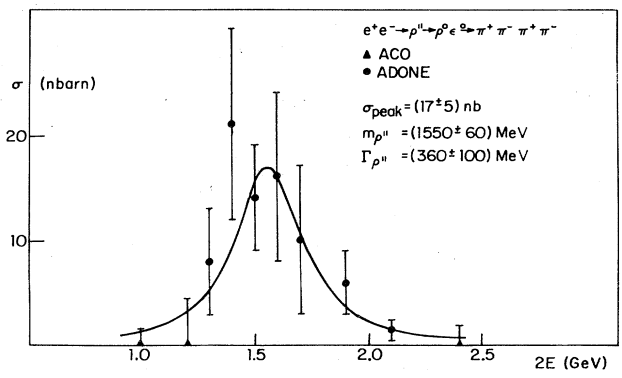

FIG. 128. Energy dependence of the cross section for the process $e^+e^- \to \pi^+\pi^-\pi^+\pi^-$ as obtained by combining "old" and "new" data collected with the apparatus of the "$\mu\pi$ group" at ADONE. These results are based on the recorded numbers of 4 C events kinematically reconstructed and on the corresponding detection efficiencies, computed by a Monte Carlo simulation of the experiment. The upper limit at $2E = 0.99$ GeV (68% confidence level) comes from ACO. The curve is a best fit of a Breit–Wigner function to the experimental points (from Conversi *et al.*, 1974).

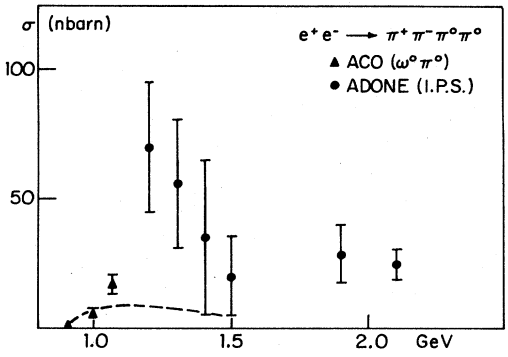

FIG. 129. Energy dependence of the cross section for the reaction $e^+e^- \to \pi^+\pi^-\pi^0\pi^0$. The points from ADONE are computed assuming a pure phase space distribution after subtraction of the $\rho''(1600) \to \rho^0\epsilon^0 \to \pi^+\pi^-\pi^0\pi^0$ resonant contribution. (The correction is negligible at 1.2 GeV and has a maximum value of ~25% at 1.5 GeV.) The points from ACO, obtained with a nearly 4π detector which allows unambiguous identification of the final states, show a clear threshold effect at the $\omega^0\pi^0$ mass. The dotted curve represents the theoretical expectation of this effect assuming only the contribution from the ρ^0 meson. Already the point at $2E = 1.076$ GeV is seen to be nearly two standard deviations above the expected value (from Conversi *et al.*, 1974).

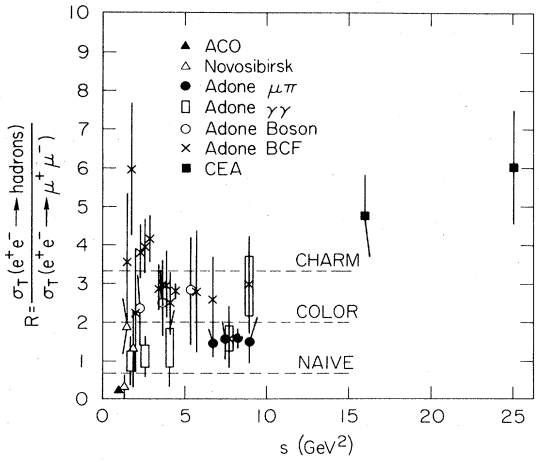

FIG. 130. Summary of measurements of $R_{e^+e^-}$ at the time of the 1973 Bonn Photon Conference (from Strauch, 1974).

The Frascati BCF group (Bernardini *et al.*, 1974b) has reported a failure to observe the $\rho''(1600)$. However, data reported by the boson group (Bartoli *et al.*, 1972) supports the original findings of the $\mu\pi$ group.

The $\mu\pi$ group (Conversi *et al.*, 1974) has combined measurements of the reaction

$$e^+e^- \to \pi^+\pi^-\pi^0\pi^0$$

from ADONE and ACO to obtain evidence for a $\rho'(1250)$ with a width of 150 MeV. Figure 129 shows a plot of the combined data. From an analysis the group obtains

$$\bar{f}^2_{\rho'}/4\pi = 7 \pm 2. \qquad (3.114)$$

Figure 121 shows later data which add further evidence for an enhancement near 1200 MeV. The interpretation of the data is unclear and more work is needed in this mass region.

Three Frascati groups (Esposito *et al.*, 1977; Bacci *et al.*, 1977; Ambrosio *et al.*, 1977) have presented evidence at ADONE for a narrow-resonance structure in hadron production for e^+e^- annihilation near 1800 MeV. For the mass and width the three groups obtained, respectively, 1812^{+7}_{-13}, $\Gamma = 34^{+21}_{-15}$; $1821 \pm 16, 31 \pm 15$; $1819 \pm 5, 24 \pm 5$. It has been suggested that this resonance is the recurrence of the ϕ. More work will be required to verify its presence and to determine its quantum numbers.

In two summary reports given at the 1977 International Conference on Lepton and Photon Interactions at High Energies (Laplanche, 1977; Bemporad, 1977) preliminary evidence was reported for several new resonances in the mass range 1.2 to 2.0 GeV. More data with greater statistics will be required to clarify the situation.

5. General features of $e^+e^- \to$ hadrons

In the region below 1100 MeV the production of hadrons is dominated by the ρ, ω, and ϕ mesons and there appears to be little evidence for production through other channels (Cosme *et al.*, 1972, 1976a). The most interesting result to emerge from higher-energy measurements at Frascati (Bartoli *et al.*, 1972; Bacci *et al.*, 1972, 1973; Grilli *et al.*, 1973; Ceradini *et al.*, 1972, 1973; Bernardini *et al.*, 1974a) and the Cambridge Electron Accelerator (Litke *et al.*, 1973; Tarnopolosky *et al.*, 1974) is the increase in the ratio to μ pairs. Figure 130 shows a plot of $R_{e^+e^-}$ at the time of the Bonn Symposium in 1973. Subsequent to the Symposium, measurements were made at SLAC with SPEAR I and SPEAR II up to a center-of-mass energy of 7.6 GeV (Schwitters, 1975; Augustin *et al.*, 1975). The most exciting discoveries made in this energy range are generally well known and will be described briefly later; here we review the more conventional features. Figure 131 shows a plot of $R_{e^+e^-}$ results (with ψ and ψ' removed) from the SLAC–Lawrence Berkeley Laboratory collaboration. Below 3.5 GeV, $R_{e^+e^-}$ is roughly constant, with a value around 2.5. Above 5 GeV, R is again roughly constant, with a value around 5.5. Between the two regions there

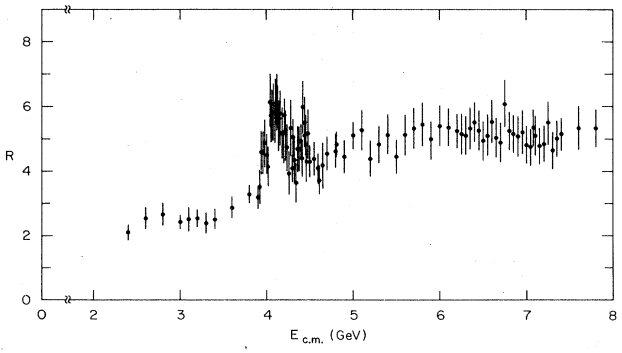

FIG. 131. $R_{e^+e^-}$ results (with ψ and ψ' removed) (from Schwitters, 1975).

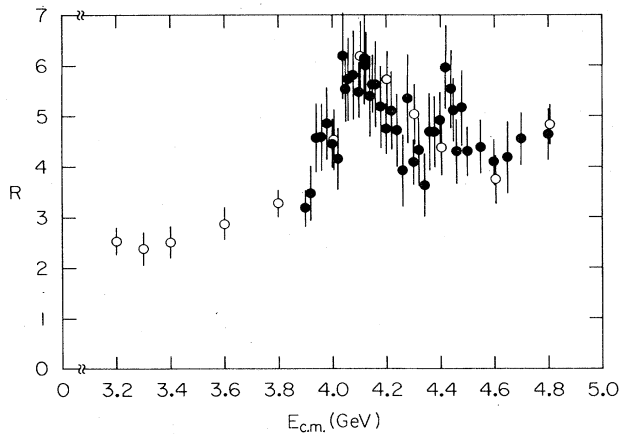

FIG. 132. Details of the charm threshold region in $R_{e^+e^-}$ (from Feldman and Perl, 1977).

is a transition region with a complicated structure. Figure 132 shows the transition region in greater detail.

The values of $R_{e^+e^-}$ have great significance for the quark model; also, as will be described in Sec. VI.B, they place constraints on the GVD models. The quark model with a triplet of fractionally charged colored quarks predicts an asymptotic value of 2 for $R_{e^+e^-}$. This is comparable to 2.5, which indicates the saturation of the u, d, s quark contributions by 3 GeV. The increase in $R_{e^+e^-}$, together with the appearance of the new resonances, is attributed to the entrance of new degrees of freedom such as charm. However, a colored charmed quark would naively give an increase of only 4/3. The somewhat larger increase could be due to the production of heavy leptons (Perl *et al.*, 1975).

A review of the main features of the hadronic final states was given by Schwitters (1975). Here we can present only a very brief summary:

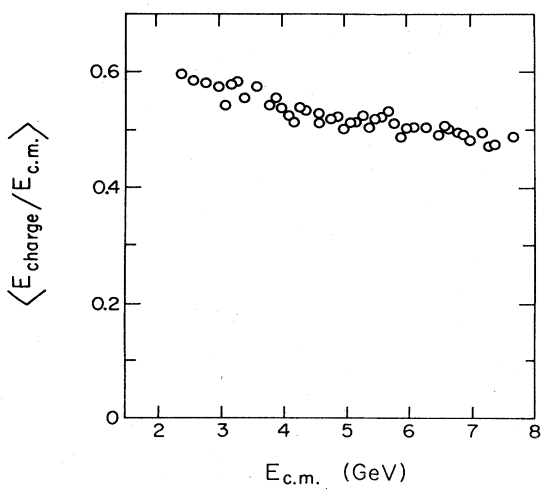

FIG. 133. Average fraction of total center-of-mass energy appearing in charged particles vs. $E_{c.m.}$, for ≥ three-prong events, assuming pion masses. The data have been corrected for acceptance and analysis losses (from Schwitters, 1975).

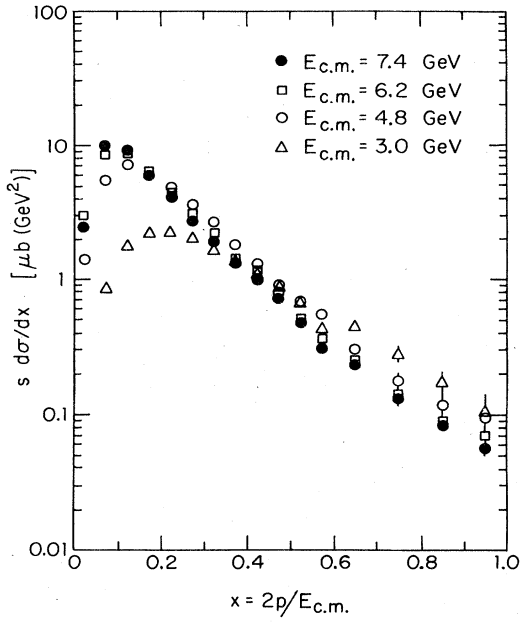

FIG. 134. $sd\sigma/dx$ vs. x for $E_{c.m.} = 3.0$ GeV, 4.8 GeV, and 7.4 GeV. Here $x \equiv 2p/E_{c.m.}$ (from Schwitters, 1975).

(1) The mean charged multiplicity and the mean charged energy rise with increasing s; however, as seen in Fig. 133, the fraction of the energy in charged particles falls.

(2) In Fig. 134 are shown plots of $sd\sigma/d\bar{x}$ vs $\bar{x}$, where $\bar{x} = 2P/\sqrt{s}$ is a scaling variable. The data exhibit Bjorken scaling for large $\bar{x}$; and as s increases, the scaling extends to smaller values of $\bar{x}$.

(3) At 7.4 GeV, the inclusive angular distribution of hadrons was measured with the aid of polarized incident beams (Schwitters *et al.*, 1975), and the results used to determine σ_T and σ_L in (3.93). Particles with low $\bar{x}$ are produced isotropically ($\sigma_L = \sigma_T$), while those with $\bar{x} > 0.2$ are produced with a predominantly transverse cross section as shown in Fig. 135.

(4) There is strong evidence for jet structure in hadron production by e^+e^- annihilation (Hanson *et al.*, 1975). For events with three or more prongs, an axis is found which minimizes the sum of squares of perpendicular momenta; and a quantity called sphericity (S) is defined as a measure of jetlike behavior by

$$S = \frac{3}{2}\left(\sum p_i^2 / \sum p^2\right). \tag{3.115}$$

Figure 136 shows the sphericity distribution. At 7.4 GeV, the angular distribution of the jet axis, integrated over azimuthal angles, is given by $[1 + (0.78 \pm 0.12)\cos^2\theta]$. It is noteworthy, but by no means conclusive, that these results are well described by a model where the e^+e^- annihilates into a quark–antiquark pair which then evolves into the final physical state. Gilman (1975) has given a critical appraisal of this interpretation.

While measuring the total hadron cross section, the SLAC–LBL group discovered a narrow resonance at a mass of 3095 MeV (Augustin *et al.*, 1974a) which they called the ψ. This resonance was reported simultaneously by a Brookhaven–MIT group (Aubert *et al.*, 1974), and

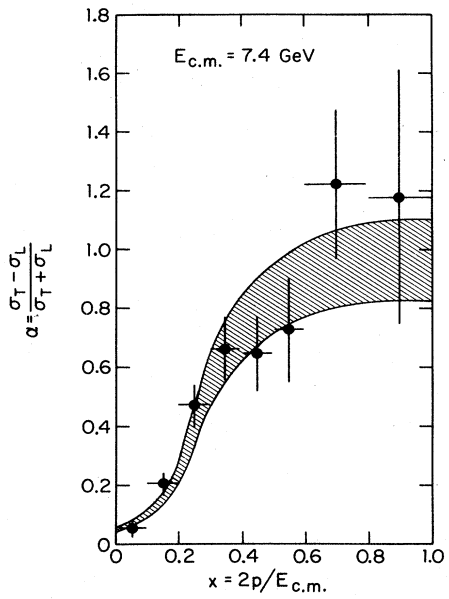

FIG. 135. Observed inclusive α vs. x for particles with $|\cos\theta| \leq 0.6$ in hadronic events at $E_{c.m.} = 7.4$ GeV. The prediction of the jet model Monte Carlo simulation for a jet axis angular distribution with $\alpha = 0.97 \pm 0.14$ is represented by the shaded band (from Schwitters, 1975).

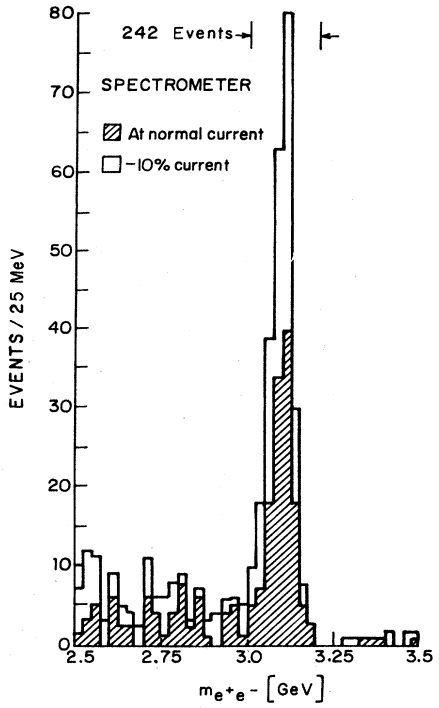

FIG. 137. Mass spectrum showing the existence of J. Results from two spectrometer settings are plotted showing that the peak is independent of spectrometer currents. The run at reduced current was taken two months later than the normal run (from Aubert *et al.*, 1974).

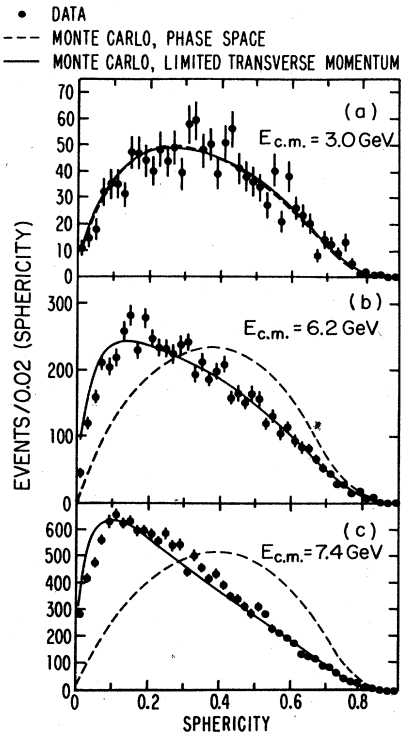

FIG. 136. Sphericity distributions for ≥3-prong hadronic events at various center-of-mass energies. The solid curves are the jet model predictions (with $\langle p_\perp \rangle = 315$ MeV); dashed curves are the invariant phase space Monte Carlo predictions (from Feldman and Perl, 1977).

called the J. The Brookhaven–MIT group used a precision pair spectrometer system and studied the reaction

$$p + \mathrm{Be} \rightarrow e^+ + e^- + \text{anything} .$$

Figure 137 shows the data from the Brookhaven–MIT group; Fig. 138 shows somewhat later measurements on the J/ψ by the SLAC–LBL group (Boyarski *et al.* 1975b). This resonance was immediately confirmed by measurements at ADONE (Bacci *et al.*, 1974) and DORIS (Braunschweig *et al.*, 1974). Subsequent to the discovery of the J/ψ the SLAC–LBL group made a systematic search and found a second narrow resonance at 3684 MeV (Abrams *et al.*, 1974, 1975). Figure 139 shows excitation curves for the $\psi(3684)$. The SLAC–LBL group made a systematic study of these two resonances using methods similar to those employed earlier with the vector mesons. For each of the resonances the quantum numbers J^{PC} are 1^{--}. Each of these particles has decays which are consistent with isospin 0 and odd G parity. The study of these particles and their decays rapidly mushroomed. Two early reviews are Abrams (1975) and Feldman (1975). The accepted interpretation is that they are a manifestation of "hidden charm"; they are bound states of charmed quark pairs below the threshold to produce charmed particles. Table XXVIII summarizes the gross properties of the ψ and ψ'.

The SLAC–LBL group systematically searched for narrow resonances up to $\sqrt{s} = 7.6$ GeV (Boyarski *et al.*, 1975a). They found no other narrow resonances. They observed a resonancelike structure in the total cross

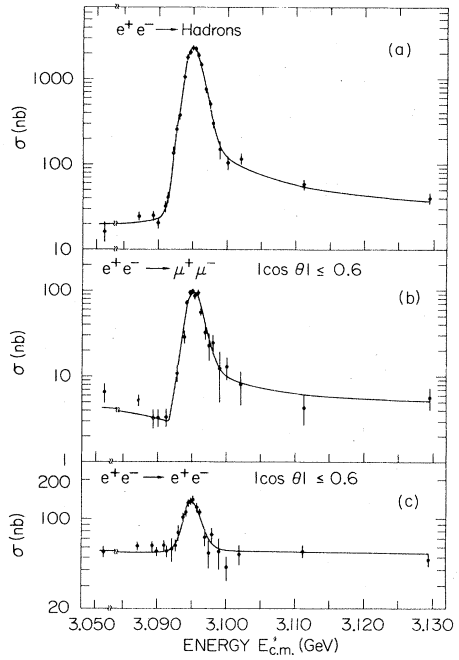

FIG. 138. Excitation curves for the ψ resonance in e^+e^- annihilation (from Boyarski *et al.*, 1975b).

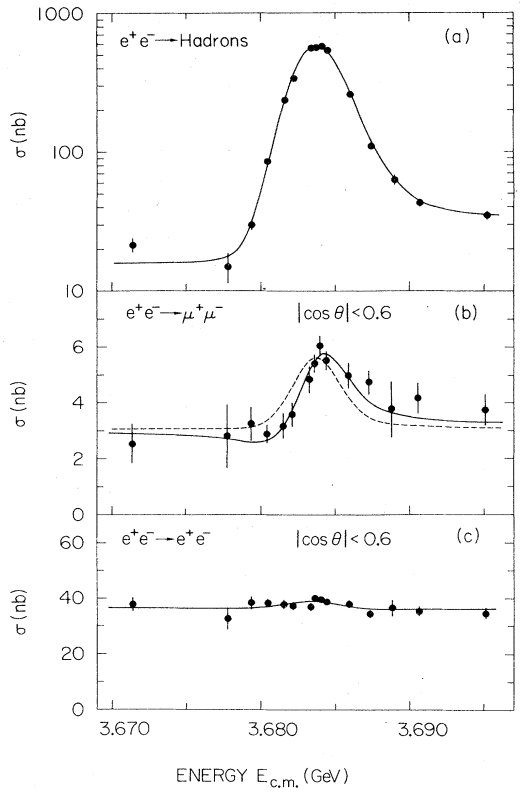

FIG. 139. Excitation curves for the ψ' resonance in e^+e^- annihilation (from Lüth *et al.*, 1975).

section for hadron production at a mass of 4414 ± 7 MeV with a total width $\Gamma = (33 \pm 10)$ MeV with a partial width to electron pairs of (440 ± 140) eV (Siegrist *et al.*, 1976). Subsequently at SPEAR a SLAC–LBL–Northwestern–Hawaii group made a detailed study of the region near 3.8 GeV and observed a narrow resonance at (3.772 ± 6) GeV with a total width of (28 ± 5) MeV, and a partial width to electron pairs of (370 ± 90) eV. (Rapidis *et al.*, 1977).

The observed states of the ψ family indicate that the threshold for production of charmed particles should be about 3.9 GeV. Above this energy, new particles produced in pairs with the properties expected for charmed mesons have been observed (Goldhaber *et al.*, 1976; Peruzzi *et al.*, 1976). For recent reviews see Born and Wiik, 1977; Feldman and Perl, 1977.

J/ψ photoproduction has been observed in several laboratories (see Sec. III.G), and there is evidence for the photoproduction of charmed baryons (Knapp *et al.*, 1976).

A Columbia–FNAL–Stony Brook collaboration (Herb *et al.*, 1977; Innes *et al.*, 1977) has obtained evidence for the production of a 9.5 GeV dimuon resonance in 400 GeV proton–nucleus collisions at FNAL. There appear to be at least two states, and the observed width is consistent with that expected from the apparatus alone. It is generally believed that these states, which have been dubbed the Υ and Υ', are due to a higher-mass quark and are the analogs for the new quark of the ψ and ψ'. For a general treatment of the new spectroscopies the reader is referred to the invited paper presented by Gottfried (1977) at the 1977 International Symposium on Lepton and Photon Interactions.

TABLE XXVIII. Properties of the J/ψ and the $\psi'(3684)$.

	J/ψ	$\psi'(3684)$
Mass	3.095 ± 0.004 GeV	3.684 ± 0.05 GeV
J^{PC}	1^{--}	1^{--}
Γ_e	4.8 ± 0.6 keV	2.1 ± 0.3 keV
Γ_μ/Γ_e	1.00 ± 0.05	•••
Γ_h	59 ± 14 keV	224 ± 56 keV
Γ	69 ± 15 keV	228 ± 56 keV
Γ_e/Γ	0.069 ± 0.009	0.0093 ± 0.0016
Γ_h/Γ	0.86 ± 0.02	0.981 ± 0.003
$\Gamma_{\gamma h}/\Gamma$	0.17 ± 0.04	0.029 ± 0.004
$f_\psi^2/4\pi$	11.5 ± 1.4	31.2 ± 4.5

G. Photoproduction of heavy vector mesons

The first attempts to detect the photoproduction of higher-mass vector mesons were made by looking for high-mass pion pairs in the reaction

$$\gamma N \to \pi^+\pi^- N$$

(Hicks *et al.*, 1969; McClellan *et al.*, 1969d; Bulos *et al.*, 1971; Alvensleben *et al.*, 1971e; Ballam *et al.*, 1972, 1973; Eisenberg *et al.*, 1972a; Park *et al.*, 1972). Figure 140 shows the mass spectrum observed by the MIT–DESY group (Alvensleben *et al.*, 1971e) with a car-

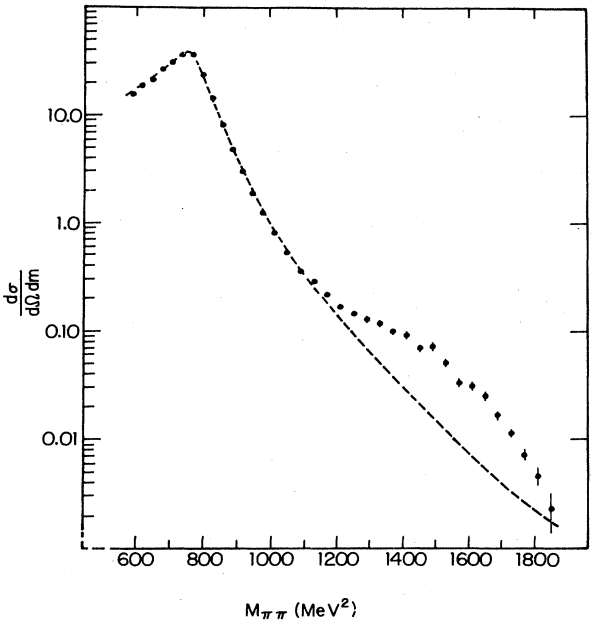

FIG. 140. The two-pion mass spectrum obtained by the MIT–DESY group (Alvensleben *et al.*, 1971e) using a two-arm magnetic spectrometer system and a 7.5 GeV bremsstrahlung beam (from Alvensleben *et al.*, 1971e).

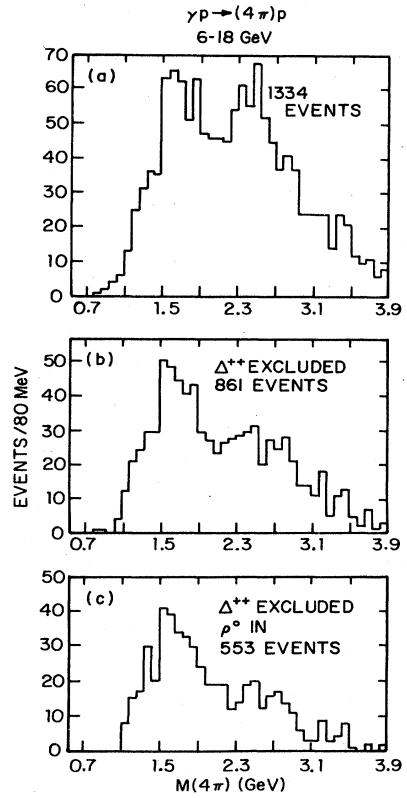

FIG. 141. The mass distribution for the reaction $\gamma p \to \pi^+\pi^-\pi^+\pi^- p$ for $6 < E_\gamma < 16$ GeV obtained by the SLAC streamer group (Davier *et al.*, 1973). (a) all events; (b) events not including Δ^{++}; (c) events not containing a Δ^{++} and including a ρ^0 (from Davier *et al.*, 1973).

bon target and a 7.5 GeV bremsstrahlung beam. No distinct high-mass structure characteristic of a resonance was observed, but there was a broad enhancement in the region $1.3 < MM < 1.8$ GeV. This result is typical.

1. $\rho''(1600)$

The first evidence for the photoproduction of the $\rho''(1600)$ was obtained by the SLAC streamer chamber group (M. Davier *et al.*, 1973) in an experiment with an 18 GeV bremsstrahlung beam incident on a hydrogen target. They observed a broad enhancement in the 4π invariant mass near 1.6 GeV in the reaction

$$\gamma p \to \pi^+\pi^-\pi^+\pi^- p\,.$$

Figure 141 shows the observed enhancement and the effect upon it of various cuts.

Davier *et al.* (1973) used Monte Carlo generated events to determine the shape of the background, and fitted the 4π mass spectrum to a nonrelativistic Breit–Wigner to determine the parameters of the resonance. They found:

(a) apparent mass $M = (1620 \pm 20)$ MeV; and width $\Gamma = (310 \pm 70)$ MeV

(b) a roughly energy-independent production cross section

$$(1.23 \pm 0.43)\ \mu\text{b} \quad \text{for } 6 < E_\gamma < 12 \text{ GeV}$$

$$(1.07 \pm 0.34)\ \mu\text{b} \quad \text{for } 12 < E_\gamma < 18 \text{ GeV}. \qquad (3.116)$$

(c) peripheral production with

$$d\sigma/dt \propto e^{(5.8 \pm 0.4)t'}$$

(d) predominant $\rho^0\pi^+\pi^-$ decay mode

(e) quantum numbers $I^G(J^P)C = 1^+(1^-)^-$.

These findings, when taken in conjunction with the evidence for a 4π resonance seen in the Frascati colliding beams (Sec. III.F), gave strong evidence for a heavy vector meson analogous to the ρ^0.

The SLAC–Berkeley bubble chamber collaboration (Bingham *et al.*, 1972) studied the reaction $\gamma p \to 2\pi^+ 2\pi^- p$ using a 9.3 GeV polarized beam and the SLAC 208 cm bubble chamber. They obtained evidence for a peripherally produced $(\sim e^{6t})4\pi$ resonance with quantum numbers $I^G(J^P)C = 1^+(1^-)^-$. The state decays primarily into $\rho^0\pi^+\pi^-$ with the $\pi^+\pi^-$ in an s-wave isospin-zero state. They presented evidence for s-channel helicity conservation in the production and found from a maximum-likelihood fit to the data a mass of (1.43 ± 0.05) GeV and a width of (0.65 ± 0.1) GeV. The photoproduction occurred via natural-parity exchange with a cross section $\sigma(\gamma p \to p\rho'' \to p\rho^0\pi^+\pi^-) = (1.6 \pm 0.4)\ \mu$b.

Alexander *et al.* (1975) used the dueterium-filled SLAC 208 cm bubble chamber exposed to a linearly polarized photon beam at 7.5 GeV to study coherent ρ, ω, and $\rho''(1600)$ production from deuterium. Figure 142 shows the mass distribution obtained for $\pi^+\pi^-$, $\pi^+\pi^-\pi^0$, and $\pi^+\pi^+\pi^-\pi^-$ production from deuterium. The fit to the four-pion data of a Breit–Wigner shape, modified by a mass skewing factor to describe the ρ'' and by a peri-

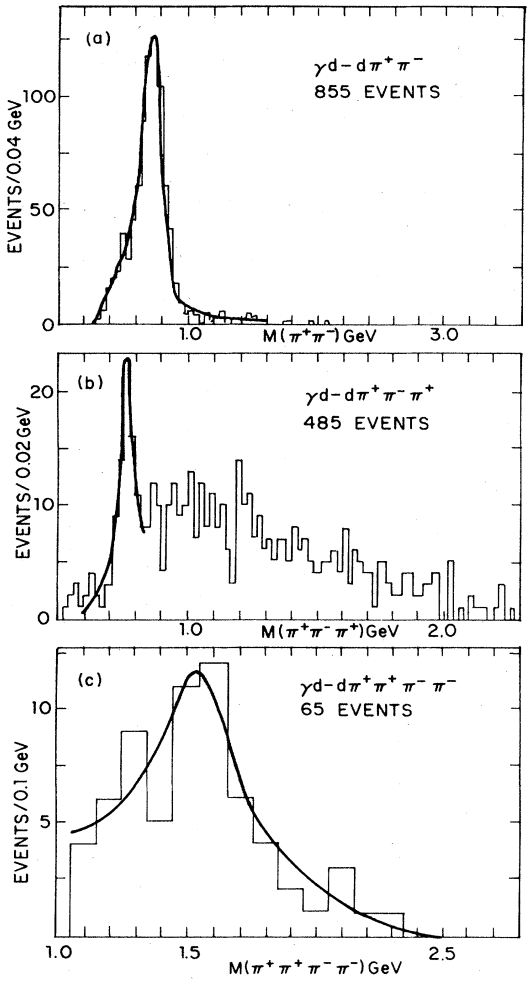

FIG. 142. Mass distributions obtained by Alexander *et al.* (1975) for coherently produced ρ, ω, and ρ'' on deuterium at 7.5 GeV. (a) $M(\pi^+\pi^-)$ for $\gamma d \to d\pi^+\pi^-$, satisfying $|t| < 0.2$ GeV^2. (b) $M(\pi^+\pi^-\pi^0)$ for $\gamma d \to d\pi^+\pi^-\pi^0$ for events having a visible deuteron recoil and $|t| < 0.2$ GeV^2. (c) $M(\pi^+\pi^+\pi^-\pi^-)$ for the reaction $\gamma d \to d\pi^+\pi^+\pi^-\pi^-$ with $|t| < 0.2$ GeV^2 (from Alexander *et al.*, 1975).

pheral phase space factor to describe the background, gave $M_{\rho''} = (1.57 \pm 0.06)$ GeV and $\Gamma_{\rho''} = (0.34 \pm 0.09)$ GeV. Using the relation $\Gamma(\rho'' \to \rho^0\pi^0\pi^0) = \frac{1}{2}\Gamma(\rho'' \to \rho^0\pi^+\pi^-)$ they obtained

$$\sigma(\gamma d \to \rho'' d) = (0.84 \pm 0.18)\ \mu\text{b}$$

for $|t_{\min}| < |t| < 0.2$ GeV^2.

Figure 143 shows the differential cross section for the coherently produced vector mesons ρ^0, ω, and ρ''. A fit to the data of the expression

$$d\sigma/dt = A_v \exp(Bt)[F(t)]^2 , \tag{3.117}$$

where $F(t)$ is the deuteron form factor, and B was taken to be 7.5 (GeV)$^{-2}$ (corresponding to the average measured slope for vector mesons photoproduced from hydrogen), gave

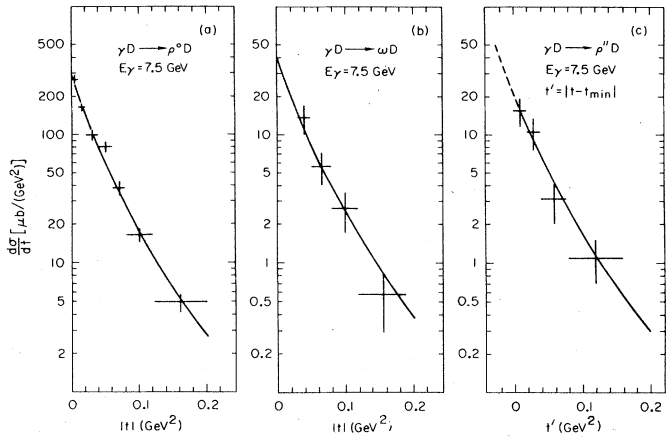

FIG. 143. The differential cross sections for coherent ρ^0, ω, and $\rho''(1600)$ production from deuterium observed by Alexander *et al.* (1975). (a) The differential cross section, $d\sigma/dt$, of the reaction $\gamma d \to \rho^0 d$. (b) $d\sigma/dt$ for the reaction $\gamma d \to \omega d$. (c) $d\sigma/dt'$, where $t' = |t - t_{\min}|$, for the reaction $\gamma d \to \rho'' d$. The curves are fits to $d\sigma/dt = A_v \exp(7.5t)[F(t)]^2$, where F is the deuteron form factor (from Alexander *et al.*, 1975).

$$A_\rho = (300 \pm 11)\ \mu\text{b/GeV}^2$$
$$A_\omega = (42 \pm 9)\ \mu\text{b/GeV}^2$$
$$A_{\rho''} = (50 \pm 10)\ \mu\text{b/GeV}^2 . \tag{3.118}$$

If the ρ'' photoproduction is described as depicted in Fig. 144 by an elastic amplitude $T_{\rho''}$ and a diffractive transition amplitude $D_{\rho\rho''}$, the ratio of the forward cross section from deuterium for ρ and ρ'' can be expressed in the form

$$R = \frac{A_\rho}{A_{\rho''}} = \frac{(1/\hat{f}_\rho^2)\,|T_\rho|^2}{|(1/\hat{f}_{\rho''})T_{\rho''} + (1/\hat{f}_\rho)D_{\rho\rho''}|^2} . \tag{3.119}$$

Experimentally this ratio is 6.0 ± 1.2. The e^+e^- experiments give, for the ratio $(\bar{f}_{\rho''}/\bar{f}_\rho)^2$, 6.6 ± 2.0. This suggests that $T_{\rho''} \sim T_\rho$ and $D_{\rho\rho''}$ is small. Neglecting $D_{\rho\rho''}$ and using the colliding-beam measurement, $\bar{f}^2_{\rho''}/4\pi = 17 \pm 5$ (Grilli *et al.*, 1973), for $\hat{f}^2_{\rho''}/4\pi$ gives

$$\sigma_T(\rho'' d) = (47 \pm 6)\ \text{mb} . \tag{3.120}$$

This is to be compared with the values

$$\sigma_T(\rho^0 d) = (54 \pm 2)\ \text{mb}$$
$$\sigma_T(\omega d) = (56 \pm 5)\ \text{mb} \tag{3.121}$$

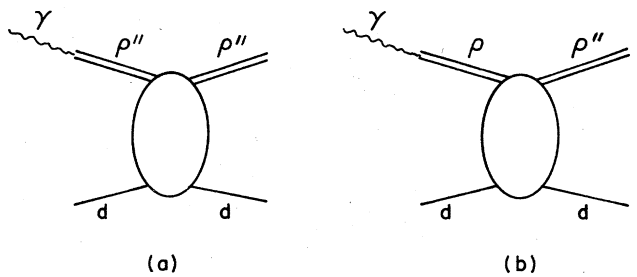

FIG. 144. Diagrams for coherent ρ'' photoproduction. (a) Elastic amplitude; (b) diffractive transition amplitude.

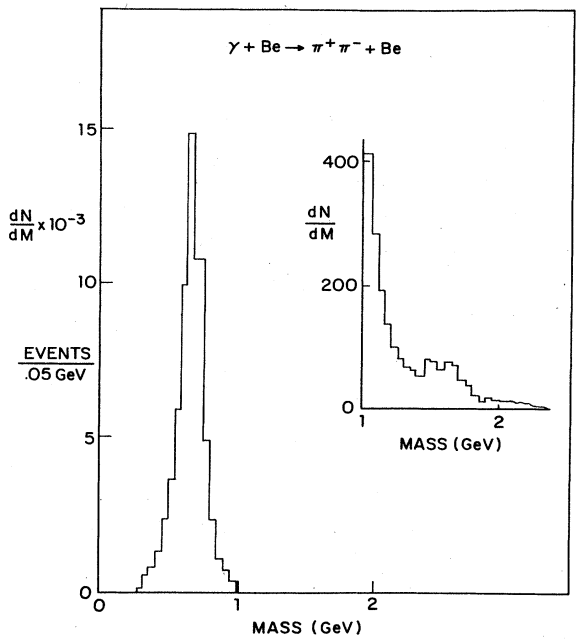

FIG. 145. The $\pi^+\pi^-$ mass plot obtained by the Columbia–Illinois group at Fermilab. The $\rho''(1600)$ is evident (from Silverman, 1975).

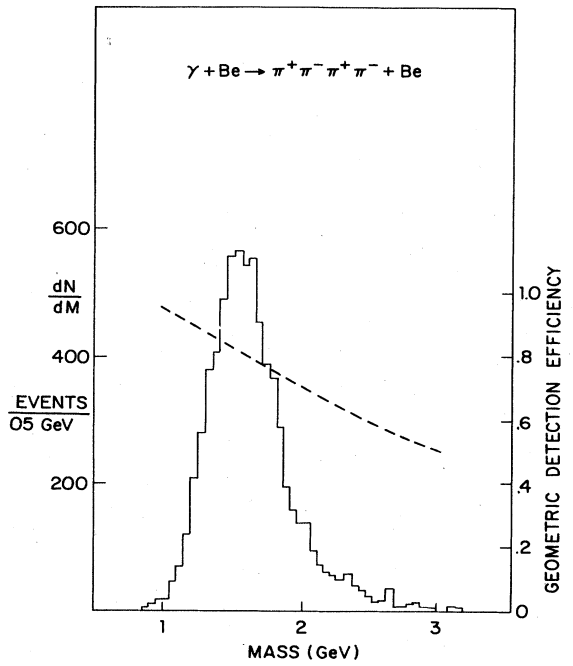

FIG. 146. The $\pi^+\pi^-\pi^+\pi^-$ mass plot obtained by the Columbia–Illinois group with the same setup as used for the data shown in Fig. 139 (from Silverman, 1975).

obtained for the ρ^0 and ω by a similar procedure.

Independent evidence for the ρ'' comes from phase-shift analysis of the reaction

$$\pi^- p \to \pi^+\pi^- n\,.$$

There is a p-wave resonance at ~1600 MeV with a total width of 180 MeV and an elasticity of 0.25 ± 0.05 (Hyams *et al.*, 1973). It is difficult to reconcile the large branching ratio for $\rho''(1600) \to 2\pi$ with the results of the photoproduction experiments. This situation has been further analyzed by Johnson *et al.* (1976).

Eisenberg *et al.* (1973) searched for ρ'' production in $\pi^+ p$ interactions at 5 GeV in a high-statistics experiment carried out with the SLAC 208 cm hydrogen bubble chamber. They did not detect the $\rho''(1600)$, and they obtained an upper limit of 0.006 for the ratio $\pi^+\rho \to \Delta^{++}\rho''/\Delta^{++}\rho^0$, with $\rho'' \to \rho^0\pi^+\pi^-$. Assuming one-pion exchange this leads to $f^2_{\rho''\pi\pi}/f^2_{\rho\pi\pi} < 0.02$.

In an experiment carried out at Fermilab with an 80 GeV photon beam and a beryllium target, a Columbia–Illinois group [private communication by W. Lee included in Silverman (1975)] has reported the detection of the two-pion decay mode for the $\rho''(1600)$. Figure 145 shows the observed mass plot for two pions; Figure 146 shows the mass plot for $\pi^+\pi^-\pi^+\pi^-$. The assumption that the 4π mass peak is entirely due to the $\rho''(1600)$ gives the $\pi^+\pi^-$ branching ratio

$$\Gamma(\pi^+\pi^-)/\Gamma(\pi^+\pi^+\pi^-\pi^-) = 0.05\,.$$

Langacker and Segrè (1976) have reexamined the evidence for the $\rho''(1600)$ and concluded that they could not account for the data without invoking a resonance. They then reanalyzed the available data assuming vector-meson dominance and found the $\rho'' p$ total cross section to be (23 ± 4) mb. With the further assumption that the ρ'' always decays into $\rho\pi\pi$, they found

$$\hat{f}^2_{\rho''}/4\pi \approx 21 \pm 10\,, \tag{3.122}$$

which is to be compared with $\hat{f}^2_\rho/4\pi \approx 2.3$ (see Table XXXI).

Further details concerning the $\rho''(1600)$ are given in the the reviews by Wolf (1972), Moffeit (1974), and Silverman (1975).

2. $\rho'(1250)$

Some evidence for an enhancement in the $\omega\pi^0$ channel near 1.2 GeV has been presented by the SLAC–Berkeley bubble chamber collaboration (Ballam *et al.*, 1974b). Those authors find a total cross section for $\gamma p \to p\rho'(1250) \to \pi^+\pi^-\pi^0\pi^0 p$ of $(1-3)$ μb with a width of 150 to 310 MeV. Langacker and Segrè (1976) concluded that they cannot account for this enhancement other than as a resonance, but that the parameters of the $\rho'(1250)$ are not sufficiently well determined to extract the $\rho'(1250)$ p total cross section in the VMD model. From their colliding-beam measurements Conversi *et al.* (1974) found $\bar{f}^2_{\rho'}(1250)/4\pi = 7 \pm 2$. More work on this resonance is merited.

3. J/ψ and $\psi(3700)$

Subsequent to the discovery of the J/ψ and the recognition of the coupling to the e^+e^- and $\mu^+\mu^-$ channels, several groups undertook experiments to study J/ψ photoproduction. Unsuccessful searches were carried out at

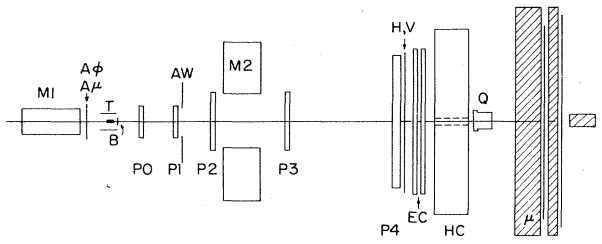

FIG. 147. Schematic diagram of the apparatus used by the Columbia–Hawaii–Cornell–Illinois–Fermilab group (Knapp *et al.*, 1975) to study J/ψ photoproduction from Be through the observation of μ pairs. M_1 and M_2 are magnets; P_0 through P_4 are multiwire proportional chambers; C is an electron calorimeter; H is a hadron calorimeter; μ is a muon identifier (from Knapp *et al.*, 1975).

Cornell by a Rochester–Cornell group (Andrews *et al.*, 1975a, b) and at SLAC by a SLAC–MIT group (Martin *et al.*, 1975). Successful experiments were reported by a Columbia–Hawaii–Cornell–Illinois–Fermilab group (Knapp *et al.*, 1975), a SLAC–Wisconsin group (Camerini *et al.*, 1975), a Cornell group (Gittelman *et al.*, 1975), a Fermilab–Lebedev–Santa Barbara–Toronto group (Nash *et al.*, 1976), and a SLAC–University of Massachusetts group (Dakin *et al.*, 1975).

The first Fermilab experiment (Knapp *et al.*, 1975) used a photon beam obtained from a zero-degree neutral beam, which was produced by interactions of 300 GeV protons in a 30.5 cm Be target, to study the reaction

$$\gamma + \mathrm{Be} \to \mu^+ + \mu^- + X .$$

Figure 147 shows a schematic diagram of their apparatus. The muon identifier consisted of a steel shield which was 120 cm thick, a 22-element horizontal scintillation-counter hodoscope, a second steel shield which was 60 cm thick, and an eighteen-element vertical scintillation-counter hodoscope. Figure 148 shows the raw mass spectrum for all events with momenta greater than 80 GeV and the momentum-transfer distribution for events in the mass interval $2.8 < M_{\mu\mu} < 3.4$ GeV^2. There is a clear peak at the J/ψ mass and the t distribution shows evidence for coherent ψ production. The curve shown in Fig. 148(b) is the assumed

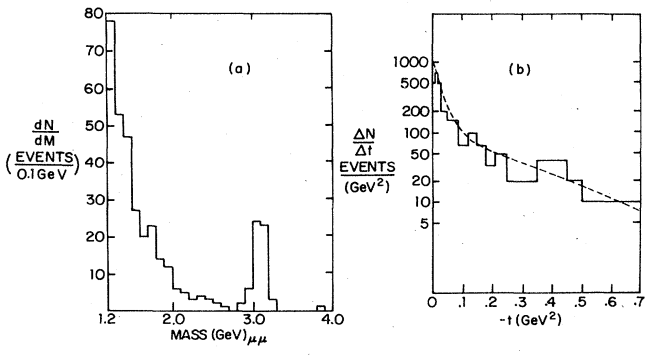

FIG. 148. (a) Diagram of invariant mass distribution observed by Knapp *et al.* (1975) above 1.2 GeV for events with momenta greater than 80 GeV. (b) Observed t distribution for events in (a) with $2.8 < M_{\mu\mu} < 3.4$ GeV (from Knapp *et al.*, 1975).

t distribution (3.123), corrected for acceptance and resolution. It was found that the form

$$d\sigma/dt(\gamma + \mathrm{Be} \to \psi + X) \propto A^2 e^{40t} + A e^{4t} \qquad (3.123)$$

was consistent with the data. For the total cross section, they obtained

$$\sigma(\gamma + \mathrm{Be} \to \mu\mu(3.1) + X) = (16 \pm 5)\ \mathrm{nb/nucleus} . \qquad (3.124)$$

Inferring from the observed t distribution the existence of a coherent peak, the differential cross section per nucleon was determined from the coherent production of the J/ψ at $t = 0$ to be

$$\left.\frac{d\sigma}{dt}\right|_{t=0} (\gamma N \to \psi N) = (56 \pm 19)\ \mathrm{nb/GeV^2} \qquad (3.125)$$

with a systematic uncertainty in normalization of about 15%.

Using VMD and the optical theorem, and assuming that the $\gamma - \psi$ coupling constant is independent of Q^2, one obtains for the ψ-nucleon total cross section,

$$(1 + \alpha_\psi^2)^{1/2} \sigma_\psi = (1.3 \pm 0.25)\ \mathrm{mb} , \qquad (3.126)$$

where α_ψ is the ratio of the real to the imaginary part of the forward scattering amplitude. It was concluded from this value of the cross section that the J/ψ is a diffractively produced hadron.

The Wisconsin–SLAC group (Camerini *et al.*, 1975) used the SLAC 8 GeV and 20 GeV spectrometers in coincidence to detect the electron and muon pairs from J/ψ decay. They measured the s and t dependence of incoherent J/ψ production from deuterium, and $\psi(3700)$ and J/ψ production from hydrogen. Among other things, they found:

(a) Production from neutron and proton targets were similar.

(b) Indications of a significant inelastic contribution to the cross section.

(a) A rise in $d\sigma/dt$ (extrapolated to $t = 0$) from ~7.6 nb/GeV^2 at $k = 13$ GeV to ~20 nb/GeV^2 at 21 GeV.

(d) At 19 GeV a t distribution with slope parameter $B = (2.9 \pm 0.3)$ GeV^{-2}.

(e) At t_{min} for $k = 21$ GeV the ratio of J/ψ production to $\psi(3700)$ production given by

$$\frac{d\sigma(J/\psi)/dt}{d\sigma(\psi(3700))/dt} = 6.8 \pm 2.4 \qquad (3.127)$$

(f) From a VMD argument an upper limit for $\sigma_{\mathrm{tot}}(\psi N)$ of 0.8 mb.

The Cornell group (Gittelman *et al.*, 1975) used a pair of lead-glass Cerenkov hodoscopes to study the photoproduction of the J/ψ from a beryllium target with an 11.6 GeV bremsstrahlung beam. If the elastic cross section for a single nucleon is expressed in the form Ae^{Bt}, their results at 11 GeV are

$$A = (1.01 \pm 0.20)\ \mathrm{nb/GeV^2} ,$$
$$B = (1.25 \pm 0.20)\ \mathrm{GeV^{-2}} . \qquad (3.128)$$

This is a surprisingly small cross section.

At Fermilab the Fermilab–Lebedev–Santa Barbara–Toronto group used a tagged photon beam in conjunction with a lead-glass based spectrometer to measure the photoproduction of J/ψ from deuterium at a mean photon

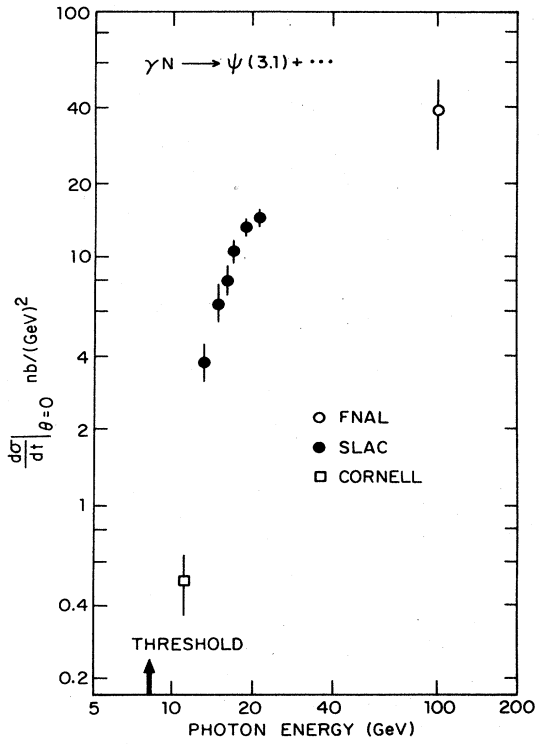

FIG. 149. Summary of results for $d\sigma/dt$ at $t=t_{\min}$ for $\gamma p \to \psi p$. This figure includes only data obtained in coincidence experiments (from R. Anderson, 1976).

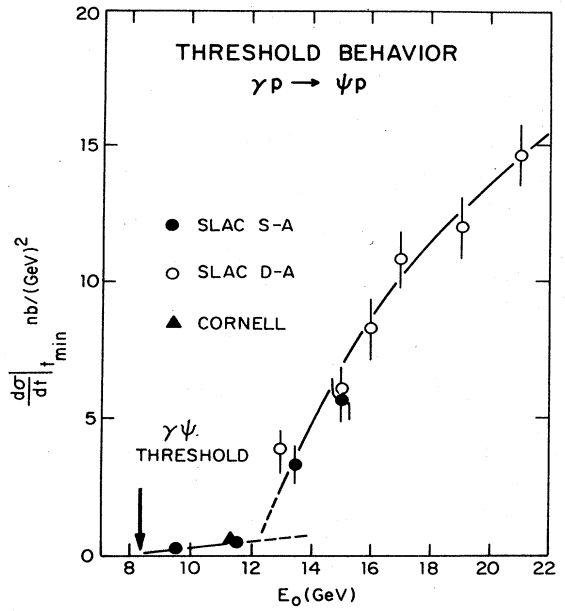

FIG. 150. Threshold behavior of $t=t_{\min}$ for J/ψ photoproduction. SLAC–S-A refers to the single-arm measurements of Anderson *et al.* (1977); SLAC D–A refers to the double-arm measurements reported by Anderson (1976) (figure from Anderson, 1976).

energy of 55 GeV. They found for the differential cross section per nucleon

$$\left.\frac{d\sigma}{dt}\right|_{t=0} = (68 \pm 19)\exp[(1.8 \pm 0.4)t]\ \text{nb/GeV}^2\,, \quad (3.129a)$$

and for the total cross section

$$[37.5 \pm 8.2(\text{statistical}) \pm 4(\text{systematic})]\ \text{nb}\,. \quad (3.129b)$$

Figure 149 shows a plot versus energy of $d\sigma/dt$ at $\theta=0$ for the reaction $\gamma p \to \psi p$. Table XXIX summarizes the data obtained from coincidence experiments in which e^+e^- or $\mu^+\mu^-$ were observed.

In a second experiment the SLAC–Wisconsin group (R. Anderson, 1976) studied the J/ψ production by observing the yield of single muons at large transverse momentum. Figure 150 shows the study of the threshold production using the single-arm data together with the SLAC and Cornell coincidence measurements. The SLAC–Wisconsin group (R. Anderson *et al.*, 1977) also used the single-arm spectrometer technique to measure the ratio of the total cross sections per nucleon for Be and Ta targets. They found

$$\sigma(\text{Be})/\sigma(\text{Ta}) = 1.25 \pm 0.05\,. \quad (3.130a)$$

They then used a simple optical model to determine from this ratio

$$\sigma_{\psi N} \approx 3.5\ \text{mb}\,. \quad (3.130b)$$

TABLE XXIX. J/ψ photoproduction versus energy. In the three columns on the right, the value of B is fixed and used with the total production cross section $\sigma_{\gamma\psi}$ to infer $d\sigma_{\gamma\psi}/dt|_{t=0}$ (indicated ←) or with $d\sigma_{\gamma\psi}/dt|_{t=0}$ to infer $\sigma_{\gamma\psi}$ (indicated →).

Experiment	$\langle E_\psi \rangle$ (GeV)	$k_{\max}$ (GeV)	A_{tgt}	B (GeV^{-2})	$d\sigma_{\gamma\psi}/dt\|_{t=0}$ per nucleon (nb/GeV^2)		$\sigma_{\gamma\psi}$ (nb)
Cornell	11.0	11.8	9	1.25 ± 0.2	1.01 ± 0.2	$B=1.25$ →	0.67 ± 0.21
SLAC	13	13.5	2		7.5 ± 1.7		
	19	20	2	2.9 ± 0.3	19.4 ± 1.3	$B=2.9$ →	5.2 ± 0.6
	19	19.5	2		15.5 ± 1.4		
	19	19.5	1		13.9 ± 1.4		
Fermi Lab (tagged γ)	55	31–80	2	1.8 ± 0.4	68 ± 19	←$B=1.8$	37.5 ± 8.2
Fermi Lab (broadband γ)	116	50–210	9	≃2	59 ± 19	$B=2$ →	~28

However, due to the very crude optical model used and the experiment's large t_{min}, this value must be regarded as very tentative.

H. Incoherent production from nuclei

Additional information concerning the hadronic nature of the photon is given by the energy and A dependence of incoherent rho and incoherent pion production (Gottfried and Yennie, 1969; Gottfried, 1972). The theory of the hadronic photon predicts that there is a transition from a low-energy region ($\lesssim 4$ GeV), where the nucleus acts as an object transparent to the photon, to a high-energy region, where the photon appears to be strongly absorbed and its ability to interact decreases as it proceeds through the nucleus. It is useful to compare the cross section for a production process on a nucleus with the cross section on a single nucleon. Depending on the nature of the process, the ratio of the cross sections is called A_{eff} (for approximately equal production cross sections from neutrons and protons), Z_{eff} (for production only from protons), or N_{eff} (for production only from neutrons); generically we use A_{eff}. According to photon shadowing theory, A_{eff}/A will decrease from 1 at low energy to a small value at high energy. Figure 203a, b, c in Sec. V.D shows various theoretical predictions for A_{eff} for several nuclei. Qualitatively, the important prediction of vector dominance is that A_{eff} should fall with energy in the transition region, with the fall being more dramatic for heavy nuclei. This energy dependence is attenuated by the fact that the ρ^0-nucleon cross section decreases as the energy increases. In this section we will report the measurements; the theoretical interpretation is discussed in Sec. V.D.

Five experiments have been carried out to study the energy and A dependence for incoherent production. A Cornell group (McClellan *et al.*, 1969c) used a pair spectrometer system to measure the A dependence for incoherent production of rho mesons with average energies of 4 and 8 GeV at a fixed value for the momentum transfer, $|t| = 0.1$ GeV^2. They made measurements with deuterium, carbon, copper, and silver targets of approximate thickness 0.1 radiation length. At $|t| = 0.1$ GeV^2 the "coherent" production has dropped to a negligible value for these nuclei. At the machine energies at which they ran, the inelastic rate was 15% of the total rate. Figure 151 shows a plot of A_{eff} versus A together with the VMD calculation of von Bochmann, Margolis, and Tang (1970). The data are not inconsistent qualitatively with photon shadowing. The observed energy dependence appears to be somewhat smaller than the predicted energy dependence. The data give clear evidence for shadowing in incoherent rho production. A residual uncertainty in the analysis is a possible suppression of the cross section due to the effects of nuclear correlations (see Sec. V.D).

In an experiment in which the principal object was a measurement of coherent rho production from complex nuclei, a DESY–Columbia group (Asbury *et al.*, 1967a) also measured the incoherent ρ^0 production from copper and lead targets for an average photon energy of 2.7 GeV. They used a double-arm magnetic spectrometer in conjunction with a 4.35 GeV bremsstrahlung beam.

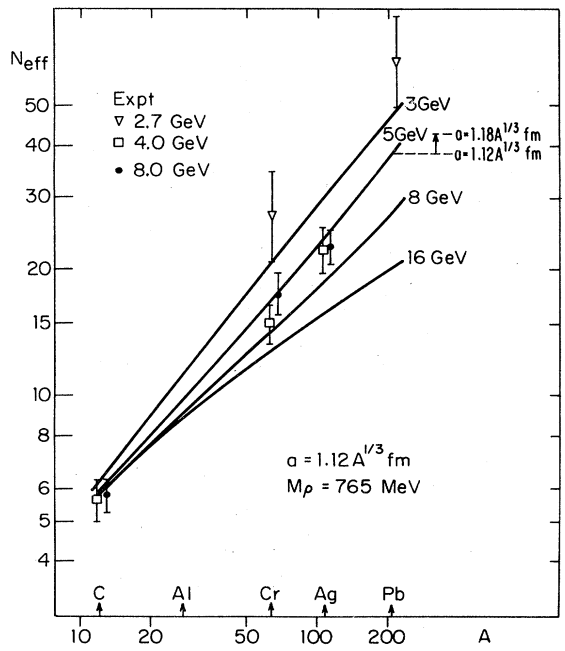

FIG. 151. The experimental and theoretical values of A_{eff} for incoherent ρ^0 photoproduction for several energies as a function of A. The effect of a change in nuclear radius from $a = 1.12A^{1/3}$ F to $a = 1.18A^{1/3}$ F is shown for $A = 200$ at $E_\gamma = 5$ GeV (from von Bochmann *et al.*, 1970).

Those measurements are shown together with the Cornell measurements in Fig. 151. The combination of the DESY–Columbia and the Cornell measurements gives evidence for the energy dependence predicted by VMD.

The third experiment was a study of single $\pi^\pm$ and K^+ production from complex nuclei carried out by a SLAC group (Boyarski *et al.*, 1969). Data were obtained with targets of CH_2, Be, C, Al, Cu, Ag, and Pb at laboratory photon energies of 8 and 16 GeV. Charged mesons were detected and momentum analyzed with the SLAC 20-GeV spectrometer system. By working close to the bremsstrahlung end-point energy, the single-meson production events were separated from multi-meson production through energy conservation. The experimental resolution was much too coarse to detect the excitation of individual nuclear levels, and all nuclear final states with excitations of less than about 100 MeV were accepted. Concentrating on the π^+, the relevant parameter is Z_{eff}, which is defined by the equation

$$Z_{eff} = \frac{d\sigma(\gamma A \to \pi^+ A^*)/dt}{d\sigma(\gamma p \to \pi^+ n)/dt} \tag{3.131}$$

Figure 152 shows a plot of Z_{eff} versus A for π^+ production. The data from complex nuclei, taken in the range of momentum transfer from 0.01 to 0.45 GeV^2, show very little dependence on t, in contrast to the t dependence (e^{3t}) observed for the hydrogen data. (The hydrogen cross section has in fact a sharp peak at small t; however, the area under this peak is not important for the experiments discussed here.) Thus the values of Z_{eff} showed a dependence on t which was not adequately explained by the theory. The t-dependent Pauli suppres-

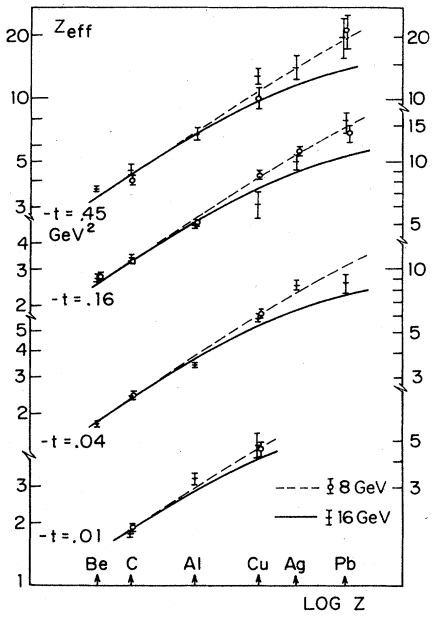

FIG. 152. The A dependence of Z_{eff} in π^+ production for four different momentum transfers. The normalization of the calculated cross section for each value of momentum transfer is fitted to the experimental data (from von Bochmann *et al.*, 1970).

sion of incoherent events would not be expected to play an important role in the upper part of the t range. Since the theory was inadequate and in particular did not include momentum-transfer-dependent correlation effects, the normalization of the calculated cross section for each value of momentum transfer was fitted to the experimental data. The normalization factors (experiment/theory) were 1.55, 1.25, 0.92, and 0.71 at $-t = 0.45$, 0.16, 0.04, and 0.01, respectively. On average the data are consistent with some shadowing but do not show the energy dependence predicted by VMD. Figure 152 shows the results of an analysis by von Bochmann *et al.* (1970).

By appropriately normalizing to the number of neutrons in the target nucleus this group also found a close parallel between π^- photoproduction and the results described above for π^+ production. Data were also taken for K^+ photoproduction at small momentum transfers; they showed an increase of Z_{eff} relative to π^+ photoproduction with increasing A. In view of the smaller $K-N$ absorption cross section and the absence of exclusion principle suppression for this process, this was not entirely unexpected.

A second Cornell experiment (Meyer *et al.*, 1972) studied the incoherent photoproduction of π^0 mesons from D_2, Be, C, Al, Cu, Ag, and Pb targets with peak bremsstrahlung energies of 4.25, 5.6, 7.8, and 9.6 GeV. They used two lead-glass hodoscopes to detect the gamma rays from the decay of the π^0. The detector gave a well separated π^0 peak with little background. The four-momentum transfers were in the range $0.1 < |t| < 0.25$ GeV^2. The resolution was not good enough to isolate the elastically produced π^0's. However, by using the data near the upper end of the spectrum only, they excluded π^0's arising from the decay of other particles and included

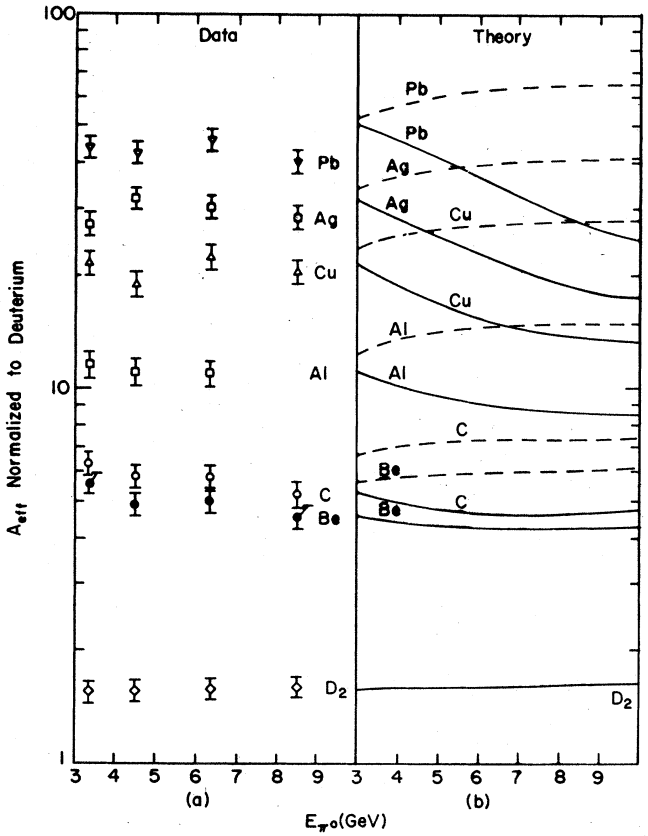

FIG. 153. A_{eff} versus E_{π^0} for π^0 photoproduction. (a) The data normalized to deuterium. (b) Model calculations explained in Sec. V.D. The dashed line is for "no photon shadowing," and the solid line is for pure vector dominance (from Meyer *et al.*, 1972, slightly rearranged).

only π^0's produced directly, either elastically or with nucleon isobars. Figure 153 shows the observed variation with energy of A_{eff}, together with the VMD and no photon shadowing predictions (Sec. V.D). The data indicate shadowing but show very little energy dependence.

A Yerevan group (Abrahamian *et al.*, 1972) has extended the studies of single-pion photoproduction from complex nuclei down to 2 and 3 GeV. They employed a magnetic spectrometer system and used a technique similar to that employed by the SLAC group to make measurements at $|t| = 0.3$ and 0.58 (GeV)^2. Allowing for the difference in momentum transfer, the values of Z_{eff} are in rough agreement with those obtained by the SLAC group, possibly indicating that Z_{eff} is independent of energy from 2 to 16 GeV.

In summary, all of the measurements of incoherent rho and incoherent pion production show the presence of shadowing, in qualitative agreement with our ideas about the photon's hadronic structure. The observed energy dependence of A_{eff} is in all cases smaller than that predicted by VMD.

I. Inelastic electron and muon scattering

Inelastic lepton scattering gives a method for studying the behavior of spacelike photons and in particular allows

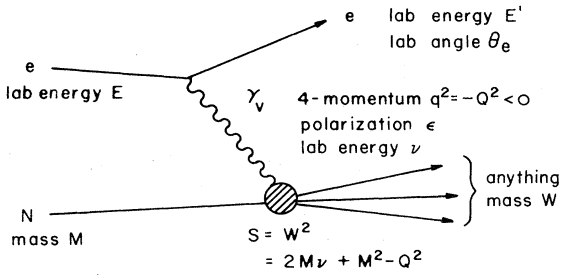

FIG. 154. The one-photon exchange diagram which is assumed to dominate inelastic electron scattering.

one to vary ν and Q^2 independently. Figure 154 shows the one-photon exchange diagram that is assumed to dominate this process, and partially defines the notation that we shall use. With the assumption of one-photon exchange, the differential cross section in the laboratory frame can be written in the form (Hand, 1963)

$$\frac{d^2\sigma(\theta,E,E')}{d\Omega dE'} = \Gamma_T[\sigma_T(Q^2,W^2) + \epsilon\sigma_L(Q^2,W^2)], \quad (3.132a)$$

$$\Gamma_T = \frac{\alpha}{4\pi^2}\left(\frac{W^2-M^2}{2M}\right)\frac{1}{Q^2}\left(\frac{E'}{E}\right)\frac{2}{1-\epsilon}, \quad (3.132b)$$

$$\epsilon = \frac{1}{1+2(1+\nu^2/Q^2)\tan^2(\frac{1}{2}\theta)}, \quad 0 \leq \epsilon \leq 1. \quad (3.132c)$$

Here M is the mass of the proton, E is the energy of the incident electron, E' is the energy of the scattered electron, θ is the angle through which the electron is scattered, ϵ is the polarization parameter. $\nu = E - E'$ is the energy transfer, $Q^2 = 4EE'\sin^2(\theta/2)$ is the mass of the virtual photon, and $W^2 = M^2 + 2\nu M - Q^2$ is the square of the total center-of-mass energy of the final hadronic state. The ratio R of the longitudinal cross section to the transverse cross section is defined by

$$R = \sigma_L/\sigma_T. \quad (3.133)$$

The differential cross section can also be written in the form

$$\frac{d^2\sigma}{d\Omega dE'} = \frac{4\alpha^2(E')^2}{Q^4}[W_2(Q^2,W^2)\cos^2(\theta/2) + 2W_1(Q^2,W^2)\sin^2(\theta/2)] \quad (3.134a)$$

or in the equivalent form

$$\frac{d^2\sigma}{d\Omega dE'} = \sigma_M[W_2(Q^2,W^2) + 2W_1(Q^2,W^2)\tan^2(\theta/2)], \quad (3.134b)$$

where σ_M is the Mott cross section for elastic scattering from a point spinless particle. The two structure functions, W_1 and W_2, are related to σ_L and σ_T by comparing Eqs. (3.132) and (3.134). The result is Eq. (2.13).

1. Critique of the one-photon exchange approximation

●Since the use of the one-photon exchange approximation is crucial to the analysis of the data, several experiments have been carried out to determine experimentally the validity of this hypothesis. There are two ways in which one can test this assumption. If one makes a series of measurements with the same W and Q^2, but different electron scattering angles and hence different polarization parameters ϵ, the data should fall on a straight line of the form

$$A + B\tan^2(\theta/2). \quad (3.135)$$

A deviation from such a line indicates the presence of two-photon exchange components. (This is the standard technique for separately determining W_1 and W_2 and hence for determining R.) The available measurements are not, however, sufficient to use this method to make a definitive test of the one-photon exchange hypothesis.

●A second method for seeking evidence for the two-photon terms is to measure precisely the ratio of positron to electron scattering from a hydrogen target. This cross section ratio is given approximately by $1 + 4\,\mathrm{Re}(T_2/T_1)$, where T_1 and T_2 are, respectively, the one- and two-photon exchange amplitudes. Several groups have made careful measurements of the e^+/e^- ratio in an effort to set a limit on the two-photon exchange component. A Rochester–Columbia group (Jöstlein *et al.*, 1974) used a muon beam and a wire spark chamber spectrometer at Brookhaven National Laboratory to make measurements in the Q^2 range from 0.5 to 2.0 GeV^2. A SLAC group (Rochester *et al.*, 1976) used the SLAC 20-GeV spectrometer to measure the ratio of positron to electron inelastic scattering from hydrogen and deuterium for Q^2 between 2.4 and 14.9 GeV^2. A Santa Barbara group (Fancher *et al.*, 1976) used a large-acceptance (±5 GeV and 2.1 millisteradian) spectrometer set at a mean scattering angle of 8° to compare the electron and positron inelastic scattering over the range $1.2 < Q^2 < 3.3$ GeV^2, $2 < \nu < 9.5$ GeV. Figure 155 summarizes the measured ratios of antilepton to lepton inelastic

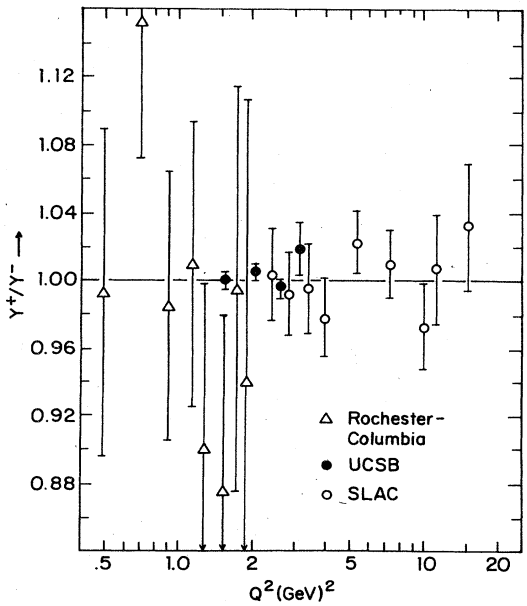

FIG. 155. Ratio of antilepton to lepton inelastic scattering from hydrogen as a function of square of four-momentum transfer (Q^2) (from Fancher *et al.*, 1976).

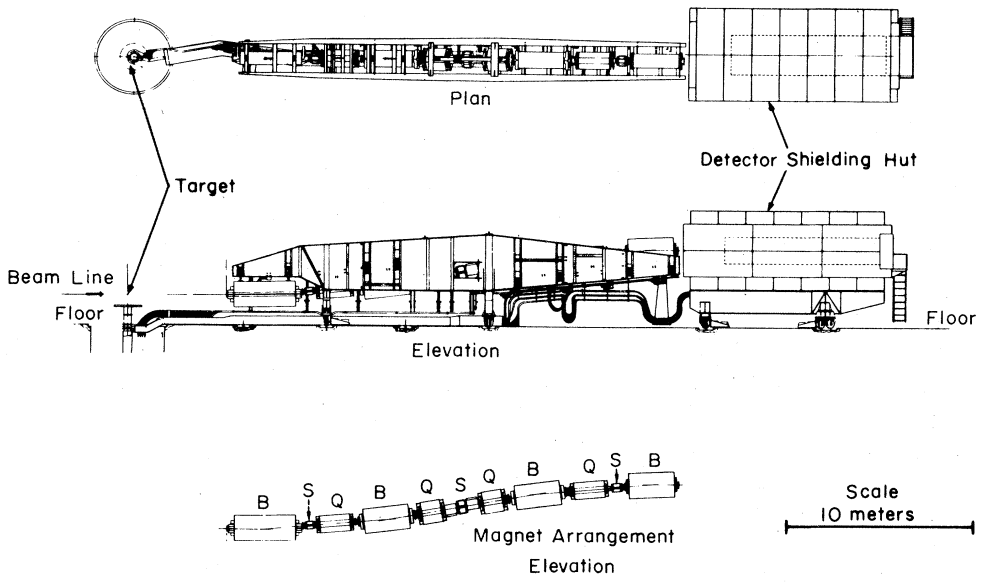

FIG. 156. A schematic diagram of the SLAC 20 GeV spectrometer (from Stein *et al.*, 1975).

scattering from hydrogen as a function of Q^2 for all these reported experiments. By integrating their results over the entire Q^2, ν range, the Santa Barbara group found

$$e^+/e^- = 1.0027 \pm 0.0035 . \tag{3.136}$$

The SLAC group found the e^+/e^- ratio was consistent with 1 within errors of a few percent for both hydrogen and deuterium targets. In summary there are, at the one or two percent level, no indications of two-photon exchange contributions; and it is accordingly justified to neglect them when analyzing the data.

2. General features of experiments

Early inelastic electron scattering experiments in which the main object of interest was the excitation of nucleon resonances such as the $\Delta(1236)$ were carried out at Stanford, Cornell, CEA, and DESY. The first systematic study of the inelastic continuum was carried out at SLAC by the SLAC–MIT group. More recently. measurements have been made using the high-energy muon beam at the Fermi National Accelerator Laboratory.

The measurements at SLAC have been carried out with the 20 GeV, 8 GeV, and 1.6-GeV spectrometers. Figures 156 and 157, respectively, show diagrams of the

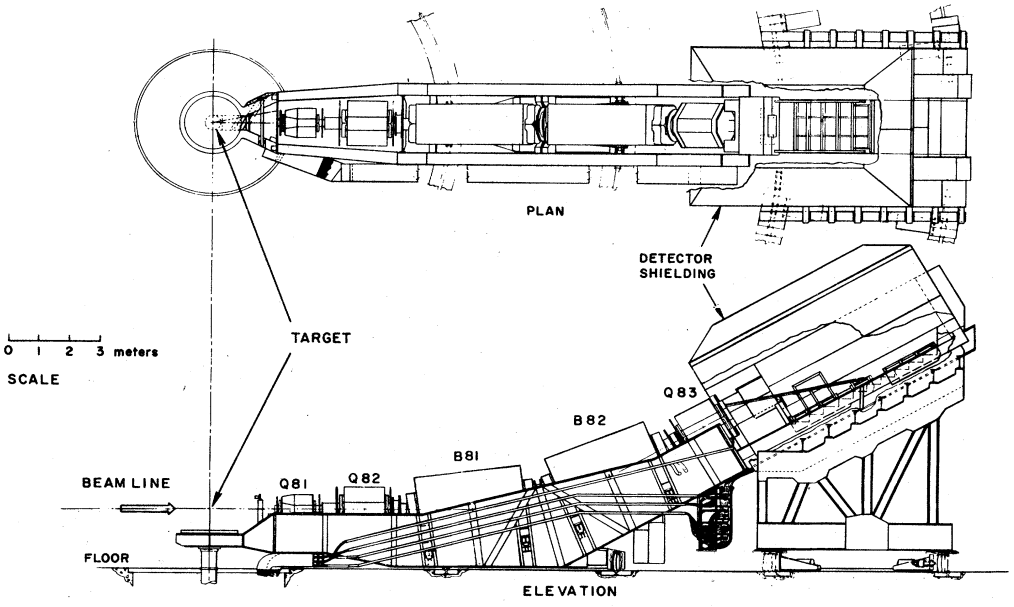

FIG. 157. A schematic diagram of the SLAC 8 GeV spectrometer (courtesy of R. Taylor).

20- and 8-GeV spectrometers; Fig. 66 shows a diagram of the 1.6-GeV spectrometer. All three of these spectrometers are focusing spectrometers which are equipped with counter systems for distinguishing electrons from pions. More recently they have been partially equipped with proportional chambers for determining the trajectories of the particles. The spectrometers have been carefully calibrated and cross-calibrated through the direct use of electrons as a probe and through studies of elastic electron scattering. In order to separately determine σ_L and σ_T, or equivalently W_1 and W_2, it is necessary to make measurements with different ϵ such that W and Q^2 are the same. This, in general, requires measurements with a different electron scattering angle; and in order to obtain sufficient counting rate, larger-aperture spectrometers are required at the larger angles. Thus separation of σ_L and σ_T usually requires combining data taken with two different spectrometers. It is, in general, only possible to make this separation over a limited range in the W, Q^2 plane with a given accelerator.

Figure 158 shows typical spectra observed at SLAC (Miller *et al.*, 1972) with a fixed energy for the incident electron beam, a fixed angle for the spectrometer, and a changing energy setting of the spectrometer. The large peak due to elastic electron scattering has been suppressed. The dominant features are the prominent resonances and the large, broad, and featureless peak directly above them in W. The breadth, large integrated area, and weak Q^2 dependence of this peak were the original experimental motivation for the parton model picture described in Sec. II.D.

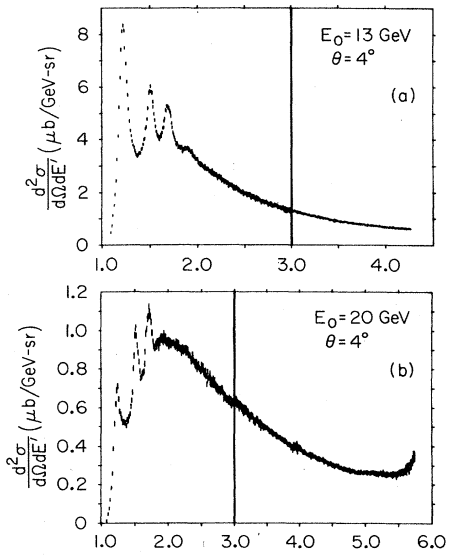

FIG. 158. Inelastic electron scattering cross sections versus the total energy in the virtual photon target proton system for incident electrons of 13 and 20 GeV scattered at 4°. A slight normalization discrepancy exists across the vertical bar which separates two data samples. The disturbance at $W=3.9$ GeV in the second spectrum occurs where two scans were joined, and is thought to be an instrumental effect.

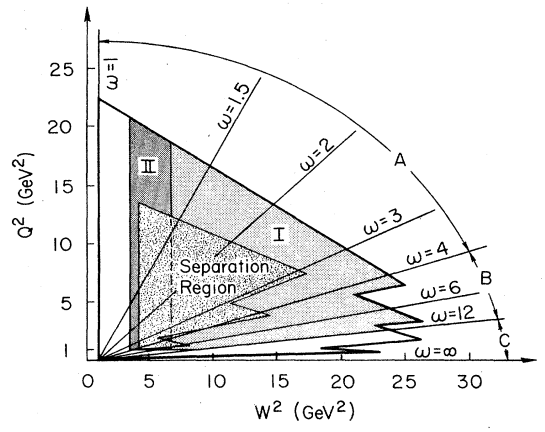

FIG. 159. The kinematic plane in Q^2 and W^2 is shown along with the lines of constant $\omega \equiv 2M_p\nu/Q^2$. The heavy line bounds all data points measured at 6, 10, 18, 26, and 34 degrees. The region marked "Separation Region" includes all points where data at three or more angles exist. Various values of ω are indicated with $\omega=\infty$ coinciding with the $Q^2=0$ abscissa and $\omega=1$ corresponding to elastic scattering ($W^2=0.88$ GeV^2). Region I indicates the region where the data seem consistent with scaling in ω. Region II indicates the possible extension of the scaling region if the data are plotted against $\omega'=1+W^2/Q^2$ (from Miller *et al.*, 1972).

3. General features of the data and scaling

In their initial measurements at 6 and 10 degrees using the 20 GeV spectrometer (Bloom *et al.*, 1969a; Breidenbach *et al.*, 1969), the SLAC–MIT group found that, with the assumption of a predominantly transverse electromagnetic cross section (i.e., the ratio R is small), νW_2 depended only on the ratio of Q^2 and ν over a substantial range of the data. To be precise the data were consistent with

$$\nu W_2 = F_2(\omega),$$

where (3.137)

$$\omega \equiv \frac{2M\nu}{Q^2} \equiv \frac{1}{x},$$

and $F_2(\omega)$ is universal function of ω. Figure 15 shows plots of νW_2 and $2MW_1$, versus x. This behavior, which is known as "scaling," was predicted by Bjorken (1969) to occur in the asymptotic kinematic region reached by letting Q^2 and ν go to infinity with ω held constant. In terms of the parton model such behavior is indicative of pointlike constituents.

In a subsequent experiment (Miller *et al.*, 1972), the SLAC–MIT group used the 8-GeV spectrometer to make measurements at 18, 26, and 34 degrees, and used these data in conjunction with the earlier measurements to determine R over the region shown in Fig. 159. They found the data consistent with R having the fixed value, $R=0.18$. They then used this value of R to determine W_1 and W_2 over the full range in which data were available. As a byproduct of studying the large-angle data at small ω, it was found that, for the whole range in ω, the scaling was extended from $W=2.6$ GeV down to $W \simeq 1.8$ GeV, if a new variable $\omega' \equiv \omega + a/Q^2$ was introduced. They found in particular that one could obtain a good fit

with $a = M_p^2$, so that

$$\omega' = \omega + M_p^2/Q^2 = 1 + W^2/Q^2 . \quad (3.138)$$

Subsequently, an MIT–SLAC group used data taken with the 8-GeV spectrometer at 18, 26, and 34 degrees, in conjunction with data taken at 6 and 10 degrees with the 20 GeV spectrometer, to expand the measurements of R to a wider kinematic range (Riordan *et al.*, 1974b).

4. Proton-neutron difference

In a separate set of experiments, the SLAC–MIT group used measurements made at 18, 26, and 34 degrees with the 8-GeV spectrometer and a deuterium target to determine the structure functions for the neutron (Bodek *et al.*, 1973; Poucher *et al.*, 1974; Taylor, 1975a). They found that the deuterium cross sections scaled; and they used the procedure developed by Atwood and West (1973) and West (1971, 1972) to determine the cross sections for the neutron. Figure 160 shows the combined data for the ratio of the neutron cross section to the proton cross section. This plot includes data taken at 4 degrees with the 20-GeV spectrometer, and data taken at 50 and 60 degrees with the 1.6-GeV spectrometer. The decrease in the ratio with x is surprisingly large and a challenge to all the models.

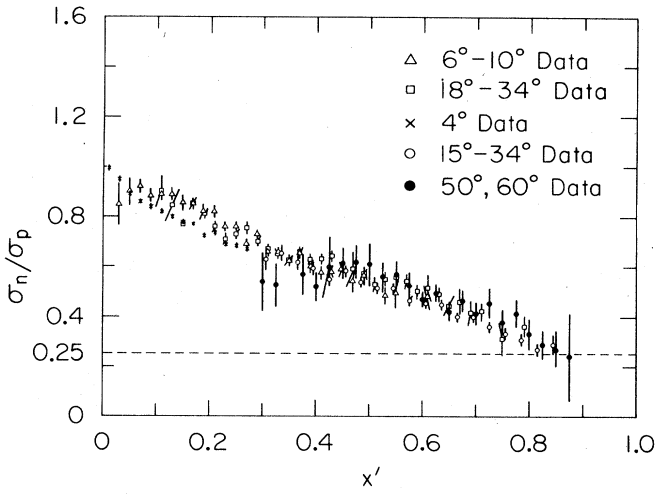

FIG. 160. The ratio of the neutron cross section (as extracted from D_2 data) to the proton cross section. The effects of Fermi motion in deuterium increase the systematic errors (not included) as $x' \to 1$ (from Taylor, 1975b).

5. Systematic studies of scaling

The MIT–SLAC group used earlier data (Bodek *et al.*, 1973; Poucher *et al.*, 1974) that allowed a complete separation of W_1 and W_2 to make a more definitive check of scaling (Riordan *et al.*, 1974a). There were clear deviations from scaling in the region $1.5 < \omega < 3.0$, $2 < Q^2 < 15$ GeV^2.

An interesting attempt was made to circumvent the limitations of a "low-energy" experiment. In the measurements at 4 degrees, a SLAC group (Stein *et al.*, 1975) studied the low-Q^2 behavior of the data with $\omega' > 6$. They theorized that the turn-on to scaling can be approximated by a single function of Q^2. Figure 17 shows a plot of νW_2 versus Q^2 for this region. They then used a particular parametrization of this turn-on to extrapolate the data for $\omega' > 8$ to the high-Q^2 limit. This procedure extended the νW_2 curve to $\omega = 100$ through extrapolation of the low-energy data. The results of such an extrapolation should be regarded with some skepticism since the functional dependence on Q^2 is likely to depend to some extent on ω.

The MIT–SLAC group (Riordan *et al.*, 1975) and a SLAC group (Atwood *et al.*, 1976) subsequently undertook to make more extensive measurements, and to make a more comprehensive analysis of the available data. Table XXX summarizes the details of the data sets that were used. Seventy-five kinematic points in the range $3.5 < W^2 < 23$ GeV^2, $1 < Q^2 < 16$ GeV^2 were chosen for determination of the structure function by the MIT–SLAC group.

Figure 161 shows the values of R_p and R_d obtained for all 75 kinematic points. For simple models with spin-$\frac{1}{2}$ constituents, as $Q^2 \to \infty$, R_p should vanish as $1/Q^2$, or $1/\log Q^2$ for asymptotically free theories. The results of the analyses are consistent with this limiting behavior, but also with R_p = constant. The value of the constant is 0.14 with a statistical uncertainty of ±0.011 and a possible systematic error of ±0.056. For the deuterium data, $\bar{R}_d = 0.175$ with a statistical uncertainty of ±0.009 and a possible systematic error of ±0.060. The values of $\bar{R}$ for deuterium and hydrogen are not significantly different.

The MIT–SLAC group further tested for differences between R_d and R_p by forming the ratio of σ_d/σ_p for each ϵ at each of the 75 values of (W, Q^2), and searching for Q^2 dependence of the ratio. Using all the data they found

TABLE XXX. A summary of the data sets used in the most recent studies of scaling by the SLAC–MIT and SLAC groups (from Taylor, 1975a).

Data set	Scattering angle θ (deg)	Spectrometers used	Target	Incident energy range E_0 (GeV)	Polarization parameter range (ϵ)	Extracted quantities
MIT–SLAC(SFG)	6, 10	20-GeV				
	18, 26, 34	8-GeV	H_2, D_2	4.5–19.5	0.24–0.98	$R, \nu W_2, W_1$
	15, 19, 26, 34					
SLAC (Group A)	50, 60	1.6-GeV	H_2, D_2	6.5–19.5	0.08–0.25	W_1

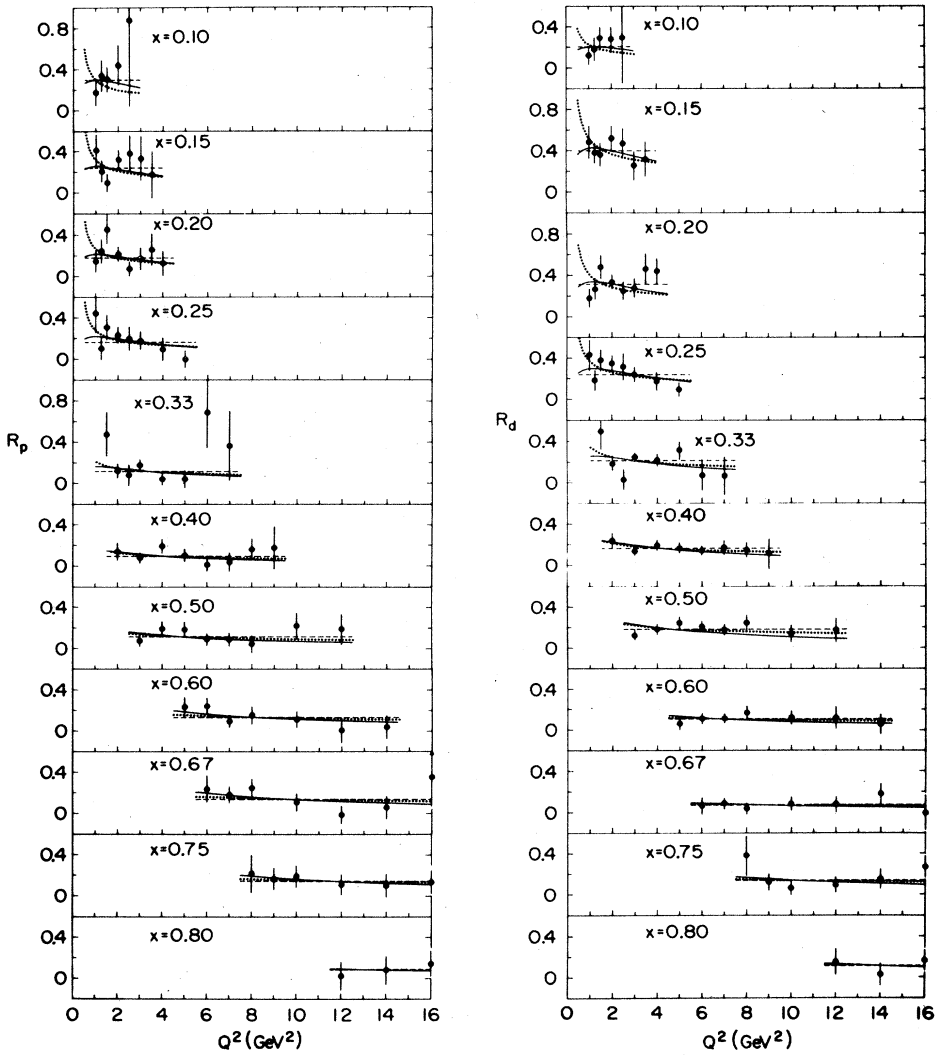

FIG. 161. Values of R_p and R_d. The dashed lines are the best fit of the form R_p = constant to the data at a given value of x. The solid and dotted lines represent fits of the form

$$R = C(x)\frac{Q^2}{(Q^2+d^2)^2}$$

and

$$R = \frac{\alpha^2(x)}{\ln(Q^2/\beta^2)}\ ,$$

respectively. There are some systematic sources of error in addition to the errors shown in the figure (from Taylor, 1975a).

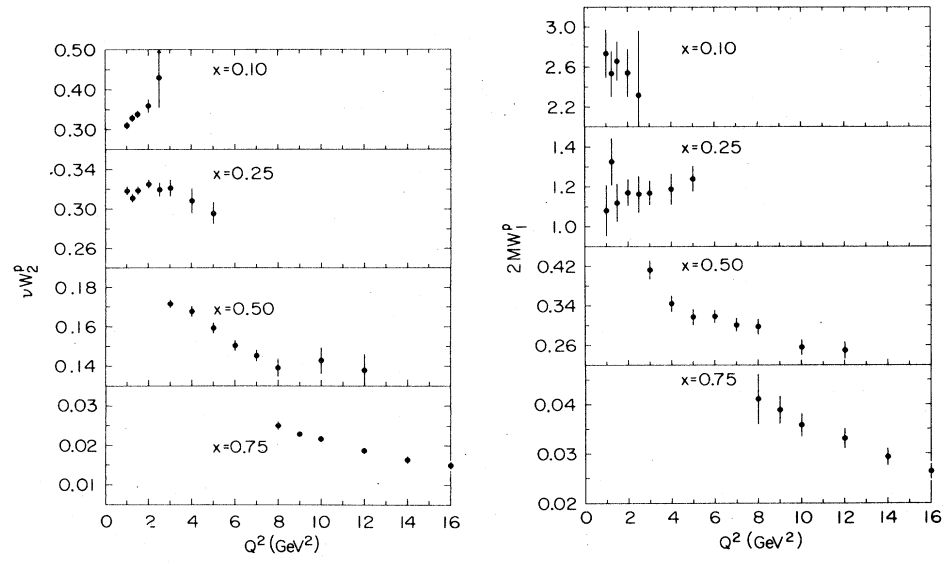

FIG. 162. The νW_2^p and $2MW_1^p$ structure functions for the proton for selected values of x. It is clear that neither structure function is scaling in x, i.e., there is Q^2 dependence of the structure function at constant x (from Taylor, 1975a).

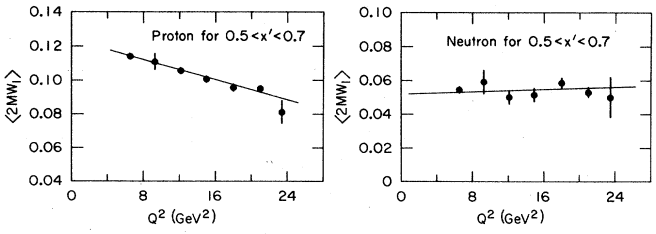

FIG. 163. Q^2 dependence of $2MW_1$. Data for proton and neutron at 50 and 60 degrees in the range $0.5 < x' < 0.7$ for various Q^2 values (from Taylor, 1975a).

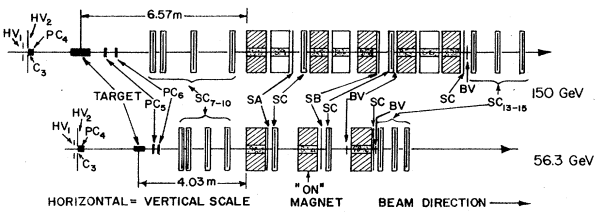

FIG. 164. Apparatus for the scaling tests used at FNAL by the Cornell–Michigan State collaboration. Shaded magnets are on, others are degaussed. The spark chamber modules have four planes each and are labeled SC_i. Multiwire proportional chambers of two planes each are shown as PC; upstream PC and scintillation counters are not shown (from Fox *et al.*, 1974).

$\bar{R}_d - \bar{R}_p = 0.031$ with a statistical error of ±0.015 and a possible systematic error of ±0.036. There was thus no evidence for a difference, and in their subsequent analysis they assumed $R_d = R_n = R_p$. It is interesting to point out that the data, plotted in Fig. 18 for R_p and R_d in the small-x domain, is significantly higher than the value 0.14. As discussed in Sec. II.C, such behavior is expected in hadronic photon models. Figure 162 shows the structure function for the proton determined by the analysis of the MIT–SLAC group. Similar results were obtained for deuterium.

The SLAC group (Atwood *et al.*, 1976) analyzed the measurements taken at 50 and 60 degrees using the 1.6-GeV spectrometer to determine W_1 through the equation

$$W_1 = \frac{d\sigma/d\Omega dE'}{\sigma_{\text{Mott}}} \frac{1}{2\tan^2\theta/2} \frac{1-\epsilon}{1+\epsilon R}. \tag{3.139}$$

In the region where their new data overlapped the separation region of the MIT–SLAC experiment, they used the MIT–SLAC measurements of R. Outside this region, where the small values of ϵ make the determination of W_1 insensitive to the value of R, they assumed $R = 0.18$. The data for a proton target showed a clear deviation from scaling that was somewhat smaller when x' was used as the scaling variable. Figure 163 shows plots of $2MW_1$ versus Q^2 for both proton and neutron targets. There appears to be a difference in the scale-breaking behavior for the neutron and proton.

In a report (Hand, 1977) given at the 1977 International Symposium on Lepton and Photon Physics at High Energies it was stated that new measurements carried out at SLAC indicated a higher value of R near 0.30. This change was attributed in part to a difference in the radiative corrections. This discrepancy attests to the difficulty of measuring R and reinforces the importance of good measurements using well understood spectrometer systems.

6. Inelastic muon scattering

Two experiments with muons have been carried out at Fermilab. The first, a Cornell–Michigan State collaboration, was designed specifically to test scaling. The second, a Chicago–Harvard–Illinois–Oxford collaboration, which used hydrogen and deuterium targets together with a spectrometer system based on the Chicago Cyclotron, was designed primarily to study the final-state hadrons produced in muon–nucleon collisions.

Figure 164 shows a schematic diagram of the apparatus used by the Cornell–Michigan State collaboration (Fox *et al.*, 1974; Watanabe *et al.*, 1975; Chang *et al.*, 1975). The group made tests of scaling based on two techniques. The first test was made by comparing distributions of kinematic quantities at two incident muon energies, 56.3 and 150 GeV, with the large-aperture spectrometer changed with energy so as to keep the acceptance and resolution constant. This method has the advantage that it does not require a detailed Monte Carlo calculation; and, because it does not require the comparison of FNAL data with SLAC data, it avoids dependence on the relative normalizations of different experiments. Figure 164 shows the realization of the two scaling geometries. Longitudinal distances scale as $(E_0)^{1/2}$; Q^2 and E' scale as E_0. The counting ratio scales as E_0^{-1} and is compensated by scaling the target material (233g/cm² at 56.3 to 622 g/cm² at 50 GeV). The relative momentum resolution of 14% is held constant by using three degaussed magnets as extra scattering material in the 150 GeV configuration. Fifty-six GeV events were selected so as to produce agreement between the beam distributions. Figure 165 shows plots of the ratio

$$r = E\frac{d^2\sigma}{dxdy}(E=150) \Big/ E\frac{d^2\sigma}{dxdy}(E=56) \tag{3.140}$$

versus x and ω. Here $y = \nu/E$, and in terms of x and y the cross section can be expressed in the form

$$\frac{d^2\sigma}{dxdy} = \frac{4\pi\alpha^2}{2ME}\frac{\nu W_2(x,Q^2)}{x^2y^2}\left(1 - y + \frac{y^2}{2(1+R)}\right). \tag{3.141}$$

There is a clear deviation from scaling which can be parametrized in the form

$$r = (\omega/\omega_0)^n, \tag{3.142a}$$

with

$$n = 0.096 \pm 0.028,$$

and (3.142b)

$$\omega_0 = 6.08^{+8.86}_{-3.61}$$

The scale-breaking parameter

$$b = \partial^2[\ln(\nu W_2)]/\partial[\ln(\omega')]\partial[\ln(Q^2)] \tag{3.143}$$

is nearly equal to the exponent of the power law fit to r versus ω(3.142). If b is assumed to be ω independent, then $b = 0.098 \pm 0.028$. This implies that νW_2 can be parametrized in the form

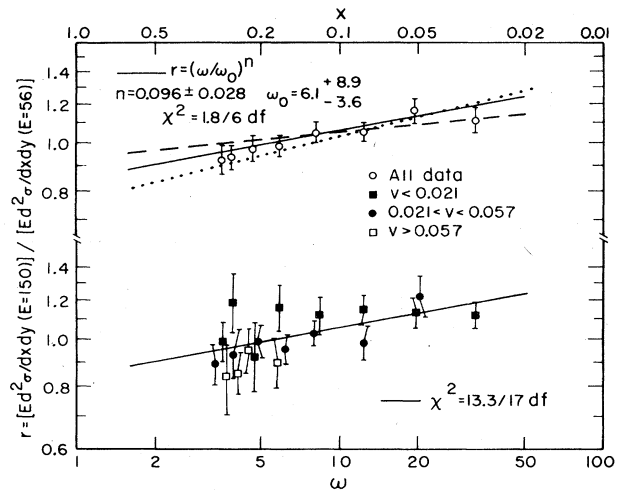

FIG. 165. A plot of the ratio r versus ω and x for the data of the Cornell–Michigan State group. The errors are statistical. There is an additional normalization error of ±7%. Solid lines are power law fits to the combined data. The effects of increasing E' at 150 GeV by 1% are indicated by the dashed lines; the effects of assuming scaling in ω rather than ω' in the Monte Carlo simulation is shown by the dotted lines (from Watanabe *et al.*, 1975).

$$\nu W_2(Q^2, \omega) = F(\omega)(Q^2/Q_0^2)^{b \ln(\omega/\omega_0)}. \tag{3.144}$$

In a separate analysis (Chang *et al.*, 1975), the Cornell–Michigan State group compared data at 56 and 150 GeV with a Monte Carlo calculation based on the structure function $\nu W_2(\omega')$ determined by the SLAC–MIT group with $R = 0.18$. They found that the ratio of the observed to simulated event rate showed a rising trend with Q^2 at high ω, and a falling trend at low ω. They found that this scale breaking could be parametrized by the value $b = 0.099 \pm 0.018$ as in (3.143). This is in good agreement with the first analysis.

Figure 166 shows a schematic diagram of the muon scattering spectrometer used by the Chicago–Harvard–Illinois–Oxford collaboration (H. L. Anderson *et al.*, 1976) at Fermilab. Positive muons strike a 122 cm long liquid hydrogen or liquid deuterium target, and the apparatus is triggered when the counter logic condition $B\bar{M}GM$ is satisfied. This group first reported measurements with a deuterium target (H. L. Anderson *et al.*, 1976). These data were analyzed with the assumption that $R = 0.18$, and they showed the same trends that were observed in the Cornell–Michigan State data. For $\omega > 10$, νW_2 increased as Q^2 increased; for $\omega < 4$, νW_2 decreased as Q^2 increased. A fit of all the data in the range $0 < Q^2 < 50$ GeV^2 and $3 < \omega < 80$ to the form

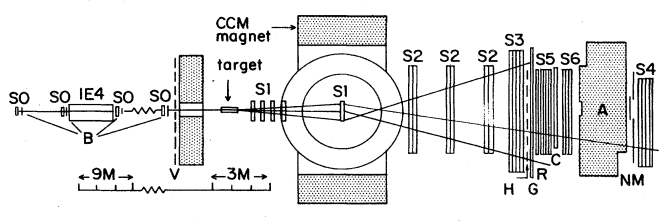

FIG. 166. Schematic layout of muon scattering spectrometer used by Chicago–Harvard–Illinois–Oxford collaboration. S0 and S1 are multiwire proportional chambers; S2, S3, S4, S5, and S6 are multiwire spark chambers; B, G, H, M, N, and V are counter hodoscopes; IE4 and CCM are magnets; R, C, and A are absorbers (from H. L. Anderson *et al.*, 1976).

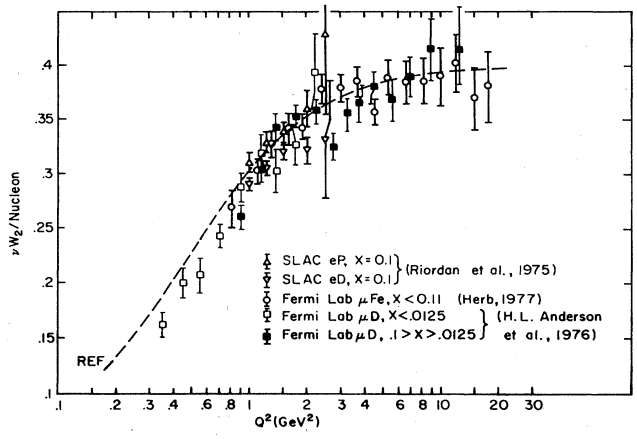

FIG. 167. A plot versus Q^2 of the high-ω data from SLAC, Cornell–Michigan State, and Chicago–Harvard–Illinois–Oxford.

$$\nu W_2(\omega, Q^2) = \nu W_2(\omega, Q_0^2)[1 + a \ln(Q^2/Q_0^2) \ln(\omega/\omega_0)] \tag{3.145}$$

gave $a = 0.072 \pm 0.038$, with $\chi^2 = 16.9$ for 23 degrees of freedom, and ω_0 and Q_0^2 fixed at 6 and 3 GeV^2, respectively. This parametrization is essentially the same as that of Chang *et al.*, (1975), who found $a = 0.099 \pm 0.018$ for data in the range $3 < \omega < 80$ and $1 < Q^2 < 50$ GeV^2. In a subsequent paper, H. L. Anderson *et al.* (1977) reported measurements with both hydrogen and deuterium targets.

As discussed in Sec. II.C, D, the hadronic structure of the photon should be most readily observable in the small-x(large-ω) region, where νW_2 should be primarily a function of Q^2. SLAC data illustrating this behavior is shown in Fig. 17. Figure 167 shows high-ω data from the MIT–SLAC collaboration, the Cornell–Michigan State collaboration [from the thesis of S. Herb (1977)], and the Chicago–Harvard–Illinois–Oxford collaboration. Figure 168 shows plots versus ω for fixed Q^2 of the more recent data from the Chicago–Harvard–Illinois–Oxford collaboration. The evidence for a universal dependence on Q^2 with little dependence on ω is striking.

Figure 169 shows a plot of the hydrogen data of the Chicago–Harvard–Illinois–Oxford group as a function of x for various ranges in Q^2, together with the data from MIT–SLAC (Riordan *et al.*, 1975). The smooth curves are fits to the data using the form

$$F_2^p(x, Q^2) = \sum_{i=3}^{5} a_i (1-x)^i. \tag{3.146}$$

If these fits are used to extrapolate into regions not covered by the data points, then

$$\int_0^1 F_2^p(x, Q^2) dx = 0.18 \pm 0.01 \tag{3.147}$$

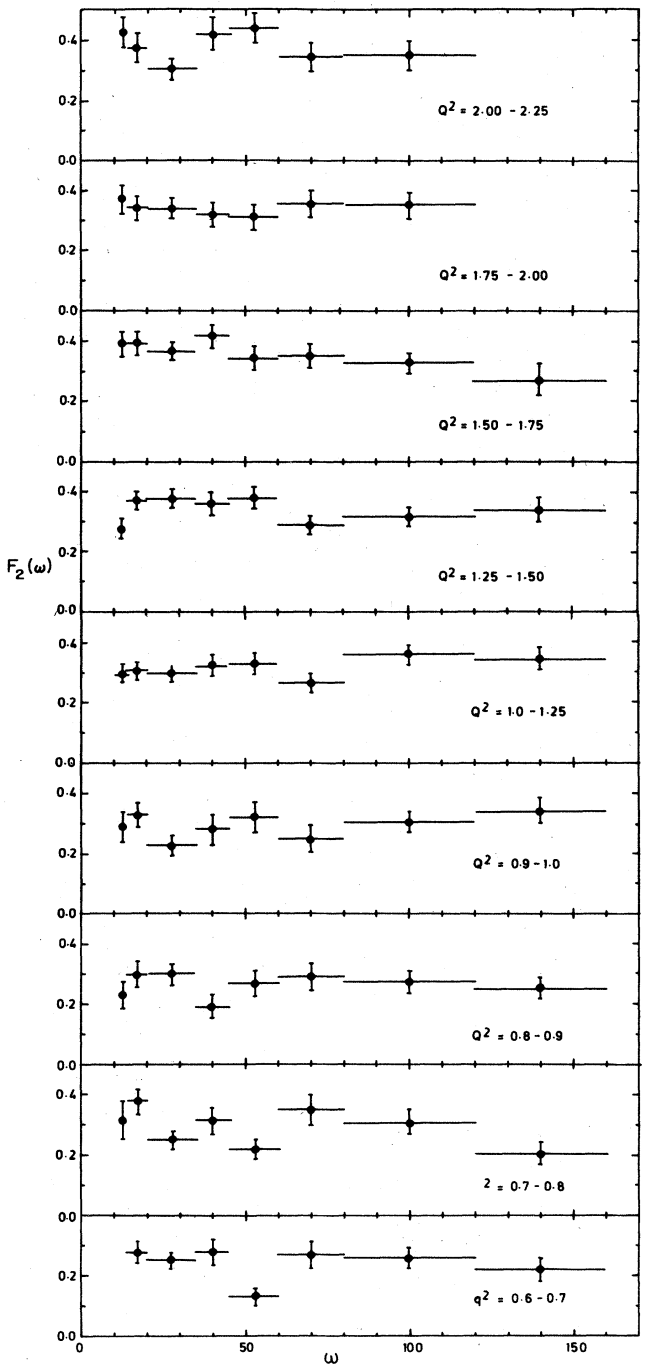

FIG. 168. A plot versus ω for different Q^2 values of νW_2 using the data of the Chicago–Harvard–Illinois–Oxford collaboration (from H. Anderson *et al.*, 1977).

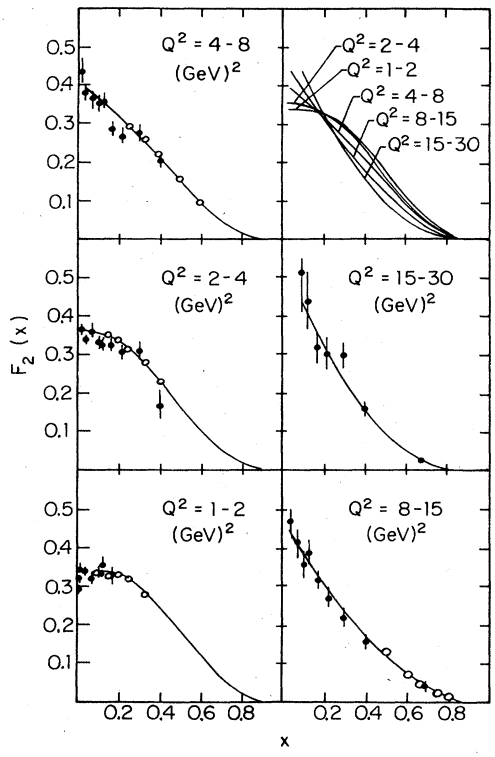

FIG. 169. Plots versus x showing νW_2 for different Q^2 ranges.

for each Q^2 region. The constancy of this area integral reflects the properties of the current commutator in Eq. (A6) near the tip of the light cone. The behavior of various "moment" integrals (powers of x^2 inserted) provides information about "anomalous dimensions" or "asymptotic freedom." It is also possible that the increase with Q^2 of νW_2 at small x could be due to the introduction of new channels such as charm, as a threshold effect.

We can summarize our knowledge of inelastic electron scattering as follows:

(1) There is no evidence for two-photon exchange contributions, and thus the analysis in terms of one-photon exchange appears legitimate.

(2) νW_2^p and $2MW_1^p$ show some scale breaking in x and x'; and, for $x > 0.25$, they break scaling in the same manner and decrease as Q^2 increases. For $x < 0.25$, νW_2^p increases with Q^2. The behavior of $2MW_1^p$ is not known for $x < 0.25$.

(3) For $x > 0.25$, the neutron structure function breaks scaling in a different manner from the proton structure function. The behavior of the neutron structure function is not well known experimentally for $x < 0.25$.

(4) For large $x(\gtrsim 0.25)$, R_p is consistent with a constant value of 0.14 ± 0.06 (and is also consistent with $1/Q^2$ and $1/\log Q^2$ behavior).

(5) $R_d = R_p$ within experimental errors.

(6) Measurements of νW_2 for large Q^2 are consistent with

$$\int_0^1 F_2(x, Q^2)dx = \text{constant, independent of } Q^2.$$

(7) At small $x(\leq .2)$, some general features of the hadronic photon model are confirmed. At small Q^2, R_p and R_d are significantly above the value of 0.14. In the turn-on region where νW_2 is increasing with Q^2, νW_2 is a "universal" function of Q^2, dependent only weakly on x (or ω).

J. Shadowing of virtual photons

Another expected manifestation of the hadronic nature of the photon is the shadowing of virtual photons. For virtual photons of sufficiently high energy, at low Q^2 the shadowing should be essentially the same as that observed for photoproduction; but with increasing Q^2, the shadowing should decrease (see Sec. V.E.). For the observation of shadowing by virtual photons, it is thus important to have high-energy virtual photons with small Q^2, and small $x(\equiv Q^2/2M\nu \lesssim 0.1)$. This makes the measurement difficult with the available electron accelerators since these kinematics necessitate a low-energy scattered electron leading to a large radiative correction. The radiative correction is further increased by the high Z of the nuclei which must be studied.

The experimental technique used to measure the total cross section for virtual photons usually differs considerably from that used for real photons. The usual procedure is to use a single-arm spectrometer to observe the inelastically scattered lepton and then to correct the data for radiation to obtain the virtual photoproduction cross section. In order to reduce the uncertainty due to the radiative corrections, a Cornell group (Eickmeyer *et al.*, 1976) has used, in addition to the single-arm spectrometer for detecting the scattered electrons, a counter system for detecting one or more of the electroproduced hadrons.

The various groups have used various mathematical forms to describe and analyze the expected shadowing effects. In this section we report the analyses made by the experimental groups themselves. A somewhat more unified analysis will be found in Sec. V.E.

The first measurements of the A dependence of high-energy inelastic electron–nucleus scattering were reported by the MIT–SLAC collaboration (Kendall, 1972; Ditzler *et al.*, 1975). Those experimenters used the SLAC 20-GeV spectrometer to measure at 6 degrees the inelastic electron scattering for H, D, Be, Al, Cu, and Au, for incident energies ranging from 4.5 to 19.5 GeV, and scattered electron energies ranging from that corresponding to elastic e-p scattering down to about 2.5 GeV. The data spanned ranges in four-momentum transfer of $3.7 > Q^2 > 0.1$ GeV^2, in electron energy loss of $17.0 > \nu > 0.1$ GeV, and in the mass of the unobserved final hadronic state of $5.7 > W > M_p$ GeV. Uncertainties, due to both radiative corrections at low E' and resonance enhancements at small W, caused them to present data only for the restricted kinematic range $E' > 5$ GeV and $W > 2$ GeV, thus limiting ν and Q^2 by: $13.6 > \nu > 2.0$ GeV and $3.3 > Q^2 > 0.4$ GeV^2.

They presented their results in terms of the shadowing factor

$$F(A) = \sigma_A/[N\sigma_d - (N-Z)\sigma_p(d)], \tag{3.148}$$

where $\sigma_A \equiv d^2\sigma_A/d\Omega dE'$ is the differential cross section for e-A scattering, the nucleus of atomic number A contains Z protons and N neutrons, σ_d is the e-d scattering cross section, and $\sigma_p(d) \equiv \sigma_p/S_{pd}$ is the effective e-p cross section for scattering from a proton bound in a deuteron. They calculated the correction factor S_{pd} for proton motion in the deuteron according to the theory of Atwood and West (1973) as modified by Bodek (1973). (No correction was made for shadowing in deuterium, which should be an effect comparable to that of S_{pd}.) Figure 170 shows a plot of $F(A)$ vs ν and Q^2, together with the results from photoproduction experiments (Caldwell *et al.*, 1973; Brooks *et al.*, 1973) and the predictions of the generalized vector-dominance model of Schildknecht (1973). It is clear that there is little evidence for shadowing; they concluded that for nuclear targets in the Q^2 region $0.4\ \text{GeV}^2 < Q^2 < 3.7\ \text{GeV}^2$, the electron scattering cross section is equal to the sum of the cross sections for scattering from the constituent nucleons. This experiment is marginal as a test of shadowing because it does not measure a low enough Q^2 for sufficiently large ν. Figure 170 is deceptive in that it does not clearly delineate the correlation in ν and Q^2. The portion of their data with small Q^2 ($\lesssim 1$) and small x ($\lesssim 0.1$) will be shown again in Sec. V.E, Fig. 206. In the x region of greatest interest, the radiative corrections are large and uncertain; these data were discarded.

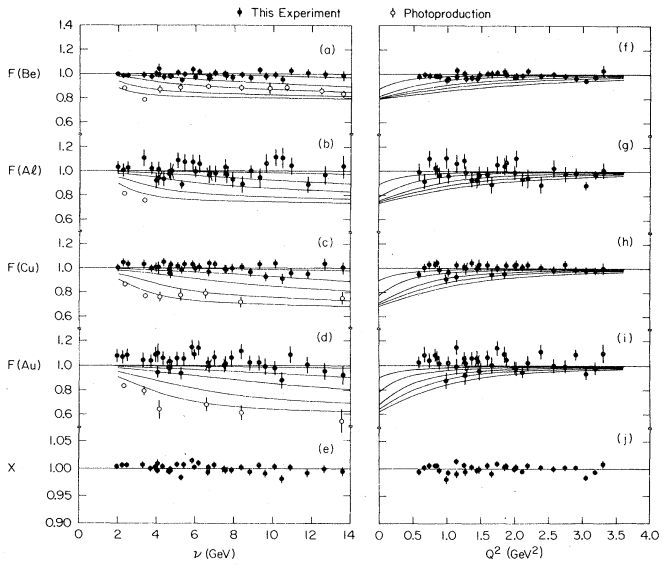

FIG. 170. Shadowing factors $F(A)$ (3.148) obtained by Ditzler *et al.* (1975) for Be, Al, Cu, and Au. Also shown are A-dependence exponents, X, from fitting the four $F(A)$ at each ν and Q^2 with the function $F(A) = A^{X-1}$. In (a)–(e) these are shown versus energy loss ν, and in (f)–(j) versus Q^2. Note that the zeros on all vertical scales are suppressed. The cross sections used incorporate radiative corrections and the errors include statistical and quasirandom components. The five curves shown are calculated from the generalized-vector-dominance model of Schildknecht (1973). On (a)–(d), the lowest curve is for $Q^2 = 0$, the next for $Q^2 = 0.25$, then 0.75, 1.5, and 4.0 GeV^2. On (f)–(i), the lowest curve is for $\nu = 14$, the next for $\nu = 10$, then 7, 4, and 2 GeV. No curves are shown on (e) or (j) because the GVD predictions are not well represented by the parametrization $F(A) = A^{X-1}$. The photoproduction results for 4 GeV are from Brookes *et al.* (1973), the rest are from Caldwell *et al.* (1973). The photoproduction results in (a) are for carbon and in (d) are for lead (figure from Ditzler *et al.*, 1975).

In a second experiment, a SLAC group (Stein *et al.*, 1975) used the 20-GeV spectrometer at 4 degrees to measure, with incident electron energies of 13 and 20 GeV, the inelastic electron scattering from hydrogen, deuterium, beryllium, aluminum, copper, and gold tar-

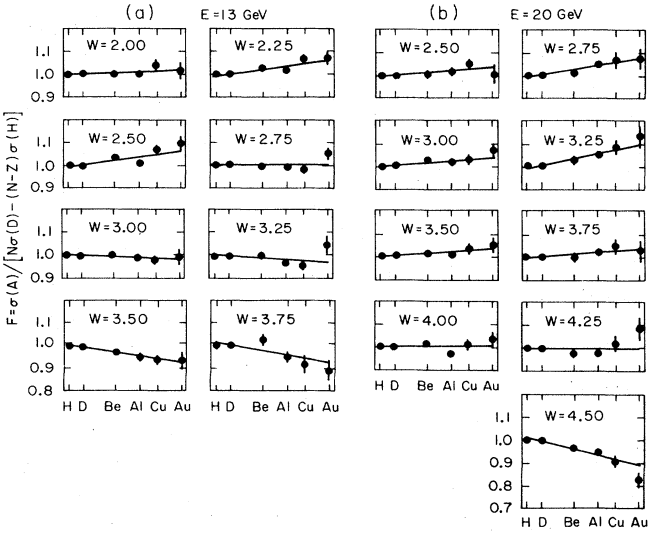

FIG. 171. The shadowing factor $F(A)$ (3.149) vs A for each kinematic point in the experiment of Stein *et al.* (1975). The lines are fits to the form $a_0 A^\epsilon$ for each plot. Only statistical errors are shown. For (a) the incident electron energy is 13 GeV; for (b), 20 GeV (from Stein *et al.*, 1975).

gets. They rejected data points where the radiative elastic tail subtractions were greater than 25 percent and made no inelastic radiative corrections for any of the targets. They calculated a shadowing factor from the expression

$$F(A) = \frac{\sigma(A)}{N\sigma(\mathrm{D}) - (N-Z)\sigma(\mathrm{H})}\,, \tag{3.149}$$

where $\sigma(\mathrm{D})$ and $\sigma(\mathrm{H})$ are the measured deuterium and hydrogen cross sections, N is the average number of neutrons, and Z the number of protons in the nucleus. No corrections for proton smearing were made to $\sigma(\mathrm{H})$, since it affects the value of F by ~0.5 percent. Figure 171 shows a plot of F vs A for each of the kinematic points. They also fitted the results for each Q^2 to the expression

$$F = a_0 A^\epsilon\,. \tag{3.150}$$

Figure 172 shows a plot of ϵ vs Q^2 for this and other measurements that will be reported shortly. There appears to be some evidence for shadowing at low Q^2, but it is considerably less than that found in the photoproduction experiments. A portion of this data will be shown in Fig. 206 (Sec. V.E).

The Columbia–Rochester–Harvard–Fermilab collaboration (May *et al.*, 1975) used at Brookhaven the 7.2-GeV muon beam, and a wire spark chamber magnetic spectrometer positioned at 16 degrees with a ±8 degree acceptance, to measure the inelastic muon scattering from H_2, D_2, C, Al, Cu, Sn, and Pb targets in the momentum transfer range $0.6 < Q^2 < 6.0$ GeV^2 (Entenberg *et al.*, 1974; Kim *et al.*, 1974; May *et al.*, 1975). They used the expression

$$\frac{A_{eff}}{A} = \frac{\sigma_A(x')}{(Z + (A-Z)\langle\sigma_n/\sigma_p\rangle)\sigma_p(x')}\,, \tag{3.151a}$$

with the assumption

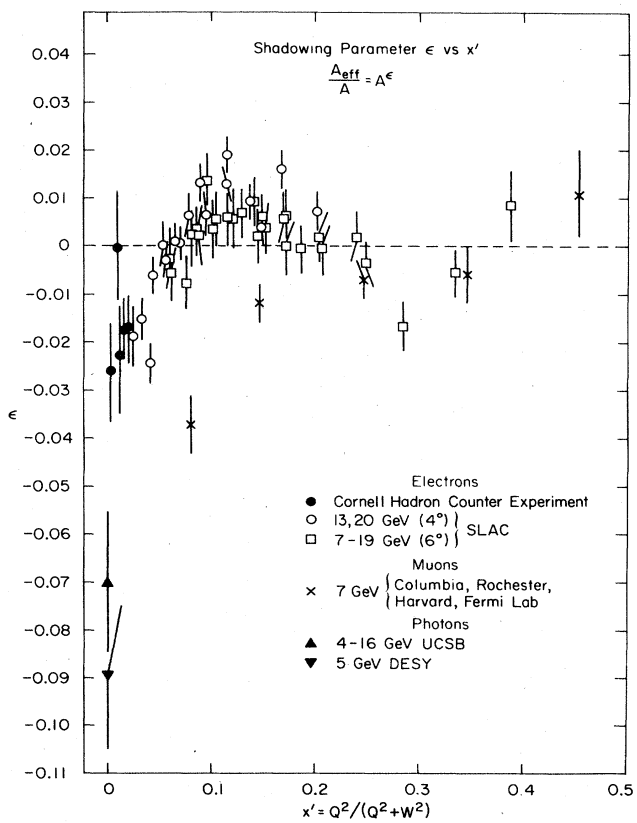

FIG. 172. A summary of the coefficient ϵ [in Eq. (3.150)] for several leptoproduction and photoproduction experiments (from Taylor, 1975).

$$\langle\sigma_n/\sigma_p\rangle = 1 - x' \tag{3.151b}$$

to determine the shadowing factor. They then used a fit of the form

$$A_{eff} = a_0 A^\rho \tag{3.152}$$

to parametrize the data. Figure 173 shows a plot of their data for various regions of x' in terms of A_{eff} vs A and A_{eff}/A vs A. They found that the cross sections could be well represented as an incoherent sum of muon-proton and muon-neutron scattering except in the region $x' < 0.1$. Their data is also shown in Fig. 172. They find clear evidence for shadowing for small x', of an amount considerably less than that observed in photoproduction. Their data are not in good agreement with that obtained in the electron scattering experiments. A portion of these data will be compared with theory in Fig. 206.

A Cornell group (Eickmeyer *et al.*, 1976) has carried out two experiments studying nuclear shadowing at low Q^2. They employed an experimental setup in which an electron spectrometer, consisting of a 182 cm long dipole magnet bending vertically through 11°, between two vertically focusing quadrupoles, was used to observe the scattered electrons. A counter system was used to detect one or more of the electroproduced hadrons. Figure 174a shows a schematic diagram of the electron spectrometer; Fig. 174b shows a schematic diagram of

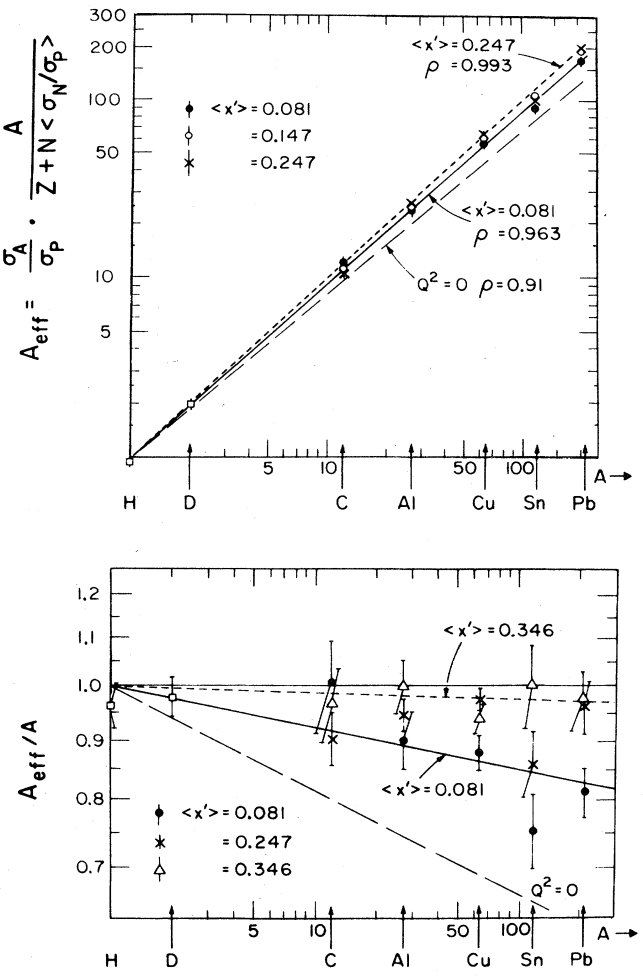

FIG. 173. The data of May *et al.* (1975): (a) Plot of $A_{\rm eff}$ versus A for different intervals of x'. (b) Plot of $A_{\rm eff}/A$ versus A for different intervals of x'. The lines are fits with the form $A_{\rm eff} = A^{\rho}$. See Eq. (3.151) for the definition of "$A_{\rm eff}$" (from May *et al.*, 1975).

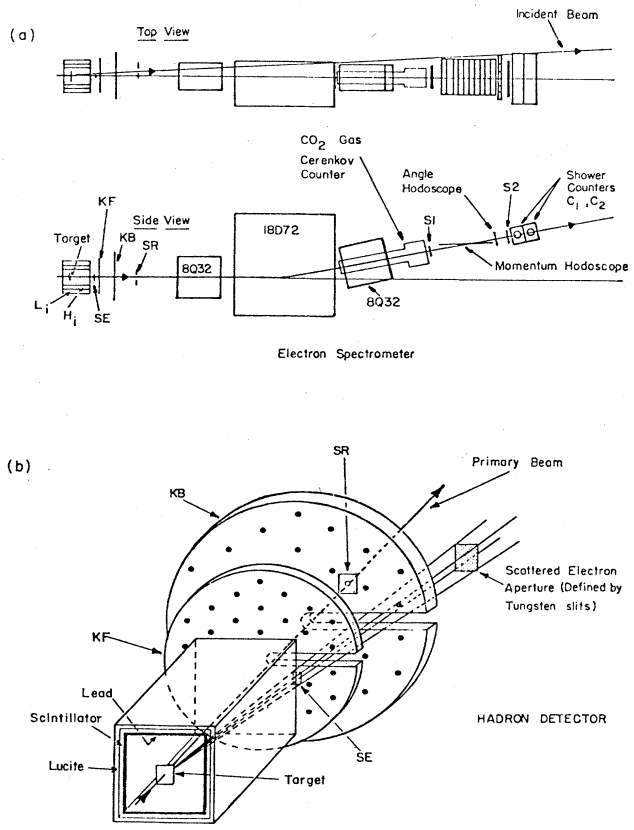

FIG. 174. (a) Schematic view of the electron spectrometer used by the Cornell group. (b) Perspective view of the hadron detector used by the Cornell group (Eickmeyer *et al.*, 1976b), with the scattered-electron aperture shown schematically. The box around the target is formed of 6 mm of Pb, followed by scintillation counters H_i and Lucite counters L_i. The forward counters KF, KB consist of two large circular disks of scintillator each viewed by 36 phototubes. A 12 mm thick lead radiator is placed between KF and KB to convert photons (from Taylor, 1975).

the hadron detector. In order to reduce the uncertainties due to radiative corrections, they measured the hadronic cross section directly by detecting at least one hadron in coincidence with the scattered electron, thus rejecting radiative elastic and quasielastic scattering events.

This group reported data for virtual photon energies $\nu = 3$, 4, 5, and 8.5 GeV, for hydrogen (0.017 radiation length) and deuterium (0.020 radiation length) targets, at $Q^2 \sim 0.10$ GeV^2, and for $\nu = 2$ GeV at $Q^2 = 0.015$, 0.047, and 0.104 GeV^2. The purpose of this investigation was to study the transition from photoproduction to electroproduction for the ratio σ_d/σ_p. Earlier SLAC (Stein *et al.*, 1975) measurements had suggested a rapid Q^2 dependence at low Q^2.

The Cornell group analyzed their data in terms of the expression

$$d^2\sigma/dE'd\Omega = \Gamma_T \sigma^*, \tag{3.153}$$

where Γ_T is defined by Eq. (3.132). The decrease of σ^* with Q^2 from photoproduction is similar for the hydrogen and deuterium targets. Figure 175 shows the deuterium to hydrogen ratio, plotted as $\sigma_D^*/2\sigma_H^*$, vs ν for the Cornell experiment and two photoproduction experiments (Armstrong *et al.*, 1972a; Caldwell *et al.*, 1973). Figure 176 shows a plot of the ratio σ_d/σ_p^s vs Q^2 for several experiments (Eickmeyer *et al.*, 1976a; Stein *et al.*, 1975; Bleckwenn *et al.*, 1975). The σ_d/σ_p^s ratio appears to change smoothly from photoproduction to electroproduction as Q^2 increases, and for electroproduction at low Q^2 is consistent with the shadowing observed in photoproduction.

In a second experiment the Cornell group took data at virtual photon energies $\nu = 2.0$, 3.0, 4.0, 5.0, and 8.5 GeV, at a fixed scattering angle of 3.2 degrees, and at a fixed value of $Q^2 = 0.1$ GeV^2 for H_2, D_2, C, Al, Cu, and Ta targets. For C, Al, Cu, and Ta they found consistent results with targets which were 0.02 and 0.08 radiation lengths.

The Cornell group expressed shadowing in terms of the expression

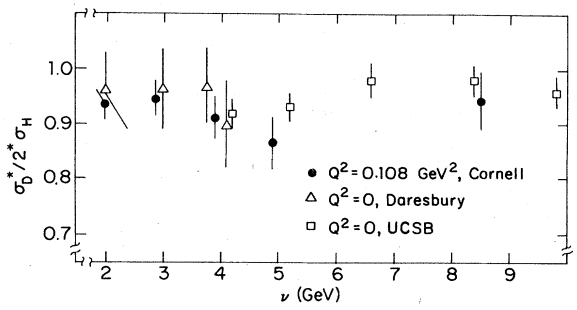

FIG. 175. The ratio $\sigma_D^*/2\sigma_H^*$ at fixed $Q^2 \sim 0.10$ as a function of ν, from data of the Cornell group (Eickmeyer *et al.*, 1976). Also shown are photoproduction data (figure after Eickmeyer *et al.*, 1976a).

$$A_{eff}/A = \sigma_A/[N\sigma_D - (N-Z)\sigma_H]$$

where σ_D and σ_H are their measured deuterium and hydrogen cross sections. This is equivalent to assuming no shadowing in the deuteron. Figure 177 shows a plot of A_{eff}/A vs ν, together with the results from the photoproduction experiment of Caldwell *et al.* (1973) and the later results for real photons obtained with essentially the same apparatus by the Cornell group (Michalowski *et al.*, 1977). The shadowing observed at low Q^2 by the Cornell group is the same as that found for real photons. The shadowing found by the Cornell group is, however, somewhat less than that found by the Santa Barbara–SLAC group—especially for the heavier elements. Figure 205 shows a plot versus Q^2 for copper using data from Caldwell *et al.* (1973), Eichmeyer *et al.* (1976), and Stein *et al.* (1975). Interpolation of the data of Michalowski *et al.* would give an additional point at $Q^2 = 0$ with $\sigma_A/[N\sigma_D - (N-Z)\sigma_H] = 0.83 \pm 0.05$. This figure shows that the results of the several experiments are consistent and indicates that the shadowing goes away rapidly as Q^2 increases.

In summary, there is evidence for shadowing of virtual photons which is somewhat less than that predicted by naive VMD and which decreases rapidly as Q^2 increases. It will require more precise measurements at high energy as a function of Q^2 to clarify further this phenomenon.

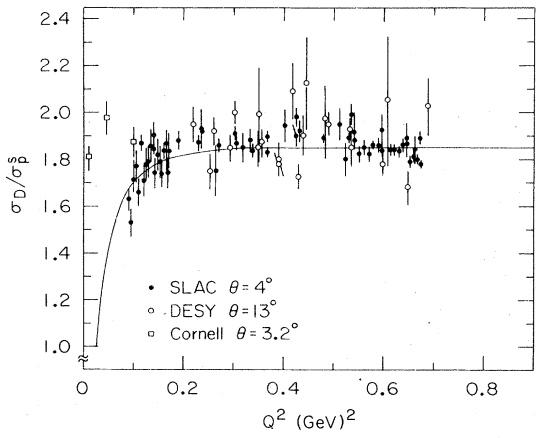

FIG. 176. Values of the ratio σ_D/σ_p^s at low Q^2 for various experiments. σ_p^s is derived from hydrogen measurements, folding in the effects of nucleon motion, and is very close to σ_p in this kinematic region. The curve should be ignored (from Eickmeyer *et al.*, 1976a).

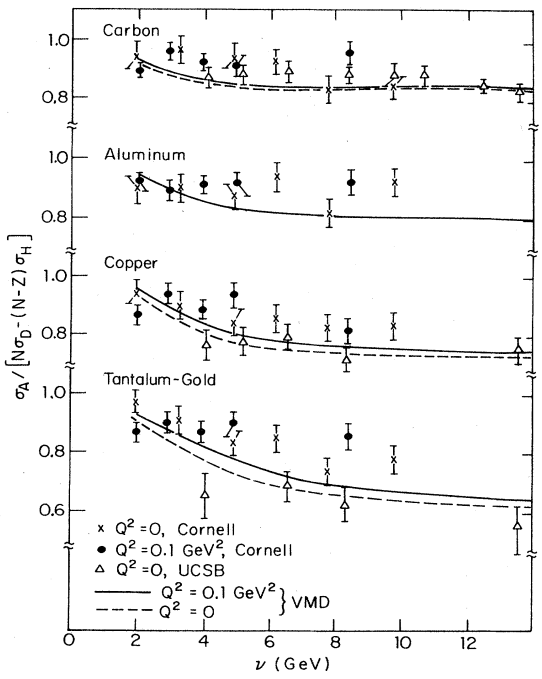

FIG. 177. The Cornell group's results (Eickmeyer *et al.*, 1976b) for the energy dependence of A_{eff}/A (3.154) at $Q^2 = 0.1$ for various nuclei. Data at $Q^2 = 0$ from Caldwell *et al.* (1973) are shown for comparison. The smooth curves are typical VMD predictions including an unshadowed contribution that is 20% of the total cross section, longitudinal vector mesons, and energy-independent vector-meson cross sections. See Sec. V.E for a more complete discussion of theoretical models (from Eickmeyer *et al.*, 1976b).

K. Electroproduction of vector mesons

Measurements of the electroproduction of vector mesons are particularly important since they determine the dependence on Q^2 and give a measure of the relative importance of the hadron-mediated and direct interactions of the photon. These experiments are more difficult than the photoproduction experiments because one has not only the new parameter Q^2, but production by longitudinal photons.

Several experimental techniques have been used to study vector-meson electroproduction. The first experiments on ρ^0 electroproduction used a missing mass technique in which the scattered electron and the recoil proton were detected in coincidence (Andrews *et al.*, 1971; Bloom *et al.*, 1972). These experiments suffered from a large background, which made the extraction of the vector-meson signal difficult. They had the further disadvantage that the ρ^0 polarization could not be measured because the decay pions were not detected. The first reported electroproduction experiment in which the two pions were detected was carried out at DESY by Driver *et al.* (1972). Their acceptance was such that

they could only observe transversely polarized rho mesons. Experiments in which the decay pions were observed over a wide range in angles were subsequently carried out at DESY using a streamer chamber (Eckardt *et al.*, 1973; Joos *et al.*, 1976, 1977), at SLAC using a wide-aperture spectrometer system (Dakin *et al.*, 1973a, b), at SLAC using a muon beam in conjunction with a hybrid bubble chamber (Ballam *et al.*, 1974a), and at SLAC using a streamer chamber system (del Papa *et al.*, 1976, 1977). A Cornell-Ithaca College group has used a refined spectrometer system to extend its measurements in which the scattered electron and the recoil proton were observed (Ahrens *et al.*, 1973; 1974).

Most recently a Harvard–Cornell group (Dixon *et al.*, 1977) reported the use of a double-arm spectrometer system to study ϕ electroproduction. In this review we shall not describe the experiments in historical order but will use a logical progression which emphasizes the physics.

1. Description of experiments

Figure 178 shows a schematic diagram of the apparatus used by the Cornell–Ithaca College group (Ahrens *et al.*, 1974) in its second study of vector-meson electroproduction. A magnetic spectrometer based on a 20*D*80 bending magnet was employed to observe the scattered electron. A wide-aperture spectrometer system based on a 72*D*18 magnet was used to observe the recoil proton. Energy loss and time of flight were used to identify pions and protons in the recoil arm; a Cerenkov counter and a lead-Lucite shower counter were used to identify electrons in the forward arm. Figure 179 shows typical missing mass spectra together with the fits used to determine the cross section. No attempt was made to separate the ρ^0 and ω. The shape of the ρ-ω peak, on which the fitting was based, was a relativistic Breit–Wigner form (with a p-wave width), multiplied by a generalized Ross–Stodolsky factor, to which was added a Breit–Wigner ω peak with an area fixed at 15% of the ρ peak. The radiative correction was calculated from a modified version of the formula given by Bartl and Urban (1966) and applied to the shape function; the result was a lowering of the peak height and the addition of a tail extending to higher masses. The shape function was then convolved with the experimental resolution function to yield the peak

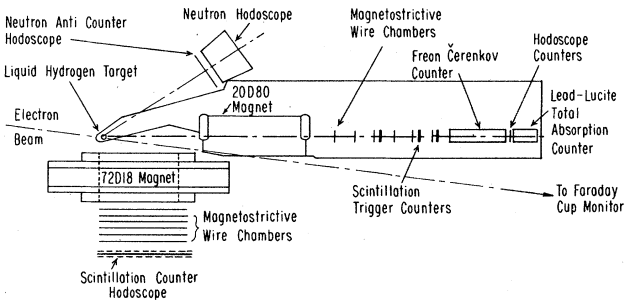

FIG. 178. Schematic diagram of the spectrometer used by the Cornell–Ithaca College group (Ahrens *et al.*, 1973, 1974) (figure from Ahrens *et al.*, 1974).

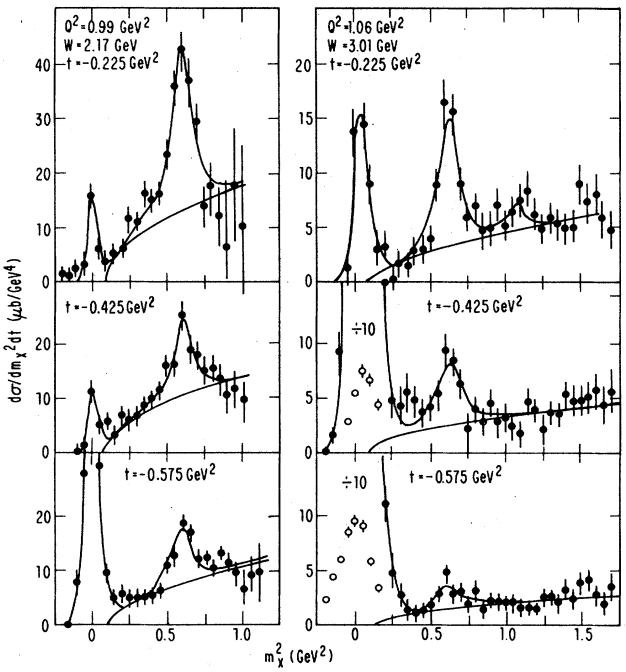

FIG. 179. Sample missing mass squared spectra for $\gamma_v + p \to p + X$ obtained by Cornell–Ithaca College group (Ahrens *et al.*, 1973, 1974) (figure from Ahrens *et al.*, 1974).

shape used in the least squares fit to the missing mass-squared spectrum.

Figure 180 shows a schematic diagram of the wide-aperture spectrometer used at SLAC (Dakin *et al.*, 1973a, b) to study ρ^0 and ϕ electroproduction by detecting the scattered electron as well as the decay products of the vector mesons. The unscattered beam and the forward electromagnetic backgrounds passed through the magnet in a field-free region created by a cylindrical superconducting tube. Two optical spark chambers were used to observe the scattered electron and the electroproduced pions. Shower counters were used for particle identification and for triggering. The appara-

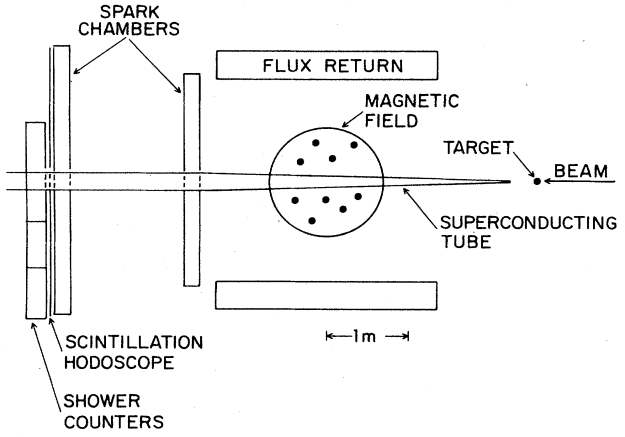

FIG. 180. Schematic elevation view of the wide-aperture spectrometer used at SLAC to study vector-meson electroproduction (Dakin *et al.*, 1973a, b) (figure from Dakin *et al.*, 1973b).

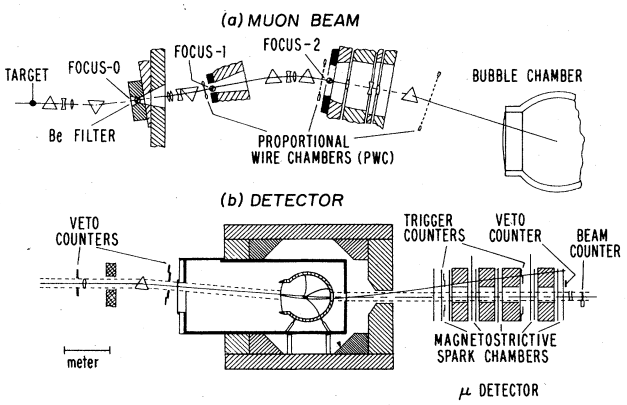

FIG. 181. Schematic representation of the muon beam hybrid bubble chamber experiment carried out at SLAC (from Ballam *et al.*, 1974a).

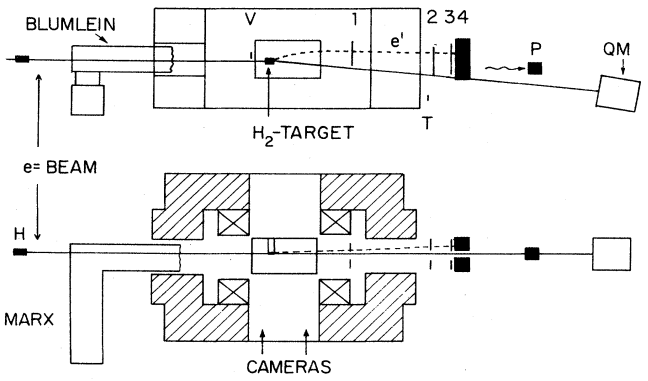

FIG. 182. Schematic diagram of the streamer chamber system used at DESY to study the electroproduction of vector mesons (from Eckardt *et al.*, 1973).

tus was triggered on the detection of a scattered electron, and there was no hadron requirement in the trigger. Cuts in missing mass squared were made at 0.2 and 1.6 GeV^2, and a one-constraint fit was made to events in this interval. There were 238 "ρ" events surviving this process in the kinematic range $0.25 < Q^2 < 2.00\,\text{GeV}^2$, $10 < s < 30\ \text{GeV}^2$, $0 < |t'| < 0.7\ \text{GeV}^2$, and $0.6 < m_{\pi\pi} < 0.9$ GeV. These events were divided into the three Q^2 bins, $0.25 < Q^2 < 0.50$, $0.50 < Q^2 < 1.0$, and $1.0 < Q^2 < 2.0$.

The data in each bin were fitted by a maximum likelihood technique to the form

$$\frac{d\sigma_\rho(Q^2, s)}{dt' d\phi_e d\psi d\cos\theta} = \sigma_{\text{tot}}(Q^2, s)\,\frac{\sigma_\rho}{\sigma_{\text{tot}}}\,Be^{Bt'}W(\phi_e, \psi, \theta)\,, \tag{3.155}$$

where $W(\phi_e, \psi, \theta)$ is the angular distribution function given in Appendix D (Schilling and Wolf, 1973). Since their data showed s-channel helicity conservation (SCHC—see Sec. III.C) to at least the 10% level, in their final analysis they assumed that SCHC holds in electroproduction and used the simplified form of W (D6). We shall return near the end of this section to a more ambitious study of the decay angular distribution.

Figure 181 shows a schematic diagram of the setup used at SLAC (Ballam *et al.*, 1974a) to study muon production of vector mesons in a hydrogen bubble chamber with a 16-GeV muon beam. A four-constraint fit was used to separate out the $\mu^- p \to \mu^- \pi^+ \pi^- p$ channel. They obtain 53, 109, and 78 events in the Q^2 ranges $0.05 < Q^2 < 0.2$ GeV^2, $0.2 < Q^2 < 0.5$ GeV^2 and $0.5 < Q^2 < 2.5$ GeV^2, respectively. The data were analyzed with a p-wave Breit–Wigner, multiplied by the usual $(m_\rho/m_{\pi\pi})^n$ mass skewing factor with n taken as a parameter to be fitted. From a general analysis of the density matrix elements, they concluded that, within one to two standard deviations, the density matrix elements were consistent with SCHC with the exception of r^1_{00} (see Appendix D), which had a 2.4 standard-deviation difference from zero. They then assumed that SCHC holds in electroproduction, and that only natural-parity exchange occurs in the t channel, for all subsequent analysis of the data. This yields the angular distribution given by Eq. (D6) in Appendix D.

Figure 182 shows a schematic diagram of the streamer chamber setup used at DESY by the DESY-Hamburg (Eckardt *et al.*, 1973) and DESY–Glasgow–Hamburg (Joos *et al.*, 1976, 1977) groups. A 7.2-GeV electron beam was directed onto a 9 cm long liquid hydrogen target inside the streamer chamber. Two arrays of trigger counters, Lucite Cerenkov counters, and lead scintillator sandwich shower counters detected the scattered electron. About 70% of the data were taken with a proportional wire chamber added to each of the two detector arms to improve the momentum and angular resolution for the scattered electron. With the exception of approximately 10% of the events in which one track was obscured by the target box or by flares, a four-constraint fit was used to separate out the reaction $ep \to ep\pi^+\pi^-$. A total of 7383 events were found in the kinematical region $1.3 < W < 2.8$ GeV, $0.3 < Q^2 < 1.4$ GeV^2. The data were analyzed using the p-wave relativistic Breit–Wigner multiplied by the $(m_\rho/m_{\pi\pi})^n$ mass skewing factor.

2. ρ^0 electroproduction

Figure 183 summarizes the values for the mass skewing factor n found in the various studies of ρ^0 electroproduction. The electroproduction value for n is consistent with that found in photoproduction, and there is some evidence that n decreases as Q^2 increases. The DESY–Glasgow–Hamburg group found that, as in photoproduction, n decreases as $|t|$ increases. An analysis of the separate variation of n with Q^2 for longitudinal and transverse rhos showed no significant Q^2 dependence for longitudinal rhos and a decrease with Q^2 for transverse rhos.

Figure 184 summarizes the ρ^0 production cross section, denoted $\sigma_{\gamma\rho}(Q^2)$, measured in the threshold region. Plotted is $\sigma_{\gamma\rho}(Q^2)/\sigma_{\gamma\rho}(0)$ vs Q^2. Data are also shown for $W > 2$ GeV. The agreement between the different experiments is good. The solid curves in Fig. 184 show a VMD prediction (labeled VDM) (Fraas and Schildknecht, 1969) given by the expression

$$\sigma^{\text{VMD}}_{\gamma\rho}(Q^2) = \frac{p^*_{in}(Q^2=0)}{p^*_{in}(Q^2)}\,\frac{1+\epsilon\xi^2 Q^2/m_\rho^2}{(1+Q^2/m_\rho^2)^2} \times \exp\{B[t_{\min}(Q^2) - t_{\min}(0)]\}\,\sigma_{\gamma\rho}(0)\,, \tag{3.156a}$$

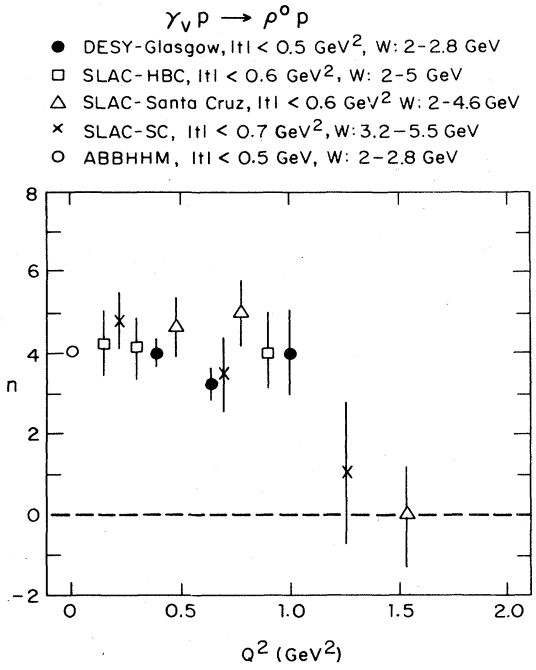

FIG. 183. A plot of the mass skewing factor n versus Q^2 for the different experiments studying rho electroproduction (from Wolf, 1972).

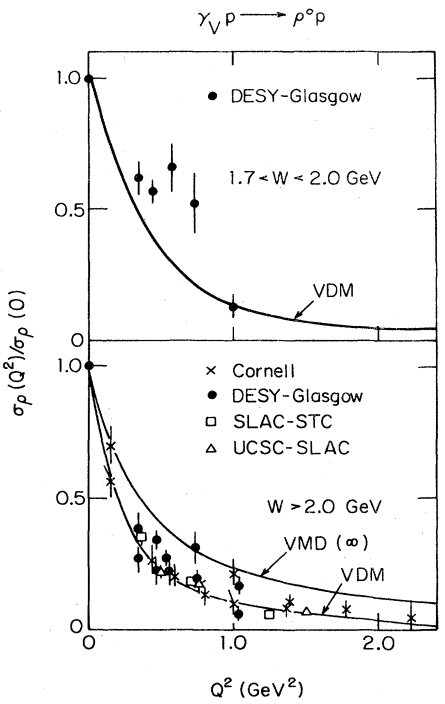

FIG. 184. Reaction $\gamma_v p \rightarrow \rho^0 p$: the ratio of $\sigma_{\gamma p}(Q^2)/\sigma_{\gamma p}(0)$ versus Q^2. The solid curves show the finite energy VMD prediction (3.156), labeled VDM, and the asymptotic VMD prediction VMD(∞).

where

$$\frac{p^*_{in}(Q^2=0)}{p^*_{in}(Q^2)} = (W^2 - M_P^2)/[(W^2 - M_P^2 - Q^2)^2 + 4W^2Q^2]^{1/2}. \tag{3.156b}$$

While this expression has a certain surface plausibility, it also serves to illustrate the ambiguities in defining VMD at nonasymptotic energies. Equation (3.156b), which tends to 1 for $W^2 \gg M_P^2$, Q^2, is a correction for the photon flux. The quantity $\epsilon\xi^2 Q^2/m_\rho^2$ represents the ratio of ρ production by longitudinal and transverse photons, where ξ is the ratio of forward amplitudes and, in general, is a function of W (even of Q^2!). The exponential factor accounts for the fact that there is a Q^2-dependent longitudinal momentum transfer; it somehow allows for the physics of the formation time (Sec. II.C). However, it is pure conjecture that B is related to the observable slope. Equation (3.156a) *assumes* the t dependence of longitudinal and transverse production are the same. If the t dependences are different, this factor would have to be modified. Factors such as (3.156b) depend on various normalization conventions and are to be regarded as suggestive rather than as theoretically derived. For example, Cho and Gounaris (1969) extrapolated off-shell in a slightly different way and introduced an extra factor $(1 - x^2)$ into (3.156a). Consequently, all analyses at low energies, and all experiments with so few events that the t dependence of longitudinal and transverse production cannot be separately determined, must be regarded as exploratory and preliminary.

To show the overall effect of the flux factor and $t_{\min}$ correction of (3.156), Fig. 184 includes a curve labeled "VMD(∞)". It is calculated for $\xi^2 = 0.5$, as suggested by Fig. 190, with a typical ϵ of 0.8, and with $W^2 \to \infty$ in the flux and $t_{\min}$ factors. The curve labeled "VDM" was calculated for the energy of the DESY-Glasgow-Hamburg experiment ($W \sim 2.5$ GeV). The flux and $t_{\min}$ corrections at this energy are seen to be appreciable. The data from all the other experiments are at a larger energy: Cornell (Ahrens *et al.*, 1974) $W = 2$–4 GeV; UCSC–SLAC (Ballam *et al.*, 1974a), $W = 2.8$ GeV; and SLAC-STC (del Papa *et al.*, 1976, 1977), $W = 4$ GeV. If (3.156) is to provide a correct description of these data, they should lie above the VDM curve and slightly below the VMD(∞) curve. The data do not show the expected variation with W. If anything, they are more like a universal function of Q^2. These results cast doubt on the validity of Eq. (3.156) as a formulation of nonasymptotic kinematics. Perhaps the drop of the data below VMD(∞) is due to a combination of threshold effects and Q^2-dependent effects such as those discussed in Sec. II.B (footnote 16).

Figures 185 and 186 show the angular distribution data obtained by the DESY–Glasgow–Hamburg group (Joos *et al.*, 1976) for the three energy regions that they observed, together with the corresponding photoproduction data from the ABBHHM and SLAC-Berkeley-Tufts bubble chamber experiments. For $W < 2$ GeV they find a center-of-mass angular distribution with two components-a forward peaked (peripheral) part which decreases with increasing Q^2, and a practically isotropic part (s-wave like) whose magnitude depends only weakly on Q^2. Both components rise steeply near threshold; the peripheral part becomes

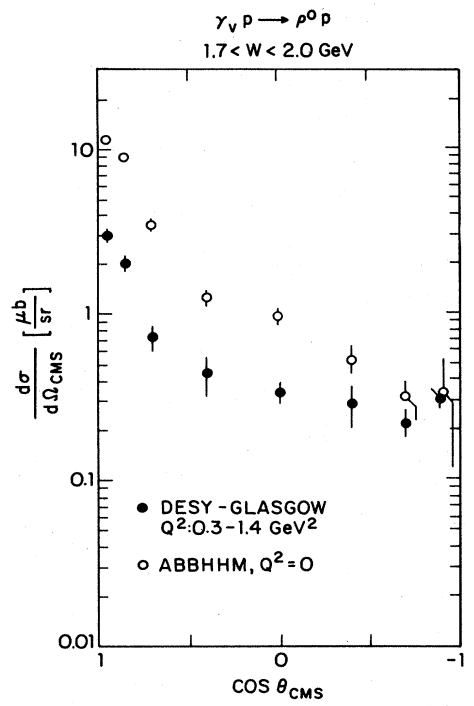

FIG. 185. $d\sigma/d\Omega_{cms}$ for $1.7 < W < 2.0$ GeV and $0.3 < Q^2 < 1.4$ GeV^2 (low energy). The open circles at $Q^2 = 0$ were obtained by refitting the data of Erbe *et al.* (1968a) with $m_\rho = 780$ MeV, $\Gamma_\rho = 150$ MeV, and $n = 4.8$ for $0.6 < \cos\theta_{cms} < 1$, $n = 0$ for $\cos\theta_{cms} < 0.6$ (from Joos *et al.*, 1976).

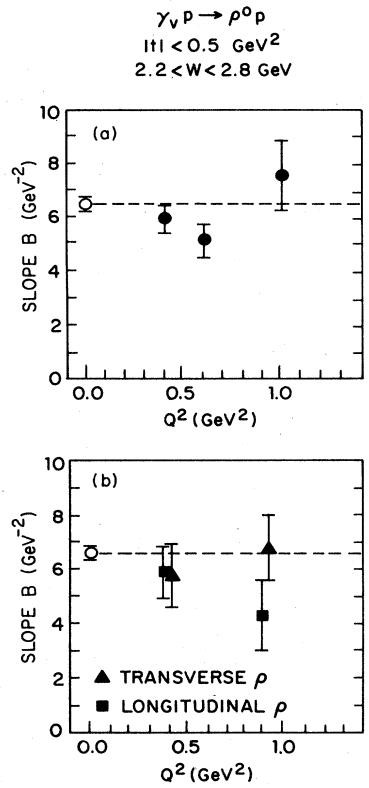

FIG. 187. The slope parameter B for ρ^0 electroproduction obtained by the DESY–Glasgow–Hamburg group (Joos *et al.*, 1976). (a) B for $2.2 < W < 2.8$ GeV and $|t| < 0.5$ GeV^2 as a function of Q^2. (b) The same as (a) but for transverse and longitudinal rhos separately (from Joos *et al.*, 1976).

nearly constant above $W = 2$ GeV, while the nonperipheral contribution falls off rapidly above $W = 2$ GeV.

Above $W = 2$ GeV the peripheral component is dominant and the differential cross section has the form

$$d\sigma/dt = A\exp(Bt)\,. \tag{3.157}$$

Fits to $d\sigma/dt$ in the W intervals 2.2–2.8 GeV and for $0.1 < |t| < 0.5$ GeV^2 give for the slope

$$B = (6.5 \pm 0.5)\,\text{GeV}^{-2} \text{ for } 0.3 < Q^2 < 0.5 \text{ GeV}^2\,,$$

$$B = (5.7 \pm 0.7)\,\text{GeV}^{-2} \text{ for } 0.5 < Q^2 < 1.4 \text{ GeV}^2\,. \tag{3.158}$$

The slope parameter was also determined from a Dalitz plot fit in which the rho term was multiplied by $\exp(Bt)$. The resulting B values are shown in Fig. 187.

In addition, the DESY–Glasgow–Hamburg group used the difference in the decay angular distribution to determine separately the slope parameter B for longitudinally and transversely polarized rho's. The weight factor $\cos^2\theta_H$ was used to project out longitudinal rho events, and the weight factor $\sin^2\theta_H(1 + \epsilon\cos 2\psi_H)$ was used to project out transverse rho events. (The subscript "H" refers to the helicity frame; see Sec. III.C.) The results of the fits to the t distribution are shown in Fig. 187(b). No statistically significant difference between the slopes for longitudinal and transverse rhos was observed. The errors, however, are large.

In an optical model, the slope parameter B measures the radius of interaction which reflects some combined size of the photon and proton. It has been argued that with increasing Q^2 the radius of the photon will shrink (Sec. VI.B), and we should observe a corresponding decrease of B. Some shrinkage may also occur if the formation time $\Delta\tau$ for the rho (see Sec. II.C) is less than the time it takes the photon to transverse a nucleon

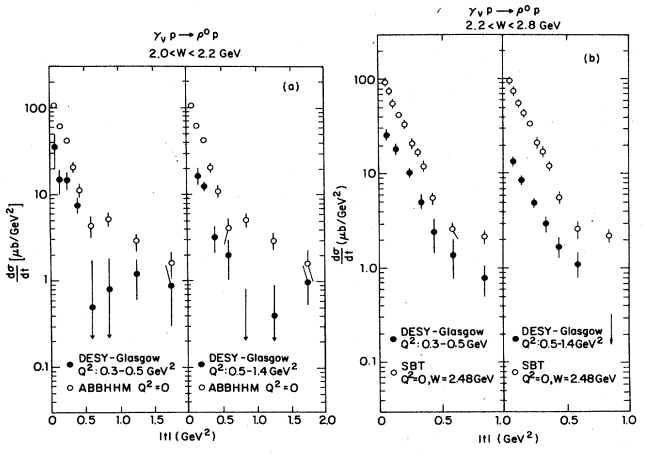

FIG. 186. $d\sigma/dt$ for the reaction $\gamma_v p \rightarrow \rho^0 p$ for different w and Q^2 regions (a) $2.0 < W < 2.2$ GeV, (b) $2.2 < W < 2.8$ GeV (high energy) (from Joos *et al.*, 1976).

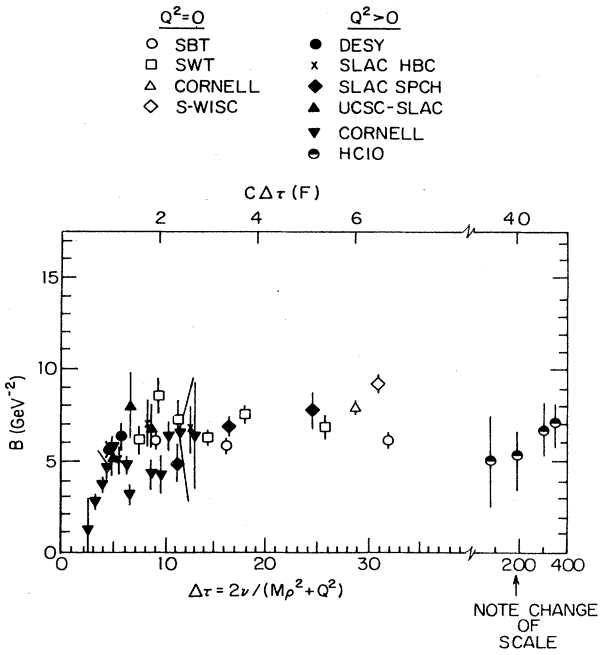

FIG. 188. Summary of the slope parameter B, defined by $d\sigma/dt \propto \exp(Bt)$ for ρ production, as a function of $\Delta\tau$.

$$\Delta\tau = 2\nu/(Q^2+m_\rho^2) \lesssim 10\ \text{GeV}^{-1}. \tag{3.159}$$

However, for such small formation times the whole qualitative VMD picture may be in doubt (Sec. II.C). Figure 188 shows the photoproduction and electroproduction measurements of B as a function of $(\Delta\tau)^{-1}$ for total ρ^0 production. The data showing strongest evidence for shrinkage are those of Ahrens *et al.* (1974). It should be noted that since this is a missing mass experiment, the B parameter corresponds to a weighted average of those for ρ^0 and ω production. All other experiments show little evidence for shrinkage. Until higher energies become available, it is not clear whether this possible shrinkage is the expected Q^2-dependent effect or a formation time effect.

The most ambitious study of the rho-decay angular distribution in electroproduction has been carried out by the DESY–Glasgow–Hamburg group (Joos *et al.*, 1976). They studied the rho decay in the s-channel helicity system and used the formalism summarized in Appendix D to analyze the data (Schilling and Wolf, 1973). Figure 189 shows scatter plots of $\cos\theta_H$ (angles are measured in the "helicity" system—Sec. III.C) versus the polarization angle $\psi_H = \phi_H - \Phi$ for events in the mass region of the rho with $|t| < 0.5$ GeV^2. At low energies ($W < 2$ GeV), production of longitudinal rhos dominates; above $W = 2$ GeV more transverse than longitudinal rho's are produced. The decay pions cluster near $\psi_H = 0°$ and 180°, thus giving evidence for dominant natural-parity exchange in the SCHC portion of the cross section.

From a study of the full density matrix, the DESY–Glasgow–Hamburg collaboration concluded that, for $W > 2.2$ GeV and $|t| < 0.5$ GeV^2, rho production conserves s-channel helicity to good accuracy. With the assumption that the ratio of the helicity single-flip to helicity

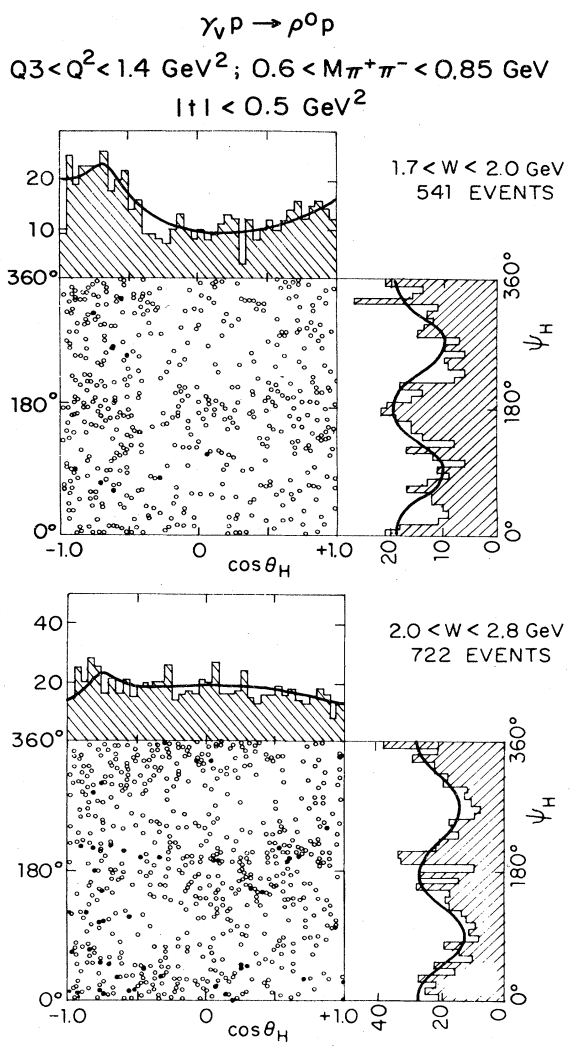

FIG. 189. Decay angular distribution for $\gamma_v p \to \pi^+\pi^- p$ in the region $0.6 < M_{\pi^+\pi^-} < 0.85$ GeV for $|t| < 0.5$ GeV^2, $0.3 < Q^2 < 1.4$ GeV^2 in the energy intervals $1.7 < W < 2.0$ GeV and $2.0 < W < 2.8$ GeV. The curves are from a maximum likelihood fit (from Joos *et al.*, 1976).

nonflip contributions is the same for longitudinal and transverse photons, they concluded that the helicity flip amplitudes are of the order of 15–20% of the nonflip amplitudes for $|t| < 0.5$ GeV^2. For photoproduction at $W = 2.48$ GeV (Ballam *et al.*, 1972) the corresponding ratio is 0.04 ± 0.02 for $|t| < 0.4$ GeV^2. The DESY–Glasgow-Hamburg group also concluded that for electroproduction the helicity double-flip amplitudes are smaller than the helicity single-flip amplitudes.

With the assumption of SCHC and natural-parity exchange, the DESY–Glasgow–Hamburg group determined the relative phase δ between the longitudinal and transverse helicity amplitudes which is defined by

$$T_{00}^* T_{11} = |T_{00}|\,|T_{11}| e^{-i\delta}. \tag{3.160}$$

Figure 190 shows $\cos\delta$ versus energy for this experiment, and the experiments of Ballam *et al.* (1974) and Dakin *et al.* (1973a, b). At W values around 2 GeV the

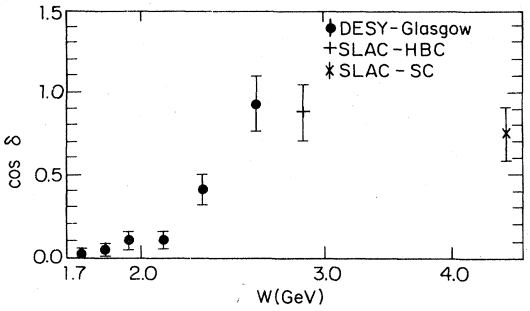

FIG. 190. The phase between the longitudinal and transverse rho production amplitudes (from Joos *et al.*, 1976).

two amplitudes are roughly 90° out of phase; with increasing energy the phase difference becomes smaller; above $W = 2.5$ GeV the rho production amplitudes from longitudinal and transverse photons are roughly in phase.

Figure 191 shows R vs Q^2 for the different regions of W as determined by the measurements of the DESY–Glasgow–Hamburg group. At fixed W, R rises linearly with Q^2. The available data are well represented by the parametrization

$$R = \xi^2 (Q^2/m_\rho^2). \tag{3.161}$$

Here ξ^2 is shown as a function of W in Fig. 192; above $W = 2$ GeV, ξ^2 is a constant and roughly equal to 0.5. ξ in Eq. (3.161) is often interpreted as the ratio of the longitudinal to the transverse ρ^0 *total cross section*. This is only true if longitudinal and transverse production have identical t dependence, as assumed for example in Eq. (3.156).

3. ω electroproduction

A small amount of data on ω electroproduction has been reported by the DESY–Glasgow–Hamburg group

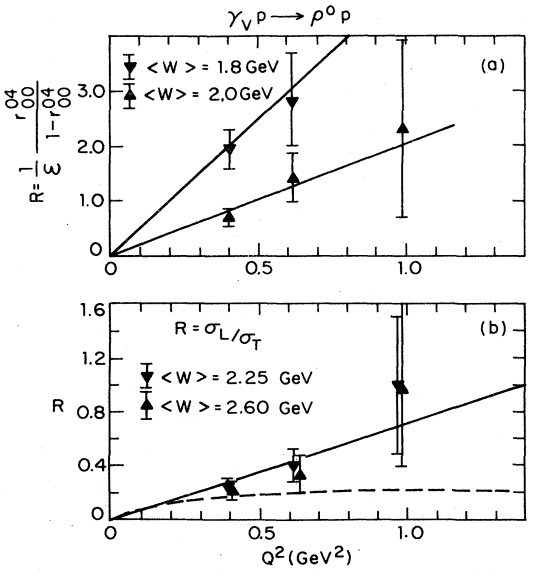

FIG. 191. The ratio R versus Q^2 for different values of w.

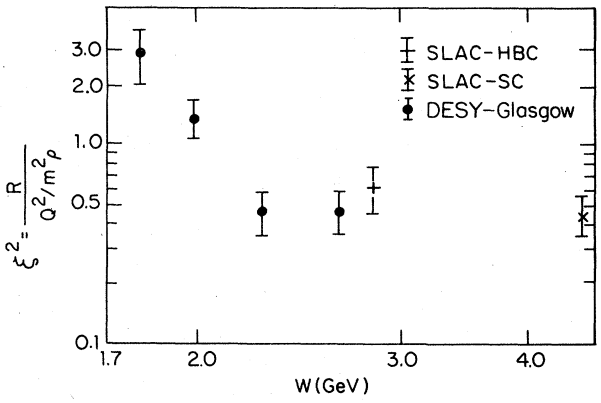

FIG. 192. The parameter ξ^2 (from Joos *et al.*, 1976).

(Joos *et al.*, 1977). Figure 193 shows the observed t distribution for $2.0 < W < 2.8$ GeV and $0.3 < Q^2 < 1.4$ GeV^2 together with the corresponding photoproduction data. One striking feature is that the Q^2 dependence at large momentum transfer is much weaker than for small $|t|$ values. The value of r_{00}^{04} for peripheral ω production is consistent with that found in photoproduction, indicating that, in contrast to ρ electroproduction, there is little increase in the production of longitudinal ω's when Q^2 changes from 0 to 0.7 GeV^2.

Figure 194 shows, as a function of Q^2, the ω production cross section, denoted by $\sigma_{\gamma\omega}(Q^2)$, together with the VMD prediction (3.156). As in rho production, $\sigma_{\gamma\omega}$ exceeds the VMD prediction for small energies but agrees with Eq. (3.156) at higher energies. Within er-

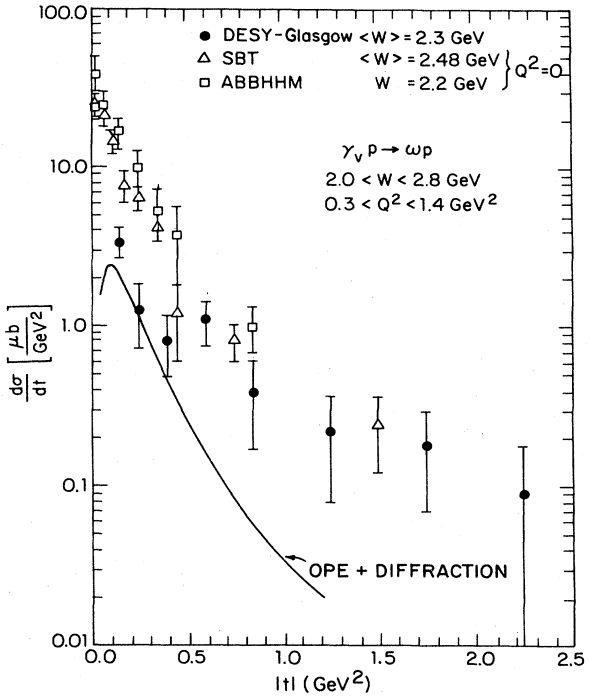

FIG. 193. Reaction $\gamma_v p \to \omega p$: $d\sigma/dt$ versus $|t|$ at $Q^2 = 0$ and $0.3 < Q^2 < 1.4$ GeV^2 (from Joos *et al.*, 1976).

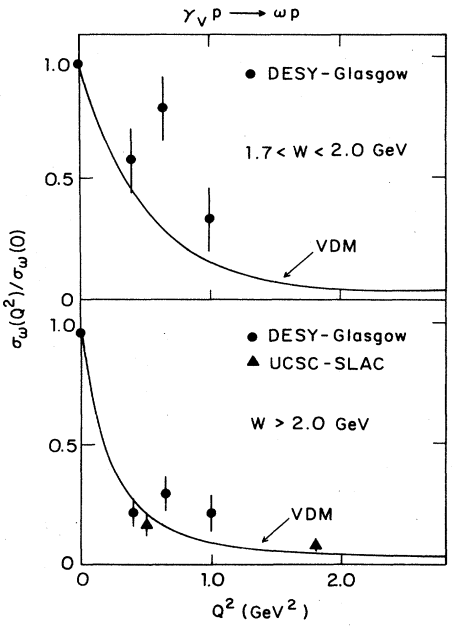

FIG. 194. The ratio of $\sigma_{\gamma\omega}(Q^2)/\sigma_{\gamma\omega}(0)$ versus Q^2. The solid curves show the VMD prediction (3.156) (from Wolf, 1975).

rors the ratio $\sigma_\omega/\sigma_\rho$ is independent of Q^2 for $0<Q^2<0.8$ GeV^2 and $W<2.8$ GeV. At large $|t|$ the ω cross section is approximately equal to the ρ cross section.

4. ϕ electroproduction

The most extensive set of data on ϕ electroproduction have been obtained by the Harvard–Cornell group with a setup using two magnetic spectrometers at the Wilson Synchrotron Laboratory. One spectrometer measured the momentum and angle of the scattered electron, thus giving the mass and energy of the virtual photon. The other spectrometer measured the two charged kaons from the decay of the ϕ. Figure 195 shows the arrangement used on the hadron arm to detect the K^+ and K^- from the decay of the ϕ. Negative pions with momenta greater than 1.3 GeV were rejected by the Freon 12 threshold Cerenkov counter. Phi electroproduction was studied at the Q^2 values of 0.23, 0.45, and 0.97 GeV^2 with $|t|$ ranging from 0.125 to 1.3 GeV^2 at each Q^2 point. The total center-of-mass energy W lay in the interval $2.10 < W < 3.55$ GeV. The overall systematic error was due primarily to the uncertainties in the corrections and was estimated to be less than 10%.

An iterative procedure was used to fit the data to the form

$$\frac{d^3\sigma}{dt d\Phi\, \Omega^*} = \frac{A}{(1+Q^2/m_\phi^2)^2} W(\theta,\phi,\Phi)\exp(Bt) \qquad (3.162)$$

with the angular distribution given by the assumption of s-channel helicity conservation and natural-parity exchange [Appendix D, Eq. (D6)] and with A, B, $\cos\delta$, and ξ^2 as free parameters. Figure 196 shows the observed t dependence together with that found in the photoproduction measurements. The electroproduction t dependence is somewhat shallower than that observed in photoproduction but there is no evidence for any dependence on Q^2 over the range $0.25 \leq Q^2 \leq 0.97$ GeV^2. The data also indicate that the Q^2 dependence is correctly given by the ϕ propagator.

Figure 197 shows the ϕ-decay distributions for the

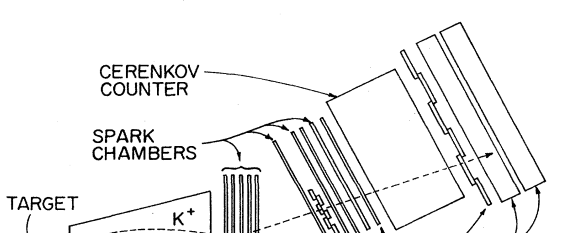

FIG. 195. A schematic diagram of the hadron arm used in the Harvard–Cornell electroproduction experiment to observe the two kaons from the decay of the ϕ. The negative particle is bent up and enters the Čerenkov counter (from Dixon *et al.*, 1977).

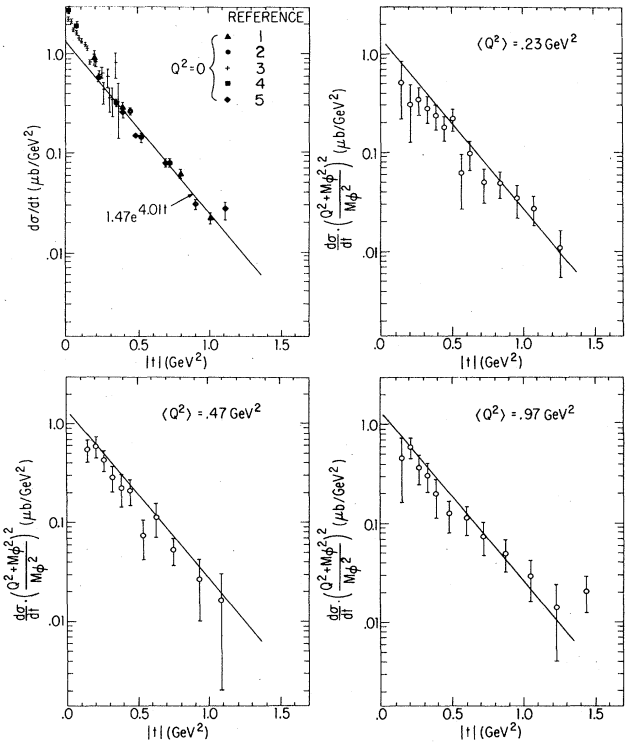

FIG. 196. The observed t dependence for ϕ photoproduction and ϕ electroproduction. The solid line in all four graphs is a fit to the photoproduction data of Besch *et al.* (1974), of the form $A\exp(Bt)$. The errors in the photoproduction data of Besch *et al.* include an estimate of the systematic error. The errors in the electroproduction data are statistical only and do not include the estimated systematic errors (~10%). In part (a) references 1,2,3,4,5 refer, respectively, to R. L. Anderson *et al.* (1973), Besch *et al.* (1974), Behrend *et al.* (1975), Berger *et al.* (1972), R. L. Anderson *et al.* (1970) (after Dixon *et al.*, 1977).

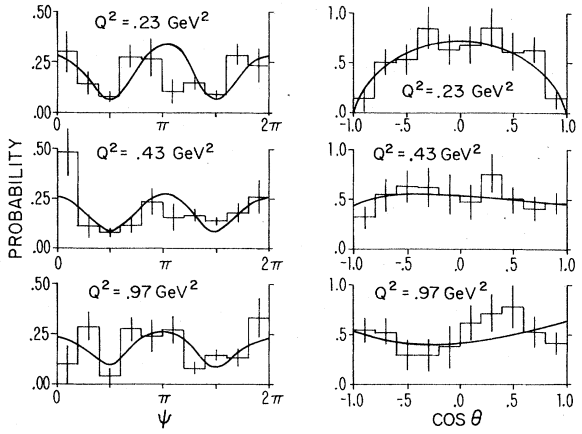

FIG. 197. The observed decay distributions for ϕ electroproduction at $Q^2 = 0.23$, 0.43, and 0.97 GeV^2. The solid curves are the fits assuming s-channel helicity conservation (from Dixon *et al.*, 1977).

three Q^2 points as a function of $\cos\theta$ and ψ. The solid lines are the fits assuming the angular distribution is that found for s-channel helicity conservation. The data are adequately fitted with the s-channel helicity conservation model and display roughly the same ratio of longitudinal to transverse components as is found in ρ electroproduction. In particular a fit to all the data gives

$$\frac{d\sigma_L/dt}{d\sigma_T/dt} = \xi^2 \frac{Q^2}{m_\phi^2} = (0.33 \pm 0.08)\frac{Q^2}{m_\phi^2} \ . \qquad (3.163)$$

IV. VECTOR-MESON PHOTOPRODUCTION FROM NUCLEI

A. Introduction

As discussed in Sec. II, vector-meson photoproduction from nuclei provides a unique opportunity for measuring forward vector-meson–nucleon scattering amplitudes. The performance and analysis of such experiments, especially in the case of the ρ^0, has, over a period of several years, occupied the time of several experimental groups and many theorists.

As originally conceived (Drell and Trefil, 1966; and Ross and Stodolsky, 1966a) the plan of attack was fairly simple. Even though the final nuclear state was not observed, the observation of a forward peak with a slope characteristic of the nuclear radius signifies a coherent process where the nucleus remains in its ground state. Under these conditions the optical model could readily be applied to calculate nuclear cross sections from assumed two-body amplitudes. By plotting the nuclear forward production cross sections against A, the number of nucleons in the nucleus, and comparing this plot with optical-model calculations, one would obtain:

(1) From the normalization of the plot, the single-nucleon forward photoproduction cross sections, $|T_{\gamma\rho}|^2$, and

(2) From the shape or A-dependence of the plot, the forward V-nucleon scattering amplitude for vector meson V, T_{VV}. No VMD assumptions are involved in this process.

Yet when confronted with high-statistics data on ρ^0 photoproduction from DESY–MIT (Asbury *et al.*, 1967a, 1968) and Cornell (McClellan *et al.*, 1969a), this sort of analysis led to contradictory and confusing results. The actual difficulties involved in analyzing high-statistics experiments on ρ^0 photoproduction are discussed in Sec. IV.C, and with the benefits of hindsight the historical confusion (Sec. III.C) on the subject is seen to have arisen from the following sources:

(1) The highly unstable nature of the ρ^0, which is observed through its decay into a wide ($\approx$155 MeV) spectrum of pion pairs.

(2) The presence of an interfering background of coherently produced nonresonant pion pairs, and other backgrounds.

(3) The sensitivity of optical-model calculations to refractive effects in ρ^0-nucleon scattering.

When such effects were taken into account in a new DESY–MIT experiment (Alvensleben *et al.*, 1970a) and a second Cornell analysis (McClellan *et al.*, 1971b), the results agreed qualitatively with the original expectations. The above complications, however, somewhat reduce our confidence in the numerical results of analysis.

In contrast, ω and ϕ photoproduction analyses have been less controversial because (1) the ω and ϕ are "narrow" resonances, and (2) there are fewer data. Results on ω and ϕ photoproduction are discussed in Sec. D.

Before delving into the details of analyzing photoproduction from complex nuclei in Secs. C and D, we briefly discuss the special significance of deuterium as a target in Sec. B. For a variety of reasons it functions as an almost independent check on our often tacit assumption of identical neutron and proton cross sections. It also provides the simplest possible test of Glauber's multiple scattering theory.

We continue in Sec. E with a brief discussion of independent experiments, in which the phases of vector-meson production amplitudes were measured through observation of leptonic decays. The results are not particularly surprising in the case of the ϕ or ρ^0, but pose a definite puzzle in our understanding of the ω.

A working model for the vector-meson scattering amplitudes is given in Sec. F.

B. Deuterium as a target

As the simplest nucleus, deuterium is singled out for special interest for several reasons:

(1) Optical-model calculations [for example, Glauber (1959) and Franco and Glauber (1966)] may proceed from "exact" wave functions.

(2) Nucleons are separated by distances of order $4F$ as opposed to distances under $2F$ in large nuclei. This makes the Glauber model hypothesis that each nucleon is an independent scatterer better here than in larger nuclei.

(3) The ratio of deuterium to hydrogen cross sections analyzed with the help of (1) and (2) above can yield information equivalent to having a free neutron target. A

critical review of this method has been given by Julius (1972a). We discuss the analysis of high-energy deuteron cross sections in Appendix B. As has already been brought out in Sec. III, there are overall theoretical uncertainties that make the assessment of "small" neutron – proton differences very difficult.

High-energy ρ^0 photoproduction from deuterium targets is a dominantly coherent process at small momentum transfer. As was discussed in Sec. III.C, comparison of deuteron and proton data, taking into account both possible deuteron breakup and a small (~5%) Glauber correction, indicates neutron and proton amplitudes to be very similar. This verifies our conjecture concerning the diffractive nature of these amplitudes. As might be expected, at lower energies, say below 5 GeV, there is evidence (McClellan *et al.*, 1969b; Hilpert *et al.*, 1970a) of nondiffractive amplitudes contributing to a neutron – proton difference (isospin exchange). A more refined theoretical analysis of these data has been given by Julius (1971).

A similar analysis can be made for ω photoproduction as was described in Sec. III.D. The qualitative difference here is the persistence to relatively high energies of a nondiffractive one-pion exchange contribution to the production (at 5 GeV it comprises nearly 50% of the cross section). Thus not only isospin exchange, but also spin flip and deuteron breakup characterize the cross sections at moderate energies.

On the other hand, ϕ photoproduction gives little indication of any neutron-proton difference, at least down to around 6 GeV (Sec. III.E). In the popular model where the ϕ is comprised predominantly of strange quarks which induce no resonant reactions in nucleons, ϕ interactions are thought to be the most purely diffractive of all the vector-meson interactions.

The simplicity of the Glauber model corrections in deuterium have been cleverly exploited by R. L. Anderson *et al.* (1971) in an experiment designed to directly measure ρ^0-nucleon elastic scattering; this was described in Sec. III.C. By making the VMD hypothesis that ρ^0 photoproduction and ρ^0 elastic scattering have the same angular distribution, they find a very reasonable ρ^0-nucleon total cross section of order 28 mb. As we shall see later, this value is consistent with high-statistics complex nuclei experiments. While the large errors quoted by Anderson *et al.* ($\gtrsim$3 mb) preclude the experiment from providing a statistically useful, independent determination of σ_ρ, it is nevertheless significant qualitative corroboration of the particular VMD and Glauber hypotheses used in the analysis, and in this sense is unique.

C. Rho-meson photoproduction from complex nuclei

High-statistics experiments on ρ^0 photoproduction at high energies from a wide range of nuclei have been done by groups at Cornell (McClellan *et al.*, 1969a, 1971b) and DESY–MIT (Alvensleben *et al.*, 1970a, b). Since these are the most complete experiments, our discussion will concentrate on them rather than on the lower-statistics SLAC (Bulos *et al.*, 1969) and Cornell–Rochester (Behrend *et al.*, 1970a) experiments, or on the earlier DESY–MIT experiment (Asbury *et al.*, 1967a, 1968). Although the final results of the Cornell and DESY-MIT experiments are similar, the original analyses differed in detail (see Sec. III.C). Therefore, in preparation for the present review, Spital and Yennie (1974) reanalyzed the data using the same theoretical models and assumptions for both experiments. The present discussion is a summary and updating of their results.

Starting with Drell and Trefil (1966) and Ross and Stodolsky (1966a), several authors have developed the formalism for photoproduction of ρ^0 mesons from nuclei and/or have carried out programs of analysis of data (Kölbig and Margolis, 1968; Gottfried and Yennie, 1969; Jurisic, 1970; Gottfried and Julius, 1970; Yennie, 1971; Moniz and Nixon, 1971; Bauer, 1971). Fortunately, the similarities between these models and calculations are more important than the differences. From the discussion of Sec. II.E and Appendix B, the reader must be aware that various approximations and assumptions must be made in order to carry through an analysis. As far as we have been able to determine, these slight qualitative differences lead to very small quantitative differences between results. Of course, their presence leads to systematic uncertainties which are hard to estimate. The most serious uncertainties appear to be the following (roughly in decreasing order of importance):

(1) Lack of independent knowledge of the ratio α_ρ of the real to imaginary parts of the ρ^0 scattering amplitude.

(2) Inadequate treatment of the incoherent ρ^0 contamination under the coherent peak.

(3) Uncertainties due to the stability of the ρ^0. Of particular importance is the uncertainty of the width which affects the overall normalization. Also, the interference with $\omega \to 2\pi$ decays seriously distorts the resonance peak while not modifying the area appreciably.

(4) Inadequate understanding of nuclear correlations, particularly in the surface.

(5) Uncertainties in the distribution of nuclear matter in the nucleus.

The importance of α_ρ to the data analysis was first emphasized by Swartz and Talman (1969). With α_ρ set equal to 0, the Cornell data had originally led to unreasonably large values of $\hat{f}_\rho^2/4\pi$ ($\approx$4) (see Table I for the definitions of the coupling constants) and the total ρ-nucleon cross section $\sigma_{\rho N}$ ($\approx$38 mb). The first DESY–MIT experiment (Asbury *et al.*, 1967a, 1968) had obtained more reasonable values while using $\alpha_\rho = 0$, but that is presumably due to some fortuitous compensation by other features of their first optical model, which was quite crude.

The theoretical model we use here is Glauber's optical model of high-energy collisions (Glauber, 1959, 1970), suitably generalized to the case of particle production. The basic ideas of this model and an indication of the derivation of expressions for the cross sections are given in Appendix B. For coherent photoproduction the well-known optical model expression is

$$\frac{d\sigma^{\rm coh}}{dt}(\gamma A \to \rho^0 A) = |T_{\gamma p}^{(A)}(t)|^2 ,$$

where

$$T_{\gamma\rho}^{(A)}(t) = T_{\gamma\rho} \int\cdots\int d^2b\, dz \exp(i\mathbf{q}_\perp \cdot \mathbf{b} + iq_\parallel z)\tilde{n}(\mathbf{b}, z) \times \exp\left[\frac{-\sigma_\rho}{2}(1 - i\alpha_\rho)\int_z^\infty \tilde{n}(\mathbf{b}, z')dz'\right], \tag{4.1}$$

and $T_{\gamma\rho}$ is the forward, single-nucleon ρ^0 photoproduction amplitude. Here $\tilde{n}(\mathbf{b}, z)$ is the nucleon number density appropriately modified to take into account the finite range of the two-body interactions; t, the four-momentum transfer squared, is given by $-(\mathbf{q}_\perp^2 + q_\parallel^2)$, where $\mathbf{q}_\perp$ is the transverse momentum transfer to the nucleus, and $q_\parallel$ is the longitudinal (minimum) momentum transfer given by $q_\parallel = k - (k^2 - m_\rho^2)^{1/2} (\approx m_\rho^2/2k$ for $k \gg m_\rho)$.

The physical interpretation of $T_{\gamma\rho}^{(A)}$ is easily read from Eq. (4.1). A photon converts to a ρ^0 meson at $(\mathbf{b}, z)$ where $\mathbf{b}$ is the impact parameter and z is the distance along the incident photon direction. The exponent corresponds to the absorption and refraction of the ρ^0 wave after production. It is assumed that $\tilde{n}$ is known for the various nuclei, and that $|T_{\gamma\rho}|^2$, σ_ρ, and α_ρ are the experimental parameters to be determined by studying the A dependence and normalization.

For the incoherent ρ^0 photoproduction background, the optical-model result assuming incoherent interaction with only one nucleon is (see Appendix B)

$$\frac{d\sigma^{\text{inc}}}{dt}(\gamma A \to \rho^0 A) = A_{\text{eff}} \frac{d\sigma}{dt}(\gamma N \to \rho^0 N), \tag{4.2a}$$

with

$$A_{\text{eff}} = \int\cdots\int d^2b\, dz \tilde{n}(\mathbf{b}, z) \exp\left(-\sigma_\rho \int_z^\infty \tilde{n}(\mathbf{b}, z')dz'\right) \times \left|1 - \int_{-\infty}^z dz'' \tilde{n}(\mathbf{b}, z'')\frac{\sigma_\rho}{2}(1 - i\alpha_\rho)e^{iq_\parallel z''} \exp\left[\frac{-\sigma_\rho}{2}(1 - i\alpha_\rho)\int_{z''}^z \tilde{n}(\mathbf{b}, z''')dz'''\right]\right|^2. \tag{4.2b}$$

Since we are here interested only in a rough estimate of this small background, VMD was used to write $T_{\gamma\rho}(t) = (e/\hat{f}_\rho)T_{\rho\rho}(t)$. We note that Eq. (4.2) is necessarily incorrect at small t, since it fails to take into account the Pauli principle which suppresses the cross section somewhat in that region. (See Appendix B for further discussion.)

Note that Eqs. (4.1) and (4.2) do not take into account the fact that the ρ^0 is an unstable particle which decays rapidly into two charged pions. Therefore, in order to make use of these equations, it is necessary first to extract from the data a cross section for ρ^0 photoproduction *as if the* ρ^0 *were stable*. The experimental data consist of values of $d\sigma/dt\, dm_{\pi\pi}$ averaged over some experimental aperture. There exists no complete theory for this doubly differential cross section, although there is good qualitative understanding of the main features of the $m_{\pi\pi}$ dependence (see Fig. 13). Some of the physics underlying the ρ^0 shape was described in Sec. II.B; some fitting procedures are described in III.C. Further complications for photoproduction from nuclei will be described below.

Spital and Yennie (1974a) discussed the problem of the ρ^0 shape and proposed

$$\frac{d\sigma}{dt} \equiv \frac{\pi\Gamma_\rho}{2}\left.\frac{d\sigma}{dt\, dm_{\pi\pi}}\right|_{m_{\pi\pi} = m_\rho} \tag{4.3}$$

as the standard definition of the "stable" ρ^0 cross section. In the narrow-resonance limit (4.3) goes smoothly over to the standard definition of a stable particle cross section. However, in our present "wide-resonance" situation, Eq. (4.3) yields, as well, a cross section minimally sensitive to inadequately understood interfering backgrounds; i.e., we believe the most important interfering background vanishes when $m_{\pi\pi} = m_\rho$.

In principle, Eq. (4.3) is to be applied in the following way, assuming that Γ_ρ and m_ρ are known from "outside": First, one fits a smooth curve to the ρ^0 part of the mass distribution and reads off the cross section at the ρ^0 mass. The formula then gives the desired cross section. In practice, this procedure is very subtle since there may be interfering and noninterfering backgrounds. In addition, the mass and width of the ρ^0 are not well known, leading to normalization uncertainties. It should be emphasized that these difficulties are theoretical and stem from the inadequate theory of the mass distribution. The difficulties associated with interfering backgrounds are described in the following two paragraphs.

●We have already seen in Sec. II.B that the $\pi^+\pi^-$ mass distribution in photoproduction from hydrogen can be qualitatively understood in terms of a picture in which the physical photon state is a superposition of a spatially localized ρ^0 component plus a loose nonresonant pion pair component. This picture is described in more detail by Yennie (1975). The nonresonant pion pair structure has an absorption cross section roughly twice that of the ρ^0. In field theoretical language, this corresponds most closely to the Drell–Söding model (Söding, 1966). It should be noted that the nonresonant contribution is defined to vanish at precisely the ρ^0 mass. This is known as the double counting correction and is due to Bauer (1970) and Pumplin (1970). The explanation of this correction is described briefly in Appendix C.3. A similar model has been discussed for production from nuclei by Bauer (1971). Here the nearly total absorption

in central collisions leads to more nearly equal cross sections for the ρ^0 and the nonresonant pion pairs. By itself, this would tend to lead to a Ross–Stodolsky (1966a) pion pair mass distribution. However, at finite energies the minimum momentum transfer to the nucleus varies across the mass distribution, tending to suppress the peak more than the low-mass tail. Beyond these considerations, we should, as in Sec. II.E, consider the fact that scattering in the nucleus can induce transitions between the ρ^0 and the nonresonant pairs, and that these transitions can also take place between scatterings (Gottfried and Julius, 1970; Chapline, 1970). At asymptotic energies time dilation could suppress such transitions, but all this suggests that a more complete theory would deal with the complete dipion system propagating through the nucleus. Since this is likely to be inordinately difficult, the expedient of using Eq. (4.3) seems to be the most practical approach. Ambiguities associated with the $\rho^0 - \pi^+\pi^-$ system are described further in Appendix C.

●There is another interfering background which does not vanish at the ρ^0 mass, and which in fact produces a severe distortion of the resonance peak in just that vicinity. This is the interference with the $\pi^+\pi^-$ decay of diffractively photoproduced ω mesons. An example of the effect of such interference is shown in Fig. 13; the precipitous drop in the data at the ω mass is due to constructive interference below m_ω and destructive interference above. As mentioned in Sec. III.C, high-resolution experiments have been done to measure this effect (Alvensleben *et al.*, 1971a; Behrend *et al.*, 1971b; Biggs *et al.*, 1970b). However, nearly all mass spectra measured for the purpose of determining σ_ρ, α_ρ, and $|T_{\gamma\rho}|^2$ have much coarser resolution, say, 30 to 50 MeV mass bins. It is clear that if the interference is not taken into account, the particular arrangement of the mass bins can make a huge difference in the apparent width, and some difference in the apparent height, of the resonance peak. For example, if a bin is centered at the ω mass, the interference will largely tend to cancel and one will see an approximation of the actual ρ^0 shape. On the other hand, with one bin just below the ω mass and the next just above, the resonance will appear narrower and higher. Without a great deal of knowledge of the details of the two experiments, it is impossible to make an *a posteriori* correction for this effect, but later on we make some gross estimates which should at least indicate the level of uncertainty which may be introduced.

A detailed study of the mass distribution in photoproduction, including the possibility of extracting m_ρ and Γ_ρ, has been made by Spital and Yennie (1974a). Their main results are as follows:

(1) There appears to be no reliable procedure for analyzing individual mass distributions. Although very precise and abundant high-resolution data from the Cornell–Rochester (Behrend *et al.*, 1971b), DESY–MIT (Alvensleben *et al.*, 1971a), and Daresbury (Biggs *et al.*, 1970b) groups were used[41] (with some mass distributions having as many as 60 data points spaced 5 MeV apart!), correlations among the fitting parameters, compounded by the presence of $\rho^0 - \omega$ interference, made the results of fitting individual mass spectra hopelessly chaotic.

TABLE XXXI. Results of the overall fit (Spital and Yennie 1974a) to the DESY–MIT data (Alvensleben *et al.*, 1971a). N is the number of terms in a polynomial in $(m^2 - m_\rho^2)$ multiplying a Breit–Wigner factor. Note the strong dependence of the fitting parameters on N. There seems to be no good criterion for selecting between these fits.

N	Γ_ρ (MeV)	m_ρ (MeV)	χ^2	Degrees of freedom
3	153.9 ± 2.2	776.1 ± 0.9	1083.0	1103
4	145.0 ± 3.7	773.6 ± 1.3	1059.1	1071
5	138.4 ± 3.9	769.7 ± 2.7	1015.9	1039

(2) Reasonable results can be obtained, however, from overall fits to a large number of mass distributions. Nevertheless, the value of Γ_ρ is still very sensitive to the number of free parameters used in the fits. It should be emphasized that the difficulties here are theoretical in nature, and there is no experiment that readily presents itself that can be expected to clear up the problem. It is possible, however, that the difficulties just described are due to the somewhat narrow mass range used (~630–880 MeV), which permitted the shape parameters too much flexibility. Perhaps with a larger mass range, as available from the purely hadronic process $\pi + N \to N' + 2\pi$, these uncertainties would be reduced, and more reliable values of Γ_ρ and m_ρ obtained [$\Gamma_\rho = (150.3 \pm 2.7)$ and $m_\rho = (770.23 \pm 0.88)$ MeV; Trippe *et al.* (1976)]. For a review, see Pišut and Roos (1968). In the absence of high-statistics wide-mass-range data in photoproduction, the hadronic determinations may be the most reliable. However, there are shape uncertainties in hadronic determinations also. It is not clear to us whether they yield an apparently more unique answer because of more restrictive assumptions on the shape, or because of the broader mass range.[42] The results for various parametrizations of the ρ^0 shape in photoproduction are shown in Table XXXI. As may be seen from Table XXII in Sec. III.F, these parametrizations are compatible with storage ring results.

After the analyses had been completed for this paper, we learned of a new, more accurate experiment which has been done at Orsay (Quenzer *et al.*, 1977) (see Sec. III.F). With the improved accuracy, the data can no longer be well fitted with a simple P-wave resonance function [represented by Fig. 209(a)], but it seems to demand contributions such as those shown schematically in Fig. 209(b), (c). A model for these additional contributions, which fits the data quite well, has been given by Costa de Beauregard *et al.* (1977). It includes the effect of the intermediate π-ω channel. One consequence of these new results is that a larger value of Γ_ρ

[41] The detailed mass distributions were supplied privately and do not appear in the references cited here.

[42] One of the authors (DRY) wishes to thank Dr. Matts Roos for useful correspondence on this point. The paper by Spital and Yennie (1974a) was concerned with the problem of obtaining Γ_ρ and m_ρ from photoproduction experiments alone.

is obtained (=158.9 ± 4.7 MeV). Since this measures the ρ_0 in its purest state, without nucleon or nuclear contaminations, and also because it agrees with (or does not disagree with) other determinations, we believe a width of about 155 MeV is now more plausible than the lower values. It should be emphasized that the new result combines more accurate data with a specific theoretical model. It would be desirable to see how well one could determine the width without incorporating any theoretical prejudice (aside from appropriate analytic properties). Another consequence of the new results is that they introduce some uncertainty into the meaning and value of $\bar{f}_\rho^2$. Since this uncertainty seems to be of less importance than some other ones in photoproduction, it seems safe to ignore it until a more complete theoretical understanding is obtained.

(3) In order to extract cross sections for comparison with the optical model, the DESY–MIT mass spectra in the ρ^0 photoproduction experiment (Alvensleben *et al.*, 1970a, b) were fitted, ignoring the ρ-ω interference. As stated previously, the mass resolution in this experiment was much broader than in the ρ-ω interference experiment. However, many more nuclei were included. Fortunately for the optical-model analysis, the cross sections extracted by means of Eq. (4.3) are nearly exactly proportional to the assumed ρ^0 width. Thus ρ-ω interference and Γ_ρ uncertainties affect only the normalization parameters, $|T_{\gamma\rho}|^2$ and $\hat{f}_\rho^2/4\pi$, but not the ρ^0-meson parameters σ_ρ and α_ρ.

(4) The Cornell group (McClellan *et al.*, 1971b) used the standard procedure of Eq. (4.3), so it was not necessary to refit the Cornell mass distributions.

Interestingly, the best values of Γ_ρ obtained from both sets of low-resolution data turned out to be 124 MeV. We have subsequently tried to correct the DESY–MIT data for ρ-ω interference and find that this brings the width up to about 150 MeV! Clearly, this is not a very good way to determine the width. Although the best evidence indicates that Γ_ρ is about 155 MeV, we allow for other possible values, but assume that it lies in the range 135 to 155 MeV. We must now use our better understanding of the role of ρ-ω interference to estimate its possible effect on the cross sections of the previous analysis. We shall make this estimate for three possible values of the width: 135, 145, and 155 MeV and reasonable correlated values of m_ρ which are guessed from Table XXXI. These new combinations are shown in Table XXXII together with other parameters.

The procedure we chose was the following. We first correct all the previous cross sections to a new Γ_ρ of 155 MeV, still ignoring the ρ-ω interference. We call these the "standard reference cross sections."

Next, for each combination of Γ_ρ and m_ρ listed in Table XXXII, we refit the mass peaks including the effect of ρ-ω interference. Generally this altered the value of the ρ^0 component of the cross section at the ρ^0 mass. The combined effect of changing this "peak height" and the width are given by the normalization constants in Table XXXII. One obtains the cross sections for these Γ_ρ, m_ρ combinations by multiplying the standard reference cross sections by these constants. It should be noted that there is no systematic dependence of these constants on A, so they affect only the overall normalization. While this procedure is necessarily somewhat crude, we believe that the results give a reasonable indication of the level of systematic uncertainty in the treatment of the mass spectrum.

Turning now to the determination of σ_ρ and α_ρ, we summarize the optical-model analysis of Spital and Yennie (1974b) for photoproduction of a stable ρ^0. For each experimental measurement of $d\sigma/dt(\gamma A \to \rho^0 A)$ optical-model calculations were made for several values of σ_ρ and α_ρ. The overall normalization of the theory (i.e., $|T_{\gamma\rho}|^2$) to the experimental data was varied to minimize χ^2. The data from the two principal experiments [DESY–MIT low mass resolution (Alvensleben *et al.*, 1970a, b) and Cornell (McClellan *et al.*, 1971b)] were treated separately.

Figures 198 and 199 show χ^2 maps from the A-dependence fits for both DESY–MIT and Cornell. The outstanding feature of the maps is that χ^2 is extremely flat along a "valley" given very crudely by $\sigma_\rho(\alpha_\rho) = (32 + \alpha_\rho/0.05)$ mb. This indicates that acceptable fits to the data can be achieved for any reasonable value of σ_ρ by appropriate choice of α_ρ. This sensitivity of the calculation to α_ρ was unanticipated in early analyses and is responsible for much of the historical controversy. The precise positions of the χ^2 minima in the valleys must not be taken seriously. These are highly sensitive to small uncertainties in the theoretical model or in the ρ^0 mass.

In addition, Fig. 198 shows the effect on the χ^2 map of some very crude attempts to take into account the effects of incoherent ρ^0 photoproduction. "Full-strength" incoherent refers to that calculated by means of Eq. (4.2) (neglecting the t dependence). Since it ignores the Pauli principle, "full-strength" gives an overestimate of the data correction needed. As one can see, the qualitative picture is essentially unchanged by these corrections. In general, the valley is displaced parallel to itself toward the smaller values of α_ρ. χ^2 drops appreciably for "half-strength," indicating the presence of some incoherent ρ^0. While more involved discussions of incoherent production have been given by other authors

TABLE XXXII. Combinations of Γ_ρ and m_ρ used in fitting the data. The first row (standard reference) was used in fitting the photoproduction data (Spital and Yennie, 1974b), overlooking the effect of ρ-ω interference. The remaining combinations were used in an attempt to correct for the ρ-ω interference. The normalization is the factor by which standard reference photoproduction cross sections must be multiplied for the particular combination. [Note that the present standard reference cross sections are 1.087 times those presented in Spital and Yennie (1974b).] The remaining columns give the different phenomenological coupling parameters which are defined in Table I for each choice of the pair m_ρ, Γ_ρ. (The necessary fitting of the two-pion mass distributions was done using $N = 5$ as defined in Table XXXI.)

Γ_ρ	m_ρ	Normalization	$\bar{f}^2_{\rho\pi\pi}/4\pi$	$\hat{f}_\rho^2/4\pi$	$\bar{f}_\rho^2/4\pi$
155	770	1.00 (standard)	2.65	2.09 ± 0.04	
135	767	0.86 ± 0.04	2.61	2.43 ± 0.10	2.21 ± 0.017
145	774	0.92 ± 0.09	2.77	2.27 ± 0.23	2.20 ± 0.06
155	776	0.96 ± 0.10	2.95	2.18 ± 0.22	2.11 ± 0.06

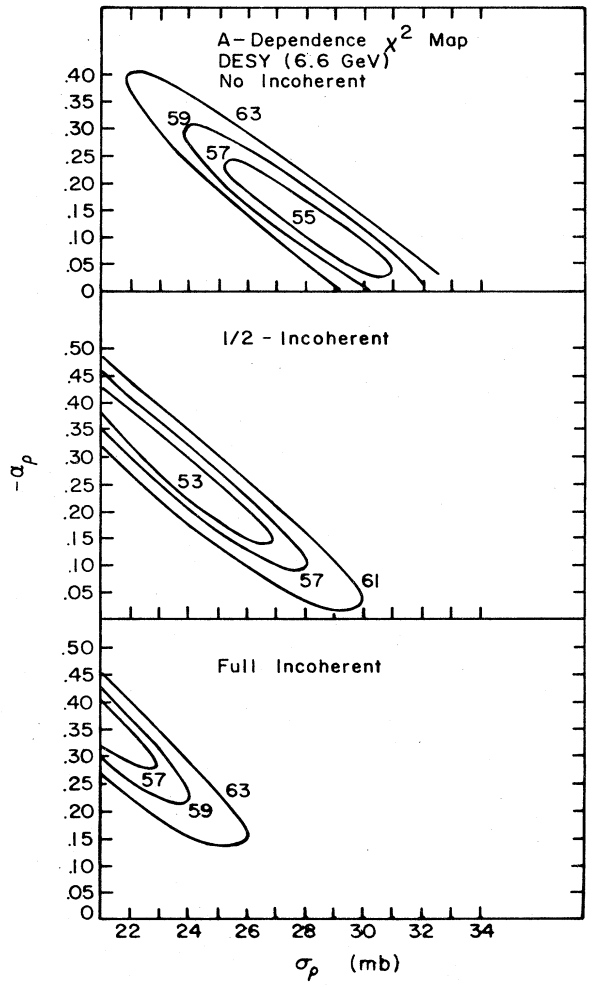

FIG. 198. χ^2 contour maps for the DESY–MIT 6.6 GeV data using various assumptions for incoherent contamination explained in the text. The number of degrees of freedom, hereafter denoted by $\langle\chi^2\rangle$, is 62 (from Spital and Yennie, 1974b).

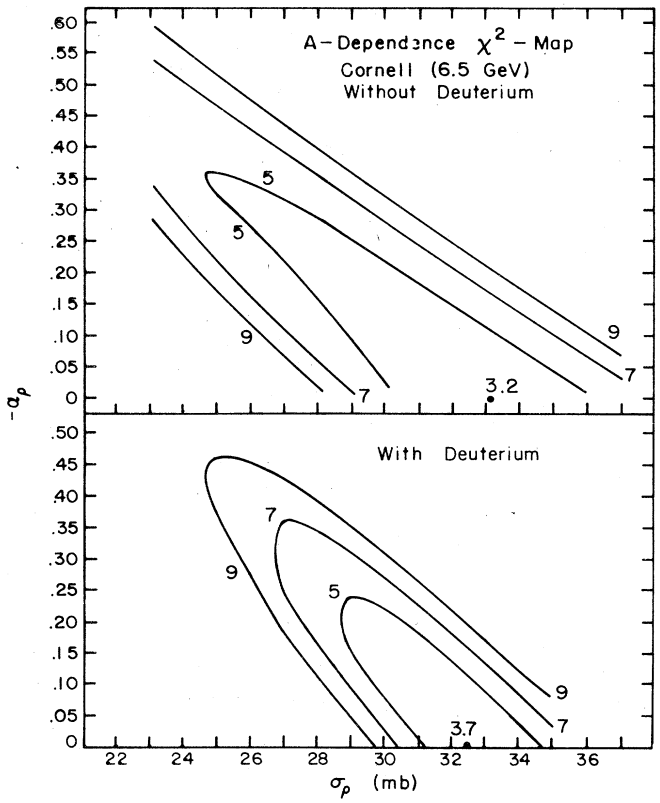

FIG. 199. χ^2 maps for the Cornell 6.5 GeV data with the deuteron omitted/included. The number of degrees of freedom is 3 with the deuteron, 2 without (from Spital and Yennie, 1974b).

(Trefil, 1969; von Bochmann, Margolis, and Tang, 1969; Yennie, 1971), we do not believe in any calculation strongly enough to warrant a more thorough analysis of incoherent effects (see Sec. V.D and Appendix B).

The major differences between the two principal experiments are as follows:

(1) DESY-MIT gives data at five values of t; Cornell gives only $\theta=0$ data (they extrapolate their data to $\theta=0$ via an optical model similar to our own). DESY–MIT had far better statistics, and more nuclei.

(2) Cornell measured photoproduction from deuterium; DESY–MIT did not.

As can be seen from Fig. 199, measurement of photoproduction from the deuteron enormously sharpens the valley, and since the precise positions of χ^2 map minima cannot be taken literally, the two experiments yield comparable information. In effect, what it lost in statistics, the Cornell group made up with the deuteron measurements. (The deuteron data are far more sensitive to the normalization $|T_{\gamma p}|^2$ than to σ_ρ and α_ρ, which

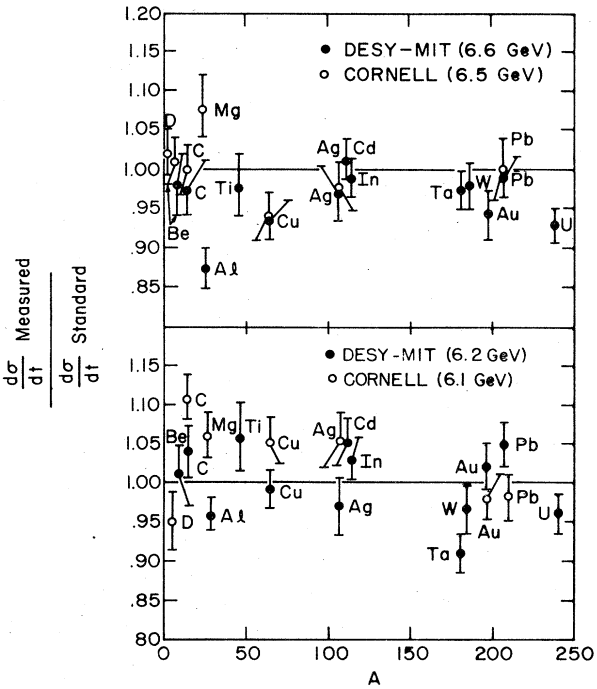

FIG. 200. Ratio of forward cross sections for DESY–MIT (Cornell) at 6.6, 6.2 (6.5, 6.1) GeV to theoretical forward cross sections calculated with certain "standard" parameters (see Spital and Yennie, 1974b).

enter only into the ~5% Glauber correction. Measuring deuteron photoproduction thus serves to tie down the normalization.)

When the data are compared at the most primitive level possible, the forward cross sections of the two groups agree. See Fig. 200. However, the results of the analyses are slightly different because of the differences noted above.

The main conclusions of the analysis are as follows:

(1) Because the precise positions of the χ^2 map minima cannot be taken literally, it is impossible to extract both σ_ρ and α_ρ from these experiments. [If one *had* confidence in the positions of these minima, a deuteron measurement combined with the massive DESY–MIT data matrix would yield very well-determined values of σ_ρ and α_ρ (see Spital and Yennie, 1974b)]. Acceptable fits can be obtained for any reasonable choice of σ_ρ or α_ρ by suitable choice of the other. Results for fixed α_ρ are given in Table XXXIII. If one takes $\alpha_\rho = -0.2$ as suggested by Compton scattering [which is consistent with quark models and observations of electron pair decays of ρ^0's photoproduced on light nuclei (see Sec. IV.E)], one obtains $\sigma_\rho = (27.1 \pm 0.3)$ mb, averaged over both experiments and all energies.

(2) The value of $\hat{f}_\rho^2/4\pi$ depends on the normalization of the data and the definition of $\hat{f}_\rho$ through $|T_{\gamma\rho}|^2 = (e^2/\hat{f}_\rho^2)^2 \times |T_{\rho\rho}|^2$, where $T_{\rho\rho} = (i/4\sqrt{\pi})\sigma_\rho(1 - i\alpha_\rho)$.[3] With the standard reference cross sections and α_ρ fixed at -0.2, the two experiments give $\hat{f}_\rho^2/4\pi = 2.09 \pm 0.04$ averaged over all energies. To adjust to one of the other (m_ρ, Γ_ρ) sets shown in Table XXXI, one must *divide* this value by the normalization constant. In the VMD hypothesis, guided by the discussion of Appendix C on "mass extrapolation effects," we would anticipate that the photoproduction constant $\hat{f}_\rho^2/4\pi$ would be closer to $\bar{f}_\rho^2/4\pi$ than to $\bar{f}_{\rho\pi\pi}^2/4\pi$ (Bauer and Yennie, 1976a). To facilitate this comparison, Table XXXI includes our Table XXV values for $\bar{f}_\rho^2/4\pi$, as well as $\bar{f}_{\rho\pi\pi}^2$ from Eq. (C.7), for each of our chosen sets (m_ρ, Γ_ρ). The consistency of these results with the VMD hypothesis is apparent. The values for the larger widths agree somewhat better than for $\Gamma_\rho = 135$; however, considering the model and theoretical uncertainties, this should not be taken as serious evidence in favor of the large widths.

TABLE XXXIII. Fixed-α_ρ A-dependence fits for the DESY–MIT (Alvensleben *et al.*, 1970a,b) and Cornell (McClellan *et al.*, 1971b) data. The errors are misleadingly small since they do not take into account the uncertainty in α_ρ. The values of $(d\sigma/dt)|_{\theta=0}$ and $\hat{f}_\rho^2/4\pi$ are for the "standard" reference cross sections. (The two-pion mass distributions for the DESY–MIT data were done using $N=5$ as defined in Table XXXI.

	$\alpha_\rho = 0$	$\alpha_\rho = -0.2$	$\alpha_\rho = -0.3$
	A. $k = 5.8$ GeV (DESY–MIT)		
σ_ρ (mb)	33.0 ±1.2	27.3 ±1	24.8 ±0.9
χ^2 (DF = 63)	69.7	69.6	70.9
$(d\sigma/dt)\|_{\theta=0}$ (μb/GeV^2)	149 ±6	138 ±4	133 ±4
$\hat{f}_\rho^2/4\pi$	2.72 ± 0.11	2.10 ± 0.08	1.87 ± 0.07
	B. $k = 6.1$ GeV (Cornell)		
σ_ρ (mb)	32.2 ±1	28.2 ±0.9	26.3 ±0.8
χ^2 (DF = 6)	21.1	12.4	9.0
$(d\sigma/dt)\|_{\theta=0}$ (μb/GeV^2)	151 ±5	146 ±4	144 ±4
$\hat{f}_\rho^2/4\pi$	2.56 ± 0.10	2.10 ± 0.08	1.93 ± 0.08
	C. $k = 6.2$ GeV (DESY–MIT)		
σ_ρ (mb)	33.3 ±0.9	27.9 ±0.7	25.4 ±0.6
χ^2 (DF = 63)	60.7	57.3	58.8
$(d\sigma/dt)\|_{\theta=0}$ (μb/GeV^2)	156 ±5	145 ±3	140 ±3
$\hat{f}_\rho^2/4\pi$	2.62 ± 0.08	2.07 ± 0.07	1.87 ± 0.06
	D. $k = 6.5$ GeV (Cornell)		
σ_ρ (mb)	32.9 ±1.4	29.6 ±1.3	27.8 ±1.2
χ^2 (DF = 4)	3.4	4.6	5.9
$(d\sigma/dt)\|_{\theta=0}$ (μb/GeV^2)	150 ±4	146 ±6	145 ±4
$\hat{f}_\rho^2/4\pi$	2.69 ± 0.16	2.29 ± 0.14	2.16 ± 0.13
	E. $k = 6.6$ GeV (DESY–MIT)		
σ_ρ (mb)	31.3 ±0.9	26.5 ±0.7	24.2 ±0.6
χ^2 (DF = 63)	57.7	56.0	58.6
$(d\sigma/dt)\|_{\theta=0}$ (μb/GeV^2)	143 ±4	134 ±4	129 ±4
$\hat{f}_\rho^2/4\pi$	2.56 ± 0.08	2.03 ± 0.07	1.84 ± 0.06
	F. $k = 8.8$ GeV (Cornell)		
σ_ρ (mb)	28.3 ±0.7	25.9 ±0.6	24.7 ±0.6
χ^2 (DF = 7)	22.1	17.5	15.9
$(d\sigma/dt)\|_{\theta=0}$ (μb/GeV^2)	128 ±3	126 ±3	124 ±2
$\hat{f}_\rho^2/4\pi$	2.32 ± 0.07	2.06 ± 0.06	2.00 ± 0.06

TABLE XXXIV. Comparison of $|T_{\gamma\rho}|^2$ in μb/GeV^2 from nuclei using the standard cross sections, and from hydrogen and deuterium (Cornell data, McClellan *et al.*, 1969b, 1971b). The hydrogen and deuterium values are obtained by fits to the energy dependence; a Glauber correction is used for deuterium.

Energy	Complex nuclei	Hydrogen	Deuterium
5.8 [a]	133 ± 4	161	135
6.1 [b]	144 ± 4	152	133
6.2 [a]	140 ± 3	150	131
6.5 [b]	145 ± 4	143	129
6.6 [a]	129 ± 3	141	129
8.8 [b]	126 ± 2	125	119

[a] DESY–MIT (Alvensleben *et al.*, 1970 a,b)
[b] Cornell (McClellan *et al.*, 1971b)

(3) When normalization differences are taken into account, the results of the Spital–Yennie analysis agree well with the results of the older analyses made by the groups themselves.

(4) In Table XXXIV the values of $|T_{\gamma\rho}|^2$ from complex nuclei using both Cornell and DESY–MIT data (standard reference cross sections) are compared with those from the forward hydrogen and deuterium cross sections from the Cornell counter experiment (we did not have sufficient information on the DESY–MIT mass distributions to reanalyze their hydrogen data). The agreement with the deuterium values is good (of course, the Cornell complex nuclei results incorporate their deuterium data). The difference between the hydrogen and deuterium values is due primarily to a $T=1$ isospin exchange (McClellan *et al.*, 1969a,b; Julius, 1971), which vanishes in elastic production from deuterium and is small for most other complex nuclei. This indicates an internal consistency in the results from counter experiments, and perhaps supports the larger hydrogen cross section for $t=0$, as compared to the bubble chamber determinations (see Sec. III.C).

D. Nuclear photoproduction of other vector mesons

Following the ρ^0 photoproduction example, experiments have also been performed on ϕ and ω photoproduction from nuclei. In principle the analysis would proceed as in Sec. IV.C and would yield appropriate values of $T_{\gamma V}(0)$, σ_V, and α_V. Nevertheless analyses here take on some different features. Because both ϕ and ω are narrow resonances, extraction of cross sections lacks the ambiguities of the ρ^0 case. However, ω production suffers from a rather hard to observe 3π dominant decay mode; and a significant incoherent contribution arising from the one-pion exchange mechanism makes it difficult to extract the diffractive part of the cross section. The optical-model analyses are also complicated by the possibility of $\phi \rightleftarrows \omega$ transitions within the nucleus. This last effect, first discussed by Ross and Stodolsky (1966b), has subsequently been largely overlooked in the literature.

A Cornell experiment (McClellan *et al.*, 1971a) on ϕ photoproduction from nuclei ranging from H_2 to Pb with photon energies between 6.4 and 9 GeV was originally analyzed ignoring ϕ-ω transitions. Extracted values of σ_ϕ and $d\sigma_{\gamma\phi}/dt|_{\theta=0}$ are both very dependent on α_ϕ and not very precise (errors of order 20%–30% for *fixed* α_ϕ). The analysis is consistent with the quark-model estimate of $\sigma_\phi \approx 12$ mb (Lipkin, 1975), and there is general agreement between complex nuclei and hydrogen for $d\sigma_{\gamma\phi}/dt|_{\theta=0}$ (see Sec. III.E) when $\alpha_\phi \approx -.3$ [this is consistent with a direct measurement of α_ϕ obtained by a DESY–MIT group from $\gamma C \to e^+e^- C$ (Alvensleben *et al.*, 1971b) and simple quark-model estimates (Krammer, 1970; Lipkin, 1975)]. The γ-ϕ coupling parameter for photoproduction is found to be $\hat{f}^2_\phi/4\pi = 23.6 \pm 9.6$, which is to be compared with the colliding-beam value of $\bar{f}^2_\phi/4\pi = 13.2 \pm 0.6$ (Table XXVII).

High-statistics Rochester experiments (Behrend *et et al.*, 1970b; Abramson *et al.*, 1976) on ω photoproduction from nuclei ranging from D_2 to Pb at photon energies between 7 and 9 GeV were analyzed after subtracting an estimate of the one-pion exchange contribution and, as before, ignoring $\phi \rightleftarrows \omega$ transitions. Again, extracted values of σ_ω and $d\sigma_{\gamma\omega}/dt|_{\theta=0}$ are strongly dependent on an assumed α_ω. *Choosing* $\alpha_\omega = -0.24$ (as suggested by Compton scattering) and fixing $\sigma_\omega = 27$ mb, they they find $d\sigma_{\gamma\omega}/dt = (8.54 \pm 0.72)\ \mu$b/GeV^2—in substantial agreement with the hydrogen cross section measured in this experiment, *but* about 20% *below* the bubble chamber measurement of Ballam *et al.* (1973). This cross section leads to $\hat{f}^2_\omega/4\pi = 30.4 \pm 4.8$, in contrast to the colliding-beam value of $\bar{f}^2_\omega/4\pi = 18.4 \pm 1.8$ (Benakas *et al.*, 1972b).

It is important to consider the effect of $\phi \rightleftarrows \omega$ transitions on both these analyses (Ross and Stodolsky, 1966b). Since no isospin exchange is involved, it is possible that this transition amplitude is diffractive. Some simple quark-model ideas (Gerasimov, 1968; Bauer and Yennie, 1976b) suggest a small negative mixing amplitude which tends to improve the normalizations (relative to VMD) of both ϕ and ω photoproduction from hydrogen.[43] Although exploratory attempts at such a reanalysis of the nuclear data have been made,[44] a clear picture of the consequences of mixing has not yet emerged. Therefore in the following paragraphs we shall describe some of the theoretical features of $\phi \rightleftarrows \omega$ mixing in nuclei.

In photoproduction from nuclei, the cross sections are modified not only by the change of the production amplitude on a single nucleon, but also by $\phi \rightleftarrows \omega$ transitions after production. At infinite photon energy a simple mixing theory would predict normal modes formed from linear combinations of ϕ and ω which would propagate independently through nuclear matter. At lower, more realistic energies, the longitudinal momentum transfer

[43] The original idea was that the mixing was associated entirely with the fact that the $\omega(\phi)$ contains a small admixture of strange (nonstrange) quark pairs, and it was assumed that diffractive scattering did not cause a transition between strange and nonstrange pairs. However, discussions with Carl Rosenzweig and Chris Schmid and correspondence with Fernand Renard have brought out the possibility that there could be such direct transitions. Hence we now feel that this amplitude ($T_{\phi\omega}$) should be left as a free fitting parameter which is expected to be of order 10% of $T_{\phi\phi}$ or $T_{\omega\omega}$.

[44] In collaboration with N. B. Mistry and E. H. Thorndike.

required by $\phi \rightleftarrows \omega$ transitions complicates the analyses; for the small values of $T_{\omega\phi}$ used, we have found it adequate to keep only terms through first order in $T_{\omega\phi}$.

At this stage we have so many parameters ($\sigma_\omega, \alpha_\omega, \hat{f}^2_\omega/4\pi, \sigma_\phi, \alpha_\phi, \hat{f}^2_\phi/4\pi, T_{\omega\phi}$, not to mention incoherent background, various nuclear effects, etc., as discussed in the case of the ρ^0) that there is no hope of determining a unique fit to the data. In fact, the separate ϕ and ω experiments already can be fit in a variety of ways without adding the complication of a new parameter. Our interest in the new parameter lies of course in its intrinsic physical importance as well as the fact that it may make it possible to attain better agreement with VMD.

To get some feeling for the possible effects of $\phi \rightleftarrows \omega$ mixing, we have performed some sample optical-model calculations to compare with both the Cornell ϕ and the Rochester ω photoproduction data.[44] The mixing can affect the A dependence as well as the overall normalization of the optical-model results. With all other parameters fixed, the fractional effect of mixing is smaller in heavier nuclei (this is essentially a shadowing of the basic mixing amplitude, similar to other shadowing effects to be discussed in Sec. V). This modification in A dependence can then be compensated by changing the other parameters. For example, with negative mixing, the A dependence can be restored approximately either by increasing σ_V or making α_V more negative; finally (for fixed α_V), the normalization can be restored by making $\hat{f}^2_V/4\pi$ smaller.

Because of the numerical values of the parameters used ($\sigma_\phi \sim \frac{1}{2}\sigma_\omega$), it turns out that the effect of $T_{\phi\omega}$ on the A dependence is stronger in the ϕ case than in the ω case. In ω photoproduction, putting in negative mixing tends to reduce $\hat{f}^2_\omega/4\pi$ and increase σ_ω slightly (for α_ω fixed). However, in the ϕ case the same mixing requires a much larger increase in σ_ϕ that actually necessitates an *increase* in $\hat{f}^2_\phi/4\pi$ (for α_ϕ fixed).

An interesting question is whether the introduction of the new parameter will make possible better agreement with VMD, i.e., bring $\hat{f}^2_{\phi,\omega}/4\pi$ closer to $\bar{f}^2_{\phi,\omega}/4\pi$. Our exploratory work indicates that this may be possible; but because of the large number of parameters, as well as model uncertainties, there is certainly no unique way to do this.

We conclude that although VMD together with mixing can probably give an adequate description of both ϕ and ω photoproduction, the determination of the physical parameters involved is a very delicate question. Probably both improved experiments (hopefully at higher energies to reduce the $t_{\min}$ effect—especially for the ϕ) and external theoretical considerations to restrict the number of free parameters will be required to complete this determination.

Another possibility should be mentioned. Aviv *et al.* (1975) have given arguments that photoproduction of higher vector mesons (J/ψ, for example) is suppressed relative to VMD. This is due to a combination of the lack of perfect overlap of different final states when produced by a photon or a vector meson and by $t_{\min}$ effects, which are different for different processes. The expected effect is large for the J/ψ (a factor of order two reduction in the diffractive amplitude relative to VMD). Presumably such effects are small in the case of the ρ^0, which has a mass well above its decay threshold. However, it is conceivable that it could begin to play a role for the ϕ, and possibly the ω, and that some of the difficulty in fitting photoproduction of these particles could be eliminated if we had an understanding of these effects at the 10%–20% level.

E. Phases of vector-meson photoproduction amplitudes: decay into lepton pairs

In this review we have used the leptonic decay of the vector mesons to determine their coupling to the photon. By studying high-energy photoproduction of lepton pairs, with invariant mass in the ρ^0, ω, and ϕ regions, it is possible to check on our notions of coherent photoproduction. The interference of the amplitude from vector-meson decay with that from ordinary quantum electrodynamics (Bethe–Heitler amplitude) permits the determination of the phases of the vector-meson production amplitudes. As alluded to in the previous section, e^+e^- pairs in the ϕ region (Alvensleben *et al.*, 1971b) contain few surprises and are consistent with a dominantly diffractive picture of production. However, because the narrow ω resonance lies right in the middle of the wide ρ^0 mass distribution, the ρ^0 and ω cases are not so simple.

DESY–MIT (Alvensleben *et al.*, 1970d, 1971b) and Daresbury (Biggs *et al.*, 1971) groups have studied with high resolution e^+e^- pairs from beryllium with 6 GeV photons (DESY) and carbon with 4 GeV photons (Daresbury) and have analyzed the interference between the ρ^0 decay and Bethe–Heitler amplitudes. They report values for α_ρ of -0.21 ± 0.08 and -0.30 ± 0.12, respectively, which are within the range of values which give reasonable fits to photoproduction. These quoted errors are statistical and a bit optimistic, as systematic errors in quantities such as m_ρ were not included. If, for example, m_ρ were really 775 MeV, the DESY and Daresbury results would both increase by about 0.08 and 0.05, respectively. An anomalously large phase angle in leptonic decay, suggested by a model taking the $\pi^+\pi^-$ continuum into account in ρ^0 photoproduction (Bauer, 1970, 1971), while not excluded by these present results, is certainly not needed to understand them.

We now look at the features of ρ^0-ω interference in e^+e^- decay and find a rather puzzling situation. While the ρ^0 production phase, at these energies, is typical of diffractive hadronic processes, the *relative* ω, ρ^0 production phase angle, i.e., the additional phase angle acquired by the coherently photoproduced ω, is disturbingly large [$41° \pm 20°$: DESY–MIT, Alvensleben *et al.* (1970c, 1971c); $100° \pm 30°$: Daresbury, Biggs *et al.* (1970a)]. These large phase angles cannot be explained by a simple VMD model where photon-vector-meson couplings are real. The unusually large values were actually suspected earlier, on the basis of low-resolution data indicating that an unexpectedly small number of lepton pairs were photoproduced in the region of the ρ^0 mass (Asbury *et al.*, 1967b; Rothwell *et al.*, 1969).

We must bear in mind that the analysis of ω photoproduction from nuclei (Sec. IV.D) and the study of ρ^0-ω interference in pion pair photoproduction (Sec. IV.C) demand no such large relative ρ^0-ω production phase.

Moreover, the total integrated number of photoproduced lepton pairs in the ρ^0 region is highly sensitive to ρ^0 parameters. The nature of the ω contribution, which is at most of order 30%, could easily be obscured by uncertainties in $\hat{f}_\rho$.[45]

In short, these experiments are very difficult to analyze, and we hesitate to draw any firm conclusions from their results at this time.

F. Model of vector-meson amplitudes for further applications

Theoretically, the real part of a hadron's scattering amplitude may be computed from a forward dispersion relation, thus relating α to the energy dependence of the total cross section. [We ignore complications arising from the instability of the particles under consideration (Bauer, 1970, 1971), which could give additional real parts.] Since the energy dependence of the vector-meson total cross sections has not been systematically measured, we adopt the following quark-model estimates (for the region of 2–30 GeV):

$$\sigma_{\rho^0} \approx \sigma_\omega \approx \frac{1}{2}(\sigma_{\pi^+ p} + \sigma_{\pi^- p}) = 20.8\left(1 + \frac{0.766}{\sqrt{p}}\right) \text{ mb} \quad (4.4a)$$

$$\sigma_\phi \approx 12 \text{ mb}. \quad (4.4b)$$

Equation (4.4a) is from a fit to the data of Foley *et al.* (1967), and is compatible with the results of Sec. IV.C for σ_ρ. These estimates for σ_ω and σ_ϕ are not contradicted by the data; but with all the uncertainties described in Sec. IV.D, our knowledge of these parameters is extremely uncertain. Equation (4.4b) is from Lipkin (1975), who also gives a quark-model estimate of the energy dependence of σ_ϕ which we choose to ignore here.

The energy dependence in Eq. (4.4) suggests the following values of α_V:

$$\alpha_\rho = \alpha_\omega = 0.766/(\sqrt{p} + 0.766), \quad (4.5a)$$

$$\alpha_\phi = 0. \quad (4.5b)$$

However, the dispersion relations for the real part of the forward scattering amplitude require at least one subtraction, introducing a new constant. In the real photon case, the corresponding term is simply the Thompson amplitude. We may allow for this additional constant by replacing (4.5) by

$$\alpha_{\rho,\omega} = -\left(\frac{0.766}{\sqrt{p}} + \frac{S_{\rho,\omega}}{p}\right) \Big/ \left(1 + \frac{0.766}{\sqrt{p}}\right) \quad (4.6a)$$

$$\alpha_\phi = -\frac{S_\phi}{p}. \quad (4.6b)$$

If the S_V are nonvanishing, there is no reason to expect that they bear a simple relationship to each other, so that the ϕ and ω could have different real parts, as suggested by the data in Sec. IV.E.

[45] In the approximation where $\hat{f}_V = \bar{f}_V = f_V$, the integrated ρ contribution is equal to the ρ^0 photoproduction cross section times something of order f_ρ^{-4}.

V. QUALITATIVE TESTS OF VMD–PHOTON SHADOWING

A. Introduction

In Sec. II.E, we described how the hadronic structure of the photon should manifest itself in the behavior of the total photon cross section for a nucleus and of individual nondiffractive photon reactions on nuclei. To recast the argument in different language, since the total hadronic photon-nucleon cross section is only ~100 μb, the nuclear mean free path of photons is of the order of 500 F, which is much greater than a nuclear radius. Thus one's first thought might be that each nucleon is equally able to participate in an interaction, and the total cross section should be the sum of the separate one-nucleon cross sections. That is, the quantity

$$\frac{A_{\text{eff}}}{A} \equiv \frac{\sigma_{\gamma A}}{Z\sigma_{\gamma p} + N\sigma_{\gamma n}} \quad (5.1)$$

should be equal to 1. However, because of its hadronic structure, we expect the photon's ability to initiate interactions to be strongly attenuated as it passes through the nucleus. After the photon has encountered one or two nucleons, its hadronic constituents will be stripped away, leaving only a bare photon that is incapable of further interaction. This is known as *photon shadowing*. When this happens, the ratio (5.1) will be noticeably smaller than unity. Photon shadowing should be an energy-dependent effect, since the formation time of a constituent, which rises linearly with ν, must be larger than the mean free path in order for shadowing to occur. An additional consequence of shadowing is some reduction of Compton scattering because the dominant imaginary part of the scattering amplitude is reduced. Qualitatively, these expected effects are present in the data, as may be seen in the figures of Secs. III.A and B.

In the case of individual nondiffractive channels, the theoretical picture is more complicated, since the outgoing particles might participate in further reactions before emerging from the nucleus. Because of an inadequate theoretical understanding of these processes, we limit our discussion to single-particle photoproduction. We assume that the desired particle is produced on a single nucleon either by a photon directly or by the hadronic component of the photon. (It is still necessary, of course, to take into account the possible loss of the particle due to absorption on the way out of the nucleus.) The resulting cross sections are again predicted to depend on the photon energy. In the absence of photon shadowing (low energies), the photon could penetrate most of the way through the nucleus before producing a particle, which could then easily get out. If the photon is shadowed (high energies), the production takes place on the edges of the nucleus; and the cross sections are accordingly reduced.

As will be seen later, under the assumption of pure VMD, the expected magnitude and energy dependence of these shadowing effects is quite dramatic. Experimentally, the shadowing is not as large as predicted and the energy dependence is not seen in particle produc-

tion. However, the quantitative failure of this simple model should not be viewed with too much disappointment as the tests are quite demanding. Because the importance of photon constituents not shadowed relative to those constituents that are shadowed increases rapidly with A (more nucleons participate in unshadowed reactions), the tests are very sensitive to VMD violations.

B. Total absorption of real photons

As mentioned in Sec. II.E, a complete analysis of this process would involve a complicated coupled-channel calculation in which all hadronic components of the photon could be involved at each stage. A discussion of this sort has been given by Gribov (1969) and Brodsky and Pumplin (1969) within the framework of generalized vector dominance. Their arguments show that there should be photon shadowing at asymptotically high energies. The amount of shadowing obtained would depend on the details of the transition amplitudes between different channels. In particular, Gribov argues that if all hadronic channels are totally absorbed on the nucleus, the total cross section should become

$$\sigma_{\gamma A} \approx 2\pi R^2(1 - Z_3), \tag{5.2}$$

where R is the nuclear radius and $1 - Z_3$ is the probability for the photon to be made of hadrons.

However, for real nuclei the "total absorption" limit may be unattainable. For one thing, peripheral hadronic collisions with finite nuclei do not show complete absorption. More fundamentally, however, the presence of destructive interference among various photon constituents could severely reduce the hadronic interaction probability, increasing the mean free path well beyond reasonable nuclear sizes. Moreover, recall that, because of their short formation time (Sec. II.C), higher-mass photon constituents may not be shadowed at finite energies, and they might therefore provide contributions equivalent to direct photon interactions.

At the present time, we have very little real evidence about the actual behavior of the higher-mass constituents of the photon other than that their net effect on the total cross section is very small ($\lesssim$20%). We seem to have good information about the ρ^0, and some strong prejudices about the ω and ϕ, as summarized in Sec. IV.F. (Our confidence in this knowledge could be misplaced, since we have ignored the possible interfering role of other constituents of the photon on these channels in photoproduction.) In the present section, we want to use the knowledge which seems reasonably firm, and save speculations about the behavior of the higher-mass constituents until Secs. V.E and VI.B.

Even though we restrict our main attention to the ρ^0, ω, and ϕ contributions, there is still more generality than we would like to deal with at the moment. For example, in addition to amplitudes involving only one vector meson, we should in principle also consider amplitudes in which transitions between the vector-meson states occur (known as "off-diagonal terms"). Naive VMD neglects off-diagonal terms,[46] thereby giving the following relations between amplitudes:[15]

$$T_{\gamma\gamma}^{(V)}(t) = \frac{e}{\bar{f}_V} T_{\gamma V}(t) = \frac{e^2}{\bar{f}_V^2} T_{VV}(t). \tag{5.3}$$

Here T_{VV} is the scattering amplitude for a vector meson V on a nucleon, $T_{\gamma V}$ is the amplitude for photoproduction of V, and $T_{\gamma\gamma}^{(V)}$ is the contribution of V to the Compton scattering amplitude. Only the right-hand equality in (5.3) is subject to experimental investigation. In principle, one determines the coupling $\bar{f}_V$ from $e^+e^- \to V$ and compares it to $\hat{f}_V$ (see Table I) extracted from the photoproduction experiments (see Secs. IV.C, D). Qualitatively, at least for the ρ^0—we consider ω and ϕ contributions relatively unimportant in our present discussion—VMD appears to play the dominant role in the connection between these amplitudes, so that the right equality is satisfied within the ambiguities described in Appendix C. Subject to those uncertainties, if one uses the left-hand equality to estimate the vector-meson contribution to the total photon cross section (2.11), the result is that they contribute about 80%.

At the current level of modeling and of experimental data, deviations from Eq. (5.3) are probably indistinguishable from other possible physical effects. In principle, we may take σ_V, $T_{\gamma V}(t)$, and σ_γ, our ingredients in shadowing calculations, directly from the photoproduction analyses of Secs. IV.C, D and the total cross-section measurements described in Sec. III.A. So, while naive VMD is certainly the theoretical picture, our *quantitative* analyses depend only weakly on Eq. (5.3) (Mennessier and Nachtmann, 1971).

In the models to be discussed below, we include, in addition to the contributions of the ρ^0, ω, and ϕ, possible unshadowed photon interactions. Physically such terms have the same properties as heavy-mass constituents that have negligible shadowing at current energies. One might also include a nonresonant two-pion contribution (Yennie, 1975), which is more effectively shadowed than the ρ^0. However, ambiguities involved in separating such a contribution from the ρ^0 itself are too large to make this refinement worthwhile. Therefore we regard the complete dipion contribution as accounted for by an effective ρ^0 contribution.

●There is one feature of the physics that must be mentioned at this point. Study of the space-time behavior of forward Compton scattering shows that the energy-independent diffractive part has the largest longitudinal range, while contributions which drop with energy have shorter ranges (suri and Yennie, 1972). This was described briefly in Sec. II.C. Thus the nondiffractive terms might be expected to be less shadowed. Our naive calculations take no account of this effect and in-

[46] At high energies $\rho^0 \rightleftarrows \omega, \phi$ transitions should be negligible as they involve I-spin interchange. On the other hand, $\phi \rightleftarrows \omega$ transitions, which involve no such I-spin interchange and could be diffractive, should also be unimportant since the total ϕ and ω contribution to the total photon cross section is small (~10%). These conjectures are made relative to what we believe to be other, more considerable uncertainties in the VMD model of photon absorption.

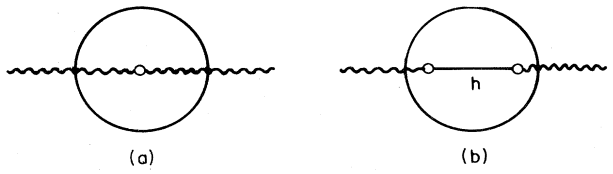

FIG. 201. High-energy photon elastically scattering from a nucleus. The imaginary part of the forward amplitude yields the total cross section. (a) The photon scatters from a single nucleon. (b) Scattering through intermediate hadronic states "h".

clude the entire (energy-dependent) V-nucleon cross section in the Glauber formalism. It is possible that at lower energies we overestimate the amount of shadowing.

The optical-model formalism based on these assumptions has been given by several authors, and the derivation from Glauber multiple scattering theory is sketched in Appendix B. Articles containing formalism relevant to photon reactions are Glauber (1959, 1970), Ross and Stodolsky (1966), Drell and Trefil (1966), von Bochmann, Margolis, and Tang (1969), Moniz and Nixon (1971), and Yennie (1971). See Sec. II.B for the early history of photon shadowing theory and experiment.

Using the optical theorem, the total cross section is given by the imaginary part of the forward Compton scattering amplitude. The Glauber multiple scattering expression for this amplitude is represented by Fig. 201. Part (a) represents the scattering from individual nucleons with amplitude $T_{\gamma\gamma}$, which is called the one-step amplitude. Part (b) is the contribution from intermediate hadronic states (approximated by vector mesons) which are produced on one nucleon, scatter through the nucleus, and change back to a photon on another nucleon, all processes being coherent. It is called the two-step amplitude. When summed over all nucleons, part (a) would clearly lead to an amplitude proportional to A or the nuclear volume. Shadowing results from a destructive interference between the two amplitudes that cancels all or most of this volume term, leaving a surface term, varying roughly as $A^{2/3}$.

The optical-model approximation to the multiple scattering expansion for $A_{\rm eff}$ is

$$A_{\rm eff}=\frac{4\sqrt{\pi}}{\sigma_\gamma}\,\mathrm{Im}\left\{A\,T_{\gamma\gamma}-\sum_V 2\sqrt{\pi}\,iT_{\gamma V}^2\int d^2b\,dz_1dz_2\tilde{n}(\mathbf{b},z_1)\tilde{n}(\mathbf{b},z_2)\right.$$
$$\left.\times\,\theta(z_2-z_1)e^{-iq_\parallel^{(V)}(z_1-z_2)}\exp\left(-\tfrac{1}{2}\sigma_V(1-i\alpha_V)\int_{z_1}^{z_2}\tilde{n}(\mathbf{b},z')dz'\right)\right\}. \tag{5.4}$$

Here $T_{\gamma\gamma}$ is a suitably weighted average of neutron and proton amplitudes, normalized so that $d\sigma_{\gamma\gamma}/dt=|T_{\gamma\gamma}|^2$, and $\sigma_\gamma\equiv 4\sqrt{\pi}\,\mathrm{Im}T_{\gamma\gamma}$. $q_\parallel^{(V)}$ is the difference between the photon and vector-meson wave numbers. For real photons

$$q_\parallel^{(V)}=k-\sqrt{k^2-m_V^2}\approx\frac{m_V^2}{2k} \tag{5.5a}$$

while for virtual photons

$$q_\parallel^{(V)}=\sqrt{Q^2+\nu^2}-\sqrt{\nu^2-m_V^2}\approx\frac{m_V^2+Q^2}{2\nu}. \tag{5.5b}$$

This is just the reciprocal of the formation time of the constituent discussed in Sec. II.C.[47]

The identification of the two terms of (5.4) with the two contributions of Fig. 201 is clear. The oscillating phase factor in (5.4) is of crucial importance in determining the energy dependence of shadowing. When $1/q_\parallel^{(V)}$ is much smaller than the mean free path (small ν or large $m_V^2+Q^2$), the factor oscillates rapidly and the integral in (5.4) will be small. V will then not contribute to shadowing. At sufficiently high energies, the phase factor may be replaced by 1 and the z_1 and z_2 integrations may be carried out explicitly with the result

$$A_{\rm eff}=A\left(1-\frac{\mathrm{Im}\sum_V T_{\gamma\gamma}^{(V)}}{\mathrm{Im}\,T_{\gamma\gamma}}\right)+\sum_V\frac{e^2}{f_V^2}\sigma_{VA}/\sigma_{\gamma\gamma}\,, \tag{5.6}$$

where

$$\sigma_{VA}=2\,\mathrm{Re}\int d^2b\;\;1-\exp\left[\left(-\frac{\sigma_V}{2}(1-i\alpha_V)\int_{-\infty}^{\infty}\tilde{n}(\mathbf{b},z')dz'\right)\right].$$

If the vector mesons saturate the total cross section, the term proportional to A vanishes, and we find that VMD in two-body reactions implies VMD for the total photon cross section on a nucleus. Since σ_{VA} is a hadronic cross section, it is expected to show shadowing, the exact amount depending on the two-body total cross section. The result (5.6) is more general than our derivation; it can be shown within the framework of the Glauber multiple scattering theory without further approximations about nuclear wave functions, etc.—see Yennie (1971).

Let us now turn to a comparison of some simple theoretical models and experiments for real photons ($Q^2=0$). The discussion for virtual photons is given later, in Sec. V.E. The experiments by groups at Cornell, Daresbury, DESY, and UCSB–SLAC to measure total photoabsorbtion cross sections from complex nuclei as well as from hydrogen and deuterium are described in Sec. III.A.

Here is a brief summary of the scope of each experiment:

[47] In addition, a VMD calculation of Eq. (5.4) for virtual photons requires the replacement of e/f_V by $e/f_V[m_V^2/(m_V^2+Q^2)]$, because of the Q^2 dependence of the vector-meson propagators.

(1) The UCSB–SLAC experiment reported shadowing results for three nuclei (C, Cu, Pb) covering an energy range from 4 to 18 GeV; their data are consistent with no energy dependence for $A_{\rm eff}/A$. The Daresbury and DESY experiments were restricted to lower energies (~2-4 GeV and ~1.5–6 GeV, respectively). The Daresbury group used a wide range of nuclei; the DESY experiment had no heavy nuclei [titanium ($A=48$) was their largest]. If one ignores the possible existence of different systematic errors between these three experiments, the overall impression one obtains is that the shadowing increases as energy increases. The Cornell experiment explores the energy region from 2–9.5 GeV with better accuracy than the previous experiments and uses several nuclei spanning the periodic table. Their results show a clear energy dependence for most nuclei.

(2) Next, let us summarize the results for a few key nuclei. C: There seems to be no basic conflict between the various experiments, but there is considerable scattering of the experimental points from the different groups. Cu: The Cornell points are marginally higher than those of UCSB–SLAC; they are also higher than the DESY results for Ti, which is a lighter nucleus. Pb(Au): The Cornell points lie higher than the UCSB–SLAC points by about two standard deviations (of UCSB–SLAC). This should be interpreted as a disagreement, but in view of the rather different systematic errors in the two experiments, not an implausibly large one.

(3) In addition to these experiments, a Cornell group (Eickmeyer *et al.*, 1976) has carried out an inelastic electron scattering experiment at small Q^2 (= 0.1 GeV^2); this is discussed in Sec. III.J. When combined with the real photon Cornell experiment, it shows a smooth Q^2 dependence in this region.

TABLE XXXV. Information for model calculations of total photon cross sections (all cross sections are averaged for proton and neutron).

1. Effective coupling constant choice

$$\frac{f_V^2}{4\pi}_{\rm eff} \equiv \left(\frac{\bar f_V^2}{4\pi}\cdot\frac{\hat f_V^2}{4\pi}\right)^{1/2}$$
$$= 2.20 \text{ for } \rho^0$$
$$= 23.6 \text{ for } \omega$$
$$= 18.4 \text{ for } \phi$$

2. VMD models

Model I (Reference model): amplitudes from (4.4) and (4.5).

$$\sigma_{\rho 0}=\sigma_\omega = 20.8\left(1+\frac{0.766}{\sqrt{p}}\right)\text{ mb};\quad \sigma_\phi = 12\text{ mb}$$

$$\alpha_{\rho 0}=\alpha_\omega = 0.766/(\sqrt{p}+0.766),\quad \alpha_\phi = 0$$

Yielding:

$$\sigma_\gamma^{(\rho^0)} = \left(69.0+\frac{52.9}{\sqrt{p}}\right)\mu\text{b}$$

$$\sigma_\gamma^{(\omega)} = \left(6.4+\frac{4.9}{\sqrt{p}}\right)\mu\text{b}$$

$$\sigma_\gamma^{(\phi)} = 4.8\ \mu\text{b}.$$

This is supplemented by an energy-independent nonshadowed (NS) contribution (adjusted to make $\sigma_\gamma = 120\ \mu$b at 6 GeV):

$$\sigma_\gamma^{\rm NS} = 16.2\ \mu\text{b}.$$

In this model

$$\sigma_\gamma^{(\rm I)} = \left(96.4+\frac{57.8}{\sqrt{p}}\right)\mu\text{b},$$

while the experimental fit from Table III is

$$\sigma_\gamma = \left((99.1\pm1.9)+\frac{51.8\pm3.6}{\sqrt{p}}\right)\mu\text{b}.$$

Model II
Like Model I except that the asymptotic values of σ_ρ and σ_ω are reduced to 19.1 mb, yielding

$$\sigma_\gamma^{(\rm II)} = \left(98.4+\frac{52.9}{\sqrt{p}}\right)\mu\text{b}$$

with

$$\sigma_\gamma^{(\rm NS)} = 24.5\ \mu\text{b}.$$

Model III
Like Model I except that only the constant parts of $\sigma_{\rho 0}$ and σ_ω are used in the shadowing calculation and the energy-dependent parts (including the α_V) are included in the nonshadowed piece which becomes

$$\sigma_\gamma^{(\rm NS)} = \left(16.2+\frac{57.8}{\sqrt{p}}\right)\mu\text{b}.$$

Model IV
Like Model I except that the decay width of the ρ^0 is taken into approximate account by adding a small negative imaginary part to m_ρ.[48] Specifically, in Eq. (5.4a) $m_\rho^2/2k$ becomes $(m_\rho^2 - im_\rho\Gamma_\rho)/2k$, where Γ_ρ is taken to be 145 MeV.

(Models V and VI are included for "historical" reference only and probably are not good representations of the complete physics.)

Model V
Like Model I except that $\sigma_\gamma^{\rm NS}$ is taken to be 0 so that

$$\sigma_\gamma \equiv \sigma_\gamma^{(\rho^0)} + \sigma_\gamma^{(\omega)} + \sigma_\gamma^{(\phi)}\ \text{(Complete VMD)}.$$

Model VI
Like Model I except all two-body cross sections are taken to be energy independent and constrained at their 6 GeV values.

$$\sigma_{\rho 0}=\sigma_\omega = 27.3\text{ mb},\quad \sigma_\phi = 12.0\text{ mb}$$

$$\alpha_{\rho 0}=\alpha_\omega = 0.24,\quad \alpha_\phi = 0$$

Yielding:

$$\sigma_\gamma^{(\rho^0)} + \sigma_\gamma^{(\omega)} + \sigma_\gamma^{(\phi)} = 104\ \mu\text{b}$$

$$\sigma_\gamma^{(\rm NS)} = 16\ \mu\text{b}$$

and

$$\sigma_\gamma = 120\ \mu\text{b}.$$

●As described in Sec.III.A, various groups have made different corrections to the deuteron cross section in determining the free neutron cross section to be used in experimental ratio (3.9). The size of these corrections is shown in Fig. 28, and a critique of them is given in Appendix B.4. Our opinion is that the total correction is approximately the sum of the Glauber and West contributions (7μb) but that the overall uncertainty is of the order of the West correction (3μb). The complete correction increases the denominator of (3.9) by about 3.5% in heavy nuclei. For uniformity, this correction has been applied to all the data.

In order to separate the comparison of the data with the theory from the discussion of the model dependence of the theory, we shall use reference models which incorporate the available information on the vector-meson cross sections and coupling constants. The parameters and features of these VMD models are given in Table XXXV as model I and II. Basically model I incorporates Eqs. (4.5) and (4.6) for the vector-meson scattering amplitudes and the left-hand equality of Eq. (5.3). $T_{\gamma V}$ is taken from experiment (this accounts for the effective $\bar{f}_V^2$ relating $T_{\gamma\gamma}^{(V)}$ and T_{VV}). To complete the total photon cross section, this model assumes a nonshadowed energy-independent contribution. Model II has slightly different parameters. In the comparison with data, Figs. 35–39, these two models are shown to allow for such model uncertainties. As can be seen, they overlap the data well for the Daresbury, DESY, and UCSB experiments, but lie somewhat below the Cornell data for the heavier nuclei.

In our subjective judgment, models I and II represent a reasonably complete treatment of the physics of the ρ^0, ω, and ϕ. However, they lump all remaining contributions together as unshadowed and energy-independent. This is certainly an oversimplification, but neglected effects may well be within the "noise" of other uncertainties. Models III and IV are crude attempts to take into account some additional refinements in the physics; model III allows only the diffractive part of the total photon cross section to be shadowed, while model IV includes a simplified treatment of ρ^0 decay within the nucleus.[48]

In addition, for reference, Table XXXV describes two models (V and VI) that approximate the physics used in early preliminary analyses. Model V is a pure VMD model with no unshadowed part; and model VI, while including some unshadowed contribution, ignores any energy dependence in the two-body amplitudes.

$A_{\rm eff}/A$ for Pb, Cu, and C has been computed over the photon energy range of 2–15 GeV for all six models and plotted in Fig. 202. The nuclear computation included realistic nuclear shapes plus two-body "smearing" and correlations (see Appendix B).

In studying models I, II, IV, and V, we note that one effect of incorporating energy-dependent vector-meson cross sections is to make $A_{\rm eff}/A$ very nearly energy independent for photon energies above 4 GeV, as first pointed out by von Bochmann, Margolis, and Tang (1970).

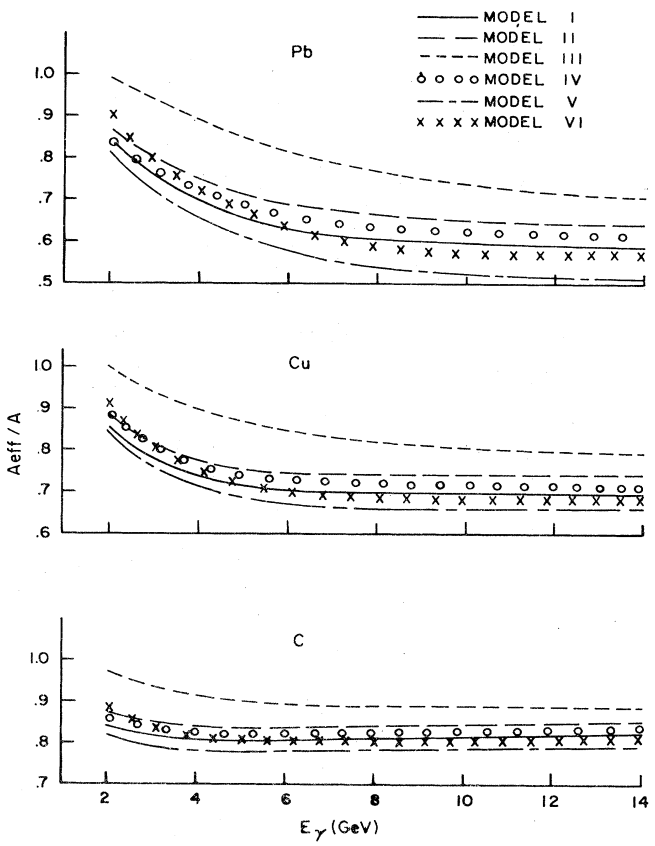

FIG. 202. Predictions of various models for $A_{\rm eff}/A$ for Pb, Cu, and C with real photons of energies 2–15 GeV. The models are as described in the text and Table XXXV.

Note also how the nonshadowed term in models I–IV acts to raise $A_{\rm eff}/A$ above that predicted by pure VMD (model V), as first pointed out by Brodsky, Close, and Gunion (1972b) and Caldwell *et al.* (1973). It is in the spirit of this section to discuss only models which are based on well-founded information about the light vector mesons (ρ^0, ω, and ϕ). Speculations about the higher-mass contributions are described in Sec.VI.B, but no comprehensive comparisons are presented in this paper. However, another simple model has recently been presented (Talman, 1977) which also emphasizes low-mass mesons (ρ^0, ω, ϕ, and ρ') and gives somewhat better agreement with the Cornell data than do models I and II.

Talman's results agree numerically quite well with our model VI, but we emphasize that the physics is very different. Practical differences between his and the models described here arise, we believe, from the use of nuclear and ρ^0, ω, or ϕ parameters different from those recommended or "favored" in this paper.

●In Talman's approach, the selection of optical-model parameters leads in the end to a result which at high energy agrees with our model II. This is probably a consequence of the fact that he restricts his nuclear radius parameter so as to fit the neutron total cross section. In our model, we use electron scattering results to determine the nuclear shape, and confirm that it correctly predicts the same cross sections. Thus,

[48]Our treatment of the ρ^0-decay effect is based on a suggestion by R. M. Talman (1977).

although the models are superficially rather different, there is suitable compensation between various rather small effects to produce agreement in cross sections where there is no longitudinal momentum transfer. Why does his cross section rise above model II at low energies? This appears to be a consequence of a different choice of vector-meson parameters. His model puts about 10% of the total photon cross section into the ρ', reducing the ρ^0, ω, and ϕ contributions accordingly. Since the ρ' is less shadowed at low energies, this can account qualitatively for the difference between the two curves. The Cornell data by themselves then suggest that moderately high-mass contributions play a more important role than our models suggest, or that the nondiffractive contributions are less shadowed than would follow from a simple VMD estimate. If so, it could be because we overestimated the ρ^0, ω, and ϕ contributions (anyhow it is difficult to get the small high-mass contributions by subtraction), or because off-diagonal contributions reduce their effect.

●We now turn to some conceptual differences between the Talman model and the one used here. His model is often referred to as a "self-absorption" model. This is an unfortunately misleading term since it seems to imply that absorption inside a single nucleon is not taken into account by the Glauber model; it is (see Appendix B). The real difference is that he treats the nucleus as a continuum of nuclear matter with the same internal density as a single nucleon. That is, he ignores the "granular" structure of the nucleus. Mathematically, this aspect of his model can be mocked by the Glauber model by choosing the correlation length to be about four times the one used in our calculations, which increases the nuclear absorption. Although this sounds like a big effect, it does not lead to a large change in the total cross section because the nucleus is already quite opaque. In any case, Talman adjusts the nuclear radius (uniform density) to obtain the correct neutron total cross sections. As mentioned in the preceding paragraph, this leads to compensations between various effects so that the total cross section of, for example, the ρ^0 meson on a nucleus would differ by at most a few percent between the two models.

C. Nuclear Compton scattering

As reported in Sec.III.B, a group at DESY (Criegee *et al.*, 1977a) measured small-angle Compton scattering from nuclei at 3 and 5 GeV. An optical model was used to extrapolate the cross sections to the forward direction, after which the quantity

$$R \equiv \left. \frac{d\sigma/dt(\gamma A \to \gamma A)}{A^2 d\sigma/dt(\gamma N \to \gamma N)} \right|_{\theta=0} \tag{5.7}$$

was calculated for comparison with theoretical predictions. In the absence of photon shadowing, R would be 1.

The optical-model expression for the nuclear forward Compton amplitude is simply the right-hand side of Eq. (5.4) multiplied by $\sigma_\gamma/4\sqrt{\pi}$ with the "Im" removed. Indeed, the real part of the nuclear amplitude is of great importance in the interpretation of this process. Specifically, the optical theorem relates the forward Compton cross section to σ_γ through

$$\left. \frac{d\sigma}{dt} \right|_{\theta=0} = \frac{\sigma_\gamma^2}{16\pi}(1+\alpha_\gamma^2) . \tag{5.8}$$

In Eq. (5.8), which applies equally well to nuclei and nucleons, α_γ is the ratio of real to imaginary parts of the forward Compton amplitude.

Figure 53 gives a comparison of the data with optical-model calculations using the preceding section's models I and II for the two-body amplitudes. Several comments are in order:

(1) All the experimental points lie well below $R=1$, confirming the existence of shadowing.

(2) At 5 GeV, model I is systematically too low. That is, model I predicts too much shadowing (see remark 5 below).

(3) At 5 GeV, model II, which includes a 20% unshadowed contribution and gives a reasonable fit to the total cross sections (see Sec.V.B), does much better than model I. It is high for some nuclei and low for others and comes close to producing an acceptable fit. (However, see 5 below.)

(4) At 3 GeV, model I gives a reasonable fit to the data while Model II is systematically high. In our opinion, this is of less significance because of the uncertainties inherent in applying the optical model at such a low energy, especially in view of the importance of the nuclear real part which is sensitive to the oscillations of the "two-step" integral (see also 5 below). It is surely true, however, that there is more energy dependence in the theory than in the data.

(5) Remarks 2 through 4 above are clouded by uncertainty about the correct value of the single-nucleon Compton cross section, $d\sigma/dt(\gamma N \to \gamma N)$, to use in the denominator of (5.7). In their latest report (Criegee *et al.*, 1977a) the DESY experimenters use a neutron-proton weighted average

$$\left[\frac{Z}{A}\left(\frac{d\sigma}{dt}(\text{proton})\right)^{1/2} + \frac{N}{A}\left(\frac{d\sigma}{dt}(\text{neutron})\right)^{1/2} \right]^2$$

where $N \equiv A - Z$. While this seems quite reasonable, it must be noted that the cross sections they used were not the ones that they subsequently measured from hydrogen and deuterium, discussed in Sec.III.B (Criegee *et al.*, 1977b).

Two striking features of the group's two-body cross sections are: (i) they are quite consistent with a neutron-proton difference of zero and (ii) they are 5% to 10% lower than the results reported in Sec.III.B from other experiments, although consistent with those experiments within errors. These two features have opposite effects on the R values calculated [(i) tends to lower them, (ii) to raise them]. In any event, there is at least 5% normalization uncertainty in the figure which can obviously have a considerable impact on the agreement of theory with experiment. The experimental data shown in Fig. 53 have been normalized to $A^2 d\sigma/dt$ (proton) with $d\sigma/dt$ (proton) (5 GeV) = (0.82 ± 0.04) μb/GeV^2 and $d\sigma/dt$ (proton) (3 GeV) = 0.98 μb/GeV^2. The first value is as reported in Criegee *et al.* (1977b). The second value was calculated to keep the same *ratio* of 3 GeV and 5 GeV cross sections as used in Criegee *et*

al. (1977), since the group supplies no measurements at 3 GeV.

(6) An objection could be raised about the extrapolations to $t=0$ done by the DESY group since they did not allow for an unshadowed contribution in their optical model. However, Dr. G. Grammer (private communication) has done the extrapolation to $\theta=0$ with a 20% unshadowed contribution, and no significant changes resulted. We are grateful to Dr. Grammer for this information.

Not shown in Fig. 53 are calculations made by the present authors for Model III of Sec.V.B. In Model III, only the energy-independent part of the photon-nucleon cross section is shadowed and, as in Sec.V.B, the results of the model are far above the data—by more than we could reasonably attribute to the normalization uncertainties discussed above.

At this point, we wish to emphasize the importance of the real part of the nuclear Compton amplitude in the above discussion (Spital, 1975). The α_γ in Eq. (5.8) is of order 0.6 at 5 GeV in a heavy nucleus! The reason for this is that the two-step term not only decreases the imaginary part of the amplitude (shadowing), but also enhances the real part of the one-step term, thereby producing very large values of α_γ. Without the nuclear real part the optical-model calculations of R would be much lower.

We conclude this section by using Eq. (5.8) to compare nuclear Compton scattering directly with total cross-section measurements. Table XXXVI shows the measured values of $A_{\rm eff}/A$. The last column of the table is the result of taking the measured value of R, the optical-model value of the nuclear real part (α_γ) (model II), and forming the quantity $[R(1+\alpha_\gamma^2(N))/(1+\alpha_\gamma^2(A))]^{1/2}$, which should be directly comparable to $A_{\rm eff}/A$. The errors in the last column are the propagation of the errors in the measured value of R and do not take into account optical-model uncertainties or the normalization uncertainties in R itself. They are therefore misleadingly small. The obvious feature of the table is that the Compton scattering results are in reasonable agreement with either of the first two total cross-section measurements, but not with those of Michalowski, *et al.* (1977).

D. Incoherent photoproduction of mesons from complex nuclei

Several experimental groups have measured incoherent photoproduction of neutral pions, charged pions, and neutral ρ's from nuclei. Their results are shown in Figs. 151–153. Pion photoproduction which involves charge exchange or a nucleon spin flip excites the nucleus intrinsically. On the other hand, we observe incoherent ρ^0 photoproduction only when the momentum transfer is too large for coherent production. In all cases, we want to work at sufficiently large momentum transfer to avoid complications introduced by the Pauli principle, but not so large as to induce complicated incoherent events (see Appendix B).

The experiments have been described in Sec.III.H. The charged-pion data (Boyarski *et al.*, 1969) are very scanty and exhibit large error bars. Neutral-pion data (Meyer *et al.*, 1972) have better statistics and cover a fair range in energy, but the possibility of inelastic π^0 photoproduction is not ruled out (this fact might not affect the qualitative features of photon shadowing but it certainly is important in fitting data with specific models). Incoherent ρ^0 data (McClellan *et al.*, 1969c) have error bars slightly larger than those of the π^0 data and were taken for only three nuclei and two energies. Theoretical curves shown in Sec.III.H are VMD-optical-model calculations similar to those described below and (on some graphs) curves marked NPS (no photon shadowing). The latter curves neglect photon absorption and

TABLE XXXVI. Comparison of total and forward Compton cross sections at 5 GeV. $A_{\rm eff}/A$ is the experimental value for the total cross section, while the last column is the prediction from Compton scattering, including a model calculation correction for the real part of the amplitude. $\alpha_\gamma(A)$ is the value of $\mathrm{Re}T_{\gamma\gamma}(A)/\mathrm{Im}T_{\gamma\gamma}(A)$, and $\alpha_\gamma(N)$ is the value for a nucleon target.

A	$A_{\rm eff}/A$	R [d]	Model II calculated $\alpha_\gamma(A)$	$[R(1+\alpha_\gamma^2(N))/(1+\alpha_\gamma^2(A))]^{1/2}$
12	0.885 ± 0.029 [a] 0.82 ± 0.04 [b] 0.95 ± 0.05 [c]	0.784 ± 0.04	−0.36	0.87 ± 0.02
64	0.779 ± 0.047 [a] 0.67 ± 0.04 [b] 0.84 ± 0.03 [c]	0.605 ± 0.02	−0.48	0.73 ± 0.01
197	0.669 ± 0.065 [a] 0.72 ± 0.11 [b] 0.83 ± 0.04 [c]	0.648 ± 0.06	−0.59	0.72 ± 0.03

[a] From Caldwell *et al.* (1973). The actual energy for $A=12$ (C) and $A=64$ (Cu) was 5.2 GeV. The value shown for $A=197$ (Au) is actually an average for $A=207$ (Pb) at 4.1 and 6.6 GeV. Au and Pb are expected to exhibit almost identical shadowing characteristics.
[b] From Heynen *et al.* (1971).
[c] From Michalowski *et al.* (1977).
[d] From Criegee *et al.* (1977a).

take into account the absorption only of the final meson.

Unlike the total photon cross section, where $A_{\rm eff}/A$ provides a qualitative test of photon shadowing, interpretation of incoherent cross sections is always dependent on optical-model calculations. Since the incoherently produced particle can be absorbed on the way out of the nucleus, one always expects the cross section to be less than the single-particle cross section times the number of nucleons in the target nucleus. Therefore a study of these processes is not a "clean" test of photon shadowing. As we shall see later on, it is hard to make *any* single optical model fit to the data. However, the normalizations predicted by our optical models are roughly correct there is substantial evidence for some shadowing. However, our detailed VMD model typically predicts too much shadowing and fails to describe the data.

The optical-model expression for the incoherent photoproduction of a meson m in VMD, including only the simplest incoherent events of single-nucleon excitation (see Appendix B), is

$$\frac{d\sigma^{\rm inc}}{dt}(\gamma A\to mA')=\int d^2b\,dz\,n^m(\mathbf{b},z)\exp\left(-\sigma_m\int_z^\infty n(\mathbf{b},z')dz'\right)$$
$$\times\left|T_{\gamma m}(t)-\sum_v\frac{e}{\bar f_v}T_{vm}(t)\int_{-\infty}^z dz''n(\mathbf{b},z'')\frac{\sigma_v}{2}(1-i\alpha_v)\exp[iq_\parallel^v(z-z'')]\right.$$
$$\left.\times\exp\left(\frac{-\sigma_v}{2}(1-i\alpha_v)\int_{z''}^z dz'''n(\mathbf{b},z''')\right)\right|^2, \tag{5.9}$$

where $T_{\gamma m}(t)$ is the one-nucleon meson photoproduction amplitude, $T_{vm}(t)$ is the amplitude for the reaction $vN\to mN$, and $n^m(\mathbf{b},z)$ is the number density of the nucleons that can participate in the process:

$$n^{\rho^0,\pi^0}(\mathbf{b},z)=n(\mathbf{b},z),n^{\pi^+}(\mathbf{b},z)$$
$$=\frac{Z}{A}n(\mathbf{b},z),n^{\pi^-}(\mathbf{b},z)=\frac{A-Z}{A}n(\mathbf{b},z)\quad.$$

(We assume that neutrons and protons have the same spatial distribution.) Amplitudes are normalized so that $|T|^2=d\sigma/dt$; e.g., $|T_{\gamma m}|^2=d\sigma/dt(\gamma\to m)$.

The effective number of participating nucleons, $A_{\rm eff}$, is defined by

$$A_{\rm eff}=\frac{d\sigma^{\rm inc}}{dt}(\gamma A\to mA)/(|T_{\gamma m}(t)|^2)\,. \tag{5.10}$$

Equation (5.9) can now be rewritten as [using VMD to write $T_{\gamma m}(t)=\sum_v e/\bar f_v T_{vm}(t)$—see Eq. (2.7)]

$$A_{\rm eff}=\frac{1}{|T_{\gamma m}(t)|^2}\int d^2b\,dz\,n^m(\mathbf{b},z)\exp\left(-\sigma_m\int_z^\infty n(\mathbf{b},z')dz'\right)$$
$$\times\left|\sum_v\frac{e}{\bar f_v}I_{vm}(t)\left\{1-\int_{-\infty}^z dz''n(\mathbf{b},z'')\frac{1}{2}\sigma_v(1-i\alpha_v)\exp[iq_\parallel^{(v)}(z-z'')]\right.\right.$$
$$\left.\left.\times\exp\left(-\frac{\sigma_v}{2}(1-i\alpha_v)\int_{z''}^z n(\mathbf{b},z''')dz'''\right)\right\}\right|^2. \tag{5.11}$$

Note that if $\{\ \}$ is independent of the vector meson, $A_{\rm eff}$ is independent of t. This cannot be correct because it ignores the Pauli principle which suppresses the cross section at small t. Such suppression has in fact been observed, but the effect should be negligible for large t.

Equation (5.11) has a, by now familiar, simple physical interpretation. The meson is produced at the point $(\mathbf{b},z)$. The photon probability incident on that point is represented by the absolute square, which takes into account the absorption of the photon's hadronic constituents. The exponential involving σ_m represents the absorption of the meson on its way out of the nucleus. The theoretical curves labeled NPS are those of Eq. (5.11) where $\sigma_v\to 0$, or where the term inside the brackets, $\{\ \},=1$.

Due to the absorption of the meson, $A_{\rm eff}$ will always be less than the total number of participating nucleons even if photon shadowing were absent. At low energies (large $q_\parallel$) the two-step contribution to the amplitude oscillates away, as before, leaving us with no shadowing. At high energies ($q_\parallel\to 0$), the absolute square in Eq. (5.11) can be simplified, giving

$$\left|\ \ \right|^2=\left|\sum_v\frac{e}{\bar f_v}T_{vm}\exp\left(-\frac{\sigma_v}{2}(1-i\alpha_v)\int_{-\infty}^z n(\mathbf{b},z'')dz''\right)\right|^2 \tag{5.12}$$

and hence the shadowing associated with νA scattering. Once again, therefore, some decrease of A_{eff} with k is anticipated.

In our computations we have assumed an energy-dependent cross section $\sigma_{\pi^0_0}^{\pm} = \sigma_\rho$ and relative real part $\alpha_{\pi^0_0}^{\pm} = \alpha_\rho$ with values similar to Model I described in Sec.V.B.[49] Since the cross sections are decreasing with energy, the energy dependence anticipated in the VMD model for A_{eff} is somewhat softened (von Bochmann and Margolis, 1969); and for no photon shadowing our results for A_{eff} actually rise with energy. In the processes under consideration, we expect that the ρ^0 and ω may be the primary contributors to the amplitude. If so, $q_{\parallel}^{(\omega)} \simeq q_{\parallel}^{(\rho^0)}$ and $\sigma_\omega \approx \sigma_\rho$, $\alpha_\omega \approx \alpha_\rho$, and Eq. (5.11) simplifies further. We have made this simplifying assumption in our calculation.

Referring back to Sec.III.H, one cannot help but notice in the data of Figs. 151–153 the absence of the dramatic energy and A dependence expected from VMD. However, we note that the VMD curves predict roughly the normalization of the incoherent ρ^0 experiment but fall below the pion data. In almost all cases "no photon shadowing" (NPS) predictions are far above the data.

Other authors (Boyarski *et al.*, 1969; von Bochmann, Margolis, and Tang, 1970; von Bochmann, 1972a) have obtained reasonable agreement between VMD and the charged-pion experiment by normalizing the theory and experiment at each value of t and/or by normalizing theory and experiment to carbon values. We consider the value of these procedures to be highly questionable. In the first place, the data of the experiment have rather large uncertainties and these normalization procedures detract even further from the experiment's information content. More importantly, we feel that it is somewhat misleading to emphasize the A-dependence aspect when the normalization discrepancies between VMD theory and experiment are so large (in carbon at 8 GeV and $-t = 0.45$, it is nearly a factor of 2). If the optical model is so poor in calculating the magnitude of A_{eff}, we see no reason to place much faith in its A-dependence predictions.

As mentioned in Appendix B, there are several known corrections to our optical model of simple incoherent events that work in the direction of decreasing shadowing. Some illustrative calculations of these effects are shown in Fig. 203 (A_{eff} is computed for the case where all A nucleons can participate in the incoherent production). One effect is called the "correlation-absorption correction". It refers to the fact that, if the projectile has an incoherent interaction with one target nucleon, there is a one-particle "hole" in the nuclear matter density nearby, which reduces the absorption of the incident and outgoing particles. A proper calculation of this effect would be very difficult (it depends sensitively on knowledge of the correlation functions). Our estimates (probably overestimates of the correction) are based on treatments by von Bochmann, Margolis, and Tang (1969) and Yennie (1971).[50] Another effect is that

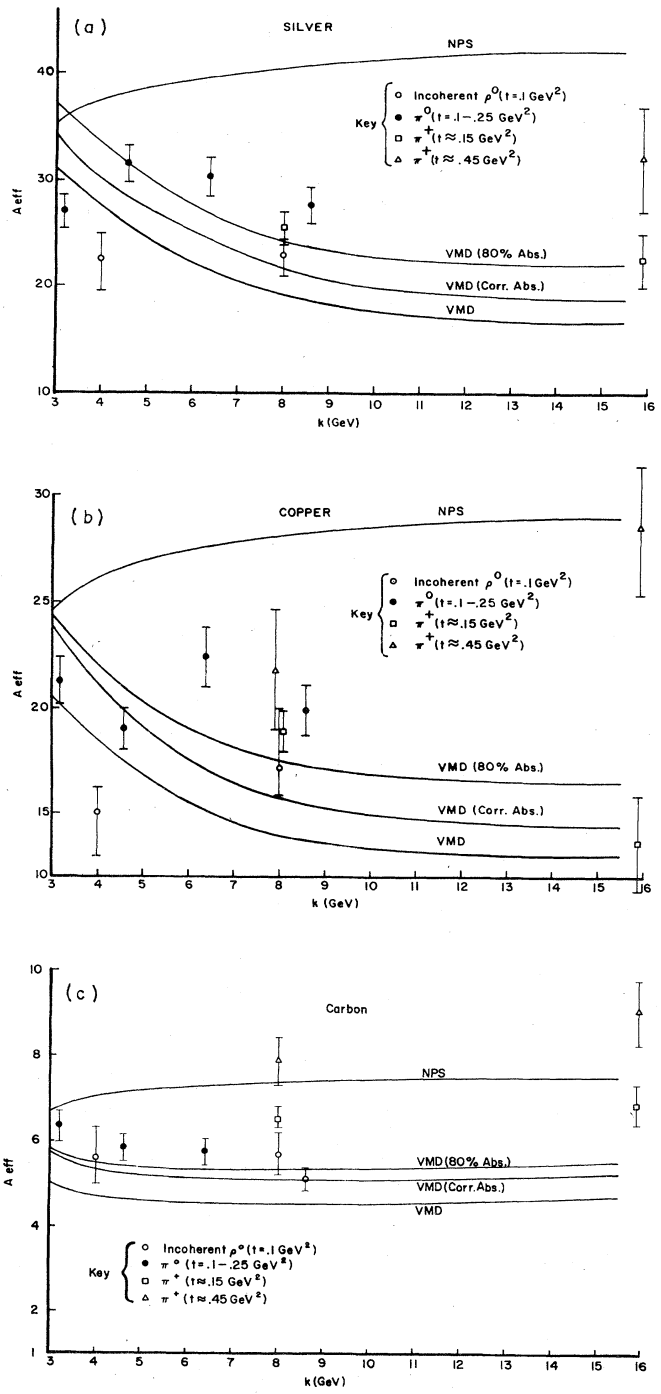

FIG. 203. (a) A_{eff} for ρ^0, π^0, and π^+ incoherent photoproduction from Ag. A_{eff} is shown as if A nucleons could participate in the process, i.e., the measured Z_{eff} for π^+ photoproduction is a factor Z/A smaller than shown here. The labels on the theoretical curves are as follows:

NPS: no photon shadowing.
VMD: production amplitude given by VMD.
VMD (Corr. Abs.): VMD with reduced absorption in vicinity of incoherent process.
VMD (80% Abs.): VMD with absorption based on $\sigma_{\text{abs}} (= \sigma_{\text{tot}} - \sigma_{\text{el}})$ rather than σ_{tot}.

(b) The same for Cu. (c) the same for C.

[49] We have assumed here that $\sigma_{\rho^0} = 22(1 + 1.15/\nu)$—in mb where ν is in GeV—and that $\alpha_{\rho^0} = \alpha_\gamma$, as given by Damashek and Gilman (1970).

[50] In these models n^m in Eq. (5.10) is enhanced by the factor $(1 + 2\sigma n^m l_c)$. $\sigma = \sigma_{\rho^0} = \sigma_{\pi^0_0}^{\pm}$ and $l_c \approx 0.3F$.

the use of the total two-body cross section overestimates the absorption of the projectile and produced particles. Clearly, elastically scattered particles are not lost to the process. They simply smear out the t distribution. The calculations labeled "80% absorption" attempt to compensate for this by using only the inelastic cross section in calculating absorption. Another procedure, better in principle, would be to calculate higher-order incoherent processes which include elastic scatterings (von Bochmann, Margolis, and Tang, 1970). However, in view of all the basic uncertainties in the model, we did not feel that the extensive effort was justified. We remind the reader that we have also not included the Pauli exclusion principle suppression of all incoherent events at small t. Such a calculation would be complicated by the fact that coherent absorption can provide a momentum transfer that permits incoherent events at small t. We see that various effects can increase or decrease the expected cross section in any basic model, affecting the normalization and A dependence of A_{eff} significantly. It is hard even to estimate quantitatively the level of reliability of our calculations.

In view of optical-model uncertainties, other approaches to the analysis of incoherent photoproduction would be useful. One possibility is to recognize that the optical-model computations of A_{eff} are essentially the same for ρ^0 and $\pi_0^{\pm}$ incoherent photoproduction. [This is aside from trivial factors of Z/A or $(A-Z)/A$ and is true as long as $\sigma_{\pi_0^{\pm},\rho 0}$ and $\alpha_{\pi_0^{\pm},\rho 0}$ are all the same and neutrons and protons are distributed identically in the nucleus.] Thus we plot, in Fig. 203, A_{eff} for all these processes on the three nuclei Ag, Cu, and C. In view of the fact that VMD seems to provide an adequate description of coherent ρ^0 photoproduction (Sec. IV.C), for a given k, t, and A we might regard the incoherent ρ^0 data as the appropriate VMD "prediction" for the pion data.[51] The pion data are "close" to the ρ^0 data, but one might read from Fig. 203 a trend for A_{eff}(pion) to be greater than $A_{eff}(\rho^0)$ that increases with A. This might be construed as evidence for some VMD violation in pion photoproduction.

This comes as no surprise, for we strongly suspect that VMD or any other model in which a low-mass hadronic constituent plays a dominant role is simply not applicable to pion photoproduction (see Sec.I.B). [Even "non-free-propagator" mass dependence in the mass extrapolation from $Q^2=-m_\rho^2$ to $Q^2=0$ using the field-current identity (as extensively discussed by Schmidt, 1969, Manweiler and Schmidt, 1970, and Schmidt and Yennie, 1969) and leading to a modified VMD result still seems to predict too much shadowing (Spital and Yennie, unpublished, quoted in Gottfried, 1972).] The situation is further complicated because of the dependence on photon polarization: the two amplitudes with ϵ_γ in or out of the production plane violate VMD in different ways (see Fig. 6). This could lead to interesting polarization effects in photoproduction from nuclei (Schmidt and Yennie, 1969; and Bertocchi and Hogaasen, 1971); such effects have not yet been tested experimentally. Such puzzles may also be associated with the fact that π photoproduction is distinct from the diffractive interactions we have discussed thus far. One must keep in mind that nondiffractive contributions to the total photon cross section fall off with increasing k, and may correspond to shorter-range behavior than is characteristic of diffractive processes (see Sec.II.C).

E. Deep-inelastic electron and muon scattering from nuclei at small Q^2

As we have seen in Sec.V.B,C,D, real photons give evidence of their hadronic structure by experiencing shadowing in nuclei. Qualitatively, the total and Compton scattering cross sections seem to be in accord with reference models in which the ρ^0, ω, and ϕ contributions dominate the interaction and the remaining, higher-mass contributions are less shadowed. Because of experimental differences and theoretical uncertainties about the relative size of the high-mass contributions, it is not possible to make a more precise statement at present. In view of the fact that the ρ^0, ω, and ϕ relative contribution to W_1 and W_2 on single nucleons drops rapidly with increasing Q^2 (Sec.II.C,D; Fig. 17; Table XXXVII), it seems plausible that one can obtain more detailed information concerning the interactions of the higher-mass contributions by investigating the shadowing effect in nuclei as a function of Q^2. Of course, we must study increasingly larger ν values so that the coherence length $2\nu/(\mathfrak{M}^2+Q^2)$ remains at least of the order of a hadronic mean free path.[52] ($\mathfrak{M}^2$ is to be regarded as typical for the photon's high-mass structure). In effect, this requirement restricts our attention to inelastic electron or muon data with x $(\equiv Q^2/2M\nu) \lesssim 0.1$.

Let us first compare the contributions of low and high masses as a function of Q^2 for x small. As has been stressed repeatedly, the determination of the VMD contribution to the total photon cross section is subject to both model and experimental uncertainties. For definiteness, we use the models from Table XXXV, appropriately extended to $Q^2 \neq 0$. The high-mass part is determined by taking the difference between the total measured cross section and the VMD prediction. With present data, this procedure seems to be most reliable for the transverse part of the cross section.[53] Typical re-

[51] This ignores the intriguing possibility of a t-dependent violation of VMD in ρ^0 photoproduction. While VMD may describe forward production rather well, wide-angle production is sensitive to scattering by the compact spatial structure probably associated with higher-mass constituents. Any such VMD violation cannot be too dramatic, however, as it would affect the analysis of wide-angle, coherent ρ^0 photoproduction from deuterium by Anderson *et al.* (1970a).

[52] In case the mean free path becomes larger than a nuclear radius, as happens in some models, the coherence length should be larger than the nuclear radius. Such contributions will be only slightly shadowed.

[53] As may be seen from the single-nucleon data in Sec. III.I and Fig. 18, σ_L/σ_T is rather poorly known experimentally. However, indications are that the shadowing of the longitudinal part of the photon-nucleus cross section will be negligible. For one thing as $Q^2 \to 0$ $\sigma_L/\sigma_T \to 0$ kinematically. At larger Q^2, ≈ 2 GeV^2, where experiment indicates σ_L/σ_T might be as large as 0.2 or 0.3, the data also point to a very small effective longitudinal vector-meson cross section or, in other words, a very long mean free path for the hadronic material involved.

TABLE XXXVII. Contributions to $\sigma_T(Q^2)$. VMD contributions are taken from the models of Table XXXV, appropriately extended to $Q^2 \neq 0$. In contrast to those in Fig. 17, these VMD contributions have been calculated for finite photon energy. The "nonshadowed" (N.S.) contribution is the difference between the experimental value of $\sigma_T(Q^2)$, as extracted from a smooth fit to the data of Fig. 17, and the VMD contributions. These *very rough estimates* are to be applied over the ν range of approximately 5–15 GeV.

	Model I (%)			Model II (%)		
Q^2	ρ,ω	ϕ	N.S.	ρ,ω	ϕ	N.S.
0	82	4	14	76	4	20
0.1	78	5	17	72	5	23
0.5	60	5	35	56	5	39
1.0	45	4	51	42	4	54
2.0	30	4	66	28	3	69

sults for the fractional contribution of the VMD terms to $\sigma_T(\nu, Q^2)$ are shown in Table XXXVII. The most important thing to be noted is that there is no abrupt change in this fraction for small Q^2. However, for $Q^2 = 1.0$ GeV^2, we would expect that only about one-half of the photon's interaction is associated with low-mass vector mesons.

What does this lead us to expect for photon shadowing in nuclei? First, for sufficiently small Q^2 ($Q^2 = 0.1$ GeV^2 qualifies), the shadowing of virtual photons should be nearly the same as for real ones. We can conceive of no mechanism which could cause a big reduction of shadowing in a small-Q^2 interval. Second, as Q^2 increases, the amount of shadowing at fixed ν should decrease for two reasons: the coherence length $2\nu/(Q^2 + m_V^2)$ decreases, and the low-mass fraction decreases. The first effect would be more important at low energies.

While the ultimate objective of virtual photon shadowing experiments is to provide information about the nature of the high-mass components, the properties of the low-mass components are not sufficiently well understood to make this feasible from data taken at small (or zero) Q^2. Moreover, at the present time, we do not even have a consistent experimental picture. Published results on real photon absorption and Compton scattering definitely show shadowing of the approximate amount expected. Virtual photon absorption, for $Q^2 \gtrsim 0.5$ GeV^2, on the other hand, shows little or no shadowing. Here we should distinguish two types of experiments. One type consists of single-arm experiments in which only the scattered electron is detected, and the other of experiments in which a hadronic trigger is required as well. As explained in Sec.III.I, the single-arm experiments are limited to a kinematic region where E'/E and Q^2 are not too small. Accordingly, they exclude the region (large ν, small Q^2) most likely to be favorable to shadowing. There is only one published experiment with a hadronic trigger (Eickmeyer *et al.*, 1976*b*). It is done at very small Q^2 (= 0.1 GeV^2), and the reported shadowing at a given photon energy ν is compatible with a slow Q^2 variation when compared with a real photon experiment done by the same group (Michalowski *et al.*, 1977). However, both experiments show less shadowing than the real photon experiments of Caldwell *et al.* (1973). Until this experimental disagreement is resolved, we

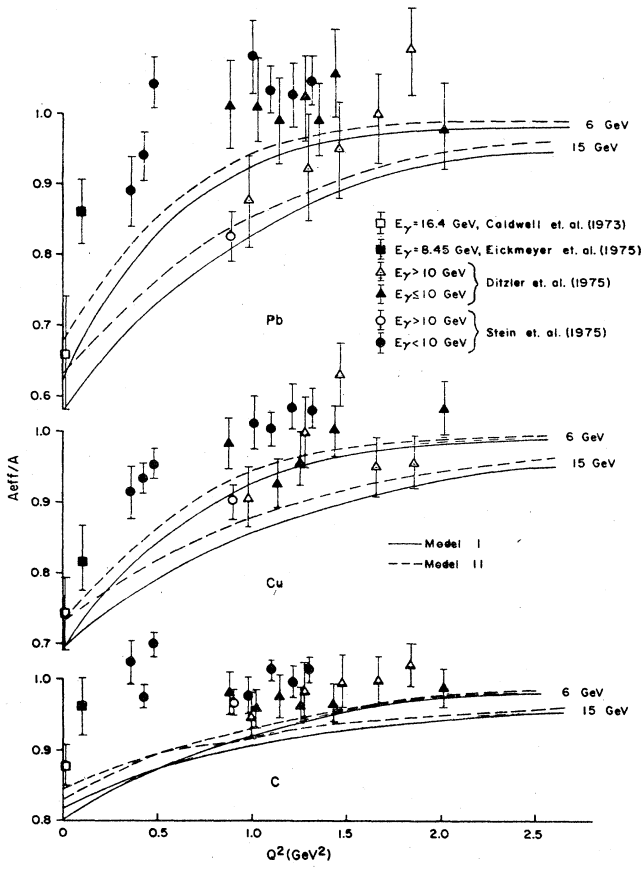

FIG. 204. Photon shadowing as a function of Q^2 for two of the models described in Table XXXV.

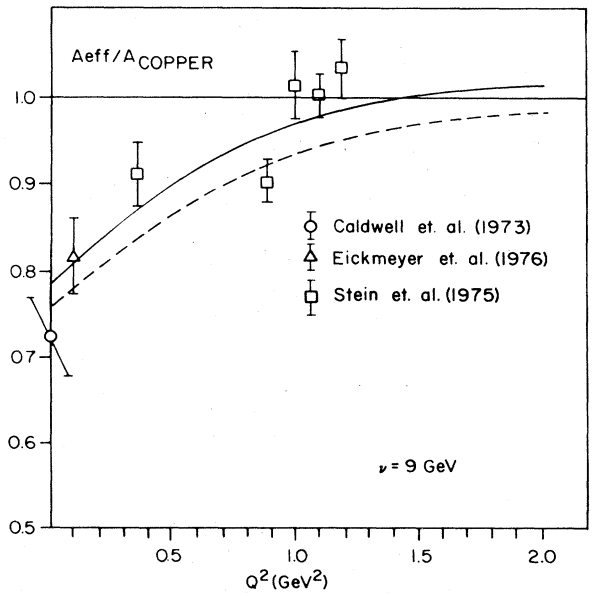

FIG. 205. Example of photon shadowing predicted by a nondiagonal GVD model. The two curves show the effects due to nuclear correlations (dashed line, effects omitted; solid line, effects included) (after Ditsas and Shaw, 1976).

are reluctant to draw any conclusions concerning the shadowing of the photon's higher-mass constituents.

Because the experimental situation is so unclear, no purpose would be served by attempting to fit the data. Instead, we show in Fig. 204 some examples of the shadowing to be expected as a function of Q^2 for some of the models of Sec.V.B. Because they completely neglect the shadowing of the higher-mass, these calculations probably do not represent the complete physics involved. For comparison, Fig. 205 shows the prediction of a generalized vector-dominance model which makes very definite assumptions about the properties and interactions of higher vector mesons. These assumptions are made on aesthetic rather than phenomenological grounds, and should be regarded primarily as a sample computation in which the higher-mass contribution to the single-nucleon cross section has certain desired properties. A description of such GVD models is given in Sec.VI.B. (It must be remarked that this particular GVD model has not been used to fit photoproduction of ρ^0's. If the parameters were constrained by such a fit, the amount of shadowing predicted here would be somewhat larger.)

VI. SUMMARY, SPECULATIONS, AND SUGGESTIONS

A. Status of our knowledge of the hadronic properties of the photon

The purpose of this section is to crystallize the main results presented in Secs.III, IV, and V. More complete details may be found there or in the original papers. Our attention will be confined exclusively to the low-mass constituents of the photon. The higher-mass constituents, which are still a matter of considerable speculation, are the topic of Sec.VI.B. In Sec.VI.C we suggest areas in which further work is needed, as well as new types of experiments which would enhance our understanding of the more subtle features of hadronic electrodynamics.

1. e^+e^- colliding-beam experiments

As discussed in Sec.II.B, these experiments provide basic information about the hadronic structure of the photon. We should recall, however, that the short-distance structure may not bear an obvious resemblance to what is observed asymptotically. The data (see Sec.III.F) have the following main features:

1. The low-mass region is strongly dominated by the relatively narrow ρ^0, ω, and ϕ resonances. The couplings $(e/\bar{f}_V)$ of the photon to these resonances are well determined (see Sec.III.F, IV.C). Interference between these resonances is seen in the final states. While ρ^0-ω mixing is of electromagnetic order, it creates difficulty in the analysis of the ρ^0 shape (see Appendix C). ϕ-ω mixing effects suggest a small admixture of nonstrange quarks in the ϕ and a corresponding admixture of strange quarks in the ω. For a variety of hypotheses, ρ^0 couplings and parameters are summarized in Tables XXIV and XXV. Couplings and parameters for the ω are summarized in Eqs. (3.109-3.111). A compendium of ϕ parameters is found in Table XXVII.

2. The data between the ϕ mass and the J/ψ mass are sketchy and not very precise. Some broad resonance structure is seen [$\rho'(1250)$, $\rho''(1600)$], and the data tend toward a scaling ratio $R_{e^+e^-} \cong 2.5$ (see Sec.III.F). There are suggestions of additional resonances in this mass region (with both narrow and wide widths) which interfere in a confusing manner. A great deal more data will be required to understand this mass region.

3. Recently discovered structure which is associated with a new quantum number, "charm," begins with the J/ψ resonance at 3.095 GeV. At a total energy of about 4 GeV, additional channels open, producing threshold behavior in $R_{e^+e^-}$ which then increases and appears to scale above 5 GeV at a value of $\cong 5$.

4. Jet structure appears in the final states at about 5 GeV total energy.

2. Diffractive photoproduction of ρ^0 mesons

This process is the largest single channel in photoproduction and a wealth of data exists for hydrogen, deuterium, and complex nuclear targets. The greatest obstacle in the interpretation of the data is a rather inadequate theoretical understanding of the very broad dipion mass spectra. Because of this difficulty, the width of the ρ^0 cannot be unambiguously determined from photoproduction experiments and must be taken from other sources. We recommend the value 155 MeV indicated by $e^+e^- \to \pi^+\pi^-$ and strong interaction experiments. We strongly advocate the use of the Spital–Yennie procedure to define the cross section; it has the advantage that different experimental results may be compared less ambiguously (Sec. IV.C).

When hydrogen data are compared using the Spital–Yennie procedure in Fig. 77, the various experiments appear to be in rough agreement in the t region where they overlap. The disagreement in the extrapolated forward cross section is probably due in part to a change of slope in the t distribution (see Sec.III.C) which is not properly accounted for in the extrapolation.

Because of very imprecise knowledge of α_ρ, photoproduction from nuclei does not permit a complete determination of the ρ^0-nucleon scattering amplitude (Sec.IV.C). Interference with Bethe–Heitler pairs has been used to measure α_ρ to within a factor of 2 (Sec.IV.E), but those coarse results do not shed much light on the nuclear experiments. However, a good fit can be obtained with $\sigma_\rho \approx \sigma_\pi$ and $\alpha_\rho \approx \alpha_\pi$ and we take this as our most plausible model (Sec.IV.F). Using these parameters, the forward cross section per nucleon obtained from complex nuclei agrees quite well with that determined from deuterium, as well as with the hydrogen forward cross section measured by the counter groups (Table XXXIV). However, the disagreement between the bubble chamber and counter groups leaves the real meaning of the hydrogen comparison in doubt. A comparison of coupling constants $\bar{f}_\rho$, $\hat{f}_\rho$, and $\bar{f}_{\rho\pi\pi}$ is made in Table XXXII.

The strength of ρ-ω mixing in photoproduction appears to be smaller than in the colliding-beam experiments. This could be due to a suppression of the ω photoproduction amplitudes as compared to VMD.

3. Diffractive photoproduction of ω mesons

Although the ω is a narrow resonance so that one is not plagued by the large width problems of the ρ^0, experimental study of ω photoproduction is complicated by a nondiffractive one-pion exchange (OPE) contribution, which is important at low energies, and by the need to detect a π^0 in the final state. The data are less detailed than in the case of the ρ^0, and although the experiments agree roughly, there is considerable spread in the measured cross sections.

Discrepancies of order 20% (see Table XIX, Sec.III.D) exist in the extrapolated forward diffractive cross sections for ω photoproduction from hydrogen. In our opinion, the difficulty lies in systematic normalization differences among the experimental groups, rather than in subtracting the OPE contribution or in measuring the t dependence. The measured t dependence agrees roughly with that of the ρ^0.

In addition, there is a very troublesome disagreement among existing experiments upon the ratio of the cross sections from hydrogen and deuterium. This makes it extremely difficult not only to determine the neutron-proton difference in ω photoproduction, but also to formulate a VMD prediction for the neutron-proton difference in the total photon cross section and Compton scattering (Table XIX and Sec.III.A, B). Even the sign of the effect is not clear from these data!

ω photoproduction data from complex nuclei are much cruder than the corresponding ρ^0 data. The two experimental groups involved agree in the A dependence, if not in normalization. A reasonable fit to the A dependence may be obtained by using $\sigma_\omega \approx \sigma_\pi$, $\alpha_\omega \approx \alpha_\pi$ as in the case of ρ^0.

The predictions of diagonal VMD for forward photoproduction which incorporate $\sigma_\omega \approx \sigma_{\rho,\pi}$, $\alpha_\omega = \alpha_\rho$, and $\bar{f}_\omega^2/4\pi$ from colliding beams agree with most experiments but disagree substantially with one (see Table XIX, the comparison of $\hat{f}_\omega^2/4\pi$ and $\bar{f}_\omega^2/4\pi$). However, we believe ω-ϕ mixing could play a role in this process and modify the diagonal VMD prediction at the 10%–20% level (such mixing would alter the σ_ω extracted from the A dependence of experiments with complex nuclei by several millibarns—see Sec.IV.D).

4. Diffractive photoproduction of ϕ mesons

The experimental study of ϕ photoproduction is made difficult by the smallness of the total production cross section and there is, as a result, only a limited amount of data. The cross section is surprisingly constant with energy and has a somewhat slower falloff with momentum transfer than that for the ρ. The slower falloff agrees with the quark-model analysis, which uses as input π^+p, π^-p, and K^+p cross sections; but the magnitude of the cross section is about a factor of two smaller. Although there are some possible explanations for this (see Sec.III.E), there is no real quantitative understanding. There are no precise measurements of the real part of the production amplitude, and the data on complex nuclei are sufficiently marginal that one cannot obtain good values for σ_ϕ or α_ϕ.

5. Total photon-nucleon cross section

The general features of σ_γ are described in Sec.II.A, and the experiments are discussed in detail in Sec.III.A. Many experiments have been carried out, and all are in basic agreement. The most recent experiment indicates that σ_γ rises with energy in a manner similar to hadronic cross sections. The resulting fits to the data are given in Tables II and III. There seems to be some evidence that $\sigma_{\gamma p}$ is slightly larger than $\sigma_{\gamma n}$ (with the difference going to zero as $k \to \infty$). However, the magnitude of the difference is probably more uncertain than quoted due to ambiguity in the theory of total deuteron cross sections. Other experiments (forward Compton scattering, some ω photoproduction experiments) even hint that the difference has the other sign (see Sec.III.D).

The information about the vector-meson parameters may be used to estimate the ρ^0, ω, and ϕ contributions to the total cross section, assuming diagonal transitions only. Examples of such estimates are given in Table XXXV, Models I and II. Asymptotically, these contributions yield about 75 to 85% of the total cross section; the ρ^0 alone provides 65% to 70%. The remainder, which is to be accounted for by heavy-mass constituents (true short-range effects do not persist to high energies; see Sec.II.C and Appendix A), is accordingly somewhat uncertain; but it is difficult to see how it could be much larger than 25% (20% at 6 GeV.) The properties of these higher-mass contributions are as yet largely unknown. Some speculations about them will be given in the following section.

6. Shadowing of the total photon cross section in nuclei

Despite the troublesome disagreement between the several experiments, a fairly consistent experimental picture of this process seems to be emerging. The amount of shadowing appears to be somewhat less than that expected from the ρ^0, ω, and ϕ constituents with the heavier-mass constituents largely unshadowed (see Figs. 35–39 and Sec.V.B.). There is good evidence for the expected energy dependence of the shadowing but there is not precise quantitative agreement with the models.

The recent experiments of the Cornell group in which they used essentially the same apparatus to measure the shadowing for both real and virtual photons have clarified the earlier discrepancy due to the failure to find shadowing for virtual photons (see Sec.III.J and V.E). The Cornell groups find a shadowing for real photons which goes away continuously when the photon becomes virtual and Q^2 increases from 0. The observed shadowing is, however, somewhat less than expected. This makes the experiment difficult and partially accounts for the failure of earlier experiments. Figures 204 and 205 in Sec.V.E. show data and theory in the region where shadowing is expected.

With the exception of the Cornell experiment, all the experiments required only the detection of the inelastically scattered electron or muon. Because of the dangerously large radiative corrections involved, they avoided kinematic regions where Q^2 and E'/E are both

small. Unfortunately these regions are the ones where shadowing effects should be most pronounced.

7. Compton scattering from nucleons and nuclei

These experiments confirm the primarily diffractive nature of high-energy photon interactions. The forward cross section on protons is compatible with what is expected from the optical theorem, taking into account the real part predicted from dispersion relations (see Sec. III.B), and confirmed experimentally (see Sec.II.B, III. B). This automatically makes them agree with a VMD model with a 15%–25% unshadowed contribution to the amplitude, since that model already accounts for the total photon cross section.

Interpretation of Compton scattering from the deuteron is more difficult since it involves the deuteron form factor as well as the Glauber and West corrections. The experimental indications are that the neutron amplitude is nearly equal to that of the proton.

Experiments on nuclei confirm photon shadowing close to the amount expected from a VMD model with an unshadowed contribution (see Fig. 53). They roughly agree with total photon cross sections using the optical theorem and calculated values of $\alpha_A[=\mathrm{Re}T_{\gamma\gamma}^{(A)}/\mathrm{Im}T_{\gamma\gamma}^{(A)}$ (see Table XXXVI)].

8. Photon shadowing in incoherent reactions

The shadowing phenomenon has been observed in incoherent ρ^0 and pion photoproduction from complex nuclei. However, the theoretical advances needed to understand these processes are prodigious. While one cannot draw any firm conclusions from the scanty ρ^0 data, there is no doubt that the VMD optical model, largely successful for coherent processes, fails to describe either the energy dependence or the normalization of the π photoproduction data (see Sec.V.D). Some of the difficulty may lie with the optical model itself (see below and Sec. V.D, Appendix B); but the fact that A_{eff} for pion photoproduction is systematically higher than for incoherent ρ^0 photoproduction is strong evidence that the physics of these diffractive and nondiffractive processes are fundamentally different.

Experimentally, A_{eff}/A for charged-pion photoproduction has a strong t dependence. (This is due to a nuclear t distribution that remains flat while hydrogen changes.) To our knowledge, no plausible theoretical explanation of this fact exists.

9. Inelastic electron scattering from nucleons

Since the general features were described in Sec.II.C (and the experiments discussed in detail in Sec III.I), we wish here only to reiterate that the small-x behavior of the structure functions (see Fig. 17) shows that the diffractive region is dominated by contributions from the hadronic structure of the photon (photon cross sections are essentially functions of Q^2 alone)—see also Fig. 167. Another expected feature of the hadronic structure is that $R(\equiv\sigma_L/\sigma_T)$ should be appreciable at small x; there is evidence for this (Fig. 18). For larger x, the scaling behavior could be attributed to hadronic structure of high mass, but the other viewpoints may be more natural in that region (e.g., the parton picture). Speculations about the role of high masses will be described in Sec. VI.B.

10. Electroproduction of ρ^0 mesons

Some scattered data is available on this process. Given the ambiguity of the model, the Q^2 dependence of the cross section agrees approximately with that expected from VMD. A separation has been made into transverse and longitudinal parts; the ratio of longitudinal to transverse production increases linearly with Q^2. Experiments on the Q^2 dependence of the slope parameter are so far inconclusive because the energies are not sufficiently high to separate this from threshold effects. A decrease of slope with Q^2 would indicate a shrinking photon effect (see Sec.VI.B). To be conclusive the slope should be determined separately for transverse and longitudinal ρ^0's, since a difference in slope for the two polarizations could falsely appear as a shrinking photon effect. One experiment makes such a separation, but at a rather low energy.

11. Optical-model calculations

The use of nuclei and the validity of the optical model have been discussed at length in Sec.II.E and Appendix B. Here we wish to remind the reader briefly about the relative reliability of various applications. Generally speaking, as the sensitivity of the analysis to the details of the optical model increases, the credibility of the analysis decreases.

We believe calculations of vector-meson photoproduction are quite reliable *in so far as off-diagonal transitions may be neglected.* If such transitions are important the determination of many parameters will become much more uncertain. (This remark is especially important for ω and ϕ photoproduction where there are theoretical arguments for $\omega \rightarrow\!\!\!\!\!- \phi$ transitions; see Sec.IV.D). As a rule, the effects of off-diagonal transitions are not easily distinguished from those of other refinements of optical models.

We believe that total photon cross section calculations are reliable except at lower energies ($\lesssim 4$ GeV), where the detailed manner in which shadowing disappears is hard to calculate. Figure 202 gives some indication of model uncertainties; each of these curves should have an uncertainty band of perhaps 10% or 15% of the shadowing (i.e., 10% or 15% of the difference between 1 and A_{eff}/A) to indicate the level of reliability of the calculations (not numerical accuracy, but true theoretical uncertainties). The Compton scattering calculations should have a similar reliability. One nagging concern is whether the nondiffractive contributions may be less shadowed than is suggested by straightforward calculation (see Secs.II.B, C; V.B,D for further discussion).

Shadowing in incoherent processes is subject to great theoretical ambiguities. However, the major effect of these difficulties should be on the normalizations; it is extremely hard to imagine how they could mask the strong energy dependence predicted by the optical model (for which there is no experimental evidence). It is much more plausible that other aspects of the physics are not well understood (see Sec.V.D).

B. Speculations about higher-mass constituents. Other viewpoints

In Sec.II.D, we gave a representation [see Eqs. (2.21) –(2.24)] of the total photon cross section from the hadron-mediated point of view. It was pointed out that such a description was sufficiently general to be compatible with any conceivable experimental results. The restrictions on the functions $I_{T,L}$ which are necessary to produce scaling and diffractive behavior were also described. These restrictions are easily satisfied, and the representation has very little predictive power. In order to obtain predictive power, one must use the available knowledge from e^+e^- experiments together with assumptions about how the hadronic constituents interact. In our discussions in Sec.V, we used the reasonably firm knowledge about the ρ^0, ω, and ϕ mesons and simply assumed that the remaining high-mass contributions contribute only a small portion (~15%–25%) of the total cross section and at present energies are effectively unshadowed. However, when virtual photon interactions are considered, the contributions from ρ^0, ω, and ϕ become relatively less important, and the predictions depend more sensitively on the details of the high-mass contributions.

1. Generalized vector dominance

Various authors have developed models for the higher-mass contributions, starting from the original idea of Gribov (1969) and Brodsky and Pumplin (1969). For other early references, see Sec.I.B. In these models it is usually assumed that the e^+e^- colliding-beam cross sections are dominated by vector-meson states which broaden and overlap with increasing mass in such a way that $\sigma(e^+e^- \to X(\mathfrak{M}))$ becomes a smooth function of $\mathfrak{M}$ for $\mathfrak{M} \gtrsim 2$ GeV (aside from the structure associated with charm which apparently smooths out at a higher energy). Since the higher-mass resonances are not separately observable, their masses (m_V) and couplings ($-em_V^2/f_V$) must be assumed, subject only to the constraint that the cross section has the correct overall $\mathfrak{M}$ dependence ($\sigma_{e^+e^-} \propto 1/\mathfrak{M}^2$) and normalization.

This rather complex situation is usually idealized as a tower of vector states associated with each of the low-mass resonances ρ^0, ω, ϕ. The higher-mass states are assumed to be uniformly spaced in $\mathfrak{M}^2$; for example, the "Regge recurrences" of the ρ^0 are given by $m_n^2 = m_\rho^2(1+an)$ with a about 2 (either fitted or assumed). The coupling of the photon to each meson is taken to satisfy $f_V^2/f_\rho^2 = (1+an)$, in order to insure that $\sigma_{e^+e^-} \propto 1/\mathfrak{M}^2$ when one averages over the various resonances [see, for example, Bramón, Etim, and Greco (1972) and Greco (1973)]. It should be emphasized that there is little experimental support for this scheme. Alternatively, one can choose a structureless continuum of high-mass states, as in Sakurai and Schildknecht (1972) and Schildkneckt (1973).

The chief virtue of these models is that they provide nontrivial constructions of the photon's hadronic component and can account for the interactions of high-energy photons—at least in the small-x region. It is especially important to note that the large magnitude of νW_2 in the small-x region can be understood completely in terms of the photon's hadronic structure, without recourse to point charges inside the nucleon (the naive parton model). In addition, these models account for the observed "precocious scaling" in inelastic electron scattering rather naturally, since the scale is set by the low-mass resonances (Gorczyca and Schildknecht 1973).

In order to obtain scaling as well as a reasonable value of the total real photon cross section (σ_γ), it is necessary that the higher masses interact with a diffractive cross section that is effectively proportional to $1/\mathfrak{M}^2$ (see Sec.II.C). This can be accomplished by letting each high-mass constituent have this behavior (Bramón *et al.*, 1972; Greco, 1973), by invoking off-diagonal transitions to make this behavior a property of the superposition (Cocho *et al.*, 1974; Fraas *et al.*, 1975a; Dominguez, 1975; Devenish and Schildknecht, 1976), or by choosing some combination of these mechanisms. Some authors have extended these concepts to include the ψ particles or "charm" (Dominguez and Greco, 1975; Schildknecht and Steiner, 1975; and Gounaris *et al.*, 1975). Clearly the possibilities are endless; and, given the present state of our knowledge, one cannot take any specific detail of these models for high-mass interactions seriously. Reviews of GVD have been given by Schildknecht (1974) and Donnachie and Shaw (1978).

The builders of GVD models have attempted to narrow the range of possibilities by using the deficit between $\sigma_\gamma^{\text{exp}}$ and $\sigma_\gamma^{\text{VMD}}$ to obtain important parameters in their theories. This, however, is still not sufficient to dictate the rather large number of arbitrary assumptions that must be made about the high-mass states. Moreover, $\sigma_\gamma^{\text{VMD}}$ has rather large theoretical and experimental uncertainties, so that the fraction of the cross section attributed to higher masses could lie between 15% and 25%. The parameters chosen are very sensitive to this amount.

One of the few *a priori* predictions made by the tower models is the absence of jets in $e^+e^- \to$ hadrons (Ferrara, Greco, and Grillo, 1970; Greco, 1973). Jets are now evident in the data (Sec.III.F). This does not rule out the tower models; interference between the vector states could account for the presence of jets, but the predictive power of these models is greatly discounted.

Given the basic flexibility of the GVD model, it is not surprising that it is able to give a reasonable account of the real and virtual photon total cross section data. Its greatest plausibility is in the small-x region, where it predicts that νW_2 should be mainly a function of Q^2; this appears to be borne out by the data, as seen in Figs. 17 and 167. The large size of νW_2 in this region is generally predicted by the ρ^0, ω, and ϕ contributions (perhaps this is optimistic), and the role of the higher masses is to cause νW_2 to level off as a function of Q^2 rather than decrease again for $Q^2 \gg m_\rho^2$. An example of such a fit is shown in Fig. 206. For larger x, further arbitrary assumptions must be introduced to account for the decrease of νW_2 as $x \to 1$. As x increases, the coherence length $2\nu/(\mathfrak{M}^2+Q^2)$ decreases and becomes smaller than a proton radius. Some cutoff (t_{min} or form-factor effect) must be introduced to account for this uncertain physics. An intuitive discussion of such effects is given by Nieh (1973).

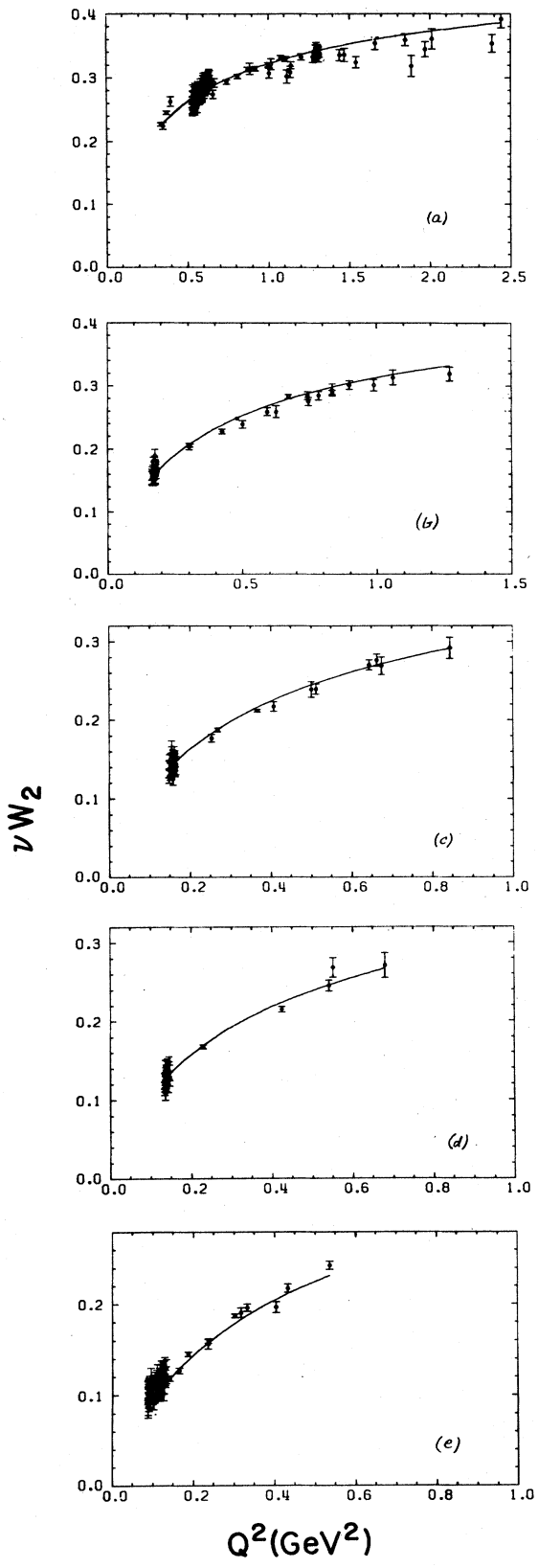

FIG. 206. An example of an off-diagonal GVD model compared with the data (a) $10<\omega'<20$; (b) $20<\omega'<30$; (c) $30<\omega'<40$; (d) $40<\omega'<50$; (e) $\omega'>50$.

Turning now to photon shadowing in nuclei, we note some general features of these models.

(1) GVD pictures may be used to calculate the shadowing effect for the photon's high-mass constituents—see Schildknecht (1973), Cocho *et al.* (1974b), Greco and Srivastava (1974), Ditsas, Read, and Shaw (1975), Ditsas and Shaw (1976). As a rule, they will predict less shadowing than naive VMD, since the higher-mass states they include have short formation times and long mean free paths (see Sec.II.C). As an example, a computation from Ditsas and Shaw (1976) is shown in Fig. 205. However, if all nuclear parameters are kept the same, our reference models of Sec. V.E should provide an upper limit to A_{eff} for all A, ν, and Q^2, since such shadowing is neglected there.

(2) Exceptions to the preceding feature could arise in an "off-diagonal" GVD model involving significant transitions between ρ^0 and ρ', ρ'', etc. (One such model calculation is that shown in Fig. 205.) We note that the strong interference with the ρ^0 state that those authors assume might not give an acceptable fit to the data on ρ^0 photoproduction from either nuclei or nucleons.) No evidence exists at present for such transitions. It is possible that off-diagonal transitions are more important for the higher-mass states since such states should be very broad resonances which overlap significantly with neighboring resonances.

(3) GVD models predict that shadowing will vanish with increasing Q^2 because increasingly higher-mass constituents dominate the interaction with their increasingly lower cross sections (in diagonal GVD this feature is incorporated directly; in off-diagonal GVD it is a property of the superposition). By contrast the aligned jet model, to be described presently, predicts some residual shadowing at small x, regardless of the value of Q^2.

2. The parton (aligned jet) model

From the discussion of Sec.II.D, we expect that the physics of the high-mass contributions may correspond, for Q^2 large, to the parton model. However, since the parton model was developed primarily to account for the large Q^2, large ν region of deep-inelastic scattering from nucleons, it needs further elaboration in order to make predictions of behavior in the small-Q^2 region where shadowing is expected to be important.

Brodsky, Close, and Gunion (1972b), using the covariant parton model of Landshoff, Polkinghorne, and Short (1971), have given a discussion of shadowing of real and virtual photons in terms of a combination of a vector-dominated contribution yielding about 78% of σ_γ together with a parton (or pointlike) contribution as illustrated in Fig. 19a. This is of course equivalent practically to the naive model used in Sec.V. The point, however, is that a specific model is now being proposed for the high-mass contribution. The resulting lack of shadowing is due to the presumed small cross section for partons to interact with nucleons. This picture also predicts that shadowing should decrease rather quickly with increasing Q^2 since the vector-dominated part of σ decreases relative to the partonlike contribution. By $Q^2=0.5$, they expect that the partonlike contributions will begin to

dominate and shadowing will be considerably reduced.

This picture is not necessarily in conflict with the GVD picture; in practice many conclusions are rather similar. However, since the jet structure described below, usually associated with parton models, is observed in $e^+e^- \to$ hadrons (Sec.III.F), there is some intuitive preference of the parton picture.

In lectures at the 1973 SLAC Summer Institute on Particle Physics, Bjorken (1973) elaborated on the "aligned jet model." In this model the jet structure in $e^+e^- \to$ hadrons (expected, but not seen at that time) would play a role in electroproduction. Although the jets in e^+e^- could be aligned in an almost random manner, he supposed that in electroproduction only jets aligned in the beam direction (limited $p_\perp$) could be absorbed by the target. He accounted then for the decreasing absorption cross section of the high masses by assuming that a fraction of the total hadronic content of order $1/\mathfrak{M}^2$ would be absorbed by a more or less normal hadronic interaction. The model also agrees with the parton model in that spin-0 leads to $\sigma_L \gg \sigma_T$ and spin-1/2 to $\sigma_T \gg \sigma_L$; this is of course a consequence of helicity conservation. (A more detailed analysis yields the result that only jets with small laboratory energy have sufficient time to dress themselves for a full interaction with the target.) Although this gives the same overall cross-section behavior as GVD on a nucleon, the physical picture is different—namely, this part of the photon's structure should experience some shadowing (but presumably less than ρ^0). Since the data in the present experimental regime can be accounted for without incorporating such shadowing, one (or more) of the following is true: shadowing of heavy masses is too small to be relevant; it has not yet set in at available energies; shadowing of lower masses should be reduced to accommodate that of the higher masses. Suggestions along a similar line have been made by Nicolaev and Zhakarov (1975), in somewhat different language.

3. Space-time picture

Although it is difficult to use space-time information from nucleons to make shadowing predictions from nuclei, the space-time picture is intuitively helpful in understanding these problems. The observable νW_2 is given as an integral transform of a space-time function $f_2(y^2, y_0)$ [see Eq. (2.24) and Fig. 14]. Because of the complementary nature of coordinate and momentum space, one cannot state a precise connection between a particular region in Q^2 and ν and an interaction region in space-time. However, as described in Sec.II.C and Appendix A, diffractive and other Regge behavior is associated with long range, i.e., $f_2 \sim 1/y_0^a$, the higher values of a being associated with terms which decrease more rapidly with increasing energy. Intuitively, we expect that the longest-range terms ($a=1$, diffractive) may be the most shadowed. An extreme model calculation, in which the nondiffractive terms are assumed to be completely unshadowed, is included in Fig. 202. We feel that this is an extreme upper limit to any reasonable GVD model of A_{eff}/A and note that at sufficiently high $\nu(Q^2=0)$ it should yield considerable shadowing.

The remainder of the discussion concerns only the diffractive ($\nu \to \infty$, fixed-Q^2) limit of photon interactions. Although one sometimes refers to high-mass contributions as pointlike, at sufficiently high energies they become long ranged with a characteristic distance $\sim 2\nu/(\mathfrak{M}^2+Q^2)$. The rapidity of variation of σ_T and σ_L with Q^2 gives a measure of the masses which are relevant. For example, in the diagonal approximation, the range associated with a single mass would be

$$L^{(\mathfrak{M})} \simeq \nu \left| \left[d\sigma_T^{(\mathfrak{M})}/dQ^2 \right] / \sigma_T^{\mathfrak{M}} \right| . \tag{6.1}$$

Unfortunately, it is very difficult to invert the information from νW_2 and MW_1 to obtain the contributions from different masses (in particular, the diagonal approximation is surely an oversimplification). The usual procedure is to invent models which fit the data on nucleons, and then to investigate their consequence for shadowing.

From the general space-time analysis, we know that the fact that σ_T is primarily a function of Q^2 in the small x region means that the longitudinal range of those interactions rises linearly with ν. We emphasize that this result is independent of the details of any particular model. If after we subtract the low-mass contributions the remainder also is primarily a function of Q^2, we can be assured that it also comes from interactions with a range proportional to ν. The simplest intuitive interpretation of this behavior is that it is associated with hadronic constituents of the photon. This means that at sufficiently high energies, the hadronic vacuum fluctuations must propagate through the nucleus. They can be unshadowed only if their mean free path is considerably larger than a nuclear radius. In the GVD models described, this is accomplished by having the effective cross section associated with a given mass region decrease as $1/\mathfrak{M}^2$. The Brodsky–Close–Gunion parton model asserts that the cross section is small, but does not specify a mass dependence. The aligned jet model asserts that the mean free path is bounded, and hence shadowing should eventually occur.

4. The shrinking photon

The transverse size of the vacuum fluctuations is of some interest and may be related to their absorption properties. A detailed study of the dipion constituent of the photon (Yennie, 1975) shows that the largest radius part (associated with nonresonant pions) shrinks with increasing Q^2, in accord with ideas expressed by Cheng and Wu (1969), Bjorken, Kogut, and Soper (1971), Kogut (1972), and Bauer (1973). The same discussion suggests that the higher the mass of the structure, the smaller its radius will be. The argument is unable to account, however, for the detailed strong interactions which give particles a finite size. For example, it is not clear whether or not the whole dipion structure (including the ρ^0-resonance part) should shrink with increasing Q^2. Nieh (1972) has argued that the ρ^0 is a well-defined object which cannot shrink with increasing Q^2. That may be so, but interference effects with the nonresonant background (called off-diagonal amplitudes) may produce the same effect. An exploratory calculation of these interference effects within the framework

of GVD has been carried out by Fraas, Read, and Schildknecht (1975b). When the interference between different initial vector mesons is destructive, the slope of ρ^0 electroproduction decreases with Q^2, as expected from the shrinking photon idea. The quantitative behavior is of course very sensitive to the specific details of the GVD model, which are rather speculative. In any case, as we have argued, the dipion constituent is an intrinsic structure which has no unique separation into resonant and nonresonant parts.

If the dipion structure of the photon shrinks, it should become manifest in a broadening of the t dependence of diffractive photoproduction of ρ^0's as a function of Q^2 (Sec.III.K). The experimental situation is unclear and complicated by the fact that energies are not high enough to avoid possible threshold effects. Moreover, the transversely and longitudinally polarized ρ^0's have not been separated as a function of t.

We can make a simple argument which suggests the transverse size of the vacuum fluctuations. The characteristic time of a vacuum fluctuation as seen in the lab is $2\nu/(\mathfrak{M}^2+Q^2)$. As seen in the rest frame of the hadrons, this time becomes $2\mathfrak{M}/(\mathfrak{M}^2+Q^2)$ (valid for $\nu \gg \mathfrak{M}$ which in any case is necessary if we are to treat this fluctuation as a hadronic constituent of the photon). The characteristic transverse size is therefore $2\mathfrak{M}/(\mathfrak{M}^2+Q^2)$. There now appear to be two extreme but naive possibilities: (a) The size of the hadronic target plays its normal role, but the photon shrinks to a point. The high-mass and/or high-Q^2 total cross section is geometric of order one-half of a typical hadronic cross section; t distributions are correspondingly broadened. (b) The complete transverse size of the interaction decreases and the total cross section becomes pointlike $\propto 4\mathfrak{M}^2/(\mathfrak{M}^2+Q^2)^2$, with extreme broadening of t distributions [for real photons, this corresponds to $\sigma(\mathfrak{M}^2) \propto 1/\mathfrak{M}^2$].

Neither of these naive pictures would be correct in the aligned jet model. In that case, the backward-moving parton (quark) in the hadronic component rest frame would move slowly in the laboratory frame, and would have sufficient time in its *own* rest frame to become dressed [the time involved in the lab is $\sim 2\nu/(\mathfrak{M}^2+Q^2)$]. The time registered by the parton's "moving clock" is appropriately dilated. Thus the interaction associated with such a "wee" parton might be similar to a dressed quark and lead to a "normal" hadronic cross section. Interesting enough, the transverse size of the fluctuation involving the "wee" parton does not shrink and is of the order of the inverse parton mass (Bauer, 1973).

Still an additional possibility exists, perhaps in conjunction with the physics discussed above, that matter is being produced in $e^+e^- \to X$ with different quantum numbers and therefore intrinsically small interactions with nucleons (e.g., "charmonium" or heavy leptons). While future clarification of this third possibility will come chiefly from storage ring experiments, it is also possible that experiments on nuclei could shed light on these mechanisms.

5. Other viewpoints

In this paper, we have emphasized the contrasting, but complementary, descriptions of photon interactions by means of the photon's hadronic structure and by the parton model. Here we shall mention briefly some other approaches which may also give viable descriptions. The oldest of these are the DGS (Deser, Gilbert, and Sudarshan, 1959, 1960) or JLD (Jost and Lehman, 1957; Dyson, 1958) representations of the forward (off-mass-shell) Compton scattering amplitude. While these are rigorous representations, their intuitive meaning is obscure. As mentioned in Appendix A, they have been of use in demonstrating the relationship between canonical singularities and scaling, but otherwise have not contributed greatly to our intuitive understanding of the process.

Several authors, motivated by a suggestion by Bloom and Gilman (1970), have pursued the formulation of deep-inelastic scattering in terms of resonance contributions. Domokos *et al.* (1971) and Moreno and Pestieau (1972) tried to describe the (somewhat poorly defined) nondiffractive part in this manner. The resulting scaling contribution to νW_2 vanishes as $x \to 0$. Elitzur (1971) and Avni and Milgrom (1973) have included Regge behavior in the discussion. The diffractive contribution is then a background which contributes at $x = 0$.

Another representation of the forward virtual-photon Compton amplitude has been given by Schwinger (1975). Based on the source theory viewpoint (described as "nonspeculative, phenomenological"), it is a double spectral representation of the amplitude, using s- and u-channel variables. By applying experimental constraints from the resonance and diffraction regions, it can account for the observed characteristics of deep-inelastic scattering.

C. Suggestions for future work

We list here the experiments which in our opinion would add the most to our understanding of the photon's hadronic structure. We take it for granted that most existing types of experiments will be extended to higher energies and mention them explicitly only when we expect them to clear up some of the puzzles of previous experiments. In view of these restrictions, we recognize that many possible interesting experiments will be omitted.

In addition, wherever possible, we try to indicate areas in which theoretical or phenomenological investigations would be helpful in interpreting both past and future experimental results.

1. ρ^0 photoproduction

It is essential to have accurate and incontrovertible measurements of $d\sigma/dt\big|_{\theta=0}$ in all energy ranges for this process in which VMD has been most successful. Not only will this information serve as a more stringent check on VMD, but, combined with cross sections for complex nuclei, it will provide a determination of $T_{\rho\rho}$ that is *independent* of the VMD connection between $T_{\gamma\rho}$ and $T_{\rho\rho}$.

High-energy measurements of the A dependence of photoproduction from complex nuclei should be made to determine σ_ρ. As $t_{\min}$ becomes negligible, the dependence on α_ρ becomes very weak, and the ambiguity caused by α_ρ should largely disappear. We emphasize

the importance of measuring deuterium cross sections in any A-dependence experiment.

As a lower-priority study, more precise measurements of α_ρ would be interesting, both in their own right and in easing the interpretation of A-dependence data.

Further studies should be made of the phenomenology of the ρ^0 mass shape. Pending a better procedure, we advocate the Spital-Yennie method for defining the cross section. It has the advantage of standardization which permits more unambiguous comparison of different experiments. Incidentally, we note that the ρ-ω interference problem can be eased by centering a mass bin at the ω mass.

2. ω photoproduction

High-energy measurements of $d\sigma/dt\,|_{\theta=0}$ on hydrogen and deuterium should not be troubled by one-pion exchange contributions and are important to resolve the remaining discrepancies at present energies.

Because of ϕ-ω mixing effects which cannot be ignored, the analysis of high-energy A-dependence measurements is more complicated than in the case of the ρ^0. However, because the real parts of the scattering amplitudes are no longer very important in the theory, there is some hope that precise high-energy data may permit disentanglement. The remaining puzzle concerning the relative ρ^0-ω photoproduction phase in leptonic decay should be resolved by measurements at higher energy.

While perhaps of lesser importance, better low-energy measurements of deuterium to hydrogen ratios are needed to generate a VMD prediction for the neutron-proton difference in total photon absorption.

3. ϕ photoproduction

While the data for $d\sigma/dt\,|_{\theta=0}$ are in reasonable agreement, the measurements should be extended to higher energy and be made more precise.

The remarks on A-dependence measurements made for the ω regarding ϕ-ω mixing apply more strongly to the ϕ. However, the need for data is more urgent here because no A-dependence experiment currently exists at small $t_{\min}$. At present σ_ϕ is very uncertain, and its magnitude is strongly correlated to an uncertain α_ϕ. At high energies ambiguities associated with both $t_{\min}$ and α_ϕ will be largely eliminated.

Efforts should be made to understand the discrepancy between the experiments and the quark–VMD model.

4. Incoherent photoproduction from nuclei

We believe that advances in understanding these difficult processes must start with theoretical studies to determine exactly what can be reliably predicted. Given reliable predictions, experimenters should concentrate on the regions of ν and Q^2 where shadowing is expected. It is important that experimentation be more systematic and thorough than in the past.

As a check on the general validity of the new theoretical work, an incoherent ρ^0 photoproduction experiment is recommended. It is likely that any VMD violations in this process will be small compared to model uncertainties.

5. Total photon cross section

Basic to any understanding of hadronic electrodynamics is the photon-nucleon total cross section, and measurements of the cross section on hydrogen and deuterium must be extended to higher energy. Since the neutron–proton difference is expected to become negligible, high-energy deuterium measurements will give us insight into the corrections involved in extracting neutron cross sections from such data. It is conceivable that such insight will allow us to make illuminating reinterpretations of low-energy deuterium results.

Of equal importance to our understanding of the hadronic structure of the photon is the behavior of photon shadowing at high energies. This important experiment bears directly on many of the questions raised in Sec. VI-B, especially whether or not the high-mass components of the photon are shadowed at sufficiently high energy.

6. Compton scattering

Compton scattering is obviously a very basic process for studying the hadronic structure of the photon. At higher energies, the forward cross section should be consistent (via the optical theorem) with the total cross-section measurements. Models which can account for the total cross section should be extended to account for the t dependence of Compton scattering. Together with diffractive photoproduction of heavy-mass vector states (see below), this should provide further insight into the nature of the high-mass constituents of the photon. We see no urgent need for new experiments, but further theoretical work may suggest such a need.

7. $e^+e^- \to$ hadrons

Obviously we hope for an exciting era of discovery in the high-mass region. In the lower-mass region, as a first priority, the $\rho'(1250)$ and $\rho''(1600)$ regions should be studied carefully, and searches made for other possible resonances. Much more detailed data in the mass range between the ϕ and the ψ are required.

8. Inelastic lepton scattering (total cross sections)

Much future effort is likely to be devoted to measurements of the deviation from scaling at large and small x. Of greatest relevance for the hadronic structure of the photon will be experiments at low Q^2 (from 0 to 1 GeV^2) and very small x ($\lesssim 0.05$), where the hadronic structure of the photon dominates and the transition away from the VMD description may be studied. Separation of σ_L and σ_T is very important in this region. As $\nu \to \infty$, each should tend to a nonzero function of Q^2 only. Careful measurements of the approach to this limit would permit the separation of other Regge-type contributions, which would be useful for comparison with the space-time picture. Shadowing measurements in the small-Q^2, large-ν region are important to clarify the present confused experimental situation; and more gen-

eral measurements at small x, large Q^2, will tell us about the interactions of the high-mass photon constituents. Measurements with a hadronic trigger, rather than single-arm-type experiments, will be helpful in keeping radiative corrections manageable.

9. Electroproduction of vector mesons from nucleons

Because of its large cross section, ρ^0 electroproduction will probably be the most completely studied of these processes. Comparison of this process with VMD predictions will be very interesting. Does the total transverse cross section vary as $(Q^2+m_\rho^2)^{-2}$ or decrease more rapidly with Q^2? It will be very important to separate the longitudinal and transverse parts in answering this question. A more rapid decrease would be expected if σ_ρ decreases with increasing Q^2, a possibility suggested by Yennie (1975). (However, an unambiguous determination of σ_ρ as a function of Q^2 requires nuclear targets; see below.) The t dependence is very important for the question of photon shrinkage (Sec.VI.B); and again, it is important to study this for the transverse and longitudinal parts separately. The total cross sections and slopes (of the t dependence) of transversely and longitudinally polarized ρ^0's need not be the same, and experiments should obtain this important information. Electroproduction of other vector mesons—ω, ϕ, and those of higher mass—will be harder to study, but those experiments will be equally interesting.

10. Electroproduction of ρ^0's from nuclei

The A dependence of ρ^0 electroproduction will provide direct information about σ_ρ as a function of Q^2, for both transverse and longitudinal ρ's $(\sigma_\rho^T, \sigma_\rho^L)$ independently of VMD assumptions. It is possible that the compact photon structure for $Q^2>0$ leads to a photoproduction amplitude that falls more rapidly than $(Q^2+m_\rho^2)^{-2}$, but that, nevertheless, the ρ^0 interacts with a normal cross section as it propagates through the nucleus. On the other hand, the compact hadronic structure produced upstream may not have time to grow to its normal transverse size, leading to an effective decrease of σ_ρ with Q^2. Perhaps this decrease of σ_ρ with Q^2 will be such that the VMD hypothesis (2.9) remains valid. This important experiment will answer these interesting questions.

Present measurements of electroproduction from nucleons already suggest a smaller σ_ρ^L than σ_ρ^T. This may point to a geometrical effect related to the dipion structure of the ρ^0. Longitudinal ρ^0's would tend to have the pion pairs aligned along the direction of flight, leading to a Glauber-type shadowing effect with a reduced cross section for their interaction. Transverse ρ^0's, on the other hand, would present a larger area for interaction. However, we cannot rule out the Q^2 dependence of the ρ^0 structure's simply being very different for σ_ρ^L and σ_ρ^T. Note that a large difference between σ_ρ^L and σ_ρ^T in the limit $Q^2\to 0$ would be incompatible with the additive quark model.

11. Diffractive photoproduction and leptoproduction of high-mass material

Our suggestions here are rather general. Any information here will be useful in assessing speculative models such as those described in Sec.VI.B. Of special interest might be forward photoproduction as a function of invariant mass, $\mathfrak{M}$, and Q^2; t dependence as a function of $\mathfrak{M}$ and Q^2; and a search for internal structure (such as jets) in the photoproduced material.

The recent discovery of new, nearly stable, photon constituents has served to underline the central theme of this paper: the photon has a rich structure that makes it far more interesting in its own right than as a mere probe of the charge distributions of other particles. We look forward to learning more about that structure in the years to come.

ACKNOWLEDGMENTS

The preparation of this paper has extended over a rather long period of time, during which we have received help and encouragement from many colleagues. Among these, Kurt Gottfried played a special role. The original basic plan of the paper was conceived with his help, and he contributed to the writing in the early stages and provided many detailed suggestions for improvement in the later stages. Stan Brodsky and Al Silverman gave freely of their time in discussing the physics and criticizing the manuscript, and the final version reflects their influence in numerous ways. Some help in specific parts of the manuscript was provided by Ed Thorndike, who wrote a useful critique of ω photoproduction experiments, and by G. Parrour and Dave Kaplan, who refit the $e^+e^-\to\pi^+\pi^-$ data as described in Sec.III.F. Many, many other colleagues have discussed various parts of the manuscript or sent us their suggestions. We thank them all and hope that we have responded appropriately. Finally, three of us wish to thank our patient wives; and all of us express our appreciation for the untiring efforts of Velma Ray at Cornell in handling all details of a very complex manuscript and of Sally Rand and Carol Davis at Harvard for their patient typing and retyping of countless drafts.

APPENDIX A: BRIEF SUMMARY OF THE SPACE-TIME FORMALISM FOR THE TOTAL PHOTON CROSS SECTION

The purpose of this appendix is to sketch the derivation of the expression for inelastic electron scattering (3.134) and its connection with current commutators; it also describes the arguments relating the properties of current commutators near the light cone to scaling and Regge behavior.

The first step is to show that the total probability for a real or virtual photon to interact with a target is described by two independent functions of Q^2 and ν (von Gehlen, 1960; Gourdin, 1961; Hand, 1961, 1963; and Drell and Walecka, 1964).

This probability may be expressed by

$$W_{\mu\nu}=(2\pi)^2\frac{P_0}{M}\sum_n[\langle n|J_\mu(0)|N\rangle^*\langle n|J_\nu(0)|N\rangle]_{\rm sa}\times(2\pi)^4\delta(P+k-P_n) \tag{A1}$$

Here $|N\rangle$ is the spin-averaged initial nucleon state (four momentum P); $|n\rangle$ is the final state (four-momentum P_n) and k is the photon's four-momentum with $Q^2\equiv -k^2$. The

cross section is then obtained by multiplying $W_{\mu\nu}$ by the appropriate tensor for real or virtual photons. By relativistic covariance and current conservation, $W_{\mu\nu}$ may be expressed in the well-known form

$$W_{\mu\nu}=\left(-g_{\mu\nu}+\frac{k_\mu k_\nu}{k^2}\right)W_1(k^2,\nu)+\frac{1}{M^2}\left(P_\mu-\frac{p\cdot k}{k^2}k_\mu\right)\left(P_\nu-\frac{p\cdot k}{k^2}k_\nu\right)W_2(k^2,\nu). \quad \text{(A2)}$$

In spite of the tensor factors, $W_{\mu\nu}$ is not singular as $k^2\to 0$. This requires the following behavior of W_1 and W_2

$$k_\mu P_\nu \text{ term: } \lim_{k^2\to 0} W_2 = o(k^2)$$

$$k_\mu k_\nu \text{ term: } \lim_{k^2\to 0}\left(W_1+\frac{\nu^2 W_2}{k^2}\right)=o(k^2). \quad \text{(A3)}$$

In the real photon limit, one finds

$$\lim_{k^2\to 0} W_1=\frac{2\nu}{8\pi^2\alpha}\sigma_{\gamma N}^T$$

$$\lim_{k^2\to 0}\frac{W_2}{-k^2}=\frac{2}{8\pi^2\alpha\nu}\sigma_{\gamma N}^T. \quad \text{(A4)}$$

More generally, the virtual photon cross sections may be separated into transverse and longitudinal parts. In this paper, we use the Hand convention (2.13).[23]

The derivation of the space-time representation of $W_{\mu\nu}$ follows conventional lines, and we simply remind the reader briefly of the main steps. The four-dimensional δ function in (A1) is first expressed in terms of its Fourier transform (the space-time variable y_μ ultimately represents the space-time separation between the annihilation of the incoming photon and creation of the outgoing photon, as illustrated in Fig. 14). Finally, space-time translation invariance is used to obtain

$$W_{\mu\nu}=(2\pi)^2\frac{P_0}{M}\int d^4y\,\langle N|J_\mu(y)J_\nu(0)|N\rangle_{\rm sa}e^{ik\cdot y}. \quad \text{(A5)}$$

In the kinematic region $\nu(\equiv k_0)>0$, one may replace the product of the currents by their commutator without changing $W_{\mu\nu}$,

$$W_{\mu\nu}=(2\pi)^2\frac{P_0}{M}\int d^4y\,e^{ik\cdot y}\langle N|\,[J_\mu(y),J_\nu(0)]\,|N\rangle_{\rm sa}. \quad \text{(A6)}$$

This follows from the fact that the reverse order of the currents leads to $\delta(P-k-P_n)$, which can never have zero argument for $\nu>0$. The result (A6) may also be obtained from the imaginary part of the forward Compton amplitude. Using the reduction formula, this amplitude may be expressed as the Fourier transform of the retarded commutator (or T bracket) of the currents, whose imaginary part is (A6). Causality implies that the commutator vanishes outside the light cone ($y^2<0$). Thus $W_{\mu\nu}$ can be expressed as the Fourier transform of a function vanishing outside the light cone.

Because the tensor factors in (A2) become differential and integral operators in coordinate space, it is not obvious that the Fourier transforms of W_1 and W_2 must vanish outside the light cone. Actually, it can be shown that these Fourier transforms can be chosen to vanish outside the light cone without loss of generality. The final result is then of the form (2.15) (taking into account space-time symmetry properties).

●In momentum space, it is easy to see that W_1 and W_2 are restricted to the kinematic region $|\nu|\geq Q^2/2M$ (when $Q^2=-k^2\geq 0$). It is well known that functions with such support properties in momentum and coordinate space can be represented by the DGS (Deser, Gilbert, and Sudarshan, 1959, 1960) or JLD (Jost and Lehmann, 1957; Dyson, 1958) representations. While these representations are helpful in discussing some of the properties of deep-inelastic scattering, they are not physically very transparent; and we do not make use of them here. Discussions of scaling and/or Regge behavior based on these representations have been given by Brown (1969) and Brandt (1969).

The remainder of this appendix will be devoted to a brief justification of some of the claims made in Sec. II.C about the relationship between canonical space-time behavior and scaling, the need for a long range to account for diffractive features of the data, and the general behavior of contributions with a power law falloff in the range. We follow the presentation of suri and Yennie (1972); some earlier references to the space-time approach scaling are Brown (1969), Jackiw, van Royen, and West (1970), Brandt (1969), Leutwyler and Stern (1970), and Mack (1971). Orzalesi (1973) has given a discussion of the long-range space-time behavior for nonforward scattering.

It is convenient to introduce light-cone variables

$$y_+=\tfrac{1}{2}(y^0+y^3),\qquad y_-=y^0-y^3, \quad \text{(A7)}$$

where y^0 and y^3 are coordinates in the laboratory frame with the 3 axis along k. Then

$$k\cdot y=\bar\nu y_- -\bar x y_+,$$

where $\bar\nu=\tfrac{1}{2}(\nu+k_3)\cong\nu$; $k_3=|\mathbf{k}|$; $\bar x=Q^2/2\bar\nu\cong Mx$. Equation (2.15) may then be rewritten

$$\nu W_2=2\pi Q^2\nu\int\int_0^\infty dy_+dy_-\sin(\bar\nu y_- -\bar x y_+)\times\int_0^{2y_+y_-}f_2(\lambda,y_+ +\tfrac{1}{2}y_-)d\lambda. \quad \text{(A8)}$$

We are interested in the large energy region ($\nu\to\infty$), with either fixed x or fixed Q^2. The aim is to see what properties of f_2 correspond to scaling or Regge behavior. Study of the asymptotic behavior of such integrals requires considerable care; here we shall proceed in a rather nonrigorous fashion.

The first point to note is that when ν is large, the integrand oscillates rapidly in y_-. This causes the major contribution to the integral to come from the vicinity of the light cone (actually, to be dominated by the behavior of f_2 near the light cone). Formally, repeated integrations by parts with respect to y_- lead to an (asym-

ptotic) expansion in inverse powers of $\bar{\nu}$.[54] As will be discussed shortly, this procedure is not useful for large values of y_+, but it is usually allowable to ignore the y_- in the second argument of f_2 (either $y_+ \gg y_-$, or the main contributing region for y_- is close to the light cone). It is now convenient to integrate *once* by parts to find

$$\nu W_2 = \frac{2\pi Q^2 \nu}{\bar{\nu}} \int\int_0^\infty dy_+ dy_- \cos(\bar{\nu} y_- - \bar{x} y_+) 2y_+ f_2(2y_+ y_-, y_+). \tag{A9}$$

We are now in a position to justify some of the points made in Sec.II.C. It can be shown that canonical singularities [referring to the behavior of the commutator in (A6) as $y^2 \to 0$] mean that f_2 remains finite when its first argument vanishes. If f_2 also goes to zero "quickly" as its second argument increases, we may integrate by parts once more and find

$$\nu W_2 = \frac{4\pi Q^2}{\nu} \int_0^\infty dy_+ y_+ \sin(x y_+) f_2(0, y_+) = F_2(x). \tag{A10}$$

This is the result of Jackiw, van Royen, and West (1970). Under these assumptions ($f_2 y_+^2 \to 0$ as $y_+ \to \infty$), it is clear that F_2 vanishes as x^2 when $x \to 0$. As remarked in Sec.II.C, this behavior is incompatible with the data. These restrictions would also yield a real photon cross section decreasing as ν^{-2}, in obvious contradiction to the data.

For these reasons, it is necessary to consider the possibility of long-range terms. A simple *ansatz* for such terms is $h^{(a)}(2y_+ y_-)/y_+^a$, and it will be seen immediately that a term with $a=1$ in f_2 can yield a constant total real photon cross section and a constant limit for F_2 as $x \to 0$. Other (larger) values of a can yield Regge behavior. With this form, it is useful to rescale the integration variables

$$\beta = \bar{\nu} y_-,$$

$$\eta = y_+ / \bar{\nu},$$

so that

$$\nu W_2^{(a)} = 2\pi \frac{Q^2}{\nu^{a-1}} \int\int_0^\infty \frac{d\eta d\beta}{\eta^a} \sin(\beta - \tfrac{1}{2} Q^2 \eta) \int_0^{2\beta\eta} h^{(a)}(\lambda) d\lambda$$

$$= \frac{Q^2}{\nu^{a-1}} G_2^{(a)}(Q^2) \tag{A11}$$

which is (2.18). It can also be shown that in the large-Q^2 limit $G_2 \to C(Q^2)^{a-2}$, so that a scaling result is obtained. The case $a=1$ obviously has the proper behavior for both the real photon case and $F_2(x \approx 0)$. It is clear that this power-law behavior in ν corresponds to Regge contributions. In space-time, they are not restricted to the light cone for fixed Q^2, since when y_+ is very large the function f_2 may vary as quickly with y_- as does the trigonometric function. Then there may be a stationary phase resulting from f_2 beating against the cosine, and the contributing region veers away from the light cone.

As we can see, the long- and short-range contributions to $W_{\mu\nu}$ have very different characteristics in both coordinate and momentum space.

APPENDIX B: GLAUBER MULTIPLE-SCATTERING THEORY AND THE OPTICAL MODEL

1. Introduction

This appendix is devoted to describing the basic ideas behind the optical model of scattering and production processes. The aim is not to provide the reader with the technical ammunition necessary to carry out elaborate calculations, but rather to give him some physical insight into the approximations and assumptions employed and a brief indication of how practical formulas are obtained. The basic reference on the formalism is Glauber (1959). Two other references of a pedagogical or review nature are Glauber (1970) and Yennie (1971); see also Bochmann (1972b). These, and many other papers, elaborate the details of the model. Multiple-scattering theory views a nuclear reaction as a succession of collisions with individual nucleons. When the nucleus is sufficiently large, the resulting formulas can be simplified with the aid of various approximations to yield a result in the form of an optical model in which the individual interactions are replaced by an effective potential interaction with the nuclear matter.

The objective of Glauber theory is to express cross sections for reactions on nuclear targets in terms of basic two-body interactions. To the extent that the latter cross sections are known, one can predict the nuclear cross sections. Conversely, by observation of nuclear cross sections, one may be able to infer information about the basic interactions. One views the nuclear interaction as arising from a succession of collisions within the nucleus. Each collision is regarded as taking place inside a "black box" region and between collisions the particles are assumed to move freely. No attempt is made to describe the short-range details of the interaction or the internal structure of the elementary particles. In the high-energy eikonal limit, one need use only a center-of-mass coordinate to describe the incident particle (or its products): b is the impact parameter and z the distance along the incident direction. Similarly the target nucleons are described by center-of-mass coordinates (and possibly also by spin and isospin). No account is taken of the interaction of the projectile with the "glue" which holds the target together.

A little reflection shows that since each target nucleon occupies a volume of order $6F^3$ inside the nucleus and its own physical size is nearly that large, the room for free motion between collisions is actually very small. Also, for some fraction of the collisions, the projectile may interact simultaneously with more than one target nucleon. We have no way of expressing such collisions in terms of known two-body interactions; hopefully they are unimportant since repulsive nuclear forces tend to keep nucleons apart.

2. Total cross section and elastic scattering

As an introduction to the more complicated production processes we consider first the elastic channel. In or-

[54] This is occasionally (and erroneously) referred to as a stationary phase approximation. In fact, the sine function does not have a stationary phase at $y_- = 0$.

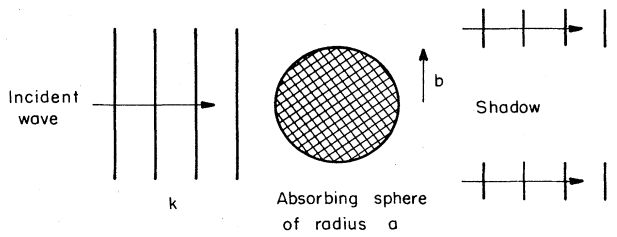

FIG. 207. Absorption of a wave by a target to produce a shadow.

der to build up nuclear scattering from two-body scattering, it is necessary to have a spatial description of the latter at very small distances, but still outside the "black box" interaction region. The accepted picture of high-energy scattering is that it is primarily shadow scattering, as illustrated in Fig. 207. In the high-energy eikonal limit where the projectile's wave number k is much larger than a^{-1} (a characterizes the interaction radius) the shadow structure persists to a very large distance ($\sim ka^2$) beyond the target. Thus in the vicinity of the target, the wave function may be written

$$\psi = [1 - \Gamma(\mathbf{b})\theta(z)]\, e^{ikz} \tag{B1}$$

where θ is a unit step function which idealizes the longitudinal buildup of the shadow in the nucleon volume; Γ is known as the profile function for elastic scattering. At larger distances, the $-\Gamma\theta$ term spreads out to give the scattered wave. Using Huygen's principle, one easily finds the scattering amplitude to be

$$T(\mathbf{p}_\perp) = \frac{ik}{2\pi} \int d^2b\, \Gamma(\mathbf{b}) e^{i\mathbf{b}\cdot\mathbf{p}_\perp} . \tag{B2}$$

$\mathbf{p}_\perp$ is the transverse momentum transfer and T is normalized so that $|T|^2 = d\sigma/d\Omega$. Nearly complete absorption corresponds to Γ approximately real and close to 1, leading to a predominantly imaginary T. The total cross section is given by

$$\sigma_{\text{tot}} = \frac{4\pi}{k} \operatorname{Im} T(0) = 2 \int d^2b\, \operatorname{Re}\Gamma(\mathbf{b}) . \tag{B3}$$

Here Γ may be inferred from experimental data by inverting (B2) (assuming the phase of T is known from experiment or from theoretical considerations).

To extend these results to nuclei, we must calculate the combined shadow from all the nucleons. This is done by assuming that the individual nucleons are "frozen" in position throughout the collision and that each one independently modifies the piece of the incident wave passing through it by a factor

$$1 - \Gamma(\mathbf{b} - \mathbf{s}) ,$$

where $\mathbf{s}$ is the transverse position of the nucleon. Thus the overall modification of the wave is given by the factor

$$1 - \Gamma_A(\mathbf{b}) = \prod_{i=1}^{A} [1 - \Gamma(\mathbf{b} - \mathbf{s}_i)] . \tag{B4}$$

Clearly, only those nucleons actually in the vicinity of impact parameter $\mathbf{b}$ influence the shadow there.

The expression (B4) is really an operator on the initial nuclear state $|0\rangle$; and the amplitude for excitation to nuclear state $|f\rangle$, when the projectile traverses the nucleus at impact parameter $\mathbf{b}$, is

$$\langle f | \Gamma_A(\mathbf{b}) | 0 \rangle = \delta_{f0} - \left\langle f \left| \prod_{i=1}^{A} [1 - \Gamma(\mathbf{b} - \mathbf{s}_i)] \right| 0 \right\rangle . \tag{B5}$$

In the case of elastic scattering ($|f\rangle = |0\rangle$) this may be converted to the form of an optical-potential result with the aid of a few further approximations. The first is to assume that the nuclear ground-state joint density distribution $|\psi_0(r_1, \ldots r_A)|^2$ is well approximated by the independent particle model (IPM):

$$|\psi_0|^2 \approx \prod_{i=1}^{A} \rho_1(\mathbf{r}_i) . \tag{B6}$$

The nucleon number density is defined by $n(\mathbf{b}, z) = A\rho_1(\mathbf{b}, z)$. Equation (B5) may then be written for this case

$$\begin{aligned} \langle 0 | \Gamma_A(\mathbf{b}) | 0 \rangle &= 1 - \left[1 - \int \Gamma(b - s)\rho_1(\mathbf{s}, z) d^2s dz\right]^A \\ &\approx 1 - \exp\left[-\int \Gamma(\mathbf{b} - \mathbf{s}) n(\mathbf{s}, z) d^2s dz\right], \end{aligned} \tag{B7}$$

where we have used $A \gg 1$. The final approximation is to note that since the shadows from individual nucleons have a smaller transverse size than typical nuclear dimensions, the integral in (B7) may be approximated using $n(\mathbf{s}, z) \to n(\mathbf{b}, z)$. Thus the exponent in (B7) becomes

$$\frac{2\pi i}{k} T(0) \int_{-\infty}^{\infty} n(\mathbf{b}, z) dz ,$$

where $T(0)$ is the two-body forward elastic scattering amplitude. The imaginary part of $T(0)$ gives the mean free path of the projectile in nuclear matter:

$$\lambda = \left(\frac{4\pi}{k} \operatorname{Im} T(0) n(\mathbf{b}, z)\right)^{-1} = \frac{1}{\sigma_{\text{tot}} n} . \tag{B8}$$

The real part of T of course corresponds to refraction.

The various approximations used can be "undone," or corrections estimated. For example, one may take the finite size of the shadow into account in (B7) by replacing n by an effective "smeared" density $\bar{n}$. The approximation of going from the power form to the exponential form in (B7) is unnecessary but customary. To some extent, the errors made tend to be compensated by corrections to the independent particle model (Yennie, 1971). Finally, as an improvement on the IPM, one may study the role of nuclear correlations. The main direction of the effect is easy to see. Without correlations, the model would permit two nucleons to be at the same place some portion of the time, leaving "holes" through which the projectile might pass without absorption. The correlations keep the nucleons apart, tending to reduce these holes. The effect is modeled by decreasing λ in a way which depends on the local density. Generally λ is decreased by $\lesssim 10\%$, leading to a change of less than 10% in the calculated cross section. The point is that the center of the nucleus is almost totally black anyway, while the modification is small for the periphery. In this paper, we use corrections estimated from the correlation function of Moniz and Nixon (1971).

Having obtained expressions for the profile function for elastic scattering [$|f\rangle = |0\rangle$ in (B5)], one may finally

calculate the elastic scattering and total cross section from (B2) and (B3). As reviewed by Gottfried (1972), this model gives a generally good account of total cross sections (for example, of neutrons at 5.7 GeV), and of small momentum-transfer elastic scattering. However, at larger momentum transfer incoherent scattering becomes important. As will be described in the following paragraphs, this incoherent scattering may be pictured as a residual scattering from individual nucleons rather than from the average matter density.

●In addition to strictly elastic scattering, there occur experimentally indistinguishable processes in which the projectile scatters with nuclear excitation. In this case, it is possible to use the closure approximation, which takes advantage of the high energy of the projectile to neglect the energy of excitation. To obtain a cross section, we must Fourier-transform $\langle f|\Gamma_A(\mathbf{b})|0\rangle$ to transverse momentum space, then square. The resulting incoherent cross section is then

$$\left(\frac{d\sigma}{d\Omega}\right)_{\text{inel}} = \frac{k^2}{4\pi^2}\int\cdots\int d^2b\,d^2b'\,e^{i\mathbf{p}_\perp\cdot(\mathbf{b}-\mathbf{b}')}Q(\mathbf{b}'-\mathbf{b})\,, \quad \text{(B9)}$$

where

$$\begin{aligned}Q(\mathbf{b}',\mathbf{b}) &= \sum_{|f\rangle\neq|0\rangle}\langle 0|\Gamma_A^\dagger(\mathbf{b}')|f\rangle\langle f|\Gamma_A(\mathbf{b})|0\rangle\\ &= \langle 0|\Gamma_A^\dagger(\mathbf{b}')\Gamma_A(\mathbf{b})|0\rangle - \langle 0|\Gamma_A^\dagger(\mathbf{b}')|0\rangle\langle 0|\Gamma_A(\mathbf{b})|0\rangle\\ &= \langle 0|\prod_{i=1}^{A}[1-\Gamma^\dagger(\mathbf{b}'-\mathbf{s})-\Gamma(\mathbf{b}-\mathbf{s}_i)\\ &\qquad +\Gamma^\dagger(\mathbf{b}'-\mathbf{s})\Gamma(\mathbf{b}-\mathbf{s}_i)]|0\rangle\\ &\quad -\langle 0|\prod_{i=1}^{A}[1-\Gamma^\dagger(\mathbf{b}'-\mathbf{s}_i)]|0\rangle\\ &\qquad \times\langle 0|\prod_{j=1}^{A}[1-\Gamma(\mathbf{b}-\mathbf{s}_j)]|0\rangle\,. \end{aligned}\quad \text{(B10)}$$

The simplest approximation to this is to again assume the independent particle model, which gives

$$\begin{aligned}Q(\mathbf{b},\mathbf{b}') &= \Big\{1-\int[\Gamma^\dagger(\mathbf{b}'-\mathbf{s})+\Gamma(\mathbf{b}-\mathbf{s})]\rho_1(s,z)d^2s\,dz\\ &\qquad +\int\Gamma^\dagger(\mathbf{b}'-\mathbf{s})\Gamma(\mathbf{b}-\mathbf{s})\rho_1(\mathbf{s},z)d^2s\,dz\Big\}^A\\ &\quad -\Big\{1-\int[\Gamma^\dagger(\mathbf{b}'-\mathbf{s})+\Gamma(\mathbf{b}-\mathbf{s})]\rho_1(\mathbf{s},z)d^2s\,dz\\ &\qquad +\int\Gamma^\dagger(\mathbf{b}'-\mathbf{s})\rho_1(\mathbf{s},z)d^2s\,dz\\ &\qquad \times\int\Gamma(\mathbf{b}-\mathbf{s}')\rho_1(\mathbf{s}',z')d^2s'\,dz'\Big\}^A\,. \end{aligned}\quad \text{(B11)}$$

The complicated brackets differ only in their last terms. Imagine now expanding out this expression in powers of this difference

$$\begin{aligned}P(\mathbf{b}',\mathbf{b}) &= \int\Gamma^\dagger(\mathbf{b}'-\mathbf{s})\Gamma(\mathbf{b}-\mathbf{s})\,\rho_1(\mathbf{s},z)d^2s\,dz\\ &\quad -\int\Gamma^\dagger(\mathbf{b}'-\mathbf{s})\rho_1(\mathbf{s},z)d^2s\,dz\\ &\qquad \times\int\Gamma(\mathbf{b}-\mathbf{s}')\rho_1(\mathbf{s}',z')d^2s'\,dz' \end{aligned}\quad \text{(B12)}$$

times powers of

$$S(\mathbf{b}',\mathbf{b}) = 1-\int[\Gamma^\dagger(\mathbf{b}'-\mathbf{s})+\Gamma(\mathbf{b}-\mathbf{s})]\rho_1(\mathbf{s},z)d^2s\,dz\,. \quad \text{(B13)}$$

We want to give a physical interpretation to the resulting expansion. Suppose we have one power of P and consider the resulting contribution to Eq. (B9). If we momentarily ignore the powers of S, the first term of P yields precisely the elastic differential cross section for projectile scattering from a free nucleon! The powers of S correspond to shadowing of the projectile before and after this single scattering. The second term of P corrects free nucleon scattering for elastic nuclear scattering and tends to suppress the single scattering cross section for small $\mathbf{p}_\perp$. Ignoring S we cannot excite the nucleus without some momentum transfer, so at $\mathbf{p}_\perp = 0$ the two terms of P completely cancel. Physically, the factors of S can absorb momentum transfer coherently, permitting excitation of the nucleus even when the projectile is undeflected. In any case, the suppression from the second term applies to small values of momentum transfer $|\mathbf{p}_\perp| \lesssim 1/R_{\text{nucl}}$. For larger transfers, single scattering should be observable. Clearly, the various powers of P correspond to real, incoherent scatterings from individual nucleons, as opposed to a "smooth" interaction with nuclear matter or an equivalent optical potential.

The use of the IPM cannot account correctly for the Pauli principle and other correlation effects. When this is worked out in detail to single scattering order [see, for example, Yennie (1971), p. 339], the second term of P is replaced by an expression involving two-body correlations. The conclusion is that the second term still tends to cancel the first term at small $\mathbf{p}_\perp$, roughly under conditions where the momentum transfer is too small to kick the nucleon outside the Fermi sphere. Here, cancellation occurs for $p_\perp \lesssim 1/l_c$, where l_c is the correlation length as opposed to $p_\perp \lesssim 1/R_{\text{nucl}}$ in the IPM case. (Again, the shadowing factors S can modify this approximate picture considerably.) Another complicated correction which we shall not attempt to explain here, but which has a simple interpretation, is that correlations give an enhancement of incoherent events by keeping shadowing nucleons away from the scattering nucleon. This may increase certain cross sections by as much as 40% (von Bochmann, Margolis, and Tang, 1969; Yennie, 1971). Finally, it must not be forgotten that incoherent processes take place predominantly at the edges of the nucleus ($|\mathbf{b}|$ large) where S is close to 1. However, it is in just this region where nuclear wave functions are most uncertain.

If the reader feels that the subject is getting very complicated, and questions the reliability of the underlying assumptions to describe such incoherent processes ac-

curately, his intuition is, in our view, entirely justified! In spite of this concern, there are examples of calculations of multiple incoherent scatterings which agree very successfully with the data [Glauber (1970); note that these calculations are of the most simple type employing no nuclear correlations].

3. Generalization to production processes and Compton scattering from nuclei

We only sketch the necessary modifications of Glauber theory for these processes since many of the basic assumptions have already been described in connection with elastic and quasielastic scattering. For the basic two-body interactions, we assume that the outgoing particle(s) are amenable to some simple description in the vicinity of the target, and represent the transition from incident particle a to produced particle b by a profile function $\Gamma_{ab}(\mathbf{b})$. That is, an incident wave $e^{ik_a z}$ for particle a is changed to a final wave $-\Gamma_{ab}(\mathbf{b})e^{ik_b z}$ for particle b. The production amplitude is defined by the analogue of Eq. (B2). In general, $k_a \neq k_b$, and there is a phase difference between the a and b waves behind the target. Note that the b wave need not be physically the same as the asymptotic state finally observed. For example, it may be a ρ^0 which later decays to a two-pion system. (On the other hand, the nonresonant part of the dipion structure of the photon may lead to a genuine two-pion state behind the target.)

In the simplest cases, Γ_{ab} is "coherent" on the nucleon, i.e., spin and isospin independent. In this case the treatment for nuclear targets will resemble elastic scattering. However, in certain processes such as photoproduction of charged pions it is incoherent, the production will excite the nucleus, and the treatment for nuclei will be similar to the one given in the final paragraphs of Sec. B.2.

As our first example of a production process on a nucleus, we consider ρ^0 photoproduction. A ρ^0 wave of profile $\Gamma_{\gamma\rho}(\mathbf{b}-\mathbf{s}_i)$ is induced on nucleon "i" and subsequently scattered by the remaining A-1 downstream nucleons with an elastic ρ^0-nucleon profile $\Gamma_\rho(\mathbf{b})$ (we ignore any difference between neutrons and protons). We neglect any longitudinal structure in the shadows cast by individual nucleons, but take into account that the wave vector $\mathbf{k}_\rho$ of the produced ρ^0 differs from that of the incident photon, $\mathbf{k}$, by $\Delta_{\gamma\rho} \equiv |\mathbf{k}| - |\mathbf{k}_\rho| \approx m_\rho^2/2k$ for $k \gg m_\rho$. We then find for the nuclear production profile

$$\langle f\,|\,\Gamma^A_{\gamma\rho^0}(\mathbf{b})\,|\,0\rangle = \sum_i \langle f\,|\prod_{j\neq i}[1-\theta(z_j-z_i)\Gamma_\rho(\mathbf{b}-\mathbf{s}_j)] \times \Gamma_{\gamma\rho^0}(\mathbf{b}-\mathbf{s}_i)e^{i\Delta_{\gamma\rho}z_i}\,|\,0\rangle\,. \tag{B14}$$

The θ functions insure that the ρ^0 scatters only from the nucleons downstream from the production point. To calculate the amplitude for elastic photoproduction ($|f\rangle = |0\rangle$) we proceed exactly as in Sec. B.2. In the IPM, Eq. (B14) becomes

$$\langle 0\,|\,\Gamma^A_{\gamma\rho^0}(\mathbf{b})\,|\,0\rangle = \int\left[1-\int\theta(z'-z)\Gamma(\mathbf{b}-\mathbf{s}')\rho_1(\mathbf{s}',z')d^2s'dz'\right]^{A-1}\Gamma_{\gamma\rho^0}(\mathbf{b}-\mathbf{s})n(\mathbf{s},z)e^{i\Delta_{\gamma\rho}z}\,d^2s\,dz\,. \tag{B15}$$

With the further approximations discussed in Sec. B.2, this easily reduces to Eq. (4.1). The effects of correlations, smearing, etc., can be incorporated approximately, as before.

Incoherent ρ^0 photoproduction is discussed in the same way as incoherent scattering, but is somewhat more complicated in detail. In place of the first term of Eq. (B12) there are now four terms corresponding to production or scattering on a given nucleon:

$$\Gamma^\dagger_{\gamma\rho^0}(\mathbf{b}'-\mathbf{s})\Gamma_{\gamma\rho^0}(\mathbf{b}-\mathbf{s}),\quad \Gamma^\dagger_\rho(\mathbf{b}'-\mathbf{s})\Gamma_{\gamma\rho^0}(\mathbf{b}-\mathbf{s}),$$
$$\Gamma^\dagger_{\gamma\rho^0}(\mathbf{b}'-\mathbf{s})\Gamma_\rho(\mathbf{b}-\mathbf{s}),\quad \Gamma^\dagger_\rho(\mathbf{b}'-\mathbf{s})\Gamma_\rho(\mathbf{b}-\mathbf{s}).$$

These are multiplied by factors giving the optical-model absorption of the ρ^0 wave from its point of production. The result may be summarized as follows: There is one nucleon on which an incoherent scattering takes place. The effective amplitude for this to happen is a sum of two terms. The first, called a "one-step" contribution, has the nucleon on which production occurs recoil incoherently. In the second, "two-step" contribution, the ρ^0 is produced coherently, scatters coherently, and then scatters incoherently from the same nucleon as in the one-step contribution. These two contributions are illustrated in Fig. 208a, b. As in Sec. B.2, there are compensating effects which tend to suppress incoherent photoproduction with small momentum transfer. Multiple incoherent scatterings are also possible (see next paragraph).

Photoproduction of single pions is also an incoherent

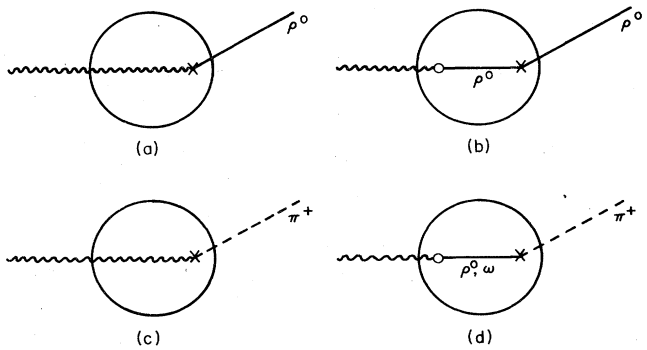

FIG. 208. Examples of incoherent photoproduction. X represents an incoherent interaction and 0 a coherent transformation. (a) one-step incoherent ρ^0 photoproduction. (b) two-step incoherent ρ^0 photoproduction, which interferes with (a). (c) one-step incoherent π^+ photoproduction. (d) two-step incoherent π^+ photoproduction mediated by ρ^0 and ω mesons. (c) and (d) interfere.

process (except for π^0's at very small $p_\perp$) which is described by the similar "one-step" and "two-step" contributions, illustrated in Fig. 208c,d. In the two-step contribution, the photon converts coherently to a superposition of vector mesons which scatters coherently before creating a pion incoherently. Higher-order incoherent multiple scatterings of the outgoing pion are likely now to be of some relative importance. Roughly speaking, they reduce the effective cross section for removing pions by allowing elastically scattered pions to be counted as produced particles. An estimate of such corrections is included in calculations made by von Bochmann, Margolis, and Tang (1970). A crude way to include the effect is to reduce σ_π by σ_π^{el}. The cautionary remarks at the end of Sec. B.2 are even more relevant here.

Returning now to coherent processes, we consider Compton scattering, which includes total photon absorption through the optical theorem. Because of the small two-body total cross section, photon scattering on a nucleus is calculated to lowest order in e. As illustrated in Fig. 201, there are two contributions: coherent photon scattering on a single nucleon (one-step) and coherent photoproduction of hadrons on one nucleon followed by the inverse process on another. Together these give

$$\langle 0|\Gamma_\gamma^A(\mathbf{b})|0\rangle = \sum_i \langle 0|\Gamma_\gamma(\mathbf{b}-\mathbf{s}_i)|0\rangle + \sum_{i,k} \langle 0|\Gamma_{\gamma h}(\mathbf{b}-\mathbf{s}_i) e^{i\Delta_{\gamma h}(z_i-z_k)} \times \sum_{j\neq i,k} [1-\theta(z_j-z_k)\theta(z_i-z_j)\Gamma_h(\mathbf{b}-\mathbf{s}_j)] \times \Gamma_{\gamma h}(\mathbf{b}-\mathbf{s}_k)|0\rangle . \quad \text{(B16)}$$

The first term alone would give a total cross section proportional to A. The second term provides the compensation corresponding to shadowing. Following the usual procedures, this may be reduced to Eq. (5.4).

In all our discussions, we have obviously neglected an infinite number of possible chains of reactions that could lead to the desired final states. If sufficiently complex chains were important, the usefulness of the model would be destroyed. Past successes of the model, as well as theoretical arguments discussed in Sec. II. E, indicate that amplitudes with a small number of hadronic steps usually provide a good approximation.

Regrettably, none of the more refined effects of correlations that are important for incoherent processes have been reliably calculated. The simple models used for incoherent processes either ignore these problems completely or put in very crude corrections. Experimentally, these simple models have not been a total failure, but the weight of evidence in their favor is not nearly as impressive as in the case of coherent processes. Since our theoretical treatments are so clearly inadequate, flaws in the optical model for these processes simply cannot be ruled out.

4. Particle production and Compton scattering from deuterium

We have reviewed the motivation for using a deuterium target in Sec. IV.B. Here we summarize briefly the notations used in this paper. The reader is cautioned that there is a variety of conventions and approximations employed in the literature.

Most analyses depend on the deuteron's ground-state density function $|\psi(\mathbf{r})|^2$. We use the convention that $\mathbf{r}$ is measured from the center-of-mass of the deuteron, while some authors use $\mathbf{r}$ for the separation of the neutron and proton. Thus some formulas in this paper will have a different appearance from those in the references quoted.

The best procedure to determine $|\psi(\mathbf{r})|^2$ is by elastic electron scattering. The actual quantity determined is $|F_d^{em}(q^2)|^2$ (we ignore complications arising from the magnetic and quadrupole moments) where F_d^{em} is the Fourier transform of the charge distribution (normalized so that $F_d^{em}(0)=1$). Since the charge density is a convolution of $|\psi(\mathbf{r})|^2$ and the internal charge density of the nucleons, one should really divide F_d^{em} by the electromagnetic form factor of the proton before deriving $|\psi(\mathbf{r})|^2$. Typically, this seems not to be done. In addition, many papers use a rather crude fit to the electromagnetic form factor, namely,

$$F_d^{em}(t) = e^{14t} \quad (t \text{ in GeV}^2) . \quad \text{(B17)}$$

We have not tried to trace the origin of this expression. It gives a rough agreement with electron scattering for $|t|<0.1$, but then falls far below the actual data (Buchanan and Yearian, 1965). We have found that the following form

$$F_d^{em}(t) = [1+6.69|t|]^{-2.5} \quad (t \text{ in GeV}^2) \quad \text{(B18)}$$

gives reasonable agreement with the data out to $|t|\sim 0.4$ GeV^2, where F_d^{em} is small enough to be neglected for most applications. Franco and Varma (1974) also give an improved expression for the deuteron form factor. We have not attempted to reanalyze the various data with the better fit (B18) or with the proton form-factor correction, but we expect that this could change some of the results slightly.

The calculation of various high-energy interactions using a deuteron target follows along the same lines as outlined for nuclei except that the independent particle model is no longer relevant; the neutron and proton positions are correlated through $|\psi(\mathbf{r})|^2$. Calculating the elastic profile and using the optical theorem, one finds for the total cross section of projectile a

$$\sigma_{ad} = \sigma_{ap} + \sigma_{an} - \delta\sigma_{ad} , \quad \text{(B19a)}$$

where σ_{ap} and σ_{an} are the contributions where the projectile interacts with a single nucleon, and $\delta\sigma_{ad}$ (called the Glauber shadowing correction) is that where it interacts with both. A crude approximation for $\delta\sigma_{ad}$, which is useful for estimates, is given by

$$\delta\sigma_{ad} \approx \frac{1}{16\pi}\sigma_{ap}\sigma_{an}\left\langle\frac{1}{r^2}\right\rangle_d \quad \text{(B19b)}$$

where $\langle 1/r^2\rangle_d$ is the mean inverse square of a nucleon distance from the center of mass (in other papers the factor in front is usually $1/4\pi$, and r is the neutron-proton separation). Equation (B19b) is valid only if, among other restrictions, the elastic scattering amplitudes are purely imaginary, and if the individual nucleon profiles have a spatial extent much smaller than the deuteron

size. For pions, the correction amounts to around 5%. A more complete and accurate discussion of the subject is provided by Franco and Glauber (1966).

Analogously to (B19a), the expression for an elastic scattering or production amplitude on deuterium will take the form

$$T_d(t) = F_d(t)\,[T_p(t) + T_n(t)] + \delta T_d(t)\,. \tag{B20}$$

Here $F_d(t)$ is the nonrelativistic deuteron form factor defined by

$$F_d(t) \equiv \int e^{i\mathbf{q}\cdot\mathbf{r}} |\psi(r)|^2 d^3r \tag{B21}$$

$$t = -\mathbf{q}^2\,.$$

As mentioned before, this should be $F_d^{\rm em}(t)$ divided by the proton's electromagnetic form factor. Here $\delta T_d(t)$ is the multiple-scattering contribution. Since it arises from the part of the wave function where the neutron and proton are oriented along the incident direction, $\delta T_d(t)$ has a broader t distribution than the first term. In fact, it becomes the dominant term in the R. L. Anderson *et al.* (1971) experiment on wide-angle ρ^0 elastic photoproduction from deuterium (see Sec. III.C).

More usually, one measures cross sections where the final deuteron is not observed. In that case, one may use closure to sum over the final states of the two nucleons, giving

$$\left(\frac{d\sigma}{dt}\right)_{\rm clos} = |T_p(t)|^2 + |T_n(t)|^2 + 2F(4t)\,{\rm Re}(T_n(t)T_p^*(t)) + (\text{mult. scatt. contr.}). \tag{B22}$$

Complete expressions for (B19), (B20), and (B22) may be found in Franco and Glauber (1966).

For the application of this formalism to vector-meson photoproduction (Secs. III.C, D), see the complete discussion by Julius (1971, 1972a, b). The applications to the total photon cross section (Sec. III.A) and Compton scattering (Sec. III.B) are discussed by Brodsky and Pumplin (1969). The formalism may also be extended to describe nondiffractive, inelastic photoproduction involving charge exchange and/or spin-dependent contributions (e.g., charged-pion photoproduction). Here the Pauli principle may be important in the final states (see Franco and Glauber, 1966, and Julius, 1972a, b).

Serious questions arise concerning the finer details of the model. As deuterons provide our simplest neutron target, the temptation exists to extract precise values for neutron cross sections. However, great theoretical uncertainty exists at the level of the multiple-scattering corrections.

As pointed out by Franco and Glauber (1966), calculation of multiple-scattering corrections depends critically on the poorly known, short-distance behavior of the deuteron wave function [N.B., the appearance of $\langle 1/r^2\rangle_d$ in Eq. (B19b)]. Elaborating on such difficulties, West (1971) has pointed out that it is also necessary to correct for the "Fermi" motion in the deuteron. The correction is complicated and has several aspects. First, there is the shift in the total center-of-mass energy due to the motion of the constituent nucleons; second, there is a change in the flux of the incident particles in the rest frame of the struck nucleons; third, there is a restriction in the available phase space due to the fact that the constituents are not free nucleons but bound nucleons; fourth, there is general ignorance as to how to treat scattering by off-mass-shell particles. These effects depend crucially upon the distribution of nucleon momenta and in particular upon the tail of the momentum distribution in the deuteron. With the assumption that the deuteron is a simple bound state of two nucleons, this problem has been analyzed by Atwood and West (1973) and by Dominguez, Gunion, and Suaya (1972). These new corrections are found to be of the same order of magnitude as those of high-energy multiple-scattering theory. In our opinion, no one really knows how to calculate the part of the cross section associated with the situation where the target nucleons are overlapping since this cannot be reduced to simple two-body interactions. We feel that this leaves a residual uncertainty of the same size as the West correction itself. Frankfurt and Strickman (1976) also question the validity of the West correction.

APPENDIX C: MASS EXTRAPOLATION CORRECTIONS

Assuming the validity of the field-current identity (FCI), any deviation from VMD in its simplest form (2.7) may be called a "mass extrapolation correction" since it results from a dependence of the amplitude on the external masses. The importance of such corrections was mentioned in Sec. I.B, in connection with the analysis of photoproduction of pions. Other such effects are discussed qualitatively in Secs. II.B and IV.C in connection with the strong coupling of the ρ^0 to the $\pi^+\pi^-$ continuum. In this appendix, we shall discuss in more detail how the strong coupling of a vector meson to other channels leads to renormalization and other modifications of its propagator and scattering amplitudes. It will become clear that these modifications lead to some ambiguity in the interpretation of VMD; but we shall be able to choose a "most plausible" interpretation, and also give an estimate of the level of uncertainty introduced by this type of correction.

The bulk of our discussion will concern the ρ^0 and pion pair continuum since, as mentioned repeatedly throughout the paper, it provides the dominant low-mass contribution to the total photon cross section. The corrections here are therefore of very great practical importance. Also, for most purposes the coupling of the ρ^0 to other channels can be ignored, and the dipion system can be analyzed rather completely (see Yennie, 1975). Finally, we shall discuss briefly mass extrapolations in the $\phi - \omega$ system, a system made interesting (but complicated) by possible mixing effects.

We should make very clear at the outset the very tenuous nature of our discussion. The uncertainties produced by mass extrapolations could be dominated by other ones — for example, our uncertain knowledge of the width of the ρ^0 (that important parameter which influences both the determination of the coupling constants and normalization of the photoproduction cross section). In all cases, the couplings of the vector mesons to continuum channels are taken to be structureless, and

only the simplest channels are taken into account. The presence of form factors and the effects of other channels could make considerable quantitative changes in the results (Renard, 1974). In vector-meson photoproduction our "most plausible" VMD estimate, obtained by using the $\gamma - V$ coupling as determined by the $e^+ - e^-$ decay width $\Gamma_{V\to e^+e^-}$, arises rather naturally from the formalism, and we are thus able to bypass many uncertainties.

1. The ρ^0 propagator and the $\pi^+\pi^-$ continuum

Let us discuss first an approximation in which the finite width of the ρ^0 is taken into account, but other possible breakdowns of VMD are ignored. The reaction $e^+e^-\to\pi^+\pi^-$ is then pictured as in Fig. 209(a) where $f_{\rho\pi\pi}$ and $g_{\gamma\rho}$ are constants, but the ρ propagator contains all vacuum polarization bubbles arising from states coupling to the ρ^0. The propagator then takes the form

$$D_\rho(m^2)=\frac{1}{m^2-m_\rho^2+\Pi_\rho(m^2)}. \tag{C1}$$

The function $D_\rho(m^2)$ has a pole on the second, unphysical sheet when $m^2=\overline{m}_\rho^2-i\overline{m}_\rho\overline{\Gamma}_\rho$, where $\overline{m}_\rho,\overline{\Gamma}_\rho$ are the parameters which give the mass and width of the resonance. However, it is more convenient to specify the resonance by the position where the real part of the denominator vanishes. We define this to be m_ρ^2 and require

$$\mathrm{Re}\Pi_\rho(m_\rho^2)=0. \tag{C2}$$

(This corresponds to mass renormalization for stable particles.) In addition, it is necessary to specify a normalization convention for D_ρ (or, equivalently, the ρ^0's wave function). Two such conventions are in common usage:

Normalization Convention I:

$$D_\rho(m^2\approx m_\rho^2)\cong\frac{1}{m^2-m_\rho^2+im_\rho\Gamma_\rho}, \tag{C3a}$$

corresponding to

$$\mathrm{Re}\frac{d}{dm}\overline{\Pi}_\rho(m^2)\Big|_{m_\rho^2}=0. \tag{C3b}$$

Normalization Convention II: $D_\rho(0)=-\frac{1}{m_\rho^2}$, (C4a)

corresponding to

$$\Pi_\rho(0)=0. \tag{C4b}$$

From now on, *coupling constants* and propagator functions using Convention I will be labeled with a bar ($\bar{}$) and similar quantities in Convention II will be unlabeled.

In common with the usual treatment of stable particles, we shall, in this paper, normalize at the ρ^0 mass (Convention I). Motivated by theoretical behavior of amplitudes near $m^2=0$, Convention II is the one chosen by Kroll, Lee, and Zumino (1967) and is most natural when emphasizing the field-current identity (FCI). In studying the literature, the reader must take care to note which convention is employed, since sizeable differences between numerical values of coupling constants can occur in different conventions. The connection between the propagators in the two conventions is

$$D_\rho(m^2)=\left(1-\frac{\overline{\Pi}_\rho(0)}{m_\rho^2}\right)\overline{D}_\rho(m^2), \tag{C5a}$$

so that

$$\Pi_\rho(m^2)=\frac{m_\rho^2\overline{\Pi}_\rho(m^2)+(m^2-m_\rho^2)\overline{\Pi}_\rho(0)}{m_\rho^2-\overline{\Pi}_\rho(0)}. \tag{C5b}$$

The couplings in Convention I are related to those in Convention II by associating $\{1-[\overline{\Pi}_\rho(0)/m_\rho^2]\}^{1/2}$ with the coupling at each end of the ρ^0 propagator. Thus

$$\overline{g}_{\gamma\rho}=\left(1-\frac{\overline{\Pi}_\rho(0)}{m_\rho^2}\right)^{1/2}g_{\gamma\rho};\quad \overline{f}_{\rho\pi\pi}=\left(1-\frac{\overline{\Pi}_\rho(0)}{m_\rho^2}\right)^{1/2}f_{\rho\pi\pi}. \tag{C5c}$$

In either convention the imaginary part of Π_ρ is related to the width:

$$\mathrm{Im}\overline{\Pi}_\rho(m^2)=m_\rho\Gamma_\rho(m^2), \tag{C6a}$$

$$\mathrm{Im}\Pi_\rho(m^2)=m_\rho\Gamma_\rho\Big/\left(1-\frac{\overline{\Pi}_\rho(0)}{m_\rho^2}\right). \tag{C6b}$$

Ignoring other decay channels in the vicinity of the ρ^0, the width is given by

$$m_\rho\Gamma_\rho(m^2)=\frac{1}{3}\frac{\overline{f}_{\rho\pi\pi}^2}{4\pi}\frac{q_\pi^3}{\omega_\pi}=\frac{1}{3}\frac{f_{\rho\pi\pi}^2}{4\pi}\frac{q_\pi^3}{\omega_\pi}\left(1-\frac{\overline{\Pi}_\rho(0)}{m_\rho^2}\right), \tag{C7}$$

where $\omega_\pi=\frac{1}{2}m$, $q_\pi=(\omega_\pi^2-m_\pi^2)^{1/2}$, and $\overline{f}_{\rho\pi\pi}(f_{\rho\pi\pi})$ is the coupling of the ρ^0 to two pions using Convention I (II). Thus the measured width may be regarded as giving an experimental determination of the coupling of ρ^0 to two pions at the ρ^0 mass shell. The experimental uncertainty in this width is one of the most important weak links in our whole analysis.

Consistently with the field-current identity (FCI) (Sec. II.B), if we regard Fig. 209(a) as describing the theory exactly with constant couplings $\overline{g}_{\gamma\rho}$ and $\overline{f}_{\rho\pi\pi}$ (or $g_{\gamma\rho}$ and $f_{\rho\pi\pi}$), the values of these couplings in Convention I are related by the pion form factor at zero momentum trans-

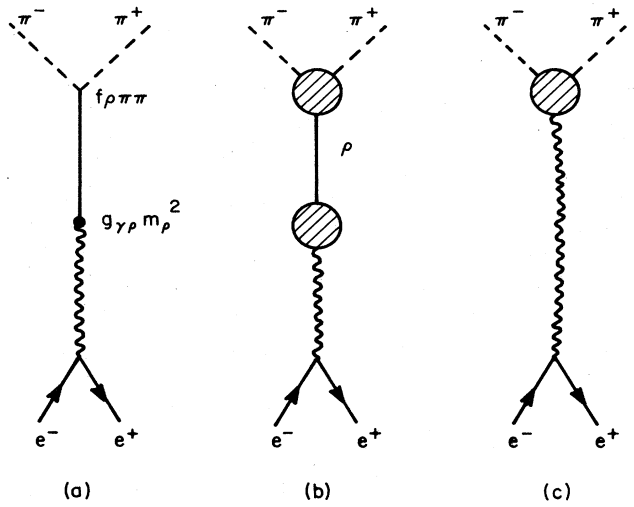

FIG. 209. Various possible contributions to $e^+e^-\to\pi^+\pi^-$. (a) Through a ρ^0, with pointlike couplings. (b) Through a ρ^0, with mass-dependent couplings. (c) Through states other than the ρ^0.

fer by

$$m_\rho^2 \frac{\bar{g}_{\gamma\rho}\bar{f}_{\rho\pi\pi}}{-m_\rho^2+\bar{\Pi}_\rho(0)} = e \tag{C8}$$

or

$$\bar{g}_{\gamma\rho} \equiv -\frac{e}{\bar{f}_\rho} = -\frac{e}{\bar{f}_{\rho\pi\pi}}\left(1-\frac{\bar{\Pi}_\rho(0)}{m_\rho^2}\right), \tag{C9a}$$

and in Convention II

$$g_{\gamma\rho} \equiv -\frac{e}{f_\rho} \equiv -\frac{e}{f_{\rho\pi\pi}}. \tag{C9b}$$

Note from (C5c), the various connections between coupling constants

$$\frac{f_\rho^2}{4\pi} = \frac{\bar{f}_\rho^2}{4\pi}\left(1-\frac{\bar{\Pi}_\rho(0)}{m_\rho^2}\right); \quad \frac{f_{\rho\pi\pi}^2}{4\pi} = \frac{\bar{f}_{\rho\pi\pi}^2}{4\pi}\left(1-\frac{\bar{\Pi}_\rho(0)}{m_\rho^2}\right)^{-1};$$
$$\frac{f_\rho^2}{4\pi} = \frac{f_{\rho\pi\pi}^2}{4\pi}; \quad \frac{\bar{f}_\rho^2}{4\pi} = \frac{\bar{f}_{\rho\pi\pi}^2}{4\pi}\left(1-\frac{\bar{\Pi}_\rho(0)}{m_\rho^2}\right)^{-2}. \tag{C10}$$

In this paper, we prefer Convention I since those couplings may be inferred directly from experiment, independently of the complications to be discussed in the following few paragraphs. For instance $\bar{f}_{\rho\pi\pi}$ is determined from the ρ^0 width (C7), and $\bar{f}_\rho$ is determined from the leptonic width by

$$\frac{\bar{f}_\rho^2}{4\pi} = \frac{\alpha^3}{3}\frac{m_\rho}{\Gamma_{\rho\to e^+e^-}}. \tag{C11}$$

Experimentally, this corresponds to measuring the strength of the ρ^0 resonance in $e^+e^-\to$ hadrons or the branching ratio of ρ^0 to e^+e^- or $\mu^+\mu^-$.

The factor $1-[\bar{\Pi}_\rho(0)/m_\rho^2]$ which appears repeatedly in these expressions is known as the Gounaris-Sakurai (1968) finite-width correction factor. This correction was also derived by Vaughn and Wali (1968). Since Π_ρ is analytic in the cut m^2 plane (cut: $4m_\pi^2 \le m^2 \le \infty$), $\mathrm{Re}\Pi_\rho$ can be determined from Im Π_ρ by using dispersion relations. In case Eq. (C7) is exactly true for all m, $\bar{\Pi}_\rho$ may be expressed in terms of a simple analytic function. Some useful formulas are given by Gounaris and Sakurai (1968) and by Yennie (1975). In this case, we find for $m_\rho = 0.77$ GeV

$$1-\frac{\bar{\Pi}_\rho(0)}{m_\rho^2} = 1+0.48\frac{\Gamma_\rho}{m_\rho}. \tag{C12}$$

It is physically clear that Fig. 209(a) represents an idealization of the process $e^+e^-\to\pi^+\pi^-$ and that, at some level, the corrections suggested by Figs. 209(b),(c) must play a role. Figure 209(c) represents contributions in which the γ couples to the pion through states other than the ρ^0 (e.g., higher mesons) in violation of the FCI. Figure 209(b) indicates an indirect coupling of the photon to the ρ^0 through other states; phenomenologically these latter contributions can make $\bar{g}_{\gamma\rho}$ a function of m^2; this, too, would violate the FCI. Finally, the upper blob of Fig. 209(b) also indicates an indirect coupling of the ρ^0 to pions; such contributions do not violate the FCI, and they are surely present (e.g., $\gamma\to\rho^0\to N\bar{N}\to\pi^+\pi^-$). Phenomenologically, these last contributions can be incorporated into the previous analysis by introducing a form factor for the $\rho\pi\pi$ coupling

$$\bar{f}_{\rho\pi\pi}\to\bar{f}_{\rho\pi\pi}F_{\rho\pi\pi}(m^2), \tag{C13}$$

where $|F_{\rho\pi\pi}(m_\rho^2)|=1$ in order to preserve Eq. (C7). The connection between $\bar{f}_\rho$ and $\bar{f}_{\rho\pi\pi}$ is now more complicated since $F_{\rho\pi\pi}(0)$ may not equal 1; and further, $\bar{\Pi}_\rho(0)$ will depend on $F_{\rho\pi\pi}(m^2)$ and on other decay channels, which can no longer be ignored.

Modifications represented by Fig. 209(c), which violate the FCI, would be very hard to distinguish from the effects of $F_{\rho\pi\pi}$. Renard (1974) and Bonneau and Martin (1973), and more recently Costa de Beauregard *et al.* (1977) have studied these questions extensively. Because of the final-state interaction theorem (phase of the pion form factor must be the same as that of $\pi^+\pi^-$ scattering), the complete amplitude from Fig. 209 should have the phase factor associated with the ρ^0 propagator.[55] Thus phenomenologically Fig. 209(c) is contained in Fig. 209(b). We shall not attempt to review these studies here. Suffice it to say that these ambiguities introduce some theoretical uncertainties in any determination of couplings from the data. They can for example give a normalization effect which would correspond to a deviation from the simplest form of VMD, and they could also skew the ρ^0 peak making the fitting somewhat uncertain. The present situation is that the theory of Costa de Beauregard *et al.* (1977), which incorporates the $\omega-\pi^0$ inelastic channel, does give a good account of the most recent experimental results (Quenzer *et al.*, 1977). Although we have been unable to make precise the effect of these refinements on the couplings ($\bar{f}_\rho^2$ and $\bar{f}_{\rho\pi\pi}^2$), it seems to be within about a 5% correction.

2. Practical analysis of $e^+e^-\to\pi^+\pi^-$

For the reasons just given, in fitting the $e^+e^-\to\pi^+\pi^-$ data in the ρ^0 region, it is best to leave the overall normalization (or $\bar{g}_{\gamma\rho}$) as a free parameter, rather than fix it by the Gounaris–Sakurai finite width factor (C9a). In effect, one determines the normalization of the p-wave Breit–Wigner portion of the data and defines the coupling in terms of the lepton pair width (C11), as in Tables XXIV and XXV. As is well known, the fitting of the peak is complicated by the presence of a small, but significant, interference with $\omega\to 2\pi$,[56] and by radiative corrections which distort its shape. When the older Orsay data were fitted by the experimental group (Benaksas *et al.*, 1972a), the values of Γ_ρ and m_ρ obtained were (1.49.6 ± 23.2) and (775.4 ± 7.3) MeV, corresponding to

[55] In our present discussion, Fig. 209 represents $e^+e^-\to\pi^+\pi^-$ in terms of field theory diagrams. The effect of final-state interactions could be to modify the Fig. 209(c) contribution by the factor $\cos\delta e^{i\delta}$ (in contrast to that of Fig. 209(a), which has the factor $\sin\delta e^{i\delta}$), giving a kind of double-counting correction at the resonant mass. The connection between such field theory diagrams and a dispersion theory calculation is not so obvious, although clearly one is trying to describe the same basic physics. One of us (D.R.Y.) wishes to thank Dr. T. N. Truong for interesting discussions of the refinements which are mentioned in this paragraph.

[56] An early review of ρ-ω mixing in various reactions was given by Goldhaber (1970). Since this is not a central subject for the present paper, we have not attempted to give a balanced status report on it.

$\bar{f}^2_{\rho\pi\pi}/4\pi = 2.85 \pm 0.50$. Other parameters are given in Sec. III.F. The $\rho - \omega$ mixing (interference) parameter ξ obtained in this fit is about twice as large as the one obtained in the experiments on photoproduction of pion pairs (Behrend *et al.*, 1971b; Alvensleben *et al.*, 1971a; and Biggs *et al.*, 1970b). A more recent, more accurate experiment (Quenzer *et al.*, 1977) has yielded a mixing parameter only 30% (±20%) larger than the photoproduction one (see Table XXVI). On the basis of our understanding of the photoproduction of vector mesons it is hard to understand a large difference between the two methods. In photoproduction the ωN scattering amplitude turns out to be nearly the same as the ρN scattering amplitude, and the $\rho \to \omega$ scattering amplitude $T_{\rho\omega}$ is quite small in a nucleus. Otherwise, the coupling constants entering the two processes are the same except for possible mass dependence of the $\gamma - V$ coupling. The photoproduction of ω's is modified slightly by $\phi - \omega$ interference, but its effect on ω photoproduction is not enough to account for a factor of 2. The new Orsay experiment eliminates this difficulty. A small reduction of the mixing effect in photoproduction is easily understandable in terms of an amplitude $T_{\gamma\omega}$ which is smaller than the VMD prediction by about 25%. This is not contradicted by experiment; perhaps it is even favored. Since we learned of these new results recently, only the old Orsay data have been refitted using a fixed value of the parameter ξ which agrees with the photoproduction value (see Sec. III.F). Results are shown in Table XXV. An acceptable χ^2 was obtained.

Clearly, the $e^+e^- \to \pi^+\pi^-$ measurement is the one which is most free of theoretical ambiguities in determining the width Γ_ρ. Until the Quenzer *et al.* (1977) experiment, however, the data were not sufficiently accurate to give a very precise value. Other experiments, suffering from theoretical ambiguities, also did not produce a "consensus" value. Therefore, throughout this paper, we have used three possible choices for the ρ^0 width, namely, 135, 145, and 155 MeV. This range probably includes the "correct" value, and the reader may interpolate in our tables to find results for his favorite value of Γ_ρ. The Quenzer *et al.* results now lead us to strongly prefer the largest value (~155 MeV — see Table XXVI).

3. Photoproduction of $\pi^+\pi^-$ and ρ^0-meson scattering

The instability of the ρ^0 can also affect photoproduction of pion pairs in various ways. Some of these have already been described in Sec. IV.C. There a practical definition (4.3) was given of the cross section which was supposed to minimize the effects of the instability, except for an overall normalization proportional to the width of the ρ^0. The aim was to determine what the cross section would be for a stable ρ^0 if all other interactions were to remain the same. Unfortunately, this procedure cannot account for all the effects of the instability. The dipion system contained in the photon is rather extended and can only approximately be regarded as two independent pieces — a ρ^0 core, and a pair of nonresonant pions. These two intimately related structures can continuously transform into each other while passing through hadronic matter.

The uncertainties due to these coupled channels come to a head in trying to decide which is the most appropriate VMD estimate for ρ^0 photoproduction. On the one hand, one might argue that the photon coupling times the ρ^0 propagator for $k^2 = 0$ is

$$\frac{e}{\bar{f}_\rho}\frac{m_\rho^2}{m_\rho^2 - \bar{\Pi}_\rho(0)} = \frac{e}{\bar{f}_{\rho\pi\pi}}$$

so that $\bar{f}_{\rho\pi\pi}$ is the appropriate coupling to use in the naive VMD formula. On the other hand, from the discussion of Sec. II.B, the amount of ρ^0 resonance in the photon structure is given by $e/\bar{f}_\rho$, making $\bar{f}_\rho$ the coupling to use. (An erroneous application of Convention II would suggest an intermediate choice, namely, f_ρ! However, when the normalization of the ρ^0 is taken into account, this would give the same result as the first viewpoint.) Because the two basic choices give cross-section predictions differing by 20% (even more for the ϕ), it is important to determine which is most plausible. As will now be described, we believe the ambiguity is to be resolved in favor of the choice $\bar{f}_\rho$.

In addition to vacuum polarization effects in the propagator, there exists an additional finite width correction indigenous to the photoproduction amplitude when the "material" in the vacuum polarization bubbles, say π pairs, scatters from the target. To be specific, consider the contributions of ρ^0 scattering shown in Fig. 210. By appropriate choice of m_1 and m_2, we can describe $T_{\rho\rho}$, $T_{\gamma\rho}$, or $T_{\gamma\gamma}$ as a sum of these two types of contributions. The loop integral in the contribution from Fig. 210(b) would be formally divergent. The divergent part of the loop integral could be lumped with the contribution from Fig. 210(a) as a kind of renormalization effect. Together they would give a contribution agreeing with VMD. The remaining finite piece from Fig. 210(b) is expected to be sensitive to the external masses. When the ρ^0 is observed by its decay into $\pi^+\pi^-$ pairs, the imaginary part of the loop integral gives an important contribution to $T_{\gamma\rho}$ which exactly cancels the Drell (1960)–Söding (1966) amplitude when the pion pair is at the ρ^0 mass shell (Bauer, 1970; Pumplin, 1970); this is known as the double-counting correction. The strength of this finite piece is easily seen to be of relative order Γ_ρ/m_ρ.

If we assume the two pions scatter from the nucleon target with an amplitude T^c and a cross section constant with energy, then in the $t = 0$ limit, as shown by Bauer and Yennie (1976a), we may estimate the contribution of the real part of the loop integral, Fig. 210(b), to be

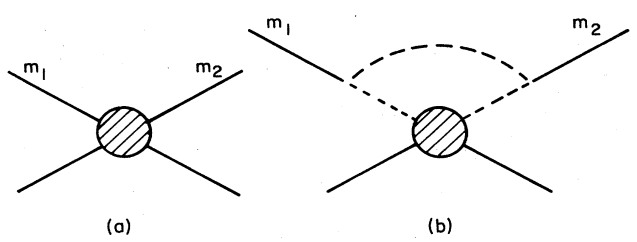

FIG. 210. Two classes of contributions to off-mass-shell vector-meson scattering. (a) Direct scattering where the blob is assumed to be independent of m_1 and m_2 [including renormalization-type contributions from (b)]. (b) A contribution from scattering of a decay channel coupled to the vector meson.

$$T^c_{m_1,m_2}=\left\{\frac{\mathrm{Re}\overline{\Pi}_\rho(m_1^2)-\mathrm{Re}\overline{\Pi}_\rho(m_2^2)}{m_1^2-m_2^2}\right\}T^c_{\rho\rho}\,. \tag{C14}$$

With the normalization conventions (C2), (C3b), $T^c_{m_1,m_2}(t)=0$ when $m_1^2=m_2^2=m_\rho^2$. So the loop integral's contribution to ρ^0 elastic scattering is already included in Fig. 210(a), which then represents the entire ρ^0 elastic scattering amplitude $T_{\rho\rho}(t)$. Equation (C14) then gives corrections for $m_1^2, m_2^2 \neq m_\rho^2$.

Applying these results to ρ^0 photoproduction, $m_1^2=0$, $m_2^2=m_\rho^2$, and (ignoring the imaginary part of the loop integral) we find

$$T_{\gamma\rho}=-\bar{g}_{\gamma\rho}T_{\rho\rho}-\frac{e}{\bar{f}_{\rho\pi\pi}}\frac{\overline{\Pi}_\rho(0)}{m_\rho^2}(T^c_{\rho\rho}-T_{\rho\rho})\,. \tag{C15}$$

Recall $\bar{g}_{\gamma\rho}\equiv e/\bar{f}_\rho$. The first term on the rhs of Eq. (C15) is the ordinary VMD expression for photoproduction, employing $e/\bar{f}_\rho$ instead of $e/\bar{f}_{\rho\pi\pi}$. *Thus, in a sense, the finite width correction in the production amplitude* (C14) *cancels out the finite width correction in the propagator*! The remaining correction on the rhs of (C15) probably gives a measure of the theory's uncertainty. As T^c is rather imperfectly known, we arbitrarily estimate this uncertainty by assuming $|T^c_{\rho\rho}-T_{\rho\rho}|\leq 0.5T_{\rho\rho}$. Numerical estimates from this model (C15) are given in Bauer and Yennie (1976a).

Applying (C14) to the ρ^0 meson's contribution to the total photon cross section (imaginary part of forward Compton scattering), we take $m_1^2=m_2^2=-Q^2$ and write (for the transverse part)

$$\sigma_\gamma(\rho)=\frac{e^2}{\bar{f}^2_{\rho\pi\pi}}\left(\frac{m_\rho^2}{Q^2+m_\rho^2}\right)^2\sigma_\rho\left\{1+\frac{\sigma_c}{\sigma_\rho}\overline{\Pi}'_\rho(-Q^2)\right\}\,. \tag{C16}$$

Except for possibly different parameters, σ_c/σ_ρ, the correction from naive VMD given by $\{\cdots\}$ is the same for the analogous longitudinal cross section. For real ($Q^2=0$) photons $\Pi'_\rho(0)\approx 0.11$, and in a model calculation (Yennie, 1975) it is found that $\sigma_c/\sigma_\rho=1.7\pm 0.5$; as above, the ± 0.5 allows for model uncertainty. Numerical estimates of (C16) are given in Bauer and Yennie (1976a).

We don't really know how to incorporate Fig. 210(b) into a nuclear calculation. In space, the amplitudes involving low-mass π pairs probably have a large longitudinal range, so each pion probably passes through several nucleons between the times the system is in its ρ^0 state. On the other hand, amplitudes involving high-mass π pairs probably have enough space to re-form a ρ^0 between collisions (see discussions in Sec. II). Thus the amplitudes $T_{\gamma\rho}(0)$ and $T_{\rho\rho}(0)$ extracted in the type of analysis described in Sec. IV may require some reinterpretation. Interestingly enough, as the question of longitudinal range is energy dependent, so may be this reinterpretation. Rough estimates indicate in the present energy range ($\leq$15 GeV) that modifications to amplitudes of interest are still within the 10% level (Bauer, 1972).

In concluding this discussion of finite width corrections to these scattering/production amplitudes, we remark that the form (C14) is more general than the specific $\rho^0 \rightleftarrows 2\pi$ model employed. For appropriate T^c, σ_c and $\Pi(m^2)$, the preceding discussion should apply as well to ω and ϕ mesons and any appropriate states to be included in the vacuum polarization bubbles.

4. Corrections to ϕ and ω amplitudes

Discussions completely analogous to the preceding may be made concerning altered normalizations of propagators and scattering amplitudes, arising from the appropriate coupling of the $\phi(\omega)$ to the isoscalar $2K$ and 3π continua. As calculated by Renard (1970), the modification of ω amplitudes is small $[\overline{\Pi}_\omega(0)/m_\omega^2\approx 0.00]$. It is, however, rather substantial in the case of the ϕ $[\overline{\Pi}_\phi(0)/m_\phi^2\approx 0.15]$, principally due to intermediate K^*K^- and $K\bar{K}$ particles. This effect could lead to a large uncertainty in the VMD prediction for ϕ photoproduction, as the second term on the right-hand side of (C15) along with the propagator/coupling constant corrections are not easily ignored. However, the 15% estimate for $\overline{\Pi}_\phi(0)/m_\phi^2$ is very sensitive to model-dependent cutoffs (Renard, 1974); so corrections to the first term on the right-hand side of (C15) are hard to assess.

Moreover, the above estimates have ignored additional corrections owing to ϕ,ω mixing. The possibility of ϕ,ω mixing actually appearing in photoproduction has already been mentioned in Secs. II.B and IV.D, but here we wish to note the possibility that intermediate $\omega(\phi)$ states might affect $\Pi_\phi(\Pi_\omega)$. Another way of viewing this effect is that at each m^2 a different transformation is needed to "diagonalize" the combined ϕ,ω system. (This is made plausible by the fact that the ϕ and ω are coupled by intermediate $2K$ and 3π states, with m^2-dependent coupling strengths.)

Unfortunately, there exists no simple and unambiguous model for unraveling the ϕ,ω superposition at all values of m^2. An ambitious attempt to analyze ϕ,ω colliding-beam cross sections that takes into account many fairly realistic alternatives was undertaken by Renard (1974). The resulting array of coupling constants found under different mixing hypotheses (SU_3 or not SU_3, high-mass cutoffs or not, etc.) probably reveals more about the uncertainties of this finite-width analysis than definitive information about mass extrapolation effects in the ϕ,ω system.

APPENDIX D: ANGULAR DISTRIBUTION OF DECAY PRODUCTS IN VECTOR-MESON PRODUCTION FROM SINGLE NUCLEONS

In this appendix, we summarize the results which are important for the analysis of present experiments. Our aim is to present the general ideas rather than a detailed treatment. For that, the reader is referred to original sources.

1. Vector-meson photoproduction

Here, as an illustrative example, we discuss the case of ρ^0 decay into $\pi^+\pi^-$ and consider the angular distribution of the π^+-momentum vector in the ρ^0's rest frame. There is no loss of generality in this approach since, in a more complicated decay scheme (e.g., ω decay discussed in Sec.III.D), the role of the π^+-momentum vector will simply be played by another vector more appropriate to the decay state being studied. A thorough treatment of the angular distribution may be found in Schilling *et al.* (1970); some useful results are also to be found in Ballam *et al.* (1972).

The relevant angles for the decay are shown in Fig.211 from Ballam *et al.* (1972). The x-z plane is the production plane, with the orientation of the z axis relative to the photon's momentum chosen arbitrarily. Specific choices correspond to the Gottfried–Jackson, Adair, or helicity systems described in Sec.III.C.

With a linearly polarized or unpolarized photon beam, the normalized decay distribution is given by

$$W(\cos\theta,\phi,\Phi)=\frac{3}{4\pi}\left[\tfrac{1}{2}(1-\rho^0_{00})+\tfrac{1}{2}(3\rho^0_{00}-1)\cos^2\theta-\sqrt{2}\,\mathrm{Re}\rho^0_{10}\sin2\theta\cos\phi-\rho^0_{1-1}\sin^2\theta\cos2\phi\right.$$
$$-P_\gamma\cos2\Phi(\rho^1_{11}\sin^2\theta+\rho^1_{00}\cos^2\theta-\sqrt{2}\,\mathrm{Re}\rho^1_{10}\sin2\theta\cos\phi-\rho^1_{1-1}\sin^2\theta\cos2\phi)$$
$$\left.-P_\gamma\sin2\Phi(\sqrt{2}\,\mathrm{Im}\rho^2_{10}\sin2\theta\sin\phi+\mathrm{Im}\rho^2_{1-1}\sin^2\theta\sin2\phi)\right] \tag{D1}$$

Here P_γ is the degree of linear polarization of the incident photon beam (along ϵ_γ). The ρ^α_{ik} are the spin-density matrix elements of ρ^0 decay. The i and k indices refer to the helicity of the produced ρ^0 meson and the α index (0, 1, 2) is related to the photon's polarization. The ρ^α_{ik} are defined as bilinear combinations of helicity production amplitudes $T_{\lambda_\rho\lambda_N,\lambda_\gamma\lambda_N}$. Parity conservation leads to symmetries among the ρ^α_{ik} so that there are only nine independent terms in Eq.(D1).

If it is possible to choose the z axis so that s-channel helicity is conserved, W takes a particularly simple form as a function of $\Psi\equiv\Phi-\phi$, namely

$$W(\theta,\Psi)\propto(\sin^2\theta+P_\gamma\sin^2\theta\cos2\Psi). \tag{D2a}$$

This results from the relationships

$$\rho^1_{1-1}=-\mathrm{Im}\rho^2_{1-1}=\tfrac{1}{2} \tag{D2b}$$

with all other $\rho^\alpha_{ik}=0$ in (D1).

2. Vector-meson leptoproduction

As before, without loss of generality, we discuss ρ^0 production and decay and consider the angular distribution of the π^+-momentum vector. The analysis is more complicated because the photon is virtual and has both longitudinal and transverse polarization components. A thorough discussion may be found in Schilling and Wolf (1973).

With an unpolarized incident lepton beam, Fig. 211 is still adequate to describe the decay π^+ in the decaying ρ^0's rest frame. "γ" stands for the momentum of the virtual photon, and the production plane is understood as that of virtual photoproduction. "ϵ_γ" no longer has direct meaning, but the angle Φ now denotes the angle between the production plane and the plane of the incident and scattered leptons. As depicted, Φ is the azimuthal angle of the scattered lepton relative to the direction of the virtual photon and the production plane. As before, the particular orientation of the z axis within the production plane relative to the virtual photon direction is arbitrary and corresponds to a choice of a particular frame.

The normalized distribution of π^+ decays with an unpolarized lepton beam is given by

$$W(\cos\theta,\phi,\Phi)=\frac{3}{4\pi}\left[\tfrac{1}{2}(1-r^{04}_{00})+\tfrac{1}{2}(3r^{04}_{00}-1)\cos^2\theta-\sqrt{2}\,\mathrm{Re}\,r^{04}_{10}\sin2\theta\cos\phi-r^{04}_{1-1}\sin^2\theta\cos2\phi\right.$$
$$-\epsilon\cos2\Phi\{r^1_{11}\sin^2\theta+r^1_{00}\cos^2\theta-\sqrt{2}\,\mathrm{Re}\,r^1_{10}\sin2\theta\cos\phi-r^1_{1-1}\sin^2\theta\cos2\phi\}$$
$$-\epsilon\sin2\Phi\{\sqrt{2}\,\mathrm{Im}\,r^2_{10}\sin2\theta\sin\phi+\mathrm{Im}r^2_{1-1}\sin^2\theta\sin2\phi\}$$
$$+\sqrt{2\epsilon(1+\epsilon+\Delta)}\cos\Phi\{r^5_{11}\sin^2\theta+r^5_{00}\cos^2\theta-\sqrt{2}\,\mathrm{Re}\,r^5_{10}\sin2\theta\cos\phi-r^5_{1-1}\sin2\theta\cos2\phi\}$$
$$\left.+\sqrt{2\epsilon(1+\epsilon+\Delta)}\sin\Phi\{\sqrt{2}\,\mathrm{Im}\,r^6_{10}\sin2\theta\sin\phi+\mathrm{Im}r^6_{1-1}\sin^2\theta\sin2\phi\}\right]. \tag{D3}$$

Here ϵ is the virtual photon's polarization parameter given by

$$\epsilon=\left[1+\frac{2(Q^2+\nu^2)}{\beta Q^2}\tan^2\frac{\Theta}{2}\right]^{-1} \tag{D4}$$

where Θ is the lepton scattering angle, $\beta=(1-Q^2_{\min}/Q^2)^2$, and $Q^2_{\min}$ is the value of Q^2 as $\Theta\to0$. The parameter Δ is given by

$$\Delta=\frac{2M_l^2}{Q^2}(1-\epsilon), \tag{D5}$$

where M_l is the lepton mass. The parameters $r^{04}_{ik}, r^\alpha_{ik}$

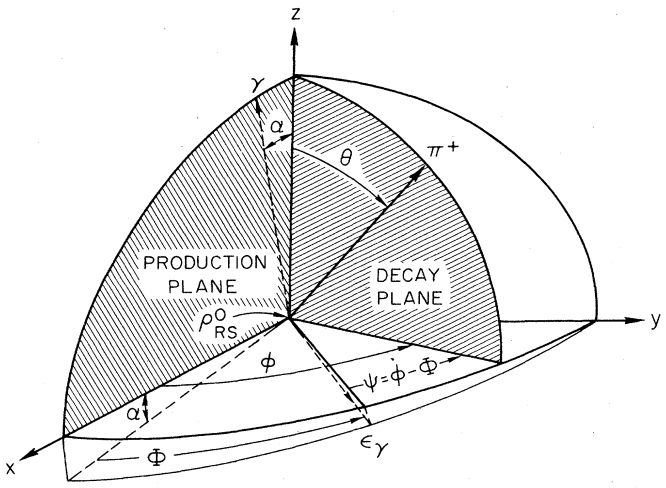

FIG. 211. Angles used in the analysis of ρ^0 decay in photoproduction. Choice of angle α specifies "system" used. These angles are also useful for describing decay in ρ^0 leptoproduction—see text (from Ballam *et al.*, 1972).

are linear combinations of density matrix elements $\rho^{\alpha}_{ik}(\alpha=0,1,\ldots 6)$, which in turn are bilinear combinations of helicity amplitudes. More of these are necessary now because of the more complicated polarization state of the photon.

As in the photoproduction case, W takes on a particularly simple form if s-channel helicity is conserved. In terms of $\Psi \equiv \Phi - \phi$, it becomes

$$W(\theta,\Psi)\propto\epsilon R\cos^2\theta+\tfrac{1}{2}\sin^2\theta(1+\epsilon\cos 2\Psi) - [\tfrac{1}{2}\epsilon R(1+\epsilon)]^{1/2}\cos\delta\sin 2\theta\cos\Psi. \quad \text{(D6)}$$

In this case, all the r^{α}_{ik} in (D3) vanish except r^4_{00}, r^1_{1-1}, $\mathrm{Im}r^2_{1-1}$, $\mathrm{Re}r^5_{10}$, and $\mathrm{Im}r^6_{10}$, and R is given by

$$R=\frac{1}{\epsilon}\frac{r^{04}_{00}}{1-r^{04}_{00}}. \quad \text{(D7)}$$

The parameters have the following significance: R is the ratio of ρ^0 production by longitudinal photons to that by transverse photons, and δ is the relative phase between these two production amplitudes.

APPENDIX E: GLOSSARY OF NOTATION

Most of the specialized notation is defined where it is needed in the text. This glossary collects for ready reference the notation which is used throughout the paper.

Coupling constants

Table I summarizes the definition of the most important constants. Couplings of the vector mesons to other channels are introduced occasionally. Normalization employed is such that $\alpha=e^2/4\pi$. In brief:

e/f_v — Coupling of the photon to the vector meson V at the vector-meson mass, in Convention I (see Appendix C).

$e/\hat{f}_v$ — Phenomenological coupling for diffractive photoproduction of V.

Total and partial cross sections

σ_a — Projectile a on a nucleon (average of proton and neutron targets).

$\sigma_{ap}, \sigma_{an}, \sigma_{ad}, \sigma_{\gamma A}$ — Target is specified as proton, neutron, deuteron, or nucleus A.

σ_L, σ_T — Projectile and target should be clear from the context, and L and T represent longitudinal and transverse cross sections (Secs. II.C, D and III.I). In Sec. III.F, $\sigma_{L,T}$ denote longitudinal and transverse features of angular distributions of hadrons in e^+e^- collisions.

$\sigma_a^{el}, \sigma_a^{N,U}$ — Superscript denotes part of total cross section: el for "elastic"; N or U for "natural- or unnatural-parity exchange part," etc.

Differential cross sections

$\frac{d\sigma}{dt}(AB\to CD)$ — Where necessary, the reaction is indicated in parentheses. If the reaction is clear from the context, the parentheses may be omitted or some simpler notation employed. Sometimes dt' ($\equiv t-t_{\min}$) or $d\Omega$ are used in place of dt (see Kinematic Variables, below).

Ae^{Bt+Ct^2} — An often used convenient parametrization of $d\sigma/dt$. Frequently fits are made with $C=0$; then B is called the slope. If t' is used in place of t, A is the forward differential cross section.

Deuteron form factor

$F_d(t)$ — See Appendix B for the definition. Caution should be observed in comparing different papers since, in a different convention, the argument of F_d is replaced by $\frac{1}{4}t$.

Kinematic variables

Units are GeV for energy, momentum, and mass. In most equations, we use natural units ($\hbar=c=1$).

k — Four-momentum of a real or virtual photon.

$Q^2 \equiv -k^2$ — Negative invariant squares of k.

k_0, ν, E_γ — Energy of a real or virtual photon, usually in the laboratory frame.

$|\mathbf{k}| = \sqrt{Q^2 + \nu^2}$ — Magnitude of photon momentum.

P — A particle four-momentum, with energy E, momentum p. Labels may be added for further specification. Without a label, it refers to the target.

s — Square of total center-of-mass energy of a collision.

W^2 — Same as s, applied to a real or virtual photon collision with a nucleon ($W^2 = M^2 + 2M\nu - Q^2$).

$q_\parallel, q_\perp$ — Spatial momentum transferred to a target by a projectile, parallel and perpendicular to the incident direction. For high-energy forward virtual photoproduction of particle b, $q_\parallel \approx (Q^2 + M_b^2)/2\nu$.

$t, t_{\min}, t'$ — t is the invariant formed from the four-momentum transfer to the nucleon. *At high energies*: $t \approx -(q_\parallel^2 + q_\perp^2)$, $t_{\min} = t(q_\perp^2 = 0)$, and $t' = t - t_{\min}$ (approximation is good provided $|t| \ll 4M^2$).

$x \equiv \frac{1}{\omega} \equiv Q^2/2k\cdot P = Q^2/2M\nu$ — A scaling variable for inelastic electron scattering (M = target mass).

$x' \equiv \frac{1}{\omega'} \equiv Q^2/(P^2 + 2k\cdot P) = Q^2/(M^2 + 2M\nu)$ — Another scaling variable for inelastic electron scattering.

Scattering amplitudes

T_{ab} — Amplitude for projectile a to turn into particle b on a nucleon (unspecified). In various contexts the "ab" label may be dropped and other details may be specified by additional subscripts or superscripts or parentheses. Normalization is chosen so that $|T|^2 = d\sigma/dt$ or $d\sigma/d\Omega$, whichever is more convenient in context. Then

$$T_{aa}(t=0) = \frac{i}{4\sqrt{\pi}}\sigma_a(1 - i\alpha_a), \quad \text{first normalization}$$

$$= \frac{ik}{4\pi}\sigma_a(1 - i\alpha_a), \quad \text{second normalization}$$

where α_a (or α_{ap}, α_{an}, etc.) is the ratio of the real to imaginary part of the forward amplitude for a scattering on a nucleon (more specifically, proton, neutron, etc.)

REFERENCES

Abrahamian, L. O., A. O. Aganiants, F. V. Adamian, V. D. Danielian, N. A. Damiokhina, S. R. Gevorkian, M. Kh. Israelian, G. Kh. Kazarin, A. G. Khudaverdian, L. S. Khurshoodian, A. N. Lebediev, J. V. Manukian, E. G. Muradian, A. M. Sirunian, H. A. Vartapetien, and A. L. Vatian, 1972, Phys. Lett. B **38**, 544.

Abrams, G. S., D. Briggs, W. Chinowsky, C. E. Friedberg, G. Goldhaber, R. J. Hollebeek, J. A. Kadyk, A. Litke, B. Lulu, F. Pierre, B. Sadoulet, G. H. Trilling, J. S. Whitaker, J. Wiss, J. E. Zipse, J.-E. Augustin, A. M. Boyarski, M. Breidenbach, F. Bulos, G. J. Feldman, G. E. Fischer, D. Fryberger, G. Hanson, B. Jean-Marie, R. R. Larsen, V. Lüth, H. L. Lynch, D. Lyon, C. C. Morehouse, J. M. Paterson, M. L. Perl, B. Richter, P. Rapidis, R. F. Schwitters, W. Tanenbaum, and F. Vannucci, 1974, Phys. Rev. Lett. **33**, 1453.

Abrams, G. S., D. D. Briggs, W. Chinowsky, C. E. Friedberg, G. Goldhaber, J. A. Kadyk, A. M. Litke, B. A. Lulu, F. M. Pierre, B. Sadoulet, G. H. Trilling, J. S. Whitaker, J. E. Wiss, J. E. Zipse, A. M. Boyarski, M. Breidenbach, F. Bulos, G. J. Feldman, G. E. Fischer, D. Fryberger, G. Hanson, B. Jean-Marie, R. R. Larsen, V. Lüth, H. L. Lynch, D. Lyon, C. C. Morehouse, J. M. Paterson, M. L. Perl, P. Rapidis, B. Richter, R. F. Schwitters, W. Tanenbaum, and F. Vannucci, 1975, Phys. Rev. Lett. **34**, 1181.

Abrams, G. S., 1975, in *Proceedings of the 1975 International Symposium on Lepton and Photon Interactions at High Energies*, edited by W. T. Kirk (SLAC, Stanford, Calif.), p. 25.

Abramson, J., D. E. Andrews, J. Harvey, F. Lobkowicz, E. N. May, C. A. Nelson, Jr., M. Singer, E. H. Thorndike, and M. E. Nordberg, Jr., 1976, Phys. Rev. Lett. **36**, 1428.

Ahrens, L., K. Berkelman, G. S. Brown, D. G. Cassel, W. R. Francis, P. H. Garbincius, D. Harding, D. L. Hartill, J. L. Hartmann, R. L. Loveless, R. C. Rohlfs, D. H. White, and A. J. Sadoff, 1973, Phys. Rev. Lett. **31**, 131.

Ahrens, L., K. Berkelman, G. S. Brown, D. G. Cassel, W. R. Francis, P. H. Garbincius, D. Harding, D. L. Hartill, J. L. Hartmann, R. L. Loveless, R. C. Rohlfs, D. H. White, and A. J. Sadoff, 1974, Phys. Rev. D **9**, 1894.

Alexander, G., J. Gandsman, A. Levy, D. Lissauer, and L. M. Rosenstein, 1974, Nucl. Phys. B **69**, 445.

Alexander, G., O. Benary, J. Gandsman, D. Lissauer, A. Levy, Y. Oren, and L. M. Rosenstein, 1975, Phys. Lett. B **57**, 487.

Alexander, G., O. Benary, J. Gandsman, A. Levy, D. Lissauer, and Y. Oren, 1976, Nucl. Phys. B **104**, 397.

Alles-Borelli, V., M. Bernardini, D. Bollini, P. L. Brunini, E. Fiorentino, T. Massam, L. Monari, F. Palmonari, and A. Zichichi, 1972, Nuovo Cimento A **7**, 330.

Alvensleben, H., U. Becker, W. K. Bertram, M. Chen, K. J. Cohen, T. M. Knasel, R. Marshall, D. J. Quinn, M. Rohde, G. H. Sanders, H. Schubel, and S. C. C. Ting, 1969, Phys. Rev. Lett. **23**, 1058.

Alvensleben, H., U. Becker, W. K. Bertram, M. Chen, K. J. Cohen, T. M. Knasel, R. Marshall, D. J. Quinn, M. Rohde, G. H. Sanders, H. Schubel, and S. C. C. Ting, 1970a, Phys. Rev. Lett. **24**, 786.

Alvensleben, H., U. Becker, W. K. Bertram, M. Chen, K. J. Cohen, T. M. Knasel, R. Marshall, D. J. Quinn, M. Rohde, G. H. Sanders, H. Schubel, and S. C. C. Ting, 1970b, Nucl. Phys. B **18**, 333.

Alvensleben, H., U. Becker, W. K. Bertram, M. Chen, K. J. Cohen, R. T. Edwards, T. M. Knasel, R. Marshall, D. J. Quinn, M. Rohde, G. H. Sanders, H. Schubel, and S. C. C. Ting, 1970c, Phys. Rev. Lett. **25**, 1373.

Alvensleben, H., U. Becker, M. Chen, K. J. Cohen, T. M. Knasel, R. Marshall, D. J. Quinn, M. Rohde, G. H. Sanders, H. Schubel, and S. C. C. Ting, 1970d, Phys. Rev. Lett. **25**, 1377.

Alvensleben, H., U. Becker, W. Busza, M. Chen, K. J. Cohen, R. T. Edwards, P. M. Mantsch, R. Marshall, T. Nash, M. Rohde, H. F. W. Sadrozinski, G. H. Sanders, H. Schubel, S. C. C. Ting, and Sau Lan Wu, 1971a, Phys. Rev. Lett. **27**, 888.

Alvensleben, H., U. Becker, W. Busza, M. Chen, K. J. Cohen, R. T. Edwards, P. M. Mantsch, R. Marshall, T. Nash, M. Rohde, H. F. W. Sadrozinski, G. H. Sanders, H. Schubel, Samuel C. C. Ting, and Sau-Lan Wu, 1971b, Phys. Rev. Lett. **27**, 444.

Alvensleben, H., U. Becker, W. K. Bertram, M. Chen, K. J. Cohen, R. T. Edwards, T. M. Knasel, R. Marshall, D. J. Quinn, M. Rohde, G. H. Sanders, H. Schubel, and S. C. C. Ting, 1971c, Nucl. Phys. B **25**, 333.

Alvensleben, H., U. Becker, M. Chen, K. J. Cohen, R. T. Edwards, T. M. Knasel, R. Marshall, D. J. Quinn, M. Rohde, G. H. Sanders, H. Schubel, and S. C. C. Ting, 1971d, Nucl. Phys. B **25**, 342.

Alvensleben, H., U. J. Becker, W. K. Bertram, M. Chen, K. J. Cohen, R. T. Edwards, T. M. Knasel, R. Marshall, D. J. Quinn, M. Rohde, G. M. Sanders, H. Schubel, and S. C. C. Ting, 1971e, Phys. Rev. Lett. **26**, 273.

Alvensleben, H., U. Becker, P. Biggs, M. Binkley, W. Busza, M. Chen, K. J. Cohen, E. Coleman, R. T. Edwards, P. M. Mantsch, R. Marshall, T. Nash, D. J. Quinn, M. Rohde, H. F. W. Sadrozinski, G. H. Sanders, H. Schubel, S. C. C. Ting, and Sau Lan Wu, 1972, Phys. Rev. Lett. **28**, 66.

Alvensleben, H., U. Becker, P. J. Biggs, W. Busza, M. Chen, R. T. Edwards, P. M. Mantsch, T. P. McCorriston, T. Nash, M. Rohde, H. F. W. Sadrozinski, H. Schubel, S. C. C. Ting, and S. L. Wu, 1973, Phys. Rev. Lett. **30**, 328.

Amaldi, U., R. Biancastelli, C. Bosio, G. Matthiae, J. V. Allaby, W. Bartel, G. Cocconi, A. N. Diddens, R. W. Dobinson, and A. M. Wetherell, 1973, Phys. Lett. B **44**, 112.

Amati, D., A. Stanghellini, and S. Fubini, 1962, Nuovo Cimento **26**, 896.

Ambrosio, M., G. Barbarino, G. Barbiellini, A. Barletta, C. Bemporad, R. Biancastelli, G. Brosco, M. Calvetti, M. Castellano, F. Costantini, G. R. Giannini, L. Lariccia, G. Paternoster, S. Patricelli, L. Tortora, and U. Troya, 1977, Phys. Lett. B **68**, 397.

Amendolia, S. R., G. Bellettini, P. L. Braccini, C. Bradaschia, R. Castaldi, V. Cavasinni, C. Cerri, T. Del Prete, L. Foa, P. Giromini, P. Laurelli, A. Menzione, L. Ristori, G. Sanguinetti, M. Valdata, G. Finocchiaro, P. Grannis, D. Green, R. Mustard, and R. Thun, 1973, Phys. Lett. B **44**, 119.

Amman, F., R. Andreani, M. Bassetti, M. Bernardini, A. Cattoni, V. Chimenti, G. F. Corazza, D. Fabiani, E. Ferlenghi, A. Massarotti, C. Pellegrini, M. Placidi, M. Puglisi, F. Soso, S. Tazzari, F. Tazzioli, and G. Vignola, 1969, Nuovo Cimento Lett. **1**, 729.

Anderson, H. L., V. K. Bharadwaj, N. E. Booth, R. M. Fine, W. R. Francis, B. A. Gordon, R. H. Heisterberg, R. G. Hicks, T. B. W. Kirk, G. I. Kirkbride, W. A. Loomis, H. S. Matis, L. W. Mo, L. C. Myrianthopoulos, F. M. Pipkin, S. H. Pordes, T. W. Quirk, W. D. Shambroom, A. Skuja, L. J. Verhey, W. S. C. Williams, R. Wilson, and S. C. Wright, 1976, Phys. Rev. Lett. **37**, 4; **37**, 1034(E).

Anderson, H. L., V. K. Bharadwaj, N. E. Booth, R. M. Fine, W. R. Francis, B. A. Gordon, R. H. Heisterberg, R. G. Hicks, T. B. W. Kirk, G. I. Kirkbride, W. A. Loomis, H. S. Matis, L. W. Mo, L. C. Myrianthopoulos, F. M. Pipkin, S. H. Pordes, T. W. Quirk, W. D. Shambroom, A. Skuja, M. A. Staton, W. S. C. Williams, L. J. Verhey, Richard Wilson, and S. C. Wright, 1977, Phys. Rev. Lett. **38**, 1450.

Anderson, R. L., D. Gustavson, J. Johnson, I. Overman, D. Ritson, and B. H. Wiik, 1969, Phys. Rev. Lett. **23**, 721.

Anderson, R. L., D. Gustavson, J. Johnson, I. Overman, D. Ritson, B. W. Wiik, R. Talman, J. K. Walker, and D. Worcester, 1970a, Phys. Rev. Lett. **25**, 1218.

Anderson, R. L., D. Gustavson, J. Johnson, D. Ritson, B. H. Wiik, W. G. Jones, D. Kreinick, F. Murphy, and R. Weinstein, 1970b, Phys. Rev. D **1**, 27.

Anderson, R. L., D. Gustavson, J. Johnson, I. Overman, D. M. Ritson, B. H. Wiik, R. Talman, and D. Worcester, 1971, Phys. Rev. D **4**, 3245.

Anderson, R. L., B. Gottschalk, D. B. Gustavson, D. M. Ritson, G. A. Weitsch, B. H. Wiik, H. J. Halpern, R. Prepost, and D. H. Tompkins, 1973a, Phys. Rev. Lett. **30**, 149.

Anderson, R. L., B. Gottschalk, D. B. Gustavson, D. M. Ritson, G. A. Weitsch, H. J. Halpern, R. Prepost, and D. H. Tompkins, 1973b, Phys. Rev. Lett. **30**, 627.

Anderson, R. L., 1976, in *Proceedings of the International Conference on the Production of Particles with New Quantum Numbers*, edited by D. B. Cline and J. J. Kolonko (University of Wisconsin, Madison), p. 102.

Anderson, R. L., W. W. Ash, D. B. Gustavson, T. Reicholt, D. M. Ritson, D. J. Sherten, C. K. Sinclair, U. Camerini, J. C. Learned, R. Prepost, and D. E. Wiser, 1977, Phys. Rev. Lett. **38**, 263.

Andrews, D. E., K. Berkelman, D. G. Cassel, D. L. Hartill, J. Hartmann, R. Kerchner, E. Lazarus, R. M. Littauer, R. L. Loveless, R. Rohlfs, D. H. White, and A. J. Sadoff, 1971, Phys. Rev. Lett. **26**, 864.

Andrews, D. E., J. Harvey, F. Lobkowicz, E. N. May, C. A. Nelson, Jr., E. H. Thorndike, and M. E. Nordberg, Jr., 1975a, Phys. Rev. Lett. **34**, 231.

Andrews, D. E., J. Harvey, F. Lobokowicz, E. N. May, C. A. Nelson, Jr., E. H. Thorndike, and M. E. Nordberg, Jr., 1975b, Phys. Rev. Lett. **34**, 1134.

Armstrong, T. A., W. R. Hogg, G. M. Lewis, A. W. Robertson, G. R. Brookes, A. S. Clough, J. M. Freeland, W. Galbraith, A. F. King, W. R. Rawlinson, N. R. S. Tait, J. C. Thompson, and D. W. L. Tolfree, 1971, Phys. Lett. B **34**, 535.

Armstrong, T. A., W. R. Hogg, G. M. Lewis, A. W. Robertson, G. R. Brookes, A. S. Clough, J. H. Freeland, W. Galbraith, A. F. King, W. R. Rawlinson, N. R. S. Tait, J. C. Thompson, and D. W. L. Tolfree, 1972a, Phys. Rev. D **5**, 1640.

Armstrong, T. A., W. R. Hogg, G. M. Lewis, A. W. Robertson, G. R. Brookes, A. S. Clough, J. H. Freeland, W. Galbraith, A. F. King, W. R. Rawlinson, N. R. S. Tait, J. C. Thompson, and D. W. L. Tolfree, 1972b, Nucl. Phys. B **41**, 445.

Asbury, J. G., U. Becker, W. K. Bertram, P. Joos, M. Rohde, A. J. S. Smith, C. L. Jordan, and S. C. C. Ting, 1967a, Phys. Rev. Lett. **19**, 865; **20**, 1134(E) (1968).

Asbury, J. G., U. Becker, W. K. Bertram, P. Joos, M. Rohde, A. J. S. Smith, C. L. Jordan, and S. C. C. Ting, 1967b, Phys. Rev. Lett. **19**, 869.

Asbury, J. G., U. Becker, W. K. Bertram, M. Binkley, E. Coleman, C. L. Jordan, M. Rohde, A. J. S. Smith, and S. C. C. Ting, 1968, Phys. Rev. Lett. **20**, 227.

Atwood, W. B., and G. B. West, 1973, Phys. Rev. D **7**, 773.

Atwood, W. B., E. D. Bloom, R. L. A. Cottrell, H. DeStaebler, M. Mestayer, C. Y. Prescott, L. S. Rochester, S. Stein, R. E. Taylor, and D. Trines, 1976, Phys. Lett. B **64**, 479.

Aubert, J. J., U. Becker, J. P. Biggs, J. Burger, M. Chen,

G. Everhart, P. Goldhagen, J. Leong, T. McCorriston, T. G. Rhoades, M. Rohde, Samuel C. C. Ting, Sau Lan Wu, and Y. Y. Lee, 1974, Phys. Rev. Lett. **33**, 1404.

Augustin, J. E., J. C. Bizot, J. Buon, J. Haissinski, D. Lalanne, P. C. Martin, J. Perez-y-Jorba, F. Rumpf, E. Silva, and S. Tavernier, 1968, Phys. Rev. Lett. **20**, 126.

Augustin, J. E., J. C. Bizot, J. Buon, J. Haissinski, D. Lalanne, P. Marin, H. Nguyen Ngoc, J. Perez-y-Jorba, F. Rumpf, E. Silva, and S. Tavernier, 1969a, Phys. Lett. B **28**, 508.

Augustin, J. E., D. Benaksas, J. Buon, F. Fulda, V. Gracco, J. Haissinski, D. Lalanne, F. Laplanche, J. Lefrancois, P. Lehmann, P. C. Marin, J. Perez-y-Jorba, F. Rumpf, and E. Silva, 1969b, Nuovo Cimento Lett. **2**, 214.

Augustin, J. E., D. Benaksas, J. Buon, V. Gracco, J. Haissinski, D. Lalanne, F. Laplanche, J. Lefrancois, P. Lehmann, P. Marin, F. Rumpf, and E. Silva, 1969c, Phys. Lett. B **28**, 513.

Augustin, J. E., J. C. Bizot, J. Buon, B. Delcourt, J. Haissinski, J. Jeanjean, D. Lalanne, P. C. Marin, H. Nguyen Ngoc, J. Perez-y-Jorba, F. Richard, F. Rumpf, and D. Treille, 1969d, Phys. Lett. B **28**, 517.

Augustin, J. E., A. M. Boyarski, M. Breidenbach, F. Bulos, J. T. Dakin, G. J. Feldman, G. E. Fischer, D. Fryberger, G. Hanson, B. Jean-Marie, R. R. Larsen, V. Lüth, H. L. Lynch, D. Lyon, C. C. Morehouse, J. M. Paterson, M. L. Perl, B. Richter, P. Rapidis, R. F. Schwitters, W. M. Tanenbaum, F. Vannucci, G. S. Abrams, D. Briggs, W. Chinowsky, C. E. Friedberg, G. Goldhaber, R. J. Hollebeek, J. A. Kadyk, B. Lulu, F. Pierre, G. H. Trilling, J. S. Whitaker, J. Wiss, and J. E. Zipse, 1974a, Phys. Rev. Lett. **33**, 1406.

Augustin, J. E., A. M. Boyarski, M. Breidenbach, F. Bulos, J. T. Dakin, G. J. Feldman, G. E. Fischer, D. Fryberger, G. Hanson, B. Jean-Marie, R. R. Larsen, V. Lüth, H. L. Lynch, D. Lyon, C. C. Morehouse, J. M. Paterson, M. L. Perl, B. Richter, R. F. Schwitters, F. Vannucci, G. S. Abrams, D. Briggs, W. Chinowsky, C. E. Friedberg, G. Goldhaber, R. J. Hollebeek, J. A. Kadyk, G. H. Trilling, J. S. Whitaker, and J. E. Zipse, 1975, Phys. Rev. Lett. **34**, 233.

Auslander, V. L., G. I. Budker, Ju. N. Pestov, V. A. Sidorov, A. N. Skrinsky, and A. G. Khabakpashev, 1967, Phys. Lett. B **25**, 433.

Auslender, V. L., G. I. Budker, E. V. Pakhtusova, Yu. N. Pestov, V. A. Sidorov, A. N. Skrinskii, and A. G. Khabakhpashev, 1969, Yad. Fiz. **9**, 114 [Sov. J. Nucl. Phys. **9**, 69 (1969)].

Aviv, R., Y. Goren, D. Horn, and S. Nussinov, 1975, Phys. Rev. D **12**, 2862.

Avni, Y., and M. Milgrom, 1973, Phys. Rev. D **7**, 1463.

Bacci, C., G. Penso, G. Salvini, B. Stella, R. Baldini-Celio, G. Capon, C. Mencuccini, G. P. Murtas, A. Reale, and M. Spinetti, 1972, Phys. Lett. B **38**, 551.

Bacci, C., G. Parisi, G. Penso, G. Salvini, B. Stella, R. Baldini-Celio, G. Capon, C. Mencuccini, C. P. Murtas, M. Spinetti, and A. Zallo, 1973, Phys. Lett. B **44**, 530.

Bacci, C., R. Baldini-Celio, M. Bernardini, G. Capon, R. Del Fabbro, M. Grilli, E. Iarocci, L. Jones, M. Locci, C. Mencuccini, G. P. Murtas, G. Penso, G. Salvini, M. Spano, M. Spinetti, B. Stella, V. Valente, B. Bartoli, D. Bisello, B. Esposito, F. Felicetti, P. Monacelli, M. Nigro, L. Paoluzi, I. Peruzzi, G. Piano Mortari, M. Piccolo, F. Ronga, F. Sebastiani, L. Trasatti, F. Vanoli, G. Barbarino, G. Barbiellini, C. Bemporad, R. Biancastelli, M. Calvetti, M. Castellano, F. Cevenini, F. Costantini, P. Lariccia, S. Patricelli, P. Parascandalo, E. Sassi, C. Spencer, L. Tortora, U. Troya, and S. Vitale, 1974, Phys. Rev. Lett. **33**, 1408; **33**, 1649(E).

Bacci, C., R. Baldini-Celio, G. Capon, R. DelFabbro, G. DeZorzi, E. Iarocci, G. P. Murtas, G. Penso, M. Spinetti, and B. Stella, 1977, Phys. Lett. B **68**, 393.

Balakin, V. E., G. I. Budker, E. V. Pakhtusova, V. A. Sidorov, A. N. Skrinsky, and G. M. Tumaikin, and A. G. Khabakhpashev, 1971a, Phys. Lett. B **34**, 328.

Balakin, V. E., G. I. Budker, L. M. Kurdadze, A. P. Onuchin, E. V. Pakhtusova, S. I. Serednyakov, V. A. Sidorov, A. N. Skrinsky, and A. G. Khabakhpashev, 1971b, Phys. Lett. B **37**, 435.

Balakin, V. E., G. I. Budker, L. M. Kurdadze, A. P. Onuchin, E. V. Pakhtusova, S. I. Serednyakov, V. A. Sidorov, A. N. Skrinsky, 1972, Phys. Lett. B **41**, 205.

Ballam, J., G. B. Chadwick, Z. G. T. Guiragossián, P. Klein, A. Levy, M. Menke, E. Pickup, P. Seyboth, T. H. Tan, and G. Wolf, 1968a, Phys. Rev. Lett. **21**, 1541.

Ballam, J., G. B. Chadwick, Z. G. T. Guiragossián, P. Klein, A. Levy, M. Menke, E. Pickup, P. Seyboth, T. H. Tan, and G. Wolf, 1968b, Phys. Rev. Lett. **21**, 1544.

Ballam, J., G. B. Chadwick, R. Gearhart, Z. G. T. Guiragossián, P. R. Klein, A. Levy, M. Menke, J. J. Murray, P. Seyboth, G. Wolf, C. K. Sinclair, H. H. Bingham, W. B. Fretter, K. C. Moffeit, W. J. Podolsky, M. S. Rabin, A. H. Rosenfeld, and R. Windmolders, 1969a, Phys. Rev. Lett. **23**, 498; **23**, 817(E).

Ballam, J., G. B. Chadwick, Z. G. T. Guiragossián, A. Levy, M. Menke, P. Seyboth, and G. Wolf, 1969b, Phys. Lett. B **30**, 421.

Ballam, J., G. B. Chadwick, R. Gearhart, Z. G. T. Guiragossián, M. Menke, J. J. Murray, P. Seyboth, A. Shapira, C. K. Sinclair, I. O. Skillicorn, G. Wolf, R. H. Milburn, H. H. Bingham, W. B. Fretter, K. C. Moffeit, W. J. Podolsky, M. S. Rabin, A. H. Rosenfeld, and R. Windmolders, 1970, Phys. Rev. Lett. **24**, 960; **24**, 1467(E).

Ballam, J., G. B. Chadwick, R. Gearhart, Z. G. T. Guiragossián, M. Menke, J. J. Murray, P. Seyboth, A. Shapira, C. K. Sinclair, I. O. Skillicorn, G. Wolf, R. H. Milburn, H. H. Bingham, W. B. Fretter, K. C. Moffeit, W. J. Podolsky, M. S. Rabin, A. H. Rosenfeld, and R. Windmolders, 1970a, Phys. Rev. Lett. **24**, 1364; **26**, 155(E) (1971).

Ballam, J., G. B. Chadwick, R. Gearhart, Z. G. T. Guiragossián, J. J. Murray, P. Seyboth, C. K. Sinclair, I. O. Skillicorn, H. Spitzer, G. Wolf, H. H. Bingham, W. B. Fretter, K. C. Moffeit, W. J. Podolsky, M. S. Rabin, A. H. Rosenfeld, R. Windmolders, and R. H. Milburn, 1972, Phys. Rev. D **5**, 545.

Ballam, J., G. B. Chadwick, Y. Eisenberg, E. Kogan, K. C. Moffeit, P. Seyboth, I. O. Skillicorn, H. Spitzer, G. Wolf, H. H. Bingham, W. B. Fretter, W. J. Podolsky, M. S. Rabin, A. H. Rosenfeld, and G. Smadja, 1973, Phys. Rev. D **7**, 3150.

Ballam, J., E. D. Bloom, J. T. Carroll, G. B. Chadwick, R. L. A. Cottrell, M. Della Negra, H. DeStaebler, L. K. Gershwin, L. P. Keller, M. D. Mestayer, K. C. Moffeit, C. Y. Prescott, and S. Stein, 1974a, Phys. Rev. D **10**, 765.

Ballam, J., G. B. Chadwick, Y. Eisenberg, E. Kogan, K. C. Moffeit, I. O. Skillicorn, H. Spitzer, G. Wolf, H. H. Bingham, W. B. Fretter, W. J. Podolsky, M. S. Rabin, A. H. Rosenfeld, G. Smadja, and P. Seyboth, 1974b, Nucl. Phys. B **76**, 375.

Bapu, P., R. Endorf, B. Meadows, M. M. Nussbaum, H. O. Cohn, W. M. Bugg, G. T. Condo, and E. L. Hart, 1977, Phys. Rev. D **15**, 26.

Baranov, P. S., L. I. Slovokhotov, G. A. Sokol, and L. N. Shtarkov, 1961, Zh. Eksp. Teor. Fiz. **41**, 1713 [Sov. Phys.—JETP **14**, 1219 (1962)].

Baranov, P. S., L. I. Slovokhotov, G. A. Sokol, and L. N. Shtarkov, 1966, Zh. Eksp. Teor. Fiz. **50**, 364 [Sov. Phys.—JETP **23**, 242 (1966)].

Baranov, P. S., G. M. Buĭnov, V. G. Godin, V. A. Kuznetsova, V. A. Petrun'kin, L. S. Tatarinskaya, V. S. Shirchenko, L. N. Shtarov, V. V. Yurchenko, and Yu. P. Yanulis, 1974, Zh. Eksp. Teor. Fiz. Pis'ma Red. **19**, 777 [JETP Lett. **19**, 398 (1974)].

Baranov, P. S., G. M. Buĭnov, V. G. Godin, V. A. Kuznetsova, V. A. Petrunkin, L. S. Tatarinskaya, V. S. Shirchenko, L. N. Shtarkov, V. V. Yurchenko, and Yu. P. Yanulis, 1975, Yad.

Fiz. **21**, 689 [Sov. J. Nucl. Phys. **21**, 355 (1975)].
Barber, W. C., B. Gittelman, G. K. O'Neill, W. K. H. Panofsky, and B. Richter, 1959, Stanford University Report HEPL 170.
Barber, W. C., B. Gittelman, G. K. O'Neill, and B. Richter, 1966, Phys. Rev. Lett. **16**, 1127.
Barbiellini, C., G. Capon, G. DeZorzi, and G. P. Murtas, 1968, Phys. Rev. **174**, 1665.
Barger, V., and D. Cline, 1970, Phys. Rev. Lett. **24**, 1313.
Barish, B., R. Gomez, D. Kreinick, C. Peck, J. Pine, F. Sciulli, B. Sherwood, A. Tollestrup, and K. Young, 1974, Phys. Rev. D **9**, 566.
Bartl, A., and P. Urban, 1966, Acta Phys. Austriaca **24**, 139.
Bartoli, B., F. Felicetti, H. Ogren, V. Silvestrini, G. Marini, A. Nigro, and F. Vanoli, 1972, Phys. Rev. D **6**, 2374.
Barton, J. S., P. S. L. Booth, L. J. Carroll, J. R. Holt, A. P. Hufton, J. N. Jackson, G. Moscati, J. H. Norem, and H. R. Wormald, 1972, Phys. Lett. B **42**, 297.
Bauer, T. H., 1970, Phys. Rev. Lett. **25**, 485; **25**, 704(E).
Bauer, T. H., 1971, Phys. Rev. D **3**, 2671.
Bauer, T. H., 1972, Acta Phys. Pol. B **3**, 5.
Bauer, T. H., 1973, Nucl. Phys. B **57**, 109.
Bauer, T., and D. R. Yennie, 1976a, Phys. Lett. B **60**, 165.
Bauer, T., and D. R. Yennie, 1976b, Phys. Lett. B **60**, 169.
Bayatyan, G. L., N. K. Grigoryan, S. G. Knyazyan, A. T. Margaryan, G. S. Vartanyan, A. I. Alikhanyan, and A. M. Frolov, 1975, Phys. Lett. B **56**, 197.
Becker, U., W. K. Bertram, M. Binkley, C. L. Jordan, T. M. Knasel, R. Marshall, D. J. Quinn, M. Rohde, A. J. S. Smith, and S. C. C. Ting, 1968, Phys. Rev. Lett. **21**, 1504.
Beder, D. S., 1966, Phys. Rev. **149**, 1203.
Behrend, H.-J., F. Lobkowicz, E. H. Thorndike, and A. A. Wehmann, 1970a, Phys. Rev. Lett. **24**, 336.
Behrend, H.-J., F. Lobkowicz, E. H. Thorndike, A. A. Wehmann, and M. E. Nordberg, Jr., 1970b, Phys. Rev. Lett. **24**, 1246.
Behrend, H.-J., C. K. Lee, F. Lobkowicz, E. H. Thorndike, A. A. Wehmann, and M. E. Nordberg, Jr., 1971a, Phys. Rev. Lett. **26**, 151.
Behrend, H.-J., C. K. Lee, F. Lobkowicz, E. H. Thorndike, M. E. Nordberg, Jr., and A. A. Wehmann, 1971b, Phys. Rev. Lett. **27**, 61.
Behrend, H.-J., C. K. Lee, F. Lobkowicz, E. H. Thorndike, M. E. Nordberg, Jr., and A. A. Wehmann, 1971c, Phys. Rev. Lett. **27**, 65.
Behrend, H.-J., J. Bodenkamp, W. P. Hesse, D. C. Fries, P. Heine, H. Hirschmann, W. A. McNeely, Jr., A. Markou, and E. Seitz, 1975, Phys. Lett. B **56**, 408.
Bell, J. S., 1964, Phys. Rev. Lett. **13**, 57.
Belousov, A. S., N. P. Budanov, Ya. A. Vazdik, B. B. Govorkov, A. I. Lebedev, E. I. Malinovskiĭ, E. V. Minarik, I. V. Mikhaĭlov, V. P. Plaksin, S. V. Rusakov, V. I. Sergienko, E. I. Tamm, A. M. Frolov, P. A. Cerenkov, and P. N. Shareĭko, 1975, Yad. Fiz. **21**, 556 [Sov. J. Nucl. Phys. **21**, 289 (1975)].
Bemporad, C., W. Beusch, A. C. Melissinos, E. Polgár, D. Websdale, J. D. Wilson, J. P. Dufey, K. Freudenreich, R. Frosch, F. X. Gentit, P. Mühlemann, J. Codling, J. G. Lee, M. Letheren, G. Bellini, M. diCorato, and G. Vegni, 1971, Nucl. Phys. B **33**, 397.
Bemporad, C., 1975, in *Proceedings of the 1975 International Symposium on Lepton and Photon Interactions at High Energies*, edited by W. T. Kirk (SLAC, Stanford, Calif.), p. 113.
Bemporad, C., 1977, in *Proceedings of the 1977 International Symposium on Lepton and Photon Interactions at High Energies*, edited by F. Gutbrod (DESY, Hamburg), p. 165.
Benaksas, D., G. Cosme, B. Jean-Marie, S. Jullian, F. Laplanche, J. LeFrancois, A. D. Liberman, G. Parrour, J. P. Repellin, and G. Sauvage, 1972a, Phys. Lett. B **39**, 289.
Benaksas, D., G. Cosme, B. Jean-Marie, S. Jullian, F. Laplanche, J. LeFrancois, A. D. Liberman, G. Parrour, J. P. Repellin, and G. Sauvage, 1972b, Phys. Lett. B **42**, 507.
Benz, P., O. Braun, H. Butenschön, H. Finger, D. Gall, U. Idschok, C. Kiesling, G. Knies, H. Kowalski, K. Müller, P. Nellen, R. Schiffer, P. Schlamp, H. J. Schnackers, V. Schulz, P. Söding, H. Spitzer, J. Stiewe, F. Storim, and J. Weigl, 1973, Nucl. Phys. B **65**, 158.
Benz, P., O. Braun, H. Butenschön, D. Gall, U. Idschok, C. Kiesling, G. Knies, K. Müller, B. Nellen, R. Schiffer, P. Schlamp, P. Söding, and F. Storim, 1974, Nucl. Phys. B **79**, 10.
Berger, C., N. Mistry, L. Roberts, R. Talman, and P. Walstrom, 1972, Phys. Lett. B **39**, 659.
Berman, S. M., and S. D. Drell, 1964, Phys. Rev. **133**, 791B.
Bernardini, C., G. F. Corazza, G. Ghigo, and B. Touschek, 1960, Nuovo Cimento, **18**, 1293.
Bernardini, C., U. Bizzarri, G. F. Corazza, G. Ghigo, R. Querzoli, and B. Touschek, 1962, Nuovo Cimento **23**, 202.
Bernardini, C., G. F. Corazza, G. DiGiugno, J. Haissinski, P. Marin, R. Querzoli, and B. Touschek, 1964, Nuovo Cimento **34**, 1473.
Bernardini, C., 1972, in *Proceedings of the 1971 International Symposium on Electron and Photon Interactions at High Energies*, edited by N. B. Mistry (Laboratory of Nuclear Studies, Cornell University, Ithaca, New York), p. 37.
Bernardini, G., A. O. Hanson, A. C. Odian, T. Yamagata, L. B. Auerbach, and I. Filosofo, 1960, Nuovo Cimento **18**, 1203.
Bernardini, M., D. Bollini, P. L. Brunini, E. Fiorentino, T. Massam, L. Monari, F. Palmonari, F. Rimondi, and A. Zichichi, 1973a, Phys. Lett. B **44**, 393.
Bernardini, M., D. Bollini, P. L. Brunini, E. Fiorentino, T. Massam, L. Monari, F. Palmonari, F. Rimondi, and A. Zichichi, 1973b, Phys. Lett. B **46**, 261.
Bernardini, M., D. Bollini, P. L. Brunini, E. Fiorentino, T. Massam, L. Monari, F. Palmonari, F. Rimondi, and A. Zichichi, 1973c, Phys. Lett. B **45**, 510.
Bernardini, M., D. Bollini, P. L. Brunini, E. Fiorentino, T. Massam, L. Monari, F. Palmonari, F. Rimondi, and A. Zichichi, 1974a, Phys. Lett. B **51**, 200.
Bernardini, M., D. Bollini, P. L. Brunini, E. Fiorentino, T. Massam, L. Monari, F. Palmonari, F. Rimondi, and A. Zichichi, 1974b, Phys. Lett. B **53**, 384.
Beron, B. L., J. F. Crawford, R. L. Ford, R. Hofstadter, E. B. Hughes, R. Kose, P. LeCoultre, T. W. Martin, L. H. O'Neill, R. E. Rand, L. Resvanis, R. F. Schilling, and J. W. Simpson, 1974, Phys. Rev. Lett. **33**, 663.
Bertanza, L., V. Brisson, P. L. Connolly, E. L. Hart, I. S. Mittra, G. C. Moneti, R. R. Rau, N. P. Samios, I. O. Skillicorn, S. S. Yamamoto, M. Goldberg, L. Gray, J. Leitner, S. Lichtman, and J. Westgard, 1962, Phys. Rev. Lett. **9**, 180.
Bertocchi, L., and H. Högaasen, 1971, Nuovo Cimento A **1**, 536.
Besch, H. J., G. Hartmann, R. Kose, F. Krautschneider, W. Paul, and U. Trinks, 1974, Nucl. Phys. B **70**, 257.
Beusch, W., 1972, Acta. Phys. Pol. B **3**, 679.
Białas, A., and K. Zalewski, 1969, Phys. Lett. B **28**, 436.
Biggs, P. J., D. W. Braben, R. W. Clifft, E. Gabathuler, P. Kitching, and R. E. Rand, 1969, Phys. Rev. Lett. **23**, 927.
Biggs, P. J., D. W. Braben, R. W. Clifft, E. Gabathuler, P. Kitching, and R. E. Rand, 1970a, Phys. Rev. Lett. **24**, 1197.
Biggs, P. J., R. W. Clifft, E. Gabathuler, P. Kitching, and R. E. Rand, 1970b, Phys. Rev. Lett. **24**, 1201.
Biggs, P. J., D. W. Braben, R. W. Clifft, E. Gabathuler, and R. E. Rand, 1971, Phys. Rev. Lett. **27**, 1157.
Bingham, H. H., W. B. Fretter, K. C. Moffeit, W. J. Podolsky, M. S. Rabin, A. H. Rosenfeld, J. Ballam, G. B. Chadwick, R. Gearhart, Z. G. T. Guiragossián, M. Menke, J. J. Murray, P. Seyboth, A. Shapira, C. K. Sinclair, I. O. Skillicorn, and G. Wolf, 1970, Phys. Rev. Lett. **24**, 955.

Bingham, H. H., W. B. Fretter, W. J. Podolsky, M. S. Rabin, A. H. Rosenfeld, G. Smadja, G. P. Yost, J. Ballam, G. B. Chadwick, Y. Eisenberg, E. Kogan, K. C. Moffeit, P. Seyboth, I. O. Skillicorn, H. Spitzer, and G. Wolf, 1972, Phys. Lett. B **41**, 635.

Bizot, J. C., J. Buon, Y. Chatelus, J. Jeanjean, D. Lalanne, H. Nguyen Ngoc, J. P. Perez-y-Jorba, P. Petroff, F. Richard, F. Rumpf, and D. Treille, 1970, Phys. Lett. B **32**, 416.

Bjorken, J. D., 1969, Phys. Rev. **179**, 1547.

Bjorken, J. D., J. B. Kogut, and D. E. Soper, 1971, Phys. Rev. D **3**, 1382.

Bjorken, J. D., 1973, SLAC Report No. **167**, Vol. I, 1.

Bjorken, J. D., 1974, in *Proceedings of the 6th International Symposium on Electron and Photon Interactions at High Energies*, edited by H. Rollnik and W. Pfeil (North-Holland, Amsterdam), p. 25.

Bjorken, J. D., and E. A. Paschos, 1969, Phys. Rev. **185**, 1975.

Blechschmidt, H., J. P. Dowd, B. Elsner, K. Heinloth, K. H. Höhne, S. Raither, J. Rathje, D. Schmidt, J. H. Smith, and J. H. Weber, 1967, Nuovo Cimento A **52**, 1348.

Bleckwenn, J., M. Kobberling, J. Moritz, K. H. Schmidt, D. Wegener, D. Zeller, G. Huber, and F. H. Heimlich, 1975, Contributed paper No. 273 to the *Proceedings of the International Symposium on Lepton and Photon Interactions at High Energies*, edited by W. T. Kirk (SLAC, Stanford, Calif.).

Bloom, E. D., D. H. Coward, H. DeStaebler, J. Drees, G. Miller, L. W. Mo, R. E. Taylor, M. Breidenbach, J. I. Friedman, G. C. Hartmann, and H. W. Kendall, 1969a, Phys. Rev. Lett. **23**, 930.

Bloom, E. D., R. L. Cottrell, D. H. Coward, H. DeStaebler, Jr., J. Drees, G. Miller, L. W. Mo, R. E. Taylor, J. I. Friedman, G. C. Hartmann, and H. W. Kendall, 1969b, SLAC Report No. SLAC–PUB–653 (unpublished).

Bloom, E. D., and F. J. Gilman, 1970, Phys. Rev. Lett. **25**, 1140.

Bloom, E. D., R. L. A. Cottrell, H. DeStaebler, C. L. Jordan, G. Miller, H. Piel, C. Prescott, R. Siemann, C. K. Sinclair, S. Stein, and R. E. Taylor, 1972, Phys. Rev. Lett. **28**, 516.

von Bochmann, G., B. Margolis, and C. L. Tang, 1969, Phys. Lett. B **30**, 254.

von Bochmann, G., B. Margolis, and C. L. Tang, 1970, Phys. Rev. Lett. **24**, 483.

Bochmann, G. V., 1972a, Phys. Rev. D **5**, 266.

Bochmann, G. V., 1972b, Phys. Rev. D **6**, 1938.

von Bochmann, G., and B. Margolis, 1969, Phys. Rev. Lett. **23**, 939.

Bodek, A., 1973, Phys. Rev. D **8**, 2331.

Bodek, A., M. Breidenbach, D. L. Dubin, J. E. Elias, J. I. Friedmann, H. W. Kendall, J. S. Poucher, E. M. Riordan, M. R. Sogard, and D. H. Coward, 1973, Phys. Rev. Lett. **30**, 1087.

Bonneau, G., and F. Martin, 1973, Nuovo Cimento A **13**, 413.

Borgia, B., F. Ceradini, M. Conversi, L. Paoluzi, R. Santonico, G. Barbiellini, M. Grilli, P. Spillantini, R. Visentin, and F. Grianti, 1972, Nuovo Cimento Lett. **3**, 115.

Boyarski, A. M., F. Bulos, W. Busza, R. Diebold, S. D. Ecklund, G. E. Fischer, J. R. Rees, and B. Richter, 1968, Phys. Rev. Lett. **20**, 300.

Boyarski, A. M., R. Diebold, S. D. Ecklund, G. E. Fischer, Y. Murata, B. Richter, and M. Sands, 1969, Phys. Rev. Lett. **23**, 1343.

Boyarski, A. M., D. H. Coward, S. Ecklund, B. Richter, D. Sherden, R. Siemann, and C. Sinclair, 1971, Phys. Rev. Lett. **26**, 1600; **30**, 1098(E) (1973).

Boyarski, A. M., M. Breidenbach, F. Bulos, G. J. Feldman, G. E. Fischer, D. Fryberger, G. Hanson, B. Jean-Marie, R. R. Larsen, V. Lüth, H. L. Lynch, D. Lyon, C. C. Morehouse, J. M. Paterson, M. L. Perl, P. Rapidis, B. Richter, R. F. Schwitters, W. Tanenbaum, F. Vannucci, G. S. Abrams, D. Briggs, W. Chinowsky, C. E. Friedberg, G. Goldhaber, J. A. Kadyk, A. Litke, B. Lulu, F. Pierre, B. Sadoulet, G. H. Trilling, J. S. Whitaker, J. Wiss, and J. E. Zipse, 1975a, Phys. Rev. Lett. **34**, 762.

Boyarski, A. M., M. Breidenbach, F. Bulos, G. J. Feldman, G. E. Fischer, D. Fryberger, G. Hanson, B. Jean-Marie, R. R. Larsen, D. Lüke, V. Lüth, H. L. Lynch, D. Lyon, C. C. Morehouse, J. M. Paterson, M. L. Perl, P. Rapidis, B. Richter, R. F. Schwitters, W. Tanenbaum, F. Vannucci, G. S. Abrams, D. D. Briggs, W. Chinowsky, C. E. Friedberg, G. Goldhaber, J. A. Kadyk, A. M. Litke, B. A. Lulu, F. M. Pierre, B. Sadoulet, G. H. Trilling, J. S. Whitaker, F. Winkelmann, and J. E. Wiss, 1975b, Phys. Rev. Lett. **34**, 1357.

Braccini, P. L., C. Bradaschia, R. Castaldi, L. Foa, K. Lübelsmeyer, and D. Schmitz, 1970, Nucl. Phys. B **24**, 173.

Brall, U., G. Reimann, W. Bothin, H. Böttcher, K. Lanius, A. Meyer, A. Pose, J. Moebes, B. Nellen, W. Tejessy, D. Cords, G. Harigel, G. Horlitz, E. Lohrmann, H. Meyer, M. W. Teucher, G. Wolf, D. Lüke, D. Pollmann, W. Rau, P. Söding, H. Spitzer, H. Beisel, H. Filthuth, H. Kolar, P. Steffen, P. Freund, N. Schmitz, P. Seyboth, and J. Seyerlein, 1966, Nuovo Cimento A **41**, 270.

Bramón, A., and M. Greco, 1972, Nuovo Cimeno Lett. **3**, 693.

Bramón, A., E. Etim, and M. Greco, 1972, Phys. Lett. B **41**, 609.

Brandt, R. A., 1969, Phys. Rev. Lett. **23**, 1260.

Brandt, R. A., 1970, Phys. Rev. D **1**, 2808.

Braunschweig, W., C. L. Jordan, U. Martyn, H. G. Sander, D. Schmitz, W. Sturm, W. Wallraff, K. Berkelman, D. Cords, R. Felst, E. Gadermann, G. Grindhammer, H. Hultschig, P. Joos, W. Koch, U. Kötz, H. Krehbiel, D. Kreinick, J. Ludwig, K.-H. Mess, K. C. Moffeit, D. Notz, G. Poelz, K. Sauerberg, P. Schmüser, G. Vogel, B. H. Wiik, G. Wolf, G. Buschhorn, R. Kotthaus, U. E. Kruse, H. Lierl, H. Oberlack, S. Orito, K. Pretzl, M. Schliwa, T. Suda, Y. Totsuka, and S. Yamada, 1974, Phys. Lett. B **53**, 393.

Breidenbach, M., J. I. Friedman, H. W. Kendall, E. D. Bloom, D. H. Coward, H. DeStaebler, J. Drees, L. W. Mo, and R. E. Taylor, 1969, Phys. Rev. Lett. **23**, 935.

Brodsky, S. J., and J. Pumplin, 1969, Phys. Rev. **182**, 1794.

Brodsky, S. J., F. E. Close, and J. F. Gunion, 1972a, Phys. Rev. D **5**, 1384.

Brodsky, S. J., F. E. Close, and J. F. Gunion, 1972b, Phys. Rev. D **6**, 177.

Brodsky, S. J., F. E. Close, and J. F. Gunion, 1973, Phys. Rev. D **8**, 3678.

Brookes, G. R., S. Hinds, W. R. Rawlinson, M. D. Rousseau, D. W. L. Tolfree, and A. G. Wardle, 1970, Nucl. Instrum. Methods **85**, 125.

Brookes, G. R., A. S. Clough, J. H. Freeland, W. Galbraith, A. F. King, T. A. Armstrong, W. R. Hogg, G. M. Lewis, A. W. Robertson, W. R. Rawlinson, N. R. S. Tait, J. C. Thompson, and D. W. L. Tolfree, 1973, Phys. Rev. D **8**, 2826.

Brown, Lowell, S., 1969, in *Lectures in Theoretical Physics*, edited by K. Mahanthappa and W. Brittin (Gordon and Breach, New York), Vol. XII, p. 201.

Buchanan, C. D., and M. R. Yearian, 1965, Phys. Rev. Lett. **15**, 303.

Bulos, F., W. Busza, R. Giese, R. R. Larsen, D. W. G. S. Leith, B. Richter, V. Perez-Mendes, A. Stetz, S. H. Williams, M. Beniston, and J. Rettberg, 1969, Phys. Rev. Lett. **22**, 490.

Bulos, F., W. Busza, R. Giese, E. E. Kluge, R. R. Larsen, D. W. G. S. Leith, B. Richter, S. H. Williams, B. Kehoe, M. Beniston, and A. Stetz, 1971, Phys. Rev. Lett. **26**, 149.

Buschhorn, G., L. Criegee, L. Dubal, G. Franke, C. Geweniger, P. Heide, R. Kotthaus, G. Poelz, U. Timm, K. Wegener, H. Werner, M. Wong, and W. Zimmerman, 1970, Phys. Lett. B **33**, 241.

Buschhorn, G., L. Criegee, G. Franke, P. Heide, R. Kotthaus, G. Poelz, U. Timm, G. Vogel, K. Wegener, H. Wer-

ner, and W. Zimmermann, 1971a, Phys. Lett. B **37**, 207.
Buschhorn, G., L. Criegee, G. Franke, P. Heide, R. Kotthaus, G. Poelz, U. Timm, G. Vogel, K. Wegener, H. Werner, and W. Zimmermann, 1971b, Phys. Lett. B **37**, 211.
Caldwell, D. O., V. B. Elings, W. P. Hesse, G. E. Jahn, R. J. Morrison, F. V. Murphy, and D. E. Yount, 1969, Phys. Rev. Lett. **23**, 1256; **24**, 796(E).
Caldwell, D. O., V. B. Elings, W. P. Hesse, R. J. Morrison, F. V. Murphy, B. W. Worster, and D. E. Yount, 1970, Phys. Rev. Lett. **25**, 609; **25**, 902(E).
Caldwell, D. O., V. B. Elings, W. P. Hesse, R. J. Morrison, F. V. Murphy, and D. E. Yount, 1973, Phys. Rev. D **7**, 1362.
Caldwell, D. O., J. P. Cumalat, A. M. Eisner, A. Lu, R. J. Morrison, F. V. Murphy, S. J. Yellin, P. J. Davis, M. G. Donnelly, R. M. Egloff, G. Luste, J. Martin, J. D. Prentice, and T. Nash, 1977, Paper No. 138 contributed to the 1977 International Symposium on Lepton and Photon Interactions at High Energies.
Callan, C. G., and D. J. Gross, 1969, Phys. Rev. Lett. **22**, 156.
Camerini, U., J. G. Learned, R. Prepost, C. M. Spencer, D. E. Wiser, W. W. Ash, R. L. Anderson, D. M. Ritson, D. J. Sherden, and C. K. Sinclair, 1975, Phys. Rev. Lett. **35**, 483.
Capps, R. H., and W. G. Holladay, 1955, Phys. Rev. **99**, 931.
Carroll, A. S., I-H. Chiang, T. F. Kycia, K. K. Li, P. O. Mazur, P. Mockett, D. C. Rahm, R. Rubinstein, W. F. Baker, D. P. Eartly, G. Giacomelli, P. F. M. Koehler, K. P. Pretzl, A. A. Wehmann, R. L. Cool, and O. Fackler, 1974, Phys. Rev. Lett. **33**, 928.
Ceradini, F., R. Santonico, M. Conversi, L. Paoluzi, M. Grilli, E. Iarocci, P. Spillantini, V. Valente, R. Visentin, and M. Nigro, 1972, Phys. Lett. B **42**, 501.
Ceradini, F., M. Conversi, S. D'Angelo, L. Paoluzi, and R. Santonico, 1973, Phys. Lett. B **47**, 80.
Chadwick, G., Y. Eisenberg, and E. Kogan, 1973, Phys. Rev. D 8, 1607.
Chambers, E. E., and R. Hofstadter, 1956, Phys. Rev. **103**, 1454.
Chang, C., K. W. Chen, D. J. Fox, A. Kotlewski, P. F. Kunz, L. N. Hand, S. Herb, A. Russell, Y. Watanabe, S. C. Loken, M. Strovink, and W. Vernon, 1975, Phys. Rev. Lett. **35**, 901.
Chanowitz, M. S., and S. D. Drell, 1974, Phys. Rev. D **9**, 2078.
Chapline, G., 1970, Phys. Rev. D **1**, 949.
Chasan, B. M., G. Cocconi, V. T. Cocconi, R. M. Schectman, and D. H. White, 1960, Phys. Rev. **119**, 811.
Cheng, H., and T. T. Wu, 1969, Phys. Rev. **183**, 1324.
Chew, G. F., R. Karplus, S. Gasiorowicz, and F. Zachariasen, 1958, Phys. Rev. **110**, 265.
Chew, G. F., and F. E. Low, 1959, Phys. Rev. **113**, 1640.
Cho, C. F., and G. J. Gounaris, 1969, Phys. Rev. **186**, 1619.
Cocho, G., M. Gregorio, J. Leon, and P. Rotelli, 1974a, Phys. Lett. B **48**, 63.
Cocho, G., M. Gregorio, J. Leon, and P. Rotelli, 1974b, Nucl. Phys. B **78**, 269.
Coddington, P., M. Atkiss, T. J. Brodbeck, D. H. Locke, J. V. Morris, D. Newton, and T. Sloan, 1975, Nucl. Phys. B **95**, 249.
Coffin, C. T., N. Dikmen, L. Ettlinger, D. Meyer, A. Saulys, K. Terwilliger, and D. Williams, 1967, Phys. Rev. **159**, 1169.
Conversi, M., L. Paoluzi, F. Ceradini, S. d'Angelo, M. L. Ferrer, R. Santonico, M. Grilli, P. Spillantini, and V. Valente, 1974, Phys. Lett. B **52**, 493.
Cordier, A., B. Delcourt, P. Eschstruth, F. Fulda, G. Grosdidier, J. Maissinski, J. Jeanjean, M. Jeanjean, R. Madaras, J. L. Masnou, J. Perez-Y.-Jorba, A. Quenzer, F. Rumpf, J. L. Bertrand, J. C. Bizot, and R. L. Chase, 1976, Nucl. Instrum. Methods **133**, 237.
Cornwall, J., D. Corrigan, and R. Norton, 1970, Phys. Rev. Lett. **24**, 1141.
Cornwall, J., D. Corrigan, and R. Norton, 1971, Phys. Rev. D **3**, 536.
Cosme, G., B. Jean-Marie, S. Jullian, F. Laplanche, J. Lefrancois, A. D. Liberman, G. Parrour, J. P. Repellin, G. Sauvage, and G. Szklarz, 1972, Phys. Lett. B **40**, 685.
Cosme, G., B. Jean-Marie, S. Jullian, F. Laplanche, J. Lefrancois, A. D. Liberman, G. Parrour, J. P. Repellin, and G. Sauvage, 1974a, Phys. Lett. B **48**, 155.
Cosme, G., B. Jean-Marie, S. Jullian, F. Laplanche, J. Lefrancois, and G. Parrour, 1974b, Phys. Lett. B **48**, 159.
Cosme, G., A. Courau, B. Dudelzak, B. Grelaud, B. Jean-Marie, S. Jullian, D. Lalanne, F. Laplanche, G. Parrour, R. Riskalla, Ph. Roy, and G. Szklarz, 1976a, Phys. Lett. B **63**, 349.
Cosme, G., A. Courau, B. Dudelzak, B. Grelaud, B. Jean-Marie, S. Jullian, D. Lalanne, F. Laplanche, G. Parrour, R. Riskalla, Ph. Roy, and G. Szklarz, 1976b, Phys. Lett. B 63, 352.
Costa de Beauregard, B., T. N. Pham, B. Pire, and Tran N. Truong, 1977a, Phys. Lett. B **67**, 213.
Costa de Beauregard, B., T. N. Pham, B. Pire, and Tran N. Truong, 1977b, Paper No. 203 contributed to the 1977 International Symposium on Lepton and Photon Interactions at High Energies.
Cozzika, G., Y. Ducros, A. Gaidot, A. de Lesquen, J. P. Merlo, and L. Van Rossum, 1972, Phys. Lett. B **40**, 281.
Creutz, M. J., S. D. Drell, and E. A. Paschos, 1969, Phys. Rev. **178**, 2300.
Criegee, L., M. H. Garrell, C. Gottfried, A. Krolzig, G. Loeffler, A. Saulys, K. P. Schüler, U. Timm, W. Zimmermann, H. Werner, G. B. Collins, P. W. Dougan, E. Von Goeler, and R. A. Carrigan, Jr., 1968, Phys. Lett. B **28**, 282.
Criegee, L., G. Franke, G. Löffler, K. P. Schüler, U. Timm, W. Zimmermann, W. Werner, and P. W. Dougan, 1970, Phys. Rev. Lett. **25**, 1306.
Criegee, L., G. Franke, A. Giese, Th. Kahl, G. Poelz, U. Timm, H. Werner, and W. Zimmermann, 1977a, Nucl. Phys. B **121**, 31.
Criegee, L., G. Franke, A. Giese, Th. Kahl, G. Poelz, U. Timm, H. Werner, and W. Zimmermann, 1977b, Nucl. Phys. B **121**, 38.
Crouch, H. R., Jr., R. Hargraves, B. Kendall, R. E. Lanou, A. M. Shapiro, M. Widgoff, G. E. Fischer, A. E. Brenner, M. E. Law, E. E. Ronat, K. Strauch, J. C. Street, J. J. Szymanski, J. D. Teal, P. Bastien, Y. Eisenberg, B. T. Feld, V. K. Fischer, I. A. Pless, A. Rogers, C. Rogers, L. Rosenson, T. L. Watts, R. K. Yamamoto, L. Guerriero, and G. A. Salandin, 1964a, Phys. Rev. Lett. **13**, 636.
Crouch, H. R., Jr., R. Hargraves, B. Kendall, R. E. Lanou, A. M. Shapiro, M. Widgoff, G. E. Fischer, A. E. Brenner, M. E. Law, E. E. Ronat, K. Strauch, J. C. Street, J. J. Szymanski, J. D. Teal, P. Bastien, Y. Eisenberg, B. T. Feld, V. K. Fischer, I. A. Pless, A. Rogers, C. Rogers, L. Rosenson, T. L. Watts, R. K. Yamamoto, L. Guerriero, and G. A. Salandin, 1964b, Phys. Rev. Lett. **13**, 640.
Crouch, H. R., Jr., R. Hargraves, B. Kendall, R. E. Lanou, A. M. Shapiro, M. Widgoff, G. E. Fisher, C. Bordner, Jr., A. E. Brenner, M. E. Law, U. Maor, T. A. O'Halloran, Jr., F. D. Rudnick, K. Strauch, J. C. Street, J. J. Szymanski, P. Bastien, B. T. Feld, V. K. Fischer, I. A. Pless, A. Rogers, C. Rogers, E. E. Ronat, L. Rosenson, T. L. Watts, R. K. Yamamoto, G. Calvelli, F. Gasparini, L. Guerriero, J. Massimo, G. A. Salandin, L. Ventura, C. Voci, F. Waldner, A. Brandstetter, Y. Eisenberg, and A. Levy, 1966, Phys. Rev. **146**, 994.
Crouch, H. R., Jr., R. Hargraves, B. Kendall, R. E. Lanou, A. M. Shapiro, M. Widgoff, G. E. Fischer, C. A. Bordner, Jr., A. E. Brenner, M. E. Law, U. Maor, T. A. O'Halloran, Jr., F. D. Rudnick, K. Strauch, J. C. Street, J. J. Szymanski, P. Bastien, B. T. Feld, V. K. Fischer, I. A. Pless,

A. Rogers, C. Rogers, L. Rosenson, T. L. Watts, R. K. Yamamoto, G. Calvelli, F. Gasparini, L. Guerriero, J. Massimo, G. A. Salandin, L. Ventura, C. Voci, F. Waldner, A. Brandstetter, Y. Eisenberg, A. Levy, and E. E. Ronat, 1967a, Phys. Rev. **155**, 1468.

Crouch, H. R., Jr., R. Hargraves, B. Kendall, R. E. Lanou, A. M. Shapiro, M. Widgoff, G. E. Fischer, C. A. Bordner, Jr., A. E. Brenner, M. E. Law, U. Maor, T. A. O'Halloran, Jr., F. D. Rudnick, K. Strauch, J. C. Street, J. J. Szymanski, P. Bastien, B. T. Feld, V. K. Fischer, I. A. Pless, A. Rogers, C. Rogers, L. Rosenson, T. L. Watts, R. K. Yamamoto, G. Calvelli, F. Gasparini, L. Guerriero, J. Massimo, G. A. Salandin, L. Ventura, C. Voci, F. Waldner, A. Brandstetter, Y. Eisenberg, A. Levy, and E. E. Ronat, 1967b, Phys. Rev. **155**, 1477.

Cumming, J., and H. Osborn, 1971, eds., *Hadronic Interactions of Electrons and Photons* (Academic, New York/London).

Dakin, J. T., G. J. Feldman, W. L. Lakin, F. Martin, M. L. Perl, E. W. Petraske, and W. T. Toner, 1973a, Phys. Rev. Lett. **30**, 142.

Dakin, J. T., G. J. Feldman, W. L. Lakin, F. Martin, M. L. Perl, E. W. Petraske, and W. T. Toner, 1973b, Phys. Rev. D **8**, 687.

Dakin, J. T., M. N. Kreisler, A. M. Lopez, C. Bolon, D. Luckey, J. F. Martin, L. S. Osborne, D. G. Rath, F. B. Helle, D. E. Lyon, M. L. Perl, and T. Pun, 1975, Phys. Lett. B **56**, 405.

Damashek, M., and F. J. Gilman, 1970, Phys. Rev. D **1**, 1319.

Dass, G. V., and H. Fraas, 1975, Ann. Phys. (N.Y.) **92**, 315.

Davier, M., I. Derado, D. Drickey, D. Fries, R. Mozley, A. Odian, F. Villa, D. Yount, and R. Zdanis, 1968, Phys. Rev. Lett. **21**, 841.

Davier, M., I. Derado, D. Drickey, D. Fries, R. Mozley, A. Odian, F. Villa, and D. Yount, 1969a, Phys. Lett. B **28**, 619.

Davier, M., I. Derado, D. Drickey, D. Fries, R. Mozley, A. Odian, F. Villa, and D. Young, 1970, Phys. Rev. D **1**, 790.

Davier, M., 1972, Phys. Lett. B **40**, 369.

Davier, M., I. Derado, D. E. C. Fries, F. F. Liu, R. F. Mozley, A. Odian, J. Park, W. P. Swanson, F. Villa, and D. Yount, 1973, Nucl. Phys. B **58**, 31.

de Lesquen, A., B. Amblard, R. Beurtey, G. Cozzika, J. Bystricky, J. Deregel, Y. Ducros, J. M. Fontaine, A. Gaidot, M. Hansroul, F. Lehar, J. P. Merlo, S. Miyashita, J. Movchet, and L. Van Rossum, 1972, Phys. Lett. B **40**, 277.

dePagter, J. K., J. I. Friedman, G. Glass, R. C. Chase, M. Gettner, E. von Goeler, Roy Weinstein, and A. Boyarski, 1966, Phys. Rev. Lett. **16**, 35.

del Papa, C., D. Dorfan, S. M. Flatté, C. A. Heusch, B. Lieberman, G. Luxton, H. Meyer, L. Moss, T. Schalk, A. Seiden, K. Bunnell, M. Duong-van, R. Mozley, A. Odian, F. Villa, and L. C. Wang, 1976, Phys. Rev. D **13**, 2934.

del Papa, C., D. Dorfan, S. M. Flatté, C. A. Heusch, B. Lieberman, H. Meyer, L. Moss, T. Schalk, A. Seiden, K. Bunnell, M. Duong-van, R. Mozley, A. Odian, F. Villa, and L. C. Wang, 1977, Phys. Rev. D **15**, 2425.

Deser, S., W. Gilbert, and E. C. G. Sudarshan, 1959, Phys. Rev. **115**, 731.

Deser, S., W. Gilbert, and E. C. G. Sudarshan, 1960a, Phys. Rev. **117**, 266.

Deser, S., W. Gilbert, and E. C. G. Sudarshan, 1960b, Phys. Rev. **117**, 273.

Deutsch, M., L. Golub, P. Kijewski, D. Potter, D. J. Quinn, and J. Rutherfoord, 1972, Phys. Rev. Lett. **29**, 1752.

Deutsch, M., K. J. Cleetus, L. Golub, D. F. Jacobs, P. Kijewski, E. Loh, G. Marini, P. M. Patel, D. Potter, R. Stiening, and K. Tsipis, 1973, Phys. Rev. D **8**, 3828.

Devenish, R., and D. Schildknecht, 1976, Phys. Rev. D **14**, 93.

Dewey, P., and B. Humpert, 1971a, Nuovo Cimento Lett. **1**, 651.

Dewey, P., and B. Humpert, 1971b, Nucl. Phys. B **33**, 589.

DeWire, J. W., M. Feldman, V. L. Highland, and R. Littauer, 1961, Phys. Rev. **124**, 909.

Diambrini-Palazzi, G., G. McClellan, N. Mistry, P. Mostek, H. Ogren, J. Swartz, and R. Talman, 1970, Phys. Rev. Lett. **25**, 478.

Diddens, A. N., 1972, in *Proceedings of the Fourth International Conference on High Energy Collisions, Oxford, England, 1972* (Rutherford High Energy Laboratory, Chilton, Didcot, Berkshire, England), p. 127.

Ditsas, P., B. J. Read, and G. Shaw, 1975, Nucl. Phys. B **99**, 85.

Ditsas, P., and G. Shaw, 1976, Nucl. Phys. B **113**, 246.

Ditzler, W. R., M. Breidenbach, J. I. Friedman, H. W. Kendall, J. S. Poucher, E. D. Bloom, R. L. A. Cottrell, D. H. Coward, H. DeStaebler, C. L. Jordan, H. Piel, and R. E. Taylor, 1975, Phys. Lett. B **57**, 201.

Dixon, R., R. Galik, M. Herzlinger, S. D. Holmes, D. Larson, F. M. Pipkin, S. Raither, A. Silverman, and R. L. Wagner, 1977, Phys. Rev. Lett. **39**, 516.

Dominguez, C. A., 1975, Nuovo Cimento Lett. **13**, 704.

Dominguez, C. A., C. Ferro Fontán, and R. Suaya, 1970, Phys. Lett. B **31**, 365.

Dominguez, C. A., J. F. Gunion, and R. Suaya, 1972, Phys. Rev. D **6**, 1404.

Dominguez, C. A., and M. Greco, 1975, Nuovo Cimento Lett. **12**, 439.

Domokos, G., S. Kovesi-Domokos, and E. Schonberg, 1971, Phys. Rev. D **3**, 1184, 1191.

Donnachie, A., and G. Shaw, 1978a, eds., *Electromagnetic Interactions of Hadrons* (Plenum, New York).

Donnachie, A., and G. Shaw, 1978, in *Electromagnetic Interactions of Hadrons*, edited by A. Donnachie and G. Shaw (Plenum, New York), Vol. II.

Drell, S. D., 1958, in *Proceedings of the 1958 Annual International Conference on High Energy Physics at CERN*, edited by B. Ferretti (CERN, Geneva), p. 27.

Drell, S. D., 1960, Phys. Rev. Lett. **5**, 278.

Drell, S. D., and F. Zachariasen, 1961, *Electromagnetic Structure of Nucleons* (Oxford University, London).

Drell, S. D., and J. D. Walecka, 1964, Ann. Phys. (N.Y.) **28**, 18.

Drell, S. D., and J. S. Trefil, 1966, Phys. Rev. Lett. **16**, 552; **16**, 832(E).

Drell, S. D., D. J. Levy, and T.-M. Yan, 1969a, Phys. Rev. Lett. **22**, 744.

Drell, S. D., D. J. Levy, and T.-M. Yan, 1969b, Phys. Rev. **187**, 2159.

Drell, S. D., D. J. Levy, and T.-M. Yan, 1970a, Phys. Rev. D **1**, 1035.

Drell, S. D., D. J. Levy, and T.-M. Yan, 1970b, Phys. Rev. D **1**, 1617.

Drell, S. D., and T.-M. Yan, 1971, Ann. Phys. (N.Y.) **66**, 578.

Driver, C., K. Heinloth, K. Höhne, G. Hofmann, F. Janata, P. Karow, D. Schmidt, G. Specht, and J. Rathje, 1972, Nucl. Phys. B **38**, 1; **53**, 643(E) (1973).

Duerr, H. P., 1956, Phys. Rev. **103**, 469.

Dyson, F. J., 1958, Phys. Rev. **111**, 1717.

Eckardt, V., H. J. Gebauer, P. Joos, H. Meyer, B. Naroska, D. Notz, W. J. Podolsky, G. Wolf, S. Yellin, G. Drews, H. Nagel, and E. Rabe, 1973a, Phys. Lett. B **43**, 240.

Eckardt, V., H. J. Gebauer, P. Joos, H. Meyer, B. Naroska, D. Notz, W. J. Podolsky, G. Wolf, S. Yellin, H. Dau, G. Drews, D. Greubel, W. Meincke, H. Nagel, and E. Rabe, 1973b, Nuovo Cimento Lett. **6**, 551.

Eckardt, V., H. J. Gebauer, P. Joos, H. Meyer, B. Naroska, D. Notz, W. J. Podolsky, G. Wolf, S. Yellin, H. Dau, G. Drews, D. Greubel, W. Meincke, H. Nagel, and E. Rabe, 1973c, Nucl. Phys. B **55**, 45.

Eickmeyer, J., S. Michalowski, N. Mistry, R. Talman, and K. Ueno, 1976a, Phys. Lett. B **63**, 104.

Eickmeyer, J., S. Michalowski, N. Mistry, R. Talman, and

K. Ueno, 1976b, Phys. Rev. Lett. **36**, 289.
Eisenberg, Y., 1974, Phys. Rev. D **9**, 2187.
Eisenberg, Y., B. Haber, Z. Carmel, E. Peleg, E. E. Ronat, A. Shapira, G. Vishinsky, R. Yaari, and G. Yekutieli, 1969, Phys. Rev. Lett. **22**, 669.
Eisenberg, Y., B. Haber, E. E. Ronat, A. Shapira, and G. Yekutieli, 1970, Phys. Rev. Lett. **25**, 764.
Eisenberg, Y., B. Haber, E. Kagan, E. E. Ronat, A. Shapira, and G. Yekutieli, 1971, Nucl. Phys. B **25**, 499.
Eisenberg, Y., B. Haber, E. E. Ronat, A. Shapira, Y. Stahl, G. Yekutieli, J. Ballam, G. Chadwick, M. M. Menke, P. Seyboth, S. Dagan, and A. Levy, 1972a, Phys. Rev. D **5**, 15.
Eisenberg, Y., B. Haber, E. Kogan, E. E. Ronat, A. Shapira, and G. Yekutieli, 1972b, Nucl. Phys. B **42**, 349.
Eisenberg, Y., U. Karshon, J. Mikenberg, S. Pitluck, E. E. Ronat, A. Shapira, and G. Yekutieli, 1973, Phys. Lett. B **43**, 149.
Eisenberg, Y., B. Haber, E. Kogan, U. Karshon, E. E. Ronat, A. Shapira, and G. Yekutieli, 1976, Nucl. Phys. B **104**, 61.
Elitzur, M., 1971, Phys. Rev. D **3**, 2166.
Entenberg, A., H. Jöstlein, I. Kostoulas, A. C. Melissinos, L. M. Lederman, P. Limon, M. May, P. Rapp, H. Gittleson, T. Kirk, M. Murtagh, M. J. Tannenbaum, J. Sculli, T. White, and T. Yamanouchi, 1974, Phys. Rev. Lett. **32**, 486.
Erbe, R., G. Reimann, E. Schüttler, W. Bothin, K. Lanius, A. Meyer, A. Pose, J. Moebes, H. Mück, B. Nellen, W. Tejessy, G. Harigel, G. Horlitz, E. Lohrmann, H. Meyer, W. P. Swanson, G. Wolf, S. Wolff, D. Lüke, D. Pollmann, W. Rau, P. Söding, H. Spitzer, H. Beisel, H. Filthuth, H. Kolar, P. Steffen, P. Freund, K. Gottstein, N. Schmitz, P. Seyboth, and J. Seyerlein, 1966, Nuovo Cimento A **46**, 795.
Erbe, R., G. Reimann, E. Schüttler, H. Böttcher, A. Meyer, A. Pose, J. Schreiber, J. Moebes, H. Mück, W. Tejessy, G. Harigel, G. Horlitz, E. Lohrmann, H. Meyer, W. P. Swanson, M. W. Teucher, G. Wolf, D. Lüke, H. Woidtke, P. Söding, H. Spitzer, H. Beisel, H. Filthuth, H. Kolar, P. Steffen, P. Freund, N. Schmitz, J. Seyerlein, and P. Seyboth, 1967, Nuovo Cimento A **48**, 262.
Erbe, R., H. G. Hilpert, E. Schüttler, W. Struczinski, K. Lanius, A. Meyer, A. Pose, H.-J. Schreiber, K. Böckmann, J. Moebes, H. Mück, B. Nellen, W. Tejessy, G. Horlitz, E. Lohrmann, H. Meyer, W. P. Swanson, M. W. Teucher, G. Wolf, S. Wolff, D. Lüke, P. Söding, H. Spitzer, F. Storim, H. Beisel, H. Filthuth, P. Steffen, P. Freund, K. Gottstein, N. Schmitz, P. Seyboth, and J. Seyerlein, 1968a, Phys. Rev. **175**, 1669.
Erbe, R., H. G. Hilpert, E. Schüttler, W. Struczinski, K. Lanius, A. Meyer, A. Pose, H. J. Schreiber, K. Böckmann, J. Moebes, H. H. Nagel, B. Nellen, W. Tejessy, G. Horlitz, E. Lohrmann, H. Meyer, W. P. Swanson, G. Wolf, S. Wolff, Ch. Eliessbach, D. Lüke, H. Spitzer, F. Storim, H. Beisel, H. Filthuth, P. Steffen, P. Freund, N. Schmitz, P. Seyboth, and J. Seyerlein, 1968b, Phys. Lett. B **27**, 54.
Erbe, R., H. G. Hilpert, E. Schüttler, W. Struczinski, K. Lanius, A. Meyer, A. Pose, H. J. Schreiber, W. Johnssen, J. Moebes, B. Nellen, W. Tejessy, G. Horlitz, E. Lohrmann, H. Meyer, W. P. Swanson, M. W. Teucher, G. Wolf, S. Wolff, H. Alvensleben, D. Lüke, H. Spitzer, F. Storim, H. Beisel, H. Filthuth, H. Kolar, P. Steffen, P. Freund, K. Gottstein, N. Schmitz, P. Seyboth, and J. Seyerlein, 1969, Phys. Rev. **188**, 2060.
Erwin, A. R., R. March, W. D. Walker, and E. West, 1961, Phys. Rev. Lett. **6**, 628.
Esposito, B., R. Bernabei, S. D'Angelo, F. Felicetti, A. Marini, P. Monacelli, M. Moricca, A. Nigro, M. Nigro, L. Paoluzi, L. Pescara, G. Piano-Mortari, F. Ronga, A. Sciubba, F. Sebastiani, B. Sechi-Zorn and G. T. Zorn, 1977, Phys. Lett. B **68**, 389.
Fancher, D. L., D. O. Caldwell, J. P. Cumalat, A. M. Eisner, T. P. McPharlin, R. J. Morrison, F. V. Murphy, and S. J. Yellin, 1976, Phys. Rev. Lett. **37**, 1323.
Federbush, P., M. L. Goldberger, and S. B. Treiman, 1958, Phys. Rev. **112**, 642.
Feldman, G., and P. T. Matthews, 1963, Phys. Rev. **132**, 823.
Feldman, G., 1975, in *Proceedings of the 1975 International Symposium on Lepton and Photon Interactions at High Energies*, edited by W. T. Kirk (SLAC, Stanford, Calif.), p. 39.
Feldman, G. J., and M. L. Perl, 1975, Phys. Rep. **19**, 233.
Feldman, G. J., and M. L. Perl, 1977, Phys. Rep. **33**, 285.
Ferrara, S., M. Greco, and A. F. Grillo, 1970, Nuovo Cimento Lett. **4**, 1.
Ferrari, E., and F. Selleri, 1961, Phys. Rev. Lett. **7**, 387.
Feynman, R. P., 1969, Phys. Rev. Lett. **23**, 1415.
Feynman, R. P., 1972, *Photon-Hadron Interactions* (Benjamin, Reading, Mass.).
Foley, K. J., S. J. Lindenbaum, W. A. Love, S. Ozaki, J. J. Russell, and L. C. L. Yuan, 1963a, Phys. Rev. Lett. **10**, 543.
Foley, K. J., S. J. Lindenbaum, W. A. Love, S. Ozaki, J. J. Russell, and L. C. L. Yuan, 1963b, Phys. Rev. Lett. **11**, 425.
Foley, K. J., S. J. Lindenbaum, W. A. Love, S. Ozaki, J. J. Russell, and L. C. L. Yuan, 1963c, Phys. Rev. Lett. **11**, 503.
Foley, K. J., R. S. Jones, S. J. Lindenbaum, W. A. Love, S. Ozaki, E. D. Platner, C. A. Quarles, and E. H. Willen, 1967, Phys. Rev. Lett. **19**, 330.
Frazer, W. R., and J. R. Fulco, 1959, Phys. Rev. Lett. **2**, 365.
Frazer, W. R., and J. R. Fulco, 1960, Phys. Rev. **117**, 1609.
Fretwell, L. J., Jr., and J. H. Mullins, 1967, Phys. Rev. **155**, 1497.
Freund, P. G. O., 1966, Nuovo Cimento A **44**, 411.
Freund, P. G. O., 1967, Nuovo Cimento A **48**, 541.
Friedman, J., and H. Kendall, 1972, Annu. Rev. Nucl. Sci. **22**, 203.
Frishman, Y., 1972, in *Proceedings of the XVI International Conference on High Energy Physics*, edited by J. D. Jackson and A. Roberts (NAL, Batavia, Ill.), Vol. 4, p. 119.
Fujikawa, K., 1971, Phys. Rev. D **4**, 2794.
Gabathuler, E., 1974, in *Proceedings of the 6th International Symposium on Electron and Photon Interactions at High Energies*, edited by H. Rollnik and W. Pfeil (North-Holland, Amsterdam), p. 299.
Gell-Mann, M., and M. L. Goldberger, 1954, Phys. Rev. **96**, 1433.
Gell-Mann, M., M. L. Goldberger, and W. E. Thirring, 1954, Phys. Rev. **95**, 1612.
Gell-Mann, M., and F. Zachariasen, 1961, Phys. Rev. **124**, 953.
Gell-Mann, M., 1962, Phys. Rev. **125**, 1067.
Gell-Mann, M., D. Sharp, and W. G. Wagner, 1962, Phys. Rev. Lett. **8**, 261.
Genz, H., and W. Schmidt, 1973, Nucl. Phys. B **59**, 629.
Genzel, M., M. Jung, K. R. Rausch, R. Wedemeyer, and H. J. Weyer, 1972, Nuovo Cimento Lett. **4**, 695.
Gerasimov, S. B., 1968, Zh. Eksp. Teor. Fiz. Pis'ma Red. **8**, 205 [JETP-Lett. **8**, 123 (1968)].
Gilman, F. J., J. Pumplin, A. Schwimmer, and L. Stodolsky, 1970, Phys. Lett. B **31**, 387.
Gilman, F., 1975, in *Proceedings of the 1975 International Symposium on Lepton and Photon Interactions at High Energies*, edited by W. T. Kirk (SLAC, Stanford, Calif.), p. 131.
Gittelman, B., K. M. Hanson, D. Larson, E. Loh, A. Silverman, and G. Theodosiou, 1975, Phys. Rev. Lett. **35**, 1616.
Gladding, G. E., J. J. Russell, M. J. Tannenbaum, J. M. Weiss, and G. B. Thomson, 1973, Phys. Rev. D **8**, 3721.
Glauber, R. J., 1959, in *Lectures in Theoretical Physics*, edited by W. E. Brittin and L. G. Dunham (Wiley Interscience, New York), Vol. I, p. 315.
Glauber, R. J., 1970, in *High Energy Physics and Nuclear Structure*, edited by S. Devons (Plenum, New York), p. 207.
Goldhaber, G., 1970, in *Experimental Meson Spectroscopy*, edited by C. Baltay and A. H. Rosenfeld (Columbia U. P., New York), p. 59.

Goldhaber, G., F. M. Pierre, G. S. Abrams, M. S. Alam, A. M. Boyarski, M. Breidenbach, W. C. Carithers, W. Chinowsky, S. C. Cooper, R. G. DeVoe, J. M. Dorfan, G. J. Feldman, C. E. Friedberg, D. Fryberger, G. Hanson, J. Jaros, A. D. Johnson, J. A. Kadyk, R. R. Larsen, D. Lüke, V. Lüth, H. L. Lynch, R. J. Madaras, C. C. Morehouse, H. K. Nguyen, J. M. Paterson, M. L. Perl, I. Peruzzi, M. Piccolo, T. P. Pun, P. Rapidis, B. Richter, B. Sadoulet, R. H. Schindler, R. F. Schwitters, J. Siegrist, W. Tanenbaum, G. H. Trilling, F. Vannucci, J. S. Whitaker, and J. E. Wiss, 1976, Phys. Rev. Lett. **37**, 255.

Gorczyca, B., and D. Schildknecht, 1973, Phys. Lett. B **47**, 71.

Gottfried, K., 1970, in *Proceedings of the Third International Conference on High Energy Physics and Nuclear Structure*, edited by S. Devons (Plenum, New York), p. 783.

Gottfried, K., 1972, in *Proceedings of the 1971 International Symposium on Electron and Photon Interactions at High Energies*, edited by N. B. Mistry (Laboratory of Nuclear Studies, Cornell University, Ithaca, New York), p. 221.

Gottfried, K., and D. R. Yennie, 1969, Phys. Rev. **182**, 1595.

Gottfried, K., and D. I. Julius, 1970, Phys. Rev. D **1**, 140.

Gounaris, G. J., and J. J. Sakurai, 1968, Phys. Rev. Lett. **21**, 244.

Gounaris, G. J., E. K. Manesis, and A. Verganelakis, 1975, Phys. Lett. B **59**, 391.

Gourdin, M., 1961, Nuovo Cimento **21**, 1094.

Gourdin, M., 1971, in *Hadronic Interactions of Electrons and Photons*, edited by J. Cumming and H. Osborn (Academic, New York/London), p. 395.

Grammer, G., and J. D. Sullivan, 1978, in *Electromagnetic Interactions of Hadrons*, edited by A. Donnachie and G. Shaw (Plenum, New York), Vol. II.

Gray, E. R., and A. D. Hanson, 1967, Phys. Rev. **160**, 1212.

Greco, M., 1973, Nucl. Phys. B **63**, 398.

Greco, M., 1975, in *Lepton and Hadron Structure*, edited by A. Zichichi (Academic, New York), p. 262.

Greco, M., and Y. N. Srivastava, 1974, Phys. Lett. B **51**, 172.

Gribov, V. N., B. L. Ioffe, and I. Ya. Pomeranchuk, 1965, Yad. Fiz. **2**, 768 [Sov. J. Nucl. Phys. **2**, 549 (1966)].

Gribov, V. N., 1969, Zh. Eksp. Teor. Fiz. **57**, 1306 [Sov. Phys.—JETP **30**, 709 (1970)].

Grilli, M., E. Iarocci, P. Spillantini, V. Valente, R. Visentin, B. Borgia, F. Ceradini, M. Conversi, L. Paoluzi, R. Santonico, M. Nigro, L. Trasatti, and G. T. Zorn, 1973, Nuovo Cimento A **13**, 593.

Gross, D. J., and F. Wilczek, 1973, Phys. Rev. Lett. **30**, 1343.

Gunion, J., and R. Suaya, 1973, Phys. Rev. D **8**, 156.

Gupta, V. P., S. Y. Fung, Y. T. Oh, R. T. Poe, D. Sager, B. Shen, G. Gidal, R. Ely, R. W. Birge, and C. Scale, 1976, Phys. Rev. D **14**, 42.

Gutbrod, F., 1977, ed., *Proceedings of the 1977 International Symposium on Lepton and Photon Interactions at High Energies* (DESY, Hamburg).

Halpern, H. J., R. Prepost, D. H. Tompkins, R. L. Anderson, B. Gottschalk, D. B. Gustavson, D. M. Ritson, G. A. Weitsch, and B. H. Wiik, 1972, Phys. Rev. Lett. **29**, 1425.

Hand, L. N., 1961, Ph.D. Thesis, Stanford University.

Hand, L. N., 1963, Phys. Rev. **129**, 1834.

Hand, L., 1977, in *Proceedings of the 1977 International Symposium on Lepton and Photon Interactions at High Energies*, edited by F. Gutbrod (DESY, Hamburg), p. 417.

Hanson, G., G. S. Abrams, A. M. Boyarski, M. Breidenbach, F. Bulos, W. Chinowsky, G. J. Feldman, C. E. Friedberg, D. Fryberger, G. Goldhaber, D. L. Hartill, B. Jean-Marie, J. A. Kadyk, R. R. Larsen, A. M. Litke, D. Lüke, B. A. Lulu, V. Lüth, H. L. Lynch, C. C. Morehouse, J. M. Paterson, M. L. Perl, F. M. Pierre, T. P. Pun, P. A. Rapidis, B. Richter, B. Sadoulet, R. F. Schwitters, W. Tanenbaum, G. H. Trilling, F. Vannucci, J. S. Whitaker, F. C. Winkelmann, and J. E. Wiss, 1975, Phys. Rev. Lett. **35**, 1609.

Harari, H., 1967, Phys. Rev. **155**, 1565.

Harari, H., 1971, in *Hadronic Interactions of Electrons and Photons*, edited by J. Cumming and H. Osborn (Academic, New York/London), p. 529.

Hartung, D., P. Blackall, B. Elsner, A. C. Helmholtz, W. C. Middelkoop, B. Powell, B. Zacharov, P. Zanella, P. Dalpiaz, M. N. Focacci, S. Focardi, G. Giacomelli, L. Monari, J. A. Bleaney, R. A. Donald, P. Mason, L. W. Jones, and D. O. Caldwell, 1965, Nuovo Cimento **38**, 60.

Hendrick, R. E., and B. Lautrup, 1975, Phys. Rev. D **11**, 529.

Herb, S., 1977, private communication, based on Chang *et al.* (1975) and Watanabe *et al.* (1975).

Herb, S. W., D. C. Hom, L. M. Lederman, J. C. Sens, H. D. Snyder, J. K. Yoh, J. A. Appel, B. C. Brown, C. N. Brown, W. R. Innes, K. Ueno, T. Yamanouchi, A. S. Ito, M. Jöstlein, D. M. Kaplan, and R. D. Kephard, 1977, Phys. Rev. Lett. **39**, 252.

Hesse, W. P., D. O. Caldwell, V. B. Elings, R. J. Morrison, F. V. Murphy, B. W. Worster, and D. E. Yount, 1970, Phys. Rev. Lett. **25**, 613; **25**, 902(E), 979(E).

Heynen, V., H. Meyer, B. Naroska, and D. Notz, 1971, Phys. Lett. B **34**, 651.

Hicks, N., A. Eisner, G. Feldman, L. Litt, W. Lockeretz, F. M. Pipkin, J. K. Randolph, and K. C. Stanfield, 1969, Phys. Lett. B **29**, 602.

Hilpert, H. G., P. Lauscher, M. Matziolis, U. Idschok, K. Müller, A. Kolb, D. Lüke, P. Raulefs, H. Spitzer, F. Storim, G. Knies, S. Brandt, O. Braun, J. Stiewe, P. Schlamp, and J. Weigl, 1970a, Nucl. Phys. B **23**, 45.

Hilpert, H. G., P. Lauscher, U. Idschok, H. Kowalski, K. Müller, B. Nellen, E. Paul, P. Benz, H. Spitzer, F. Storim, H.-J. Willutzki, P. Söding, S. Brandt, O. Braun, J. Stiewe, H. Finger, P. Schlamp, and J. Weigl, 1970b, Nucl. Phys. B **21**, 93.

Höhler, G., and H. P. Jakob, 1972, Karlsruhe preprint TKP 23/72.

Höhler, G., and H. P. Jakob, 1974, Z. Phys. **268**, 75.

Holladay, W. G., 1956, Phys. Rev. **101**, 1198.

Hughes, D. J., J. A. Harvey, M. D. Goldberg, and M. J. Stafne, 1953, Phys. Rev. **90**, 497.

Hyams, B. D., W. Koch, D. Pellett, D. Potter, L. Von Lindern, E. Lorenz, G. Lütjens, U. Stierlin, and P. Weilhammer, 1967, Phys. Lett. B **24**, 634.

Hyams, B., C. Jones, P. Weilhammer, W. Blum, H. Dietl, G. Grayer, W. Koch, E. Lorenz, G. Lütgens, W. Märmer, J. Meissburger, W. Ochs, and U. Stierlin, 1973, Nucl. Phys. B **64**, 134.

Hyman, L. G., R. Ely, D. H. Frisch, and M. A. Wahlig, 1959, Phys. Rev. Lett. **3**, 93.

Innes, W. R., J. A. Appel, B. C. Brown, C. N. Brown, K. Ueno, T. Yamanouchi, S. W. Herb, D. C. Hom, L. M. Lederman, J. C. Sens, H. D. Snyder, J. K. Yok, R. J. Fisk, A. S. Ito, M. Jöstlein, D. M. Kaplan, and R. D. Kephart, 1977, Phys. Rev. Lett. **39**, 1240.

Ioffe, B. L., 1969, Phys. Lett. B **30**, 123.

Jackiw, R., R. van Royen, and G. B. West, 1970, Phys. Rev. D **2**, 2473.

Jackson, J. D., 1967, in *Proceedings of the XIIIth International Conference on High-Energy Physics*, edited by M. Alston-Garnjost (University of California, Berkeley), p. 149.

Jaffe, R. L., 1972, Phys. Rev. D **5**, 2622.

Jeanjean, J., M. Jeanjean, R. Madaras, J. L. Masnou, J. Perez-Y.-Jorba, Q. Quenzer, F. Rumpf, J. I. Bertrand, J. C. Bizot, R. L. Chase, A. Cordier, B. Delcourt, P. Eschstruth, and G. Grosdidier, 1974, Nucl. Instrum. Methods **117**, 349.

Johnson, R. C., A. D. Martin, and M. R. Pennington, 1976, Phys. Lett. B **63**, 95.

Jones, W. G., D. Kreinick, R. Anderson, D. Gustavson,

J. Johnson, D. Ritson, F. Murphy, M. Gettner, and R. Weinstein, 1968, Phys. Rev. Lett. **21**, 586.
Joos, H., 1967a, Acta Phys. Austriaca, Suppl. IV., p. 320.
Joos, H., 1967b, Phys. Lett. B **24**, 103.
Joos, P., A. Ladage, H. Meyer, P. Stein, G. Wolf, S. Yellin, C. K. Chen, J. Knowles, D. Martin, J. M. Scarr, I. O. Skillicorn, K. Smith, C. Benz, G. Drews, D. Hoffmann, J. Knobloch, W. Kraus, H. Nagel, E. Rabe, C. Sander, W.-D. Schlatter, H. Spitzer, and K. Wacker, 1976, Nucl. Phys. B **113**, 53.
Joos, P., A. Ladage, H. Meyer, P. Stein, G. Wolf, S. Yellin, C. K. Chen, J. Knowles, D. Martin, J. M. Scarr, I. O. Skillicorn, K. Smith, C. Benz, G. Drews, D. Hoffman, J. Knobloch, W. Kraus, H. Nagel, E. Rabe, C. Sander, W.-D. Schlatter, H. Spitzer, and K. Wacker, 1977, Nucl. Phys. B **122**, 365.
Jost, R., and H. Lehmann, 1957, Nuovo Cimento **5**, 1598.
Jöstlein, H., I. J. Kim, K. Königsman, A. C. Melissinos, P. Mühlemann, E. Aslanides, and P. Limon, 1974, Phys. Lett. B **52**, 485.
Julius, D. I., 1971, Nucl. Phys. B **33**, 558.
Julius, D. I., 1972a, Daresbury Lecture Note Series No. 8 (Daresbury Nuclear Physics Laboratory, Daresbury, Lancashire, England).
Julius, D. I., 1972b, Nucl. Phys. B **40**, 409.
Jurisic, N., 1970, Ph.D. Thesis, Cornell University.
Kabe, S., T. Fujii, T. Kamei, R. Yamada, T. Yamagata, S. Kato, I. Kita, and T. Kiyoshima, 1972, Nucl. Phys. B **50**, 17.
Kajantie, K., and J. S. Trefil, 1967, Phys. Lett. B **24**, 106.
Kemp, M. A. R., and R. Marshall, 1975, DNPL/P226.
Kendall, H., 1972, in *Proceedings of the 1971 International Symposium on Electron and Photon Interactions at High Energies*, edited by N. B. Mistry (Laboratory of Nuclear Studies, Cornell University, Ithaca, New York), p. 247.
Khachaturyan, M. N., M. A. Azimov, A. M. Baldin, A. S. Belousov, I. V. Chuvilo, R. Firkowski, J. Hladký, M. S. Khvastunov, J. Manc, A. T. Matyushin, V. T. Matyushin, G. A. Ososkov, L. N. Shtarkov, and L. I. Zhuravleva, 1967, Phys. Lett. B **24**, 349.
Kim, K. J., A. Entenberg, H. Jöstlein, K. Königsmann, I. Kostoulas, A. C. Melissinos, F. Aslanides, L. Lederman, P. Limon, M. May, P. Rapp, H. Gittleson, T. Kirk, M. Murtagh, M. J. Tannenbaum, J. Sculli, T. White, and T. Yamanouchi, 1974, Phys. Rev. Lett. **33**, 551.
Kirk, W. T., 1975, ed., *Proceedings of the 1975 International Symposium on Lepton and Photon Interactions at High Energies* (SLAC, Stanford, Calif.).
Knapp, B., W. Lee, P. Leung, S. D. Smith, A. Wijangco, J. Knauer, D. Yount, D. Nease, J. Bronstein, R. Coleman, L. Cormell, G. Gladding, M. Gormley, R. Messner, T. O'Halloran, J. Sarracino, A. Wattenberg, D. Wheeler, M. Binkley, R. Orr, J. Peoples, and L. Read, 1975, Phys. Rev. Lett. **34**, 1040.
Knapp, B., W. Lee, P. Leung, S. D. Smith, A. Wijangco, J. Knauer, D. Yount, J. Bronstein, R. Coleman, G. Gladding, M. Goodman, M. Gormley, R. Messner, T. O'Halloran, J. Sarracino, A. Wattenberg, M. Binkley, I. Gaines, and J. Peoples, 1976, Phys. Rev. Lett. **37**, 882.
Kogan, E., 1975, Ph.D. Thesis, Weizmann Institute, Rehovot, Israel (unpublished).
Kogut, J. B., 1972, Phys. Rev. D **5**, 1152.
Kogut, J., and L. Susskind, 1973, Phys. Rep. **8**, 75.
Kogut, J., and L. Susskind, 1974, Phys. Rev. D **9**, 697.
Kölbig, K. S., and B. Margolis, 1968, Nucl. Phys. B **6**, 85.
Kramer, G., 1972, Z. Phys. **250**, 413.
Kramer, G., and H. R. Quinn, 1971, Nucl. Phys. B **27**, 77.
Kramer, G., and J. L. Uretsky, 1969, Phys. Rev. **181**, 1918.
Krammer, M., 1970, Acta Phys. Austriaca **32**, 395.
Kroll, N. M., T. D. Lee, and B. Zumino, 1967, Phys. Rev. **157**, 1376.
Kugler, M., and M. Milgrom, 1971, Ann. Phys. (N.Y.) **66**, 335.
Kuti, J., and V. F. Weisskopf, 1971, Phys. Rev. D **4**, 3418.
Lakin, W. L., T. J. Braunstein, J. Cox, B. D. Dieterle, M. L. Perl, W. T. Toner, T. F. Zipf, and H. C. Bryant, 1971, Phys. Rev. Lett. **26**, 34.
Landshoff, P. V., J. C. Polkinghorne, and R. D. Short, 1971, Nucl. Phys. B **28**, 225.
Langacker, P., and G. Segrè, 1976, Phys. Rev. D **13**, 697.
Lanzerotti, L. J., R. B. Blumenthal, D. C. Ehn, W. L. Faissler, P. M. Joseph, F. M. Pipkin, J. K. Randolph, J. J. Russell, D. G. Stairs, and J. Tenenbaum, 1965, Phys. Rev. Lett. **15**, 210.
Lanzerotti, L. J., R. B. Blumenthal, D. C. Ehn, W. L. Faissler, P. M. Joseph, F. M. Pipkin, J. K. Randolph, J. J. Russell, D. G. Stairs, and J. Tenenbaum, 1968, Phys. Rev. **166**, 1365.
Laplanche, F., 1977, in *Proceedings of the 1977 International Symposium on Lepton and Photon Interactions at High Energies*, edited by F. Gutbrod (DESY, Hamburg), p. 189.
Lasinski, T. A., R. Levi-Setti, B. Schwarzschild, and P. Ukleja, 1972, Nucl. Phys. B **37**, 1.
Lee, W. Y., 1977, in *Proceedings of the 1977 International Symposium on Lepton and Photon Interactions at High Energies*, edited by F. Gutbrod (DESY, Hamburg), p. 555.
Leith, D. W. G. S., 1971, in *Hadronic Interactions of Electrons and Photons*, edited by J. Cumming and H. Osborn (Academic, New York/London), p. 195.
Leith, D. W. G. S., 1973, SLAC–PUB–1263. Paper presented at the Eighth Rencontre de Moriond, Meribel-les-Alleres France, March 4–16, 1973.
Leith, D. W. G. S., 1978, in *Electromagnetic Interactions of Hadrons*, edited by A. Donnachie and G. Shaw (Plenum, New York), Vol. I, 345.
Leutwyler, H., and J. Stern, 1970, Nucl. Phys. B **20**, 77.
Lipkin, H. J., 1966, Phys. Rev. Lett. **16**, 1015.
Lipkin, H., 1975, Phys. Rev. D **11**, 1827.
Litke, A., G. Hanson, A. Hofmann, J. Koch, L. Law, M. E. Law, J. Leong, R. Little, R. Madaras, H. Newman, J. M. Paterson, R. Pordes, K. Strauch, G. Tarnopolsky, and Richard Wilson, 1973, Phys. Rev. Lett. **30**, 1189.
Liu, F. F., M. Davier, I. Derado, D. Fries, R. F. Mozley, A. C. Odian, J. Park, W. P. Swanson, F. Villa, and D. Yount, 1972, Nucl. Phys. B **47**, 1.
Llewellyn-Smith, C., 1975, in *Proceedings of the 1975 International Symposium on Lepton and Photon Interactions at High Energies*, edited by T. Kirk (SLAC, Stanford, Calif.), p. 709.
Low, F. E., 1954, Phys. Rev. **96**, 1428.
Lüth, V., A. M. Boyarski, H. L. Lynch, M. Breidenbach, F. Bulos, G. J. Feldman, D. Fryberger, G. Hanson, D. L. Hartill, B. Jean-Marie, R. R. Larsen, D. Lüke, C. C. Morehouse, J. M. Paterson, M. L. Perl, T. P. Pun, P. Rapidis, B. Richter, R. F. Schwitters, W. Tanenbaum, F. Vannucci, G. S. Abrams, W. Chinowsky, C. E. Friedberg, G. Goldhaber, J. A. Kadyk, A. M. Litke, B. A. Lulu, F. M. Pierre, B. Sadoulet, G. H. Trilling, J. S. Whitaker, F. C. Winkelmann, and J. E. Wiss, 1975, Phys. Rev. Lett. **35**, 1124.
Mack, G., 1971, Phys. Lett. B **35**, 234.
Maglić, B. C., L. W. Alvarez, A. H. Rosenfeld, and M. L. Stevenson, 1961, Phys. Rev. Lett. **7**, 178.
Manweiler, R., and W. Schmidt, 1970, Phys. Lett. B **33**, 366.
Manweiler, R. W., and W. Schmidt, 1971, Phys. Rev. D **3**, 2752.
Margolis, B., and C. L. Tang, 1969, Nucl. Phys. B **10**, 329.
Marshall, R., 1977, in *Proceedings of the 1977 International Symposium on Lepton and Photon Interactions at High Energies*, edited by F. Gutbrod (DESY, Hamburg), p. 11.
Martin, J. F., C. Bolon, R. L. Lanza, D. Luckey, L. S. Osborne, D. G. Roth, J. T. Dakin, G. F. Feldman, G. Hanson, D. E. Lyon, M. L. Perl, and T. Pun, 1975, Phys. Rev. Lett.

34, 288.
May, M., E. Aslanides, L. M. Lederman, P. Limon, P. Rapp, A. Entenberg, H. Jöstlein, I. J. Kim, K. Königsman, I. G. Kostoulas, A. C. Melissinos, H. Gittleson, T. Kirk, M. Murtagh, M. J. Tannenbaum, J. Sculli, T. White, and T. Yamanouchi, 1975, Phys. Rev. Lett. **35**, 407.
McAllister, R. W., and R. Hofstadter, 1956, Phys. Rev. **102**, 851.
McClellan, G., N. Mistry, P. Mostek, H. Ogren, A. Silverman, J. Swartz, and R. Talman, 1969a, Phys. Rev. Lett. **22**, 377.
McClellan, G., N. Mistry, P. Mostek, H. Ogren, A. Silverman, J. Swartz, R. Talman, K. Gottfried, and A. I. Lebedev, 1969b, Phys. Rev. Lett. **22**, 374.
McClellan, G., N. Mistry, P. Mostek, H. Ogren, A. Osborne, A. Silverman, J. Swartz, R. Talman, and G. Diambrini-Palazzi, 1969c, Phys. Rev. Lett. **23**, 554.
McClellan, G., N. Mistry, P. Mostek, H. Ogren, A. Osborne, A. Silverman, J. Swartz, R. Talman, and G. Diambrini-Palazzi, 1969d, Phys. Rev. Lett. **23**, 718.
McClellan, G., N. Mistry, P. Mostek, H. Ogren, A. Osborne, J. Swartz, R. Talman, and G. Diambrini-Palazzi, 1971a, Phys. Rev. Lett. **26**, 1593.
McClellan, G., N. Mistry, P. Mostek, H. Ogren, A. Silverman, J. Swartz, and R. Talman, 1971b, Phys. Rev. D **4**, 2683.
McClellan, G., N. Mistry, B. Sandler, J. Swartz, R. Talman, P. Walstrom, and G. Diambrini-Palazzi, 1971c, Phys. Rev. Lett. **26**, 1597.
McIntyre, J. A., 1956, Phys. Rev. **103**, 1464.
McIntyre, J. A., and R. Hofstadter, 1955, Phys. Rev. **98**, 158.
McLeod, D., S. Richert, and A. Silverman, 1961, Phys. Rev. Lett. **7**, 383.
Melkonian, E., B. M. Rustad, and W. W. Havens, Jr., 1956, Phys. Rev. **114**, 1571.
Mennessier, G., and O. Nachtmann, 1971, Phys. Lett. B **34**, 309.
Meyer, H., B. Naroska, J. H. Weber, M. Wong, V. Heynen, E. Mandelkow, and D. Notz, 1970, Phys. Lett. B **33**, 189.
Meyer, W. T., A. Browman, K. Hanson, A. Osborne, A. Silverman, F. E. Taylor, and N. Horwitz, 1972, Phys. Rev. Lett. **28**, 1344.
Michalowski, S., D. Andrews, J. Eickmeyer, T. Gentile, N. Mistry, R. Talman, and K. Ueno, 1977, Phys. Rev. Lett. **39**, 737.
Miklavc, A., and C. H. Woo, 1973, Phys. Rev. D **7**, 3754.
Miller, G., E. D. Bloom, G. Buschhorn, D. H. Coward, H. DeStaebler, J. Drees, C. L. Jordan, L. W. Mo, R. E. Taylor, J. I. Friedman, G. C. Hartmann, H. W. Kendall, and R. Verdier, 1972, Phys. Rev. D **5**, 528.
Mistry, N. B., ed., 1972, *Proceedings of the 1971 International Symposium on Electron and Photon Interactions at High Energies* (Laboratory of Nuclear Studies, Cornell University, Ithaca, New York).
Mo, L. W., 1975, in *Proceedings of the 1975 International Symposium on Lepton and Photon Interactions at High Energies*, edited by W. T. Kirk (SLAC, Stanford, Calif.), p. 651.
Moffat, J. W., and V. G. Snell, 1972, Phys. Rev. D **6**, 859.
Moffeit, K. C., H. H. Bingham, W. B. Fretter, W. J. Podolsky, M. S. Rabin, A. H. Rosenfeld, R. Windmolders, J. Ballam, G. B. Chadwick, R. Gearhart, Z. G. Guiragossian, M. Menke, J. J. Murray, P. Seyboth, A. Shapira, C. K. Sinclair, I. O. Skillicorn, G. Wolf, and R. M. Milburn, 1971, Nucl. Phys. B **29**, 349.
Moffeit, K. C., J. Ballam, G. B. Chadwick, M. Della-Negra, R. Gearhart, J. J. Murray, P. Seyboth, C. K. Sinclair, I. O. Skillicorn, H. Spitzer, G. Wolf, H. H. Bingham, W. B. Fretter, W. J. Podolsky, M. S. Rabin, A. H. Rosenfeld, R. Windmolders, G. P. Yost, and R. H. Milburn, 1972, Phys. Rev. D **5**, 1603.
Moffeit, K., 1974, in *Proceedings of the 6th International Symposium on Electron and Photon Interactions at High Energies*, edited by H. Rollnik and W. Pfeil (North-Holland, Amsterdam), p. 313.
Moniz, E. J., and G. D. Nixon, 1971, Ann. Phys. (N.Y.) **67**, 58.
Moreno, H., and J. Pestieau, 1972, Phys. Rev. D **5**, 1210.
Morris, J. V., T. J. Brodbeck, P. Coddington, D. Newton, and T. Sloan, 1976, Nucl. Phys. B **119**, 420.
Mostek, P., E. Eisenhandler, G. McClellan, N. Mistry, H. Ogren, A. Silverman, J. Swartz, and R. Talman, 1968, Phys. Rev. Lett. **20**, 1057.
Murphy, F. V., and D. E. Yount, 1971, Sci. Amer. **225**, 94 (July).
Nachtmann, O., 1977, in *Proceedings of the 1977 International Symposium on Lepton and Photon Interactions at High Energies*, edited by F. Gutbrod (DESY, Hamburg), p. 811.
Nagoshima, Y., 1964, INSJ-81 (Tokyo).
Nambu, Y., 1957, Phys. Rev. **106**, 1366.
Naroska, B., 1970, Ph.D. thesis, Hamburg University (DESY Report No. DESY-F1-7013) (unpublished).
Nash, T., A. Belousov, B. Govorkov, D. O. Caldwell, J. P. Cumalat, A. M. Eisner, R. J. Morrison, F. V. Murphy, S. J. Yellin, P. J. Davis, R. M. Egloff, G. Luste, and J. D. Prentice, 1976, Phys. Rev. Lett. **36**, 1233.
Nauenberg, M., 1969, Phys. Rev. Lett. **22**, 556.
Newman, H., R. Averill, J. Eshelman, L. Law, M. E. Law, J. Leong, R. Little, H. Mieras, K. Strauch, G. Tarnopolsky, R. Wilson, and H. Winick, 1974, Phys. Rev. Lett. **32**, 483.
Nicolaev, N. N., and V. I. Zakharov, 1975, Phys. Lett. B **55**, 397.
Nieh, H. T., 1970, Phys. Rev. D **1**, 3161.
Nieh, H. T., 1972, Phys. Lett. B **38**, 100.
Nieh, H. T., 1973, Phys. Rev. D **7**, 3401.
Ogren, H. O., 1970, Ph.D. thesis, Cornell University.
O'Neill, G. K., 1956, Phys. Rev. **102**, 1418.
O'Neill, L. H., B. L. Beron, R. L. Carrington, R. L. Ford, E. Hilger, R. Hofstadter, E. B. Hughes, A. D. Liberman, T. W. Martin, J. W. Simpson, and L. K. Resvanis, 1976, Phys. Rev. Lett. **37**, 395.
Orzalesi, C. A., 1973, Phys. Rev. D **7**, 488.
Osborne, L. S., 1965, in *Proceedings of the International Symposium on Electron and Photon Interactions at High Energies*, edited by G. Höhler, G. Kramer, and H. Meyer-Berkhout (Deutsche Physikalische Gesellschaft, Hamburg), p. 91.
Oxley, C. L., and V. L. Telegdi, 1955, Phys. Rev. **100**, 435.
Oxley, C. L., 1958, Phys. Rev. **110**, 733.
Panofsky, W. K. H., 1968, in *Proceedings of the 14th International Conference on High-Energy Physics*, Vienna, edited by J. Prentki and J. Steinberger (CERN, Geneva), p. 23.
Park, J., M. Davier, I. Derado, D. C. Fries, F. F. Liu, R. F. Mozley, A. C. Odian, W. P. Swanson, F. Villa, and D. Yount, 1972, Nucl. Phys. B **36**, 404.
Parrour, G., B. Grelaud, G. Cosme, A. Courau, B. Dudelzak, B. Jean Marie, S. Jullian, D. Lalanne, F. Laplanche, R. Riskalla, Ph. Roy, and G. Szklarz, 1976a, Phys. Lett. B **63**, 357.
Parrour, G., B. Grelaud, G. Cosme, A. Courau, B. Dudelzak, B. Jean-Marie, S. Jullian, D. Lalanne, F. Laplanche, R. Riskalla, Ph. Roy, and G. Szklarz, 1976b, Phys. Lett. B **63**, 362.
Perl, M. L., T. Braunstein, J. Cox, F. Martin, W. T. Toner, B. D. Dieterle, T. F. Zipf, W. L. Lakin, and H. C. Bryant, 1969, Phys. Rev. Lett. **23**, 1191.
Perl, M. L., G. S. Abrams, A. M. Boyarski, M. Breidenbach, D. D. Briggs, F. Bulos, W. Chinowsky, J. T. Dakin, G. J. Feldman, C. E. Friedberg, D. Fryberger, G. Goldhaber, G. Hanson, F. B. Heile, B. Jean-Marie, J. A. Kadyk, R. R. Larsen, A. M. Litke, D. Lüke, B. A. Lulu, V. Lüth, D. Lyon, C. C. Morehouse, J. M. Paterson, F. M. Pierre, T. P. Pun, P. A. Rapidis, B. Richter, B. Sadoulet, R. F. Schwitters, W. Tanenbaum, G. H. Trilling, F. Vannucci, J. S. Whitaker, F. C. Winkelmann, and J. E. Wiss, 1975, Phys. Rev. Lett.

35, 1489.
Peruzzi, I., M. Piccolo, G. J. Feldman, H. K. Nguyen, J. E. Wiss, G. S. Abrams, M. S. Alam, A. M. Boyarski, M. Breidenbach, W. C. Carithers, W. Chinowsky, R. G. DeVoe, J. M. Dorfan, G. E. Fischer, C. E. Friedberg, D. Fryberger, G. Goldhaber, G. Hanson, J. A. Jaros, A. D. Johnson, J. A. Kadyk, R. R. Larsen, D. Lüke, V. Lüth, H. L. Lynch, R. J. Madaras, C. C. Morehouse, J. M. Paterson, M. L. Perl, F. M. Pierre, T. P. Pun, P. Rapidis, B. Richter, R. H. Schindler, R. F. Schwitters, J. Siegrist, W. Tanenbaum, G. H. Trilling, F. Vannucci, and J. S. Whitaker, 1976, Phys. Rev. Lett. **37**, 569.
Pestieau, J., P. Roy, and H. Terazawa, 1970, Phys. Rev. Lett. **25**, 402; **25**, 704(E).
Pestieau, J., and J. Urias, 1973, Phys. Rev. D **8**, 1552.
Pišút, J., and M. Roos, 1968, Nucl. Phys. B **6**, 325.
Politzer, H. D., 1973, Phys. Rev. Lett. **30**, 1346.
Poucher, J. S., M. Breidenbach, R. Ditzler, J. I. Friedman, H. W. Kendall, E. D. Bloom, R. L. A. Cottrell, D. H. Coward, H. DeStaebler, C. L. Jordan, H. Piel, and R. E. Taylor, 1974, Phys. Rev. Lett. **32**, 118.
Powell, J. L., 1949, Phys. Rev. **75**, 32.
Preparata, G., 1974, in *Proceedings of the 6th International Symposium on Electron and Photon Interactions at High Energies*, edited by H. Rollnik and W. Pfeil (North-Holland, Amsterdam), p. 467.
Pugh, G. E., D. H. Frisch, and L. Gomez, 1954, Phys. Rev. **95**, 590.
Pugh, G. E., R. Gomez, D. H. Frisch, and G. Sargent Janes, 1957, Phys. Rev. **105**, 982.
Pumplin, J., 1970, Phys. Rev. D **2**, 1859.
Pumplin, J., and L. Stodolsky, 1970, Phys. Rev. Lett. **25**, 970.
Quenzer, A., F. Rumpf, J. L. Bertrand, J. C. Bizot, R. L. Chase, A. Cordier, B. Delcourt, P. Eschstruth, F. Fuldo, G. Grosdidier, J. Haissinski, J. Jean-jean, M. Jean-jean, R. Madaras, J. L. Masnous, and J. Perez-y-Jorba, 1975, Orsay L.A.L. 1282, paper submitted to 1975 International Symposium on Lepton and Photon Interactions at High Energies, Stanford, 1975.
Quenzer, A., 1977, PhD thesis, University of Paris, Sud.
Quenzer, A., M. Ribes, F. Rumpf, J. L. Bertrand, J. C. Bizot, R. L. Chase, A. Cordier, B. Delcourt, P. Eschstruth, F. Fulda, G. Grosdidier, J. Haissinski, J. Jeanjean, M. Jeanjean, R. J. Madaras, J. L. Masnous, and J. Perez-Y.-Jorba, 1977, Paper No. 140 contributed to 1977 *International Symposium on Lepton and Photon Interactions at High Energies*.
Rand, R. E., R. F. Frosch, C. E. Littig, and M. R. Yearian, 1967, Phys. Rev. Lett. **18**, 469.
Rapidis, P. A., B. Gobbi, D. Lüke, A. Barbari-Goltieri, J. M. Dorfan, R. Ely, G. J. Feldman, J. M. Feller, A. Fong, G. Hanson, J. A. Jaros, B. P. Kwan, P. Lecomte, A. M. Litke, R. J. Madaras, J. F. Martin, T. S. Mast, D. H. Miller, S. I. Parker, M. L. Perl, I. Peruzzi, M. Piccolo, T. P. Pun, M. T. Ronan, R. R. Ross, B. Sadoulet, T. G. Trippe, V. Vuillemin, and D. E. Yount, 1977, Phys. Rev. Lett. **39**, 526.
Reid, R. V., 1968, Ann. Phys. (N.Y.) **50**, 411.
Renard, F. M., 1970, Nucl. Phys. B **15**, 118.
Renard, F. M., 1974, Nucl. Phys. B **82**, 1.
Richter, B., 1974, in *Proceedings of the XVII International Conference on High Energy Physics*, London, edited by J. R. Smith (Science Research Council, Rutherford Laboratory, Chilton, Didcot, England), p. IV–37.
Riordan, E. M., A. Bodek, M. Breidenbach, D. L. Dubin, J. E. Elias, J. I. Friedman, H. W. Kendall, J. S. Poucher, M. R. Sogard, and D. H. Coward, 1974a, Phys. Lett. B **52**, 249.
Riordan, E. M., A. Bodek, M. Breidenbach, D. L. Dubin, J. E. Elias, J. I. Friedman, H. W. Kendall, J. S. Poucher, M. R. Sogard, and D. H. Coward, 1974b, Phys. Rev. Lett. **33**, 561.
Riordan, E. M., A. Bodek, M. Breidenbach, D. L. Dubin, J. E. Elias, J. I. Friedman, H. W. Kendall, J. S. Poucher, and M. R. Sogard, 1975, SLAC–PUB–1634 (unpublished).
Ritson, D. M., 1971, Phys. Rev. D **3**, 1267.
Rochester, L. S., W. B. Atwood, E. D. Bloom, R. L. A. Cottrell, D. H. Coward, H. DeStaebler, M. Mestayer, C. Y. Prescott, S. Stein, R. E. Taylor, and D. Trines, 1976, Phys. Rev. Lett. **36**, 1284.
Rollnik, H., and W. Pfeil, eds., 1974, *Proceedings of the 6th International Symposium on Electron and Photon Interactions at High Energies*, Bonn, 1973 (North-Holland, Amsterdam).
Rosenfeld, A. H., and P. Söding, 1973, in *Properties of the Fundamental Interactions*, edited by A. Zichichi (Editrice Compositori, Bologna), Vol. 9, Part C, p. 883 [1971 Erice Summer School].
Ross, M., and L. Stodolsky, 1966a, Phys. Rev. **149**, 1172.
Ross, M., and L. Stodolsky, 1966b, Phys. Rev. Lett. **17**, 563.
Rothwell, P. L., R. C. Chase, D. R. Earles, M. Gettner, G. Glass, G. Lutz, E. von Goeler, and R. Weinstein, 1969, Phys. Rev. Lett. **23**, 1521.
Roy, P., 1975, *Theory of Lepton-Hadron Processes at High Energies—Partons, Scale Invariance and Light-cone Physics* (Oxford University, London).
Rust, D. R., E. Eisenhandler, P. J. Mostek, A. Silverman, C. K. Sinclair, and R. M. Talman, 1965, Phys. Rev. Lett. **15**, 938.
Sachs, R. G., and L. L. Foldy, 1950, Phys. Rev. **80**, 824.
Sakurai, J. J., 1960, Ann. Phys. (N.Y.) **11**, 1.
Sakurai, J. J., 1966, Phys. Rev. Lett. **17**, 1021.
Sakurai, J. J., 1968, in *Boulder Lectures in Theoretical Physics XI*, edited by K. T. Mahanthappa, W. E. Brittin, and A. O. Barut (Gordon and Breach, N.Y., London, Paris), p. 1.
Sakurai, J. J., 1969a, in *Proceedings of the 4th International Symposium on Electron and Photon Interactions at High Energies*, edited by D. W. Braben (Daresbury Nuclear Physics Laboratory, Daresbury, Lancashire, England), p. 91.
Sakurai, J. J., 1969b, *Currents and Mesons* (University of Chicago, Chicago).
Sakurai, J. J., 1969c, Phys. Rev. Lett. **22**, 981.
Sakurai, J. J., 1973, in *Properties of the Fundamental Interactions*, edited by A. Zichichi (Editrice Compositori, Bologna), Vol. 9, Part A, p. 243 [1971 Erice Summer School].
Sakurai, J. J., 1975, in *Laws of Hadronic Matter*, edited by A. Zichichi (Academic, New York), p. 291.
Sakurai, J. J., and D. Schildknecht, 1972a, Phys. Lett. B **40**, 121.
Sakurai, J. J., and D. Schildknecht, 1972b, Phys. Lett. B **41**, 489.
Sakurai, J. J., and D. Schildknecht, 1972c, Phys. Lett. B **42**, 216.
Satz, H., and K. Schilling, 1970a, Nuovo Cimento A **67**, 511.
Satz, H., and K. Schilling, 1970b, Nuovo Cimento Lett. **3**, 723.
Schiffer, R., H. H. J. Schnackers, V. Valdmanis, U. Idschok, K. Müller, P. Benz, R. Riebensahm, V. Schulz, F. Storim, G. Ullrich, G. Knies, O. Braun, J. Stiewe, H. Finger, C. Kiesling, P. Schlamp, and J. Weigl, 1972, Nucl. Phys. B **38**, 628.
Schildknecht, D., 1969, Z. Phys. **229**, 278.
Schildknecht, D., 1972, *Springer Tracts in Modern Physics* (Springer, Berlin), Vol. 63, p. 57.
Schildknecht, D., 1973, Nucl. Phys. B **66**, 398.
Schildknecht, D., 1975, in *Lepton and Hadron Structure*, edited by A. Zichichi (Academic, New York), p. 448.
Schildknecht, D., and F. Steiner, 1975, Phys. Lett. B **56**, 36.
Schilling, K., P. Seyboth, and G. Wolf, 1970, Nucl. Phys. B **15**, 397; **18**, 332(E).
Schilling, K., and G. Wolf, 1973, Nucl. Phys. B **61**, 381.
Schmidt, W., 1969, Phys. Rev. **188**, 2458.
Schmidt, W., and D. R. Yennie, 1969, Phys. Rev. Lett. **23**,

623; 23, 946(E).
Schwinger, J., 1975, Proc. Nat. Acad. Sci. U.S.A. 72, 1.
Schwitters, R. F., 1975, in *Proceedings of the 1975 International Symposium on Lepton and Photon Interactions at High Energies*, edited by W. T. Kirk (SLAC, Stanford, Calif.), p. 5.
Schwitters, R. F., 1977, in *Proceedings of the XVIII International Conference on High Energy Physics*, Tbilisi, July 1976 (Dubna), Vol. II, p. B34.
Schwitters, R. F., A. M. Boyarski, M. Briedenbach, F. Bulos, G. J. Feldman, G. Hanson, D. L. Hartill, B. Jean-Marie, R. R. Larsen, D. Lüke, V. Lüth, H. L. Lynch, C. C. Morehouse, J. M. Paterson, M. L. Perl, T. P. Pun, P. Rapidis, B. Richter, W. Tanenbaum, F. Vannucci, F. M. Pierre, G. S. Abrams, W. Chinowsky, C. E. Friedberg, G. Goldhaber, J. A. Kadyk, A. M. Litke, B. A. Lulu, B. Sadoulet, G. H. Trilling, J. S. Whitaker, F. C. Winkelmann, and J. E. Wiss, 1975, Phys. Rev. Lett. 35, 1320.
Schwitters, R. F., and K. Strauch, 1976, Annu. Rev. Nucl. Sci. 26, 89.
Sellen, J. M., G. Cocconi, V. T. Cocconi, and E. L. Hart, 1959, Phys. Rev. 113, 1323.
Shephard, W. D., J. T. Powers, N. N. Biswas, N. M. Cason, V. P. Kenney, R. R. Riley, D. W. Thomas, J. W. Elbert, and A. R. Erwin, 1971, Phys. Rev. Lett. 27, 1164; 1972, 28, 260 (E).
Shibasaki, I., T. Minamikawa, and T. Watanabe, 1971, Prog. Theor. Phys. 46, 173.
Siegrist, J., G. S. Abrams, A. M. Boyarski, M. Breidenbach, F. Bulos, W. Chinowsky, G. J. Feldman, C. E. Friedberg, D. Fryberger, G. Goldhaber, G. Hanson, D. L. Hartill, J. Jaros, B. Jean-Marie, J. A. Kadyk, R. R. Larsen, D. Lüke, V. Lüth, H. L. Lynch, R. Madaras, C. C. Morehouse, H. K. Nguyen, J. M. Paterson, M. L. Perl, I. Peruzzi, F. M. Pierre, M. Piccolo, T. P. Pun, P. Rapidis, B. Richter, B. Sadoulet, R. F. Schwitters, W. Tanenbaum, G. M. Trilling, F. Vannucci, J. S. Whitaker, F. C. Winkelmann, and J. E. Wiss, 1976, Phys. Rev. Lett. 36, 700.
Silverman, A., 1969, in *Proceedings of the 4th International Symposium on Electron and Photon Interactions at High Energies*, edited by D. W. Braben and R. E. Rand (Daresbury Nuclear Physics Laboratory, Daresbury, Lancashire, England), p. 71.
Silverman, A., 1975, in *Proceedings of the 1975 International Symposium on Lepton and Photon Interactions at High Energies*, edited by W. T. Kirk (SLAC, Stanford, Calif.), p. 355.
Silvestrini, V., 1972, in *Proceedings of the XVI International Conference on High Energy Physics*, edited by J. D. Jackson and A. Roberts (NAL, Batavia, Ill.), Vol. 4, p. 1.
Söding, P., 1966, Phys. Lett. 19, 702.
Spital, R., and D. R. Yennie, 1974a, Phys. Rev. D 9, 126.
Spital, R., and D. R. Yennie, 1974b, Phys. Rev. D 9, 138.
Spital, R., 1975, Contribution to the 1975 International Symposium on Lepton and Photon Interactions at High Energies, Stanford, California (unpublished).
Spital, R., and D. R. Yennie, 1976, Nucl. Phys. B 106, 269.
Stein, S., W. B. Atwood, E. D. Bloom, R. L. A. Cottrell, H. DeStaebler, C. L. Jordan, H. G. Piel, C. Y. Prescott, R. Siemann, and R. E. Taylor, 1975, Phys. Rev. D 12, 1884.
Stichel, P., 1964, Z. Phys. 180, 170.
Stichel, P., and M. Scholz, 1964, Nuovo Cimento 34, 1381.
Stiening, R. F., E. Loh, and M. Deutsch, 1963, Phys. Rev. Lett. 10, 536.
Stodolsky, L., 1964, Phys. Rev. 134, 1099B.
Stodolsky, L., 1967, Phys. Rev. Lett. 18, 135.
Stodolsky, L., 1970, in *Summer School in Elementary Particle Physics—Weak and Electromagnetic Interactions*, edited by R. F. Peierls (BNL, Upton, New York), p. 371.
Strauch, K., 1974, in *Proceedings of the 6th International Symposium on Electron and Photon Interactions at High Energies*, edited by H. Rollnik and W. Pfeil (North-Holland, Amsterdam), p. 1.
Struczinski, W., H. Meyer, B. Naroska, D. Notz, J. Knobloch, E. Rabe, E. Maier-Reimer, S. Brandt, M. Grimm, D. Pollmann, I. Derado, G. Kronseder, and P. Schacht, 1972, Nucl. Phys. B 47, 436.
Struczinski, W., P. Dittmann, V. Eckardt, P. Joos, A. Ladage, H. Meyer, D. Notz, J. Knobloch, E. Rabe, M. Grimm, D. Pollman, I. Derado, R. Meinke, P. Schacht, and H. Strobl, 1973, Nucl. Phys. B 57, 1.
Struczinski, W., P. Dittmann, V. Eckardt, P. Joos, A. Ladage, H. Meyer, D. Notz, G. Hetschel, J. Knobloch, E. Rabe, E. Taureg, M. Grimm, I. Derado, R. Meinke, and P. Schacht, 1976, Nucl. Phys. B 108, 45.
suri, Ashok, 1971, Phys. Rev. D 4, 570.
suri, A., and D. R. Yennie, 1972, Ann. Phys. (N.Y.) 72, 243.
Swartz, J., and R. Talman, 1969, Phys. Rev. Lett. 23, 1078.
Tait, N. R. S., and J. N. J. White, 1972, Nucl. Phys. B 43, 27.
Talman, R., 1977, Phys. Rev. D 15, 1260.
Tarnopolsky, G., J. Eshelman, M. E. Law, J. Leong, H. Newman, R. Little, K. Strauch, and R. Wilson, 1974, Phys. Rev. Lett. 32, 432.
Taylor, R. E., 1975a, in *Proceedings of the 1975 International Symposium on Lepton and Photon Interactions at High Energies*, edited by W. T. Kirk (SLAC, Stanford, California), p. 679.
Taylor, R. E., 1975b, SLAC–PUB–1613. (Presented at International Conference in High Energy Physics, sponsored by European Physical Society, Palermo, Italy, June 23–28, 1975).
Teller, E., 1956, in *Proceedings of the Sixth Annual Rochester Conference on High-Energy Physics* (Interscience, New York), Chap. VII, p. 18.
Ting, S. C. C., 1975, in *Laws of Hadronic Matter*, edited by A. Zichichi (Academic, New York), p. 759.
Trefil, J. S., 1969, Nucl. Phys. B 11, 330.
Trippe, T. G., A. Barbaro-Galtieri, R. L. Kelley, A. Rittenberg, A. H. Rosenfeld, G. P. Yost, N. Barash-Schmidt, C. Bricman, R. J. Hemingway, M. J. Losty, M. Roos, V. Chaloupka, and B. Armstrong, 1976, Rev. Mod. Phys. 48, S1.
Uretsky, J. L., 1973, Phys. Rev. D 7, 140.
Vaughn, M., and K. Wali, 1968, Phys. Rev. Lett. 21, 938.
von Gehlen, G., 1960, Phys. Rev. 118, 1455.
Watanabe, Y., L. N. Hand, S. Herb, A. Russell, C. Chang, K. W. Chen, D. J. Fox, A. Kotlewski, P. F. Kunz, S. C. Loken, M. Strovink, and W. Vernon, 1975, Phys. Rev. Lett. 35, 898.
Wehmann, A. A., E. Engels, Jr., L. N. Hand, C. M. Hoffman, P. G. Innocenti, Richard Wilson, W. A. Blanpied, D. J. Drickey, and D. G. Stairs, 1966, Phys. Rev. Lett. 17, 1113.
Wehmann, A. A., E. Engels, Jr., C. M. Hoffman, P. G. Innocenti, Richard Wilson, W. A. Blanpied, D. J. Drickey, L. N. Hand, and D. G. Stairs, 1969, Phys. Rev. 178, 2095.
Weise, W., 1974, Phys. Rep. 13, 53.
West, G. B., 1971, Phys. Lett. B 37, 509.
West, G. B., 1972, Ann. Phys. (N.Y.) 74, 464.
West, G. B., 1975, Phys. Rep. 18, 263.
Wiik, B. H., and G. Wolf, 1977, Lectures given at the Les Houches Summer School, 1976, DESY Report DESY 77/01.
Wilson, K. G., 1969, Phys. Rev. 179, 1499.
Wilson, K. G., 1972, in *Proceedings of the 1971 International Symposium on Electron and Photon Interactions at High Energies*, edited by N. B. Mistry (Laboratory of Nuclear Studies, Cornell University, Ithaca, New York), p. 115.
Wolf, G., 1969, Phys. Rev. 182, 1538.
Wolf, G., 1971, in *Springer Tracts in Modern Physics* (Springer, Berlin), Vol. 59, p. 77.
Wolf, G., 1972, in *Proceedings of the 1971 International Symposium on Electron and Photon Interactions at High Energies*, edited by N. B. Mistry (Laboratory of Nuclear Studies, Cornell University, Ithaca, New York), p. 189.

Wolf, G., 1975, in *Proceedings of the 1975 International Symposium on Lepton and Photon Interactions at High Energies*, edited by W. T. Kirk (SLAC, Stanford, Calif.), p. 795.
Yan, T.-M., 1976, Annu. Rev. Nucl. Sci. **26**, 199.
Yang, C. N., and R. L. Mills, 1954, Phys. Rev. **96**, 191.
Yennie, D. R., M. Lévy, and D. G. Ravenhall, 1957, Rev. Mod. Phys. **29**, 144.
Yennie, D. R., 1971, in *Hadronic Interactions of Electrons and Photons*, edited by J. Cummings and H. Osborn (Academic, New York/London), p. 321.
Yennie, D. R., 1975, Rev. Mod. Phys. **47**, 311.
Yennie, D. R., 1976, Acta Phys. Pol. B **7**, 897.
Yennie, D. R., 1977, in *Cargèse Lectures in Physics, Vol. 7*, edited by M. Levy (Gordon and Breach, New York), p. 331.
Zdanis, R. A., L. Madansky, R. W. Kraemer, S. Hertzbach, and R. Strand, 1965, Phys. Rev. Lett. **14**, 721.